

Stainless Steel Strands and Lightweight Concrete for Pretensioned Concrete Girders

FDOT Contract No. BDV30-977-22
FSU Project No. 041063

Submitted to:

Florida Department of Transportation
Research Center
605 Suwannee Street
Tallahassee, Florida 32399-0450

Vickie Young, P.E.
Project Manager
FDOT Structures Design Office



FAMU-FSU
College of
Engineering

Prepared by:

Michelle Rambo-Roddenberry, Ph.D., P.E.
Principal Investigator

Anwer Al-Kaimakchi
Graduate Research Assistant

FAMU-FSU College of Engineering
Department of Civil and Environmental Engineering
2525 Pottsdamer Street
Tallahassee, FL 32310-6046

December 2020

Final Report A – Stainless Steel Strands

DISCLAIMER

The opinions, findings, and conclusions expressed in this publication are those of the authors and not necessarily those of the State of Florida Department of Transportation.

SI* (MODERN METRIC) CONVERSION FACTORS

APPROXIMATE CONVERSIONS TO SI UNITS

SYMBOL	WHEN YOU KNOW	MULTIPLY BY	TO FIND	SYMBOL
LENGTH				
in.	inches	25.4	millimeters	mm
ft	feet	0.305	meters	m
yd	yards	0.914	meters	m
mi	miles	1.61	kilometers	km
AREA				
in²	square inches	645.2	square millimeters	mm ²
ft²	square feet	0.093	square meters	m ²
yd²	square yard	0.836	square meters	m ²
ac	acres	0.405	hectares	ha
mi²	square miles	2.59	square kilometers	km ²
VOLUME				
fl oz	fluid ounces	29.57	milliliters	mL
gal	gallons	3.785	liters	L
ft³	cubic feet	0.028	cubic meters	m ³
yd³	cubic yards	0.765	cubic meters	m ³
NOTE: volumes greater than 1000 L shall be shown in m ³				
MASS				
oz	ounces	28.35	grams	g
lb	pounds	0.454	kilograms	kg
T	short tons (2000 lb)	0.907	megagrams	Mg (or "t")
TEMPERATURE (exact degrees)				
°F	Fahrenheit	5(F-32)/9 or (F-32)/1.8	Celsius	°C
ILLUMINATION				
fc	foot-candles	10.76	lux	lx
fl	foot-Lamberts	3.426	candela/m ²	cd/m ²
FORCE and PRESSURE or STRESS				
kip	1000 pound force	4.45	kilonewtons	kN
lbf	pound force	4.45	newtons	N
lbf/in²	pound force per square inch	6.89	kilopascals	kPa

*SI is the symbol for the International System of Units. Appropriate rounding should be made to comply with Section 4 of ASTM E380.

SI* (MODERN METRIC) CONVERSION FACTORS

APPROXIMATE CONVERSIONS FROM SI UNITS

SYMBOL	WHEN YOU KNOW	MULTIPLY BY	TO FIND	SYMBOL
LENGTH				
mm	millimeters	0.039	inches	in.
m	meters	3.28	feet	ft
m	meters	1.09	yards	yd
km	kilometers	0.621	miles	mi
AREA				
mm²	square millimeters	0.0016	square inches	in ²
m²	square meters	10.764	square feet	ft ²
m²	square meters	1.195	square yards	yd ²
ha	hectares	2.47	acres	ac
km²	square kilometers	0.386	square miles	mi ²
VOLUME				
mL	milliliters	0.034	fluid ounces	fl oz
L	liters	0.264	gallons	gal
m³	cubic meters	35.314	cubic feet	ft ³
m³	cubic meters	1.307	cubic yards	yd ³
MASS				
g	grams	0.035	ounces	oz
kg	kilograms	2.202	pounds	lb
Mg (or "t")	megagrams (or "metric ton")	1.103	short tons (2000 lb)	T
TEMPERATURE (exact degrees)				
°C	Celsius	1.8C+32	Fahrenheit	°F
ILLUMINATION				
lx	lux	0.0929	foot-candles	fc
cd/m²	candela/m ²	0.2919	foot-Lamberts	fl
FORCE and PRESSURE or STRESS				
kN	kilonewtons	0.225	1000 pound force	kip
N	newtons	0.225	pound force	lbf
kPa	kilopascals	0.145	pound force per square inch	lbf/in ²

*SI is the symbol for the International System of Units. Appropriate rounding should be made to comply with Section 4 of ASTM E380.

TECHNICAL REPORT DOCUMENTATION PAGE

1. Report No.	2. Government Accession No.	3. Recipient's Catalog No.	
4. Title and Subtitle Stainless Steel Strands and Lightweight Concrete for Pretensioned Concrete Girders (Final Report A – Stainless Steel Strands)		5. Report Date December 2020	
		6. Performing Organization Code	
7. Author(s) Michelle Rambo-Roddenberry, Anwer Al-Kaimakchi		8. Performing Organization Report No.	
9. Performing Organization Name and Address FAMU-FSU College of Engineering Department of Civil and Environmental Engineering 2525 Pottsdamer St., Rm. A129 Tallahassee, FL 32310-6046		10. Work Unit No. (TRAVIS)	
		11. Contract or Grant No. BDV30-977-22	
12. Sponsoring Agency Name and Address Florida Department of Transportation 605 Suwannee Street, MS 30 Tallahassee, FL 32399-0450		13. Type of Report and Period Covered Final Report December 2020	
		14. Sponsoring Agency Code	
15. Supplementary Notes			
16. Abstract Durability of prestressed concrete bridges in extremely aggressive environments is of increasing concern because of corrosion of the carbon steel strands. One solution to overcome the early deterioration of coastal bridges is to use corrosion-resistant strands, such as duplex high-strength stainless steel (HSSS) strands. The use of HSSS strands in flexural members has been hindered by the lack of full-scale test results and design guidelines. This report investigated the use of HSSS strands in flexural members. A total of thirteen (13) 42-ft-long AASHTO Type II girders were designed, fabricated, and tested in flexure and/or shear. Ten (10) girders were prestressed with HSSS strands, while the other three (3) were prestressed with carbon steel strands and served as control girders. This research program also included experimental activities to determine the mechanical and bond strength characteristics, prestress losses, and transfer length of 0.6-in.-diameter HSSS strands. A stress-strain equation is proposed for the 0.6-in.-diameter HSSS strands. Experimental flexural and shear results showed that the post-cracking behavior of girders prestressed with HSSS strands continued to increase up to failure with no discernible plateau, which reflects the stress-strain behavior of the HSSS strands. In addition, flexural results revealed that, although HSSS strands have low ductility and all composite girders failed due to rupture of strands, the girders provided significant and substantial warning through large deflection, as well as well-distributed and extensive flexural cracking, before failure. Although the developed analytical model gave better predictions, the developed iterative numerical approach is slightly conservative and is easier to use for design – designers prefer to use an equation type of approach to perform preliminary designs. Therefore, equations were developed to calculate the nominal flexural resistance for flexural members prestressed with HSSS strands. Flexural design guidelines were proposed for the use of HSSS strands in flexural members. For I-girders, rupture of strands failure mode is recommended by assuring that concrete in the extreme compression fiber reaches considerable inelastic stresses, at least $0.7f'_c$. For beams (e.g., Florida Slab Beam), crushing of concrete failure mode is recommended by assuring that the net tensile strain in the HSSS strand is greater than 0.005. The recommended maximum allowable jacking stress and stress immediately prior to transfer are 75% and 70%, respectively. A resistance factor of 0.75 is recommended for both rupture of strand and crushing of concrete failure modes. AASHTO equations conservatively estimated the measured transfer length and prestress losses of 0.6-in.-diameter HSSS strands. The ACI 318-19 and AASHTO LRFD conservatively predicted the shear capacity of concrete girders prestressed with HSSS strands.			
17. Key Word Corrosion-resistant strands, stainless steel strands, HSSS strands, transfer length, prestress losses, full-scale girders, flexural tests, shear tests, design guidelines		18. Distribution Statement No restrictions.	
19. Security Classif. (of this report) Unclassified.	20. Security Classif. (of this page) Unclassified.	21. No. of Pages 372	22. Price

Form DOT F 1700.7 (8-72)

Reproduction of completed page authorized

ACKNOWLEDGMENTS

The authors wish to express their gratitude and sincere appreciation to the Florida Department of Transportation (FDOT) for funding this project. The authors would like to thank Vickie Young, Will Potter, Sam Fallaha, Steve Nolan, and Bruno Vasconcelos for their technical input and support throughout the project. Also, the authors would like to thank Christina Freeman, Steve Eudy, Justin Robertson, Paul Tighe, Ben Allen, Miguel Ramirez and Michael Waters at the FDOT Structures Research Center in Tallahassee, and Richard DeLorenzo, Juan Coz Sanchez and Andrew Pinkham at FDOT State Materials Office in Gainesville for their assistance in testing specimens. The work was enjoyable and well executed because of everyone's expertise and enthusiasm.

EXECUTIVE SUMMARY

Prestressed concrete is used in structures because of its versatility, adaptability, and durability. Durability of prestressed concrete bridges in extremely aggressive environments is of increasing concern because of corrosion of the carbon steel strands that are typically used for prestressing. Concrete is a permeable material where chloride ions can penetrate through and reach the internal reinforcement, and carbon steel strands are highly susceptible to corrosion. Thus, prestressed concrete bridges located in areas with high exposure to environmental factors (e.g., marine environments) deteriorate due to corrosion of carbon steel strands. For example, Florida has a long coastline, with many concrete bridges over coastal water. Among the 12,518 bridges in Florida, 6,303 are prestressed concrete, and almost half of them are older than 40 years. One solution to overcome the early deterioration of coastal bridges is to use corrosion-resistant strands, such as Duplex High-Strength Stainless Steel (HSSS) strands.

HSSS strands have high corrosion resistance and are an alternative to carbon steel strands in concrete bridges in extremely aggressive environments. The growing interest in using stainless steel strands has led to the development of the ASTM A1114. In 2020, ASTM A1114 was released as a standard specification for low-relaxation, seven-wire, Grade 240, stainless steel strands for prestressed concrete. Stainless steel is made from different alloys compared to carbon steel, and thus the mechanical properties of stainless steel strands are fundamentally different than those of carbon steel strands. The most significant difference is in the guaranteed ultimate strain: the value for stainless steel strands is only 1.4%.

Several departments of transportation (DOTs) have already used or allowed the use of HSSS strands in prestressed piles. As of 2020, a total of 17 projects have used stainless steel strands, a majority of them in piles. Those projects are in areas with high exposure to environmental factors. The use of HSSS strands in flexural members has been hindered by the lack of full-scale test results, structural design approaches, and/or design guidelines. The main concern in using HSSS strands in flexural members is their low ductility. Concrete members prestressed with HSSS strands, if not properly designed, might fail suddenly without adequate warning. There have been no attempts to address this problem in full-scale research studies.

The goals of this research project were to investigate the use of HSSS strands in flexural members and to develop design guidelines that could be used by bridge engineers. A total of thirteen (13) 42-ft-long AASHTO Type II girders were designed, fabricated, and tested in flexure or shear. Ten (10) girders were prestressed with HSSS strands, while the other three (3) were prestressed with carbon steel strands and served as control girders. This research program included experimental activities to determine the mechanical and bond strength characteristics, prestress losses, and transfer length of 0.6-in.-diameter HSSS strands.

Twenty HSSS strands from two spools were tested in direct tension. A stress-strain equation is proposed for the 0.6-in.-diameter HSSS strands, which satisfied all ASTM A1114 requirements. The measured bond strength of 0.6-in.-diameter HSSS strands was greater than the bond strength of carbon steel strands proposed by other researchers. The maximum measured transfer length of 0.6-in.-diameter HSSS strands was 21.5 in., which was less than the value predicted by AASHTO LRFD Bridge Design Specifications' equation for carbon steel strands.

Experimental flexural and shear results showed that the post-cracking behavior of girders prestressed with HSSS strands continued to increase up to failure with no discernible plateau. The behavior is attributed to the stress-strain behavior of the HSSS strands. Also, flexural results revealed that, although HSSS strands have low ductility and all composite girders failed due to rupture of strands, the girders exhibited large reserve deflection and strength beyond the cracking load and provided significant and substantial warning through large deflection, as well as well-distributed and extensive flexural cracking, before failure. A non-linear analytical model and an iterative numerical model were developed to predict the flexural behavior of concrete members prestressed with HSSS strands. Although the analytical model gave better predictions, the iterative numerical approach is slightly conservative and is easier to use for design – designers prefer to use an equation type of approach to perform preliminary designs. Numerical equations were developed to calculate the nominal flexural resistance for flexural members prestressed with HSSS strands. The proposed equations are only valid for rectangular sections. In the case of flanged sections, iterative numerical approaches were also introduced.

Because HSSS strand is a brittle material, the design must consider the strain capacity of the strand and must be balanced between flexural strength and ductility. Based on the flexural design philosophy for using carbon steel strands in prestressed concrete girders, along with experimentally-observed behaviors and analytical results for concrete members prestressed with

HSSS strands, flexural design guidelines were developed for the use of HSSS strands in flexural members. For I-girders, rupture of strands failure mode is recommended by assuring that concrete in the extreme compression fiber reaches considerable inelastic stresses, at least $0.7f'_c$. In addition, the recommended maximum allowable jacking stress is 70%. For slab beams (e.g. Florida Slab Beam), crushing of concrete failure mode is recommended by assuring that the net tensile strain in the HSSS strand is greater than 0.005. The recommended maximum allowable jacking stress and stress immediately prior to transfer are 75% and 70%, respectively. A resistance factor of 0.75 is recommended for both rupture of strand and crushing of concrete failure modes. AASHTO equations conservatively estimated the measured transfer length and prestress losses of 0.6-in.-diameter HSSS strands. The ACI 318-19 and AASHTO LRFD conservatively predicted the shear capacity of concrete girders prestressed with HSSS strands.

TABLE OF CONTENTS

Disclaimer	ii
SI (modern metric) conversion factors	iii
Technical report documentation page	v
Acknowledgments.....	vi
Executive summary.....	vii
List of tables.....	xiv
List of figures	xvi
List of symbols.....	xxiii
Chapter 1 Introduction.....	1
1.1 Introduction	1
1.2 Research motivation.....	3
1.3 Problem statement.....	4
1.4 Research goals.....	4
1.5 Research objectives.....	4
1.6 Organization.....	5
Chapter 2 Literature review.....	6
2.1 Introduction	6
2.2 Mechanical properties and corrosion resistance performance	7
2.3 Guaranteed mechanical properties for stainless steel strands	8
2.4 Galvanic corrosion	8
2.5 Research conducted by state departments of transportation (DOTs).....	8
2.6 Current stainless steel design guidelines.....	9
2.7 Projects utilized stainless steel reinforcing materials.....	9
2.7.1 Stainless steel rebars	9
2.7.2 Stainless steel strands.....	10
Chapter 3 Mechanical and bond strength properties	12
3.1 Introduction	12
3.2 Comparison of carbon steel and HSSS strands	12
3.3 Tensile tests.....	14
3.3.1 Preparation of specimens	14
3.3.2 Test setup	16
3.3.3 Results.....	17

3.3.4	Differences in tensile testing HSSS strands.....	21
3.4	Stress-strain model.....	22
3.4.1	Background.....	22
3.4.2	Proposed model for 0.6-in.-diameter HSSS strands	23
3.5	Bond strength tests.....	25
3.5.1	Preparation of specimens	26
3.5.2	Test setup	26
3.5.3	Results.....	26
3.6	Summary	29
Chapter 4	Girder design and fabrication.....	32
4.1	Introduction.....	32
4.2	First set of girders	32
4.2.1	Design objective.....	32
4.2.2	Design method	33
4.2.3	Design matrix.....	33
4.2.4	Materials	36
4.2.5	Fabrication	39
4.3	Second set of girders	47
4.3.1	Design of girders.....	47
4.3.2	Design matrix.....	50
4.3.3	Materials	50
4.3.4	Fabrication	51
Chapter 5	Transfer length.....	55
5.1	Introduction.....	55
5.2	First set of girders	56
5.2.1	Preparation of specimens	56
5.2.2	Method of prestress release.....	58
5.2.3	Instrumentation	59
5.2.4	Analyzing measured concrete strain.....	60
5.2.5	Results.....	62
5.2.6	Comparison of test data with literature.....	67
5.3	Second set of girders.....	69
5.3.1	Preparation of specimens	69
5.3.2	Method of prestress release.....	69
5.3.3	Instrumentation	69
5.3.4	Results.....	71
5.3.5	Comparison with first set of girders.....	73
5.3.6	Prediction of transfer length.....	73
5.4	Summary	74
Chapter 6	Flexural test.....	76
6.1	Introduction.....	76

6.2 First set of girders	76
6.2.1 Test setup	76
6.2.2 Test instrumentation.....	79
6.2.3 Prestress losses.....	79
6.2.4 Experimental results.....	84
6.3 Second set of girders	90
6.3.1 Test setup	90
6.3.2 Test instrumentation.....	92
6.3.3 Prestress losses.....	93
6.3.4 Experimental results.....	98
6.4 Summary	105
Chapter 7 Prediction of experimental flexural results	108
7.1 Introduction	108
7.2 Analytical model	108
7.2.1 Validation of analytical model.....	109
7.2.2 Prediction of flexural moment using ASTM A1114 values	114
7.2.3 Parametric study.....	115
7.3 AASHTO LRFD	128
7.4 Iterative numerical model	131
7.5 Summary	136
Chapter 8 Development of flexural design equations	138
8.1 Introduction	138
8.2 Desired flexural failure mode	138
8.2.1 Rupture of strand.....	139
8.2.2 Crushing of concrete.....	141
8.3 Balanced failure condition	142
8.4 Design equations for nominal flexural resistance	144
8.4.1 Rupture of strand failure mode	145
8.4.2 Crushing of concrete failure mode.....	149
8.5 Validation of proposed numerical equations	153
8.6 Summary	155
Chapter 9 Flexural design guidelines	156
9.1 Introduction	156
9.2 Nominal resisting moment	156
9.2.1 Strain compatibility approach	156
9.2.2 Numerical approach	156
9.3 Recommended failure mode	157
9.4 Recommended reinforcement limits	161
9.5 Recommended strength resistance factors	162
9.6 Recommended stress limit	165
9.7 Summary	166

Chapter 10	Shear test.....	168
10.1	Introduction.....	168
10.2	Literature review	169
10.2.1	Glass Fiber Reinforced Polymer rebars	169
10.2.2	Stainless steel rebars.....	171
10.3	Experimental program.....	171
10.3.1	Material properties	171
10.3.2	Specimen fabrication.....	172
10.3.3	Test setup.....	173
10.3.4	Instrumentation.....	175
10.4	Interface shear reinforcement.....	177
10.5	Experimental results.....	178
10.5.1	Girders prestressed with carbon steel strands	181
10.5.2	Girder prestressed with stainless steel strands	192
10.6	Code predictions	195
10.6.1	AASHTO LRFD Bridge Design Specifications.....	196
10.6.2	ACI 318-19.....	199
10.7	Summary	201
10.7.1	Effect of using GFRP rebars	202
10.7.2	Effect of using stainless steel strands.....	203
Chapter 11	Summary and conclusions	205
11.1	Summary	205
11.2	Conclusions.....	206
11.2.1	Conclusions drawn from experimental testing.....	206
11.2.2	Conclusions drawn from analytical model.....	210
11.3	Suggestions for future research.....	211
References	212

APPENDICES

APPENDIX A	Mill certificates for HSSS strands and carbon steel strands	A1
APPENDIX B	Design details drawings	B1
APPENDIX C	Construction of girders	C1
APPENDIX D	Test setup and instrumentation plans	D1
APPENDIX E	Concrete strain measurements	E1
APPENDIX F	Design examples	F1

LIST OF TABLES

Table 2-1 Projects that used HSSS strands in the United States.....	11
Table 3-1 Minimum required mechanical properties of 0.52-in.- and 0.62-in.-diameter strands.	14
Table 3-2 Test matrix of the tensile test.....	16
Table 3-3 Statistical summary of test results for specimens from the first spool.....	17
Table 3-4 Statistical summary of test results for specimens from the second spool	18
Table 3-5 Mechanical properties for 0.6-in.-diameter HSSS strands	19
Table 3-6 Mechanical properties of stainless steel strands using grout coating and chuck devices	20
Table 3-7 Power formulas for low-relaxation carbon steel strands Grade 270	23
Table 3-8 Coefficient of modified Ramberg-Osgood function for HSSS strands	24
Table 4-1 Design matrix of first set of girders.....	34
Table 4-2 Mechanical properties for carbon steel strands	36
Table 4-3 Mechanical characteristics of stainless steel bars.....	37
Table 4-4 Chemical composition of stainless steel bars	38
Table 4-5 Mechanical properties of GFRP bars	38
Table 4-6 Concrete compressive strength on testing day of the flexural test of first set of girders	39
Table 4-7 Fabrication activities schedules for first set of girders.....	41
Table 4-8 Concrete test results.....	43
Table 4-9 Casting date of composite girders of first set of girders.....	47
Table 4-10 Interior girder moments at midspan	48
Table 4-11 Concrete mixture proportions for second set of girders	51
Table 4-12 Concrete compressive strength on testing day of flexural tests of second set of girders	52
Table 5-1 Test matrix for transfer length.....	57
Table 5-2 Concrete compressive strength for first set of girders.....	57
Table 5-3 Transfer length results for HSSS and carbon steel strands.....	65
Table 5-4 Transfer length estimates of the tested specimens at release	72
Table 6-1 Flexural tests results of first set of girders.....	87
Table 6-2 Prestress losses of HSSS strands using VWSGs	94
Table 6-3 Prestress losses of HSSS strands using decompression method	97
Table 6-4 Comparison of prestress losses.....	97

Table 6-5 Flexural test results of second set of girders	101
Table 7-1 Calculation of flexural strength using modified AASHTO LRFD equations	130
Table 7-2 Flexural strength of concrete girders prestressed with HSSS strands	136
Table 8-1 Calculation of flexural strength using proposed numerical equations	154
Table 10-1 Mechanical properties of the HSSS and carbon steel strands	172
Table 10-2 Test matrix for shear testing	172
Table 10-3 Cracking shear force.....	179
Table 10-4 Experimental shear results.....	180
Table 10-5 Concrete compressive strength at testing day of shear tests.....	180
Table 10-6 Experimental results for test specimens	195
Table 10-7 Experimental and AASHTO LRFD predicted capacities for test specimens.....	199
Table 10-8 Experimental and ACI predicted capacities for test specimens	201

LIST OF FIGURES

Figure 1-1 Percentage of prestressed concrete bridges from total number of bridges (NBI. 2020)	1
Figure 1-2 Age of prestressed concrete bridges in Florida (NBI. 2020)	3
Figure 1-3 Comparison of surface layer of carbon steel spool (left) and stainless steel spool (right)	3
Figure 3-1 Comparing stress-strain diagram of stainless steel strands versus carbon steel strands	13
Figure 3-2 Preparation and testing of specimens using grout	15
Figure 3-3 Stress-strain curves of the tested stainless steel specimens using coating approach	18
Figure 3-4 Stress-strain curves of specimens using grout coating and chuck devices	20
Figure 3-5 Preparation and testing of specimens using chuck devices	21
Figure 3-6 Comparison of measured and calculated stress-strain curves of stainless steel strands	24
Figure 3-7 Comparing stress-strain model of the proposed equation versus experimental stress-strain models	25
Figure 3-8 Six HSSS specimens prepared for bond strength test	27
Figure 3-9 Test setup for the bond strength test	27
Figure 3-10 Compressive strength of concrete mortar cubes	28
Figure 3-11 Pull-out test results of 0.6-in.-diameter HSSS strands	28
Figure 4-1 Reinforcement layout for first set of girders	34
Figure 4-2 Casting bed layout for first set of girders	40
Figure 4-3 Running cables in the bed	41
Figure 4-4 Monitoring applied force on electronic cell	41
Figure 4-5 Seated stainless strands in the chucks	41
Figure 4-6 Shielding two strands in Girder B2	41
Figure 4-7 Stainless steel confinement reinforcement	42
Figure 4-8 Tying stainless steel stirrups	42
Figure 4-9 Lifting loop	42
Figure 4-10 Concrete slump test	43
Figure 4-11 Concrete air content test	43
Figure 4-12 Casting concrete	44
Figure 4-13 Concrete cylinders	44
Figure 4-14 Removing side forms	44
Figure 4-15 Releasing stainless steel strands using flame	44

Figure 4-16 Strand detensioning sequence (not to scale)	45
Figure 4-17 Bed end after breakage of the HSSS strand	45
Figure 4-18 Notching effect of grips on fractured HSSS strands	46
Figure 4-19 Girder before casting deck slab.....	47
Figure 4-20 Girder after casting deck slab.....	47
Figure 4-21 Bridge prototype.....	48
Figure 4-22 Cross section of an interior girder.....	49
Figure 4-23 Cross section of modified interior girder (specimens in this study)	49
Figure 4-24 Reinforcement layout for second set of girders	50
Figure 4-25 Casting bed layout for second set of girders. a) Position of girders in the casting bed; (b) midspan cross section for specimens with 11 HSSS strands; (c) midspan cross section for specimens with nine HSSS strands; (d) midspan cross section for specimens with seven HSSS strands.	52
Figure 4-26 Stainless steel and carbon steel spools	53
Figure 4-27 Twist of HSSS strands after cut	54
Figure 5-1 Casting bed layout and detensioning sequence for first set of girders. a) girders with carbon steel strands; and (b) girders with HSSS strands	58
Figure 5-2 ERSGs and DEMEC points locations	60
Figure 5-3 Concrete strains measured by strain gages during strands release at end 3	61
Figure 5-4 Determination of transfer length at End 3 by 95% Average Maximum Strain (AMS) method.....	62
Figure 5-5 Smoothed strain profiles measured by DEMEC points over time at End 9.....	62
Figure 5-6 Measured transfer length at release by DEMEC and strain gages	63
Figure 5-7 Measured transfer length by DEMEC points over time for HSSS strands	63
Figure 5-8 Measured transfer length by DEMEC points over time for carbon steel strands.....	64
Figure 5-9 Comparison of measured transfer length of HSSS strands with equations from literature	68
Figure 5-10 Comparison of measured transfer length of carbon steel strands with equations from literature	69
Figure 5-11 Installation of internal Fiber Optic Sensors for transfer length.....	70
Figure 5-12 Installation of external Fiber Optic Sensors for transfer length.....	70
Figure 5-13 Installation of strain gages for transfer length.....	71
Figure 5-14 Smoothed strain distribution of the tested specimens	72
Figure 5-15 Strain distribution from the external fiber optic at internal ends	73

Figure 6-1 Flexural test setup a) for non-composite specimens; and (b) for composite specimens	77
Figure 6-2 Flexural test setup for Girder B2.....	77
Figure 6-3 External post-tensioning of threaded rods.....	78
Figure 6-4 Test instrumentation for monolithic girders.....	80
Figure 6-5 Test instrumentation for composite girders.....	80
Figure 6-6 VWSG attached to the bottom layer of strands in Girder A2	81
Figure 6-7 Measured elastic shortening losses	82
Figure 6-8 Effective prestress with time	83
Figure 6-9 Prestress losses estimation with time	84
Figure 6-10 Measured prestress losses of non-composite girders 63 days after start of building control girders	85
Figure 6-11 Load-deflection relationships of non-composite girders in the first set of girders ...	85
Figure 6-12 Load-deflection relationships of composite girders in the first set of girders.....	86
Figure 6-13 Crack patterns at ultimate load for Girder C2 and Girder C3	89
Figure 6-14 Crushing of concrete failure mode (Girder B3)	91
Figure 6-15 Rupture of strands failure mode (Girder B2)	91
Figure 6-16 Loading scheme	92
Figure 6-17 Test instrumentation of composite girders (second set).....	92
Figure 6-18 VWSGs attached to the bottom layer of HSSS strands in Girder E1.....	93
Figure 6-19 Measured prestress losses of HSSS strands in second set of girders	94
Figure 6-20 First flexural crack	95
Figure 6-21 Load-strain relationship for decompression method (gages S14 and S16 were installed on opposite sides of the crack).....	96
Figure 6-22 Estimated / measured elastic shortening and total prestress losses.....	97
Figure 6-23 Load-midspan deflection relationship for second set of girders	98
Figure 6-24 Tested girders at failure (second set of girders)	100
Figure 6-25 Reinforcement ratio vs. cracking and ultimate loads	101
Figure 6-26 Reinforcement ratio vs. deflection at cracking and ultimate loads	101
Figure 6-27 Deflection along length of the specimen.....	103
Figure 6-28 Load-top fiber strain relationship for second set of girders	104
Figure 7-1 Experimental and analytical load-deflection relationships of Girder A3.....	110
Figure 7-2 Experimental load-concrete top fiber strain relationship for Girders A3 and C3	111

Figure 7-3 Experimental and analytical load-deflection relationships of Girder C3	112
Figure 7-4 Experimental and analytical deflections along Girder C3 at failure load	112
Figure 7-5 Comparison of experimental and analytical load-deflection curves	113
Figure 7-6 Comparison of experimental and analytical moment-top fiber strain curves	114
Figure 7-7 Predicted flexural moment using analytical model	115
Figure 7-8 Predicted curvature as a function of prestressing reinforcement ratio and mechanical properties of HSSS strand	117
Figure 7-9 Predicted flexural strength as a function of prestressing reinforcement ratio and mechanical properties of HSSS strand	118
Figure 7-10 Curvature normalized reinforcement ratio for I-girders with guaranteed mechanical properties of HSSS strands	119
Figure 7-11 Analytical strain distribution for crushing of concrete and rupture of strand failures	119
Figure 7-12 Cross sections of two girders: 14 HSSS strands with rupture of strands failure and 21 HSSS strands with crushing of concrete failure	120
Figure 7-13 Analytical moment-curvature relationship for crushing of concrete and rupture of strand failure modes	120
Figure 7-14 Analytical deflections along girders at failure, for crushing of concrete and rupture of strand failure modes	121
Figure 7-15 Analytical load-deflection relationship, for crushing of concrete and rupture of strand failure modes	121
Figure 7-16 Analytical neutral axis depth vs. reinforcement ratio, for girder with carbon steel strands and girder with HSSS strands	123
Figure 7-17 Analytical curvature vs. reinforcement ratio, for girder with carbon steel strands and girder with HSSS strands	124
Figure 7-18 Analytical flexural strength vs. reinforcement ratio, for girder with carbon steel strands and girder with HSSS strands	125
Figure 7-19 Analytical initial prestressing force vs. reinforcement ratio, for girder with carbon steel strands and girder with HSSS strands	126
Figure 7-20 Cross sections of two girders: 11 carbon steel strands with crushing of concrete failure and 13 HSSS strands with rupture of strands failure	126
Figure 7-21 Analytical moment vs. curvature, for girder with carbon steel strands and girder with HSSS strands	127
Figure 7-22 Analytical deflections along girders at failure, for girder with carbon steel strands and girder with HSSS strands	127
Figure 7-23 Analytical applied load vs. deflection, for girder with carbon steel strands and girder with HSSS strands	128

Figure 7-24 Comparison of experimental moments and moments calculated using modified AASHTO LRFD equations.....	131
Figure 7-25 Proposed flexural design flowchart for concrete members prestressed with HSSS strands and designed to fail due to rupture of strand	133
Figure 7-26 Comparison of experimental moments and moments calculated using iterative numerical model.....	134
Figure 7-27 Simplified iterative model to calculate the flexural strength of concrete girders prestressed with HSSS strands and designed to fail due to rupture of strand.....	135
Figure 8-1 Strength resistance factor for carbon steel strands (AASHTO LRFD).....	139
Figure 8-2 Design of carbon and stainless steel prestressed concrete girders	140
Figure 8-3 Concrete compressive stress-strain curves.....	141
Figure 8-4 Strain and stress distributions for balanced failure condition.	143
Figure 8-5 Prediction of stress block factors	144
Figure 8-6 Strain and stress distributions for strands rupture failure condition.	145
Figure 8-7 Variation in ratio of neutral axis depth to prestressing reinforcement depth, k_{pu} , for strand rupture failure condition.....	147
Figure 8-8 Variation of reinforcement ratio for stainless steel prestressed concrete member designed to fail due to rupture of strands.....	148
Figure 8-9 Variation in c/d for stainless steel prestressed concrete member designed to fail due to rupture of strands	149
Figure 8-10 Strain and stress distributions for concrete crushing failure condition.	150
Figure 8-11 Variation in ratio of neutral axis depth to prestressing reinforcement depth, k_{pu} , for concrete crushing failure condition.....	151
Figure 8-12 Comparison of stress in the prestressing reinforcement at failure	152
Figure 8-13 Variation of reinforcement ratio for stainless steel prestressed concrete members designed to fail due to crushing of concrete	153
Figure 8-14 Experimental and numerical flexural strengths.....	155
Figure 9-1 Design flowchart for concrete rectangular beam prestressed with HSSS strands and designed to fail due to rupture of strand	158
Figure 9-2 Iterative design procedure for concrete member prestressed with HSSS strands and designed to fail due to rupture of strand	159
Figure 9-3 Design flowchart for concrete rectangular beam prestressed with HSSS strands and designed to fail due to crushing of concrete	160
Figure 9-4 Iterative design procedure for concrete member prestressed with HSSS strands and designed to fail due to crushing of concrete	161
Figure 9-5 Strength resistance factors for CFRP and AFRP tendons.....	163

Figure 9-6 Stress-strain relationship of AFRP and CFRP tendons and stainless steel strands...	164
Figure 9-7 Recommended strength resistance factors for HSSS strands.....	164
Figure 10-1 Test sequence Girder A2.....	174
Figure 10-2 Test sequence Girder A3.....	174
Figure 10-3 Test sequence Girder B3.....	175
Figure 10-4 Shear test setup.....	175
Figure 10-5 Strain gages attached to the stirrups.....	176
Figure 10-6 Strain gages at the top of the slab.....	176
Figure 10-7 Rosette strain gages at the shear span.....	176
Figure 10-8 End-slip gages.....	176
Figure 10-9 Shaft gages.....	177
Figure 10-10 Deflection gages.....	177
Figure 10-11 Principal strains for test specimens.....	179
Figure 10-12 Load-deflection relationship for Girder A2.....	181
Figure 10-13 Load-stirrups strain for Girder A2_1.....	183
Figure 10-14 Load-stirrups strain for Girder A2_2.....	183
Figure 10-15 Strand slip response in Girder A2_1.....	184
Figure 10-16 Strand slip response in Girder A2_2.....	184
Figure 10-17 Horizontal interface displacement (Girder A2_1).....	186
Figure 10-18 Horizontal interface displacement (Girder A2_2).....	186
Figure 10-19 Concrete crushing and rupture of GFRP for Girder A2_1.....	187
Figure 10-20 Concrete crushing and rupture of GFRP for Girder A2_2.....	187
Figure 10-21 Types of failure of GFRP bars.....	188
Figure 10-22 Girder A2_3 at failure.....	189
Figure 10-23 Load-deflection relationship for Girder A3.....	190
Figure 10-24 Load-stirrups strain for Girder A3_1.....	190
Figure 10-25 Load-stirrups strain for Girder A3_2.....	190
Figure 10-26 Flexure-shear failure of Girder A3_1.....	192
Figure 10-27 Crushing of concrete of Girder A3_1.....	192
Figure 10-28 Shear force versus deflection for Girder B3.....	193
Figure 10-29 Load-stirrups strain for Girder B3_1.....	194
Figure 10-30 Load-stirrups strain for Girder B3_2.....	194
Figure 10-31 Web shear failure of Girder B3_1.....	195

Figure 10-32 Web shear failure of Girder B3_2..... 195

LIST OF SYMBOLS

A_{ct}	area of concrete on the flexural tension side of the girder, in ²
A_{cv}	area of concrete considered to be engaged in interface shear transfer, in ²
A_{fv}	area of GFRP transverse reinforcement within distance s , in ²
A_v	area of stirrups, in ²
A_{vf}	area of interface shear reinforcement crossing the shear plane within the area A_{cv} , in ²
A_{ps}	area of prestressing strand, in ²
a	depth of equivalent rectangular stress block, in.
b	width of compression face of member, in.
b_v, b_w	effective web width, in.
c	distance from extreme compression fiber to the neutral axis, in.; cohesion factor, ksi
c_b	distance from extreme compression fiber to the neutral axis at balanced condition, in.
d_1	distance from the extreme compression fiber to bottom layer of prestressing strands, in.
d_b	diameter of prestressing strand, in.; diameter of GFRP rebars, in.
d_{avg}	distance from the extreme compression fiber to centroid of prestressing strands, in.
d_v	effective shear depth, in.
E_c	modulus of elasticity of concrete, ksi
E_f	modulus of elasticity of GFRP reinforcement, ksi
E_{ps}	elastic modulus of the prestressing strand, ksi
f_c	concrete compressive strength at ϵ_{cf} , ksi
f'_c	concrete compressive strength, ksi
f_{cr}	cracking stress of concrete in tension, ksi
f_{fb}	design tensile strength of bent portion of GFRP reinforcement, ksi
f_{fd}	design tensile strength of GFRP reinforcing rebar, ksi
f_{fv}, f_{yv}	design tensile strength of GFRP transverse reinforcement, ksi
f_p	stress in the stainless steel prestressing strand at nominal flexural resistance, ksi
f_{pi}	initial prestressing level in the strand, ksi
f_{pe}	effective stress in stainless steel strand after losses, ksi

f_{ps}	average stress in the carbon steel strands at nominal flexural resistance, ksi
f_t	concrete tensile stress when concrete strain reaches ε_t , ksi
f_{pt}	stress in the prestressing strand immediately after transfer, ksi
f_{pu}	ultimate tensile strength of prestressing strand, ksi
f_{py}	yield stress in the prestressing strand, ksi
f_{se}	effective stress in the strand, ksi
f_y	yield stress of stirrups, ksi
f_{yt}	specified yield strength of stainless steel transverse reinforcement, ksi
f_{po}	jacking stress of the strand, ksi
K_L	factor accounting for type of steel
k_{pu}	corresponding ratio of depth of the neutral axis to the depth of bottom layer of prestressing strands
k_{pub}	corresponding ratio of depth of the neutral axis to the depth of bottom layer of prestressing strands at balanced condition
l_d	transfer length, in.
M_n	nominal flexural resistance, kip-ft
M_u	ultimate bending moment at distance d_v from face of support, kip-ft
P_c	permanent net compressive force normal to the shear plane
r_b	internal radius of bent GFRP reinforcement rebar, in.
s	spacing of stirrups, in.
V_c	nominal shear strength resistance of the concrete, kip
V_{ci}	flexural-shear nominal shear resistance, kip
V_{cr}	experimental shear capacity provided by concrete, kip
V_{cw}	web-shear nominal shear resistance, kip
V_f	nominal shear resistance provided by GFRP transverse reinforcement, kip
V_{ni}	nominal interface shear resistance, kip
$V_{n,AASHTO}$	nominal shear resistance at the critical section according to the general method in AASHTO LRFD, kip
V_s	nominal shear resistance provided by steel transverse reinforcement, kip
V_u	ultimate shear force at distance d_v from face of support, kip; shear force at loading point, kip
V_{ui}	experimental interface shear force, kip

V_{ult}	experimental ultimate shear capacity, kip
β_c	factor relating effect of longitudinal strain on the shear capacity of concrete
α and β	compressive stress block factors at ϵ_{cf}
α_1 and β_1	compressive stress block factors at ϵ_{cu}
Δf_{pES}	prestress elastic shortening loss, ksi
Δf_{pR}	prestress relaxation loss, ksi
σ	stress in the prestressing strand, ksi
ϵ_{cf}	compressive concrete strain, in./in.
ϵ_{cr}	cracking strain of concrete in tension, in./in.
ϵ_{cu}	ultimate concrete strain in compression, in./in.
ϵ'_c	strain in concrete when the compressive stress reaches f'_c , in./in.
ϵ_p	strain in the stainless steel prestressing strands at nominal flexural resistance, in./in.
ϵ_{pe}	strain in the prestressing strand due to effective stress, in./in.
ϵ_{pu}	ultimate tensile strain in strand, in./in.
ϵ_s	net longitudinal tensile strain at centroid of the tension reinforcement, in./in.
ϵ_t	ultimate concrete strain in tension, in./in.
Θ	angle of inclination of diagonal compressive stresses
λ	concrete density factor
ρ_{ssb}	balanced reinforcement ratio for concrete member prestressed with stainless steel strands
$\rho_{ss,min}$	minimum prestressing reinforcement ratio for concrete members prestressed with stainless steel strands
$\rho_{ss,max}$	maximum prestressing reinforcement ratio for concrete members prestressed with stainless steel strands

CHAPTER 1 INTRODUCTION

1.1 Introduction

Prestressed concrete has been used in bridge construction for decades. Prestressed concrete was first integrated into long-span bridges in the United States in the 1950s. The Walnut Lane Memorial Bridge in Philadelphia, PA, is the first prestressed concrete bridge built in the United States (Zollman et al. 1992); it was opened to traffic in 1951. Since then, new materials, innovations and technologies have been developed, which led to the growth of the prestressed concrete industry. Based on data provided by the National Bridge Inventory (NBI. 2020), the percentage of prestressed concrete bridges from the total number of bridges in the United States has increased dramatically in the last seven decades, as shown in Figure 1-1. In the most recent decade, the 2010s, prestressed concrete bridges represent more than 45% of the total bridges in the United States. This percentage has increased by more than 50% in the last five decades. The increase in number of prestressed concrete bridges is attributed to their versatility, adaptability, reliability, and durability.

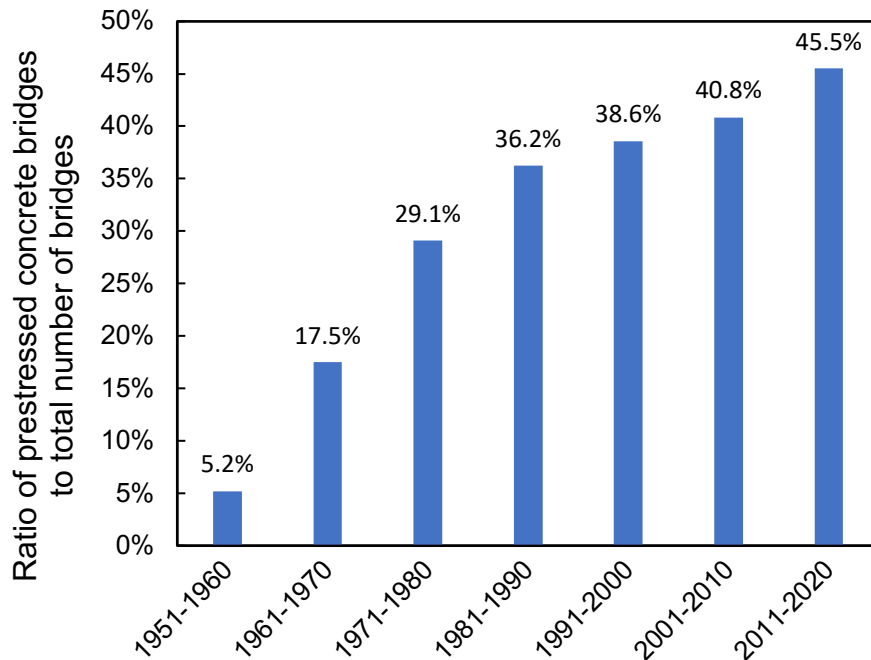


Figure 1-1 Percentage of prestressed concrete bridges from total number of bridges (NBI. 2020)

Durability of concrete structures can be maintained by protecting the internal reinforcement – for example, by increasing concrete cover and minimizing concrete crack width. Yet, concrete is a permeable material and thus chloride ions can penetrate through and reach the internal

reinforcement, particularly in extremely aggressive environments. Therefore, these measures may not be adequate to protect the internal reinforcement in concrete structures.

Carbon steel reinforcing materials are highly susceptible to corrosion. Therefore, concrete bridges located in extremely corrosive environments, such as in coastal waters, deteriorate due to corrosion of carbon steel reinforcing materials. For example, Florida has a long coastline, with many concrete bridges over coastal water. Note that corrosion of reinforcing materials could also occur in low-level bridges over water than may not be necessarily be on the coast. Among the 12,518 bridges in Florida, 6,303 are prestressed concrete (NBI. 2020). Figure 1-2 shows the age of prestressed concrete bridges in Florida, where almost half of the bridges are older than 40 years. The prestressed concrete bridges that are in extremely aggressive environments require more resources for additional inspection and maintenance, rehabilitation, and/or replacement. One solution to overcome the early deterioration of those bridges is to use corrosion-resistant strands, such as stainless steel strands, which will significantly enhance their durability.

Stainless steel material has high corrosion resistance and can be used in seven-wire prestressing strands. Stainless steel strands are a new technology and option for the construction of durable, low-maintenance concrete bridges, and they are being promoted as a good alternative to carbon steel strands in concrete bridges in extremely aggressive environments. The surface of stainless steel strands does not tend to rust as carbon steel strands do, as shown in Figure 1-3. Also, stainless steel strands extend the service life of prestressed concrete bridges compared to those built with carbon steel strands. So, utilizing stainless steel strands could be more economical in the long run. Currently, Duplex High-Strength Stainless Steel (HSSS) strands (corrosion-resistant) and Carbon Fiber Reinforced Polymer (CFRP) strands (corrosion-free) are the required reinforcement for Florida vehicular bridge 18-inch square piles in extremely aggressive environments (2020).

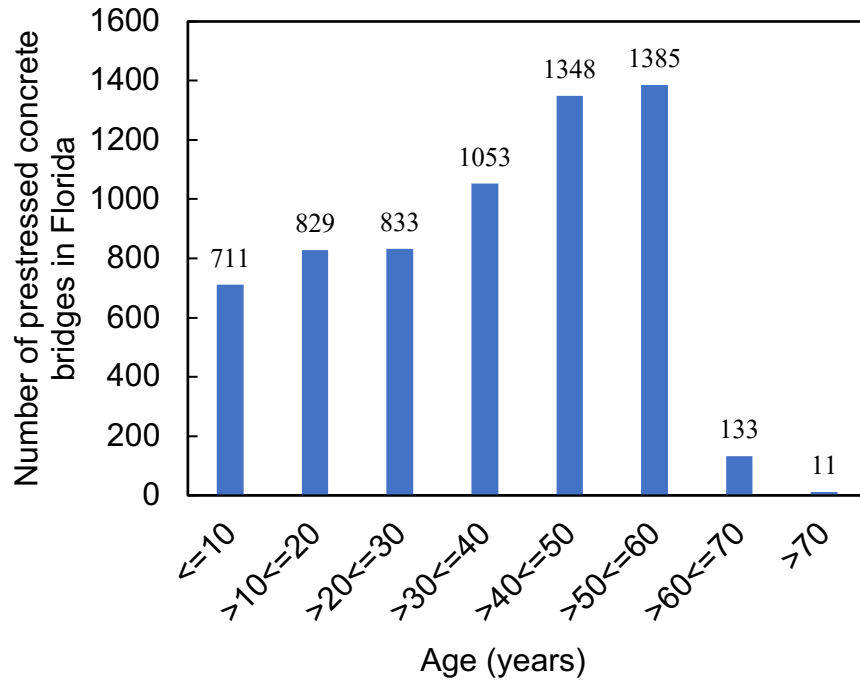


Figure 1-2 Age of prestressed concrete bridges in Florida (NBI. 2020)



Figure 1-3 Comparison of surface layer of carbon steel spool (left) and stainless steel spool (right)

1.2 Research motivation

Stainless steel strand has a superior corrosion-resistant property compared to carbon steel strand, and it is proposed as an alternative to carbon steel strand in prestressed concrete bridges in extremely aggressive environments. HSSS strand has been successfully deployed in piles in many bridges around the United States. In prestressed concrete bridges in environments that are extremely aggressive primarily due to chlorides, the superstructure components, i.e. slabs and

girders, are also susceptible to corrosion damage. Therefore, to mitigate the corrosion problems in the whole concrete bridge, HSSS strands may be implemented in superstructure prestressed concrete components as well.

1.3 Problem statement

The main design concern in using HSSS strand in flexural members is their low ductility. Flexural members prestressed with HSSS strands, if not properly designed, might fail suddenly without adequate warning. There have been no attempts to address this problem in full-scale research studies. Thus, the use of HSSS strand in flexural members has been hindered by the lack of full-scale test results and structural design approaches. For Florida Department of Transportation (FDOT) and bridge designers to use HSSS strands in flexural members in lieu of carbon steel strands, some study and testing are needed.

1.4 Research goals

The goals of this research project were as follows.

1. To determine if HSSS strands are a viable alternative to carbon steel strands in flexural members;
2. To investigate the use of HSSS strand in flexural members; and
3. To develop design guidelines that could be used by FDOT and bridge engineers to design flexural members prestressed with HSSS strands.

The research goals were attained by conducting several experiments. Positive results would give confidence to FDOT and bridge designers in deploying HSSS strands in flexural members.

1.5 Research objectives

The objectives of this research project were as follows.

1. To determine the mechanical characteristics of HSSS strands and propose a stress-strain equation that could be used by bridge engineers to design and analyze concrete girders prestressed with HSSS strands;
2. To quantify the bond strength of 0.6-in.-diameter HSSS strands;
3. To document construction activities of concrete girders prestressed with HSSS strands;
4. To measure transfer length of 0.6-in.-diameter HSSS strands and compare results with design provisions;
5. To investigate the flexural behavior of concrete girders prestressed with HSSS strands; and
6. To investigate the shear behavior of concrete girders prestressed with HSSS strands.

To accomplish the aforementioned objectives, several tasks were completed. Twenty-five 0.6-in.-diameter HSSS strands from two spools were tested in tension, and six 0.6-in.-diameter HSSS strands were tested for bond strength. Ten (10) and three (3) 42-ft-long AASHTO Type II girders prestressed with HSSS strands and carbon steel strand, respectively, were designed and cast. Precasting operations for girders prestressed with HSSS were observed, documented, and compared with girders prestressed with carbon steel strands. The transfer length of 0.6-in.-diameter HSSS strands was measured from most girders using multiple sensing technologies. The girders were tested either in flexure or shear to determine their capacity. An analytical model was developed using strain compatibility and force equilibrium and was validated with experimental results.

1.6 Organization

This research project is organized into chapters as follows. Chapter 2 gives background information and studies related to stainless steel strands. Chapter 3 presents the test program and results of tensile tests and bond strength tests of 0.6-in.-diameter HSSS strands. Design objectives and construction of the test girders are explained in Chapter 4. Chapter 5 discusses experimental results for transfer length of 0.6-in.-diameter HSSS strands. The flexural test setup and instrumentation are described in Chapter 6. Chapter 6 also includes discussion on prestress losses and flexural tests results. Chapter 7 presents models used to estimate the flexural strength of girders. Chapter 8 presents proposed equations to estimate nominal flexural resistance. Chapter 9 presents design guidelines for concrete bridge beams prestressed with HSSS strands. The shear test setup and instrumentation are described in Chapter 10. Chapter 10 also includes discussion on shear tests results. Finally, Chapter 11 gives a summary and conclusions.

CHAPTER 2 LITERATURE REVIEW

2.1 Introduction

Stainless steel is not a single type of steel, but rather a combination of a group of metallic materials and alloys containing, but not limited to, chromium, nickel, molybdenum, manganese, copper and nitrogen (2017). Mechanical and corrosion resistance properties of stainless steel are directly affected by the proportion of the elements. The stainless steel gets its improved corrosion resistance from the chromium content, which forms a very thin passive film layer to resist atmospheric or electrochemical corrosion. A minimum chromium content of 10.5% is required to consider the material as stainless steel (Dundu 2018). The corrosion resistance of the stainless steel is enhanced by the nickel and molybdenum proportions.

One of the earliest structural uses of stainless steel was in the renovation activities of St Paul's Cathedral in London in 1925 (Baddoo 2008). A stainless steel reinforcing chain was used to stabilize the dome. Although the cost of stainless steel is high compared to other materials, the rate of growth of the annual consumption of stainless steel has increased significantly in the last three decades (Baddoo 2008). It was estimated that approximately 4 billion tons of stainless steel were used worldwide in construction applications in 2006.

Multiple stainless steel alloys (i.e. austenitic, ferritic and duplex) are available, and each of them can be used to form a reinforcing bar or seven-wire prestressing strand. The chemical composition of any developed stainless steel bar or strand shall be within the range specified by ASTM A276 (2017). Stainless steel reinforcing materials are viable options, offering durability and potentially less maintenance work. The main limitation of the use of stainless steel in structural applications is its high cost. Stainless steel reinforcing materials are more expensive than carbon steel reinforcing materials. Therefore, careful consideration and efficient use of stainless steel is needed. The price of stainless steel varies, as it depends on the availability of the raw material and the manufacturing process (Gedge 2008; Medina et al. 2015; Salomon and Moen 2014). Duplex stainless steel is cheaper than austenitic stainless steel because of its lower nickel content; it is one of the most highly available types. Stainless steel material has been used in the construction industry for many decades in the form of reinforcing rebars. Around a decade ago, stainless steel material was introduced to the construction industry in the form of seven-wire prestressing strands.

2.2 Mechanical properties and corrosion resistance performance

Multiple types of stainless steel strands have been developed, and researchers have evaluated their mechanical properties and/or corrosion resistance performance. Moser et al. (Moser et al. 2013; Moser et al. 2012) conducted a preliminary investigation to evaluate the mechanical properties of six different high strength stainless steel wires and their corrosion resistance performances in alkaline and carbonated concrete solutions. The six stainless steel wires were austenitic Grades 304 and 316, martensitic Grade 17-7, and duplex Grades 2101, 2304 and 2205. It was proven that it is possible to obtain mechanical properties of carbon steel strand by tensile testing a single wire taken from the strand (Moser 2011). Thus, tensile tests were performed on a single wire of stainless steel strands for all six specimens, and stress-strain curves were plotted. The diameter of a single wire was 0.16 in., which is comparable to a single wire from a 0.5-in.-diameter carbon steel strand. (Mullins et al. 2014) evaluated the mechanical and corrosion resistance properties of three different stainless steel strands (Grade 316, XM29 and duplex Grade 2205) and carbon steel strand Grade 270, as the control. Schuetz (Schuetz 2013) evaluated the mechanical properties of duplex Grades 2205 and 2304 prestressing strands.

Results from previous studies have revealed that all tested stainless steel strands, regardless of their type, had rounded stress-strain curves once the elastic modulus is deviated. The degree of roundedness, level of strain hardening, ultimate stress, ultimate strain, and corrosion resistance property varied among types. The differences in roundedness of the stress-strain curves for six types of stainless steel strands can be found in a report done by (Moser et al. 2013). The degree of roundness depends on many factors such as chemical composition, heat treatment and level of cold work (Gardner 2005). Unlike carbon steel strands, stainless steel strands have a rounded stress-strain curve with early nonlinearity. The early nonlinear behavior is due to the presence of residual stress from the cold-drawing process where steel does not receive a stabilizing heat treatment (Moser 2011). Therefore, the presence of residual stresses results in a lower elastic modulus. The level of cold work has a significant effect on not only the degree of roundness but also on mechanical properties, specifically ultimate strength. The cold-drawing process is essential to achieve high tensile strength but it decreases ultimate strain (Nürnberg and Wu 2008). All previous research has concluded that Duplex High-Strength Stainless Steel (HSSS) strand Grade 2205 is the best option because of its high strength and corrosion resistance properties.

2.3 Guaranteed mechanical properties for stainless steel strands

As with all new products, the lack of a standard specification on guaranteed mechanical properties of stainless steel strands has delayed their implementation in structural applications despite their desired corrosion resistance property. Stainless steel strand is made from different alloys compared to carbon steel strand and thus mechanical properties specified for carbon steel strand by ASTM A416 (2017) cannot be applied to stainless steel strand. The growing interest in using stainless steel strand has led to the development of ASTM A1114, which was released in 2020. ASTM A1114 specifies the minimum required mechanical properties of Grade 240 stainless steel strands, which are different than those for carbon steel strands.

Note that the mechanical properties of stainless steel strand might vary from spool to spool due to multiple reasons such as the wire rod used to make prestressing strands is not perfectly identical from heat to heat, chemistry variances of the elements alloyed, and processing variances. The release of ASTM A1114 makes it easier for bridge owners to implement stainless steel strands in their projects because the design of any stainless steel prestressed concrete members will be based on the guaranteed acceptable values specified by ASTM A1114.

2.4 Galvanic corrosion

Galvanic corrosion occurs when two dissimilar materials are used together. Several studies have shown that the rate of corrosion will not increase when carbon steel and stainless steel rebars are used in the same concrete structure, even if they are in direct electrical contact (Abreu et al. 2002; Ji et al. 2005). Therefore, hybrid use of stainless steel and carbon steel rebars was considered as a viable option to optimize cost and increase durability of concrete structures. In multiple projects, stainless steel reinforcement was placed in the outermost reinforcement layers, which are the most exposed regions to chloride, and the remaining layers were carbon steel reinforcement (Markeset et al. 2006).

2.5 Research conducted by state departments of transportation (DOTs)

Many state DOTs have shown interest in stainless steel strands by sponsoring research projects. In 2014, Florida Department of Transportation (FDOT) completed a research study investigating the use of different types of stainless steel strands in prestressed concrete piles (Mullins et al. 2014). The conclusion was to allow the use of HSSS strands in piles. Georgia Department of Transportation (GDOT) conducted a study on constructability and evaluation of prestressed concrete piles using HSSS strands (Paul et al. 2015). The study finished in 2015 and concluded

that design requirements and construction procedures used for carbon steel strands in prestressed concrete piles can be used for stainless steel strands. Virginia Department of Transportation (VDOT) conducted a pilot study to monitor fabrication and driving of HSSS strand in prestressed concrete piles in new bridges in Virginia (Troconis et al. 2020). The study finished in 2020, and it permitted the use of HSSS strands in bridge elements in Virginia where it is needed, but it did not provide any design guidelines for this new material in flexural members. After successful research projects by Florida, Georgia, and Virginia DOTs, many other state DOTs have already used or allowed the use of HSSS strand in prestressed piles. Much of the previous work has focused on the constructability, fabrication, and evaluation of stainless steel prestressed concrete piles. So, apparently, very limited research has been performed on the application of HSSS strand in flexural members.

2.6 Current stainless steel design guidelines

Current design guidelines for carbon steel and carbon fiber reinforced polymer (CFRP) strands in prestressed concrete are based on the results of decades of research work, large-scale experiments, and lessons learned from field applications. Stainless steel strands have different stress-strain behavior compared to that for carbon steel and CFRP strands. Stainless steel strand shares only one mechanical property with CFRP strand, which is low ductility. Thus, the design provisions developed for concrete members with carbon steel strands or CFRP strands are not necessarily applicable to those with stainless steel strand. The design methodology must account for the stress-strain behavior of the stainless steel strand.

Because stainless steel strands are relatively new to the construction industry, few studies and experimental tests have been conducted. Therefore, no design guidelines or codes have been drafted yet to assist engineers in the design of the stainless steel prestressed concrete flexural members.

2.7 Projects utilized stainless steel reinforcing materials

2.7.1 Stainless steel rebars

One of the earliest uses of the austenitic stainless steel rebars was in the construction of Progreso Pier in Mexico in the 1940s, where around 200 tons of stainless steel bars were used (Castro-Borges et al. 2002). The Progreso Pier was constructed in a highly-corrosive environment, classified as grade 5, corrosive aggressivity, in the scale of the International Organization of Standardization (ISO) (Maldonado and Veleza 1999). Although the Progreso Pier has not received

any type of maintenance during the first 60 years of service, no signs of deterioration were observed in the pier during the inspection almost 20 years ago (Castro-Borges et al. 2002).

The earliest use of stainless steel rebars in bridge concrete decks in the United States was in 1983. After 25 years in service, the deck-slab exhibited no deterioration according to the inspection report (Kahl 2011). Therefore, it can be inferred that using stainless steel, even in highly-corrosive environments, can significantly reduce demand for inspection and maintenance. A restriction of 1.5-in. concrete cover, to keep the existing geometry and roadway approach, pushed the choice of stainless steel as the main reinforcement in a bridge deck in Michigan (Kahl 2011).

Stainless steel rebars have already been utilized worldwide in multiple structures such as bridges, retaining walls, and foundations (Baddoo and Kosmac 2010; Markeset et al. 2006; Rabi et al. 2019).

2.7.2 Stainless steel strands

Stainless steel strands do not have a long history in the construction industry compared to stainless steel rebars. Stainless steel seven-wire prestressing strands became available to the bridge industry around a decade ago. Stainless steel strands are an attractive choice for state departments of transportation (DOTs), especially DOTs with bridges in extremely aggressive environments. For example, in Florida, so many prestressed concrete bridges will be constructed in extremely aggressive marine environments in the future.

Stainless steel strands have been utilized in piles in multiple projects around the United States to extend the service life of the substructure. The earliest use of HSSS strands in concrete piles in the United States was in 2013. As of 2020, a total of 17 projects have used stainless steel strands. Table 2-1 provides information about projects that used stainless steel strands in the United States. The growing interest by state DOTs in using stainless steel piles has increased in recent years.

The use of HSSS strands was mostly in piles. The delay of implementation of HSSS strands in flexural members can be attributed to two factors. First, limited research and/or full-scale experimental work have been conducted to evaluate the flexural behavior of concrete members prestressed with stainless steel strands. Second, there is a lack of design guidelines and codes.

Table 2-1 Projects that used HSSS strands in the United States

Number	Project name	Owner	Year	Application
1	Nimmo Parkway	VDOT	2013	Piling
2	Riceboro Creek	GDOT	2016	Piling
3	Satilla River	GDOT	2016	Piling
4	LA 1 Grand Isle	LADOT	2017	Piling
5	Cedar Key Bridge	FDOT	2018	Piling
6	High Rise Bridge	VDOT	2018-2019	Piling
7	Arlington Bridge	EFL*	2018-2019	Deck panels
8	Wilmington River Bridge	GDOT	2018-2019	Piling
9	Jimmy Delouch Parkway	GDOT	2018-2019	-
10	Queens Creek	VDOT	2019	Piling
11	Seneca 19	ODOT	2019	Box girder beams
12	Sterling Creek Bridge	GDOT	2019	Piling
13	Pipe Makers Canal	GDOT	2019	Piling
14	Skyway Bridge 19025	FDOT	2019	Sheet pile
15	Island Parkway	GDOT	2019	Piling
16	Brick Kiln Creek Bridge	VDOT	2019	Piling
17	US41/Tamiami Trail	FDOT	2019	Piling

* Eastern Federal Land

CHAPTER 3 MECHANICAL AND BOND STRENGTH PROPERTIES

3.1 Introduction

Many parameters are involved in the design of prestressed concrete members such as: mechanical properties of the strands, concrete strength, and effective prestress. The mechanical properties of the strands can be determined from tensile tests. HSSS strands are relatively new to the construction industry. Thus, mechanical properties of HSSS strands need to be evaluated.

In pretensioned concrete members, the prestressing force is transferred from strand to concrete through bonding. This bonding depends on many parameters such as: concrete strength, surface condition of the strand, and type and size of the strand. For the surface condition of the strand, any lubricant residue left from the manufacturing process can affect both the chemical adhesion and friction of the strand (Polydorou et al. 2016). In some cases, residue materials on the strand's surface cannot be identified by visual inspection. The strand is bonded to the concrete through chemical adhesion on the surface of the strand before slippage occurs between the strand and the concrete (Riding et al. 2016). However, once slippage occurs, the bonding is controlled by friction. Unlike carbon steel strands, HSSS strands are shiny and do not hold rust on their surface. Therefore, HSSS strands can be classified as smooth compared to carbon steel strands. Thus, the bond strength of HSSS strands needs to be evaluated.

This chapter investigates the mechanical properties of 0.6-in.-diameter HSSS strands. Tensile tests were performed on 25 0.6-in.-diameter HSSS strands from two spools. A stress-strain equation was developed and is proposed for HSSS strands. The proposed equation satisfies ASTM A1114 requirements and is in good agreement with experimental results. Also, this work evaluates the bond strength properties of 0.6-in.-diameter HSSS strands where six HSSS strands were tested for bond strength following ASTM A1081 (2015).

3.2 Comparison of carbon steel and HSSS strands

Because HSSS strands are made from different alloys compared to carbon steel strands, their stress-strain relationship is fundamentally different than that of carbon steel strands. The HSSS strands have early nonlinearity with a rounded stress-strain curve once the elastic modulus is deviated, and thus they exhibit no discernable yield plateau as shown in Figure 3-1.

The minimum required mechanical properties of the carbon steel strands are specified by ASTM A416 for both Grade 250 and Grade 270. Recently, ASTM A1114 was published defining the minimum required mechanical properties of the stainless steel strands Grade 240. The decrease

in the Grade from 270 in ASTM A416 to 240 in ASTM A1114 is attributed to the chemical composition of the strand. Some alloying elements, used to make stainless steel strands, control the ultimate tensile strength. ASTM A1114 specifies two sizes for stainless steel strands, 0.52-in. and 0.62-in. diameter.

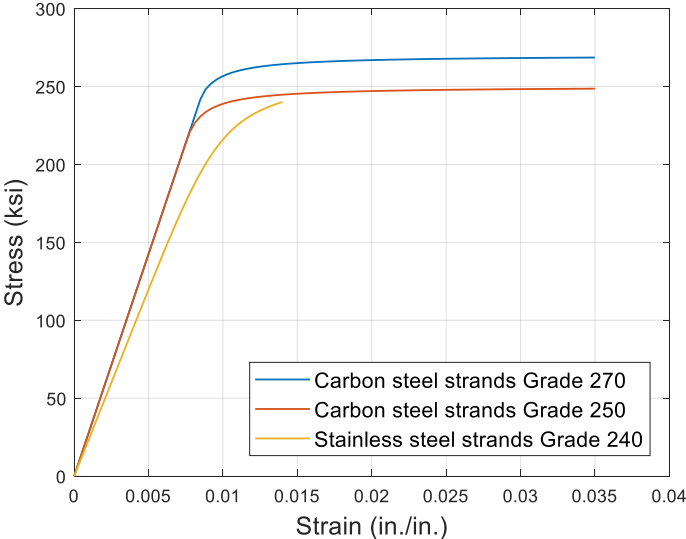


Figure 3-1 Comparing stress-strain diagram of stainless steel strands versus carbon steel strands

Table 3-1 lists the minimum requirements for 0.52-in.- and 0.62-in.- diameter strands from ASTM A416 Grade 270 and ASTM A1114 Grade 240. The area and weight of stainless steel strands Grade 240 are equal to those of the carbon steel strands Grade 270. The strength at 1% elongation, breaking strength, and elongation are lower than those of the carbon steel strands Grade 270. The most significant difference between stainless steel and carbon steel strands is elongation. The minimum guaranteed elongation of carbon steel strands is 2.5 times greater than that of stainless steel strands. Thus, stainless steel strands exhibit almost no strain hardening compared to carbon steel strands. This reduction in elongation significantly affects the design philosophy when using stainless steel strands in prestressed concrete members.

Table 3-1 Minimum required mechanical properties of 0.52-in.- and 0.62-in.-diameter strands

Parameters	ASTM A416 Grade 270		ASTM A1114 Grade 240	
	0.52	0.62	0.52	0.62
Nominal diameter (in.)	0.52	0.62	0.52	0.62
Area (in ²)	0.167	0.231	0.167	0.231
Strength @ 1% extension (lbf)	40,500	56,520	36,100	49,860
Breaking strength (lbf)	45,000	62,800	40,100	55,400
Elongation (%)	3.5	3.5	1.4	1.4
Weight of strand lb/1000 ft	570	780	570	780

3.3 Tensile tests

3.3.1 Preparation of specimens

Two 0.6-in.-diameter HSSS strand spools were received, at different times, in ideal condition free of rust and any visible defects. It was stored at the FDOT Structures Research Center (SRC) and protected from damage such as oil, excessive bending, and any physical damage. A mill test certificate for each spool was provided by the manufacturer, specifying the mechanical properties of the HSSS strands. The mill test certificate for both spools can be found in Appendix A. The mechanical behavior of HSSS strands might vary from spool to spool due to multiple reasons such as the wire rod used to make prestressing strands is not perfectly identical from heat-to-heat, chemistry variances of the elements alloyed, and processing variances. Therefore, tensile tests were performed on multiple samples that were taken from the two spools. Both spools were manufactured by Sumiden Wire. The samples from the two spools were referred to as first spool and second spool throughout this work. It is recommended to test three specimens per material size or type (Mullins et al. 2014).

Fifteen HSSS strand specimens were taken from the first spool. Ten specimens were taken from the beginning of the spool. Then the strand in the spool was used to fabricate several pretensioned concrete beams. The other five specimens were taken from the strand's leftover at the end of the precasting bed after releasing the strands. Ten HSSS strand specimens were taken from the second spool. Five specimens were taken directly from the spool, and the other five specimens were taken from the strand's leftover at the end of the precasting bed. All specimens were sent to the FDOT State Materials Office (SMO) for tensile testing.

There are multiple methods for gripping strands in the tensile test. HSSS strands exhibit grip slippage and have complications with the gripping mediums such as stress concentration and

premature failure. Therefore, the ends of the strands were coated with high modulus epoxy and 80 grit silicon carbide to create a friction grip and prevent grip slippage as shown in Figure 3-2a and Figure 3-2b. This coating approach seems to be the best available method to transfer force from the grips to HSSS strands because it aims to eliminate failure at the strand's ends. All specimens were tensile tested using the grout coating approach except for five specimens, which were taken directly from the first spool. Those specimens were tensile tested using chucks as a primary gripping device. Table 3-2 shows the test matrix of the tensile tests in this experimental program.



(a) coating end of a specimen with epoxy



(b) specimens prepared to be tensile tested



(c) seating the end of the specimen in the grip



(d) preload to align the strand and seat the ends in the grips



(e) attached extensometer to measure strain up to 1% elongation



(f) failure of the specimen close to the grip

Figure 3-2 Preparation and testing of specimens using grout

Table 3-2 Test matrix of the tensile test

Number of specimens			
Source of strand	Beginning of spool		Leftover from bed
Testing method	Grout coating	Chuck devices	Grout coating
First spool	5	5	5
Second spool	5	-	5

3.3.2 Test setup

3.3.2.1 Using coating approach

A universal testing machine (UTM) was used for the tensile tests. The length of each specimen was 50 in., and the minimum required strand length to be inserted in the grips is 8 in. as shown in Figure 3-2c. This embedded length allows for a full transfer of the load from the grips to the strand. A preload of around 10% of breaking strength was applied to align the strand and seat the ends in the grips, Figure 3-2d. Once the strand was aligned and tight, a 24-in. extensometer was attached to the strand leaving a 5-in. clear distance between the jaws and the extensometer, Figure 3-2e. The extensometer measured strain up to around 1% extension with an accuracy of 0.01% and then it was removed to prevent possible damage, as HSSS Grade 2205 strands have low ultimate strain. Once the extensometer was removed, the machine was reloaded, and the data collection was switched from the extensometer to the UTM. The UTM calculates strain by measuring displacement between the machine’s crossheads.

3.3.2.2 Using chuck devices

The objective of these tests was only to verify that regular chucks can be used to tension HSSS strands in the casting yard. Several methods can be used to grip the strands for the tensile test. The type of strand and tensile testing machine determine which gripping method to use. ASTM A1061 (2016) does not specify a single gripping method for all types of strands and tensile testing machines, but rather leaves it to the tester to decide which method is more suitable. It is clearly stated that chucks shall not be used as a primary gripping device in the tensile tests. However, chucks are used in the field for normal tensioning procedures. Therefore, chucks were used as the primary devices in the tensile tests to ensure that they can be used to tension HSSS strands in casting beds.

3.3.3 Results

3.3.3.1 Using coating approach

Tensile tests were performed on 20 0.6-in.-diameter HSSS strands, ten from each spool. All specimens were tensioned until breakage, which is defined as failure state. Failure of all strands happened at one end, close to the jaw as shown in Figure 3-2f. The failure of all strands was categorized as pure rupture. The measured area for the first spool was 0.230 in² and for the second spool was 0.228 in². Statistical summaries of tested strands are presented in Table 3-3 and Table 3-4 for specimens from the first and second spools, respectively. Experimental results of two strands from the second spool were excluded from the summary in Table 3-4. The first one was excluded because the specimen length was shorter than the required length, and the extensometer could not be installed to measure elongation. The second one was excluded because the specimen was not seated perfectly in the grips, which significantly affected the experimental results.

Table 3-3 Statistical summary of test results for specimens from the first spool

Specimen type	Specimen no.	Load at 1% (kip)	f_{py} (ksi)	Ultimate load (kip)	f_{pu} (ksi)	$\frac{f_{py}}{f_{pu}}$ (%)	Elongation (%)	E_{ps} (ksi)
Beginning of spool	1	52.52	228.34	60.25	261.93	87.2	1.87	24,100
	2	52.61	228.72	60.35	262.40	87.2	1.85	24,500
	3	52.50	228.27	60.12	261.40	87.3	1.83	24,600
	4	51.72	224.86	60.31	262.22	85.8	1.89	23,900
	5	52.47	228.11	60.07	261.16	87.3	1.86	24,400
Leftover from bed	6	53.41	232.23	60.14	261.47	88.8	1.76	25,200
	7	53.88	234.27	59.99	260.81	89.9	1.69	25,900
	8	53.43	232.32	60.36	262.43	88.5	1.80	25,200
	9	53.42	232.25	60.01	260.89	89.0	1.75	25,600
	10	53.41	232.23	60.11	261.35	88.9	1.78	25,800
Maximum						89.8	1.89	25,900
Minimum						85.8	1.69	23,900
Average		52.94	230.16	60.17	261.61	88.0	1.81	24,920
Standard deviation		0.667	2.900	0.139	0.602	1.218	0.064	716

Stress-strain plots of the tested HSSS strands are shown in Figure 3-3; note that the stress-strain behavior is different between specimens from the first spool and second spool. This difference is attributed to the chemical composition of alloys used to manufacture the strands. Tensile test results showed that the HSSS strands exhibit a rounded stress-strain curve once the elastic modulus slope is deviated with early nonlinearity. Figure 3-3 shows a small drop in stress

at around 1% strain. This drop occurred due to unloading the strand to remove the extensometer. It should be noted that this drop was unavoidable, but it could have been minimized by removing the extensometer more quickly and reloading the UTM.

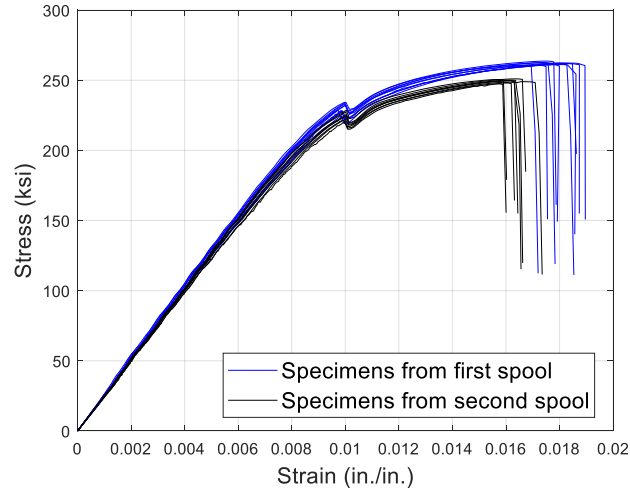


Figure 3-3 Stress-strain curves of the tested stainless steel specimens using coating approach

Table 3-4 Statistical summary of test results for specimens from the second spool

Specimen type	Specimen no.	Load at 1% (kip)	f_{py} (ksi)	Ultimate load (kip)	f_{pu} (ksi)	$\frac{f_{py}}{f_{pu}}$ (%)	Elongation (%)	E_{ps} (ksi)
Beginning of spool	1	51.06	223.96	56.87	249.42	89.8	1.62	24,500
	2	50.62	222.02	56.66	248.51	89.3	1.63	24,200
	3	50.18	220.10	56.77	248.97	88.4	1.71	24,200
	4	50.58	221.83	56.41	247.42	89.7	1.59	24,600
Leftover from bed	5	51.40	225.44	56.95	249.80	90.3	1.63	25,300
	6	52.06	228.33	57.12	250.52	91.1	1.59	25,300
	7	51.21	224.61	57.02	250.10	89.8	1.64	24,800
	8	51.84	227.37	57.22	250.97	90.6	1.66	25,400
Maximum							1.71	25,400
Minimum							1.59	24,200
Average		51.12	224.21	56.88	249.46	89.9	1.63	24,788
Standard deviation		0.645	2.831	0.262	1.150	0.826	0.036	494

Table 3-5 gives ASTM A1114 and FDOT requirements (2020), mill certificates provided by the manufacturer for each spool, and average experimental results. All specimens from the first and second spools satisfied ASTM A1114 and FDOT requirements. The areas of the tested specimens were slightly lower than the required value by ASTM A1114 because the diameter of the tested specimens was 0.6 in. while ASTM A1114 provides minimum required mechanical

properties only for 0.62-in. diameter. Note that the tested strands were produced before the release of ASTM A1114.

Table 3-5 Mechanical properties for 0.6-in.-diameter HSSS strands

		Area (in ²)	Yield strength (kip)	Breaking strength (kip)	Ultimate stress (ksi)	Elongation (%)	Elastic modulus (ksi)
Standard requirements	ASTM A1114	0.2310	≥ 49.86	≥ 55.400	≥ 240	≥ 1.4	-
	FDOT	0.2310	≥ 49.86	≥ 55.400	≥ 240	≥ 1.4	-
First spool	Manufacturer	0.2328	52.92	59.76	256.65	1.90	24,400
	Average tensile tests	0.2300	52.94	60.17	261.61	1.81	24,920
Second spool	Manufacturer	0.2306	50.59	55.47	240.56	1.60	23,900
	Average tensile tests	0.2280	51.12	56.88	249.46	1.63	24,788

3.3.3.2 Using chuck devices

Five specimens from the first spool were tested by using chucks as a primary gripping device at the FDOT SMO. The chucks were attached to the ends of the strands and neither epoxy nor 80 grit silicon carbide were used to coat the ends of the strands. The strands were preloaded to 10% of breaking strength and then an extensometer was attached. The UTM was unloaded at 1% extension to remove the extensometer, to avoid damage. Once the extensometer was removed, the strand was reloaded again until failure. The stress-strain curves of specimens tested using grout coating and chuck devices are illustrated in Figure 3-4. Average mechanical properties of the five tested strands are reported in Table 3-6. A reduction in all parameters was observed (breaking strength, load at 1% extension, ultimate strain and modulus of elasticity) when strands were tested with chucks. This is clear evidence that using chucks for tensile tests does not produce the full capacity of strands and should not be used as stated by ASTM A1016. The behavior of the strands before yielding was not significantly affected compared to after yielding. Usually strands in the casting bed are tensioned within its elastic limit, below yield strength. It can be concluded from Figure 3-4 that the strands lost some of their mechanical behavior due to stress concentration from the grips at the ends of the strands. Figure 3-5a shows a HSSS strand tensile tested using chucks as primary gripping devices. Failure of all five specimens happened at one end at the point where the chucks gripped the strands, as shown in Figure 3-5b. Figure 3-5c shows a notching effect of

the grips, which resulted in failure of the strand. To conclude, chucks can be used to initially stress HSSS Grade 2205 strands for prestressed concrete member fabrication.

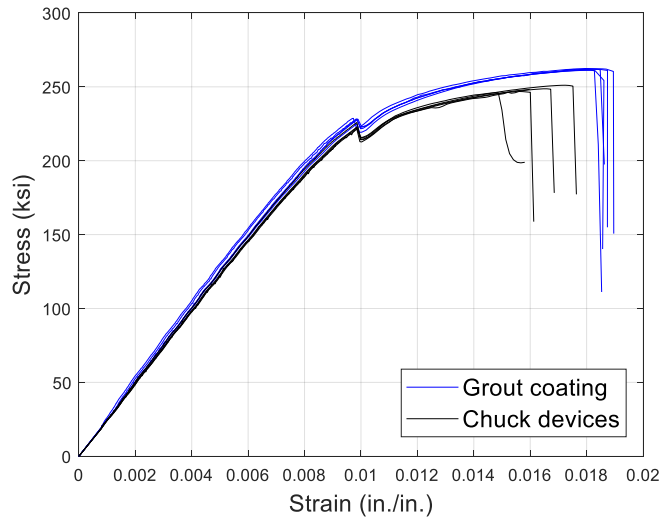


Figure 3-4 Stress-strain curves of specimens using grout coating and chuck devices

Table 3-6 Mechanical properties of stainless steel strands using grout coating and chuck devices

Parameters	Using grout coating	Using chuck devices	Reduction (%)
Area (in ²)	0.2328	0.2328	0
Strength @ 1% extension (lbf)	52,937	51,918	1.92
Breaking strength (lbf)	60,169	57,792	3.95
Elongation (%)	1.81	1.60	11.60
Elastic modulus (ksi)	24,920	23,900	4.09

3.3.3.1 Yield strength

There are multiple methods to determine the yield strength of prestressing strands. The most common ones are the extension under load (EUL) and the offset methods. ASTM A416 and ASTM A1114 propose EUL method for seven-wire prestressing strand. Those ASTMs define the yield strength as the stress when the total strain reaches 1%, and the yield strength must be at least 90% of the ultimate strength. The average values of the yield and breaking strength of specimens from both spools were higher than the required values by ASTM A1114 as shown in Table 3-5. However, Table 3-3 and Table 3-4 show that all specimens from the first spool and some specimens from the second spool did not meet the 90% yield strength requirement. The average

ratio of the yield strength to breaking strength was 88.0% and 89.9% for specimens in the first spool and second spool, respectively.

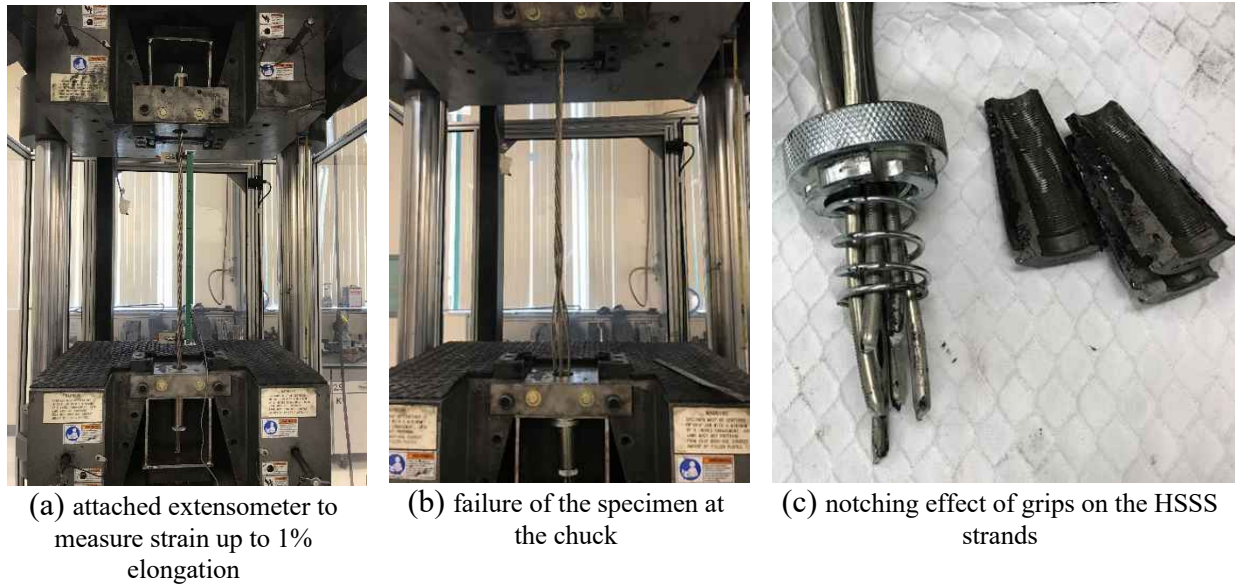


Figure 3-5 Preparation and testing of specimens using chuck devices

The offset method defines the yield stress as the intersection of the stress-strain curve with a line that starts at a specified strain value and runs parallel to the linear region of the stress-strain curve. Eurocode2 specifies the start strain value as 0.1%; this method is called the 0.1% offset method (2004). The 0.2% offset method is recommended by Korean Concrete Institute, which specifies the start strain value as 0.2% (2012). Schuetz suggested to use 1.2% extension method or 0.2% offset method to determine the yield strength of HSSS Grade 2205 strands (Schuetz 2013). In this research, yield strengths calculated using 1.2% extension method or 0.2% offset method were higher than 90% of the ultimate strength, which satisfies the 90% yield strength requirement by ASTM A1114.

3.3.4 Differences in tensile testing HSSS strands

The professional technician who performed the tests reported multiple differences between tensile testing of carbon steel strands and HSSS strands. First, the HSSS strands kept their shape as bent on the spool, which resulted in difficulties seating both ends of the specimen in the top and bottom grips. Second, the location of the break of the HSSS specimens was in close proximity to the grip in all specimens tested, while the carbon steel strands broke at random locations. Third, the epoxy coating, Figure 3-2a, peels from HSSS specimens. Fourth, the HSSS specimens failed faster than the carbon steel strands, where the plastic strain was vastly smaller than that of the

carbon steel strands. Fifth, special attention was needed when removing the extensometer (after reaching 1% extension) because the HSSS specimens might break while removing the extensometer due to its short plastic strain.

3.4 Stress-strain model

3.4.1 Background

The stress-strain behavior of HSSS strands is different from that of carbon steel strands. Therefore, a new stress-strain equation needs to be developed. The stress-strain formula is necessary for strength design and numerical analysis of prestressed concrete members. A widely accepted method for describing stress-strain behavior of a material is the Ramberg-Osgood model (Ramberg and Osgood 1943). The original model was developed for aluminum alloys and was not valid and accurate for materials with highly nonlinear stress-strain relationships. Many researchers, afterwards, have modified the model for either different materials or to better fit experimental tests. One of the most widely-used analytical formulas, known as the power formula, was derived from the modified Ramberg-Osgood function (Collins and Mitchell 1991). The power formula was proposed by Mattock (Mattock 1979) and has been proven suitable for highly-nonlinear materials. It consists of four curve fitting constants as shown in Equation 3-1. The methodology behind this formula is to divide the stress-strain curve into two straight lines connected by a curve. The first line is for the elastic region, and the second line is for the inelastic region; the two lines are connected by a curve, which is around the yield point. As long as the actual stress-strain curve is available, either from the manufacturer or actual tests, those four curve-fitting variables can be calculated. A detailed procedure for calculating curve-fitting constants for the power formula is given in (Collins and Mitchell 1991).

$$\sigma = E_{ps} * \varepsilon \left\{ A + \frac{1-A}{[1+(B * \varepsilon)^C]^{1/C}} \right\} \quad \text{Equation 3-1}$$

where

σ = stress in strand, ksi

E_{ps} = modulus of elasticity of strand, ksi

ε = strain in strand, in./in.

$A, B, \text{ and } C$ = constant

Researchers have developed power formulas for all available low-relaxation carbon steel strand sizes. Table 3-7 shows power formulas for three sizes of carbon steel strand Grade 270. (Devalapura and Tadros 1992) studied 56 stress-strain curves for low-relaxation carbon steel strand Grade 270; half of the stress-strain curves were obtained from the manufacturers, while the

other half were tested by the researchers. The specimens were made from different types of steel and were tested by different machines. A statistical lower-bound curve was derived from the 56 curves. The study resulted in proposed curve fitting constants for the power formulas for 0.5-in.-diameter low-relaxation carbon steel strands. The proposed power formula curve was as close as possible to the experimental lower-bound curve and satisfied the yield strength requirements of ASTM A416. (Collins and Mitchell 1991) proposed curve fitting constants for the power formula for 0.6-in.-diameter carbon steel strand Grade 270. The power formula is not limited to certain strand diameters; (Morcous et al. 2011) recently proposed a power formula for 0.7-in.-diameter carbon steel strand Grade 270. The curve fitting constants for the proposed power formula were calculated after testing 40 strands from two different producers and by two different machines. All proposed power formulas result in a conservative curve which lies below the actual stress-strain curves. This is mainly because the proposed power formulas were developed to fit the lower-bound curve of tested strands. PCI Design Handbook (2010) provides approximated equations for 7-wire low-relaxation strands. The PCI equations are divided into two parts: the first part is for the elastic region, and the second one is for the plastic region.

Table 3-7 Power formulas for low-relaxation carbon steel strands Grade 270

Author	Diameter (in.)	Modulus of elasticity (ksi)	Proposed stress-strain equation
(Devalapura and Tadros 1992)	0.5	28,500	$\sigma = E_{ps} * \varepsilon \left\{ 0.031 + \frac{0.969}{[1 + (112.4 * \varepsilon)^{7.36}]^{\frac{1}{7.36}}} \right\}$
(Collins and Mitchell 1991)	0.6	29,000	$\sigma = E_{ps} * \varepsilon \left\{ 0.025 + \frac{0.975}{[1 + (118 * \varepsilon)^{10}]^{\frac{1}{10}}} \right\}$
(Morcous et al. 2011)	0.7	28,500	$\sigma = E_{ps} * \varepsilon \left\{ 0.02 + \frac{0.98}{[1 + (\frac{E * \varepsilon}{1.03 * f_{py}})^{7.33}]^{\frac{1}{7.33}}} \right\}$

3.4.2 Proposed model for 0.6-in.-diameter HSSS strands

The format of the modified Ramberg-Osgood function, given in Equation 3-1, was used for the stress-strain models of the two HSSS spools.

3.4.2.1 Tensile tests

As mentioned previously, ten 50-in.-long specimens from each spool were tested in direct tension. The three coefficients (*A*, *B*, and *C*) in Equation 3-1 were calculated to obtain a best fit

with the lower-bound curve of the tested strands. Table 3-8 summarizes the proposed coefficients. Figure 3-6 shows the measured stress-strain curves as well as the curves from the proposed equations.

Table 3-8 Coefficient of modified Ramberg-Osgood function for HSSS strands

Specimen ID	A	B	C
Spool no. 1	0.065	100	6.5
Spool no. 2	0.050	102	7.0

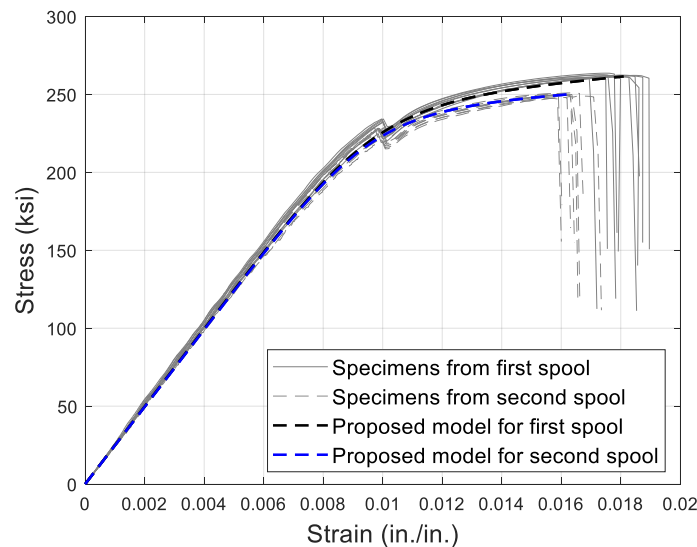


Figure 3-6 Comparison of measured and calculated stress-strain curves of stainless steel strands

3.4.2.1 Design purposes

ASTM A1114 requirements represent the minimum guaranteed mechanical properties for stainless steel strands. Thus, the proposed stress-strain equation for design purposes shall represent the ASTM A1114 minimum requirements and have the same shape as the tested specimens. This means that for 1% strain and 1.4% strain, the proposed equation shall result in a stress of 216 ksi and 240 ksi, respectively. The curve-fitting constants in Equation 3-1 were determined to adequately match the ASTM A1114 requirements as well as have the same stress-strain shape as the tested specimens. The proposed stress-strain equation for 0.6-in.-diameter HSSS strands is given in Equation 3-2; where σ is stress in the strands and ε is the strain in the strand.

$$\sigma = 24,000 * \varepsilon \left\{ 0.06 + \frac{0.94}{[1+(101*\varepsilon)^{6.45}]^{1/6.45}} \right\} \quad \text{Equation 3-2}$$

Figure 3-7 provides a visual representation of the proposed equation along with the average stress-strain curves from the experimental results of the two spools. The proposed equation fits the lower-bound curve of the tested strands in the elastic region; this was achieved by taking the elastic modulus equal to 24,000 ksi. The proposed equation is parallel to the shape of the curves for the two spools in the plastic region. The proposed equation is conservative and underestimates the strand behavior of the two spools, and it is conservative compared to the actual behavior of the HSSS strands because the manufacturers will always produce HSSS strands that have mechanical properties higher than the minimum requirements in ASTM A1114.

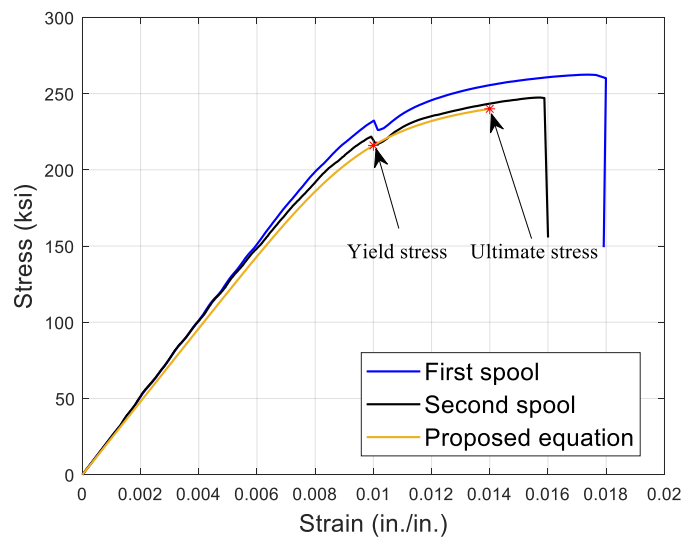


Figure 3-7 Comparing stress-strain model of the proposed equation versus experimental stress-strain models

3.5 Bond strength tests

Bond strength quantifies the bonding between a strand and the surrounding concrete in a pretensioned concrete member. The strand bond strength can be evaluated by either performing a bond test of a single strand in a mortar, or by measuring transfer and development lengths in pretensioned concrete members (Dang et al. 2018). A test procedure to measure strand bond strength is provided by ASTM A1081 (2015), which was adopted from North America Strand Producers (NASP), where the strand is pulled out from a sand-cement mortar (Dang et al. 2018; Morcouc et al. 2011). However, the bond strength test does not simulate the practical behavior of a prestressed concrete member because the strand is not prestressed. The transfer and development lengths have been estimated from the bond strength test, where strength from the Hoyer effect was added (Brandes and Kurama 2018).

3.5.1 Preparation of specimens

The bond strength tests were performed according to ASTM A1081 protocol (2015). The test requires a minimum of six strands and 15 mortar cubes. Six HSSS strands were taken from the first spool, in as-received condition and preserved from foreign substances. Six specimens were prepared by casting sand-cement mortar in a steel pipe around a single 0.6-in.-diameter HSSS strand as shown in Figure 3-8. The steel tube was 5-in.-diameter and 24 in. tall. A 2-in.-long steel breaker was placed at the bottom of the can. This steel breaker is used to debond the strand and reduces the confinement pressure acting on the strand. The specimens were cured in an environmental chamber until testing. The dimensions of the mortar cube were 2 in. x 2 in. x 2 in. Per ASTM A1081, three mortar cubes shall be tested each hour at 22-26 hours after casting until an average compressive strength of 4500-5000 psi is reached for the three cubes. Once reached, bond strength tests can be performed. Mortar mix design was validated before the experiment, and it was expected to have a compressive strength of 4500-5000 psi at 24 hours. Mortar strength has an influence on the bond strength of the strand.

3.5.2 Test setup

The test setup and apparatus used for the bond strength test are shown in Figure 3-9. The live end of the strand was connected to the gripping device where the force was applied. A linear variable displacement transducer (LVDT) was mounted at the dead end to measure displacement. The rate of pull-out force at the gripping device was 0.1 in./min. The loading rate did not exceed 8500 lb/min. Tensile and bond strength tests were performed by professional technicians at the FDOT SMO in Gainesville, Florida.

3.5.3 Results

Three mortar cubes were tested each hour starting at 22 hours after casting. Figure 3-10 shows the average hourly compressive strength results of mortar cubes, which did not meet minimum required compressive strength of 4500 psi by ASTM A1081. The average compressive strength after 26 hours of casting was 4452 psi which was 98.93% of the minimum required strength. A mean mortar strength less than 4500 psi is acceptable by ASTM A1081 if the bond test result exceeds a minimum threshold value (2015). Thus, the strand bond test was continued despite the minor understrength of the mortar.



Figure 3-8 Six HSSS specimens prepared for bond strength test

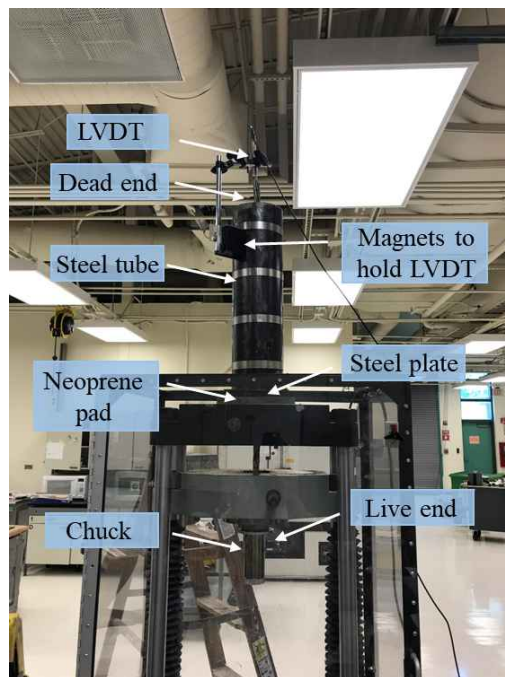


Figure 3-9 Test setup for the bond strength test

The bond strength tests were started 26 hours after casting. Six HSSS strands were tested for bond strength. Each test was terminated after the strand slip exceeded 0.1 in. at the dead end, according to ASTM A1081, and the strand bond strength was taken as the average pull-out force of six strand specimens. Force-slip displacements were measured during the test. The pull-out force at the chuck was measured in accordance with the movement of the dead end of the strand.

Figure 3-11 illustrates the force-displacement results for the six strands. The minimum and average bond strengths at 0.1 in. displacement were 15,800 lbf and 17,883 lbf, respectively. The peak tensile force was reached when the slip displacement at the dead end was around 0.0223 in. as shown in Figure 3-11. The minimum and average peak forces were 16,300 lbf and 18,633 lbf, which were about 3% and 4% greater than the minimum and average strand bond strength at 0.1 in. displacement at the dead end, respectively.

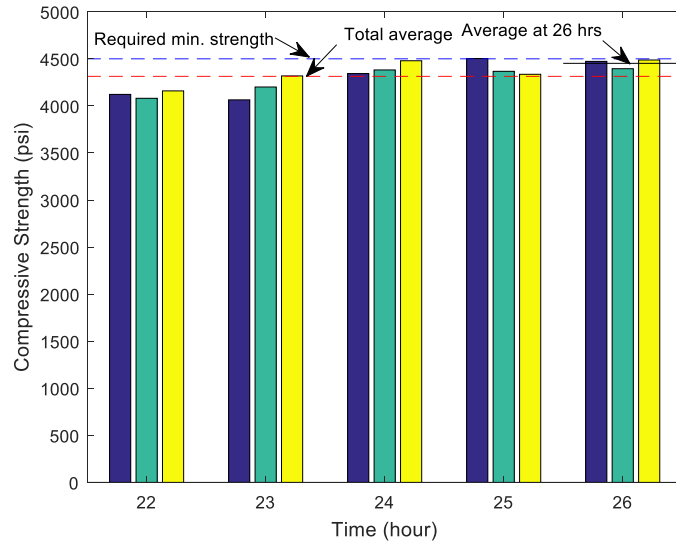


Figure 3-10 Compressive strength of concrete mortar cubes

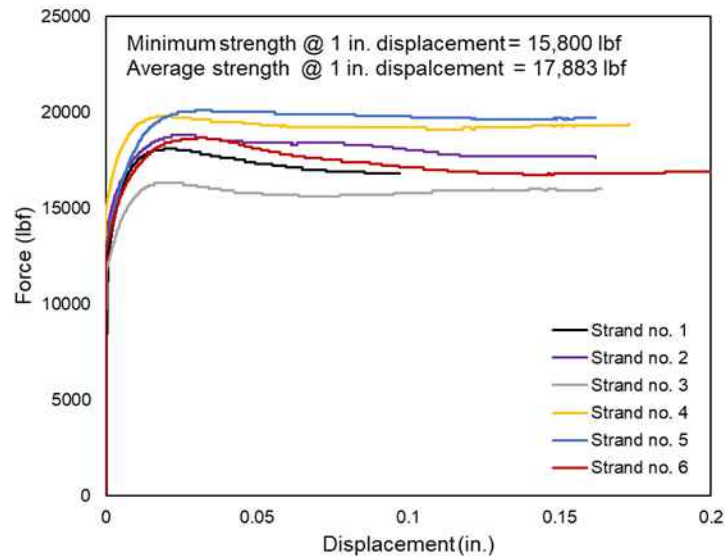


Figure 3-11 Pull-out test results of 0.6-in.-diameter HSS strands

ASTM A1081 does not specify a minimum threshold value for the bond strength of strand. In 2020, PCI Strand Bond Task Group recommended two acceptance bond strength criteria for ASTM A1081 (2020). The first criterion is that the minimum recommended average pullout value from six strands is 14,000 lb, with no strand having a pullout value less than 12,000 lb. The second criterion is that the ultimate (high bond) recommended average pullout value from six strands is 18,000 lb, with no strand having a pullout value less than 16,000 lb. Note that those acceptance bond strength values are for 0.5-in.-diameter Grade 270 carbon steel prestressing strand conforming to ASTM A416. For strands with either larger diameter or different grades, the PCI task group proposed an equation, which is given in Equation 3-3.

$$\text{Bond strength} = \text{Pullout value}_{0.5 \text{ in.}} \times 2 \times d_b \times \frac{f_{pu}}{270} \quad \text{Equation 3-3}$$

where d_b is diameter of strand in in. and f_{pu} is specified tensile strength of strand in ksi. Even though the recommended bond strength values were proposed for carbon steel strands conforming to ASTM A416, they were used here for HSSS strand conforming to ASTM A1114. In this study, the diameter and specified tensile strength for HSSS strand are 0.6 in. and 240 ksi, respectively. Using Equation 3-3, the minimum recommended average pullout value for 0.6-in.-diameter HSSS strand Grade 240 is 14,933 lb, with no strand having a pullout value less than 12,800 lb; and the ultimate (high bond) recommended average pullout value for 0.6-in.-diameter HSSS strand Grade 240 is 19,200 lb, with no strand having a pullout value less than 17,067 lb.

The minimum and average experimental ASTM 1081 pullout values were 15,800 lb and 17,883 lb, respectively, which were 23.4% and 19.8% greater than the recommended values calculated using the PCI Strand Bond Task Group recommendations. Another comparison can be made with the ultimate (high bond) pullout values measured experimentally. The minimum and average peak forces (high bond ASTM A1081 value) were 16,300 lb and 18,633 lb, which were 95.5% and 97.0%, respectively, from the recommended values calculated using the PCI Strand Bond Task Group recommendations. Note that the PCI task group specified that either the minimum ASTM A1081 value or the high bond ASTM A1081 shall be satisfied. Therefore, it can be concluded that the 0.6-in. HSSS strand used in this study has an acceptable bond strength.

3.6 Summary

This chapter presents experimental results on the mechanical and bond strength properties of 0.6-in.-diameter HSSS Grade 2205 strands. The following conclusions were made:

1. Twenty 0.6-in.-diameter HSSS strands were tensile tested from two spools. The stress-strain behavior of specimens from the two spools was different. The difference is attributed to multiple reasons such as the wire rod used to make prestressing strands is not perfectly identical from heat-to-heat, chemistry variances of the raw materials used to manufacture strands, and processing variances.
2. Specimens from both spools tested satisfied the minimum requirements specified by ASTM A1114 except area. The areas of the tested specimens were slightly lower than the required value by ASTM A1114 because the diameter of the tested specimens was 0.6 in. while ASTM A1114 provides minimum required mechanical properties only for 0.62-in.-diameter. Note that the tested strands were produced before the release of ASTM A1114.
3. The stress-strain equation is essential for the strength design and numerical analysis of prestressed concrete members. A stress-strain equation is proposed for the 0.6-in.-diameter HSSS strands. The proposed equation satisfies the ASTM A1114 requirements, fits lower-bound curves of the tested strands in the elastic region, and has a stress-strain shape similar to those of the tested strands in the plastic region.
4. The stress-strain behavior of HSSS strands is fundamentally different from that of carbon steel strands. The HSSS strands have early nonlinearity with a rounded stress-strain curve in the plastic region. The HSSS strands exhibit almost no strain hardening compared to carbon steel strands. The currently available HSSS strands have lower ultimate strain and stress and elastic modulus than those of carbon steel strands. The most significant difference is in the elongation. The minimum required elongation of the stainless steel strands is 40% of that of the carbon steel strands.
5. Five 0.6-in.-diameter HSSS strands were tested using chuck devices as the primary gripping devices. Experimental results showed that the mechanical properties of the HSSS strands are not significantly affected in the elastic region when chucks were used in the tensile tests. Thus, regular wedges can be used in the casting yard to tension HSSS strands.
6. Bond strength of the 0.6-in.-diameter HSSS strands was evaluated following ASTM A1081. The minimum and average strand bond strengths at 0.1 in. displacement of six strands were 15,800 lbf and 17,883 lbf, respectively. The peak tensile force was reached when slip displacement at the dead end was around 0.0223 in. The minimum and average

peak forces of six strands were 16,300 lbf and 18,633 lbf, respectively, which were about 3% and 4% greater than the minimum and average bond strengths, respectively.

7. The minimum and average experimental ASTM 1081 pullout values at 0.1 in. were 15,800 lb and 17,883 lb, respectively, which were 23.4% and 19.8% greater than the recommended values calculated using the PCI Strand Bond Task Group recommendations.

CHAPTER 4 GIRDER DESIGN AND FABRICATION

4.1 Introduction

This chapter discusses design and fabrication of the girder test specimens. An AASHTO Type II girder was selected for this research program for two reasons. First, this girder type allowed for a full-scale test with a practical design. Second, it is a standardized girder than can be used in low-level short- to medium-span bridges.

This research involved fabricating and testing 13 42-ft-long AASHTO Type II girders, with ten (10) girders prestressed with 0.6-in.-diameter HSSS strands and three (3) girders prestressed with 0.6-in.-diameter carbon steel strands. The girders were fabricated by a precaster, Dura-Stress, Inc., in Leesburg, FL.

The specimens in this chapter are divided into two sets. Each set was designed and cast individually. The first set consisted of eight girders. Seven of the eight girders were tested in flexure – three as monolithic and four as composite; and the eighth girder was tested in shear. The top fiber surface between the deck slab and girder was left smooth during fabrication. The shear stirrups in the monolithic girders were not embedded in the section and this resulted in reduction in the post-cracking behavior of all three non-composite girders. Two of the four composite girders had glass fiber reinforced polymer (GFRP) rebars as shear reinforcement. Because of the GFRP shear rebars and smooth surface at interface, the stiffnesses of both girders were reduced. More information about the design of the first set of girders is given in the following section.

After analyzing the experimental flexural data obtained from testing the first set of girders, no conclusion was drawn regarding use of HSSS strands in flexural members because the flexural behavior of most girders was influenced by other parameters. Therefore, it was decided to build a second set of five girders, taking into consideration all issues encountered during testing of the first set of girders.

4.2 First set of girders

4.2.1 Design objective

The objective was to design concrete girders prestressed with HSSS strands, some with the same number of strands and some with the same initial prestressing force as girders with conventional carbon steel strands, which served as the control.

4.2.2 Design method

The design of prestressed concrete members depends on concrete strength, type of prestressing strands, and effective prestressing. The HSSS strands are relatively new to the construction industry, compared to carbon steel strands. Therefore, no guidelines or codes are yet available to assist engineers in the design of concrete members prestressed with HSSS strands. Thus, the strain compatibility method was the best available option. The method can be used to design any reinforced/prestressed concrete member using any material or combination of materials, and it relies more on theory as opposed to using code equations.

4.2.3 Design matrix

A total of eight 42-ft-long AASHTO Type II girders were designed. Because HSSS strands have low ductility, it is feasible to fail a concrete member prestressed with HSSS strands by rupturing the strands. In this research program, this failure mode was achieved by adding a deck slab to the girder. The deck slab had an 8-in. thickness and a 24-in. width, and the haunch thickness was 2 in. Among the eight girders, deck slabs were added to six of them (two control and four with HSSS strands) as shown in Table 4-1. Adding a deck slab increased the compression zone, which resulted in an increase in the resultant compressive force, so the HSSS strands could reach their ultimate elongation before the concrete strain at the top fiber reached its ultimate strain of 0.003. In this case, rupture of HSSS strands would occur before the concrete crushed in the compression zone. For this design case, the ultimate moment capacity of the member was controlled by the HSSS mechanical properties. The specified concrete compressive strength for the girder and deck slab was 10 ksi and 6.5 ksi, respectively. The deck slab concrete strength was substantially greater than the minimum value specified by the FDOT, which is 4.5 ksi. The main reason for increasing the concrete strength of the deck slab was to avoid crushing of concrete in the compression zone of the composite girders prestressed with HSSS strands.

All girders were designed to resist shear and fail in flexure. Shear reinforcement (4K bars), confinement reinforcement (3D bars), and splitting reinforcement (5Z bars), all shown in Figure 4-1, were designed based on the AASHTO LRFD Bridge Design Specifications. Shear reinforcement was designed based on the mechanical properties of carbon steel rebar. The same reinforcement details and spacing were used in all the girders, regardless of material type – carbon steel, stainless steel, or GFRP. Figure 4-1 presents the transverse reinforcement layout; note that they are not identical in the two end regions.

Table 4-1 Design matrix of first set of girders

Number of strands	Section		Girder only			Composite with slab		
	Reinforcement	Transverse	Carbon steel	Stainless steel	GFRP	Carbon steel	Stainless steel	GFRP
11	Carbon steel strands		Girder A1				Girder A3	Girder A2
	HSSS strands			Girder B3				Girder B2
13	HSSS strands		Girder C1				Girder C3	Girder C2

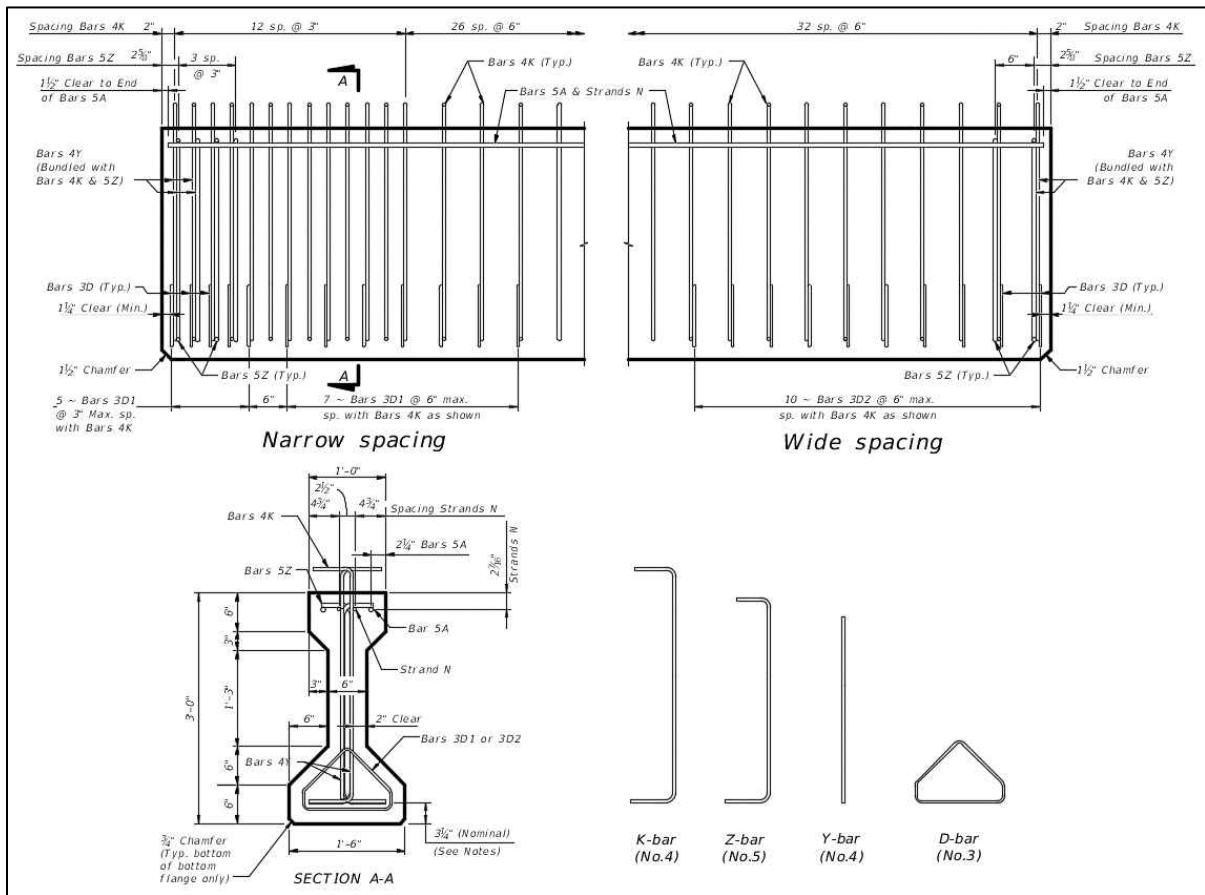


Figure 4-1 Reinforcement layout for first set of girders

The configuration in the narrow spacing end represents FDOT’s standard end region reinforcement detailing. The spacing of confinement and vertical reinforcement were increased at the other end – the wide spacing end – to investigate the spacing effect on bursting stresses at release, transfer length, and shear behavior of the member. The first shear reinforcement (4K bars) was placed at 2 in. on center from the end face of the girder. Both the 4K and 5Z bars have 90-

degree hooks at the bottom and top. Bars 4K and 5Z were bundled when spaced together, and the direction of the 90-degree hook bars was alternated. 5Z bars were within the girder, and the 4K bars extended out of the top of the girder to provide interface shear resistance between the girder and deck slab. The use of 5Z and 4Y bars was limited to regions in which bursting and spalling stresses were of concern. In the wide spacing end, the spacing of confinement reinforcement (3D bars) was 6 in. (double that the other end) for the first 12 in. as shown in Figure 4-1. The confinement reinforcement was placed along the first 56 in. from each end of the girder to resist bursting stresses when the strands were released. The confinement reinforcement was extended to more than the expected transfer length by AASHTO LRFD equation to minimize cracking in the ends of the girder.

The design matrix is given in Table 4-1, which consists of three groups. The first group was three control girders, Girder A1, Girder A2 and Girder A3. All girders had 11 carbon steel prestressing strands. Each strand was pretensioned to 43.9 kips, which is equal to 75% of its ultimate strength. The total initial prestressing force was 482.9 kips. Each girder had a different transverse reinforcement type, Table 4-1. The transverse reinforcement was carbon steel, GFRP, and stainless steel for Girder A1, Girder A2, and Girder A3, respectively. The typical shear reinforcement spacing was 6 in., providing a reinforcement ratio of 0.555% for Girder A1 and Girder A3 and 0.603% for Girder A2. These reinforcement ratios for the shear stirrups were used along the whole length of the girder except 36 in. at the narrow spacing end, where the shear stirrups were doubled as shown in Figure 4-1, and except in the mid region of the girder, where the shear reinforcement was spaced at 10 in. from either side of mid span, and then at 12 in. along a length of 4 ft towards each support.

The second group consisted of two girders prestressed with HSSS strands, Girder B2 and Girder B3, which were designed to have the same total number of strands (11) as the control girders. Each HSSS strand was pretensioned to 37.2 kips, 62.2% of their ultimate strength, resulting in an initial prestressing force of 409.2 kips. For transverse reinforcement, Girder B2 had GFRP rebar while Girder B3 had stainless steel rebar. The typical shear reinforcement spacing was 6 in., providing a reinforcement ratio of 0.603% and 0.555% for Girder B2 and Girder B3, respectively. These reinforcement ratios for the shear stirrups were used along the whole length of the girder except 36 in. at the narrow spacing end, where the shear stirrups were doubled as shown

in Figure 4-1, and except in the mid region of the girder, where the shear reinforcement was spaced at 10 in. from either side of mid span, and then at 12 in. along a length of 4 ft towards each support.

The third group, Girder C1, Girder C2 and Girder C3, was designed with HSSS strands having the same initial prestressing force (482.9 kips) as the control girders. Each HSSS strand was pretensioned to 37.2 kips, and to match the total prestressing force with the control girder, the total number of strands was 13. The total initial prestressing force was 483.6 kips. For transverse reinforcement, Girder C1, Girder C2 and Girder C3 had carbon steel, GFRP, and stainless steel, respectively. The typical shear reinforcement spacing was 6 in., providing a reinforcement ratio of 0.555% for Girder C1 and Girder C3 and 0.603% for Girder C2. These reinforcement ratios for shear stirrups were used along the whole length of the girder except 36 in. at the narrow spacing end, where the shear stirrups were doubled as shown in Figure 4-1, and except in the mid region of the girder, where the shear reinforcement was spaced at 10 in. from either side of mid span, and then at 12 in. along a length of 4 ft towards each support.

4.2.4 Materials

4.2.4.1 Prestressing strands

Two types of 0.6-in.-diameter prestressing strands were used: carbon steel and HSSS strands. The manufacturers for both carbon steel and HSSS strands provided mill test certificates, which included mechanical properties and stress-strain curves. Mill test certificates can be found in Appendix A. Table 4-2 provides ASTM 416 requirements as well as results from the manufacturer for carbon steel strands. The stress-strain equation for carbon steel strands is given in Table 3-7. The mechanical properties result for HSSS strands obtained from experiments, provided by the manufacturer and required by ASTM A1114 can be found in Table 3-5. Note that all HSSS strands used in the fabrication of the first set of girders were taken from spool no. 1. More information regarding the developed stress-strain equation for HSSS strands can be found in Section 3.4.

Table 4-2 Mechanical properties for carbon steel strands

Mechanical properties	Area (in ²)	Strength at 1% extension (kip)	Breaking strength (kip)	Ultimate stress (ksi)	Ultimate strain (in./in.)	Elastic modulus (ksi)
ASTM A416	0.2170	52.74	58.60	270.00	0.0350	-
Manufacturer	0.2184	55.50	60.90	278.85	0.0633	28,700

4.2.4.2 Reinforcing rebars

Three types of shear reinforcement were used: carbon steel, GFRP and stainless steel rebars. GFRP rebars is a possible stirrups option and stainless steel rebars is a viable stirrup option to make the entire prestressed member corrosion resistant.

All stainless steel rebars used in this study were manufactured by North American Stainless. Duplex stainless steel rebars Grade 75 were chosen for this study because of their high strength and corrosion resistance compared to other stainless steel types. Three different sizes, No. 3, No. 4 and No. 5 were used as confinement and shear reinforcement. The mechanical properties, provided by the manufacturer, of all sizes are given in Table 4-3. The stress-strain relationship of the stainless steel rebars is different than that of carbon steel rebars (Medina et al. 2015). The stainless steel rebars show no clear yield strength and therefore the 0.2% yield method is recommended to be used to define the yield strength (Dundu 2018). All stainless steel rebar sizes used in this study had stress at 0.2% yield higher than the classified stress, 75 ksi. The No. 4 bars were used as transverse reinforcement (stirrups). The No. 4 bars have a yield and ultimate strength of 83.39 ksi and 119.84 ksi, respectively. The modulus of elasticity of the bars is reported to be slightly less than that of carbon steel bars (Gedge 2008). The heat treatment condition for all stainless steel bars used in this study was hot rolled, pickled and passivated. The hot-rolled condition improves the ductility performance of the rebars (Gedge 2008).

Table 4-3 Mechanical characteristics of stainless steel bars

Size	Diameter (in.)	Area (in ²)	Yield stress (0.2%) (ksi)	Ultimate tensile strength (ksi)	Ultimate strain (in./in.)
No. 3	0.375	0.11	92.25	125.04	0.2028
No. 4	0.5	0.20	83.39	119.84	0.2646
No. 5	0.625	0.31	87.86	120.55	0.2479

Chemical analyses of the stainless steel rebars, provided by the manufacturer, were performed according to ASTM A751 (2014). Table 4-4 shows the chemical composition of the stainless steel rebars used in this study. The chemical composition of stainless steel rebars conforms to requirements of ASTM A955 (2017). Stainless steel rebars used in this study satisfied FDOT Specification 931 requirements.

Table 4-4 Chemical composition of stainless steel bars

Bar size	C	CO	CR	CU	MN	MO	N	NI	P	S	SI
No. 3	0.013	0.09	22.57	0.32	1.64	0.180	0.161	4.03	0.030	0.0006	0.46
No. 4	0.018	0.09	22.55	0.32	1.78	0.206	0.150	4.41	0.034	0.0007	0.58
No. 5	0.018	0.11	22.50	0.26	1.70	0.172	0.143	4.19	0.031	0.0013	0.55

GFRP bars have a linear stress-strain relationship up to failure, i.e., no yield point or strain hardening exist. Table 4-5 shows average mechanical properties, provided by the manufacturer, of six samples of No. 4 and No. 5 GFRP bars. Tensile tests were done according to ASTM D7205 (2011). The average ultimate tensile strength of No. 4 and No. 5 bars was 131.4 ksi and 132.3 ksi with a standard deviation of 4.3 ksi and 3.2 ksi, respectively. The average ultimate strain of No. 4 and No. 5 bars was 0.0187 and 0.0172 with a standard deviation of 0.0006 and 0.0005, respectively. GFRP rebars are light (approximately 20 to 25% the density of steel) and have high tensile strength (around double steel's yield strength). Yet, the ultimate strain of GFRP bars is very low compared to that of carbon steel rebars. In general, FRP rebars are stronger along the longitudinal direction than transverse because they are made from an anisotropic material. The transverse shear strength of No. 4 and No. 5 rebars was 6.45 ksi and 7.53 ksi, respectively. The transverse shear test was done according to ASTM D7617 (2011). The fiber content of No. 4 and No. 5 bars was 75.34% and 77.79% by weight, respectively. For both sizes, silica sand is applied to the surface during manufacturing to enhance bond performance between the bars and surrounding concrete, and the spacing of the wrap was between 0.75 and 1 in. The manufacturer did not provide mechanical properties for the No. 3 GFRP rebars.

Table 4-5 Mechanical properties of GFRP bars

Size	Diameter (in.)	Area (in ²)	Tensile strength (ksi)	Ultimate strain (in./in.)	Modulus of elasticity (ksi)
No. 4	0.5257	0.2170	131.4	0.0187	7042.6
No. 5	0.6250	0.3068	132.3	0.0172	7686.4

4.2.4.3 Concrete

Two different concrete strengths were used for the girder and deck slab. A self-consolidating concrete (SCC) was used for the girder with a specified compressive strength of 10 ksi, while the deck slab was cast with normal-weight concrete with a specified compressive strength of 6.5 ksi. Multiple concrete cylinders were taken from each concrete batch. On average,

three concrete cylinders were tested in compression for each member (girder and slab) on the day of the designated flexural test. Table 4-6 shows the average measured strength for each specimen.

Table 4-6 Concrete compressive strength on testing day of the flexural test of first set of girders

Specimen type	Specimen ID	Girder		Deck slab	
		Compressive strength (psi)	Age (days)	Compressive strength (psi)	Age (days)
Non-composite	Girder A1	10,688	67	-	-
	Girder B3	11,917	94	-	-
	Girder C1	11,128	73	-	-
Composite	Girder A3	10,945	247	8,302	54
	Girder B2	10,367	143	7,801	29
	Girder C2	11,493	175	8,662	42
	Girder C3	11,234	364	6,836	50

4.2.5 Fabrication

All eight 42-ft-long AASHTO Type II girders were constructed by a precaster, Dura-Stress, Inc., in Leesburg, FL. A fabrication check list, provided by Dura-Stress, is included in Appendix B. The specimens were built in two beds as shown in Figure 4-2. For clarity, only longitudinal prestressing is included in Figure 4-2.

4.2.5.1 At casting yard

Fabrication activities for both casting beds are presented in Table 4-7. First, strands were run in the casting beds, Figure 4-3, and then they were tensioned. The specified tension force was 43.9 kips and 37.2 kips, which were 75% and 62.2% of ultimate strength, for carbon steel and HSSS strands, respectively. A hydraulic jack was used to tension strands, and regular chucks were used to grip them. During strand tensioning, the prestressing force was monitored with an electronic cell as shown in Figure 4-4. Once the target prestressing force was reached, the strand was seated in the wedge as shown in Figure 4-5. Afterward, an elongation measurement was taken at the live end to verify the applied prestressing force.

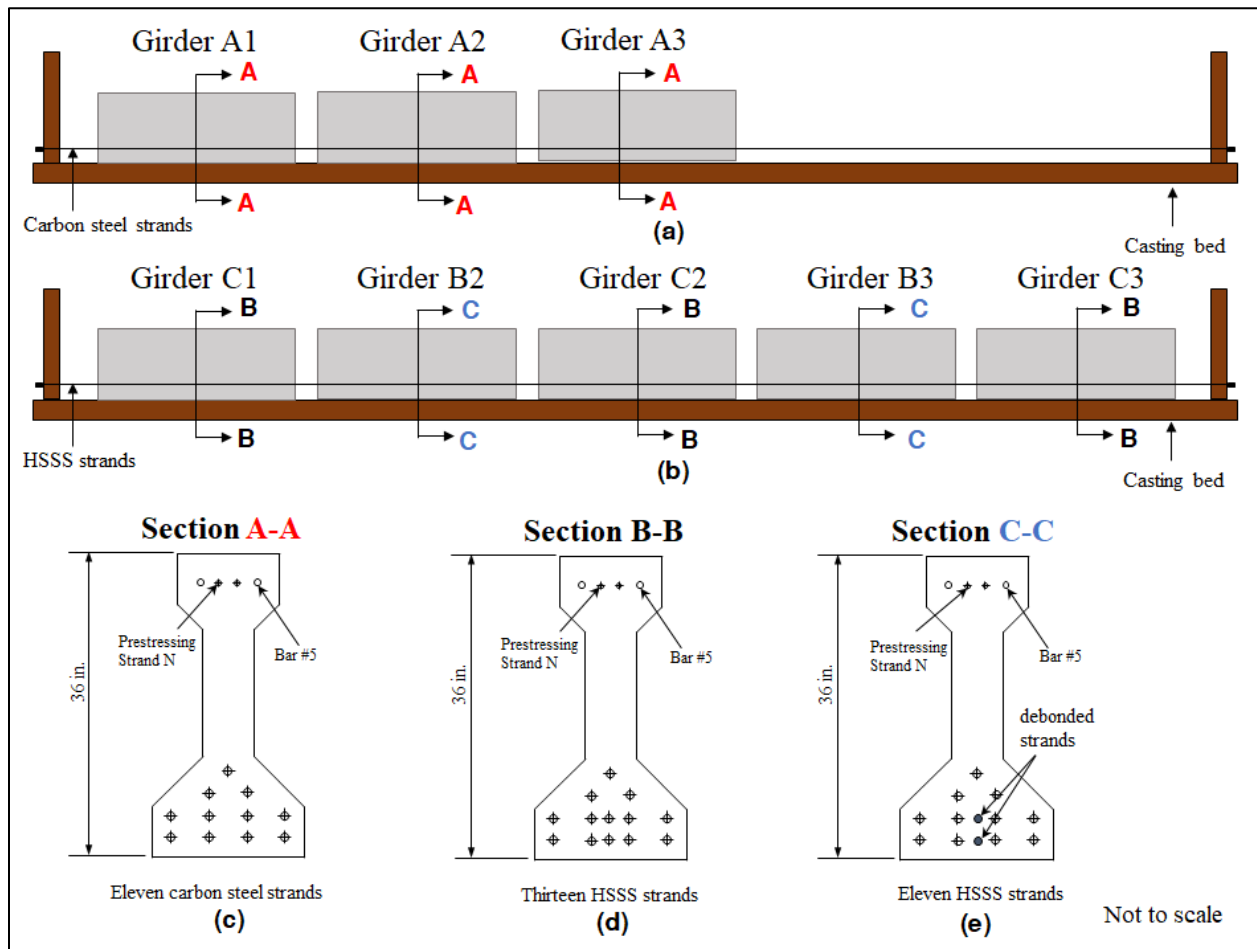


Figure 4-2 Casting bed layout for first set of girders.

(a) Position of carbon steel girders in the casting bed; (b) Position of HSSS girders in the casting bed; (c) midspan cross section for specimens with 11 carbon steel strands; (d) midspan cross section for specimens with 13 HSSS strands; and (e) midspan cross section for specimens with 11 HSSS strands.

The three carbon steel girders were cast separately in a casting bed as shown in Figure 4-2a. Midspan section for specimens with 11 fully bonded carbon steel strands is shown in Figure 4-2c. The other five girders prestressed with HSSS strands were cast in another casting bed as shown in Figure 4-2b. Two HSSS strands in Girder B2 and Girder B3 were debonded for the whole length of the girders as shown in Figure 4-6. Girder B2 and Girder B3 were placed between the girders with fully bonded strands, as shown in Figure 4-2b, to prevent slippage of debonded strands during detensioning. Figure 4-2d and Figure 4-2e present midspan section for specimens with 13 fully bonded strands and for specimens with two debonded strands, respectively.

Table 4-7 Fabrication activities schedules for first set of girders

Carbon steel strands casting bed		HSSS strands casting bed	
Date	Activity	Date	Activity
9/10/2018	Run cables, tension cables and tie reinforcement.	9/17/2018	Run cables, tension cables, tie reinforcement and set side forms.
9/11/2018	Finish instrumenting internal gages and set side forms.	9/18/2018	Cast concrete.
9/12/2018	Cast concrete.	9/19/2018	Remove forms and instrument external DEMEC points and strain gages.
9/13/2018	Remove forms and instrument external DEMEC points and strain gages.	9/20/2018	Release strands and collect data.
9/14/2018	Release strands and collect data.		



Figure 4-3 Running cables in the bed



Figure 4-4 Monitoring applied force on electronic cell



Figure 4-5 Seated stainless strands in the chucks



Figure 4-6 Shielding two strands in Girder B2

After tensioning the strands, the stirrups and confinement reinforcement were tied, as shown in Figure 4-7 and Figure 4-8. The lifting loops were placed at 38 in. from the face of the girder and consisted of four strands as shown in Figure 4-9. Although lifting loops may provide additional interface shear resistance at the end regions during shear tests, they are not considered in design.



Figure 4-7 Stainless steel confinement reinforcement



Figure 4-8 Tying stainless steel stirrups



Figure 4-9 Lifting loop

After tying all the reinforcements, side forms were set. Before casting concrete, several tests were performed on the concrete mixes such as: slump, air content, water-to-cement ratio and penetration. Concrete slump and air content tests are shown in Figure 4-10 and Figure 4-11, respectively.

Table 4-8 provides concrete mix design limits for normal-weight concretes. All concrete batches satisfied the specified mix design requirements as shown in Table 4-8. After confirming that the concrete batch satisfied the specified mix design requirements, the concrete was placed in the bed. Figure 4-12 shows concrete casting for the girders with HSSS strands. Several concrete cylinders were taken from each batch, Figure 4-13. Those cylinders were used to measure concrete strength at 28 days and on the days of flexural and shear tests. The forms were removed the next day, as shown in Figure 4-14. Ideally, strands should be released within 24 hours after casting to match industry practice. However, one day was allocated for instrumentation. Therefore, the strands were released two days after casting concrete. Figure 4-15 shows HSSS strands being cut.



Figure 4-10 Concrete slump test



Figure 4-11 Concrete air content test

Table 4-8 Concrete test results

Bed designation	Truck number	Slump (in.)	Air %	W/C	Penetration (mm)
	Design limit	24.5 - 29.5	0 - 6	≤ 0.29	25
Carbon steel strands casting bed	Truck 1	24.5/24.5	4.7	0.27	1
	Truck 2	26.5/26	3.1	0.28	2
	Truck 3	29/28	2.2	0.28	5
HSSS strands casting bed	Truck 1	28/28	5.0	0.28	2
	Truck 2	29/29	4.0	0.28	1
	Truck 3	27/27	2.0	0.28	3



Figure 4-12 Casting concrete



Figure 4-13 Concrete cylinders

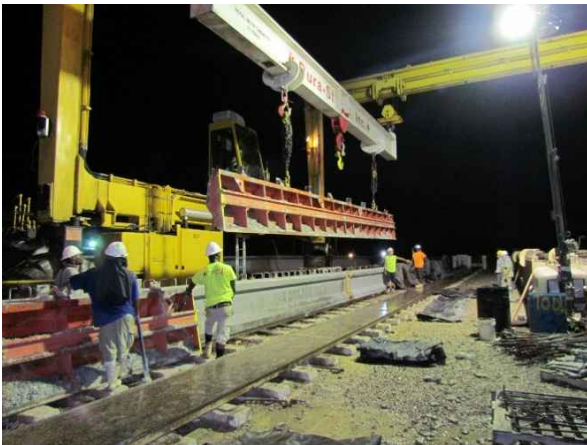


Figure 4-14 Removing side forms



Figure 4-15 Releasing stainless steel strands using flame

The orientation of the girders in the beds is illustrated in Figure 4-16. The strands were cut in the following sequence: first, at the external ends of the external girders, simultaneously; second, at the internal ends of the external girders; and third, between internal ends of the internal girders. The strands were cut starting from the bottom layer and moving upward as shown in Figure 4-16. The strand release sequence and procedure in this study represents common industry practice for AASHTO Type II girders. During cutting of the penultimate HSSS strand at one of the external ends (strand number 12 in Figure 4-16), the last HSSS strand fractured (strand number 13 in Figure 4-16). Figure 4-17 shows the fractured strands. The strand broke at the chuck device. Figure 4-18 shows the notching effect of the grips on the fractured strand. Two factors may have contributed to this incident. First, as each strand is cut, elastic shortening of the beam causes additional tension in the remaining uncut strands, between the end of the girder and the abutment. The last strand to be cut experiences the most accumulation of these tensile stresses. Because an HSSS strand has

low ductility, it reached its ultimate strain and broke. A second factor that may have contributed to the breakage is the deviation of the strand. The end abutments in the casting bed used for the girders prestressed with HSSS strands had only three layers, while the girders were designed with four layers of strands. Therefore, one strand, number 13 in Figure 4-16, had to be deviated from the girder ends to the abutments. Changing the orientation of the strand creates force concentration from the grips on one side of the strand.

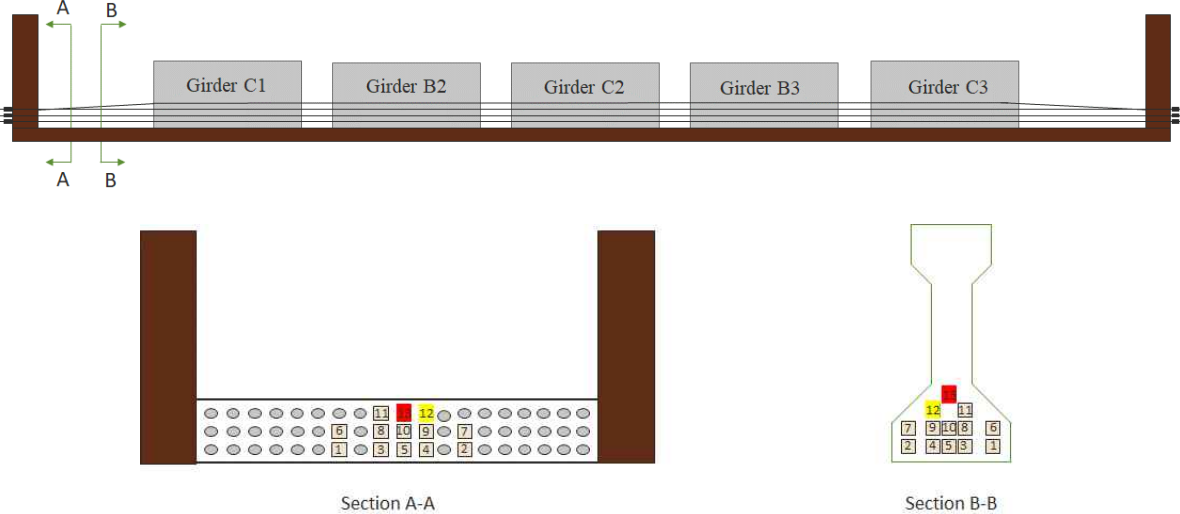


Figure 4-16 Strand detensioning sequence (not to scale)



Figure 4-17 Bed end after breakage of the HSSS strand



Figure 4-18 Notching effect of grips on fractured HSSS strands

Due to impact force from the strand failure, the external girder, Girder C1, moved approximately 2 in., and internal spacings between the girders were reduced. Based on this incident, it is recommended that HSSS strands not be deviated until further studies can be done to establish tolerance to kinks or deviations. Special attention shall be taken while cutting HSSS strands. Other than the isolated incident failure, it was demonstrated that concrete girders prestressed with HSSS strands can be constructed using the same apparatuses and procedures that are used for concrete girders prestressed with carbon steel strands.

4.2.5.2 At FDOT lab

All girders were transported to the FDOT SRC in Tallahassee, FL. At the FDOT lab, a deck slab was cast onto the six girders after testing Girders A1, B3, and C1 and determining that a deck slab was needed. Note that Girder B3 was initially tested in flexure as a non-composite section and it was unloaded before failure to be saved for future shear tests. The deck slab had an 8-in. thickness and a 24-in. width, and the haunch thickness was 2 in. Note that the concrete surface was smooth at the interface region between the girder and deck slab. Fabrication of deck slab started by setting the forms. Then, reinforcement was placed as shown in Figure 4-19. Normal-weight concrete with a specified compressive strength of 6.5 ksi was used for the deck-slab. The concrete was received from a local plant. Before placing concrete in the forms, a slump test was performed.

After confirming that the concrete batch satisfied the specified mix design requirements, the concrete was placed in the bed. Figure 4-20 shows the specimen after casting the deck slab. Note that the deck slab was covered with plastic sheets after casting. Table 4-9 provides the casting dates for both girder and deck-slab.



Figure 4-19 Girder before casting deck slab



Figure 4-20 Girder after casting deck slab

Table 4-9 Casting date of composite girders of first set of girders

Girder designation	Girder	Deck-slab
A1	9/12/2018	-
A2	9/12/2018	4/26/2019
A3	9/12/2018	3/22/2019
B2	9/18/2018	1/10/2019
B3	9/18/2018	6/17/2019
C1	9/18/2018	-
C2	9/18/2018	1/29/2019
C3	9/18/2018	7/29/2019

4.3 Second set of girders

4.3.1 Design of girders

A bridge prototype including pretensioned precast AASHTO Type II girders and cast-in-place deck slab was used to design the five girders in this study, Figure 4-21. The bridge consisted of simply-supported girders spaced at 6 ft on center that spanned 40 ft. The specified concrete compressive strength was 8.5 ksi and 4.5 ksi for the girder and deck slab, respectively. The guaranteed mechanical properties of the HSSS strands, specified by ASTM A1114, were used in

the design. The girders were designed according to AASHTO LRFD Bridge Design Specifications (2017). The design steps of an interior girder were as follows. First, maximum dead and live loads moments were calculated, Table 4-10. The dead load moments included effects from the weight of the girder, deck slab, forms, barrier, and future wearing surface. The live load moments were due to HL-93 loading (truck load and lane load). Based on AASHTO LRFD, the distribution factor for the moment was equal to 0.616 (2017). The impact factor was equal to 1.33. Second, the flexural demand on the interior girder was calculated based on the Strength I load combinations; the required number of HSSS strands was calculated accordingly. Third, the minimum reinforcement requirements were checked, and the number of HSSS strands was increased as needed. Last, the tensile and compressive stress requirements for Service I and Service III limit states were checked to be within the specified limits. The service moment for deflection control was 701.3 kip-ft with 262.4 and 438.9 due to dead and live loads, respectively. The ultimate moment for strength design was 1100.6 kip-ft. The design of an interior girder was governed by the minimum reinforcement requirements, which was 1470.3 kip-ft. The total required number of 0.6-in.-diameter HSSS strands was 11. The girder was designed to fail by rupturing of strands at ultimate load. Because the failure mode was rupture of strands, which is considered a brittle failure, a resistance factor of 0.75 was used.

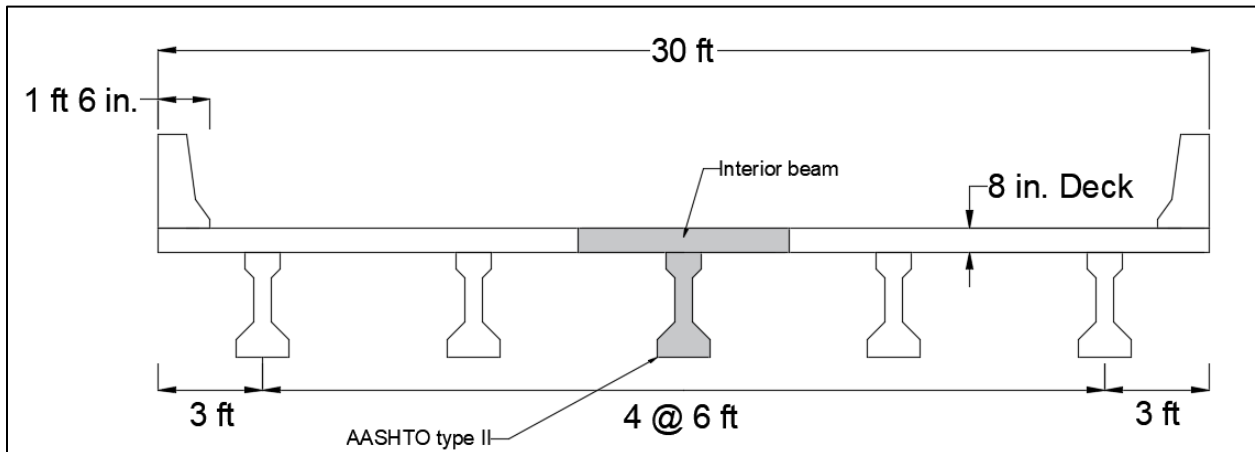


Figure 4-21 Bridge prototype

Table 4-10 Interior girder moments at midspan

Dead load (kip-ft)		Live load (kip-ft)				
Non-composite		Composite			Composite	
Beam	Slab	Forms	Barrier	Wearing	Truck load	Lane load
76.9	127.5	20.0	20.0	18.0	360.1	78.8

In this study, the cross section of the designed bridge interior girder (Figure 4-22) was modified so that it could be tested in the lab. The deck slab width was reduced from 6 ft to 2 ft. Decreasing the deck slab width reduced the ultimate capacity of the section, but the failure mode was still rupture of the strands. Figure 4-23 shows a cross section of modified interior girder. For all specimens in this study, all stress limits according to the AASHTO LRFD specifications were checked. The stresses were calculated along the length of the girder and at two stages: at the time of prestressing release, and at the time of deck slab placement.

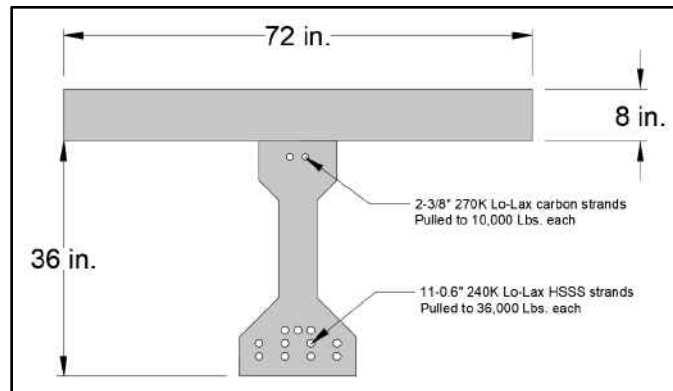


Figure 4-22 Cross section of an interior girder

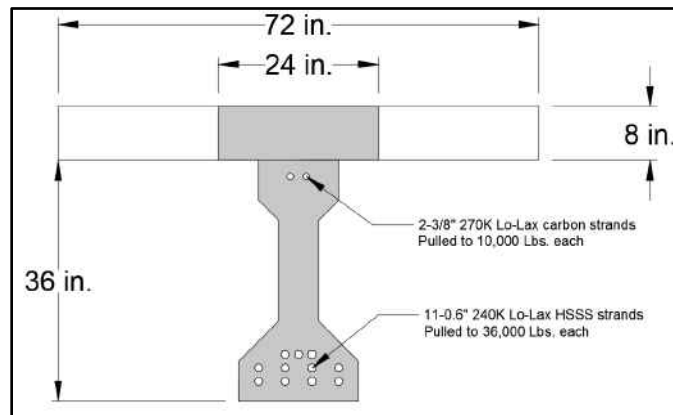


Figure 4-23 Cross section of modified interior girder (specimens in this study)

All girders were designed to resist shear and fail in flexure. Carbon steel reinforcement was used for transverse reinforcement. Figure 4-24 presents the transverse reinforcement layout. Shear reinforcement (5K bars), confinement reinforcement (3D bars), and splitting reinforcement (5Z bars), all shown in Figure 4-24, were designed based on the AASHTO LRFD Bridge Design Specifications. Shear reinforcement was designed based on the mechanical properties of carbon steel rebar. The same reinforcement details and spacing were used in all the girders. The shear reinforcement (5K bars) and the splitting reinforcement (5Z bars) have 90-degree hooks at the

bottom and top. Both the 5K and 5Z bars were bundled when spaced together, and the direction of the 90-degree hook bars was alternated. 5Z bars were within the girder, and the 5K bars extended out of the top of the girder to provide interface shear resistance between the girder and deck slab. The use of 5Z bars was limited to regions in which bursting and spalling stresses were of concern. The first shear reinforcement (5K bars) was placed at 2 in. on center from the end face of the girder.

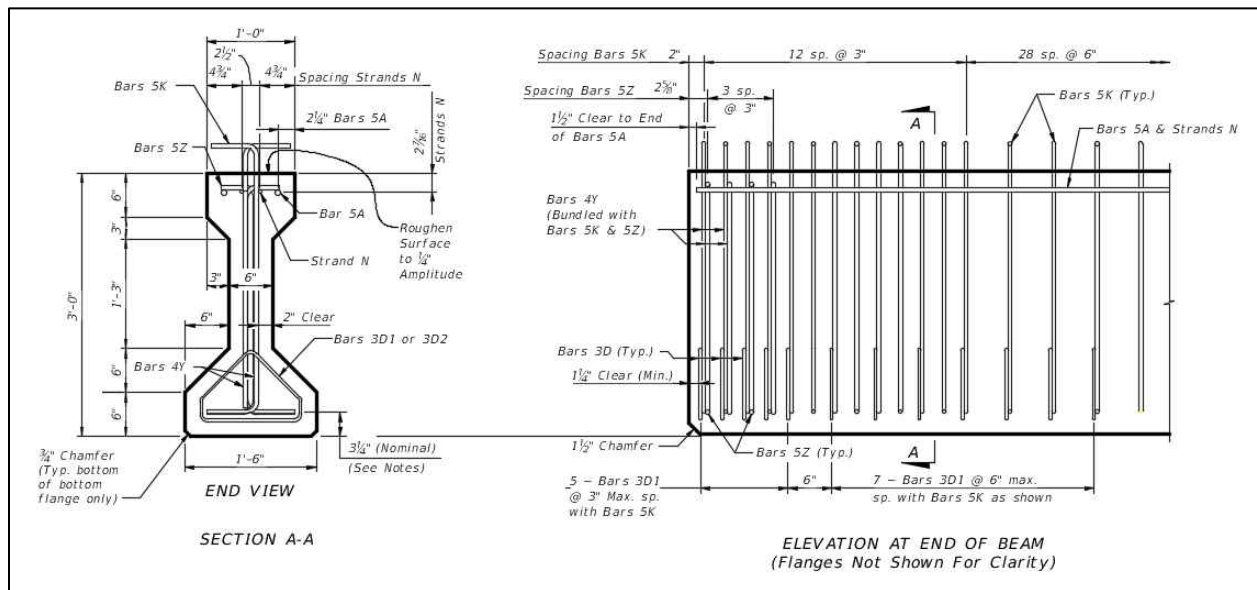


Figure 4-24 Reinforcement layout for second set of girders

4.3.2 Design matrix

A total of five 42-ft-long AASHTO Type II girders were designed and were divided into three groups. The first group consisted of two identical girders, Girder E1 and Girder E2. Each girder had 11 0.6-in.-diameter HSSS strands. The second group also consisted of two identical girders, Girder E3 and Girder E4. Each girder had nine 0.6-in.-diameter HSSS strands. The third group consisted of one girder, Girder E5, which had seven 0.6-in.-diameter HSSS strands.

4.3.3 Materials

4.3.3.1 Prestressing strands

HSSS strands from two spools (spool no.1 and spool no.2) were used to fabricate the specimens. See Section 3.4 for details regarding the stress-strain equations for the two HSSS spools.

4.3.3.2 Reinforcing rebars

Carbon steel reinforcement was used for transverse reinforcement. Three different sizes, No. 3, No. 4 and No. 5 were used as confinement and shear reinforcement.

4.3.3.3 Concrete

The specified concrete compressive strength was 8.5 ksi for the girder and 4.5 ksi for the deck slab. Self-consolidating concrete (SCC) was used for girders, while conventional concrete (CC) was used for deck slabs. Table 4-11 shows the concrete mixture design for both girder and deck slab.

Table 4-11 Concrete mixture proportions for second set of girders

Material	Units	Quantity	
		SCC (girder)	CC (deck slab)
Type II cement	lb/yd ³	735	490
Fly ash (Type F)	lb/yd ³	165	122
Crushed stone #67	lb/yd ³	1308	1765
Sand	lb/yd ³	1264	1385
Water	lb/yd ³	250	268
Water-cement ratio	-	0.340	0.547
Air entraining admixture	DAREX	oz/yd ³	1
	MB AE90		-
Set retardant admixture	DELVO	oz/yd ³	54
Water-reducing admixture	ZYLA 610	oz/yd ³	18
	ADVA 600		54
	Glenium 7920		-
			27.54

The average measured concrete compressive strengths, which are given in Table 4-12, were higher than the specified strengths. On average, three cylinders for each component (girder and slab) were tested in compression on the day of testing. However, no cylinders were tested for the deck slab on the day of testing Girders E3 and E4. A total of six cylinders from the deck slab were tested on the day of testing Girder E5. The deck slabs for Girders E3, E4, and E5 were cast using the same concrete mix from one mixing truck batch.

4.3.4 Fabrication

Five 42-ft-long AASHTO Type II girders were constructed in one bed as shown in Figure 4-25. Figure 4-26 shows the two HSSS spools used in this study as well as three other carbon steel spools at the casting yard. The surface of HSSS strands does not tend to rust as carbon steel strands do as shown in Figure 4-26. The fabrication of the girders began by placing the HSSS strands in the bed.

Two strands in Girders E3 and E4 and four strands in Girder E5 were shielded for the entire length of the girders. The designated strands were debonded using typical plastic sheathing. The girders with fully-bonded strands were placed at the ends of the bed, Figure 4-25. Then the strands were tensioned using a hydraulic jack. Regular chucks were used, and an electronic cell was used to monitor the prestressing force. Pretension was obtained by applying 36 kips to each strand, which was 65% and 62% of the ultimate strength for the bottom layer of strands (spool no. 1) and for the other two layers (spool no. 2), respectively.

Table 4-12 Concrete compressive strength on testing day of flexural tests of second set of girders

Specimen ID	Compressive strength (psi)	
	Girder	Deck slab
Girder E1	10,061	6,441
Girder E2	10,845	6,760
Girder E3	10,492	7,442
Girder E4	11,054	
Girder E5	10,710	

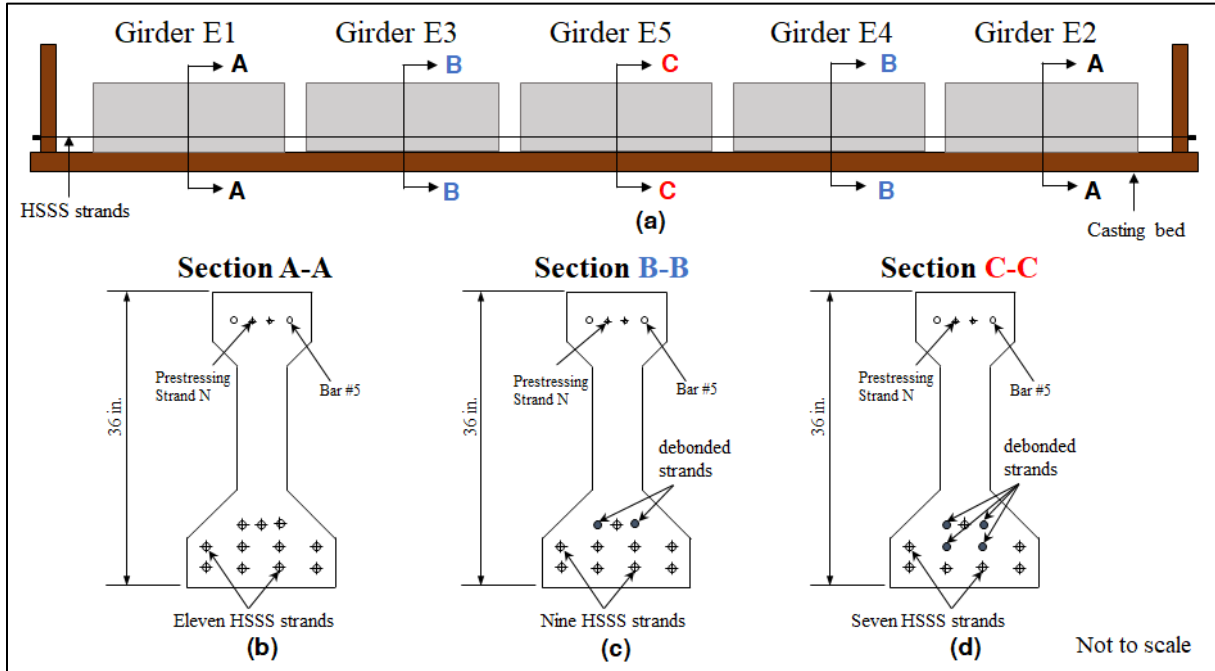


Figure 4-25 Casting bed layout for second set of girders. a) Position of girders in the casting bed; (b) midspan cross section for specimens with 11 HSSS strands; (c) midspan cross section for specimens with nine HSSS strands; (d) midspan cross section for specimens with seven HSSS strands.



Figure 4-26 Stainless steel and carbon steel spools

Then, transverse reinforcement was installed, and the forms were placed. Before placing concrete in the bed, several tests were performed on the concrete mixes such as: slump, air content, water-to-cement ratio, and penetration. After confirming that the concrete batch satisfied the specified mix design requirements, the concrete was cast. The forms were removed one day after casting. After the concrete reached the specified release strength, which was two days after casting, the HSSS strands were released using the flame cutting method. The strands were cut starting from the outer ends of the bed and moving toward the center of the bed. The HSSS strands were found twisted at the cut ends, as shown in Figure 4-27, after release. The deck slab for Girders E1 and E3 was cast on the day of the releasing prestressing strands. The deck slab for Girders E2, E4 and E5 was cast five days after release.



Figure 4-27 Twist of HSSS strands after cut

CHAPTER 5 TRANSFER LENGTH

5.1 Introduction

In pretensioned concrete members, transfer length is defined as the distance required for the strand to transfer all effective force to the surrounding concrete. It is assumed that the prestressing force is linearly distributed along the transfer length. Therefore, prediction of stress distribution at the end of the member depends on transfer length. The transfer length is important in evaluating anchorage zone stresses, shear capacity, and preventing bond slip failure. The transfer length relies mainly on bond strength between the strands and concrete. The bond strength of strands is affected by multiple factors such as strand surface condition and concrete type and/or strength. Because chemical composition of HSSS alloys is different than that of carbon steel alloys, the surface condition is also different. Strand surface condition varies with strand type and batches. This difference is attributed to the manufacturing process. Any lubricant residue films left from the manufacturing process can reduce both the chemical adhesion and friction of the strand (Polydorou et al. 2016), which can reduce bond strength, and thereby influence the transfer length of the strand.

Based on the ACI 318-19 design code, transfer length (l_d) can be calculated using Equation 5-1, where f_{se} is the effective prestress in the strand in (ksi), and d_b is the strand diameter in (in.).

$$l_d = \left(\frac{f_{se}}{3000} \right) d_b \quad \text{Equation 5-1}$$

The AASHTO LRFD Bridge Design Specifications equation for transfer length is 60 times the strand diameter ($60d_b$) (2017). However, the transfer length depends on more factors than strand diameter alone. Previous researchers have investigated the effect of various parameters on transfer length, such as size of the strand (Dang et al. 2016; Russell and Burns 1996), type of strand (Grace 2000; Lu et al. 2000; Rambo-Roddenberry et al. 2016), strand spacing (Morcouis et al. 2014; Russell and Burns 1996; Shahawy et al. 1992), effective stress in strand (Oh et al. 2014), strand surface condition (Russell and Burns 1996; Zia and Mostafa 1977), strand release technique (Carroll et al. 2017; Kim et al. 2016; Mitchell et al. 1993; Russell and Burns 1996; Salazar et al. 2018), concrete strength (Carroll et al. 2017; Dang et al. 2016; Kim et al. 2016; Mitchell et al. 1993; Oh et al. 2014; Zia and Mostafa 1977), concrete cover and consolidation around strand (Oh et al. 2014), size of stirrups (Lee 2018), and spacing and length of stirrups (Kim et al. 2016).

Transfer length can be evaluated from the longitudinal strain distribution in the end regions of pretensioned concrete members. As the strands are released, the prestress forces transfer from

the strands to the concrete, causing a compressive force in the end regions, resulting in compressive strains most notably in the bottom flange. The strain distribution is approximately linear up to a point where it converges to a nearly constant plateau, which indicates reaching full stress transfer from the strands to the concrete. Transfer length can be estimated as a distance from the beam end to the convergence point in the strain distribution. Different types of sensing technology can be used to measure the strain distribution. Types of sensing technology used in this research program were electrical strain gages (ERSG), detachable mechanical strain gages (DEMEC), and fiber optic sensors (FOS).

(Paul et al. 2017b) conducted experimental work measuring transfer and development lengths of 0.5-in.-diameter HSSS strands in prestressed concrete piles. Recently, HSSS strands became available in a new larger size, 0.6-in.-diameter. One of the objectives of this research was to experimentally measure the transfer length of 0.6-in.-diameter HSSS strands and compare it with prediction equations available in the literature.

This chapter reports transfer length results that were obtained experimentally. The first set is described in Section 5.2 and the second set in Section 5.3.

5.2 First set of girders

5.2.1 Preparation of specimens

Running and tensioning the strands in the casting bed as well as layout of the girders in the casting beds are all described in Section 4.2.5. After tensioning the strands, confinement and stirrup reinforcement were tied. To study the effect of confinement reinforcement on transfer length, three different types of internal reinforcing bars were used. They were carbon steel, GFRP, and stainless steel. Each end of each girder had different confinement and vertical detailing, resulting in 16 unique ends as shown in Table 5-1. Figure 4-1 illustrates the confinement and vertical reinforcement detailing. See Section 4.2 for more information regarding first set of the girders.

Several concrete cylinders were cast from the concrete batches used to cast the girders. Ideally, strands should be released once the concrete strength reaches 80%, or 8 ksi for this case, of the specified concrete strength (2020). After one day, girders with carbon steel strands achieved the required release concrete strength while girders with HSSS strands achieved 93% of the required release strength. One day was allocated for installing external instrumentations. The strands were released two days after casting concrete without breaking any cylinders. Dura-Stress's materials

lab tested two cylinders in compression at one day and six days of age, and three at 28 days after casting. Results of the average compressive strength of the concrete cylinders are shown in Table 5-2. The specified concrete compressive strength of concrete was achieved after six days of casting. The average 28-day concrete compressive strengths were 11.94 ksi and 11.45 ksi, approximately equal, for girders prestressed with HSSS and carbon steel strands, respectively.

Table 5-1 Test matrix for transfer length

Bed Designation	Girder Designation	No. of strands	Strand type	End region reinforcement	End region spacing	
					End	Spacing
Carbon steel strands casting bed	A1	11	carbon steel	carbon steel	End 11	Wide
					End 12	Narrow
	A2	11	carbon steel	GFRP	End 13	Wide
					End 14	Narrow
	A3	11	carbon steel	stainless steel	End 15	Wide
					End 16	Narrow
HSSS strands casting bed	C1	13	HSSS	carbon steel	End 2	Narrow
					End 1	Wide
	B2	11	HSSS	GFRP	End 8	Narrow
					End 7	Wide
	C2	13	HSSS	GFRP	End 4	Narrow
					End 3	Wide
	B3	11	HSSS	stainless steel	End 10	Narrow
					End 9	Wide
	C3	13	HSSS	stainless steel	End 6	Narrow
					End 5	Wide

Table 5-2 Concrete compressive strength for first set of girders

Time (days)	Concrete compressive strength (ksi)	
	Girders with carbon steel strands	Girders with HSSS strands
1	6.32	8.97
6	10.02	10.89
28	11.94	11.45

5.2.2 Method of prestress release

The strands release method has a significant effect on the transfer length. Strands can be released by methods such as gradual release or sudden release. For the gradual release method, all strands are released gradually at the end of bed, whereas strands are cut individually by flame in the sudden release method. The sudden release method is more often used by fabricators. Sudden release of a strand induces a dynamic impact, which causes a significant force in the anchorage zone region, resulting in a longer transfer length compared to that obtained using the gradual release method. It was reported that sudden release of strands results in approximately 20% longer transfer length than gradual release of strands (Kaar et al. 1963). The gradual release method does not induce a dynamic force on the member's end.

In this research, all strands were released by flame cutting. All prestressing force transferred to the surrounding concrete in all girders in the casting bed after cutting the strands at the external ends of the external girders. Therefore, the strands at the external ends were released using sudden release method while the strands at all other ends (internal ends of the girders) were released using gradual release method. The orientation of the girders in the beds is illustrated in Figure 5-1. More information about the strand release sequence can be found in Section 4.2.5.1.

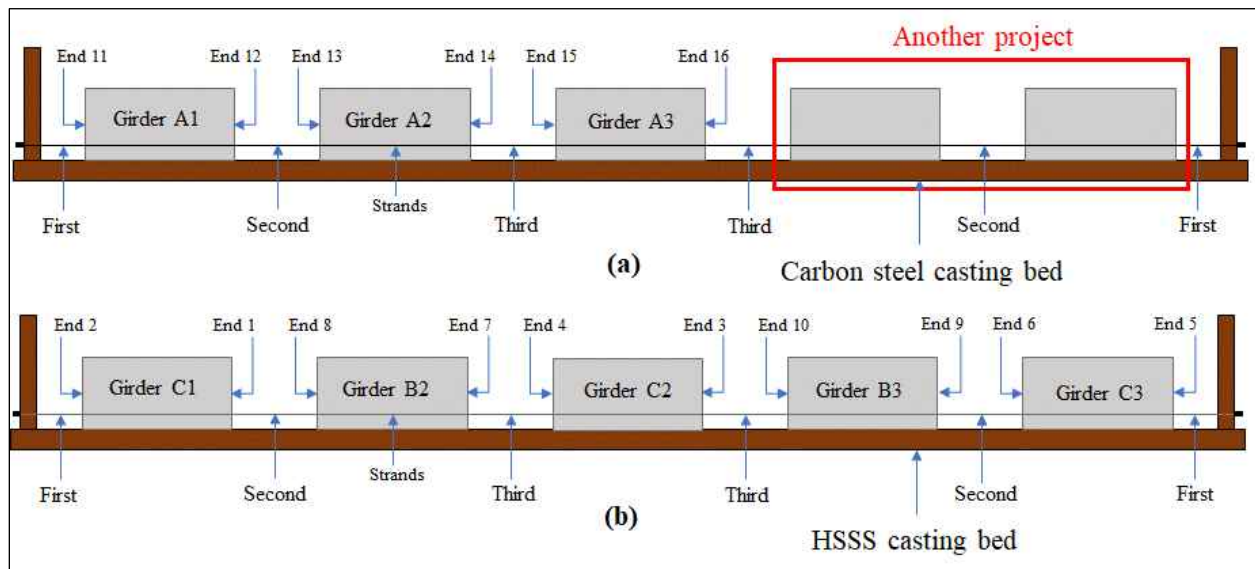


Figure 5-1 Casting bed layout and detensioning sequence for first set of girders. a) girders with carbon steel strands; and (b) girders with HSSS strands

5.2.3 Instrumentation

Transfer length can be determined from strand and/or concrete strains. Strain gages installed on strands provide a more precise strain profile than strain gages attached to a concrete surface (Salazar et al. 2018). However, they require more effort and are susceptible to damage during concrete placement. Also, a single strand strain profile, not all strands, is usually used to estimate transfer length which does not represent the full behavior of all strands. (Lee 2018) reported that transfer lengths calculated from strain gages attached to strands were slightly longer than the transfer lengths calculated from strain gages attached to the surface of concrete. However, (Lee 2018) found that both strand and concrete strain profiles were in a good agreement.

Because external strain gages attached to concrete have been proven to give realistic and similar strain profiles as gages attached to strands (Park et al. 2012), it was preferred in this study to determine transfer length using concrete strains. Two types of gages were used: electrical resistance strain gage (ERSG) and detachable mechanical strain gages (DEMEC). All eight girders were equipped with ERSGs and DEMEC points except for Girders B2 and B3, which were not instrumented with ERSGs due to limited available installation time.

The ERSG is a reliable and accurate tool to measure strain on surfaces. The ERSG comes in a short length, and this gives it the ability to accurately measure strain change, which provides a better picture for stress distribution in the vicinity of the anchorage zone. The drawbacks of ERSGs are expense and one-time use.

A DEMEC gage (caliper gage) measures change in length between two targets called DEMEC points. The DEMEC gage is the most cost-effective, practical, and most widely-used instrument for measuring transfer length. However, strain readings from DEMEC gages are time consuming and may vary from one operator to another. The precision of the caliper gage used in this work was 10 microstrain. Transfer length is a function of time, and it increases over time. This increase is primarily due to the combined effect of shrinkage and creep of concrete and due to relaxation of the prestressing strand, which takes place in the first few days after stressing (Mitchell et al. 1993; Morcous et al. 2014). The most valuable advantage of the DEMEC gage is its multiple usages, which means it can be used to measure the transfer length over time.

ERSGs and DEMEC points were installed on the concrete surface. ERSGs were installed on one side of the girder, while DEMEC points were installed on the other side of the girder. Both types of the gages were installed on the bottom flange at the level of the centroid of the strands.

Each girder was equipped with 18 2.4-in.-long (60-mm-long) ERSGs and 22 DEMEC points. Figure 5-2 shows the locations of ERSGs and DEMEC points for half of the girder. The ERSGs and DEMEC points were symmetric about the girder's midspan. For ERSGs, the first gage was placed at 2 in. from the girder's end, and the subsequent eight gages were spaced at 5 in. Strain gages were installed as follows: locations for strain gages were determined and marked; those spots were ground and cleaned with acetone; the strain gages were glued on the concrete surface. Strain readings were collected for around one hour after starting the strand detensioning process. The 11 DEMEC points (which, when placed in a row, can be used to measure ten strain readings) were placed along 40 in. at each end of each girder; they were spaced at 4 in. on center, starting at 2 in. from the end of girder. DEMEC points were installed as follows: locations for DEMEC points were determined and marked; marked places were ground to make the concrete surface smooth; those spots were cleaned with acetone; and the DEMEC points were glued to the concrete. A special gage length stick, 4 in. long, was used to reliably space the DEMEC points. Once a DEMEC point was glued to the concrete, another person used the stick to place the next DEMEC point. Reference readings were taken prior to the release of strands. These reference readings are important as they represent the initial lengths between the DEMEC points.

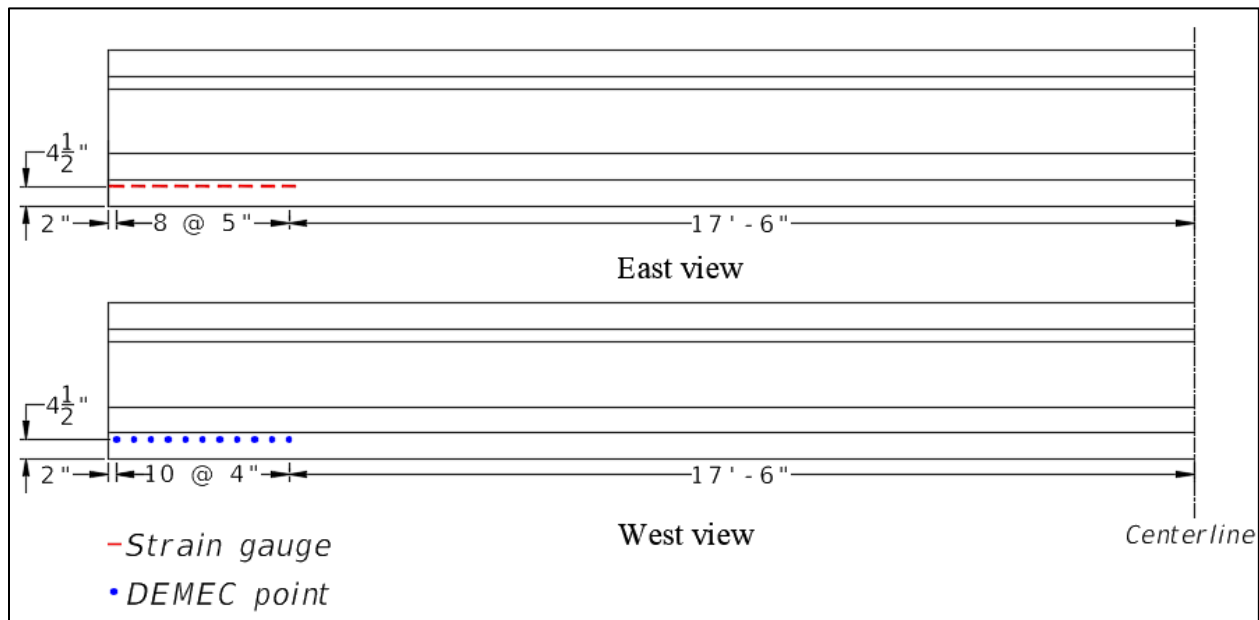


Figure 5-2 ERSGs and DEMEC points locations

5.2.4 Analyzing measured concrete strain

As stated in the previous section, concrete strains were measured using strain gages and DEMEC points. For each strain gage, strain readings were recorded for around an hour. Figure 5-3

shows readings for End 3 of Girder C2; gage S30 was closest to the end of the girder, and the 5-in.-spaced gages were sequentially numbered towards midspan. The concrete strain was calculated as the average of multiple readings once the strain readings reached a constant plateau as shown in Figure 5-3. For each DEMEC strain reading, the average of three strain measurements was calculated. Strain profiles were constructed from the measured concrete strains (strain gages) and average strain readings (DEMEC points), Figure 5-4 and Figure 5-5. The profiles were smoothed by averaging the data over three gage lengths. The smoothing technique is represented by Equation 3-1.

$$(Strain)_i = \frac{(Strain)_{i-1} + (Strain)_i + (Strain)_{i+1}}{3} \quad \text{Equation 5-2}$$

where i-1, i and i+1 represent sequence DEMEC or strain readings.

Technically, transfer length is estimated as the distance from the end of the girder to where the measured concrete strains become constant. Constant concrete strain means that the strands at that end have developed their effective stress. The transfer length was determined by using the smoothed strain profile along with the 95% Average Maximum Strain (AMS) method (Russell and Burns 1993; Russell and Burns 1996). Figure 5-4 illustrates the application of the AMS method to determine the transfer length from the smoothed strain profile of End 3; the points in this plot represent the average strains around 2500 seconds in Figure 5-3. Figure 5-5 shows the transfer lengths from DEMEC readings at End 9 at release, 1 day, 8 days, and 28 days.

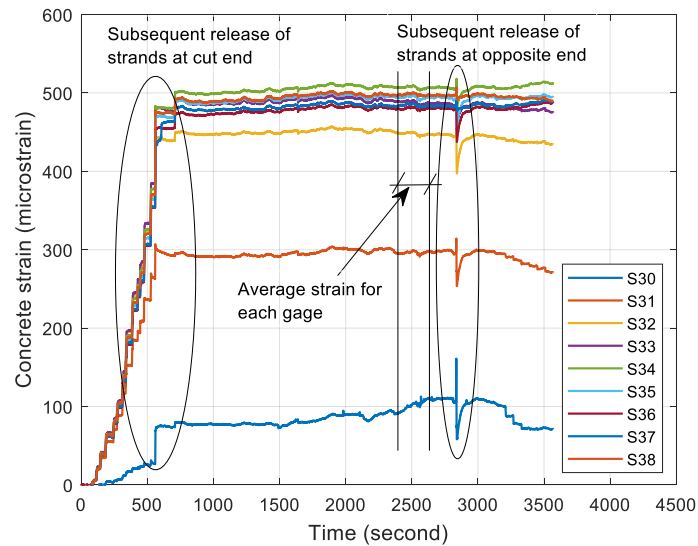


Figure 5-3 Concrete strains measured by strain gages during strands release at end 3

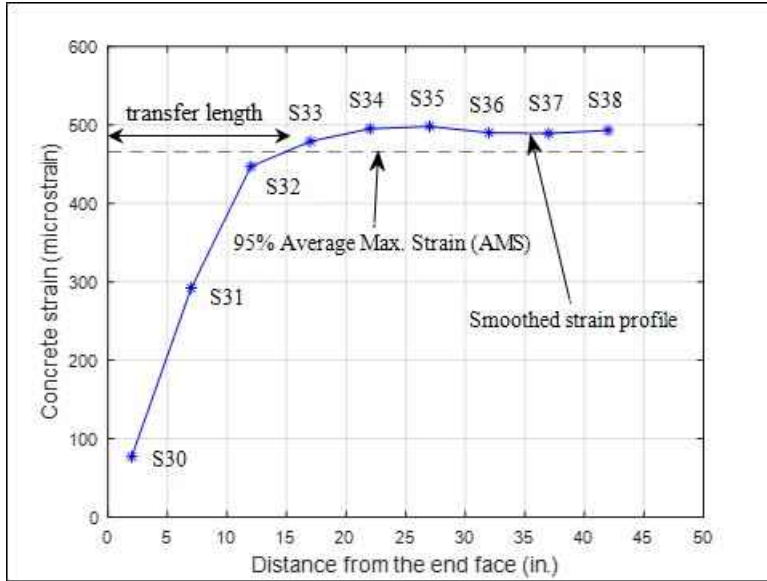


Figure 5-4 Determination of transfer length at End 3 by 95% Average Maximum Strain (AMS) method

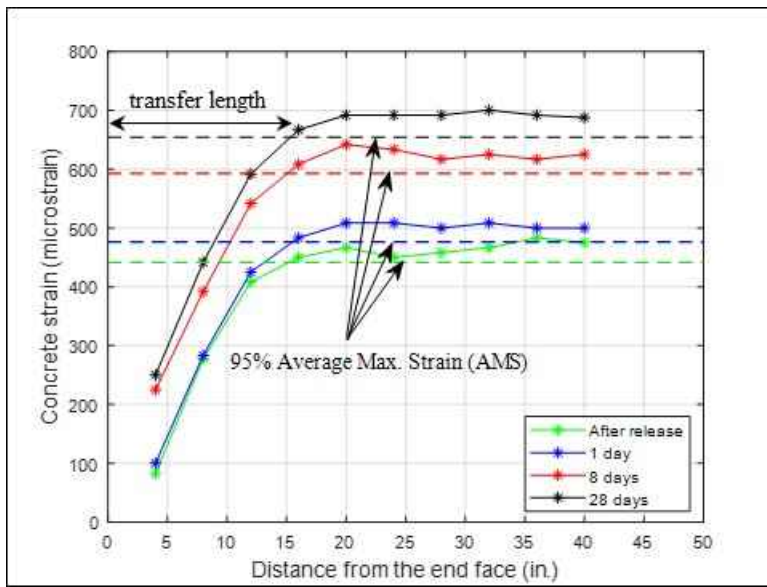


Figure 5-5 Smoothed strain profiles measured by DEMEC points over time at End 9

5.2.5 Results

5.2.5.1 Time effect

Transfer length increases over time, and to monitor this change each girder was equipped with DEMEC points. ERSGs do not hold up well over time and would require continuous monitoring so they were used to monitor the concrete strain during strand release. However, DEMEC points hold up well over time and do not require continuous monitoring. Figure 5-6 shows measured transfer lengths at release using DEMEC and strain gages. Note that Ends 7 through 10 were not

instrumented with ERSGs because of the limited available installation time. The measured transfer lengths at release from the two gage types, ERSGs and DEMEC, were found to be in good agreement, as shown in Figure 5-6. The maximum difference in transfer length between DEMEC and strain gages was approximately 15% at End 3. In some cases, measured transfer length by DEMEC gage was slightly less than the measured transfer length by strain gages, 9% maximum at End 5. Using DEMEC readings, Figure 5-7 and Figure 5-8 show the measured transfer lengths at multiple times for the HSSS and carbon steel strands, respectively.

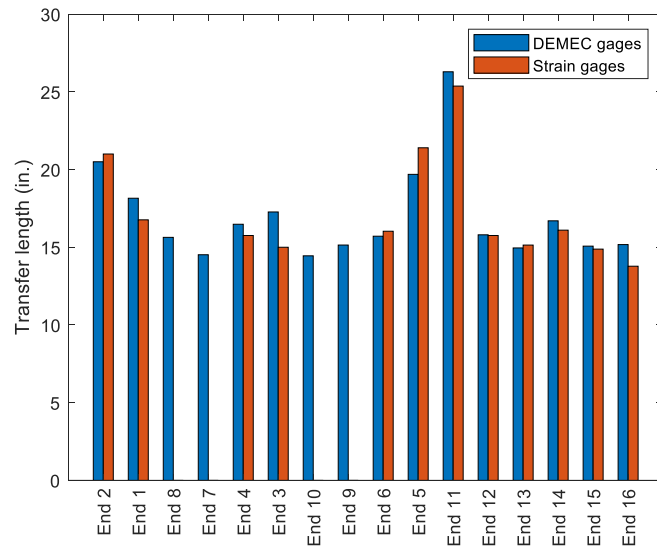


Figure 5-6 Measured transfer length at release by DEMEC and strain gages

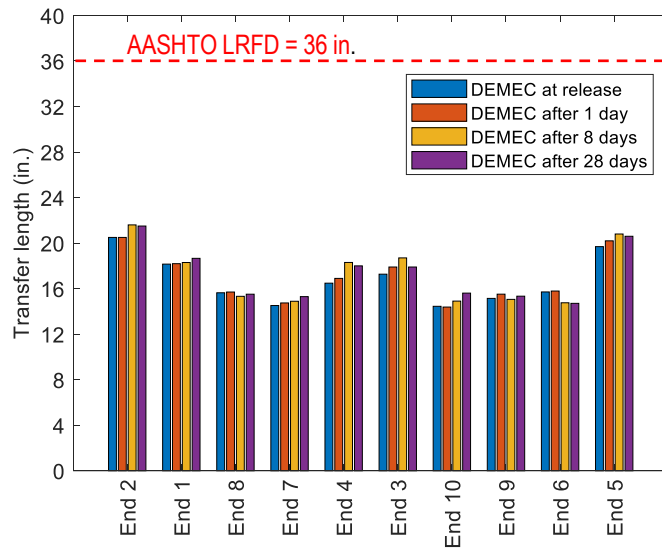


Figure 5-7 Measured transfer length by DEMEC points over time for HSSS strands

Increase in transfer length usually occurs during the first 28 days after release (Barnes et al. 2003; Dang et al. 2016). It was reported that transfer length increases by approximately 10% for the first 28 days after release for full-size members constructed with high-strength concrete (Bruce et al. 1994). In this study, transfer lengths were found to increase 3% on average after 28 days for the HSSS strands, Figure 5-7. The maximum increase in transfer length was approximately 9% in the first 28 days after release. The maximum increase in transfer length for carbon steel strands was approximately 5% in the first 35 days after release. In some cases, transfer length slightly decreased after release. As stated before, one of the disadvantages of the caliper gage is the potential for inconsistency in measuring. However, DEMEC gages are the most cost-effective method to determine transfer length with time. It can be concluded that the measured transfer lengths did not significantly change over time, and this might be due to the high initial concrete compressive strength.

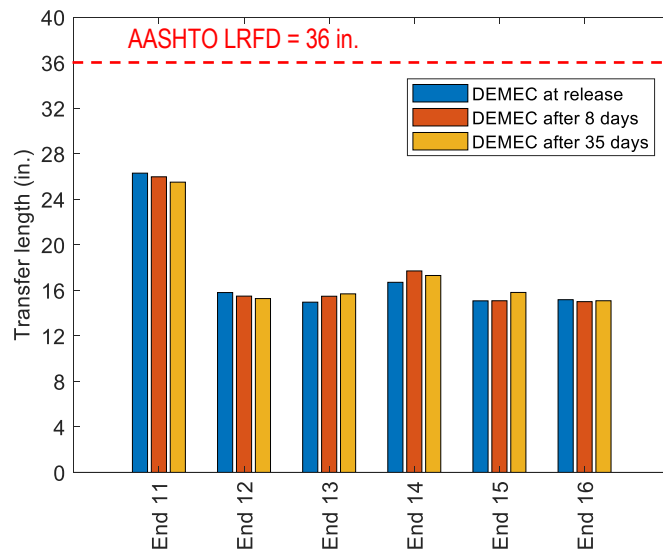


Figure 5-8 Measured transfer length by DEMEC points over time for carbon steel strands

5.2.5.2 Strand release method effect

Many previous researchers have reported that the transfer length is longer at the cut end than at the other end (Kaar et al. 1963; Oh and Kim 2000; Yang et al. 2018). The average percentage increase in transfer length is not consistent among all reported results. Moreover, the gradual prestress release method results in shorter transfer lengths than the sudden release method (Barnes et al. 2003). Effect of sudden release of strands does not only influence small transfer length test specimens but also full-scale members. The effect from sudden release of a single strand in a

concrete prism is different than that of full-size member with multiple strands (Hwan et al. 2006). Multiple strands cause higher dynamic impact force.

In this work, it was found that the cut ends always had longer transfer lengths than the opposite ends as shown in Table 5-3. The measured transfer length for carbon steel strands using ERSGs and DEMEC gages at the first cut end (End 11) was 61% and 66%, respectively, longer than those at the opposite end (End 12). This increase in transfer length is assumed to be mainly because of the impact force. Similar to carbon steel strands, HSSS strands had longer transfer lengths at the first cut ends than at the other ends. The measured transfer length for HSSS strands using ERSGs at End 2 and End 5 (first cut ends) was 25% and 34%, respectively, longer than that at End 1 and End 6 (opposite ends). The measured transfer length for HSSS strands using DEMEC gages at End 2 and End 5 (first cut ends) was 13% and 25%, respectively, longer than that at End 1 and End 6 (opposite ends).

Table 5-3 Transfer length results for HSSS and carbon steel strands

Bed designation	Girder designation	End designation		Transfer length (in.)				
				Strain gages	DEMEC reading			
					At release	At release		8 days
Carbon steel strands casting bed	A1	End 11	1 st cut	25.5	26.3		26.0	25.5
		End 12	2 nd cut	15.8	15.8		15.5	15.3
	A2	End 13	2 nd cut	15.1	15.0		15.5	15.7
		End 14	3 rd cut	16.1	16.7		17.7	17.3
	A3	End 15	3 rd cut	14.9	15.1		15.1	15.8
		End 16	3 rd cut	13.8	15.2		15.0	15.1
				At release	At release	1 day	8 days	28 days
HSSS strands casting bed	C1	End 2	1 st cut	21.0	20.5	20.5	21.5	21.5
		End 1	2 nd cut	16.8	18.2	18.2	18.3	18.7
	B2	End 8	2 nd cut	-	15.6	15.7	15.3	15.5
		End 7	3 rd cut	-	14.5	14.7	14.9	15.3
	C2	End 4	3 rd cut	15.8	16.5	16.9	18.3	18.0
		End 3	3 rd cut	15.0	17.3	17.9	18.7	17.9
	B3	End 10	3 rd cut	-	14.4	14.4	14.9	15.6
		End 9	2 nd cut	-	15.1	15.5	15.1	15.3
C3	End 6	2 nd cut	16.0	15.7	15.8	14.8	14.7	
	End 5	1 st Cut	21.5	19.7	20.2	20.8	20.6	

During cutting of the penultimate HSSS strand in casting bed, the last HSSS strand fractured. More information about this incident can be found in Section 4.2.5.1. The impact force due to fracture failure of the penultimate HSSS strand had a significant effect on the transfer length. This effect influenced first cut end (End 2) as well as the internal end (End 1) of the affected Girder C1. Exterior end (End 2) of Girder C1 had the highest transfer length compared to transfer length at all other ends. Moreover, internal end (End 1) had the highest transfer length compared to transfer length at all other internal ends. The increase in transfer length using ERSGs between End 2 and End 1 (Girder C1) was approximately double the increase that occurred at the other side of the casting bed between End 5 and End 6 (Girder C3). The increase in transfer length using DEMEC gages between End 2 and End 1 (Girder C1) was 36% higher than the increase that occurred at the other side of the casting bed between End 5 and End 6 (Girder C3).

5.2.5.3 Prestress force effect

The transfer length increases with an increase in prestressing force (Oh et al. 2014). The prestressing force in the carbon steel strands was 43.9 kips, 18.0% higher than the 37.2-kip force in the HSSS strands. Higher prestressing force results in higher impact force on the end of the member due to sudden release of the strands. Therefore, it was anticipated that the transfer length of the carbon steel strands would be higher than that of the HSSS strands. The transfer length, using ERSGs, at release at the first cut end was 25.5 in. (End 11) for carbon steel strands and 21.5 in. (End 5) for HSSS strands. Thus, transfer length for carbon steel strands was approximately 18.6% longer than that for HSSS strands. The percentage of transfer length increase was almost equal to the percentage increase of the prestressing force.

5.2.5.4 Confinement reinforcement effect

Confinement reinforcement enhances the stiffness of the end regions to resist the bursting force induced from releasing the strands. The effect of different confinement reinforcement types on transfer length were studied. Girders A1, A2, and A3 had carbon steel, GFRP, and stainless steel confinement reinforcement, respectively. The averaged-measured transfer length at 35 days was 15.3 in., 16.5 in., and 15.5 in. for Girders A1, A2, and A3, respectively. The external cut end in Girder A1 was excluded because of the effect of sudden release on transfer length. Girders B2 and B3 had GFRP and stainless steel confinement reinforcement, respectively. The averaged-measured transfer length at 28 days was 15.4 in. and 15.5 in. for Girders B2 and B3, respectively. Experimental results revealed that transfer length did not significantly change when confinement

reinforcement type was changed from carbon steel rebars to GFRP or stainless steel rebars. Note that this conclusion is based on limited sample size and further studies might be needed to fully investigate the effect of GFRP confinement on end region stresses and transfer length.

The effect of different confinement reinforcement spacing on transfer length was also studied. Confinement reinforcement spacing was different between the ends of the same girder. At one end, the confinement reinforcement spacing was doubled to FDOT's standard confinement reinforcement detailing for the first 12 in. from end face. Ends numbered with odd values refer to standard ends while ends numbered with even values represent ends with less confinement reinforcement. For Girder A3, transfer length at 35 days was 15.8 in. and 15.1 in. for End 15 and End 16, respectively. For Girder B3, transfer length at 28 days was 15.3 in. and 15.5 in. for End 7 and End 8, respectively. For Girder C3, transfer length at 28 days was 17.9 in. and 18.0 in. for End 3 and End 4, respectively. Experimental results revealed that transfer length did not significantly change when confinement reinforcement spacing was increased to double along the first 12 in. from the end face.

5.2.6 Comparison of test data with literature

Experimentally-measured transfer lengths were compared with multiple equations from literature (Barnes et al. 2003; Kose and Burkett 2005; Lane 1998; Mitchell et al. 1993; Ramirez-Garcia et al. 2016; Russell and Burns 1996; Zia and Mostafa 1977). Also, experimental values were compared with equations from design provisions such as ACI 318 and AASHTO LRFD (2017; 2019). The equations in the literature consider parameters such as higher concrete compressive strength, different prestressing force and release method, etc. Transfer length results ranged from 14.7 in. to 21.5 in. and 15.1 in. to 25.5 in. for HSSS and carbon steel strands, respectively, as shown in Table 5-3. The averaged-measured transfer length at 28 days was 17.3 for HSSS strands while the averaged-measured transfer length at 35 days was 17.5 in. To be more conservative, transfer length at the first cut end shall be compared to proposed equations from the literature. All measured transfer lengths for HSSS and carbon steel strands were lower than the calculated value from ACI 318-19 and AASHTO LRFD Bridge Design Specifications, as shown in Figure 5-9 and Figure 5-10. The ratios of maximum-measured transfer length to values obtained using ACI and AASHTO equations were, respectively, found to be 1.31 and 1.67 for HSSS strands and 1.40 and 1.41 for carbon steel strands. ACI's transfer length equation provided a better estimation for HSSS strands than AASHTO's equation since ACI considers effective prestress in

addition to the strand’s diameter in its prediction equation. Some of the predictive transfer length equations yielded a transfer length less than the measured transfer length in this work, as shown in Figure 5-9 and Figure 5-10.

This study was also compared with the experimental transfer length that was obtained by (Paul et al. 2017b) for 0.5-in.-diameter HSSS strands in prestressed piles, where the longest calculated transfer length for 0.5-in.-diameter HSSS strands at the cut end was reported to be 24 in. The initial stress of strands in this study was approximately 11.5% longer than that in (Paul et al. 2017b). The maximum-measured transfer length for 0.6-in.-diameter HSSS strands was 90% of that for 0.5-in.-diameter HSSS strands. This observation contradicted the conclusions that transfer length is longer for bigger strand diameters and increases with an increase in the initial jacking stress (Oh et al. 2014; Russell and Burns 1996). (Paul et al. 2017b) reported that difficulties were encountered when removing the pile from the bed and, therefore, a mechanical hammer was used. (Paul et al. 2017b) suggested that the vibration induced from the mechanical works may have resulted in longer transfer length values in that pile. Also, the concrete compressive strength of the piles was 8 ksi at 28 days, which is 70% of that used in this study. Because transfer length is considered to be inversely proportional to concrete compressive strength (Mitchell et al. 1993), the shorter transfer length obtained in this study for 0.6-in.-diameter strands may be attributed to the higher concrete compressive strength.

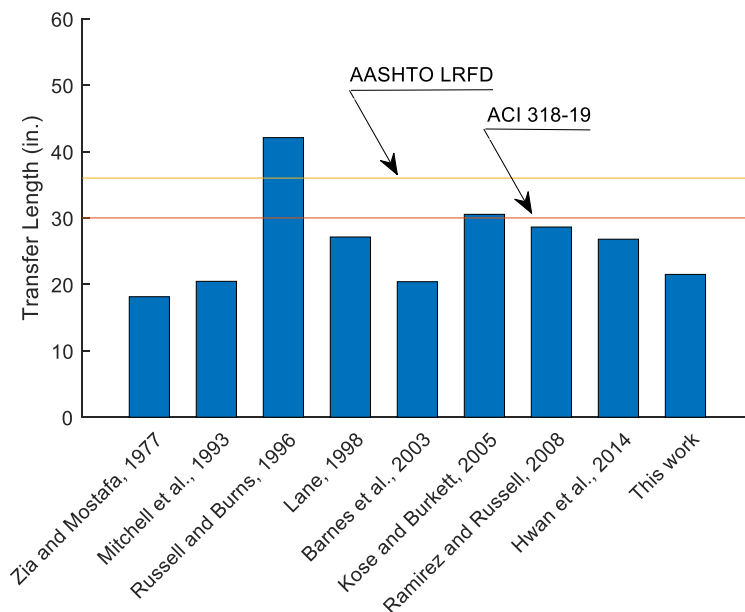


Figure 5-9 Comparison of measured transfer length of HSSS strands with equations from literature

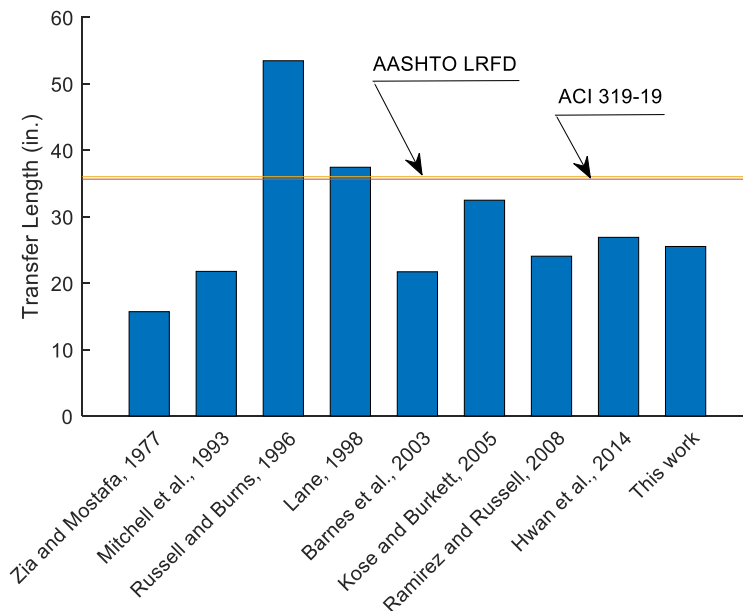


Figure 5-10 Comparison of measured transfer length of carbon steel strands with equations from literature

5.3 Second set of girders

5.3.1 Preparation of specimens

See Section 4.3.4 for information about fabrication of the specimens.

5.3.2 Method of prestress release

The strands were released using the flame cutting method. The orientation of the girders in the beds is illustrated in Figure 4-25. The strands were cut in the following sequence: first, at the external ends of the external girders, simultaneously; second, at the internal ends of the external girders; and third, between internal ends of the internal girders. The strand release sequence and procedure in this study represents common industry practice for AASHTO Type II girders.

5.3.3 Instrumentation

Fiber optic sensors (FOS) and ERSGs were used to determine the transfer length of the 0.6-in.-diameter HSSS strands. Utilizing FOS to measure strain distributions to determine transfer length has been very limited until now. The FOS used in this study was a distributed fiber optic with a gage spacing of 0.25 in. FOS were used internally and externally to measure strains at the end regions. Internal FOS were installed as follows. A 50-in.-long No. 2 GFRP bar was cut. Then, a small portion along the length of the GFRP bar was grooved. The GFRP bar was cleaned, and the fiber optic sensors were glued into the groove. After tensioning the strands, the GFRP bars

were attached to the bottom layer of strands, running parallel to the strands, as shown in Figure 5-11. The internal FOS was placed at 3 in. from the girder end and extended 40 in. After casting the concrete and removing the forms, external FOS were installed on the concrete surface at the bottom flange as shown in Figure 5-12. The external FOS was placed for 40 in. starting at 2 in. from the girder end. Due to limited channels in the data acquisition system, only three Girders (E2, E4 and E5), four end regions, were instrumented with FOS. To verify the strain measurements from the FOS, two ends of Girder E2 were instrumented with ERSGs. The ERSGs were installed on the concrete surface on the other side of the bottom flange with a spacing of 5 in. starting at 2 in. from the beam end to 42 in.; a total of eight strain gages were installed at each end as shown in Figure 5-13. Two data loggers were used for data acquisition: one was used for FOS measurements, and the other was dedicated for ERSG measurements.



Figure 5-11 Installation of internal Fiber Optic Sensors for transfer length

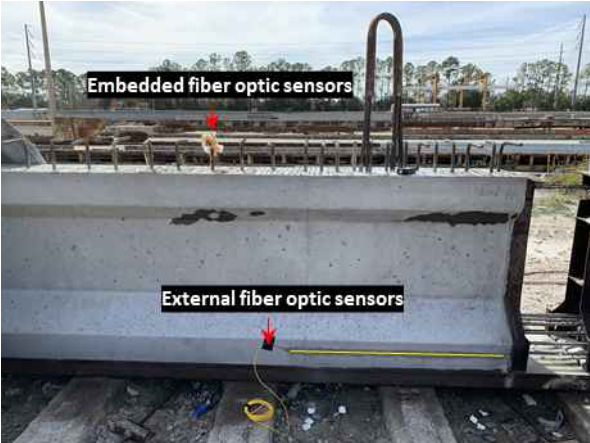


Figure 5-12 Installation of external Fiber Optic Sensors for transfer length



Figure 5-13 Installation of strain gages for transfer length

5.3.4 Results

The scope of this experimental work was to verify that transfer length can be determined using different types of sensing technology such as fiber optic sensors. In general, transfer length is estimated using strain measurements from DEMEC gages or ERSGs attached to the concrete surface. However, in this study, FOS were used to measure strain. FOS provide continuous strain measurements, which is an advantage compared to DEMEC gages and ERSGs. Figure 5-14 shows the strain distribution measured using ERSGs and FOS in all tested specimens. The magnitude of the strains in the FOS stabilized – reached a constant plateau – after a certain distance, indicating full stress transfer from the strands to the concrete, Figure 5-14. Strain values obtained by internal fiber optic sensors were always higher than those obtained by external fiber optic sensors except at the cut (external) end. In this study, the 95% average maximum strain (AMS) method was adopted to determine the convergence point and then evaluate the transfer length (Russell and Burns 1993). Table 5-4 provides a summary of all the transfer lengths obtained from ERSGs and FOS. Note that only two out of the four ends were instrumented with strain gages. The transfer length at the cut end was longer than those at the other ends. This observation was expected because the sudden release of the strands by flame cutting at the cut end is expected to generate a higher impact force than at the other ends.

The results from this study indicate that FOS provide better representation of strain distribution than strain gages. Both internal and external fiber optic sensors were found to give a good transfer length result. Therefore, FOS is an alternative option that can be used to measure transfer length. Advantages of using internal fiber optic sensors are reduced installation time at the casting yard

and reduced measurement error due to their less dependency on good concrete surface condition and adhesion.

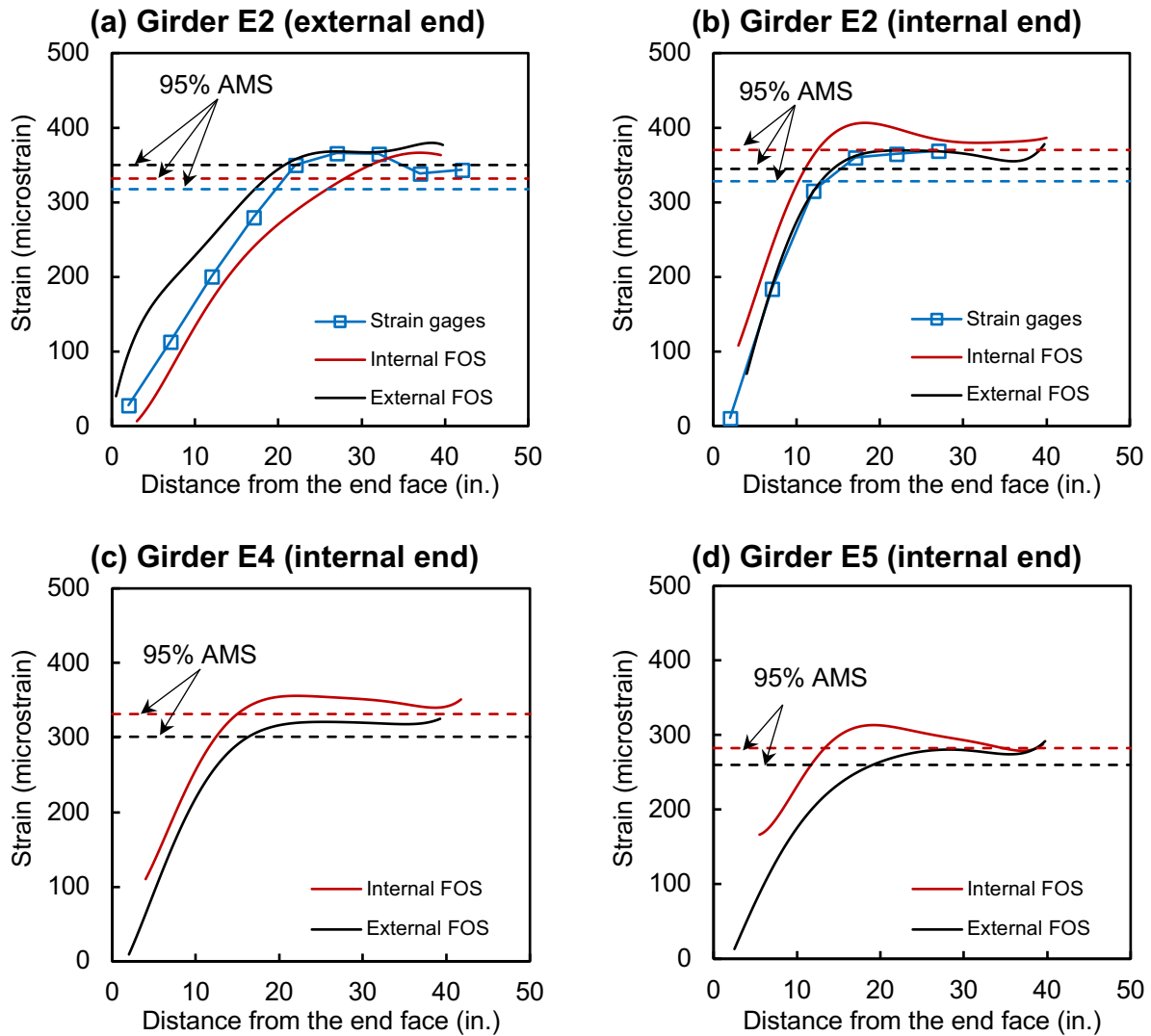


Figure 5-14 Smoothed strain distribution of the tested specimens

Table 5-4 Transfer length estimates of the tested specimens at release

Specimen	End designation	Strain gages (in.)	Internal FOS (in.)	External FOS (in.)
Girder E2	External (cut) end	19.7	24.0	20.6
	Internal end	13.0	12.8	13.2
Girder E4	Internal end	-	15.0	16.0
Girder E5	Internal end	-	13.2	15.0

As known, releasing of strands generates compressive force in the concrete. Higher compressive forces were obviously obtained at the ends that had larger total initial prestressing

forces. Compressive forces at the dead end of the specimens are depicted as compressive strain in Figure 5-15. The total initial prestressing force of Girders E2, E4 and E5 was 396, 324 and 252 kips, respectively. The average maximum strain values were approximately 369, 317 and 274 microstrain, respectively.

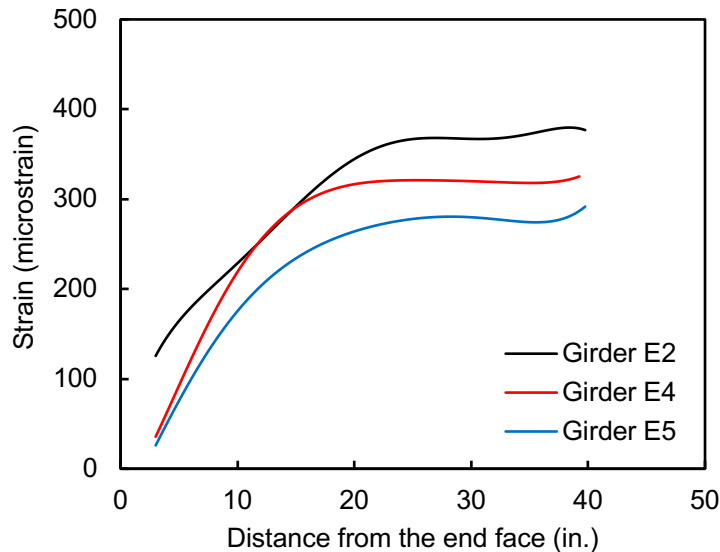


Figure 5-15 Strain distribution from the external fiber optic at internal ends

5.3.5 Comparison with first set of girders

The transfer length increases with an increase in prestressing force (Oh et al. 2014). Thus, transfer length in the first set of girders was expected to be greater than that in the second set of girders because the initial prestressing force in the first set of girders was 3.3% greater than that in the second set of girders. Transfer lengths calculated from ERSGs measurements were used in the comparison. The maximum transfer length at release at external (cut) end in the first set and second set of girders was 21.5 in. and 19.7 in., respectively. Also, the average transfer length at release at the internal end in the first set and second set of girders was 15.9 in. and 13.0 in., respectively. Thus, it can be concluded that results obtained from the first set and second set of girders are in good agreement.

5.3.6 Prediction of transfer length

AASHTO LRFD Bridge Design Specifications and ACI 318-19 were used to predict the transfer lengths (2017; 2019). The predicted transfer lengths by AASHTO LRFD and ACI 318 were 36.0 in. and 31.2 in., respectively. The transfer lengths immediately after release were generally shorter than the predictions. Note that the transfer lengths in this study were determined

only immediately after release. Transfer lengths in all specimens are expected to increase with time. However, monitoring the growth of the transfer length was not within the scope of this study.

5.4 Summary

One of the objectives of this experimental work was to determine the transfer length for 0.6-in.-diameter HSSS strands. The transfer lengths were calculated from strain profiles, which were measured by strain gages, DEMEC points, and internal and external fiber optic sensors. Based on the experimental test results, the following conclusions were drawn:

1. The maximum transfer length of HSSS and carbon steel strands was 21.5 in. and 25.5 in, respectively. The ratio of prestressing force of HSSS to carbon steel strands was 84.7%, which was approximately equal to the ratio of transfer length of HSSS to that of carbon steel strands, 84.3%. Therefore, it was concluded that the transfer length increases with an increase in prestressing force.
2. This study indicates that the transfer length at the first cut end was always higher than that at the second cut end regardless of strand type. The maximum increase of transfer length for HSSS strands between the first cut end and the second cut end was 25% and 34%, respectively, when transfer length was measured using DEMEC and ERSGs. The strands at the second cut ends were relatively gradually released.
3. By examining the measured transfer lengths, no significant change in the transfer length was observed when different types and spacing of confinement and vertical reinforcement were used.
4. Strain gages and fiber optic sensors can only be used to measure transfer length at release. The maximum transfer length at release of 0.6-in.-diameter HSSS strands using strain gages, internal FOS, and external FOS was 19.7 in., 24.0 in., and 20.6 in., respectively.
5. Transfer lengths at release of 0.6-in.-diameter HSSS strands using strain gages from the first set and second set of girders were in good agreement.
6. Transfer lengths obtained by internal and external FOSs were in good agreement with those obtained by strain gages. Internal and external FOSs provide better representation of strain distribution than strain gages.
7. This study recommends the use of internal fiber optic sensors to measure strain distribution at the end regions. Advantages of using internal fiber optic sensors are reduced installation

time at the casting yard and reduced measurement error due to their less dependency on good concrete surface condition and adhesion.

8. The current ACI 318-19 design code and *AASHTO LRFD Bridge Design Specifications* conservatively estimate the transfer length of HSSS and carbon steel strands.

CHAPTER 6 FLEXURAL TEST

6.1 Introduction

This chapter reports the flexural test results that were obtained from testing ten (10) girders prestressed with 0.6-in.-diameter HSSS strands and two (2) girders prestressed with 0.6-in.-diameter carbon steel strands. The testing matrix of the first set of girders consisted of five (5) girders prestressed with HSSS strands and two (2) girders prestressed with carbon steel strands. The testing matrix of the second set of girders included five (5) girders prestressed with HSSS strands.

6.2 First set of girders

6.2.1 Test setup

All seven girders were tested in flexure using a four-point loading scheme while the eighth girder was tested in shear, which is discussed in Chapter 10. For the flexural test, a 7-ft-long W16x100 spreader beam was used to transfer load from actuator to girder. The spreader beam was placed on the top face of the girder on two neoprene pads spaced at 6 ft. The load from the actuator was applied at the center of the spreader beam. The girder was placed on thick neoprene pads to create a simply-supported condition. The clear span was 40 ft. The test setups for the non-composite and composite specimens are shown in Figure 6-1a and Figure 6-1b, respectively. The shear reinforcement (4K bars) extended out of the girder's top face. So, for non-composite specimens, the extended part of six bars in the mid span was cut to provide space for the spreader beam as shown in Figure 6-1a. In the case of composite specimens, the shear reinforcement was embedded in the deck slab as shown in Figure 6-1b.

Girder B2 was the first to be tested among the four composite specimens as shown in Figure 6-2a. Slightly after cracking load, a shear crack initiated at the end of the girder as shown in Figure 6-2b. Thus, it was decided to unload the specimen. One solution to prevent shear failure in a member is to externally reinforce it with steel rods. (Chehab et al. 2018) used external clamped steel bars to preserve a portion of the girder from damage during the initial test, for subsequent testing. (Chehab et al. 2018) was able to test a 36-ft-long AASHTO Type II girder three times in shear by using external clamped steel bars and adjusting the support and load locations. In this experimental work, it was decided to use external post-tensioning clamped steel rods, Figure 6-2c, to reinforce the section and prevent it from failing in shear. The steel rods were not attached to the steel frame and therefore did not influence the rotation of the specimen. Girder B2 was then loaded

to failure. As mentioned before, the main objective of this experimental program was to study the flexural behavior of girders prestressed with HSSS strands. For consistency in the testing procedure, the other three composite specimens were also reinforced with the external threaded rods.

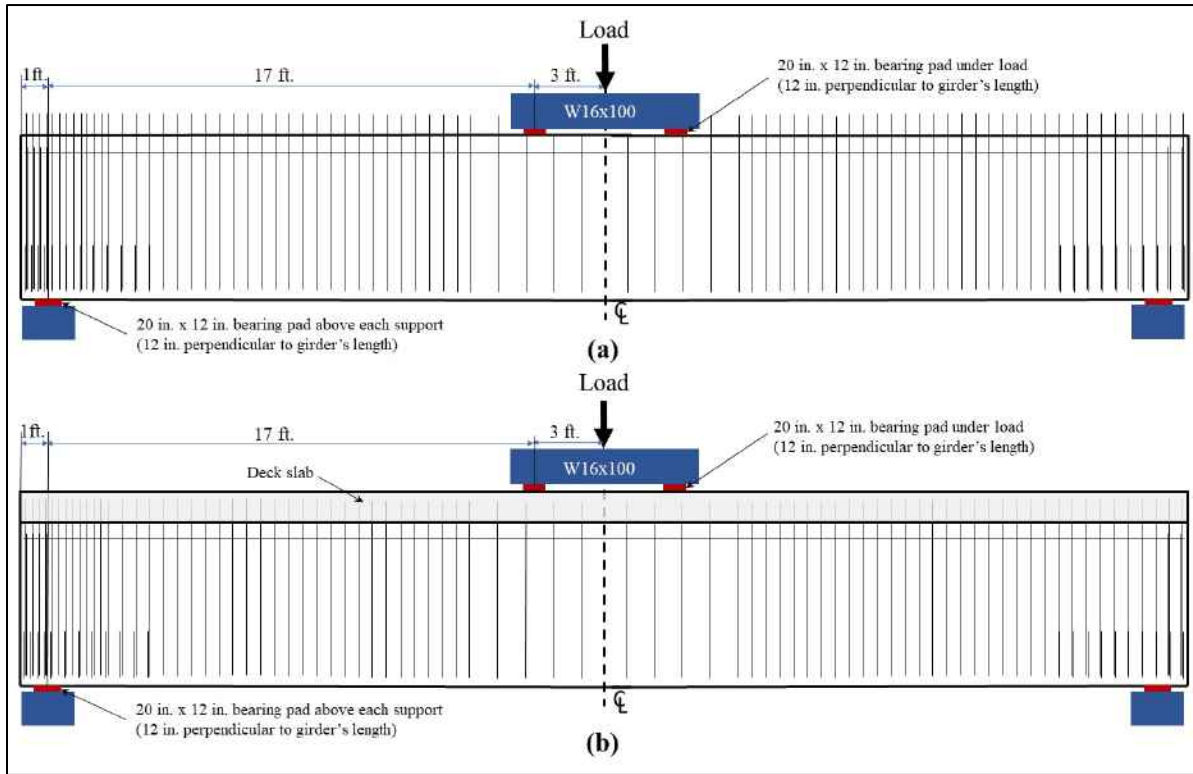


Figure 6-1 Flexural test setup a) for non-composite specimens; and (b) for composite specimens

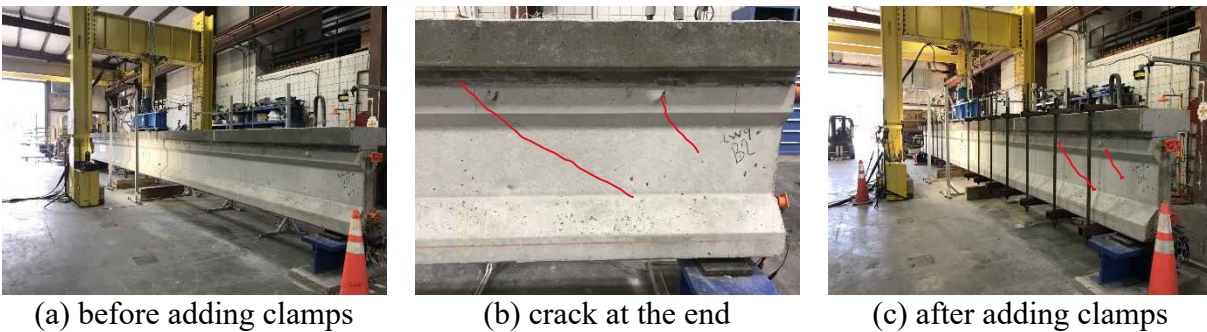


Figure 6-2 Flexural test setup for Girder B2

External post-tensioning clamped steel bars were installed as follows. First, sizes of the threaded rods and steel tubes (at the top and bottom) were determined so that they will not fail or yield during the tensioning procedure and/or testing of the girder. The dimensions of the top and bottom tubes were 3 in. x 3 in. and 4 in. x 4 in., respectively. A smaller tube was used at the top

region because the moment demand at the top region was lower than at the bottom region. Second, the threaded rods and tubes were attached to the beam. A total of 14 sets (seven sets on each side of the specimens as shown in Figure 6-2c) of external clamped steel bars were used. The first set of external clamped steel bars was installed at 22 in. from the end face of the beam. Then, the rest were installed at 29-in. spacing on-center, and the distance from the last set to the point load was 20 in. All external reinforcements were symmetrical about the girder's center line. Once all external clamped steel bars were placed, washers were installed, and nuts were tightened. Third, the threaded rods were tensioned. A system was created to apply the tension force to the threaded rods as shown in Figure 6-3. Each set, two threaded rods, was tensioned individually. The installed threaded rod was extended by attaching another threaded rod through the coupler. Then, a new steel tube (7 in. x 7 in.) was placed through the threaded rods and locked using nuts at both ends, leaving a space for the hydraulic jack to be placed between the two tubes. The hydraulic jack was positioned carefully. The force from the hydraulic jack pushed the new steel tube, and therefore the girder was vertically squeezed. As a result, the nuts at the top face of the girder were loosened. The two nuts were simultaneously tightened using a wrench, causing a tension of 5.6 kips in each threaded rod. It was assumed that approximately equal tensile forces were applied to each threaded rod. For this experiment, the discrepancy in tensile forces applied to threaded rods does not significantly affect the performance of the system. A similar procedure was used for each set of external clamped steel bars.

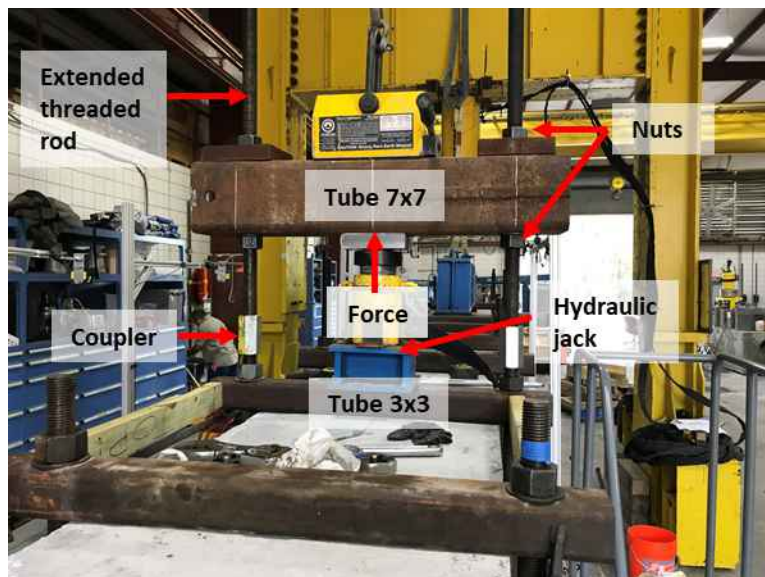


Figure 6-3 External post-tensioning of threaded rods

6.2.2 Test instrumentation

Each girder was instrumented with strain, deflection and shaft gages. Figure 6-4 and Figure 6-5 show the test instrumentation for monolithic and composite girders, respectively. Three sets of strain gages were installed on the concrete top surface at three locations (mid span cross section and 18 in. from mid span in each direction) in the constant moment region. For monolithic girders, two sets of two strain gages were installed along the depth of the section at midspan at 3 in. and 12 in. from the top face of the girder. For composite girders, three sets of two strain gages were installed along the depth of the section at mid span at 4 in., 13 in., and 22 in. from the top face of the slab. Multiple deflection gages were installed along the length of the girder, to measure the vertical displacement of the specimen during the flexural test. The strand slip gages were installed on all bottom layer strands to monitor any slip in the strands during the flexural test. The load was applied by a hydraulic jack at a rate of 0.25 kip/sec. Two load cells, placed at the center of the load frame, were used to measure the applied load.

6.2.3 Prestress losses

Limited studies have been performed regarding the prestress losses of any grade of stainless steel strands and particularly HSSS strands. (Paul et al. 2017a) investigated the prestress loss of 0.5-in.-diameter HSSS strands in piles. The HSSS strands were tensioned to 61% of their ultimate stress, which was reported as 240 ksi. (Paul et al. 2017a) reported that the total prestress losses in the 0.5-in.-diameter HSSS strands were 12.4% after 335 days. At the time of writing this report, (Paul et al. 2017a) had conducted the only study related to the prestress losses estimation of 0.5-in.-diameter HSSS strands, and no study, so far, has investigated prestress losses estimation for the new 0.6-in.-diameter HSSS strands.

For assessment of total prestress losses, two vibrating wire strain gages (VWSGs) were installed at the bottom layer of strands in the mid span of each girder as shown in Figure 6-6. The VWSGs can be embedded in concrete and measure internal concrete strain and temperature. The reference reading for each vibrating wire was collected immediately before releasing the strands. Afterward, periodic readings were taken. Perfect bonding was assumed between the strands and surrounding concrete. Thus, the change in strain of prestressing strands equals the change in strain of concrete at the same level. The measured strains, from VWSGs, were corrected by including the internal temperature of concrete and coefficient of thermal expansion of steel, which was 12.2 microstrain/C. The corrected strains were transformed into stresses by using the elastic modulus

of the strands. The stress losses by VWSGs were calculated by subtracting the measured stress in the strands from the initial prestress.

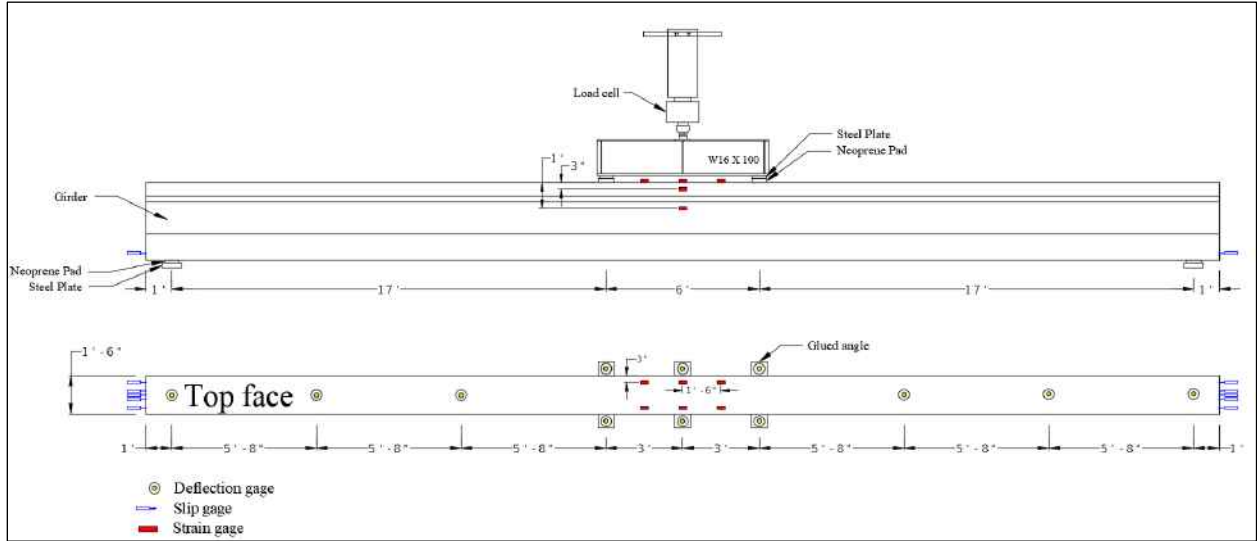


Figure 6-4 Test instrumentation for monolithic girders

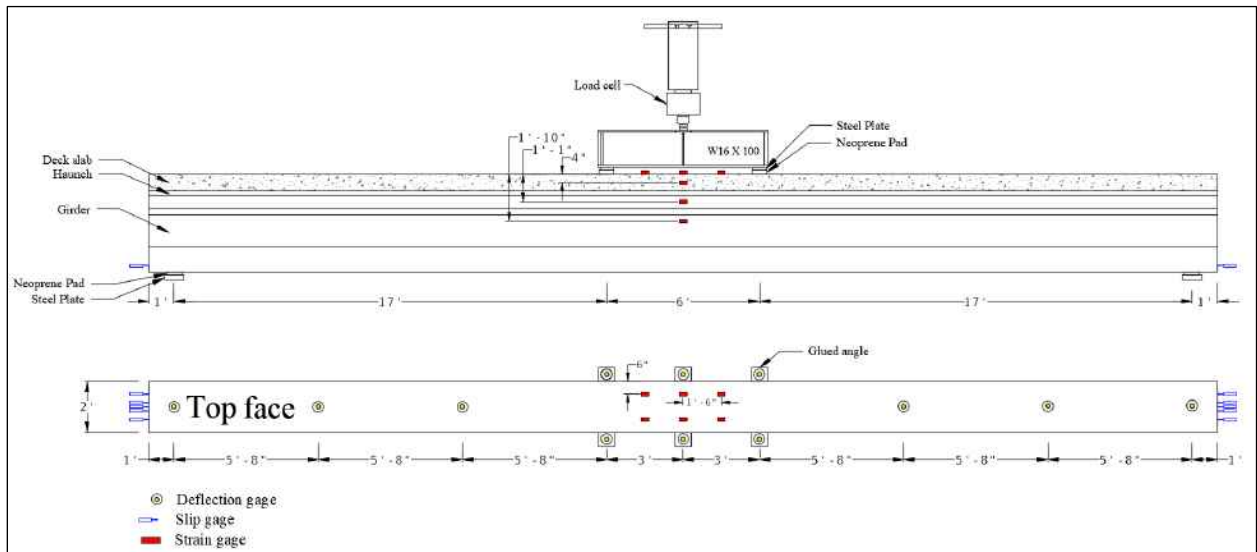


Figure 6-5 Test instrumentation for composite girders



Figure 6-6 VWSG attached to the bottom layer of strands in Girder A2

Based on the design objective of this study, the HSSS specimens were divided into two groups. The first group included HSSS specimens (Girder C1, Girder C2, and Girder C3) which had the same prestressing force as the carbon steel specimens (Girder A1 and Girder A3). The second group consisted of HSSS specimens (Girder B2 and Girder B3) which had same prestressing reinforcement ratio as the carbon steel specimens. The initial total prestressing force for the second group was approximately 84.7% of that for the carbon steel specimens. Thus, the elastic shortening losses for the second group were expected to be lower than those for the carbon steel specimens. VWSGs readings immediately after releasing the strands were used to determine the stress losses caused by elastic shortening (Δf_{pES}). Figure 6-7 shows measured elastic shortening losses. The elastic shortening losses for the second group were 86.0% on average of those for carbon steel specimens as shown in Figure 6-7.

Because VWSGs measure only change in the concrete strain, they cannot detect changes in the strands' strain caused by relaxation of strands (Garber et al. 2015). Prestress loss due to strand relaxation is best determined by a separate experiment. (Schuetz 2013) conducted experimental tests, following ASTM E38 (2013), to measure stress relaxation for 0.5-in.-diameter HSSS strands. (Schuetz 2013) tested three specimens for 1000 hours. The strand specimens were initially stressed to 70% of their ultimate tensile stress. Results revealed that the average stress relaxation loss was 2.49%, which was slightly below the acceptable limit by ASTM A1114. At the time of writing this report, Schuetz had conducted the only study related to the stress-relaxation losses of 0.5-in.-diameter HSSS strands, and no study, so far, has investigated stress-relaxation losses of the new 0.6-in.-diameter HSSS strands. Also, it was not within the scope of this study. Therefore,

AASHTO Equation 5.9.3.4.2c-1, which is given in Equation 6-1, was used to estimate the stress-relaxation losses (Δf_{pR}).

$$\Delta f_{pR} = \frac{f_{pt}}{K_L} \left(\frac{f_{pt}}{f_{py}} - 0.55 \right) \quad \text{Equation 6-1}$$

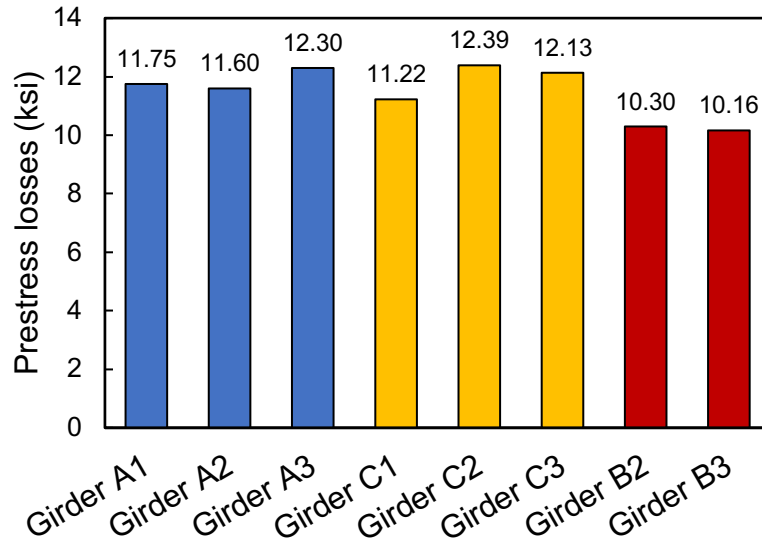


Figure 6-7 Measured elastic shortening losses

The stress immediately after transfer, f_{pt} , was calculated using Equation 6-2, where: f_{pi} is initial stress in the strands, which was 202.2 ksi and 161.7 ksi for carbon steel and HSSS strands, respectively; Δf_{pES} is elastic shortening losses, which is given in Figure 6-7; f_{py} is yield stress in the strands, which was 243 ksi and 230 ksi for carbon steel and HSSS strands, respectively; and the factor accounting for the type of steel, K_L , was taken as 30 for both carbon steel and HSSS strands.

$$f_{pt} = f_{pi} - \Delta f_{pES} \quad \text{Equation 6-2}$$

The averaged-estimated stress relaxation loss was found to be equal to 1.49 ksi and 0.52 ksi for carbon steel and HSSS strands, respectively. The estimated stress relaxation loss for HSSS was significantly lower than that for carbon steel strands because the stress in the HSSS strands immediately after transfer, f_{pt} , was lower than that in carbon steel strands. More research is needed to determine the applicability of the current AASHTO equation to determine the stress relaxation losses for HSSS strands. The total stress losses in the strands were calculated by adding the stress losses measured by VWSGs and stress-relaxation losses estimated by AASHTO (2017). For

composite girders, the estimated stress-relaxation loss was added twice: the first time after releasing the strands, and the second time after adding the deck slab.

The effective stress in the prestressing strands was calculated periodically. Figure 6-8 shows effective prestress force with time. All specimens were transported 38 days after start of building the carbon steel specimens (32 days after start of building the HSSS specimens). All specimens, shown in Figure 6-8, experienced an increase in the effective stress for approximately 18 days after arriving at the FDOT SRC. This increase is attributed to vibration of the girders while transporting. Afterward, the effective stress started to decrease. Four specimens were made composite by adding a deck slab, cast at the FDOT SRC. The deck slab produced a uniform dead load on the girder, resulting in an increase in the effective stress.

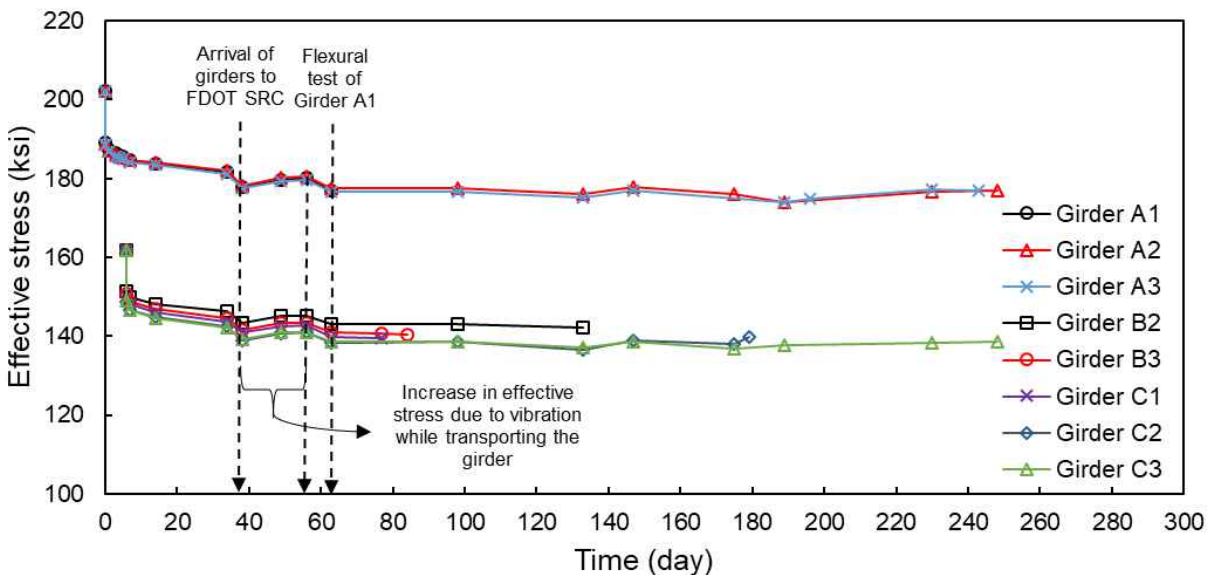


Figure 6-8 Effective prestress with time

The comparison of prestress losses between the carbon steel and HSSS strands shall be made between members with the same prestressing force and same section geometry. The comparison shall be presented in terms of percentage of prestress losses because the initial prestressing force was different between the HSSS and carbon steel strands. Figure 6-9 presents the percentage of prestress losses with time for all specimens. The first specimen (Girder A1) was tested 63 days after start of building, and others were tested later. The loss of initial prestress for all non-composite specimens, at the day of testing Girder A1, is shown in Figure 6-10. The averaged-measured prestress losses were 12.4% and 14.2% for carbon steel and HSSS strands (in the girders which had the same prestressing force as the control girders), respectively. A proper comparison

can also be made between the composite specimen Girder C2, which was tested in flexure 48 days after casting deck slab, and Girder A2, which was tested 54 days after casting deck slab. The averaged-measured prestress losses were 12.6% and 13.7% for carbon steel and HSSS strands, respectively. Even though the total initial prestressing force in the girders prestressed with carbon steel and HSSS strands was equal, the total prestressing losses were slightly higher in the HSSS strands. The measured total prestress losses of the 0.6-in.-diameter HSSS strands were higher than the reported total prestress losses of the 0.5-in.-diameter HSSS strands by (Paul et al. 2017a).

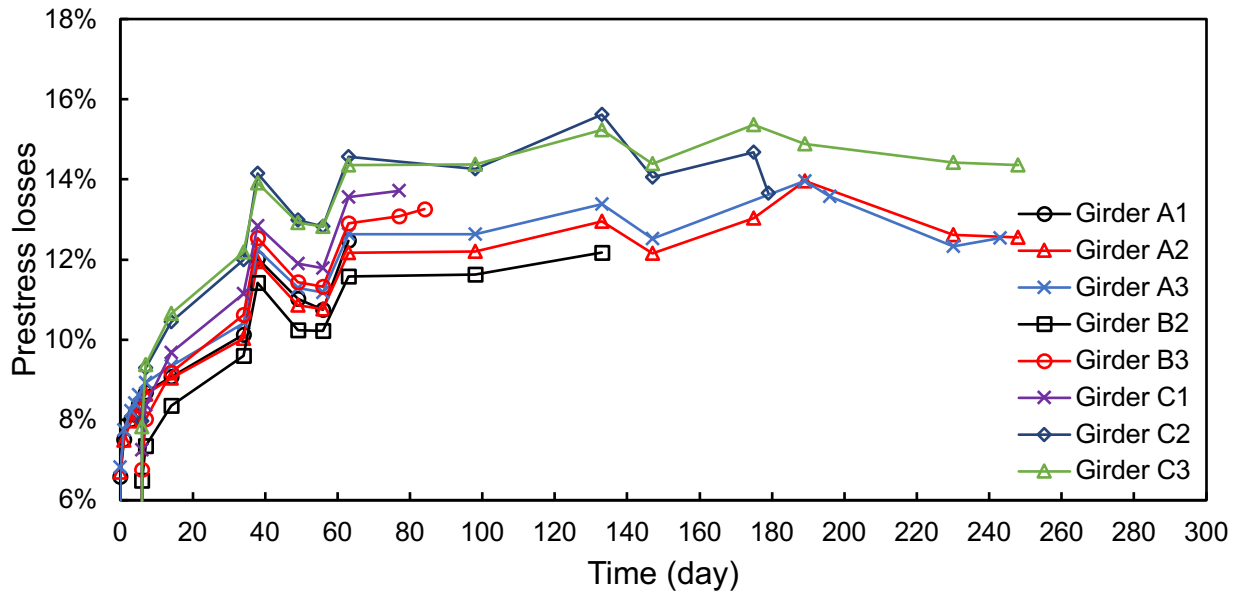


Figure 6-9 Prestress losses estimation with time

6.2.4 Experimental results

All seven specimens were tested in flexure up to failure except for Girder A3 and Girder B3, which were unloaded before failure to save them for a future shear test. The specimens were tested over a period of 12 months. Experimental mid span load-deflection curves for all tested girders are shown in Figure 6-11 and Figure 6-12 for non-composite and composite girders, respectively. The load-deflection curve is divided into two regions, separated by initiation of the first flexural cracking. All specimens behaved linearly in the pre-cracking region. All girders prestressed with HSSS strands exhibited similar post-cracking behavior up to failure, which was different than that for the control specimen. Unlike carbon steel strands where they reach plateau after yielding, HSSS strands exhibit no discernible yield plateau. The capacity of all girders prestressed with HSSS strands increased up to failure, which reflects the stress-strain behavior of the HSSS strands.

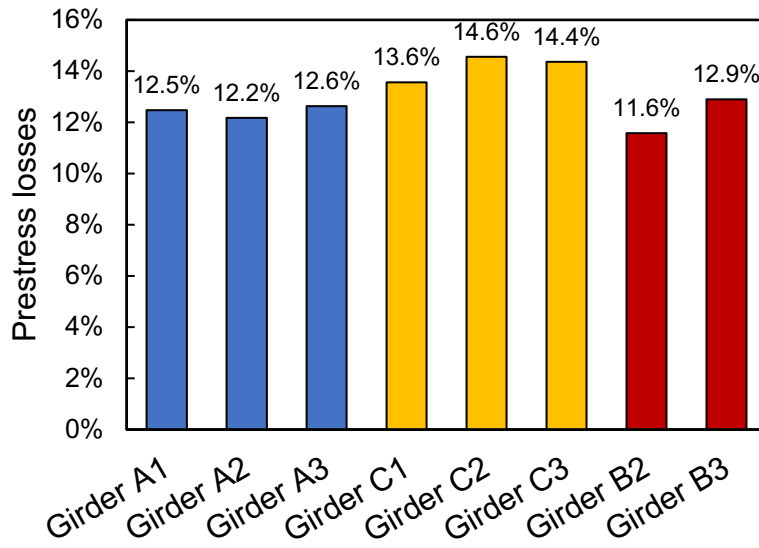


Figure 6-10 Measured prestress losses of non-composite girders 63 days after start of building control girders

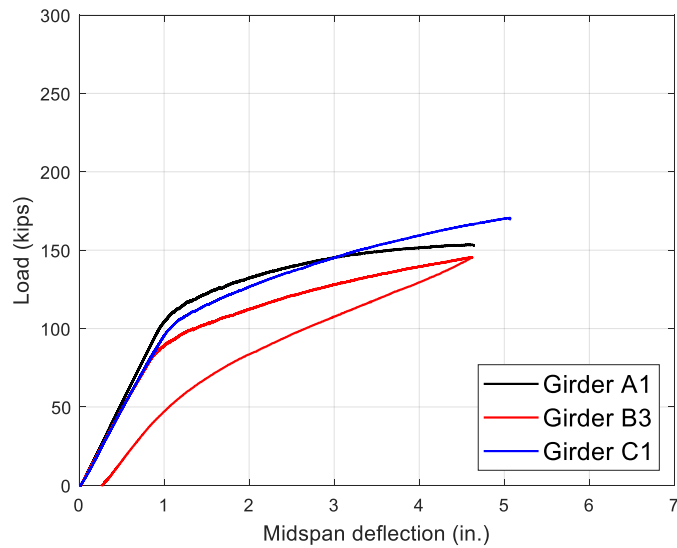


Figure 6-11 Load-deflection relationships of non-composite girders in the first set of girders

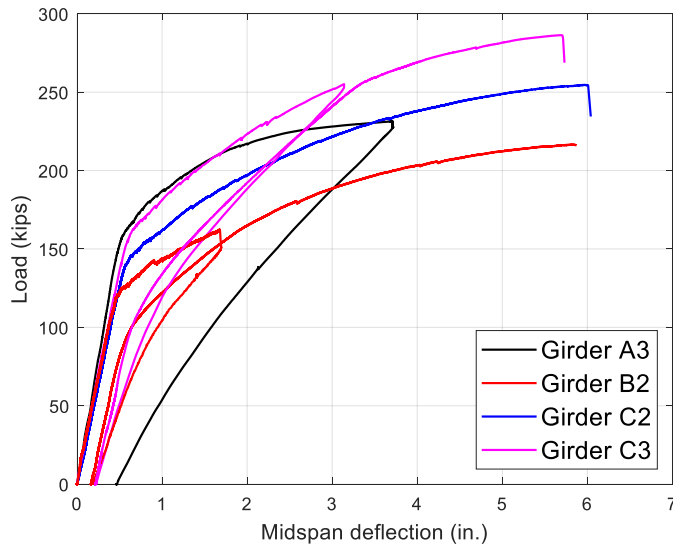


Figure 6-12 Load-deflection relationships of composite girders in the first set of girders

Shear reinforcement in all specimens extended out of the top of the girder. The extended stirrups are essential to develop dowel interlock between the girder and deck slab. The shear reinforcement had 90-degree hooks at the top and bottom to develop sufficient bonding with the surrounding concrete. Three specimens in this study were non-composite girders, and therefore the top 90-degree hook was not embedded in the concrete section. Therefore, stirrups could not develop their anticipated strength, as designed, because development length was not enough. The consequence of this effect was reduced post-cracking behavior of the member. In this experimental program, it is appropriate to compare results of all three non-composite specimens because they were all designed and tested under the same condition. However, the post-cracking behavior of the non-composite specimens would have been different than those in this experimental program if the stirrups were embedded in a concrete slab.

Among the four composite girders, two were reinforced with GFRP stirrups (Girder B2 and Girder C2). GFRP rebar has a lower elastic modulus and ultimate strain compared to carbon and/or stainless steel rebar. The stiffnesses of Girder B2 and Girder C2 were significantly reduced, and this was not taken into consideration during design. Because GFRP rebar is made from an anisotropic material, their longitudinal strength is much higher than their transverse strength. Therefore, interface shear failure was another issue in Girder B2 and Girder C2 for two reasons: GFRP rebar does not provide high strength in the transverse direction, and the interface region was smooth.

A summary of the main test results is given in Table 6-1. Discussion and comparison of the experimental results are summarized in the following sections.

Table 6-1 Flexural tests results of first set of girders

Section	Specimen ID	Cracking load (kips)	Cracking deflection (in.)	Ultimate Load (kips)	Ultimate deflection (in.)	Failure mode [analytical]	Note
Non-composite section	Girder A1 (control)	98.4	0.931	152.7	4.642	Crushing of concrete	
	Girder B3	80.2	0.840	--	--	Crushing of concrete	Unloaded before failure
	Girder C1	94.5	0.992	170.6	5.071	Crushing of concrete	
Composite section	Girder A3 (control)	143.2	0.455	--	--	Crushing of concrete	Unloaded before failure
	Girder B2	115.6	0.445	216.7	5.835	Rupture of strands	
	Girder C2	132.6	0.530	254.7	5.969	Rupture of strands	
	Girder C3	143.6	0.530	286.3	5.693	Rupture of strands	

6.2.4.1 Non-composite girders

Girder A1 was the control girder, which had 11 carbon steel strands. Girder C1 and Girder B3, which were prestressed with HSSS strands, had the same initial prestressing force and the same prestressing steel area as the control girder, respectively. The flexural behavior of all specimens was linear up to the occurrence of the first flexural crack as shown in Figure 6-11. The post-cracking behavior of specimens prestressed with HSSS strands, Girder B3 and Girder C1, was increasing load up to failure, which reflects the stress-strain behavior of the HSSS strands.

Girder B3 had the same total number of strands as the control girder, Girder A1, but a lower initial total prestressing force. The flexural behavior of Girder B3 was different and lower than that for Girder A1 as shown in Figure 6-11. The cracking load for Girder A1 was approximately 22.7% greater than that for Girder B3. The ultimate load and deflection for Girder A1 was 152.7 kips and 4.64 in., respectively. Girder B3 was loaded until the measured deflection reached the ultimate deflection of Girder A1, 4.64 in. At this deflection, the measured load for Girder B3 was approximately 95% of that for Girder A1. Girder B3 was unloaded to be saved for future shear tests.

The prestressing reinforcement ratio has a significant influence on the flexural behavior of the member. Girder C1 had the same initial total prestressing force as the control girder but a higher prestressing reinforcement ratio. Achieving the same initial total prestressing force in Girder C1

required having more prestressing strands compared to the control girder because the ultimate stress as well as the stress limit for the carbon steel strands was higher than those for the HSSS strands. Thus, the ultimate load and deflection for Girder C1 were approximately 11.7% and 9.2% greater, respectively, than those for Girder A1. The stiffness of Girder C1 was lower than that of Girder A1 up to a 3-in. deflection. After that, the stiffness of Girder C1 became greater than that of Girder A1. All non-composite girders failed by crushing of concrete as designed.

6.2.4.2 Composite girders

Girder A3 was the control girder, which had carbon steel strands. Girder B2, which was prestressed with HSSS strands, had the same reinforcement ratio as the control girder, and Girders C2 and C3, which were prestressed with HSSS strands, had the same initial total prestressing force as the control girder. The flexural behavior was linear with applied load up to initiation of the first flexural crack. After cracking load, behavior of composite girders prestressed with HSSS strands was increasing load up to failure, which reflects the stress-strain behavior of the HSSS strands. All composite girders prestressed with HSSS strands failed due to rupture of all the strands, which indicated that the capacity of the member was controlled by the ultimate strain limit of the HSSS strands.

To achieve the same initial total prestressing force in Girders C2 and C3 compared to Girder A3, the number of HSSS strands was increased in Girders C2 and C3 because HSSS strands had lower ultimate stress and stress limit than carbon steel strands. The prestressing reinforcement ratio is proportional to the bending capacity of the member. Both Girders A3 and C3 had similar pre-cracking behavior, where they cracked at almost the same load. The post-cracking behavior of Girder A3 was almost identical to Girder C3 up to a point where Girder A3 deflection increased more rapidly due to yielding of carbon steel strands; in contrast, the load on Girder C3 continued increasing up to failure. Girder A3 was unloaded once the load-deflection curve plateaued at 231.4 kips. Girder A3 had a permanent deflection of 0.460 in. after unloading. Girder C3 was unloaded once it reached 90% of the calculated analytical capacity and then loaded up to failure, 286.3 kips. It had a permanent deflection of 0.216 in. after unloading.

Girder C2 and Girder C3 were identical except that Girder C2 had GFRP stirrups while Girder C3 had stainless steel stirrups. As mentioned before, all girders were designed to resist shear and fail in flexure. Shear reinforcement was designed based on the mechanical properties of carbon steel rebar. The carbon steel shear reinforcement in Girder C1 was replaced on a one-to-one basis

with GFRP rebars in Girder C2 and with stainless steel rebars in Girder C3. Because stainless steel rebars have comparable mechanical properties to carbon steel rebars, in this study it was natural to change shear reinforcement from carbon steel to stainless steel. However, direct replacement of shear reinforcement from carbon steel rebars to GFRP rebars affects the flexural behavior of the girder because GFRP rebars have lower ultimate strain and elastic modulus than those of carbon steel rebars. Due to the use of GFRP stirrups in Girder C2, the overall flexural behavior was significantly reduced as shown in Figure 6-12. Deformation almost entirely comes from flexure, if shear deformations are assumed to be zero. An increase in deflection can also be attributed to the concrete surface condition at the interface region and to low interface shear reinforcement, which affects the composite interaction of the girder and deck slab. The cracking and ultimate loads of Girder C3 were 8.3% and 12.4% higher than those of Girder C2, respectively, even though Girder C3 and Girder C2 had the same longitudinal reinforcement type and force. However, the cracking deflection and ultimate deflection were almost equal for both girders. Visual inspection of Girder C2 and Girder C3 revealed that more cracks originated throughout the length in Girder C2 than in Girder C3. Figure 6-13 shows both Girder C2 and Girder C3 after the flexural tests. An increased number of cracks in Girder C2 contributed to the reduction in the girder's stiffness due to the use of GFRP rebar.



Figure 6-13 Crack patterns at ultimate load for Girder C2 and Girder C3

Girder B2 and Girder C2 had the same longitudinal reinforcement (HSSS strands) and same transverse reinforcement (GFRP rebars), but different prestressing reinforcement ratio. The

prestressing reinforcement ratio in Girder C2 was approximately 18.2% greater than that for Girder B2. Both girders failed at approximately the same deflection as shown in Figure 6-12. However, the ultimate capacity of Girder C2 was approximately 17.5% higher than that of Girder B2.

6.2.4.3 Failure mode

The failure mode of a prestressed concrete member depends on the type and ratio of prestressing and on the concrete compressive strength. The desired failure mode for concrete members prestressed with carbon steel strands is yielding of the prestressing strands followed by crushing of concrete. Because HSSS strands have low ductility, rupture of strands is another possible failure mode when they are used in flexural members.

All non-composite girders failed by crushing of concrete. Figure 6-14 shows Girder B3 after failure. At failure load, concrete crushed in the compression zone, but to check the integrity of the HSSS strands, the concrete in the bottom flange was removed as shown in Figure 6-14. Adding a deck-slab to the AASHTO Type II girder resulted in a decrease in the prestressing reinforcement ratio; all composite girders prestressed with HSSS strands failed by rupture of all strands. Figure 6-15 shows Girder B2 after failure, where all HSSS strands in the bottom flange broke while the concrete at the top face was still intact. Ductility is a significant measure of the performance of prestressed concrete members. One way to measure ductility is deformation. The deformations can be expressed in terms of strain, deflections, or curvatures. Rupture of strands might be considered as brittle failure; however, all HSSS composite girders failed at a large deflection, as shown in Figure 6-15, with many flexural cracks in the mid-span region. Therefore, regardless of failure mode, the girders prestressed with HSSS strands can achieve ultimate capacity and deformability as high as girders prestressed with carbon steel strands. In conclusion, design of prestressed concrete I-girders with HSSS strands to fail by rupturing of strands is a viable design option, if not the best option, among other failure modes.

6.3 Second set of girders

6.3.1 Test setup

All five 42-ft-long girders were tested in flexure under a four-point bending setup over an effective span of 40 ft as shown in Figure 6-16. A two-point loading frame was used to transfer the load from actuator to beam; each point load was located 3 ft from midspan. Steel-reinforced neoprene bearing pads were installed at loading points and supports.



Figure 6-14 Crushing of concrete failure mode (Girder B3)



Figure 6-15 Rupture of strands failure mode (Girder B2)



Figure 6-16 Loading scheme

6.3.2 Test instrumentation

Each girder was instrumented with strain, deflection, and shaft gages as shown in Figure 6-17. Strain gages were installed at these locations: six at the top fiber of the slab in the constant moment region, two at mid span, and two at 12 in. from mid span on each side. Three sets of two strain gages were installed along the depth of the section at mid span at 4 in., 11 in., and 20 in. from the top fiber of the slab. Twelve laser deflection gauges were installed along the entire length of the specimens: two gages at mid span, two gages at 36 in. from mid span on each side, one gage at each support, and one gage at 68 in. and 136 in. from the support on both sides. Shaft gages were used to monitor slip of the bottom layer of prestressing strands.

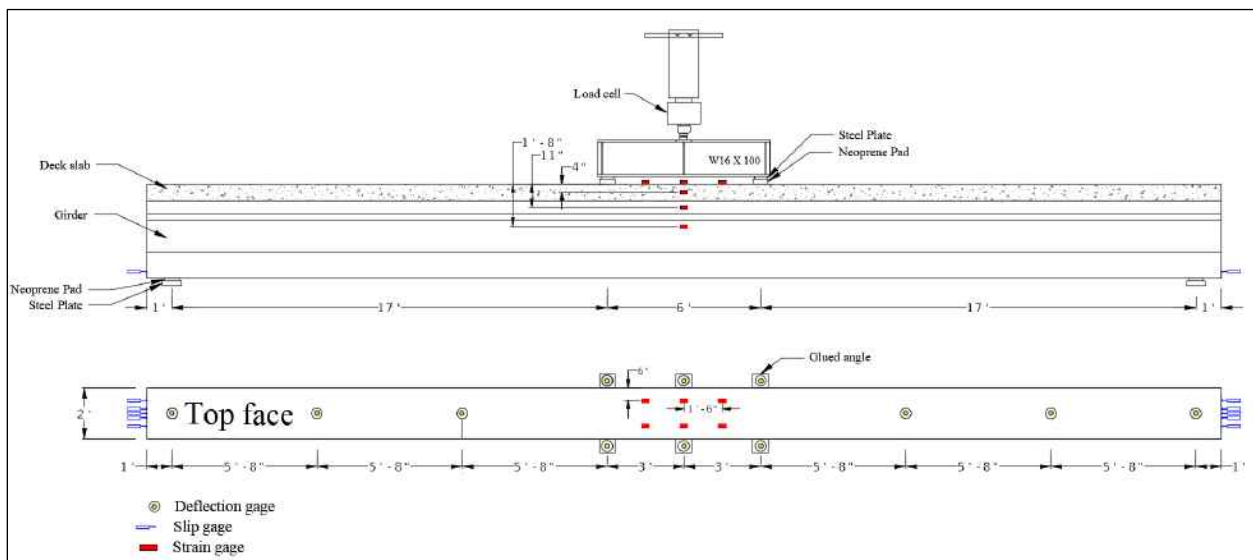


Figure 6-17 Test instrumentation of composite girders (second set)

6.3.3 Prestress losses

The prestress losses in the HSSS strands were evaluated using two different estimation procedures.

The first method to determine the stress losses in HSSS strands was using VWSGs. Each girder contained at least one VWSG attached to the bottom layer of strands at mid span as shown in Figure 6-18. Reference readings (strain measurements and internal temperature of concrete) were taken immediately before releasing the strands. Subsequent readings were taken immediately after releasing the strands and before flexural testing of the girders. The procedure to determine the stress losses from VWSGs is explained previously in this report in Section 6.2.3. The final losses in the HSSS strands before the flexural tests included losses measured by VWSGs and stress-relaxation losses estimated by AASHTO Section 5.9.3.3. The estimated stress-relaxation loss was added twice; the first time after releasing the strands and the second time after adding the deck slab. Table 6-2 shows the total prestress losses and effective prestress in the HSSS strands. The age in Table 6-2 indicates the number of days from release to flexural testing day. The averaged-measured prestress losses using VWSGs (not including losses due to relaxation of strands) was 16.2 ksi, 14.0 ksi, and 10.7 ksi for girders prestressed with 11, 9, and 7 HSSS strands, respectively. Figure 6-19 presents the percentage of total prestress losses in HSSS strands where the initial stress was 156.5 ksi. The measured prestress losses increased when the initial total prestressing force increased. The maximum measured total prestress losses in HSSS strands was 12.1% of the initial stress. The effective prestress losses in HSSS strands before the flexural test is given in Table 6-2.



Figure 6-18 VWSGs attached to the bottom layer of HSSS strands in Girder E1

Table 6-2 Prestress losses of HSSS strands using VWSGs

Specimen ID	VWSG ID	Age (days)	Initial stress (ksi)	Prestress losses (ksi)			Effective stress (ksi)	Effective / jacking stresses
				VWSGs	Stress relaxation	Total		
Girder E1	VW1	110	156.5	16.5	2.4	18.9	137.6	87.9%
Girder E2	VW7	113		15.5		17.9	138.6	88.6%
	VW8			16.2		18.6	138.0	88.2%
Girder E3	VW2	125		15.2		17.6	139.0	88.8%
Girder E4	VW5	120		13.2		15.6	141.0	90.1%
	VW6			12.4		14.8	141.8	90.6%
Girder E5	VW3	133		10.1		12.5	144.1	92.1%
	VW4			11.3		13.7	142.8	91.2%

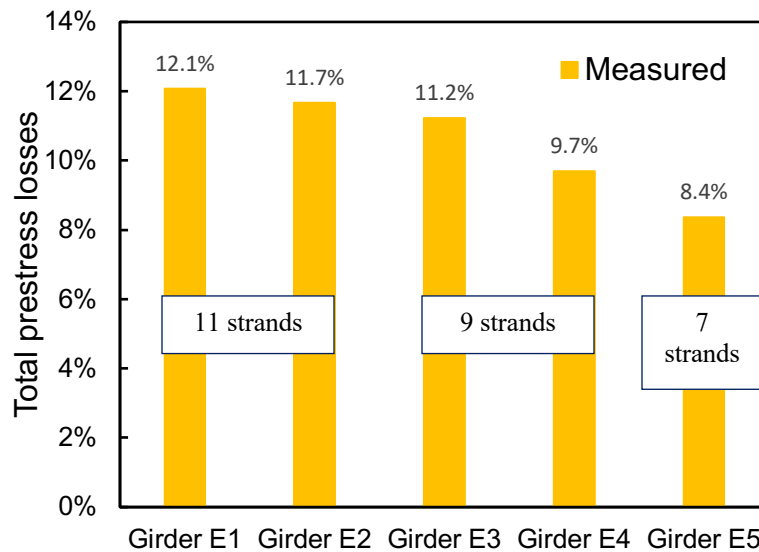


Figure 6-19 Measured prestress losses of HSSS strands in second set of girders

The second method to determine the total prestress losses in the HSSS strands was the decompression method (Pessiki et al. 1996). Note that this method requires loading the member beyond cracking, therefore, it cannot be used in the field. This method was used to validate results obtained by VWSGs. The girder was loaded until the first flexural crack formed in the constant moment region. Once a flexural crack was seen, the load was halted to mark the crack and identify its location as shown in Figure 6-20a. Then, the girder was unloaded, and the marked flexural crack closed, as shown in Figure 6-20b, due to the effect of the prestressing force. Two sets of two

strain gages were placed on opposite sides of the crack as shown Figure 6-20b. The girder was loaded again, and data was collected. The concrete strains on opposite sides of the crack increased linearly until a certain load level at which the strain reached a plateau as shown in Figure 6-21. The change in slope on the load-strain curve indicates that all the precompression in the tension zone, due to effect of the prestress force, has been overcome. Therefore, the decompression load is defined as the load when the strain no longer increases with applied load. At the decompression load, the stress at the bottom fiber of the girder is assumed to be zero. The decompression load for each beam is given in Table 6-3. To calculate the effective prestress, the tensile stresses induced by the dead and decompression load shall be equal to the compression stresses induced by the prestressing force and eccentricity. Table 6-3 provides the total prestress losses and effective prestress on the day of testing for each girder.

The prestress losses evaluation using VWSGs was more consistent than that using the decompression method. Note that the decompression method requires some subjectivity in determining the decompression load. In this research, the preferred method of measuring prestress losses was VWSGs, and the values obtained were used for further analysis.

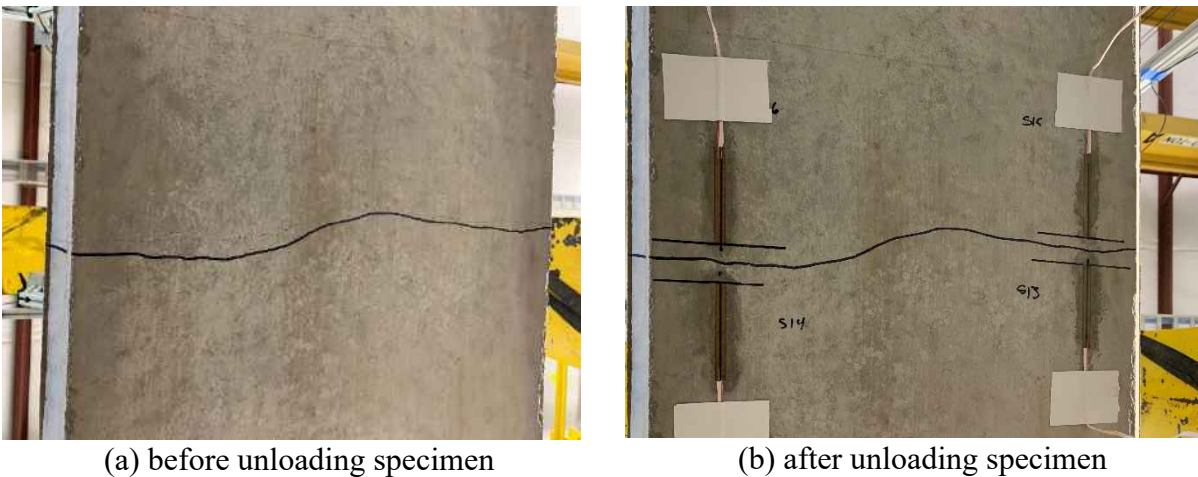


Figure 6-20 First flexural crack

Measured prestress losses using VWSGs were compared with values obtained by the AASHTO approximate method as shown in Table 6-4. VWSGs readings immediately after releasing the strands (before casting the deck slab) were used to determine the stress losses caused by elastic shortening. Both estimated / measured elastic shortening losses and estimated / measured total losses are presented in Figure 6-22. The estimated total prestress losses by AASHTO

approximate method were found to be on average 25.3% greater than the measured values, Table 6-4. In other words, AASHTO approximate method was conservative in predicting the prestress losses of 0.6-in.-diameter HSSS strands. As mentioned previously, the prestress loss estimation of HSSS strands was not the main objective of this work. Therefore, a more detailed study is recommended to determine the total prestress loss estimation of both HSSS strand sizes and determine the applicability of AASHTO equations to predict the prestress losses for HSSS strands.

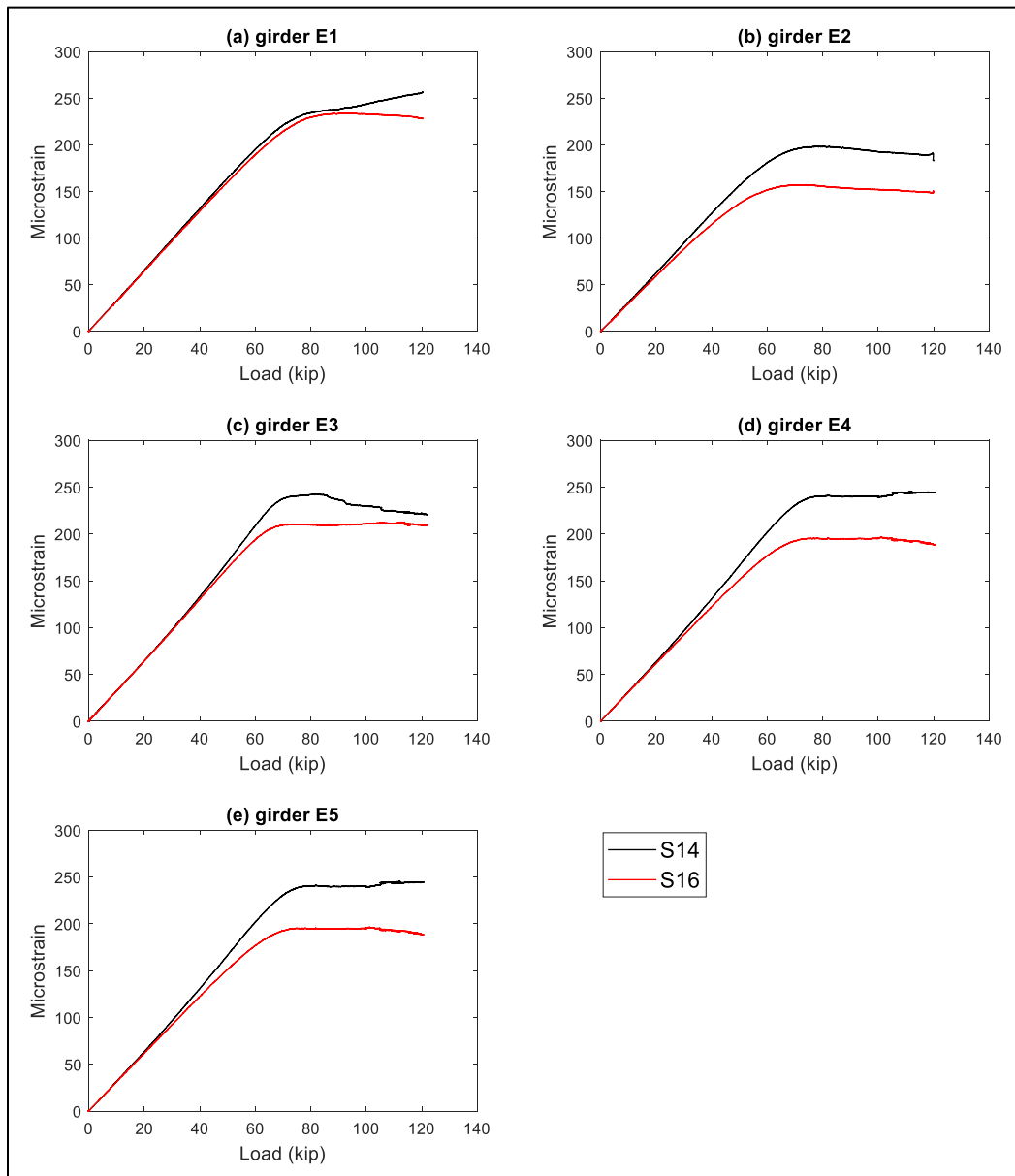


Figure 6-21 Load-strain relationship for decompression method (gages S14 and S16 were installed on opposite sides of the crack)

Table 6-3 Prestress losses of HSSS strands using decompression method

Specimen	Jacking stress (ksi)	Average decompression load (kip)	Total losses (ksi)	Effective prestress (ksi)	Effective / jacking stresses
Beam E1	156.5	85	19.9	136.7	87.3%
Beam E2		70	26.7	129.8	83.0%
Beam E3		70	26.2	130.3	83.2%
Beam E4		74	28.0	128.6	82.1%
Beam E5		58	22.3	137.2	85.7%

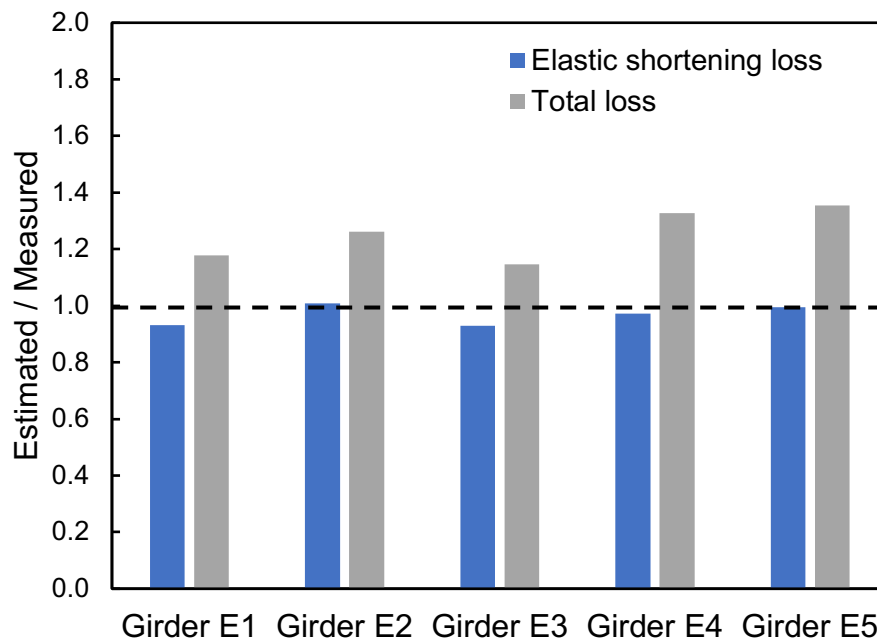


Figure 6-22 Estimated / measured elastic shortening and total prestress losses

Table 6-4 Comparison of prestress losses

Specimen	VWSGs (ksi)	Decompression method (ksi)	AASHTO LRFD (ksi)	AASHTO LRFD	AASHTO LRFD
				VWSGs	Decompression method
Girder E1	18.9	19.9	22.2	1.178	1.116
Girder E2	18.3	26.7	23.0	1.262	0.861
Girder E3	17.6	26.2	20.1	1.146	0.767
Girder E4	15.2	28.0	20.1	1.327	0.718
Girder E5	13.1	22.3	17.7	1.354	0.794

6.3.4 Experimental results

The mid span load-deflection curves of all five girders are shown in Figure 6-23. The flexural behavior of any prestressed concrete girders can be divided into two regions, separated by the formation of the first flexural crack. All girders behaved linearly up to the formation of the first flexural crack. The cracking load was determined by visual observation of the specimen while loading. Once a crack was observed, the load was halted and documented, and the crack was marked. The cracking load increased when the girders had a higher reinforcement ratio. After initiation of the first flexural crack, all girders behaved nonlinearly up to failure. The post-cracking behavior continued to increase up to failure with no discernible plateau. This response is attributed to the stress-strain behavior of HSSS strands. Analysis of this phenomenon revealed that the flexural behavior of a member prestressed with HSSS strands is fundamentally different than when prestressed with carbon steel strands.

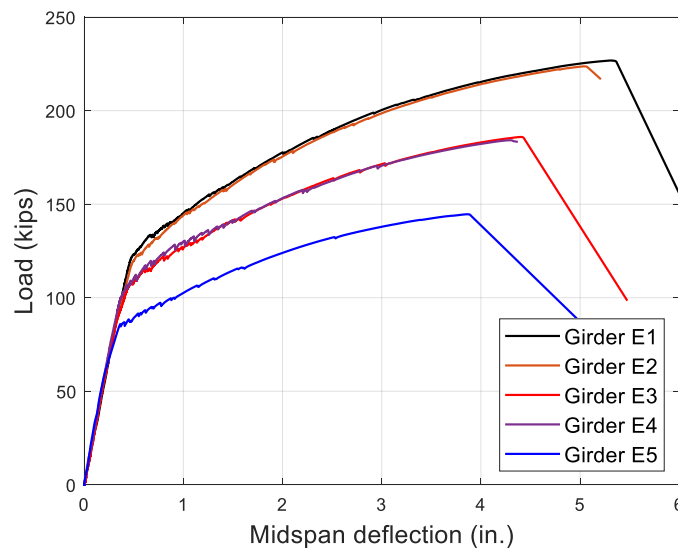


Figure 6-23 Load-midspan deflection relationship for second set of girders

In general, all five girders had similar stiffness before cracking. However, after cracking, the stiffness of all girders decreased, and the reduced stiffness was maintained. Flexural cracks were initiated in the beginning of the inelastic stage. Initially, flexural cracks occurred in the constant moment region (between loading points). Further increase in load resulted in the formation of several cracks beyond the constant moment region. After failure of each girder, the flexural cracks along the girder were mapped, Figure 6-24. All girders exhibited well-distributed flexural cracking before failure. The crack spacing was larger for specimens with a lower reinforcement ratio. More

cracks extended beyond the constant moment region as the reinforcement ratio increased; those girders exhibited higher curvatures and failed at large loads and deflections. Even though all girders failed by rupturing of all the HSSS strands, they exhibited adequate warning before failure by achieving large deflection and exhibiting many flexural cracks. The bottom layer of HSSS strands was instrumented with shaft gages to monitor slippage. Slippage of strands was nonexistent in all of the specimens.

The load-deflection relationship is dependent on the reinforcement ratio. Note that the reinforcement ratio refers here to the total area of HSSS prestressing strands divided by bd , where the width of the deck slab (b) was 24 in., and the depth from the top fiber to the bottom layer of strands (d) was 41 in. The reinforcement ratio of the first set (Girder E1 and Girder E2), second set (Girder E3 and Girder E4), and third set (Girder E5) was 0.257%, 0.210%, and 0.164%, respectively. As the reinforcement ratio increased, larger cracking load and ultimate load were obtained, as shown in Table 6-5.

The largest capacity and deflection at failure were recorded for Girders E1 and E2, which had the highest reinforcement ratio. Conversely, the smallest capacity and deflection at failure were recorded for Girder E5, which had the lowest reinforcement ratio. When the reinforcement ratio increased by 22.2%, 28.6% and 57.1%, the cracking load increased by 19.1%, 23.1% and 46.6%, and the failure load increased by 21.7%, 28.0% and 55.8%, respectively. Experimental results showed a linear correlation between reinforcement ratio and cracking and ultimate loads as shown in Figure 6-25. However, the effect of an increased reinforcement ratio is more pronounced on the ultimate capacity, where the increase in slope is larger for failure load compared to that for cracking load.

Girders prestressed with a higher reinforcement ratio achieved larger deflections at cracking and ultimate loads as shown in Figure 6-26.

The behavior of the five girders was studied at service level and at ultimate level. The following sections include a discussion and comparison of the experimental results.



(a) Girder E1



(b) Girder E2



(c) Girder E3



(d) Girder E4



(e) Girder E5

Figure 6-24 Tested girders at failure (second set of girders)

Table 6-5 Flexural test results of second set of girders

Events	Service load (68.1 kips)		Cracking load		Failure load	
	Load (kips)	Deflection (in)	Load (kips)	Deflection (in)	Load (kips)	Deflection (in)
Girder E1	68.10	0.219	118.19	0.416	226.82	5.282
Girder E2	68.10	0.224	117.56	0.408	223.67	4.972
Girder E3	68.10	0.207	100.30	0.334	185.94	4.342
Girder E4	68.10	0.218	97.58	0.315	184.18	4.239
Girder E5	68.10	0.222	80.40	0.270	144.60	3.823

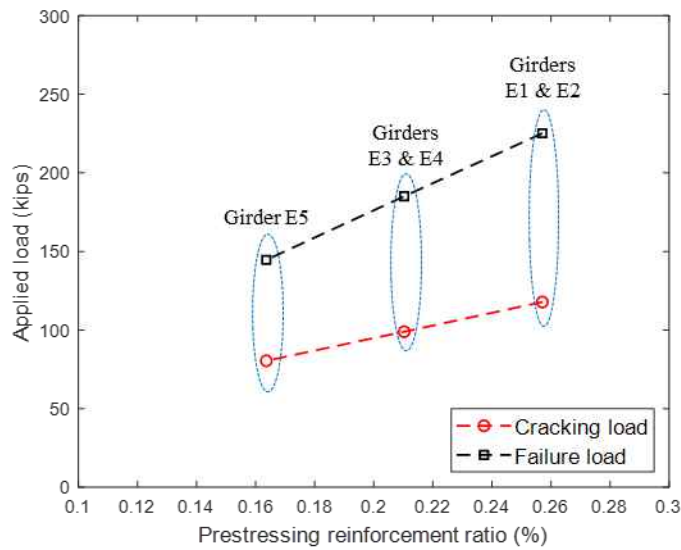


Figure 6-25 Reinforcement ratio vs. cracking and ultimate loads

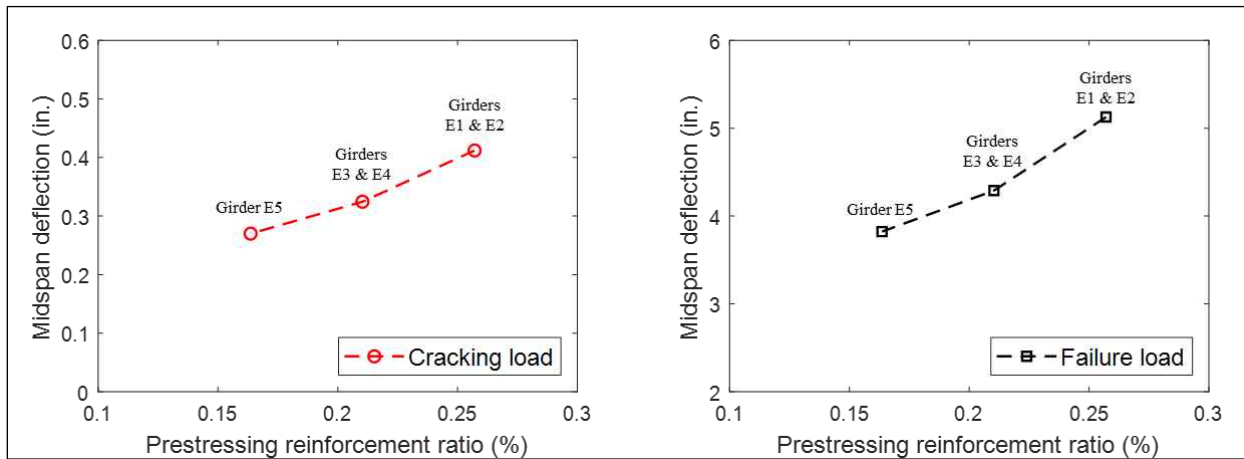


Figure 6-26 Reinforcement ratio vs. deflection at cracking and ultimate loads

6.3.4.1 Service behavior of girders

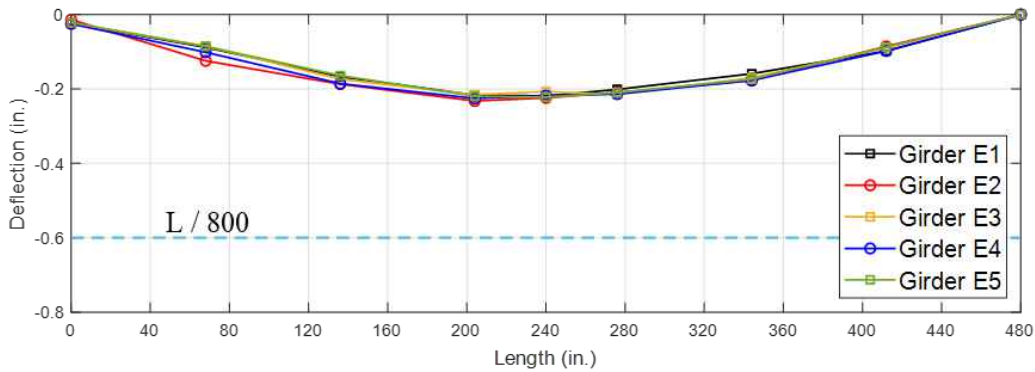
All five girders were designed as a fully prestressed section; thus, under service load moment, they should remain free from cracks, and their deflections should be the same. The service load for deflection control was 701 kip-ft, which was calculated based on maximum dead load and live load moments induced on the bridge prototype described in Section 4.3.1. This 701 kip-ft service load moment is achieved by applying a 68.1-kip load to the test setup in this study. Note that the deck slab width was reduced from 6 ft to 2 ft for the specimens used in this study; therefore, the calculated service load is overestimated (conservative). According to AASHTO LRFD Bridge Design Specifications (AASHTO 2.5.2.6), the allowable maximum vehicular load deflection is defined as the length of the span divided by 800, which equals 0.6 in. in this study (2017). Figure 6-27a shows the deflections along the length of girders under service load. The midspan deflection at 68.1 kips is given in Table 6-5. The midspan deflection was 36.5%, 37.3%, 34.5%, 36.3%, and 37.0% of the allowable deflection for Girders E1-E5, respectively.

Experimental results showed that the cracking moment of all girders was greater than the service load moment (701 kip-ft). From a serviceability point of view, the prestressed concrete girder is in the serviceability region if it is not cracked; the serviceability region finishes with the initiation of the first flexural crack. Therefore, in this study, the cracking load was treated as service load, and deflection at that load was compared with the allowable deflection specified by AASHTO LRFD. The first flexural crack was observed at moments (including effect of self-weight) equal to 1127.2, 1122.9, 975.2, 952.0 and 806.0 kip-ft for Girders E1-E5, respectively. Figure 6-27b shows the deflections along the length of the girders under cracking load. The mid span deflections at cracking loads are given in Table 6-5, which were lower than the allowable amount. The mid span deflection was 69.3%, 67.9%, 55.7%, 52.5%, and 45.0% of the allowable deflection for Girders E1-E5, respectively.

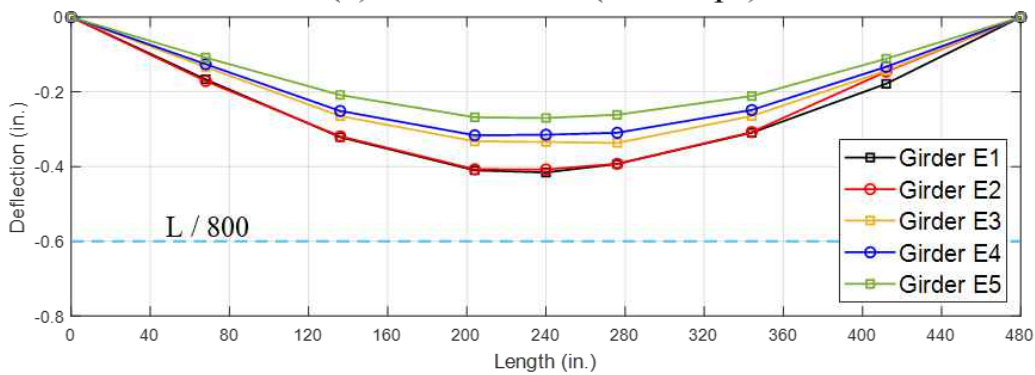
6.3.4.1 Ultimate behavior of girders

The required moment for strength design was 1470 kip-ft, which was calculated based on maximum dead load and live load moments induced on the bridge prototype described in Section 4.3.1. Note that the required moment was governed by the AASHTO LRFD minimum reinforcement requirements (2017). Because all five girders failed due to rupture of strands, a strength reduction factor of 0.75 was used in the calculation of flexural strength of the tested girders. The experimental ultimate moment strength (including moment due to self-weight) was

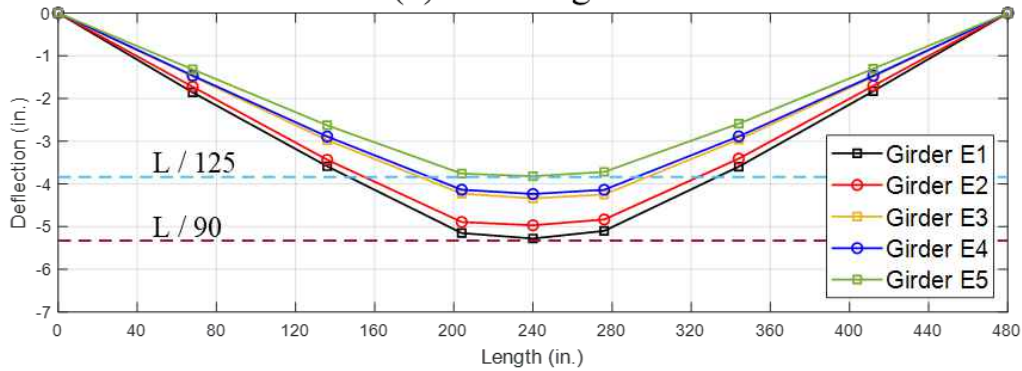
2051, 2024, 1703, 1688 and 1352 kip-ft for Girders E1-E5, respectively. Applying the strength resistance factor, the experimental flexural strength was 1538, 1518, 1277, 1266 and 1014 kip-ft for Girders E1-E5, respectively.



(a) Service load (68.1 kips)



(b) Cracking load



(c) Ultimate load

Figure 6-27 Deflection along length of the specimen

Note that the deck slab width was reduced from 6 ft in the bridge prototype to 2 ft for the specimens used in this study. Even though the slab width was reduced by 4 ft, Girders E1 and E2

had higher flexural strength than required for the original section. Note that both the original section and Girders E1 and E2 had the same number of strands, 11. The increase in the experimental flexural strength of the tested girders is attributed to two factors. First, the mechanical properties of the HSSS strands used in the tested girders were larger than those mechanical properties specified by ASTM A1114, which were used to design the original section. Second, the concrete compressive strength for the deck slab was approximately 44% greater than the specified one. Even though HSSS strands have low ductility, the girders exhibited large deflection at failure. All tested girders had an ultimate deflection in the range of $L/125$ to $L/90$; the denominator value decreases as the reinforcement ratio increases. Figure 6-27c shows the deflections along the length of the girders under ultimate load.

In this study, all five girders were designed to fail by rupturing the HSSS strands and to ensure that the concrete in the compression zone reaches considerable inelastic stresses. Concrete top fiber compressive strain was monitored during the tests by six strain gages in the constant moment region. The concrete compressive strain at the extreme fiber was expected to be less than 3000 microstrain because all five girders were designed to fail by rupturing of strands. The concrete at the top fiber exhibited inelastic stresses before failure of all five girders, and the strain at failure was 2430, 2216, 1926, 1883, and 1516 microstrain for Girders E1-E5, respectively (Figure 6-28).

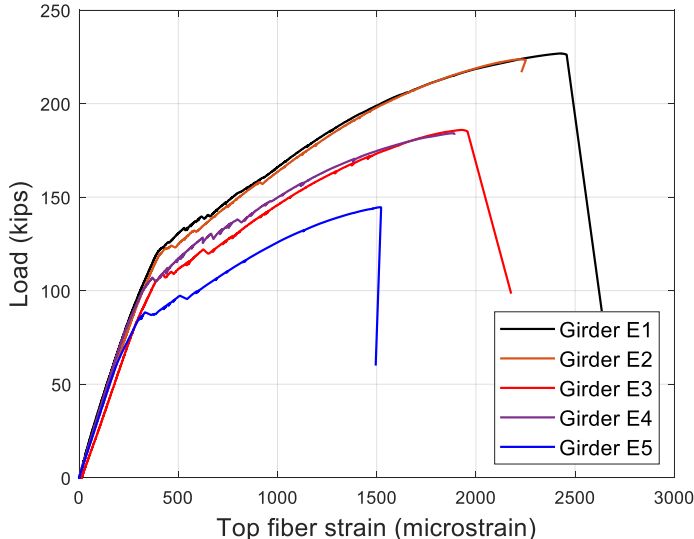


Figure 6-28 Load-top fiber strain relationship for second set of girders

6.3.4.2 Failure mode

The failure mode of concrete members prestressed with HSSS strands depends primarily on the longitudinal prestressing ratio and secondarily on the concrete compressive strength. Balanced reinforcement ratio distinguishes between rupture of strand and crushing of concrete failure modes. All five girders had a reinforcement ratio less than the balanced reinforcement ratio, which anticipated a rupture of strands failure. The failure of all five girders occurred due to rupture of HSSS strands while the concrete at the compression zone was still intact as shown in Figure 6-24. Although rupture of prestressing strand is less desirable, the tested girders provided adequate warning before failure, where many cracks formed in the mid span region as shown in Figure 6-24.

In cases where HSSS strands are used as the primary longitudinal strands in prestressed I-girders, crushing of concrete failure mode may result in high deformability and strength compared to the same I-girder designed to fail due to rupture of strands. However, crushing of concrete failure mode is less economical compared to rupture of strands failure mode because more strands would be needed to achieve crushing of concrete failure mode. In this study, all five girders failed due to rupture of strand; two of them (Girders E1 and E2) satisfied all the limit states. Therefore, the increase in deformability and strength between rupture of strand failure mode and crushing of concrete failure mode is not needed. In conclusion, based on the experimental results and observations of girders at failure, rupture of HSSS strands is the recommended failure mode in the design of pretensioned concrete I-girders utilizing HSSS strands.

6.3.4.3 Ductility

Ductility is defined as the ability of the member to sustain inelastic deformation before failure. Deformation can be expressed in terms of deflection, strain, or curvature. Deflection at mid span was measured during testing. Ductility was calculated based on the ratios of deflection at failure load to the corresponding value at cracking load. The mid span deflection at failure for Girders E1-E5 was 12.7, 12.2, 13.0, 13.5, 14.2 times deflection at cracking, respectively. The spread between the cracking load and failure load can also be used as a measure for ductility. The larger the spread, the more ductile the member. The failure load for Girders E1-E5 was 1.92, 1.90, 1.85, 1.89, 1.80 times the cracking load, respectively.

6.4 Summary

Twelve full-scale 42-ft-long AASHTO Type II girders were tested in flexure. Ten girders were prestressed with 0.6-in.-diameter HSSS strands, and two girders were prestressed with 0.6-in.-

diameter carbon steel strands. Based on the results obtained from this experimental program, the following conclusions are drawn.

1. Both girders prestressed with HSSS and carbon steel strands exhibited linear behavior up to the initiation of the first crack. The post-cracking behavior of girders prestressed with HSSS strands continued to increase up to failure with no discernible plateau, which is different compared to girders prestressed with carbon steel strands. The differences in the post-cracking behavior are attributed to the differences in mechanical properties between the two strands.
2. The flexural stiffness was higher for the girder prestressed with HSSS strands compared to the girder prestressed with carbon steel strands (control) when both girders had the same initial prestressing force. The flexural strength of the non-composite and composite girders prestressed with HSSS strands was approximately 11.7% and 23.7% higher, respectively, than girders prestressed with carbon steel strands. This increase is attributed to the increase in the reinforcement ratio in the HSSS girders.
3. The flexural strength of the girder prestressed with HSSS strands was increased by 17.5% when the reinforcement ratio was increased by 18.2%, which is equivalent to the increase in the initial prestressing force.
4. The flexural strength of the girder decreased approximately 15% when the shear reinforcement was replaced on a one-to-one basis from stainless steel rebar to GFRP rebar.
5. Under the service limit state, the mid span deflection at cracking loads for all composite girders prestressed with HSSS strands were lower than the allowable deflection specified by AASHTO LRFD Bridge Design Specifications (AASHTO 2.5.2.6).
6. At ultimate load, all composite girders prestressed with HSSS strands had ultimate deflection ranging from $L/125$ to $L/84$; the denominator value decreases as the reinforcement ratio increases.
7. Rupture of the HSSS strands controlled the flexural behavior of all composite girders prestressed with HSSS strands. The girders exhibited large deflection and many flexural cracks at failure. Regardless of failure mode, girders prestressed with HSSS strands can achieve ultimate capacity and deformability as high as those prestressed with carbon steel strands. Therefore, based on these experimental results, the

recommended failure mode of I-girders prestressed with HSSS strands is rupture of strand.

8. The measured prestress loss for carbon steel and HSSS strands was 10.5% and 13.0%, respectively, of the initial stress. Therefore, it can be concluded that HSSS strands exhibited greater prestress losses than carbon steel strands.
9. The AASHTO LRFD approximate method conservatively estimated prestress losses of HSSS strands, on average 25.3% greater than the measured values. Until further studies, AASHTO equations can be used to estimate the prestresses losses of HSSS strands.

CHAPTER 7 PREDICTION OF EXPERIMENTAL FLEXURAL RESULTS

7.1 Introduction

This chapter provides an overview of the developed analytical and iterative numerical models. The experimental flexural strengths were compared with values obtained using the developed analytical model, modified AASHTO LRFD equations, and developed iterative numerical model.

Experimental results from composite Girders A3, C3, and E1-E5 were included in the comparison in this chapter because their flexural behaviors were not influenced by other parameters.

7.2 Analytical model

A nonlinear iterative sectional analysis model was developed to determine the moment-curvature relationship for any prestressed concrete section. These basic assumptions were considered in developing the model:

1. plane sections remain plane after bending;
2. bond slip between HSSS strands and concrete is assumed to be negligible; and
3. failure of the flexural member takes place when the concrete strain reaches a crushing strain of 0.003 or the HSSS strands reach their ultimate strain (Table 3-5).

To develop the moment-curvature relationship, it is necessary to use good approximations for the stress-strain models of concrete and prestressing strands. Concrete in compression was modeled following (Collins and Mitchell 1991), which is given in Equations 7-1 through 7-5.

$$f_c = \left(\frac{n (\varepsilon_{cf}/\varepsilon'_c)}{n-1+(\varepsilon_{cf}/\varepsilon'_c)^{nk}} \right) f'_c \quad \text{Equation 7-1}$$

$$\varepsilon'_c = \frac{f'_c}{E_c} \frac{n}{n-1} \quad \text{Equation 7-2}$$

$$k = \begin{cases} 1 & \text{if } \varepsilon_{cf} < \varepsilon'_c \\ 0.67 + \frac{f'_c}{9000} & \text{if } \varepsilon_{cf} \geq \varepsilon'_c \end{cases} \quad \text{Equation 7-3}$$

$$n = 0.8 + \frac{f'_c}{2500} \quad \text{Equation 7-4}$$

$$E_c = 40,000\sqrt{f'_c} + 1,000,000 \quad \text{Equation 7-5}$$

where ε_{cf} is concrete compressive strain; f_c is concrete compressive strength at ε_{cf} (psi); f'_c is concrete compressive strength (psi); ε'_c is strain corresponding to compressive stress; k and n are factors; and E_c is the elastic modulus of concrete (psi). Concrete in tension was modeled following (Belarbi and Hsu 1994), which is given in Equations 7-6 through 7-8.

$$f_t = \begin{cases} E_c \varepsilon_t & \text{if } \varepsilon_t \leq \varepsilon_{cr} \\ f_{cr} \left(\frac{\varepsilon_{cr}}{\varepsilon_t} \right)^{0.4} & \text{if } \varepsilon_t > \varepsilon_{cr} \end{cases} \quad \text{Equation 7-6}$$

$$\varepsilon_{cr} = \frac{f_{cr}}{E_c} \quad \text{Equation 7-7}$$

$$f_{cr} = 4\sqrt{f'_c} \quad \text{Equation 7-8}$$

where ε_t is concrete tensile strain; f_t is concrete tensile stress at ε_t (psi); ε_{cr} is cracking strain of concrete in tension; and f_{cr} is cracking stress of concrete in tension (psi). Once the moment-curvature function was created, the moment-area method was used to generate the load-deflection curve.

A brief description of the iterative model to generate the moment-curvature for the section is as follows:

1. the section was divided into 0.25-in.-thick layers;
2. the top fiber strain was selected, and the neutral axis location was assumed randomly;
3. the strain in each layer was calculated based on linear strain distribution;
4. the stress in each layer was calculated from the strain using the stress-strain models of the concrete and HSSS strands;
5. the neutral axis depth was solved by iterating steps 2 through 4 until force equilibrium was achieved; and
6. the curvature of the section was calculated using selected top fiber strain (step 2) and the calculated neutral axis depth (step 5), and the corresponding bending moment was determined by summing forces about any point along the depth of the section; and
7. the iteration was terminated if the concrete and/or HSSS strands reach their ultimate strain, otherwise go to step (2) and increase the top fiber strain for the next iteration.

7.2.1 Validation of analytical model

The analytical model was validated by comparing it to the results from the experimental programs.

7.2.1.1 First set of girders

The analytical flexural strength for Girder A3 was calculated using the stress-strain equation for carbon steel strands given in PCI Design Handbook (2010), concrete compressive strength on testing day given in Table 4-6, and measured prestress losses given in Figure 6-9. Figure 7-1 shows the experimental and calculated load-deflection relationships at mid span for Girder A3. Note that

Girder A3 was loaded up to 231.4 kips, until the load-deflection curve plateaued, which indicated that the carbon steel strands yielded. Analytical calculations indicated that the strains in the bottom layer of strands at 231.4 kips and at failure load were 1.86% (greater than yield strain of 1.0%) and 2.82% (lower than the minimum specified ultimate strain of 3.5% by ASTM A416), respectively. Six strain gages were installed on the top fiber of the slab in the constant moment region. The measured concrete top fiber strain at 231.4 kips was 2064 microstrain as shown in Figure 7-2; the analytical concrete top fiber strain was 2000 microstrain. Analytical results revealed that if Girder A3 had been loaded up to failure then it would have failed by crushing of concrete in the compression zone. The predicted failure load and deflection was 232.8 kips and 5.376 in., respectively.

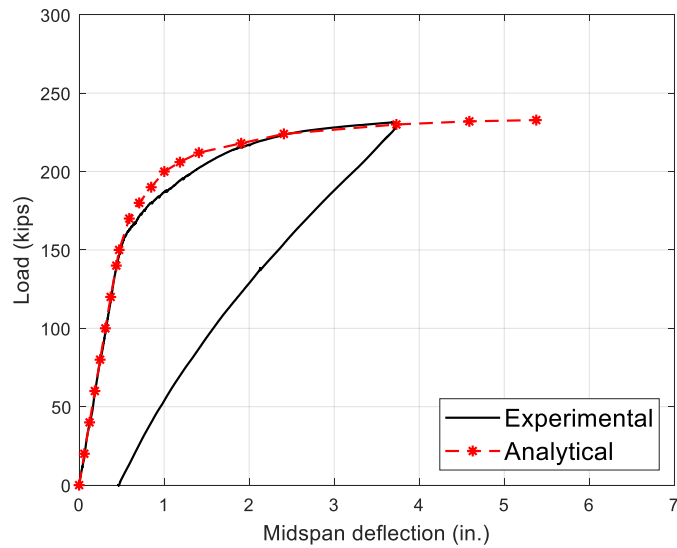


Figure 7-1 Experimental and analytical load-deflection relationships of Girder A3

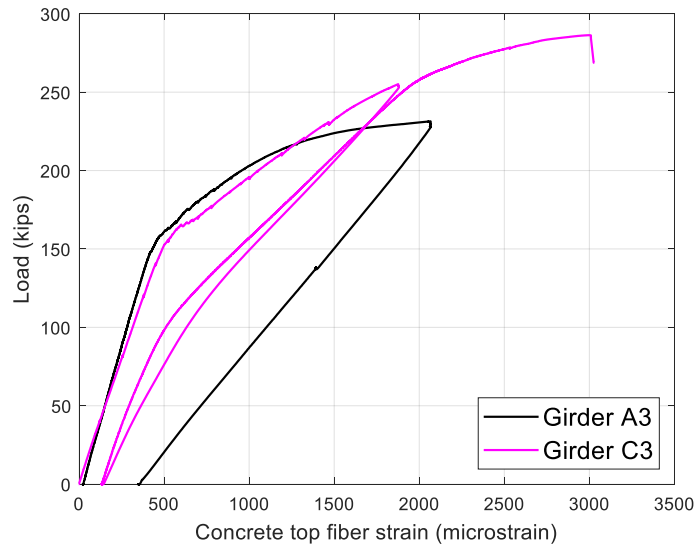


Figure 7-2 Experimental load-concrete top fiber strain relationship for Girders A3 and C3

The analytical moment-curvature relationship for Girder C3 was calculated using the stress-strain model given in Equation 3-1 after substituting coefficients from Table 3-8 and mechanical properties from Table 3-5, concrete compressive strength on testing day given in Table 4-6, and measured prestress losses given in Figure 6-9. The experimental and analytical load-deflection relationships at mid span for Girder C3 is shown in Figure 7-3. The measured concrete top fiber strain at failure load was 3009 microstrain as shown in Figure 7-2. ACI 318-19 assumes the ultimate concrete strain as 3000 microstrain. Even though the measured concrete top fiber strain was slightly higher than the ultimate specified value, Girder C3 failed by rupturing of all HSSS strands. The increase in concrete strain could be attributed to the confinement effect from the bearing pad and reinforcement in the deck slab. The analytical concrete top fiber strain was 2650 microstrain when the bottom layer of HSSS strands reached their ultimate tensile strain. The predicted ultimate load and deflection were 283.4 kips and 5.326 in., which were 99.0% and 93.6% of the experimental ultimate load and deflection, respectively. Figure 7-4 presents the experimental and analytical deflections along the length of Girder C3 at failure load. The analytical results showed good agreement with experimental results.

Analytical results revealed that even though Girder C3 failed by rupturing of all HSSS strands, it performed well in terms of capacity as well as deformability compared to Girder A3. The prestressing reinforcement ratio of Girder C3 was approximately 25.3% higher than that of Girder

A3, which was reflected in the analytical ultimate failure capacity of Girder C3 being 20.4% greater than that of Girder A3.

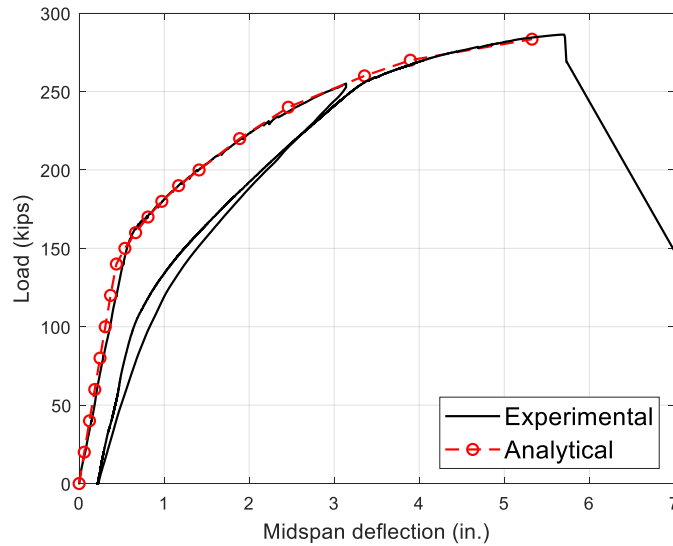


Figure 7-3 Experimental and analytical load-deflection relationships of Girder C3

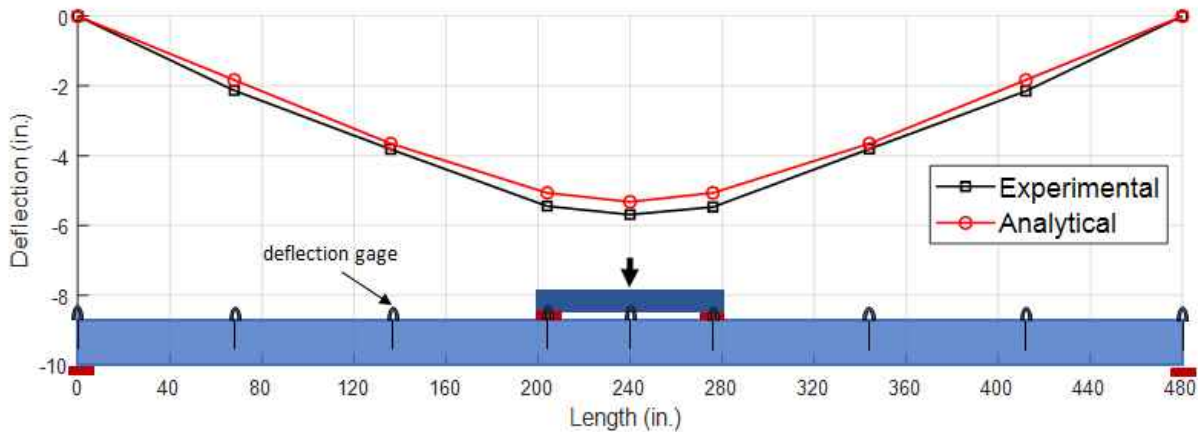


Figure 7-4 Experimental and analytical deflections along Girder C3 at failure load

7.2.1.2 Second set of girders

The measured and predicted load-midspan deflection responses for Girders E1-E5 are compared in Figure 7-5 and are in good agreement. The analysis of Girders E1-E5 predicted a flexural strength of 1990, 1993, 1673, 1672 and 1319 kip-ft, respectively. The predicted flexural strength of Girders E1-E5 was 97.0%, 98.5%, 98.2%, 99.0%, and 97.5%, respectively, of those measured experimentally. The analytical flexural strengths for Girders E1-E5 were calculated using the stress-strain model given in Equation 3-1 after substituting coefficients from Table 3-8, measured elastic modulus from Table 3-5, concrete compressive strength on testing day given in

Table 4-12, and measured prestress losses given in Table 6-2. The analytical model underestimated the deflection at failure for Girders E1 and E2; however, it accurately predicted the deflection at failure for the other girders (Figure 7-5). In addition, the measured and predicted moment-to-top fiber strain for Girders E1-E5 are compared in Figure 7-6 and are in good agreement. The analysis of Girders E1-E5 predicted concrete top fiber strain of 2160, 2110, 1825, 1810, and 1600 microstrain at failure, respectively. The predicted concrete top fiber strains of Girders E1-E5 were 87.9%, 93.7%, 93.8%, 95.8%, and 99.9%, respectively, of those measured experimentally.

Based on the aforementioned discussion, it was concluded that the results of the analytical model were remarkably close to the experimental results.

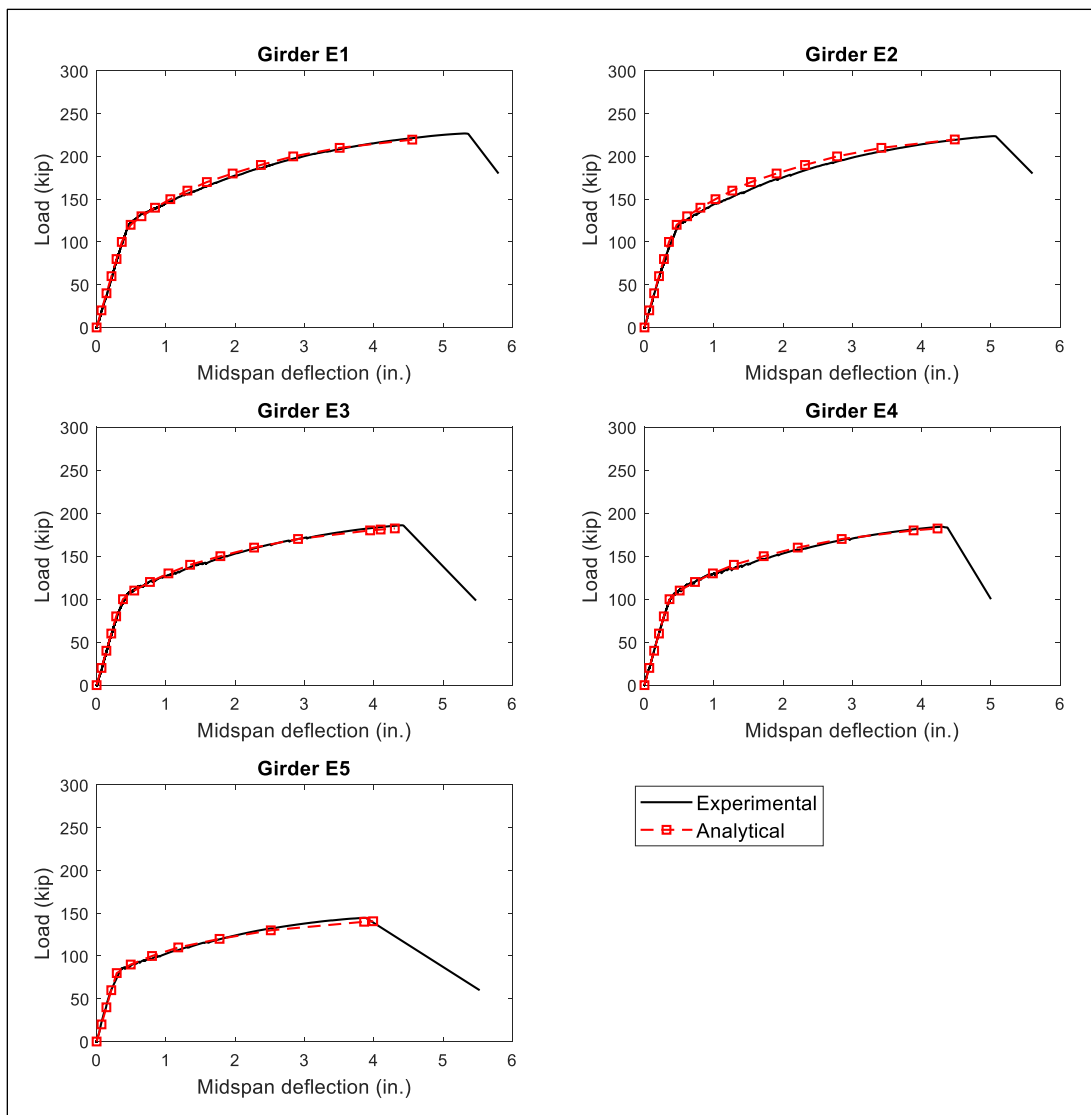


Figure 7-5 Comparison of experimental and analytical load-deflection curves

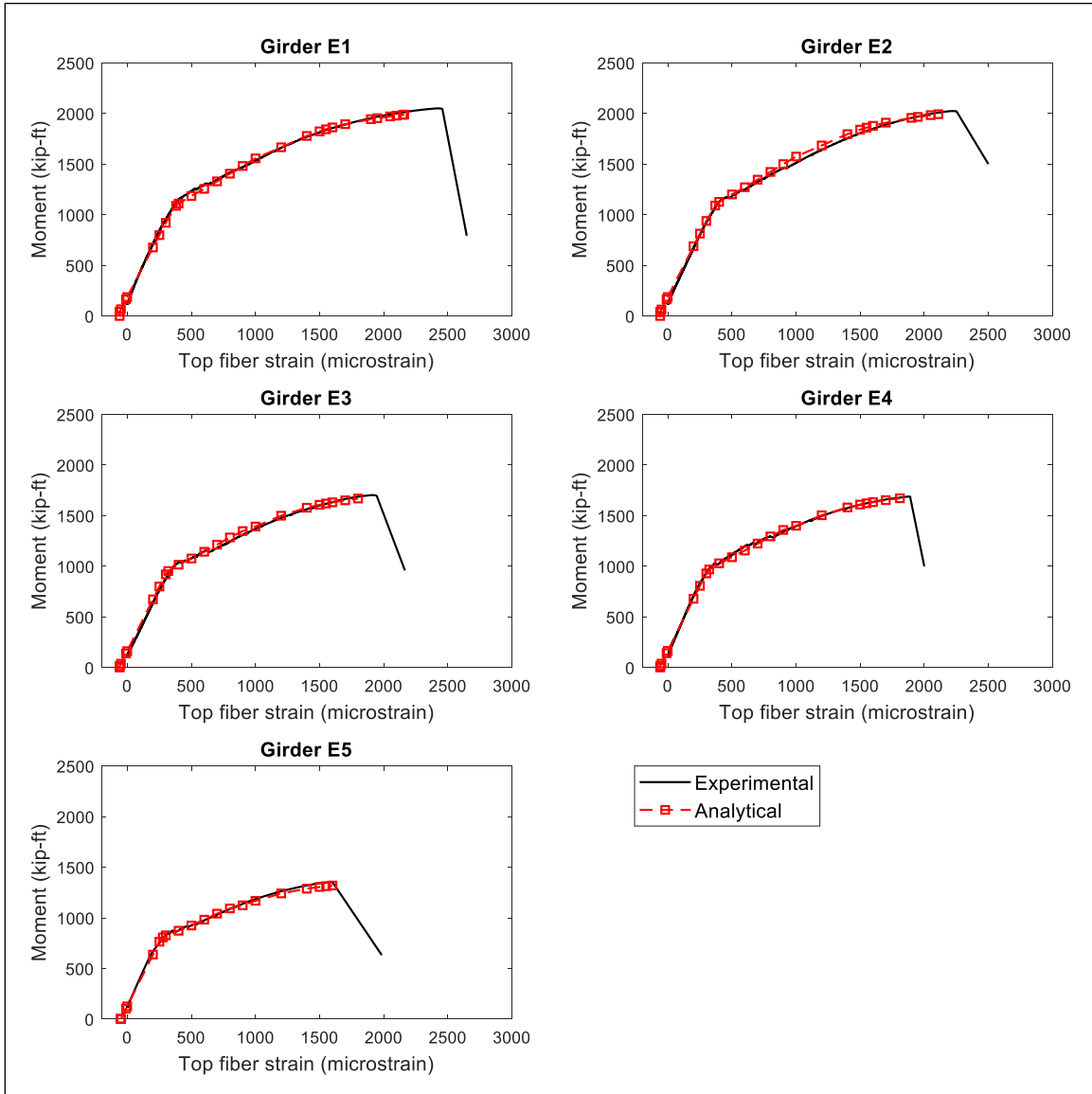


Figure 7-6 Comparison of experimental and analytical moment-top fiber strain curves

7.2.2 Prediction of flexural moment using ASTM A1114 values

The analytical model was validated; therefore, it is reasonable to extend its use to model specimens with different mechanical properties of the stainless steel strands (such as those specified by ASTM A1114).

As mentioned before, the measured mechanical properties of HSSS strands used in the study were greater than those specified by ASTM A1114 (Table 3-5). Note that bridge designers should always use guaranteed mechanical properties of stainless steel strands in the design of stainless steel prestressed concrete members. Utilizing the mechanical properties specified by ASTM A1114, the predicted flexural strength of Girders E1-E5 was 1869, 1873, 1574, 1574, 1247 kip-ft,

respectively—less than the predicted strengths when measured mechanical properties were used, as expected. The predicted flexural strengths of Girders E1-E5 using ASTM A1114 were 91.1%, 92.5%, 92.4%, 93.2%, and 92.2%, respectively, from those measured experimentally. Figure 7-7 presents comparisons between the experimental moment, analytical moment calculated using measured mechanical properties of HSSS strands, and analytical moment calculated using mechanical properties specified by ASTM A1114.

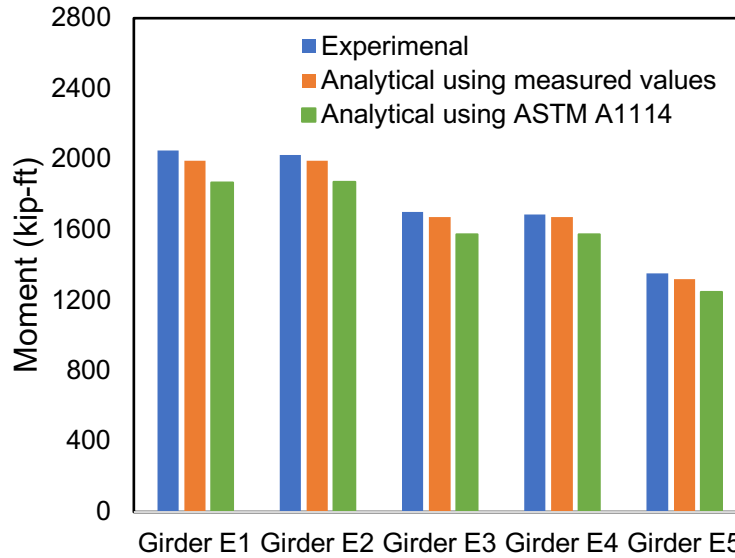


Figure 7-7 Predicted flexural moment using analytical model

7.2.3 Parametric study

The validated analytical model was used to conduct parametric studies to further understand/investigate the flexural behavior of concrete members prestressed with HSSS strands.

7.2.3.1 Effect of mechanical properties of HSSS strands

A parametric study was conducted to investigate the effect of mechanical properties of HSSS strands on behavior and capacity of members. The design variables were prestressing reinforcement ratio and mechanical properties of HSSS strands. The selected reinforcement ratio covered both rupture of strand and crushing of concrete failure modes. Two sets of mechanical properties were used: measured and guaranteed. The selected reinforcement ratio is defined in terms of the balanced reinforcement ratio. The balanced reinforcement ratio (ρ_{ssb}) is a function of concrete compressive strength and mechanical properties of HSSS strands, and it can be calculated using Equation 7-9.

$$\rho_{ssb} = 0.85\beta_1 \frac{f'_c}{f_{pu}} \frac{\varepsilon_{cu}}{\varepsilon_{cu} + \varepsilon_{pu} - \varepsilon_{pe}} \quad \text{Equation 7-9}$$

where

β_1 = the ratio of the depth of equivalent rectangular stress block to the depth of neutral axis = 0.712

f'_c = concrete compressive strength = 6.76 ksi

f_{pu} = measured and guaranteed ultimate tensile stress of HSSS strands = 249.46 ksi and 240 ksi, respectively

ε_{pu} = measured and guaranteed ultimate tensile strain of HSSS strands = 0.0163 and 0.014, respectively

ε_{pe} = effective strain in the HSSS strands due to prestress = 0.0058

ε_{cu} = ultimate compressive strain of concrete = 0.003

For measured mechanical properties, the selected prestressing reinforcement ratio (ρ) ranged from $0.278\rho_{ssb}$ to $1.222\rho_{ssb}$, while for guaranteed mechanical properties, the selected prestressing reinforcement ratio (ρ) ranged from $0.217\rho_{ssb}$ to $1.174\rho_{ssb}$. A total of 80 isolated analyses were completed. The outcomes of each analysis were analytical flexural strength and curvature for the selected prestressing reinforcement ratios and mechanical properties.

Figure 7-8 shows the curvature in terms of reinforcement ratio for measured and guaranteed mechanical properties. For reinforcement ratios lower than the balanced reinforcement ratio, the failure mode is rupture of strand, while the failure mode is crushing of concrete for reinforcement ratios higher than the balanced reinforcement ratio. By increasing the reinforcement ratio, the curvature increased up to the balanced reinforcement ratio. This increase is attributed to the increase in the concrete top fiber strain at failure. The highest curvature can be achieved at the balanced reinforcement ratio because both concrete top fiber strain and HSSS strand strain are at their highest values. The curvature decreases for reinforcement ratios beyond the balanced reinforcement ratio. This decrease is attributed to the decrease in the strands' strain at failure. The rate of curvature change is higher for reinforcement ratios beyond the balanced reinforcement ratio compared to those below the balanced reinforcement ratio as shown in Figure 7-8. The ultimate curvature was higher when measured mechanical properties were used because the measured ultimate strain of HSSS strands was 16% greater than the guaranteed ultimate strain. The ultimate curvature at the balanced condition using measured mechanical properties was 22% greater than

that using guaranteed mechanical properties. The overall behavior of the ultimate curvature-reinforcement ratio relationship did not change when different mechanical properties for HSSS strands were used.

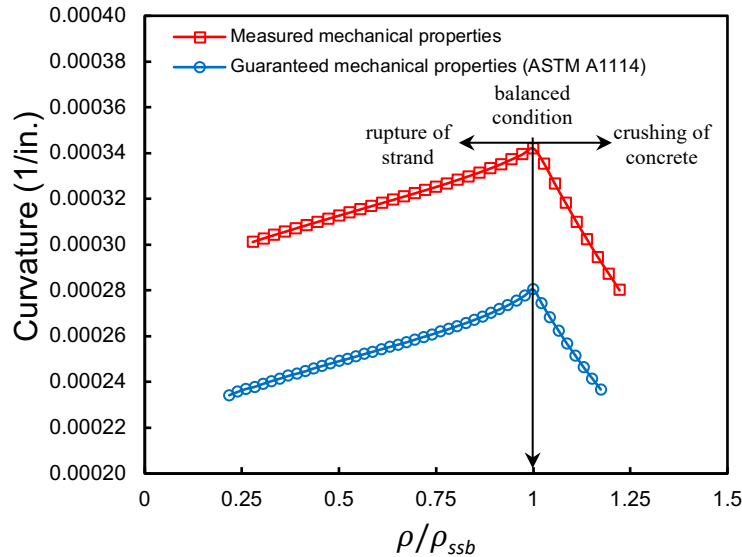


Figure 7-8 Predicted curvature as a function of prestressing reinforcement ratio and mechanical properties of HSSS strand

The flexural strength increased with increasing reinforcement ratio as shown in Figure 7-8. Mechanical properties of HSSS strands also influence the capacity of members. The flexural strength was greater when measured mechanical properties were used compared to guaranteed mechanical properties as shown in Figure 7-9.

7.2.3.2 Desired failure mode for I-girders prestressed with HSSS strands

In this parametric study, the desired failure mode for I-girders was investigated using the reinforcement ratio (ρ) as the variable, ranging from $0.217\rho_{ssb}$ to $1.174\rho_{ssb}$, which covers both rupture of strand and crushing of concrete failure modes. A concrete compressive strength of 6.44 ksi was used for the deck slab. The cross section was similar to that of the tested girders. The guaranteed mechanical properties specified by ASTM A1114 were used, to reflect the values that designers would use. The effective stress was 139.2 ksi.

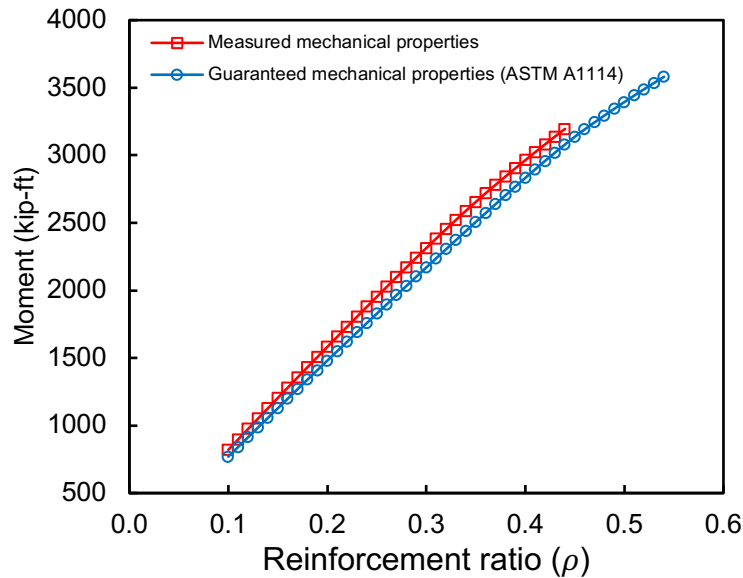


Figure 7-9 Predicted flexural strength as a function of prestressing reinforcement ratio and mechanical properties of HSSS strand

As shown in Figure 7-10, the same curvature can be achieved for two different reinforcement ratios, one less than balanced reinforcement ratio (rupture of strands failure) and one larger than the balanced reinforcement ratio (crushing of concrete failure). Figure 7-11 demonstrates this observation for curvature equal to 0.000262 (1/in.), using guaranteed mechanical properties of HSSS strands. The slope of the strain distributions is equal; however, the top and bottom strains are different (Figure 7-11). The number of HSSS strands was 14 and 21 for the less-than-balanced and larger-than-balanced reinforcement ratios, respectively, which is equivalent to prestressing reinforcement areas of 3.234 in² and 4.851 in², respectively. Thus, to change the failure mode from rupture of strand to crushing of concrete, the number of HSSS strands was increased by seven strands (or prestressing reinforcement area increased by 50%). Adding seven more HSSS strands resulted in a 38% increase in the moment strength. The layout of the HSSS strands for less-than-balanced and more-than-balanced sections is shown in Figure 7-12. Analytical moment-curvature plots for both sections are presented in Figure 7-13. Note that the rate of increase in moment after cracking is slightly greater in crushing of concrete failure mode compared to that of rupture of strand failure mode. Because the layout of the moment-curvature relationship did not significantly change when the failure mode was changed from rupture of strand to crushing of concrete, and both failure modes have the same ultimate curvature, the ultimate deflections of both sections are expected to be roughly the same.

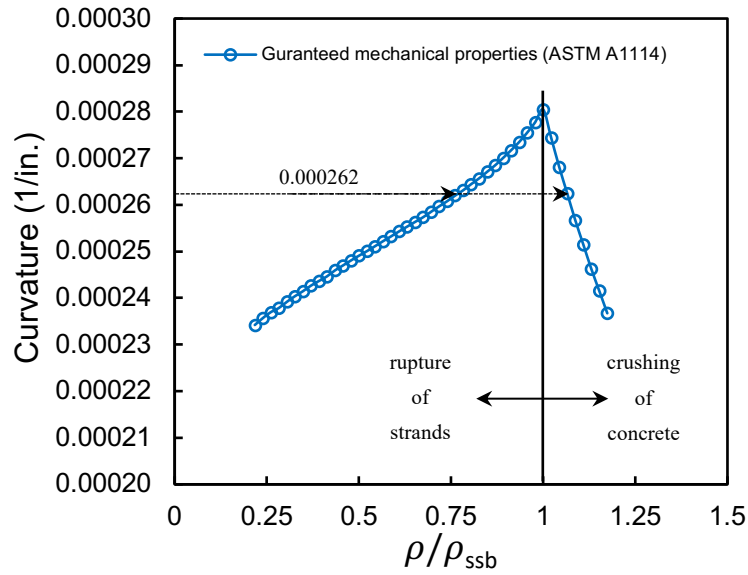


Figure 7-10 Curvature normalized reinforcement ratio for I-girders with guaranteed mechanical properties of HSSS strands

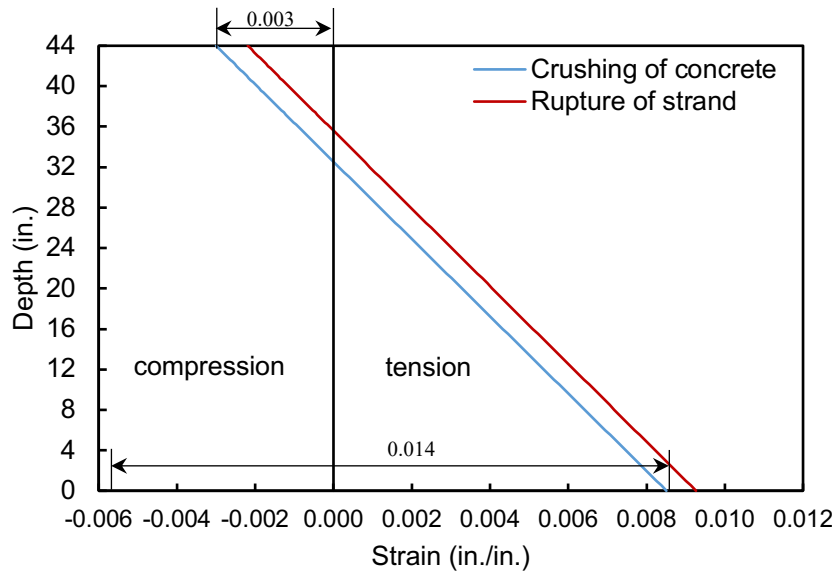


Figure 7-11 Analytical strain distribution for crushing of concrete and rupture of strand failures

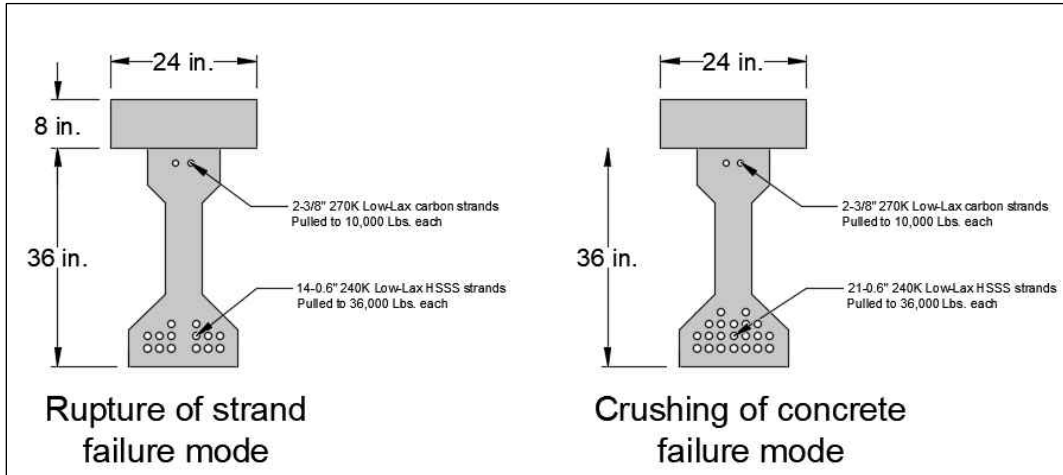


Figure 7-12 Cross sections of two girders: 14 HSSSS strands with rupture of strands failure and 21 HSSSS strands with crushing of concrete failure

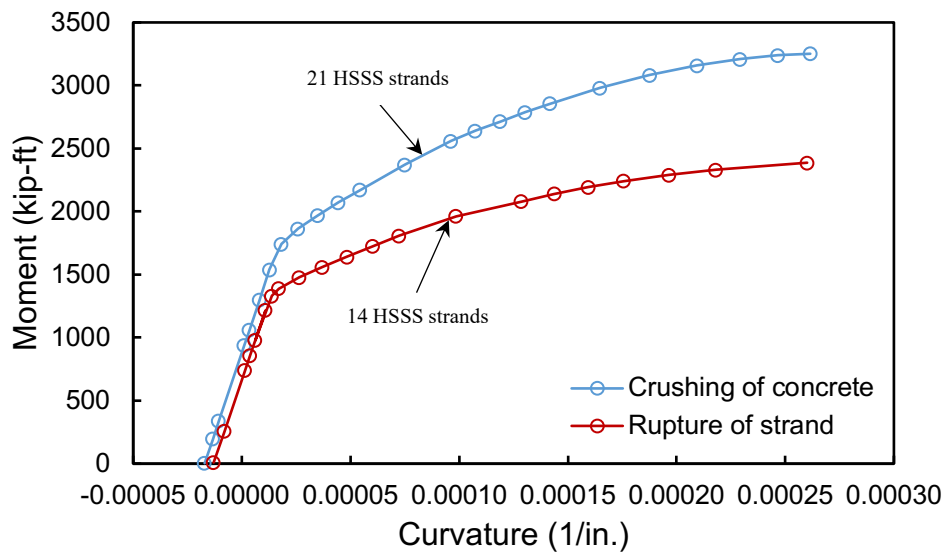


Figure 7-13 Analytical moment-curvature relationship for crushing of concrete and rupture of strand failure modes

Figure 7-14 presents the analytical deflection along the 40-ft-long girders at failure loads. The loading scheme was four-point bending, where the point load is 17 ft from the support. Figure 7-15 shows the load-deflection relationship for both sections at mid span. The ultimate deflection at mid span was 7.3% greater, and the flexural strength was 38.3% greater, for the section that failed by crushing of concrete than for the section that failed by rupture of strands. Although more strength was achieved with the addition of seven strands, if the additional strength were not needed, then one could argue that it is not worth the expense to gain only 7.3% more deflection.

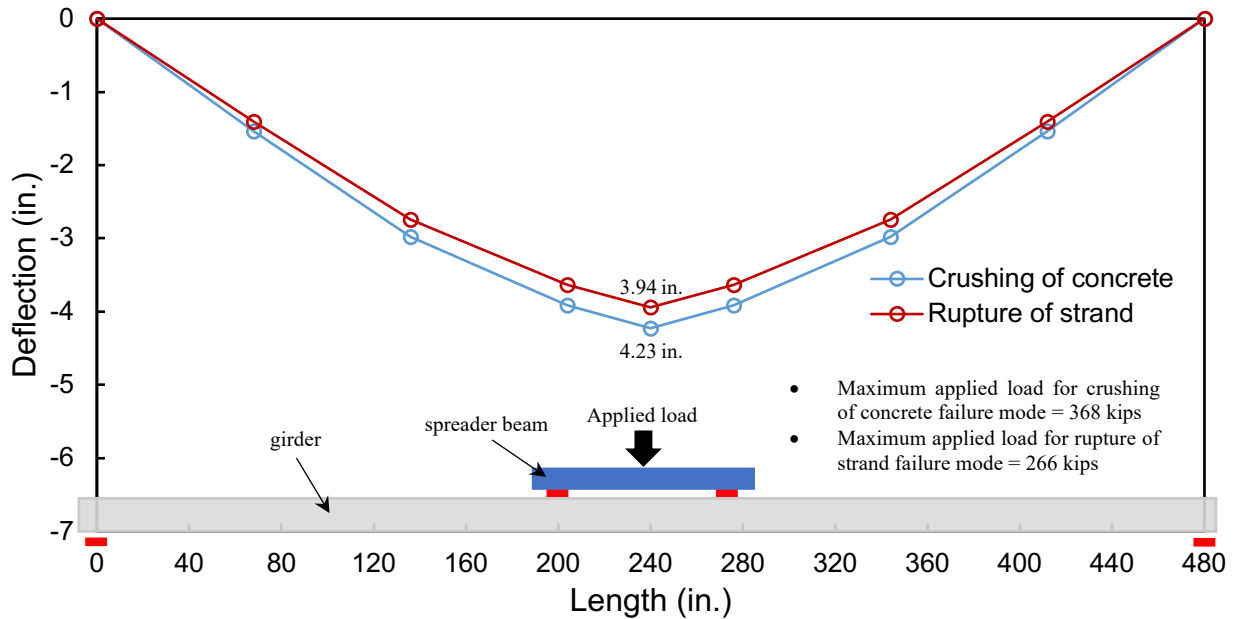


Figure 7-14 Analytical deflections along girders at failure, for crushing of concrete and rupture of strand failure modes

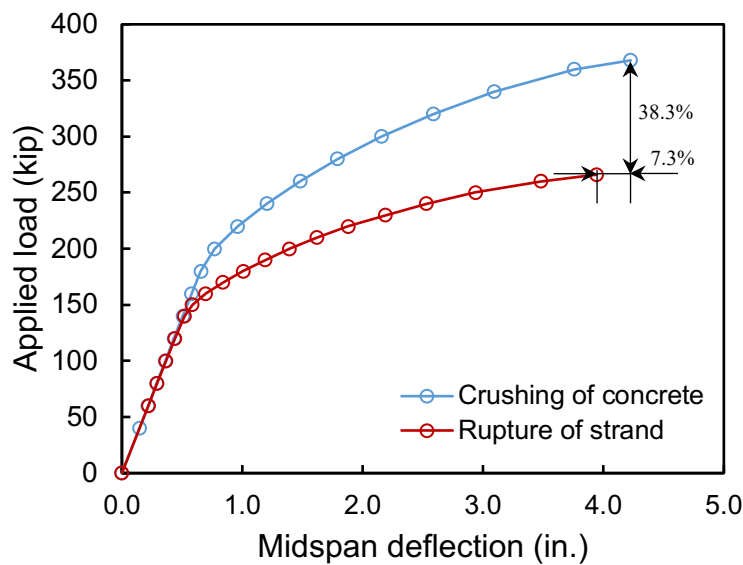


Figure 7-15 Analytical load-deflection relationship, for crushing of concrete and rupture of strand failure modes

Analytical results revealed that concrete girders designed to fail due to rupture of strand can exhibit large deflection at failure load. The deflection of 3.94 in. at mid span in Figure 7-14 will be accompanied by many flexural cracks, giving warning before the member reaches its capacity. Designing for crushing of concrete failure mode may not be necessary unless it is controlled by the design limit states where a higher prestressing reinforcement area is required. Thus, rupture of

strand failure mode is more economical than crushing of concrete failure mode because the same curvature can be achieved in both failure modes. In conclusion, the recommended failure mode for I-girders is rupture of HSSS strands.

7.2.3.3 Comparison of HSSS strands and carbon steel strands in I-girders

A parametric study was conducted to investigate the effect of the type of prestressing reinforcement on ultimate curvature (deformability) and flexural capacity of members. The cross section of the member was similar to that of the tested girders. The design variables were prestressing reinforcement ratio, ρ , and type of prestressing reinforcement, carbon steel and HSSS. The selected reinforcement ratio ranged from 0.13% to 0.54%. Reinforcement ratio refers to the total area of prestressing reinforcement divided by bd , where the width of the deck slab (b) was 24 in., and the depth from the top fiber to the prestressing strand (d) was 40 in. A total of 84 isolated analyses were completed. The outcomes of each analysis were analytical flexural strength and curvature. As mentioned previously, HSSS strands have lower elastic modulus, as well as lower ultimate stress and strain, than carbon steel strands. Lower ultimate strain of HSSS strands influences the failure mode and ultimate curvature of the members. Lower ultimate stress of HSSS strands influences the ultimate capacity of the members.

Figure 7-16 shows the neutral axis depth in terms of prestressing reinforcement ratio for both carbon steel and HSSS strands. For members prestressed with carbon steel strands, the neutral axis depth increased linearly with increasing prestressing reinforcement ratio, and failure mode was crushing of concrete in the compression zone, which means that the top fiber strain was always equal to 0.003. The strain in the prestressing strands at ultimate strength decreases with increasing reinforcement ratio. Thus, curvature decreases when the prestressing reinforcement ratio increases as shown in Figure 7-17. For members prestressed with HSSS strands, the neutral axis depth increased with prestressing reinforcement ratio. However, the rate of neutral axis change is higher for reinforcement ratios beyond the balanced reinforcement ratio compared to those below the balanced reinforcement ratio as shown in Figure 7-16. Balanced reinforcement ratio is the ratio at which the member fails simultaneously due to rupture of strand and crushing of concrete. For a reinforcement ratio lower than the balanced reinforcement ratio, the strain in the HSSS strands is equal to its ultimate strain of 0.014, and the concrete strain in the extreme compression fiber is lower than its assumed ultimate strain of 0.003. The concrete strain in the extreme compression fiber increases by increasing the reinforcement ratio up to the balanced reinforcement ratio. Thus,

curvature increases with an increasing reinforcement ratio up to the balanced reinforcement ratio. For a reinforcement ratio greater than the balanced reinforcement ratio, the concrete strain in the extreme compression fiber is always equal to 0.003, and the strain in the HSSS strands is lower than 0.014. The strain in the HSSS strands decreases by increasing the reinforcement ratio beyond the balanced reinforcement ratio. Therefore, curvature decreases for a reinforcement ratio greater than the balanced reinforcement ratio.

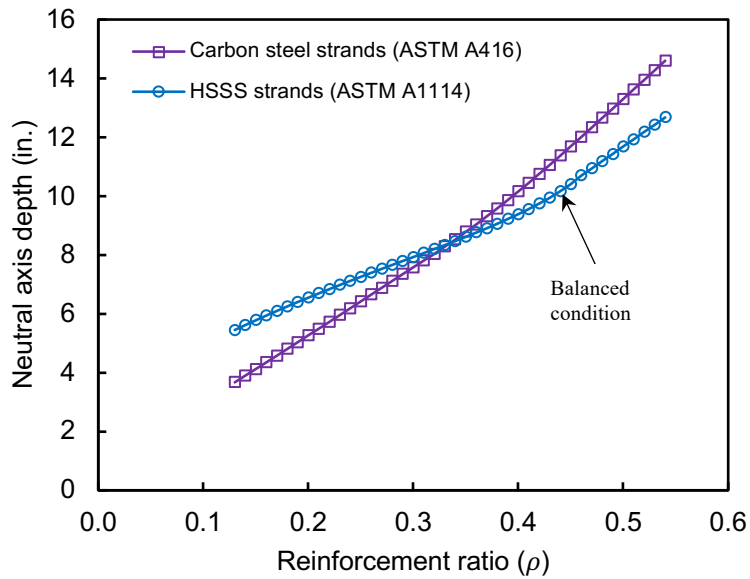


Figure 7-16 Analytical neutral axis depth vs. reinforcement ratio, for girder with carbon steel strands and girder with HSSS strands

Figure 7-17 shows the curvature in terms of reinforcement ratio for both girders prestressed with carbon steel and HSSS strands. Girders prestressed with carbon steel strands had higher curvature than those prestressed with HSSS strands up to a reinforcement ratio of 0.43. The difference in curvatures decreases when the reinforcement ratio increases as shown in Figure 7-17. For a wide range of reinforcement ratios, achieving curvatures in girders prestressed with HSSS strands as high as those in girders prestressed with carbon steel strands might not be possible.

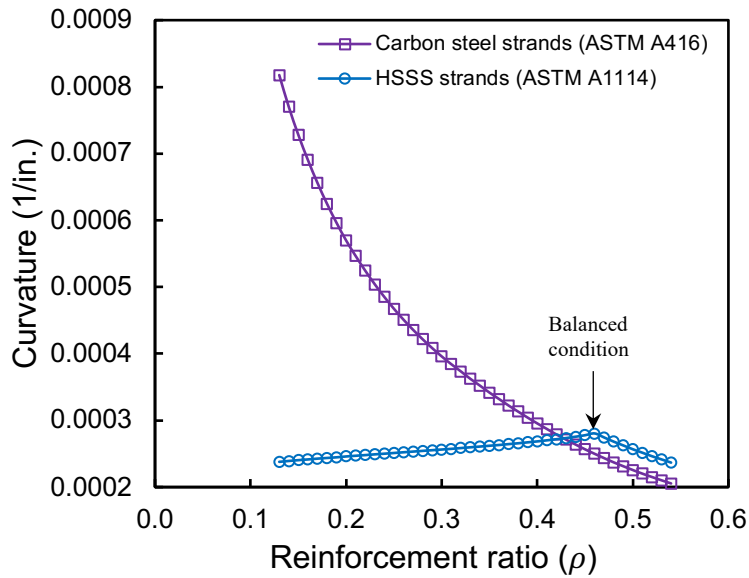


Figure 7-17 Analytical curvature vs. reinforcement ratio, for girder with carbon steel strands and girder with HSSS strands

Figure 7-18 shows the relationship of flexural strength with reinforcement ratio for girders prestressed with carbon steel and HSSS strands. The flexural strength increased with increasing reinforcement ratio. Ultimate stress in the strands influences the capacity of the members. Girders prestressed with carbon steel strands had greater flexural strengths than those prestressed with HSSS strands. The difference in flexural strength increased for higher prestressing reinforcement ratio (reinforcement ratio greater than balanced reinforcement ratio). This increase is attributed to a decrease in the stress of HSSS strands at failure (lower than ultimate stress of 240 ksi) because the failure mode is crushing of concrete. The same flexural strength can be achieved in the girder with HSSS strands by increasing the reinforcement ratio.

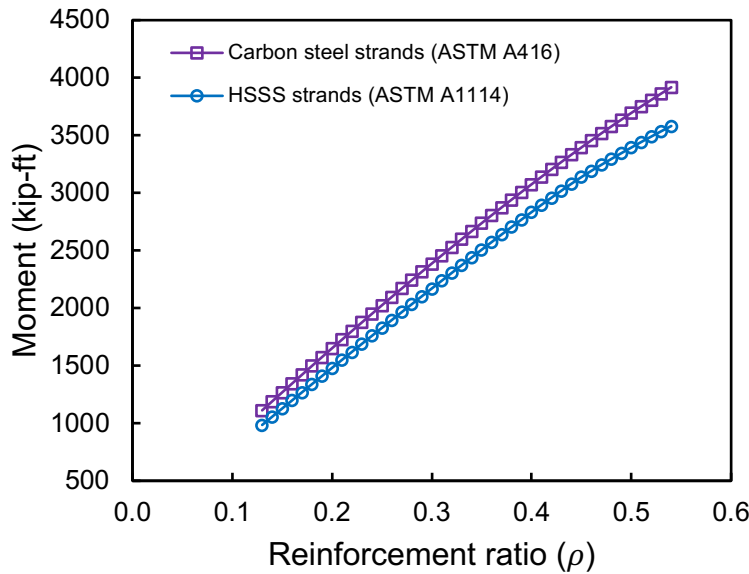


Figure 7-18 Analytical flexural strength vs. reinforcement ratio, for girder with carbon steel strands and girder with HSSS strands

Figure 7-19 shows the relationship between initial prestressing force with the reinforcement ratio for girders prestressed with carbon steel and HSSS strands. For girders with the same reinforcement ratio, the girder with the HSSS strands will have a lower initial prestressing force because of the lower jacking force that is allowed, compared to the girder with carbon steel strands. However, the same initial prestressing force can be achieved in the girder with HSSS strands by increasing the reinforcement ratio. When making comparisons between girders with HSSS and carbon steel strands, it is important to establish the same initial prestressing force in the girders.

Figure 7-20 compares two girders with the same initial prestressing force. One girder has 11 carbon steel strands stressed to 44 kips, and the other girder has 13 HSSS strands stressed to 37.2 kips. The girder prestressed with HSSS strands failed due to rupture of strands, while the girder prestressed with carbon steel strands failed due to crushing of concrete. Because of the limited ultimate strain of HSSS strands, the girder with HSSS strands had less curvature compared to the girder with carbon steel strands. Although the ultimate stress of HSSS strands is lower than for carbon steel strands, their larger area and number resulted in a larger total prestressing force at failure ($A_{ps}f_{ps}$), which resulted in a higher flexural strength. Analytical moment-curvature for both sections is presented in Figure 7-21. It can be seen in Figure 7-21 that the rate of increase in moment after cracking is greater in girder prestressed with HSSS strands because of the larger total prestressing force; however, the curvature at failure was lower because of the limited strain in the

HSSS strands. Because the layout of the moment-curvature relationship is different between girder prestressed with carbon steel and girder prestressed with HSSS strands (ultimate curvature is larger in girder prestressed with carbon steel strands), the deflection along the girder at failure in girder prestressed with carbon steel strands is expected to be larger than that in girder prestressed with HSSS strands.

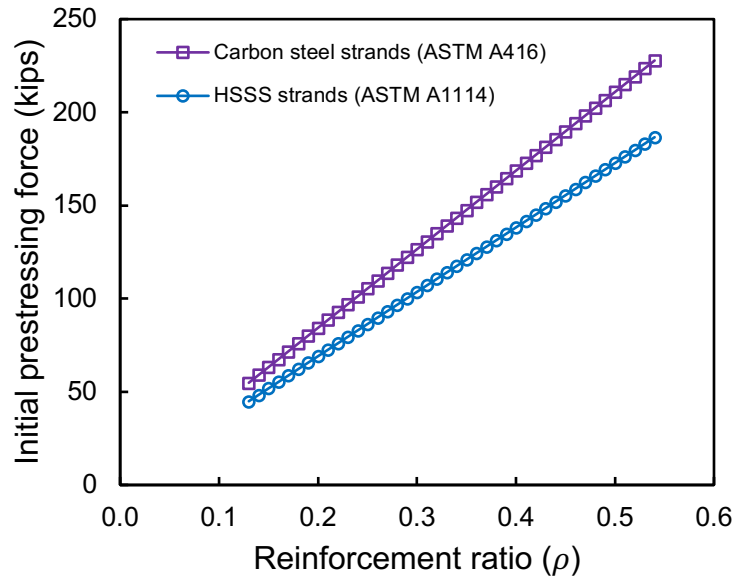


Figure 7-19 Analytical initial prestressing force vs. reinforcement ratio, for girder with carbon steel strands and girder with HSSS strands

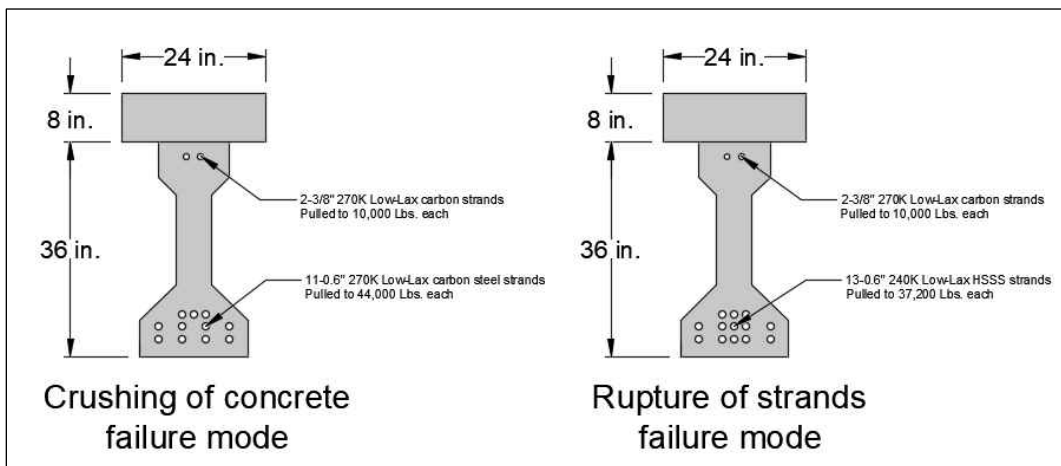


Figure 7-20 Cross sections of two girders: 11 carbon steel strands with crushing of concrete failure and 13 HSSS strands with rupture of strands failure

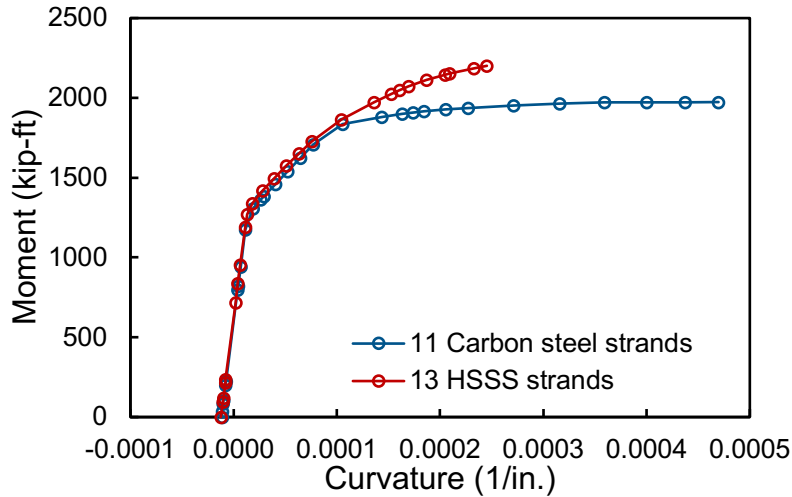


Figure 7-21 Analytical moment vs. curvature, for girder with carbon steel strands and girder with HSSS strands

Figure 7-22 presents the analytical deflection along the 40-ft-long girders at failure loads. The loading scheme was four-point bending, where the point load is 17 ft from the support. The ultimate deflection at mid span was 3.94 in. for the girder prestressed with HSSS strands. The girder prestressed with carbon steel strands exhibited more deformability; the deflection was 4.71 in., or 19.5% larger. Although the girder prestressed with HSSS strands failed due to rupture of strands, it exhibited large deflections, not as large as the girder prestressed with carbon steel strands. However, the 3.94-in. deflection of the girder with HSSS strands would be accompanied by many flexural cracks, giving warning before the member reaches its capacity.

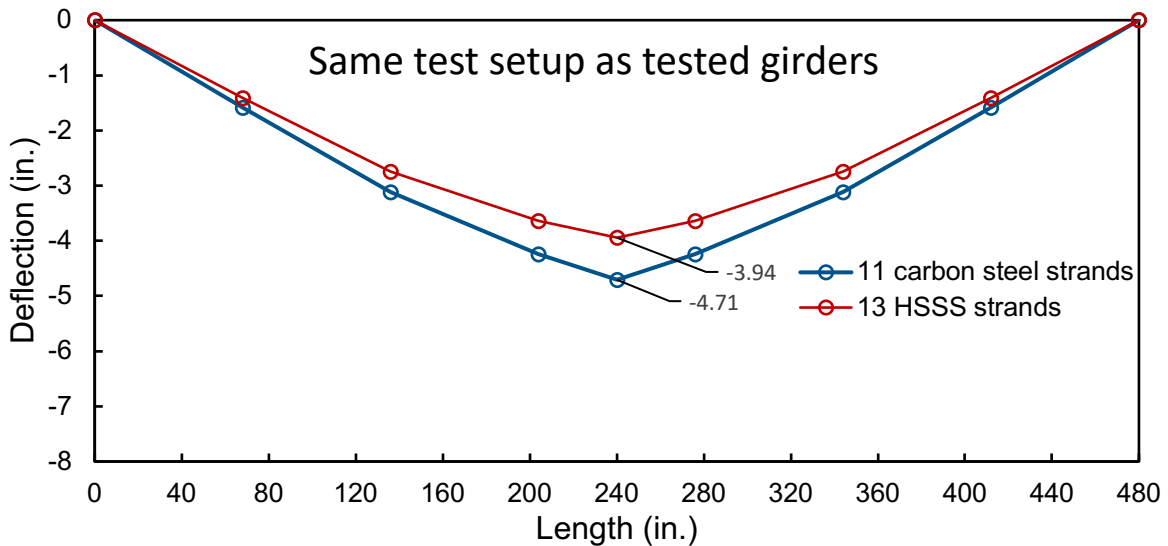


Figure 7-22 Analytical deflections along girders at failure, for girder with carbon steel strands and girder with HSSS strands

Figure 7-23 shows the load-deflection relationship for both sections at mid span. Although the deformability was less for the girder with HSSS strands, 12% more nominal flexural strength was achieved. Note that the resistance factors are not included here; girders with HSSS strands would require a lower resistance factor than for girders with carbon steel strands because of the brittle behavior of the HSSS strands.

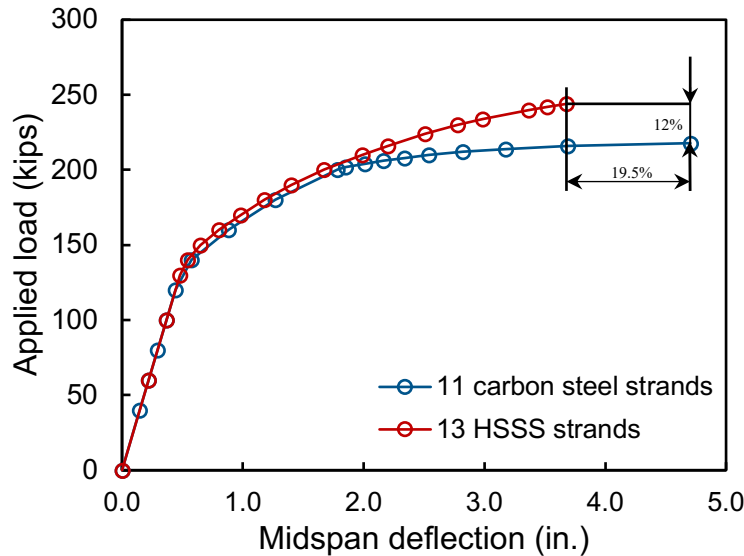


Figure 7-23 Analytical applied load vs. deflection, for girder with carbon steel strands and girder with HSSS strands

7.3 AASHTO LRFD

AASHTO LRFD Bridge Design Specifications were originally developed for concrete members prestressed with carbon steel strands, and HSSS strands have different mechanical properties compared to carbon steel strands. Experimental results were compared with the predicted values by AASHTO LRFD equations to verify their applicability for full-scale concrete girders prestressed with HSSS strands.

Carbon steel strands have high ductility, so rupture of strands is an uncommon failure mode. AASHTO LRFD equations for flexural capacities were developed on the basis that carbon steel pretensioned concrete girders are designed to fail under ultimate load by crushing of concrete in the compression zone. AASHTO Equation 5.6.3.2.2-1, which is given in Equation 7-10, is used to compute the flexural capacity of the girder. The neutral axis depth (c) can be computed using AASHTO Equation 5.6.3.1.1-4, which is given in Equation 7-11. For low-relaxation strand, the value for k shall be taken equal to 0.28 (AASHTO Table C5.6.3.1.1-1). The average stress in the prestressing strand can be computed using AASHTO Equation 5.6.3.1.1-1, which is given in

Equation 7-12. According to AASHTO Section 5.6.2.2, the stress block factors, α_1 and β_1 , can be computed using Equations 7-13 and 7-14, respectively.

$$M_n = A_{ps}f_{ps} \left(d_{ps} - \frac{a}{2} \right) \quad \text{Equation 7-10}$$

$$c = \frac{A_{ps}f_{pu}}{\alpha_1 f'_c \beta_1 b + k A_{ps} \frac{f_{pu}}{d_p}} \quad \text{Equation 7-11}$$

$$f_{ps} = f_{pu} \left(1 - k \frac{c}{d_p} \right) \quad \text{Equation 7-12}$$

$$\beta_1 = \begin{cases} 0.85 & f'_c \leq 4 \\ 0.85 - 0.05(f'_c - 4) & 4 < f'_c \leq 8 \\ 0.65 & f'_c > 8 \end{cases} \quad \text{Equation 7-13}$$

$$\alpha_1 = \begin{cases} 0.75 & f'_c \leq 10 \\ 0.75 - 0.02(f'_c - 10) & f'_c > 10 \end{cases} \quad \text{Equation 7-14}$$

In this study, Girder A3 was prestressed with carbon steel strands. All needed input design variables for Girder A3 are given in Table 7-1. The neutral axis depth was found to be 5.63 in., where: the deck slab width (b) was 24 in.; distance from extreme compression fiber to the centroid of carbon steel strands (d_p) was 41.0 in.; tensile strength of carbon steel strands (f_{ps}) was 259.6 ksi; average concrete compressive strength for deck slab on testing day was 8.3 ksi; and stress block factors α_1 and β_1 were 0.85 and 0.65, respectively. The compression flange depth (a) equals $\beta_1 c$, which was found to be 3.66 in., less than the 8-in. flange depth (h_f). So, the section was correctly analyzed as a rectangular section. The predicted flexural moment strength of Girder A3 was equal to 2,023 kip-ft, 96.6% of the experimental flexural strength of 2,095 kip-ft which includes the effect of the girder's self-weight.

Because girders prestressed with HSSS strands (C3, E1-E5) failed due to rupture of all HSSS strands, Equations 7-10 and 7-11 need to be modified as follows before they can be used to predict the flexural strength of Girders C3, and E1-E5. First, the average stress in the prestressing strands (f_{ps}) shall be taken as the ultimate tensile strength (f_{pu}) of the HSSS strands because girders failed due to rupture of HSSS strands. Second, the second term in the denominator of Equation 7-11 ($k A_{ps} \frac{f_{ps}}{d_p}$) shall be deleted. The modified version of Equations 7-10 and 7-11 for girders prestressed with HSSS strands are given in Equations 7-15 and 7-16, respectively.

$$M_n = A_{ps}f_{pu} \left(d_{ps} - \frac{\beta_1 c}{2} \right) \quad \text{Equation 7-15}$$

$$c = \frac{A_{ps}f_{pu}}{\alpha_1 f'_c \beta_1 b} \quad \text{Equation 7-16}$$

The flexural strength of girders prestressed with HSSS strands (Girders C3, and E1-E5) can be computed by applying the input parameters, which are given in Table 7-1, in the above equations. Table 7-1 also provides the procedure using numerical equations to calculate the flexural strength of the girders. The calculated flexural strength was 2500, 1934, 1940, 1634, 1634, and 1290 kip-ft for Girders C3, E1, E2, E3, E4, and E5, respectively. The calculated flexural strengths for Girders C3, E1, E2, E3, E4, and E5 were 97.6%, 94.3%, 95.9%, 95.9%, 96.8%, and 95.4%, respectively, of the experimental strengths. Figure 7-24 presents comparisons of the experimental and numerical strengths. Although the modified AASHTO equations predicted well the experimental results, it has some limitations, as follows. First, it cannot be used for a section other than a rectangular one. Second, it cannot be used in sections where HSSS strands are distributed vertically along the depth of the section. Third, it cannot be used for a section with nonprestressed tension and compression reinforcement because stress in compression reinforcement might be overestimated by assuming its yielding value. Forth, stress block factors, α_1 and β_1 , are overestimated and may result, in some cases, in overestimation of the nominal flexural resistance of the member.

Table 7-1 Calculation of flexural strength using modified AASHTO LRFD equations

Variable	Unit	Girder A3	Girder C3	Girder E1	Girder E2	Girder E3	Girder E4	Girder E5
b	in.	24						
d_{ps}	in.	41.00	41.15	39.18	39.18	36.67	36.67	39.86
A_{ps}	in ²	2.387	2.990	2.541	2.541	2.079	2.079	1.617
f'_c	ksi	8.30	6.84	6.44	6.76	7.44	7.44	7.44
f_{pu}	ksi	270	261.61	249.46				
β_1 (Eq. 7-13)	-	0.650	0.708	0.728	0.712	0.678	0.678	0.678
α_1 (Eq. 7-14)	-	0.85						
k	-	0.28	-					
f_{ps} (Eq. 7-12)	ksi	259.62	-					
c (Eq. 7-11)	in.	5.629	7.920	6.541	6.372	4.974	4.974	4.974
c (Eq. 7-16)								
a	in.	3.659	5.609	4.762	4.537	3.372	3.372	3.372
M_n (Eq. 7-10)	kip-ft	2023	2500	1934	1940	1634	1634	1290
M_n (Eq. 7-15)								

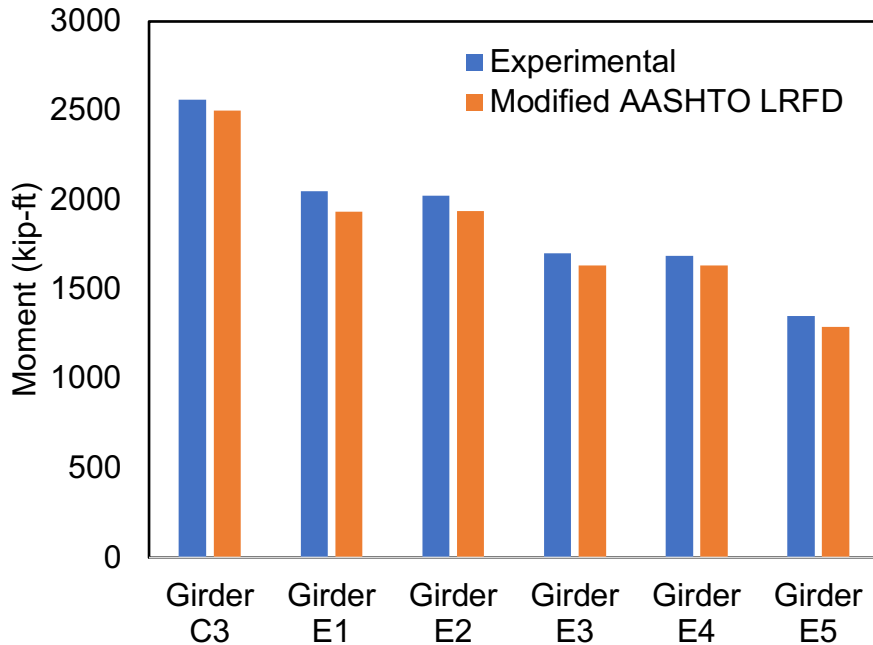


Figure 7-24 Comparison of experimental moments and moments calculated using modified AASHTO LRFD equations

7.4 Iterative numerical model

Current AASHTO equations for the stress block parameters, α_1 and β_1 , (Equations 7-13 and 7-14) are only valid when concrete top fiber strain equals 0.003. Because all composite girders prestressed with HSSS strands failed due to rupture of strand, the HSSS strands in the bottom layer reached their ultimate strain while the concrete strain in the extreme compression fiber was less than 0.003. Therefore, it is inappropriate (unconservative) to approximate the concrete compressive force using the current AASHTO equations for the stress block parameters, α_1 and β_1 .

HSSS strands and carbon fiber-reinforced polymer (CFRP) strands have low ductility compared to carbon steel strands. NCHRP Report 907 was developed for concrete bridge beams prestressed with CFRP systems (2019); rupture of CFRP strands was proposed as a feasible failure mode for prestressed concrete I-girders. In the NCHRP Report 907, equations for stress block parameters, α and β , were proposed for any strain value in the extreme compression fiber, and they are given in Equations (7-18) and (7-19), respectively, where ϵ'_c is calculated using Equation (7-20). In the case of rupture of strand failure mode, the neutral axis depth (c_1) can be determined by achieving force equilibrium, which is given in Equation (7-21). Both α and β are a function of the concrete strain at the extreme compression fiber (ϵ_{cf}) at failure, which is unknown. Therefore,

Equation (7-21) cannot be solved because it has two unknowns, α and β . The neutral axis depth (c_2) can be also determined from strain distribution by using similar triangles as shown in Equation (7-22). In this case, the neutral axis depth can only be solved through an iterative procedure.

$$\beta = \frac{4 \frac{\varepsilon_{cf}}{\varepsilon'_c}}{6 - 2 \frac{\varepsilon_{cf}}{\varepsilon'_c}} \left(-\frac{f'_c}{50} + 1.1 \right) \quad \text{Equation 7-18}$$

$$\alpha = \left(\frac{1}{\beta} \right) \left(\frac{\varepsilon_{cf}}{\varepsilon'_c} - \frac{1}{3} \left(\frac{\varepsilon_{cf}}{\varepsilon'_c} \right)^2 \right) \left(-\frac{f'_c}{60} + 1 \right) \quad \text{Equation 7-19}$$

$$\varepsilon'_c = \left(\frac{f'_c}{11} + 1.6 \right) * 10^{-3} \quad \text{Equation 7-20}$$

$$c_1 = \frac{A_{ps} f_{pu}}{\alpha f'_c \beta b} \quad \text{Equation 7-21}$$

$$c_2 = \frac{\varepsilon_{cf}}{\varepsilon_{cf} + \varepsilon_{pu} - \varepsilon_{pe}} d_1 \quad \text{Equation 7-22}$$

An iterative numerical model was developed to determine the flexural strength for concrete girders prestressed with HSSS strands and designed to fail by rupturing of strands. The procedure can be summarized in the following steps.

1. Assume top fiber strain, e.g. $\varepsilon_{cf} = 0.0005$.
2. Calculate the first neutral axis depth, c_1 , from the strain distribution using Equation 7-22.
3. Calculate the concrete stress block parameters β and α using Equations 7-18 and 7-19, respectively.
4. Calculate strain in the layers of HSSS strands using the linear strain distribution;
5. Calculated stress in the layers of HSSS using the stress-strain model given in Equation 3-1 after substituting A , B , and C coefficients and determining modulus of elasticity, E ;
6. Calculate the second neutral axis depth, c_2 , from force equilibrium; and
7. Terminate the iteration if $c_1 - c_2 = 0$, otherwise go to step (1) and increase the top fiber strain for the next iteration.
8. Calculate the nominal flexural resistance, M_n , by summing tension forces about the centroid of the compression depth.

The proposed iterative procedure is given in a form of flowchart in Figure 7-25.

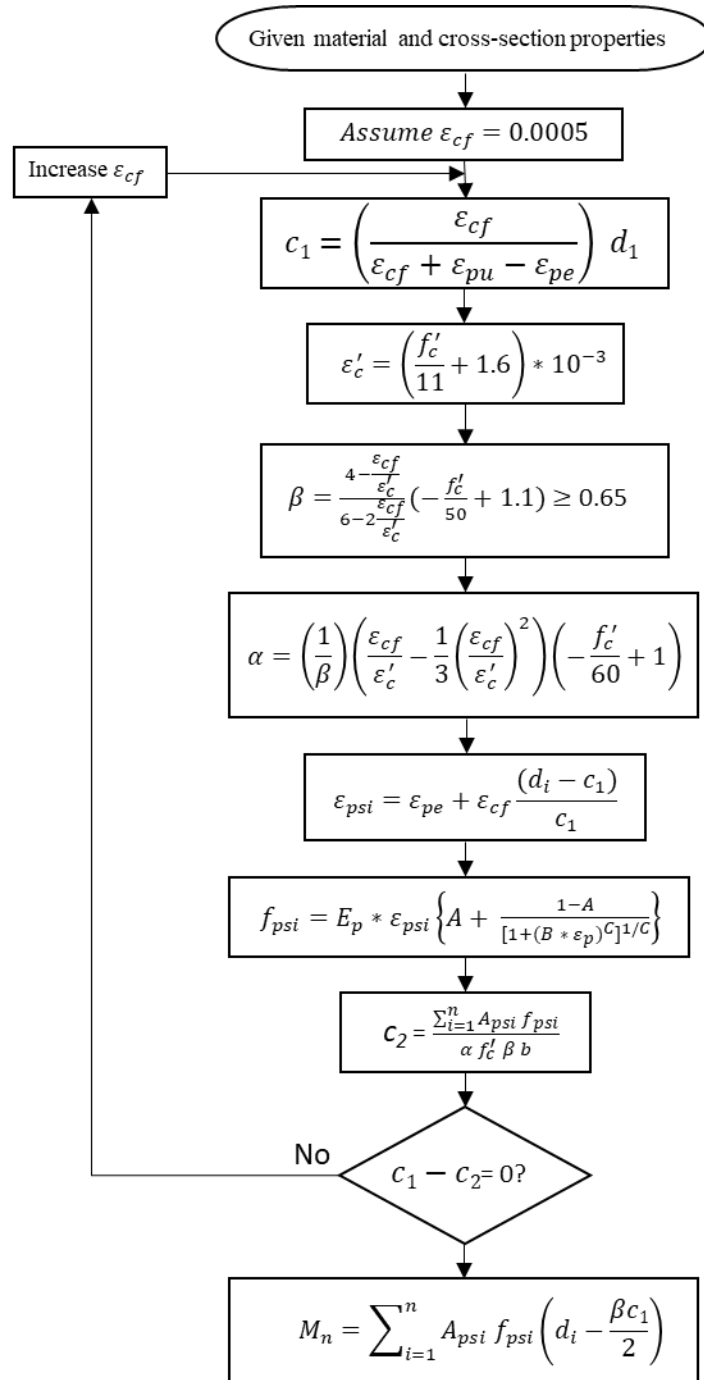


Figure 7-25 Proposed flexural design flowchart for concrete members prestressed with HSSS strands and designed to fail due to rupture of strand

To validate the detailed iterative numerical model, results from the experimental programs were compared with those obtained using the flowchart in Figure 7-25. The stress in the HSSS strands (f_{psi}) was calculated using the stress-strain model given in Equation 3-1 after substituting

coefficients from Table 3-8 and mechanical properties from Table 3-5. The measured concrete compressive strength on testing day (Table 4-6 and Table 4-12) and measured prestress losses (Figure 6-9 and Table 6-2) were used in the iterative numerical model to calculate the flexural strength. The iterative numerical analysis of Girders C1 and E1-E5 predicted a flexural strength of 2504, 1961, 1966, 1647, 1647, and 1293 kip-ft, respectively. The predicted flexural strengths of Girders C1 and E1-E5 were 97.8%, 95.6%, 97.1%, 96.7%, 97.6%, and 95.6%, respectively, from those measured experimentally. Figure 7-26 presents comparisons of the experimental moments and moments calculated using the proposed iterative numerical model. It can be concluded that the proposed iterative numerical model predicted the experimental results well. An example following this approach is given in Appendix F.

The proposed flowchart in Figure 7-25 can be slightly improved to include nonprestressed tension and compression reinforcements at any depth along the section and to cover flanged sections (provided later in this report).

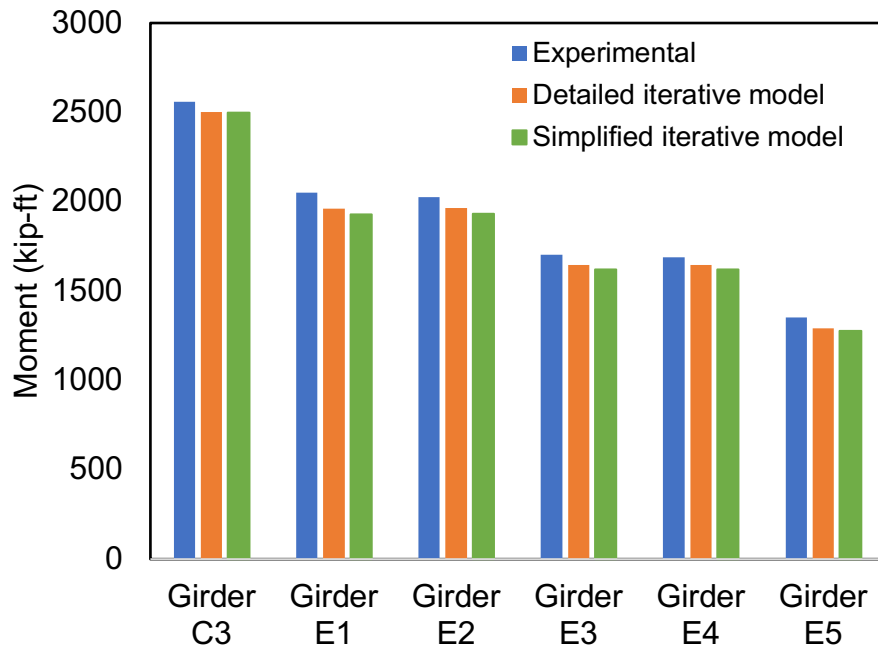


Figure 7-26 Comparison of experimental moments and moments calculated using iterative numerical model

The detailed iterative numerical model (Figure 7-25) requires calculation of the strain in each layer of strands to determine the tension force. The distance from the neutral axis to the layer of strands is used to determine the strain in the strands at that layer. So, in deep girders, the rate of increase in strain between the bottom layer and other layers is very minimal. Also, the stress-strain

curve of the HSSS strands has a very low slope in the inelastic region. This means that a small difference in the strain results in a very minimal difference in the stress. To investigate the vertical distribution of HSSS strands on the flexural strength of the girders, the iterative detailed model was simplified by assuming an equivalent area at the centroid of the strands. The simplified iterative procedure is given in a form of flowchart in Figure 7-27.

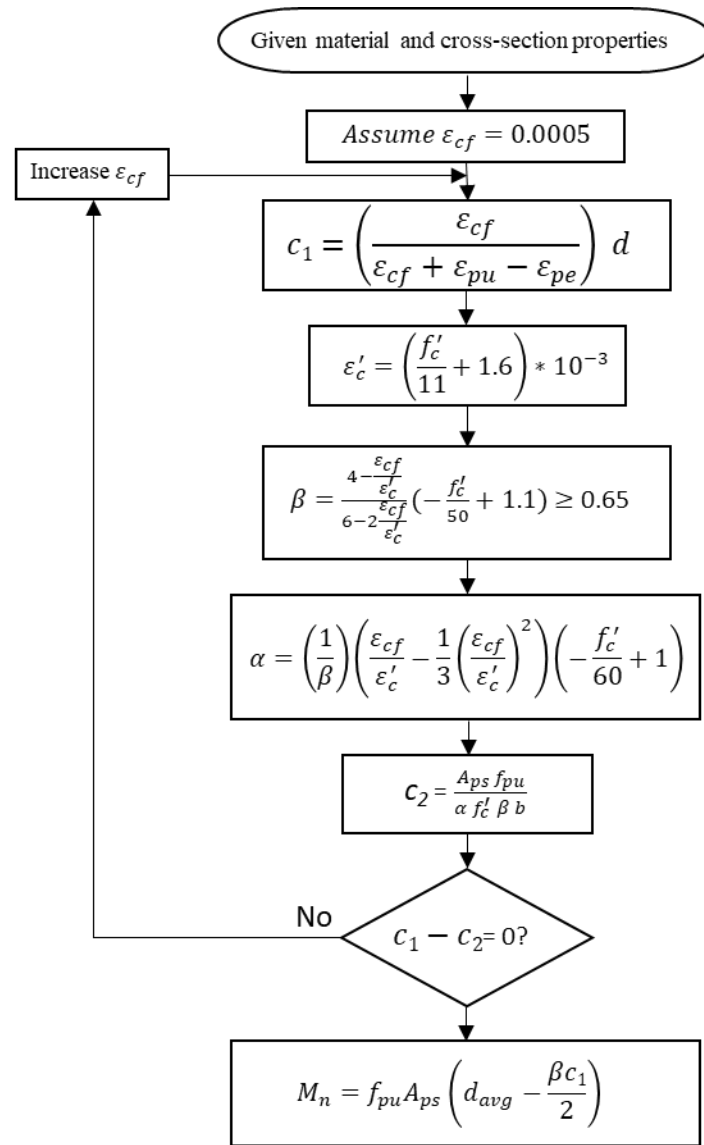


Figure 7-27 Simplified iterative model to calculate the flexural strength of concrete girders prestressed with HSSS strands and designed to fail due to rupture of strand

To validate the simplified iterative numerical model, results from the experimental programs were compared with those obtained using the flowchart in Figure 7-27. The iterative numerical

analysis of Girders C1 and E1-E5 predicted a flexural strength of 2500, 1929, 1933, 1621, 1621, and 1276 kip-ft, respectively, as shown in Figure 7-26. The predicted flexural strengths of Girders C1 and E1-E5 were 97.6%, 94.1%, 95.5%, 95.2%, 96.0%, and 94.4%, respectively, from those measured experimentally. The predicted flexural strength was calculated using measured HSSS strand properties, concrete compressive strength on testing day, and measured prestress losses. Figure 7-26 shows that assuming an equivalent area for HSSS strands at their centroid did not significantly affect the calculated moment. The difference between flexural strengths calculated using vertical (real) distribution of HSSS strands and assuming an equivalent area was less than 2%. Therefore, it can be concluded that the proposed simplified iterative model can be used to calculate the flexural strength of concrete girders prestressed with HSSS strands and designed to fail due to rupture of strand. An example following this approach is given in Appendix F.

7.5 Summary

Multiple approaches were developed to compute the flexural strength of concrete members prestressed with HSSS strands, and a summary table is below:

Table 7-2 Flexural strength of concrete girders prestressed with HSSS strands

Specimen	Experimental (kip-ft)	Strain compatibility (kip-ft)	Modified AASHTO LRFD (kip-ft)	Detailed iterative numerical model (kip-ft)	Simplified iterative numerical model (kip-ft)
Girder C3	2561	2537	2500	2504	2500
Girder E1	2051	1990	1934	1961	1929
Girder E2	2024	1993	1940	1966	1933
Girder E3	1703	1673	1634	1647	1621
Girder E4	1688	1672	1634	1647	1621
Girder E5	1352	1319	1290	1293	1276

The developed approaches are as follows:

1. A nonlinear iterative sectional analysis model, using strain compatibility, was developed to calculate the flexural strength of any prestressed concrete section. The calculated flexural strengths using analytical model for Girders C3, E1, E2, E3, E4, and E5 were 99.0%, 97.0%, 98.5%, 98.2%, 99.0%, and 97.5%, respectively, of the experimental strengths.

2. AASHTO LRFD equations cannot be used when HSSS strands are used, for two reasons. First, HSSS have different mechanical properties compared to those for carbon steel strands. Second, carbon steel strands have high ductility, so rupture of strands is an uncommon failure mode. AASHTO LRFD equations were slightly modified for the use of HSSS strands. The calculated flexural strengths using modified AASHTO equations for Girders C3, E1, E2, E3, E4, and E5 were 97.6%, 94.3%, 95.9%, 95.9%, 96.8%, and 95.4%, respectively, of the experimental strengths. Even though the modified AASHTO equations predicted well the experimental results, they have some limitations, and they may result, in some cases, in overestimation of the nominal flexural resistance of member.
3. A straightforward, iterative numerical approach was developed to calculate the flexural strength of any prestressed concrete section. The calculated flexural strengths of Girders C1 and E1-E5 were 97.8%, 95.6%, 97.1%, 96.7%, 97.6%, and 95.6%, respectively, of those measured experimentally.

CHAPTER 8 DEVELOPMENT OF FLEXURAL DESIGN EQUATIONS

8.1 Introduction

The flexural strength of concrete members prestressed with HSSS strands can be computed quite accurately through a nonlinear sectional analysis or an iterative numerical model, as discussed in Chapter 7. However, for practical design purposes, it is preferable to have simple numerical equations to compute the nominal flexural resistance.

This chapter is devoted to developing flexural design equations for concrete members prestressed with HSSS strands.

8.2 Desired flexural failure mode

The desirable behavior of any prestressed concrete member is for it to exhibit a large deflection and excessive cracking before failure, which serve as warning before the member reaches its capacity. Both deflection and cracking are functions of the strain in the extreme compression fiber and strain in the bottom layer of strands. The capacity and failure mode of a prestressed concrete member are controlled by which component – concrete in the compression zone or the bottom layer of strand – reaches its ultimate strain first. The failure mode – crushing of concrete or rupture of strand – is controlled by the mechanical properties of the strand, concrete compressive strength, and member dimensions (especially depth).

According to AASHTO Section 5.5.4.2, the flexural resistance factor depends on the net tensile strain in the strand, as shown in Figure 8-1. From a design point of view, the higher the resistance factor, the higher the capacity that can be achieved. To achieve a resistance factor of 1.0, the net tensile strain in the strand shall be not less than 0.005. Therefore, concrete flexural members prestressed with carbon steel strands are designed to have a net tensile strain in the strands greater than 0.005. In this case, the capacity of the member is controlled by concrete in the compression zone. Rupture of strand failure mode is uncommon when carbon steel strands are used because of their high ductility. The minimum guaranteed ultimate strain for carbon steel strand is 0.035, however, most carbon steel strands have an ultimate strain larger than 0.05. The ductility of the member is achieved through high strain in the carbon steel strands.

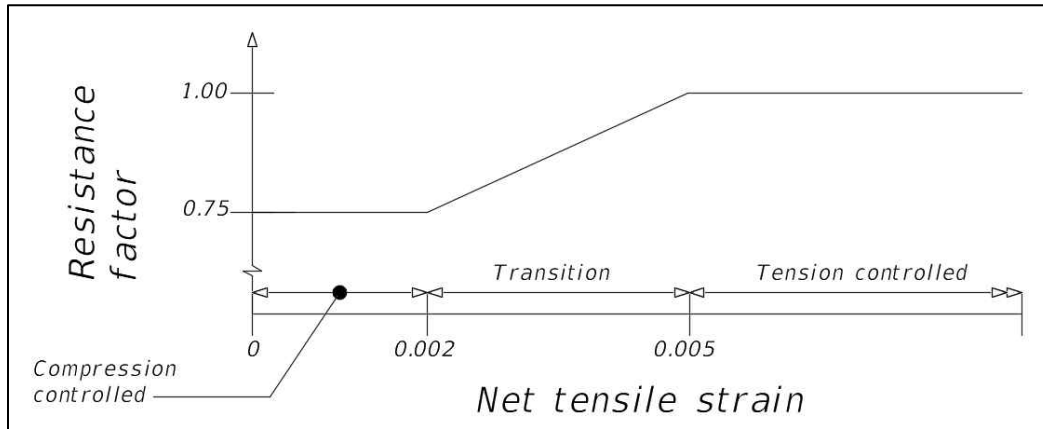


Figure 8-1 Strength resistance factor for carbon steel strands (AASHTO LRFD)

The desired flexural behavior for concrete members prestressed with carbon steel strands is not applicable for concrete members prestressed with HSSS strands because HSSS strands have low ductility compared to carbon steel strands. The minimum guaranteed ultimate strain for HSSS strand is only 0.014. Regardless of the low ductility of HSSS strand, the net tensile strain in the bottom layer of HSSS strands in flexural members is recommended to be greater than 0.005 (this will be discussed later in this report). This is important to provide adequate deformability before failure. Because of the low ductility of HSSS strands, two failure modes are feasible, and they are discussed in the following sections.

8.2.1 Rupture of strand

For the case of rupture of strands, both deflection and cracking are primarily a function of the concrete strain in the top fiber, which will be less than its ultimate value of 0.003. Thus, the design procedure of a prestressed concrete I-girder should be revised when HSSS strands are used. Instead of the prestressing strand yielding (having net tensile strain higher than 0.005), the concrete strain at the top fiber should reach inelastic strain (yielding) as shown in Figure 8-2. Ductility of a concrete flexural member prestressed with HSSS strands is obtained by ensuring considerable inelastic strain in the top fiber before rupture of the HSSS strands occurs.

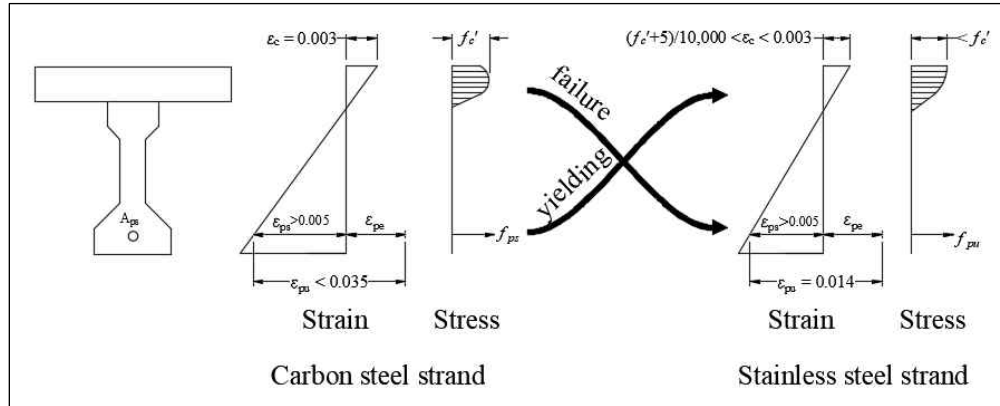


Figure 8-2 Design of carbon and stainless steel prestressed concrete girders

The stress-strain relationship of concrete is essential in determining the end of the elastic range. Figure 8-3 shows stress-strain curves of concrete of various strengths, which were developed using Equations 7-1 through 7-5 (Collins and Mitchell 1991). It was reported that concrete starts to lose stiffness after approximately $0.7f'_c$. This concrete stress ($0.7f'_c$) is considered the end of the elastic range on the concrete stress-strain curve. The strains at $0.7f'_c$ of various concrete strengths were determined and plotted in Figure 8-3. Those strains represent the start of the inelastic range of the concrete stress-strain curve. The minimum inelastic compressive stress or strain of the concrete at failure should be $0.7f'_c$ and $(f'_c+5)/10,000$, respectively, for a concrete member prestressed with HSSS strands. The required inelastic stress or strain in the extreme top fiber is to compensate for the small ductility of HSSS strands. This proposed design approach takes full advantage of HSSS strands and ensures adequate ductility by having the concrete strain in the extreme compression fiber reach the inelastic region before failure. This design type is the most economical approach for I-girder sections such as AASHTO Type II.

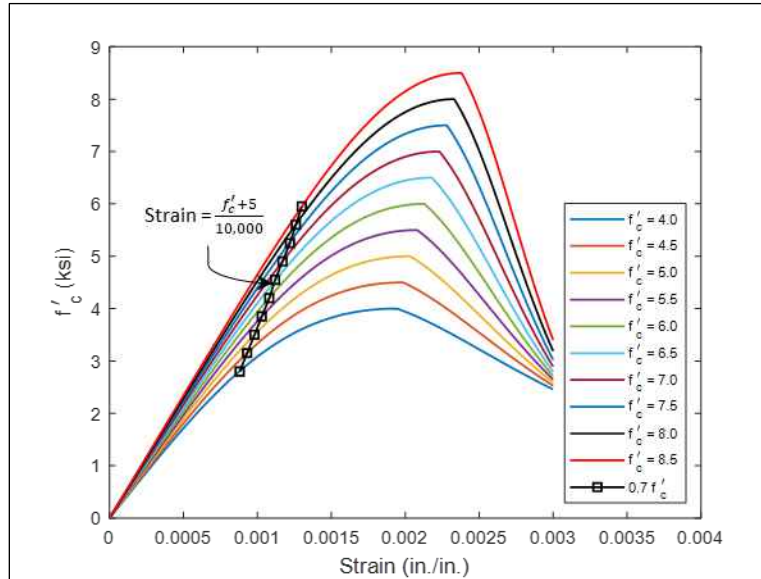


Figure 8-3 Concrete compressive stress-strain curves

8.2.2 Crushing of concrete

For the case of crushing of concrete, both deflection and cracking are primarily a function of strain in the HSSS strands at failure. This design type takes full advantage of the concrete in the compression zone; however, not as much advantage is taken from the HSSS strands. Even though designing for crushing of concrete failure mode requires a large prestressing reinforcement area compared to rupture of strand failure mode, the need for the large area might be due to service limit states, such as in the case of shallow sections such as Florida Slab Beams. The strain in the HSSS strands decreases when the reinforcement ratio increases. Thus, in the case of crushing of concrete failure mode, deformability can be obtained by ensuring that the net tensile strain in the HSSS strand is greater than 0.005. A net tensile strain lower than 0.005 is acceptable only after ensuring that the ultimate deflection of the concrete member prestressed with HSSS strands is equivalent to that of the same member prestressed with carbon steel strands. Further research is needed to establish this net tensile strain limit for design purposes. In this design type, the nominal flexural resistance of the member depends mainly on the condition and compressive strength of the concrete in the compression zone, which is in most cases the concrete in the bridge deck. Deterioration in the bridge deck slab due to weathering may result in a reduction in the member's dimension, and the resulting decrease in the nominal flexural resistance of the member could be accounted for during design.

For I-girder sections such as AASHTO Type II, this design type is impractical because of the limited space available for the strands in the section, and it is uneconomical because of the additional unnecessary strands. This design type is recommended for slab beam sections, where design is most likely controlled by the service limit state.

8.3 Balanced failure condition

Balanced failure condition occurs when strains in the extreme concrete fiber and bottom layer of HSSS strands simultaneously reach their maximum values. In other words, beams with a balanced reinforcement ratio fail by crushing of concrete and rupture of HSSS strands simultaneously as shown in Figure 8-4. The parabolic concrete stress distribution can be approximated by Whitney's rectangular stress block (Figure 8-4d), which can be defined by stress block factors, β_1 and α_1 . By considering equilibrium of internal forces, the following equation is obtained

$$\alpha_1 f'_c \beta_1 c b = A_{ps} f_{pu} \quad \text{Equation 8-1}$$

The balanced prestressing reinforcement area can be expressed as

$$A_{ps} = \rho_{ssb} b d \quad \text{Equation 8-2}$$

By substituting Equation 8-2 in Equation 8-1, one can obtain

$$\alpha_1 \beta_1 f'_c c b = \rho_{ssb} b d f_{pu} \quad \text{Equation 8-3}$$

The balanced reinforcement ratio can be obtained by rearranging Equation 8-3

$$\rho_{ssb} = \alpha_1 \beta_1 \frac{f'_c c b}{f_{pu} d} \quad \text{Equation 8-4}$$

Based on linear strain distribution shown in Figure 8-4b, one obtains

$$k_{pub} = \frac{c b}{d_1} = \frac{\epsilon_{cu}}{\epsilon_{cu} + \epsilon_{pu} - \epsilon_{pe}} \quad \text{Equation 8-5}$$

By substituting Equation 8-5 in Equation 8-10, the balanced reinforcement ratio can be expressed as

$$\rho_{ssb} = \alpha_1 \beta_1 \frac{f'_c}{f_{pu}} \frac{\epsilon_{cu}}{\epsilon_{cu} + \epsilon_{pu} - \epsilon_{pe}} \quad \text{Equation 8-6}$$

where

β_1 = stress block factor = ratio of depth of equivalent rectangular stress block to neutral axis depth

α_1 = stress block factor = ratio of equivalent rectangular concrete compressive stress block intensity to the concrete compressive strength

f'_c = concrete compressive strength

ϵ_{cu} = ultimate compressive strain of concrete, which is assumed to be 0.003 according to AASHTO

f_{pu} = ultimate tensile stress of HSSS strand

ϵ_{pe} and ϵ_{pu} = effective prestressing strain and ultimate tensile strain, respectively, in the HSSS strands

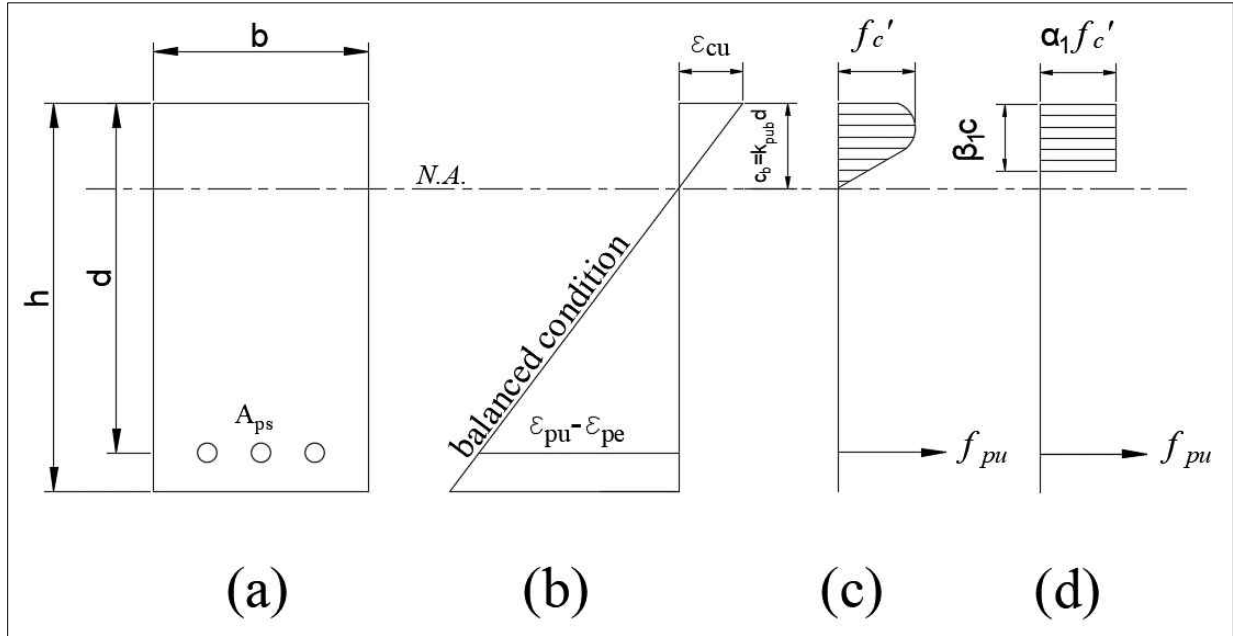


Figure 8-4 Strain and stress distributions for balanced failure condition.
 (a) cross section; (b) strain; (c) stress; and (d) stress (equivalent)

According to AASHTO Section 5.6.2.2 (2017), the stress block factor, α_1 , is equal to 0.85 for concrete compressive strength not exceeding 10 ksi; and the stress block factor, β_1 , is equal to 0.85 for concrete compressive strength not exceeding 4 ksi. For concrete strength greater than 4 ksi, the β_1 shall be reduced by 0.05 for each 1 ksi in excess of 4 ksi. The minimum value for β_1 is 0.65. Note that AASHTO provides values for stress block factors, α_1 and β_1 , only when the strain in the extreme compression fiber reaches its ultimate value of 0.003. The stress block factors, α_1 and β_1 , are functions of the concrete strain in the extreme compression fiber. (Collins and Mitchell 1991) proposed equations for stress block factors, α and β , for any strain values in the extreme compression fiber. Those equations were modified in NCHRP Project 12-97 (2019) and are given in Equation 8-7 and Equation 8-8, where ϵ'_c is calculated using Equation 8-9.

$$\beta = \frac{4 - (\epsilon_{cf} / \epsilon'_c)}{6 - 2 (\epsilon_{cf} / \epsilon'_c)} \left(-\frac{f'_c}{50} + 1.1 \right) \geq 0.65 \quad \text{Equation 8-7}$$

$$\alpha = \left(\frac{1}{\beta}\right) \left(\frac{\varepsilon_{cf}}{\varepsilon'_c} - \frac{1}{3} \left(\frac{\varepsilon_{cf}}{\varepsilon'_c}\right)^2\right) \left(-\frac{f'_c}{60} + 1\right) \quad \text{Equation 8-8}$$

$$\varepsilon'_c = \left(\frac{f'_c}{11} + 1.6\right) * 10^{-3} \quad \text{Equation 8-9}$$

The stress block factors, α and β , can be determined using the above equations when the concrete top fiber compression strain (ε_{cf}) is less than 0.003. To determine β_1 and α_1 factors when the concrete strain reaches its maximum value, ε_{cf} is taken to be equal to ε_{cu} , which is 0.003. Figure 8-5 shows the relationship between $\alpha_1\beta_1$ and concrete compressive strength when ε_{cf} equal 0.003. An equation is proposed in this study for the stress block parameters, $\alpha_1\beta_1$, and it is given in Equation 8-10.

$$\alpha_1\beta_1 = 0.77 - \frac{f'_c}{60} \quad \text{Equation 8-10}$$

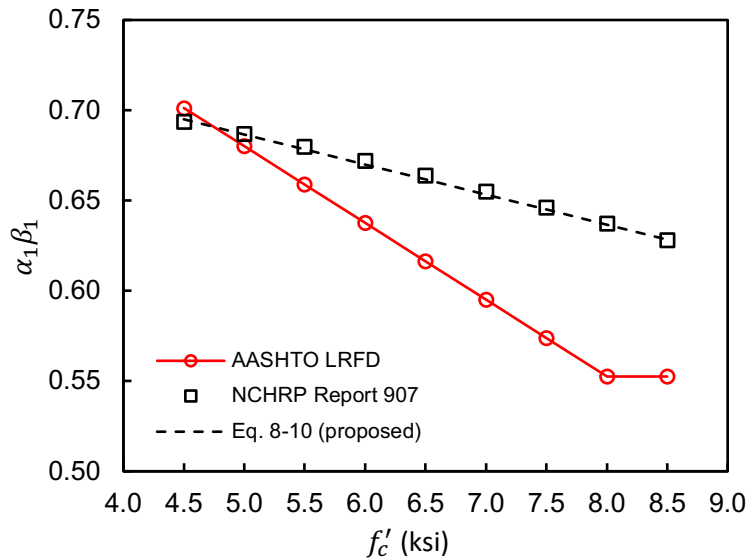


Figure 8-5 Prediction of stress block factors

The balanced reinforcement ratio, ρ_{ssb} , distinguishes between crushing of concrete failure mode and rupture of HSSS strands failure mode. The flexural capacity and deformability of concrete members prestressed with HSSS strands depend on whether the failure is governed by crushing of concrete or rupture of HSSS strand. If the HSSS reinforcement ratio is less than the balanced ratio ($\rho_{ss} < \rho_{ssb}$), the rupture of HSSS strand failure mode governs. Otherwise, crushing of concrete failure mode governs ($\rho_{ss} > \rho_{ssb}$).

8.4 Design equations for nominal flexural resistance

A nonlinear sectional analysis model was validated with experimental results in Chapter 7. The analytical model was then used to conduct parametric studies to develop analytical data covering

both crushing of concrete and rupture of strands failures. Based on analytical data, design equations were proposed for each failure mode, and they are discussed in the following sections.

8.4.1 Rupture of strand failure mode

When rupture of HSSS strand governs the design, the ultimate tensile strain of HSSS strands, ϵ_{pu} , is reached. However, the concrete top fiber compressive strain, ϵ_{cf} , does not reach the ultimate compressive strain, ϵ_{cu} , as shown in Figure 8-6b. In this case, Whitney's rectangular stress block cannot approximate the concrete stress distribution in the compression zone. The strain distribution in Figure 6b allows determination of the value for k_{pu} in terms of the available strain at failure (Equation 8-11).

$$k_{pu} = \frac{c}{d_1} = \frac{\epsilon_{cf}}{\epsilon_{cf} + \epsilon_{pu} - \epsilon_{pe}} \quad \text{Equation 8-11}$$

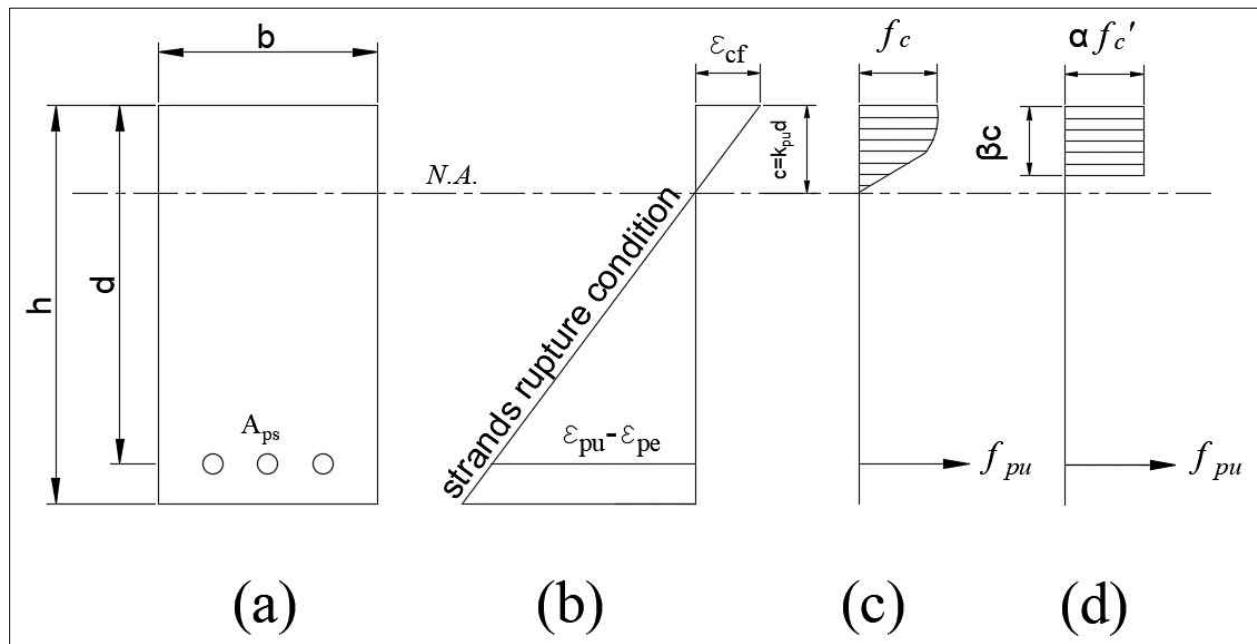


Figure 8-6 Strain and stress distributions for strands rupture failure condition.
 (a) cross section; (b) strain; (c) stress; and (d) stress (equivalent)

An analytical procedure was developed to determine the ratio of the depth of the neutral axis to the depth of bottom layer of prestressing reinforcement (k_{pu}) and to calculate the nominal flexural resistance (M_n). The procedure can be summarized in the following steps.

1. Determine the balanced reinforcement ratio, ρ_{ssb} , from the input parameters using Equation 8-6;
2. Select a reinforcement ratio, ρ_{ss} , lower than the balanced reinforcement ratio;
3. Assume a concrete strain value, ϵ_{cf} , at the extreme compression fiber (i.e. $\epsilon_{cf} = 0.0005$);

4. Increase the concrete top fiber strain (or neutral axis depth) until force equilibrium is achieved;
5. According to the strain distribution, calculate the value of k_{pu} using Equation 8-11; and
6. According to the stress distribution, calculate the nominal flexural resistance M_n .

Parametric studies were performed using the aforementioned procedure to generate analytical k_{pu} and M_n for a wide range of design parameters. The parametric studies were used to statistically derive a design approach for concrete members prestressed with HSSS strands and designed to fail by rupture of strand. The design parameters were as follows:

- Concrete compressive strength (f'_c) ranging from 4.5 ksi to 8.5 ksi;
- Effective prestress equal to 50%, 55% and 60% of the ultimate tensile strength; and
- Prestressing reinforcement ratio (ρ_{ss}) ranging from $0.2\rho_{ssb}$ to ρ_{ssb} .

A total of 540 isolated analyses were completed. A correlation analysis of the analytical k_{pu} data indicated that ρ_{ss}/ρ_{ssb} and f_{pe} have the most significant effect on k_{pu} . Based on regression analysis of the analytical k_{pu} data, Equation 8-12 was obtained.

$$k_{pu} = \left(0.7 \frac{\rho_{ss}}{\rho_{ssb}} + 0.26\right) k_{pub} \quad \text{Equation 8-12}$$

Figure 8-7 compares the k_{pu} data calculated from the analytical model and those from Equation 8-12. As shown, the proposed equation provides consistent and accurate predictions of k_{pu} .

The neutral axis depth (c) can be obtained by substituting Equation 8-5 and Equation 8-11 in Equation 8-12.

$$c = \left(0.7 \frac{\rho_{ss}}{\rho_{ssb}} + 0.26\right) c_b \quad \text{Equation 8-13}$$

The concrete strain in the extreme compression fiber (ε_{cf}) can be obtained by rearranging Equation 8-11

$$\varepsilon_{cf} = c \left(\frac{\varepsilon_{pu} - \varepsilon_{pe}}{d - c} \right) \quad \text{Equation 8-14}$$

Summing moments about the compression resultant (Figure 6d), the nominal flexural resistance can be computed by Equation 8-15 for concrete members prestressed with HSSS strands and designed to fail by rupture of strand.

$$M_n = f_{pu} A_{ps} \left(d_{avg} - \frac{\beta c}{2} \right) \quad \text{Equation 8-15}$$

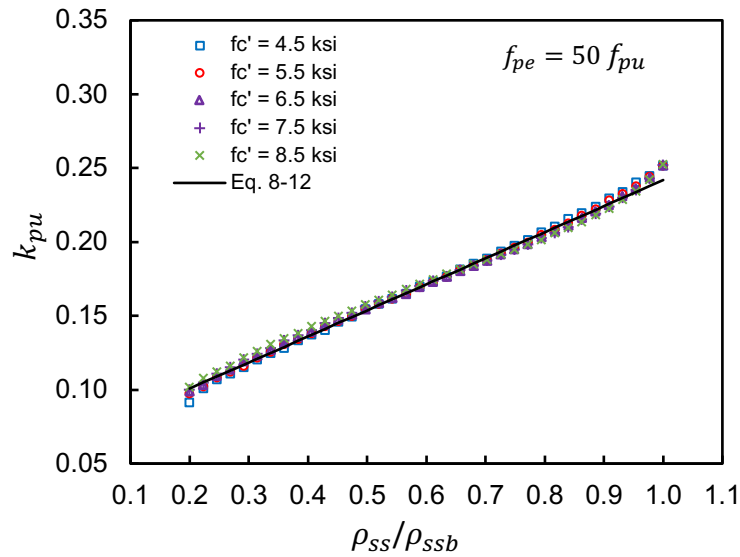
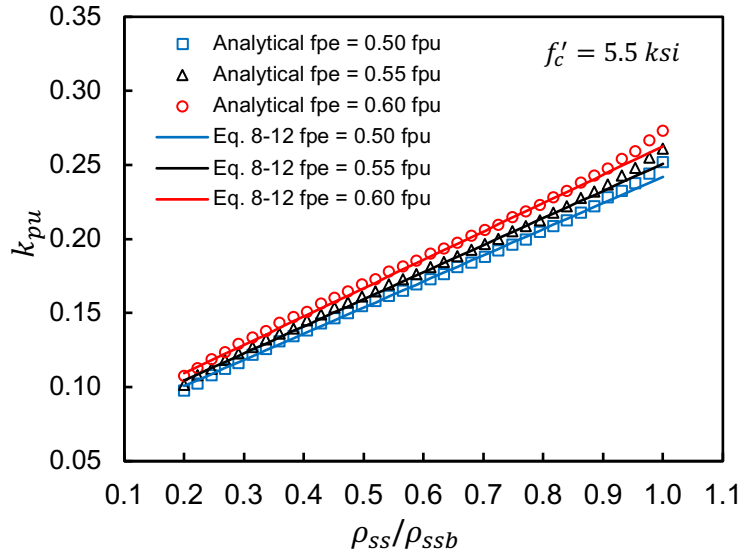


Figure 8-7 Variation in ratio of neutral axis depth to prestressing reinforcement depth, k_{pu} , for strand rupture failure condition

For concrete members prestressed with HSSS strands and designed to fail due to rupture of strand, the recommended minimum reinforcement ratio ($\rho_{ss,min}$) is the reinforcement ratio at which the concrete strain in the extreme compression fiber reaches inelastic strain, $(f'_c+5)/10,000$, before failure. Parametric studies were performed to generate analytical prestressing reinforcement ratios for a wide range of design parameters. The design parameters were as follows:

- Concrete compressive strength ranging from 4.5 ksi to 8.5 ksi; and

- Effective prestress force 50%, 55% and 60% of the ultimate tensile strength.

For each analysis, the minimum reinforcement ratio was found by satisfying the failure condition. A total of 15 isolated analyses were completed. The parametric studies were used to statistically derive an equation to specify the minimum reinforcement limit. A correlation analysis of the analytical data indicated that only f'_c has a significant effect on the minimum reinforcement ratio. Based on regression analysis of the analytical data, the minimum reinforcement ratio for concrete members prestressed with HSSS strands and designed to fail by rupture of the strand can be computed using the following equation.

$$\rho_{ss,min} = \left(\frac{50+33f'_c}{1,000} \right) \rho_{ssb} \quad \text{Equation 8-16}$$

The proposed equation is in good agreement with values obtained by the analytical model as shown in Figure 8-8. The minimum reinforcement ratio can be also expressed in terms of the ratio of the depth of the neutral axis to the depth of the bottom layer of strands (c/d). Figure 8-9 shows the relationship between c/d and concrete compressive strength (f'_c) for different effective prestress (f_{pe}). Equation 8-17 is proposed in terms of c/d as a limit for the reinforcement ratio. Figure 8-9 shows that the proposed equation provides consistent and accurate predictions of the minimum reinforcement ratios.

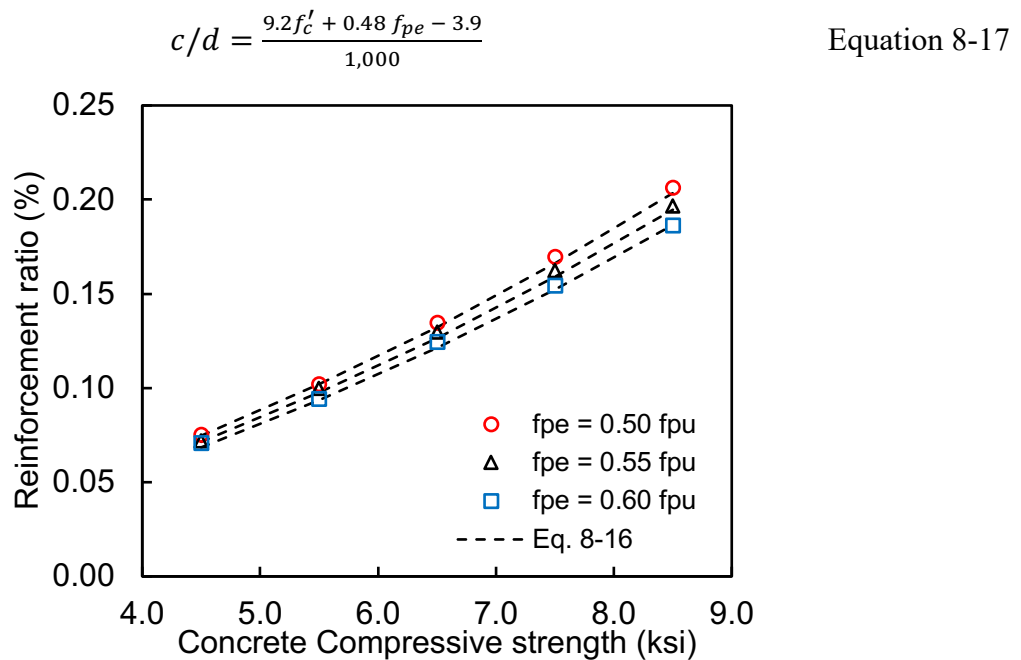


Figure 8-8 Variation of reinforcement ratio for stainless steel prestressed concrete member designed to fail due to rupture of strands

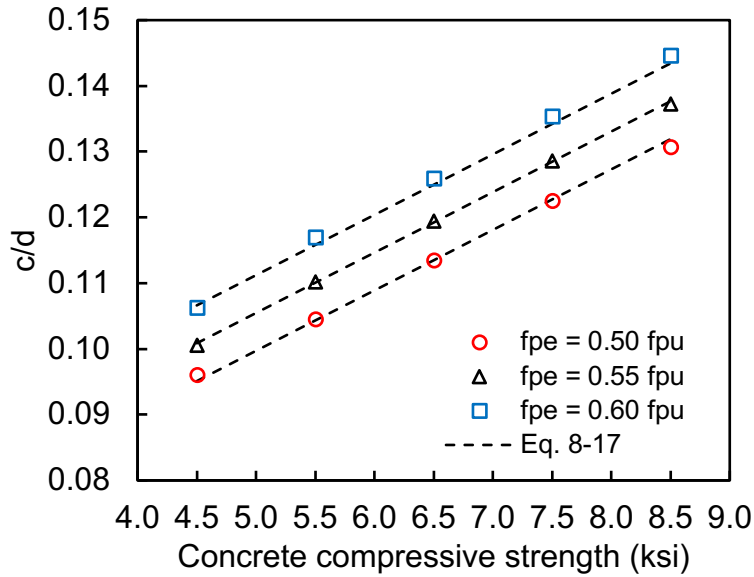


Figure 8-9 Variation in c/d for stainless steel prestressed concrete member designed to fail due to rupture of strands

8.4.2 Crushing of concrete failure mode

When crushing of concrete governs the design, the ultimate concrete compressive strain, ϵ_{cu} , at the extreme top fiber is reached. However, the strain in the HSSS strands does not reach its ultimate tensile strain, ϵ_{pu} . Therefore, the stress in the HSSS strands at failure needs to be determined. In this case, concrete stress distribution in the compression zone can be approximated by an equivalent rectangular stress block. The strain distribution in Figure 8-10 allows for the determination of k_{pu} in terms of the available strain at failure (Equation 8-18).

$$k_{pu} = \frac{c}{d_1} = \frac{\epsilon_{cu}}{\epsilon_{cu} + \epsilon_p - \epsilon_{pe}} \quad \text{Equation 8-18}$$

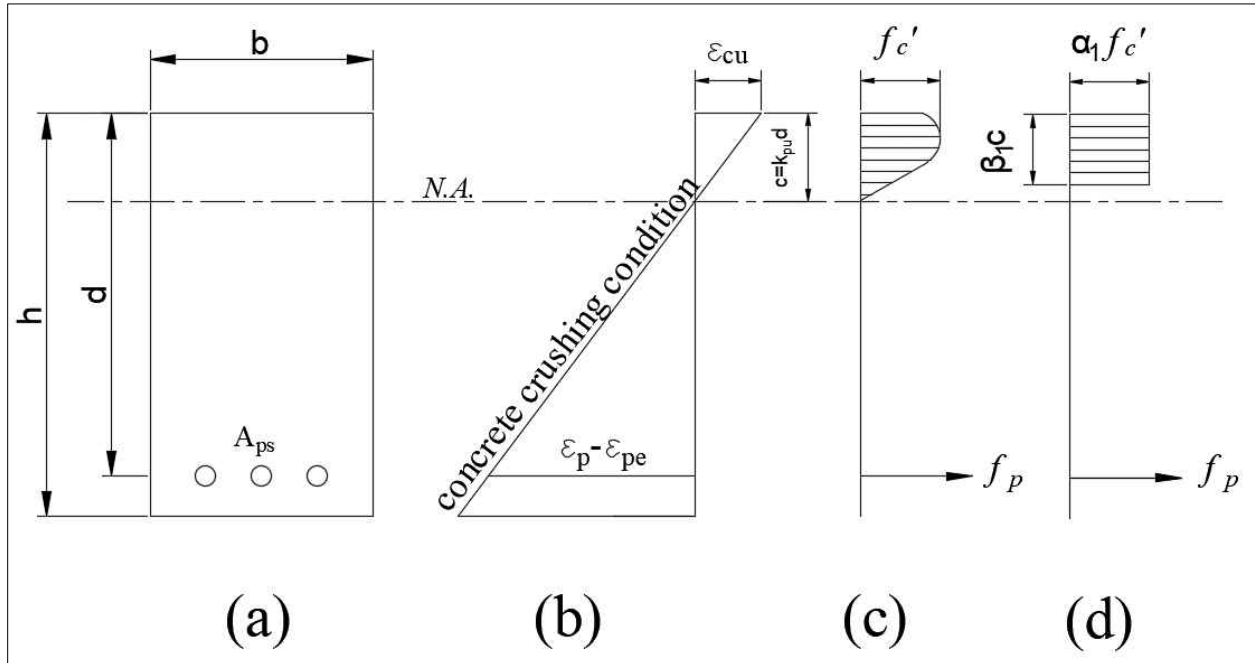


Figure 8-10 Strain and stress distributions for concrete crushing failure condition.
 (a) cross section; (b) strain; (c) stress; and (d) stress (equivalent)

An analytical procedure was developed to determine the ratio of the depth of the neutral axis to the depth of bottom layer of prestressing reinforcement (k_{pu}), the stress in the HSSS strands (f_p), and nominal flexural resistance (M_n). The procedure is summarized in the following steps.

1. Determine the balanced reinforcement ratio, ρ_{ssb} , from the input parameters using Equation 8-6;
2. Select a reinforcement ratio, ρ_{ss} , greater than the balanced reinforcement ratio;
3. Set the concrete strain value at the extreme compression fiber to be 0.003;
4. Assume the neutral axis depth, c , (i.e. $c = 0.1d$);
5. Increase the neutral axis depth until force equilibrium is achieved;
6. According to the strain distribution, calculate the value of k_{pu} using Equation 8-18; and
7. According to the stress distribution, calculate the nominal flexural resistance, M_n .

Parametric studies were performed using the aforementioned procedure to generate analytical k_{pu} and M_n for a wide range of design parameters. The parametric studies were used to statistically derive a design approach for concrete members prestressed with HSSS strands and designed to fail by crushing of concrete. The design parameters were as follows:

- Concrete compressive strength (f'_c) ranging from 4.5 ksi to 8.5 ksi;
- Effective prestress equal to 50%, 55% and 60% of the ultimate tensile strength; and

- Prestressing reinforcement ratio (ρ_{ss}) ranging from ρ_{ssb} to $1.34\rho_{ssb}$.

A total of 240 isolated analyses were completed. A correlation analysis of the analytical k_{pu} data indicated that ρ_{ss}/ρ_{ssb} and f_{pe} have the most significant effect on k_{pu} . Based on a regression analysis of the analytical k_{pu} data, Equation 8-19 was proposed.

$$k_{pu} = \left(0.8 \frac{\rho_{ss}}{\rho_{ssb}} + 0.2\right) k_{pub} \quad \text{Equation 8-19}$$

Figure 8-11 compares the k_{pu} data calculated from the analytical model and those from Equation 8-19. The proposed equation provides consistent and accurate predictions of k_{pu} for a wide range of analytical data.

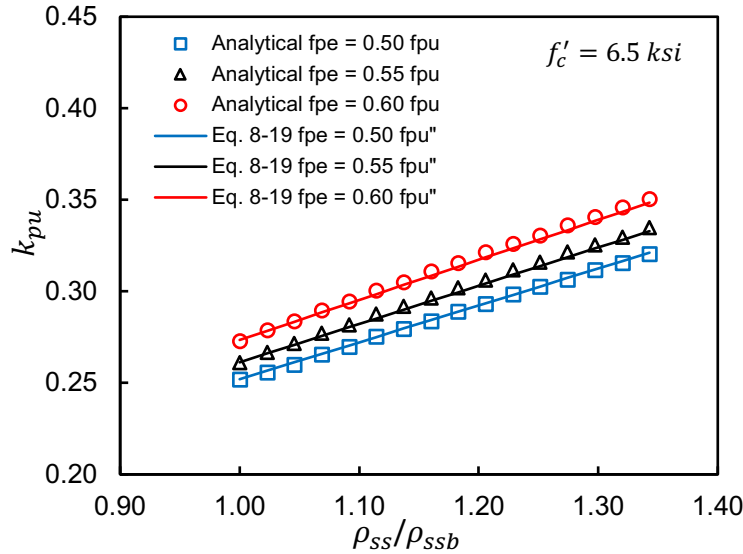


Figure 8-11 Variation in ratio of neutral axis depth to prestressing reinforcement depth, k_{pu} , for concrete crushing failure condition

The neutral axis depth (c) can be obtained by substituting Equation 8-5 and Equation 8-18 in Equation 8-19.

$$c = \left(0.8 \frac{\rho_{ss}}{\rho_{ssb}} + 0.2\right) c_b \quad \text{Equation 8-20}$$

The strain in the bottom layer of HSSS strands (ε_p) can be obtained by rearranging Equation 8-18

$$\varepsilon_p = \left(\varepsilon_{cu} \frac{d-c}{c}\right) + \varepsilon_{pe} \quad \text{Equation 8-21}$$

The stress in the prestressing strands (f_p) can be computed by using Equation 8-22

$$f_p = E_{ps} * \varepsilon_p \left\{ A + \frac{1-A}{[1+(B * \varepsilon_p)^c]^{1/c}} \right\} \quad \text{Equation 8-22}$$

where A , B , and C are coefficients, depending on the stress-strain curves of the HSSS strands. For design, A , B , and C coefficients shall be taken as 0.06, 101, and 6.45, respectively, and elastic modulus, E_{ps} , equals 24,000 ksi. More information about A , B , and C coefficients can be found in Section 3.4. Figure 8-12 compares f_p obtained from the analytical model to that obtained from Equation 8-22.

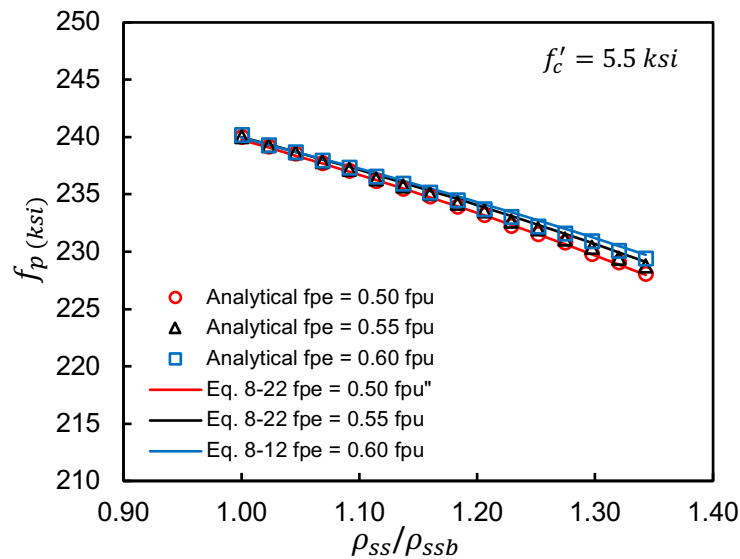


Figure 8-12 Comparison of stress in the prestressing reinforcement at failure

Once c and f_p are obtained from Equation 8-20 and Equation 8-22, respectively, the nominal flexural resistance, M_n , can be computed by Equation 8-23 for a concrete member prestressed with HSSS strands and designed to fail by crushing of concrete.

$$M_n = f_p A_{ps} \left(d_{avg} - \frac{\beta c}{2} \right) \quad \text{Equation 8-23}$$

As mentioned before, the design approach recommended herein, for crushing of concrete failure mode, is to have the net tensile strain in the HSSS strand greater than 0.005 at failure. The strain in the HSSS strands decreases when the reinforcement ratio increases; however, the nominal flexural strength increases. A maximum reinforcement limit is needed to ensure that the net tensile strain in the strand at failure is at least 0.005. As mentioned previously, further research is needed to establish this strain limit for design purposes. Parametric studies were performed to generate analytical prestressing reinforcement ratios for a wide range of design variables, and they were as follows:

- Concrete compressive strength ranging from 4.5 ksi to 8.5 ksi; and
- Effective prestress force 50%, 55% and 60% of the ultimate tensile strength.

For each analysis, the maximum reinforcement ratio was found by satisfying the failure condition. A total of 15 isolated analysis were completed. The parametric studies were used to statistically derive an equation to specify the maximum reinforcement limit. A correlation analysis of the analytical data indicated that only f_{pe} has a significant effect on the reinforcement ratio and c/d . Based on regression analysis of the analytical data, the maximum reinforcement ratio for concrete members prestressed with HSSS strands and designed to fail by crushing of concrete can be computed using the following equation.

$$\rho_{ss,max} = \left(\frac{2f_{pe}}{1,000} + 1.18 \right) \rho_{ssb} \quad \text{Equation 8-24}$$

The proposed equation provides consistent and accurate predictions of the maximum reinforcement ratios as shown in Figure 8-13. The maximum reinforcement ratio can be also expressed in terms of the ratio of the depth of the neutral axis to the depth of the bottom layer of strands (c/d), and the proposed equation is given in Equation 8-25.

$$\frac{c}{d} = \left(\frac{18f_{pe} + 1227}{10,000} \right) \quad \text{Equation 8-25}$$

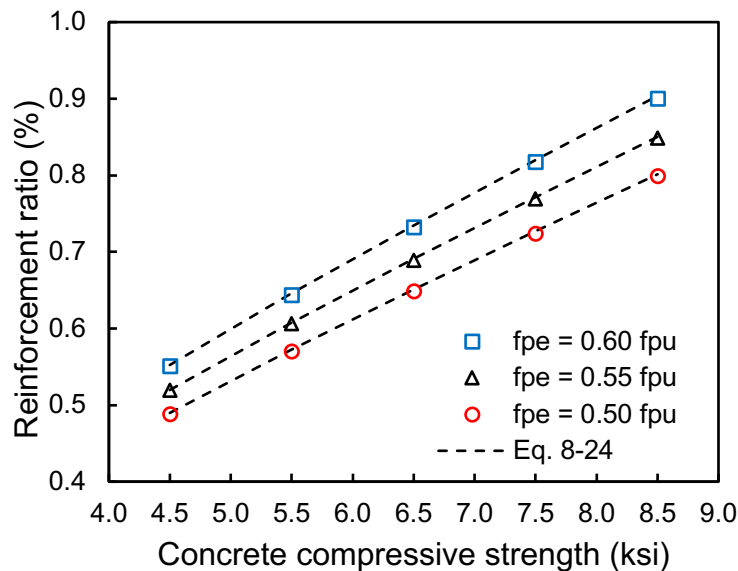


Figure 8-13 Variation of reinforcement ratio for stainless steel prestressed concrete members designed to fail due to crushing of concrete

8.5 Validation of proposed numerical equations

The proposed numerical equations were validated by comparing them to flexural strengths obtained from the experimental program. The experimental flexural strength (including moment due to self-weight) was 2561, 2051, 2024, 1703, 1688 and 1352 kip-ft for Girders C3, E1, E2, E3, E4, and E5, respectively. Note that all girders failed due to rupture of strand. Therefore, equations

given in Section 8.4.1 are used. All needed design variables for all tested girders are given in Table 8-1. Table 8-1 also provides the procedure using numerical equations to calculate the flexural strength of the girders. The proposed numerical equations are straightforward and do not require iterations. The calculated flexural strength was 2499, 1930, 1961, 1623, 1631, 1277 kip-ft for Girders C3, E1, E2, E3, E4, and E5, respectively. The calculated flexural strengths for Girders C3, E1, E2, E3, E4, and E5 were 97.6%, 94.1%, 96.9%, 95.3%, 96.6%, and 94.5%, respectively, of the experimental strengths. Figure 8-14 presents comparisons of the experimental and numerical strengths. The numerical equations predicted well the experimental results.

Table 8-1 Calculation of flexural strength using proposed numerical equations

Variable	Unit	Girder C3	Girder E1	Girder E2	Girder E3	Girder E4	Girder E5
b	in.	24					
d	in.	43	41				
d_{avg}	in.	41.15	39.18	39.18	36.67	36.67	39.86
A_{ps}	in ²	2.990	2.53	2.541	2.079	2.079	1.617
f_c'	ksi	6.84	6.44	6.76	7.44	7.44	7.44
f_{pu}	ksi	261.61	249.46				
ϵ_{cu}	in./in.	0.003					
ϵ_{pu}	in./in.	0.0181	0.0163				
ϵ_{pe}	in./in.	0.00551	0.00555	0.00558	0.00561	0.00570	0.00579
ρ_{ss} (Eq. 8-2)	-	0.00303	0.00269	0.00266	0.00217	0.00216	0.00168
$\alpha_1\beta_1$ (Eq. 8-10)	-	0.65607	0.66265	0.65733	0.64597	0.64597	0.64597
ρ_{ssb} (Eq. 8-6)	-	0.00330	0.00379	0.00395	0.00428	0.00431	0.00434
c_b (Eq. 8-5)	in.	8.276	8.945	9.092	9.111	9.177	9.235
c (Eq. 8-13)	in.	7.467	6.839	6.646	5.607	5.609	4.908
ϵ_{cf} (Eq. 8 – 14)	in./in.	0.00264	0.00215	0.00204	0.00166	0.00165	0.00140
ϵ'_c (Eq. 8 – 9)	in./in.	0.00222	0.00219	0.00221	0.00228	0.00228	0.00228
β (Eq. 8 – 7)	-	0.7540	0.7265	0.7190	0.6996	0.6990	0.6893
M_n (Eq. 8-15)	kip-ft	2499	1930	1961	1623	1631	1277

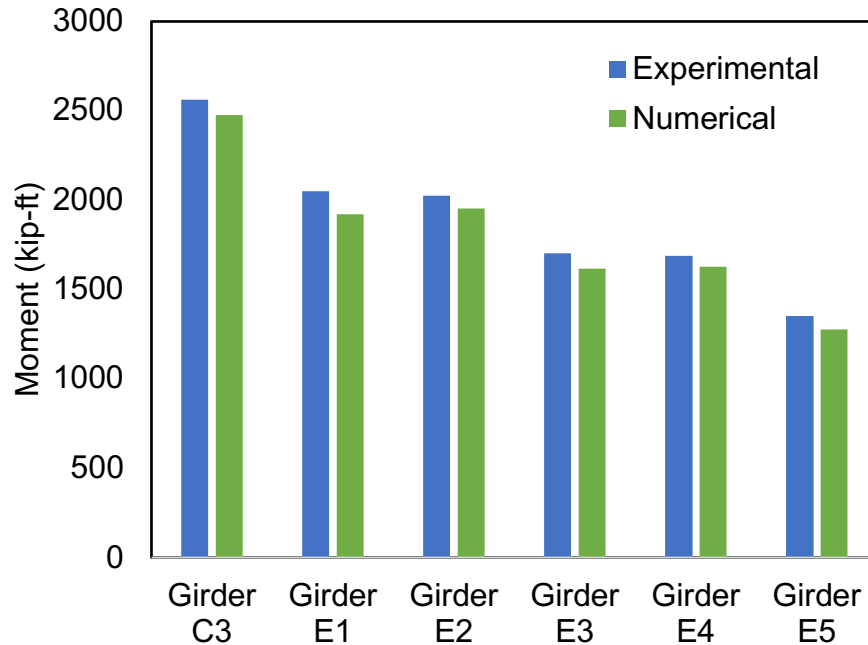


Figure 8-14 Experimental and numerical flexural strengths

8.6 Summary

For practical design purposes, designers prefer to use simple numerical equations to compute the nominal flexural resistance. Current design codes and specifications do not have numerical equations to compute the nominal flexural resistance for concrete members prestressed with HSSS strands. An analytical model was developed and validated with experimental results. Then, the model was used to perform a series of parametric studies to generate analytical data. Based on analytical data, numerical equations were developed to determine the nominal flexural resistance for concrete members prestressed with HSSS strands. The proposed numerical equations cover both crushing of concrete and rupture of strands failure modes. The proposed numerical equations were validated by comparing flexural strengths calculated using the proposed numerical equations and those obtained from the experimental program. The calculated flexural strengths of Girders C3, E1, E2, E3, E4, and E5 were 97.6%, 94.1%, 96.9%, 95.3%, 96.6%, and 94.5%, respectively, of the experimental strengths. Thus, it can be concluded that the calculated flexural strengths are in good agreement with those measured experimentally.

CHAPTER 9 FLEXURAL DESIGN GUIDELINES

9.1 Introduction

There are many differences in mechanical properties between HSSS and carbon steel strands, as discussed in Chapter 3. Therefore, design guidelines developed for concrete members prestressed with carbon steel strands (such as AASHTO LRFD) cannot be used for concrete members prestressed with HSSS strands. The flexural behavior of concrete girders prestressed with HSSS strands tend to have low deformability because of the limited ultimate strain of the strands. To use HSSS strands in flexural members, the low ultimate strain of HSSS strands shall be considered in the design procedure. However, current design codes and guidelines do not address this.

In this chapter, recommended design guidelines of concrete members prestressed with HSSS strands are discussed. This includes discussing the desired flexural failure mode, procedures, and equations to determine the nominal flexural resistance – introducing limits for minimum and maximum reinforcement, recommending strength resistance factors, and recommending the jacking stress limit.

9.2 Nominal resisting moment

9.2.1 Strain compatibility approach

The strain compatibility method, as opposed to using an equation, is a more theoretical way to calculate flexural behavior of a section, as it considers the stress-strain laws for the materials, as well as internal force equilibrium. It is recommended in multiple design codes and specifications. This approach was used to design the girders in this study and was described in Section 7.2.

9.2.2 Numerical approach

Designers prefer to use an equation type of approach to perform their preliminary designs. Equations were developed, as discussed in Chapter 8, to calculate the nominal flexural resistance for flexural members prestressed with HSSS strands. The proposed equations are only valid for rectangular sections. In the case of flanged sections, an iterative numerical approach was developed. In this research, design procedures were developed based on the failure mode of the beam, and they are given in the following sections.

9.2.2.1 Rupture of strand

The flowchart given in Figure 9-1 is proposed to determine the nominal flexural resistance of a rectangular beam designed to fail due to rupture of strand. Appendix F provides analysis and design examples of concrete members prestressed with HSSS strands following Figure 9-1.

The flowchart given in Figure 9-2 is proposed to determine the nominal flexural resistance for rectangular and flanged sections designed to fail due to rupture of strand. The proposed approach is simple and straightforward, but it requires multiple iterations to determine the nominal flexural resistance of the member.

9.2.2.1 Crushing of concrete

The flowchart given in Figure 9-3 is proposed to determine the nominal flexural resistance of a rectangular beam designed to fail due to crushing of concrete. Appendix F provides analysis and design examples of concrete members prestressed with HSSS strands following Figure 9-3.

The flowchart given in Figure 9-4 is proposed to determine the nominal flexural resistance for rectangular and flanged sections designed to fail due to crushing of concrete. The proposed approach is simple and straightforward, but it requires multiple iterations to determine the nominal flexural resistance of the member.

9.3 Recommended failure mode

Failure mode is defined here as the state where the concrete member prestressed with HSSS strands cannot withstand any further load in bending. In general, two failure modes are possible, and they are crushing of concrete in the compression zone and rupture of the strand in the tension zone. The type of failure mode is dependent on the depth of the section. For I-girder sections, the recommended failure mode is rupture of strands. For slab girders, the recommended failure mode is crushing of concrete in the compression zone.

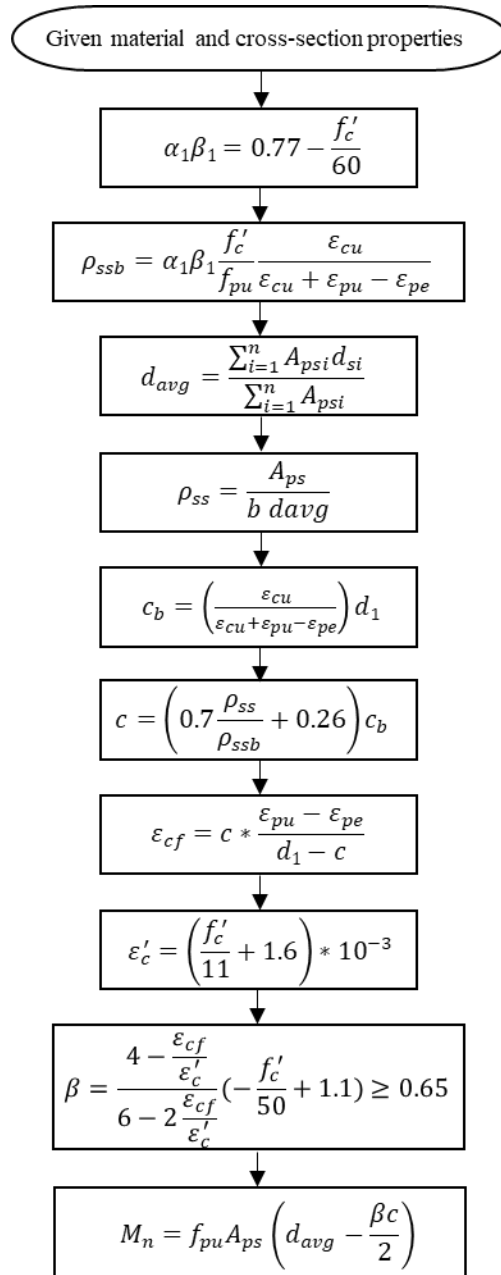


Figure 9-1 Design flowchart for concrete rectangular beam prestressed with HSSS strands and designed to fail due to rupture of strand

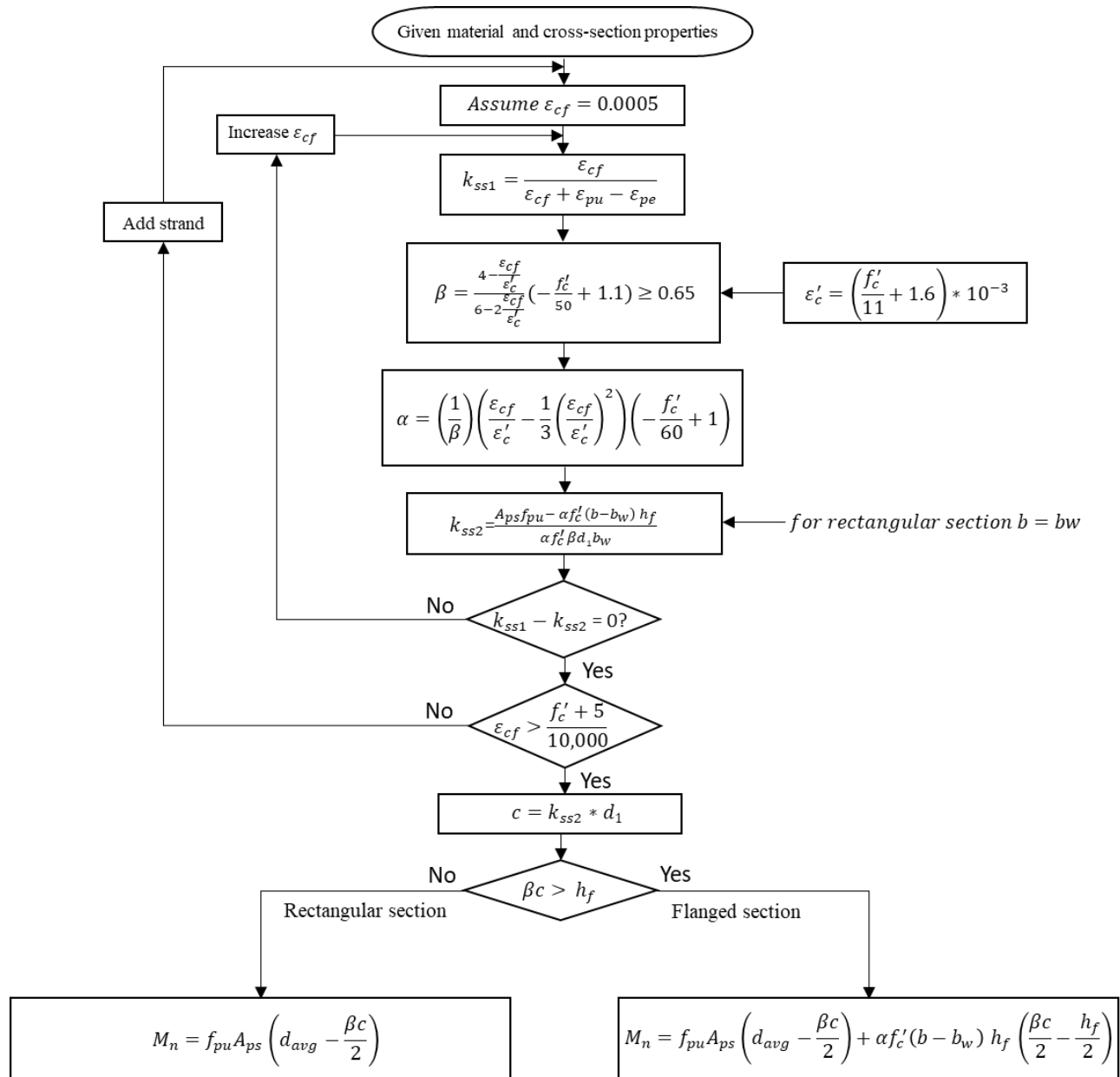


Figure 9-2 Iterative design procedure for concrete member prestressed with HSSS strands and designed to fail due to rupture of strand

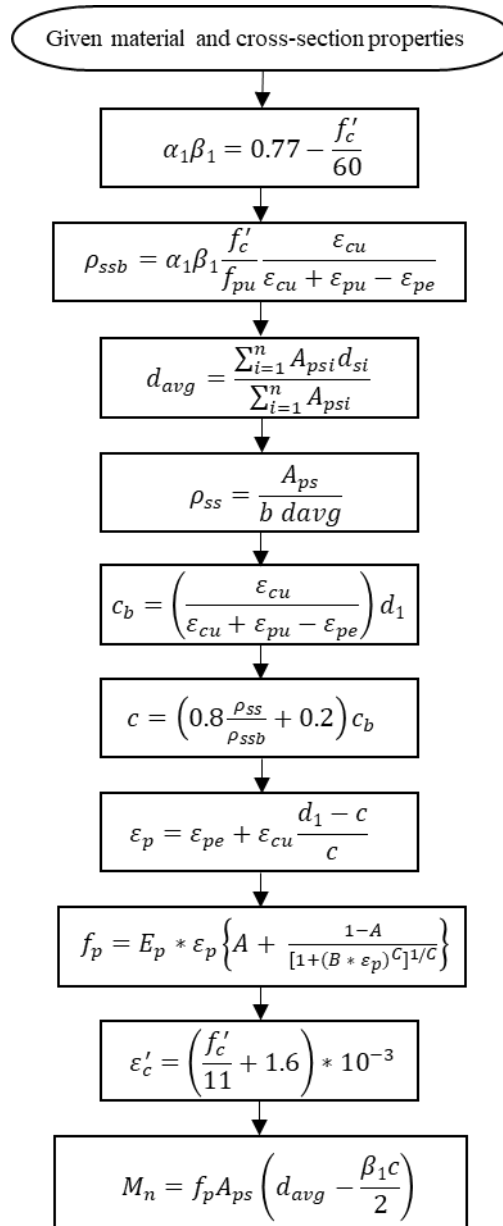


Figure 9-3 Design flowchart for concrete rectangular beam prestressed with HSSS strands and designed to fail due to crushing of concrete

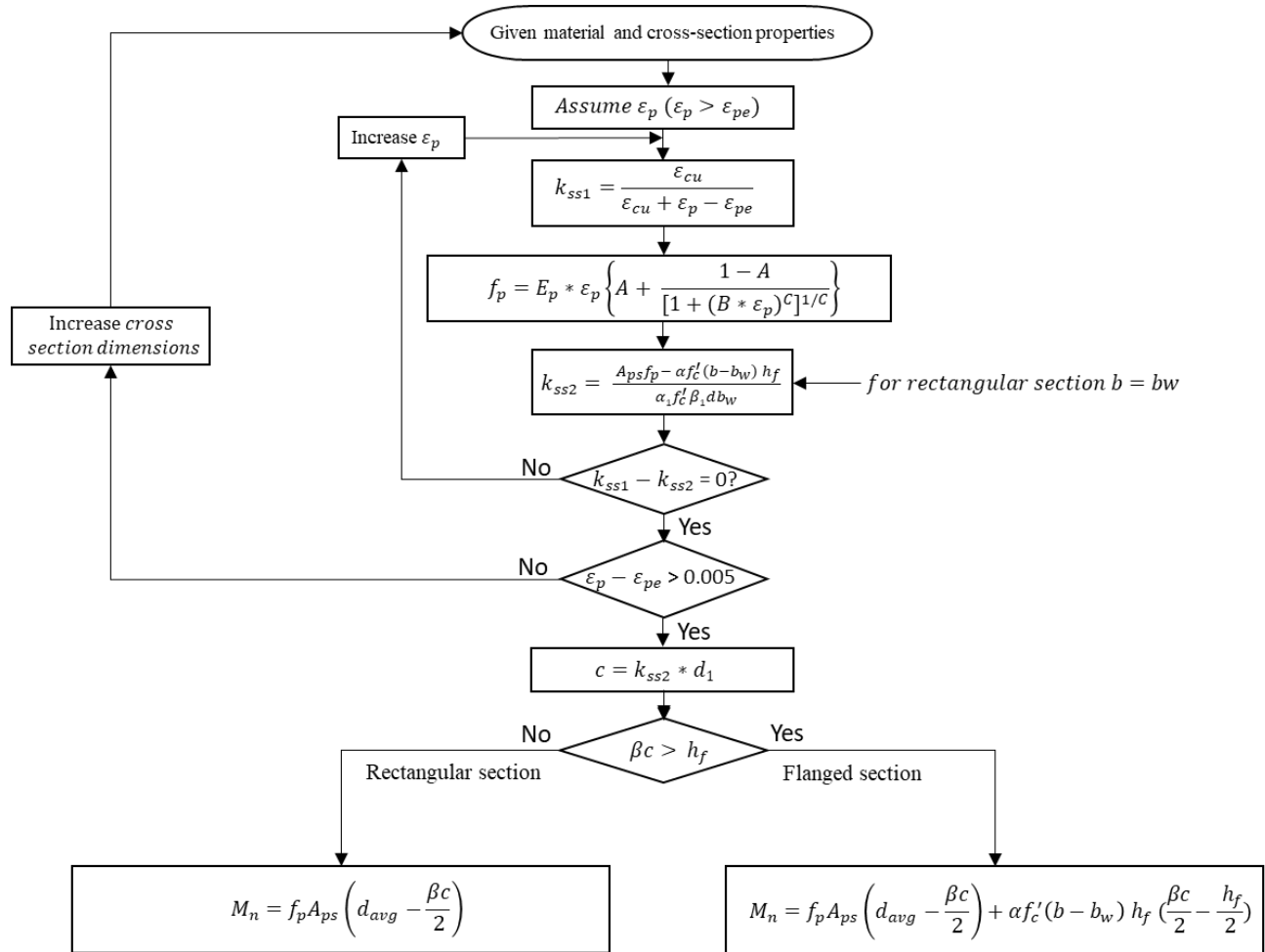


Figure 9-4 Iterative design procedure for concrete member prestressed with HSSS strands and designed to fail due to crushing of concrete

9.4 Recommended reinforcement limits

In addition to the minimum reinforcement limits in AASHTO Section 5.6.3.3, other reinforcement limits, based on failure mode of the section, are recommended in this study. The recommended reinforcement limits are to ensure adequate deformability before failure.

For concrete I-girders prestressed with HSSS and designed to fail due to rupture of strands, the deformability of the section is a function of concrete strain in the extreme compression fiber. Therefore, to ensure the concrete strain at failure is beyond the elastic limit, the prestressing reinforcement ratio in the section shall be greater than Equation 9-1. More information about development of Equation 9-1 can be found in Section 8.4.1.

$$\rho_{ss,min} = \left(\frac{50+33f'_c}{1,000} \right) \rho_{ssb} \quad \text{Equation 9-1}$$

For concrete slab beams prestressed with HSSS strands and designed to fail due to crushing of concrete, the deformability of the section is a function of strain in the bottom layer of HSSS strands. Adding prestressing reinforcement decreases the strain in the HSSS strands. Therefore, to ensure that the strain in the bottom layer of HSSS strands is higher than 0.005 (tension-controlled limit), the prestressing reinforcement ratio in the section shall not be greater than Equation 9-2. More information about development of Equation 9-2 can be found in Section 8.4.2.

$$\rho_{ss,max} = \left(\frac{2 f_{pe}}{1,000} + 1.18 \right) \rho_{ssb} \quad \text{Equation 9-2}$$

9.5 Recommended strength resistance factors

HSSS strands have different mechanical properties compared to those for carbon steel strands. The most significant difference is the ultimate strain. The minimum guaranteed elongation of an HSSS strand is 40% of the guaranteed ultimate strain of a carbon steel strand. Elongation of strand influences the deformability of the member and may control the nominal flexural resistance and behavior of the member. Therefore, strength resistance factors developed for carbon steel strands are not applicable for HSSS strands, and new strength resistance factors shall be developed to consider the strands' low ductility. Strength resistance factors are usually determined by conducting a reliability analysis covering a wide range of design parameters. However, a reliability analysis study to determine the strength resistance factors for concrete members prestressed with HSSS strands was not within the scope of this work.

HSSS strand shares the same low ductility property with fiber-reinforced polymer (FRP) tendons; i.e. Carbon and Aramid composites. Kim and Nickle (2016) proposed strength resistance factors for CFRP- and AFRP-prestressed concrete girders by conducting a robust reliability analysis (Kim and Nickle 2016). The proposed strength resistance factors for both CFRP and AFRP tendons were 0.80 when the net tensile strain is lower than 0.002 (referred to as a compression-controlled section) and 0.75 when the net tensile strain is greater than 0.005 (referred to as a tension-controlled section) as shown in Figure 9-5. Note that those strength resistance factors were determined for a reliability index of 3.5. Even though the elastic modulus and the guaranteed ultimate stress and strain of the CFRP tendon were different than those of the AFRP tendon as shown in Figure 9-6, the proposed strength resistance factors for CFRP and AFRP tendons were similar. Therefore, it can be concluded from Kim and Nickle's work that the differences in the elastic modulus and the guaranteed ultimate stress and strain between CRFP and AFRP tendons did not influence the strength resistance factors. This conclusion can be applied to

HSSS strands as their elastic modulus and guaranteed ultimate strain and stress are not much different than those for CFRP tendon or AFRP tendon as shown in Figure 9-6. HSSS strand has a lower guaranteed ultimate strain than both CFRP and AFRP tendons, but its guaranteed ultimate stress is between that of CRFP and AFRP tendons. Based on strength resistance factors for CFRP and AFRP tendons and similarities of mechanical properties of HSSS strands with CFRP and AFRP tendons, it can be concluded that the strength resistance factors for members prestressed with HSSS strands are not expected to be different than those proposed for members prestressed with CFRP or AFRP tendons. Further research is needed to determine the strength resistance factors of members prestressed with HSSS strands through a robust reliability analysis. As mentioned previously, reliability analysis was not within the scope of this project; however, it is within the scope of the NCHRP Project 12-120, which is currently in progress. Until further research, the recommended strength resistance factor for concrete members prestressed with HSSS strands is 0.75.

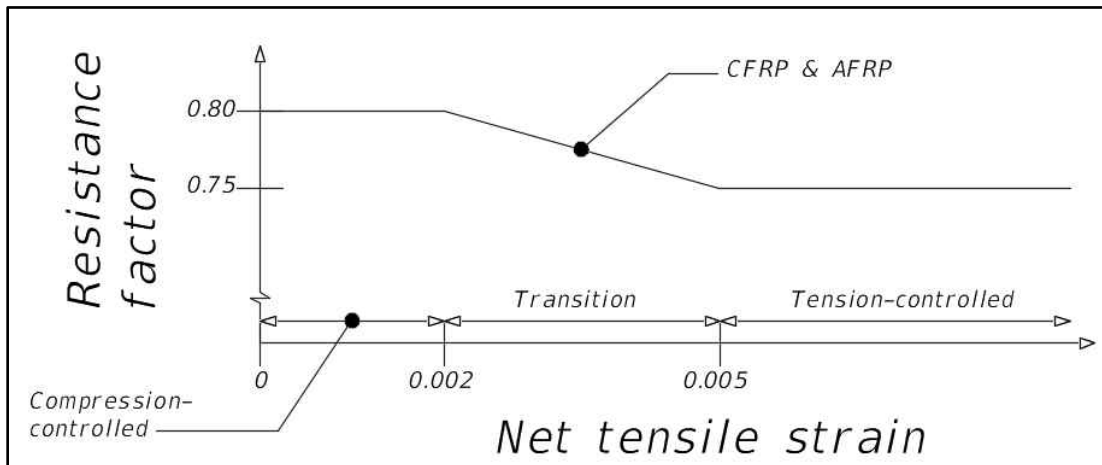


Figure 9-5 Strength resistance factors for CFRP and AFRP tendons

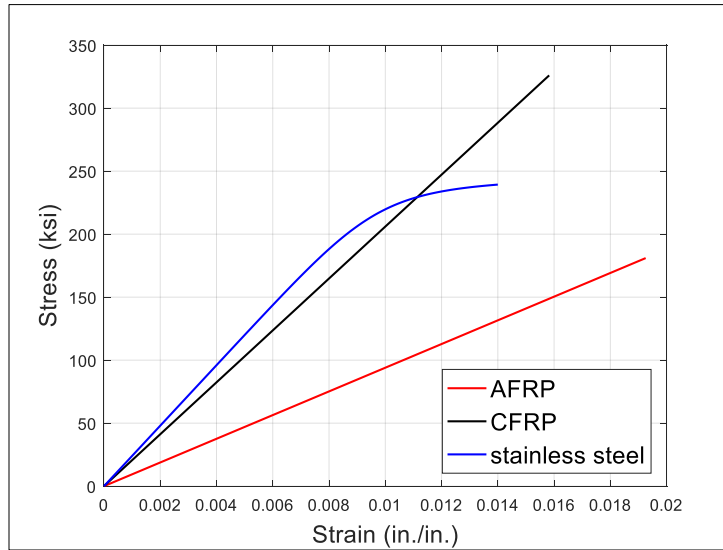


Figure 9-6 Stress-strain relationship of AFRP and CFRP tendons and stainless steel strands

The strength resistance factor is a function of the net tensile strain in the HSSS strands. Based on the proposed design approach for flexural members prestressed with HSSS strands, the net tensile strain in the HSSS strands at failure shall be greater than 0.005, as shown in Figure 9-7. In other words, both crushing of concrete and rupture of strand failures are within the tension-controlled region. For example, suppose the stress in the HSSS strands at transfer is 70% of ultimate, which is 168 ksi. Assuming prestress losses of 15%, the effective prestress in the HSSS strands is 142.8 ksi, which is equivalent to an effective strain of 0.006. As shown in Figure 9-7, crushing of concrete failure mode occurs when the net tensile strain is lower than 0.008, and rupture of strands failure mode occurs when the net tensile strain is equal to 0.008.

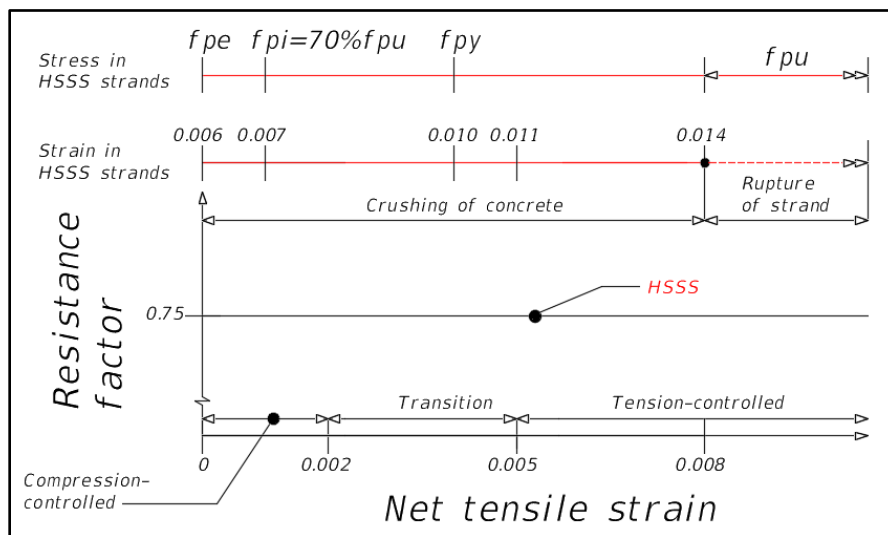


Figure 9-7 Recommended strength resistance factors for HSSS strands

The authors recommend that the terms “compression-controlled” and “tension-controlled” not be used for members prestressed with HSSS strands. Instead, the failure mode should be differentiated as either “concrete crushing failure” or “strand rupture failure”. The resistance factor, needing further study, should be dependent on the failure mode.

9.6 Recommended stress limit

The maximum stress limit for carbon steel strands immediately prior to transfer is 75% of their ultimate strength. A lower fraction of the tensile strength might need to be specified when HSSS strands are used, for two reasons. First, HSSS strands have limited strain capacity, which is significantly lower than that for carbon steel strands. Second, HSSS strands have a different stress-strain curve than carbon steel strands, and the elastic modulus deviates earlier also. The stress in HSSS strands immediately prior to transfer determines the reserved strain and stress that are available between service and strength states. In general, larger initial stress is desirable for the service limit state. However, in the case of HSSS, lower initial stress is also desirable to provide adequate deformability at failure. Thus, the strain capacity of the HSSS strands in design must be balanced between flexural strength and deformability. The stress in HSSS strands immediately prior to transfer influences the type of failure mode (rupture of strand and crushing of concrete). In this research, the HSSS strands were stressed to 65% of their ultimate strength. A higher percentage was used by the Louisiana Department of Transportation in construction of piles using HSSS strands (Brown 2018); the specified initial stress in HSSS strands was 70% of their ultimate stress. As of 2020, a total of 17 projects used HSSS strands, but information about the initial stress in HSSS strands used in other projects is not available to the authors.

The stress in carbon steel strands immediately prior to transfer is typically 75% of their ultimate strength ($0.75 \times 270 \text{ ksi} = 202 \text{ ksi}$). Typical losses are often estimated at about 25 ksi, resulting in an effective stress of about 175 ksi. This results in nearly 95 ksi ($270 \text{ ksi} - 175 \text{ ksi}$) stress available for the failure limit state. For concrete members prestressed with HSSS and designed to fail due to rupture of strand (i.e. the strand reaches 240 ksi), the HSSS strands need to provide the same 95 ksi available stress for the failure limit state. Therefore, the effective stress needs to be about 145 ksi ($240 \text{ ksi} - 95 \text{ ksi}$). Using the same assumption for prestress losses of about 25 ksi, the initial stress would be 170 ksi ($140 \text{ ksi} + 25 \text{ ksi}$). Therefore, the initial stress for rupture of strand failure mode can be estimated at 70% of the 240 ksi ultimate strength ($170/240 \approx 0.70$). Note that the reserved stress that is available between the effective stress and failure limit state is lower than 95

ksi when members are designed to fail due to crushing of concrete because the stress in the bottom layer of HSSS strands is lower than 240 ksi. However, for concrete members designed to fail due to crushing of concrete (i.e. slab girders), those members are most likely controlled by service III not strength I limit state. In other words, the required number of strands is determined to satisfy tensile stress limits, which results in a larger number of strands than strength I limit state requires. Thus, the total initial stress when service III limit state controls the design is larger than when the design is controlled by strength I limit state.

The maximum recommended stress in HSSS strands immediately prior to transfer is 70%. Note that the jacking stress may be more than the design stress because the latter must be adjusted in the construction yard to include seating losses and to accommodate compensation for temperature differences. The maximum recommended allowable jacking stress for HSSS strands is 75% of their ultimate strength.

Initial stress is more of a design variable when HSSS strands are used because of the brittle behavior of the strands. A lower initial prestress might be chosen to allow for ductility for the overload condition.

9.7 Summary

HSSS strands are new to the construction industry, and no design guidelines/specifications or codes have been drafted yet to assist engineers in the design of concrete flexural members prestressed with HSSS strands. The proposed design guidelines are summarized below.

1. Two failure modes, crushing of concrete and rupture of strands, are feasible when HSSS strands are used in flexural concrete members.
2. A non-iterative approach is proposed to determine the nominal flexural resistance of a rectangular beam prestressed with HSSS strands. For flanged sections prestressed with HSSS strands, a simple iterative approach is proposed to determine the nominal flexural resistance.
3. The recommended failure mode for I-girder sections such as AASHTO Type II is rupture of strand. In this case, the member fails due to rupture of the strands before the concrete in the compression zone reaches its ultimate strain. The ductility of the member is a function of the strain in the extreme compression fiber. Therefore, it is recommended that the concrete strain at the extreme compression fiber be greater than $(f'_c+5)/10,000$ at failure. A numerical equation is proposed to determine the minimum reinforcement ratio to ensure that the concrete strain in the extreme compression fiber reaches inelastic strain before failure.

4. The recommended failure mode for slab girders is crushing of concrete. In this case, the member fails due to crushing of concrete in the compression zone before the strands reach their ultimate stress. The ductility of the member is a function of the strain in the HSSS strands. Therefore, it is recommended that the net tensile strain in the bottom layer of HSSS strands be greater than 0.005 at failure. A numerical equation is proposed to determine the maximum reinforcement ratio to ensure that the net tensile strain in the bottom layer of strands is greater than 0.005. Net tensile strain lower than 0.005 is acceptable after ensuring that the designed section exhibits large deformability at failure equivalent to the same section designed with carbon steel strands. Further research is needed to establish this net tensile strain limit for design purposes.
5. Until further studies, a strength resistance factor of 0.75 is recommended for both crushing of concrete and rupture of strand failure modes. More research is needed to determine the strength resistance factors for HSSS strands by conducting a reliability analysis.
6. The maximum recommended stress in HSSS strands immediately prior to transfer is 70% of their guaranteed ultimate strength, and the initial jacking stress shall not be greater than 75%.

CHAPTER 10 SHEAR TEST

10.1 Introduction

The main objectives in designing any concrete structure are strength, safety and durability. The strength and safety of the structure are directly related to its durability. Durability can be maintained by protecting the internal reinforcement. In bridges in extremely aggressive environments, the superstructure components, i.e. slabs and girders, are susceptible to corrosion damage, and they deteriorate when their reinforcing materials corrode. Corrosion of reinforcing materials happens when chloride ions exist; chloride ions can penetrate through the concrete and reach reinforcement. To improve durability of concrete members in extremely aggressive environments, corrosion-resistant and/or corrosion-free materials may be implemented for both longitudinal and transverse reinforcement. Corrosion-resistant strands, e.g., HSSS, can address corrosion issues in horizontal reinforcement, but corrosion also occurs in transverse reinforcement. One available option for the transverse reinforcement is GFRP bars. The corrosion-free property of GFRP bars makes them appealing for use in prestressed concrete bridges in harsh environments. However, they are known to have low transverse shear capacity. Stainless steel bars are another viable option for the transverse reinforcement. They have high corrosion resistance and seem to be a very promising choice for use in concrete structures in severe environments. However, the high corrosion resistance of stainless steel bars comes with a price. The initial cost of stainless steel bars is significantly higher than that of carbon steel bars. On the other hand, stainless steel bars may reduce maintenance and inspection costs and associated disruptions to the public.

Even though the designed service life of a prestressed concrete member can be enhanced with the use of GFRP or stainless steel bars as shear reinforcement, the member capacity needs to be evaluated. The mechanical characteristics of GFRP or stainless steel bars can significantly influence the shear behavior, failure mode, and ultimate load carrying capacity of prestressed concrete members. Insufficient, limited information is available to practicing engineers regarding the shear performance of prestressed members reinforced with GFRP or stainless steel stirrups. The lack of large-scale experimental data has delayed the use of GFRP and stainless steel rebars as shear reinforcement in prestressed concrete flexural members.

This chapter covers an experimental program to investigate the shear behavior of pretensioned concrete I-girders with either GFRP or stainless steel rebars as shear reinforcement. Also, this experimental program investigated the effect of using stainless steel strands as the main

longitudinal strands on the shear behavior of prestressed concrete girder. The behavior of the tested girder was evaluated for the cracking and ultimate loads, load-deflection response, shear capacity, strain in the transverse reinforcement, and failure mode. The experimental shear capacities are compared with the predicted shear capacities from the current ACI and AASHTO LRFD provisions.

10.2 Literature review

10.2.1 Glass Fiber Reinforced Polymer rebars

Fiber Reinforced Polymer (FRP) bars are commercially available as reinforcement for reinforced and prestressed concrete members. The most known and used FRPs in the construction industry are carbon (CFRP), aramid (AFRP), and glass (GFRP). CFRP was first used as primary flexure and shear reinforcement in a bridge in Canada in 1994 (Rizkalla and Tadros 1995). GFRP bars have become more attractive to the construction industry due to their lower cost compared to the other types, CFRP and AFRP (Ahmed et al. 2010). Several studies have evaluated the performance of reinforced concrete members with GFRP bars as shear reinforcement in normal strength concrete (Ahmed et al. 2010; Guadagnini et al. 2006; Johnson and Sheikh 2016), high-strength concrete (El-Sayed et al. 2006), and geopolymer concrete (Maranan et al. 2017). As a result, many concrete structures have utilized GFRP bars as the primary reinforcement (Rossini and Nanni 2019). Since FRP bars have attracted the construction industry, many design codes and specifications have been developed worldwide to guide engineers in designing FRP reinforced concrete structures, such as American Concrete Institute ACI 440.1R (2015), Canadian Standards Association S806 (2012), and *AASHTO LRFD Bridge Design Specifications* (2018).

FRP bars are corrosion-free; this characteristic makes them desirable in concrete applications in extremely aggressive environments where corrosion is an issue and long-term resistance to corrosion is needed. FRP bars are nonmetallic and therefore have different bond characteristics compared to that of traditional steel bars (Ahmed et al. 2010). Moreover, FRP bars have different mechanical properties as well. Both bond and mechanical characteristics of FRP bars have a significant effect on the flexural behavior of FRP-reinforced concrete members. The flexural rigidity of an FRP-reinforced concrete beam is lower than an equivalent beam reinforced with traditional steel bars because of the lower elastic modulus of FRP bars. In addition, the shear capacity of a reinforced concrete member with FRP bars as shear reinforcement is expected to be

lower than one with traditional steel bars. Thus, FRP bars cannot directly replace traditional steel bars.

In North America, a significant number of bridges are girder-type, which consists of longitudinal girders, deck slabs, and barriers (Ahmed et al. 2009). Corrosion-free and/or corrosion-resistant bars and tendons are attractive for this type of bridge located in severe environments such as marine and cold regions where deicing salts are used. In girder-type bridges, usually prestressed concrete girders are precast off-site, and the deck slab is cast on site. The advantage of adding a composite deck slab is to increase the stiffness and load carrying capacity of the section. The vertical shear stirrups are extended out of the girder's top face and into the slab to provide interface shear capacity for the composite section. The interface shear capacity depends on multiple parameters such as the top surface finish of the girder, amount of transverse reinforcement crossing the interface, and the type and/or grade of reinforcement (Patnaik 2001). Interface shear failure happens when the two concrete sections (the slab and girder) slip at the interface joint. Once slippage occurs, the composite section loses its monolithic behavior, and the girder and deck slab act independently.

To the authors' knowledge, limited studies have been performed to investigate the shear capacity of prestressed concrete girders with GFRP bars as shear reinforcement. (Nabipay and Svecova 2013) conducted an experimental investigation on the shear behavior of CFRP prestressed concrete T-beams with GFRP as shear reinforcement. (Alkatan 2016) studied the interface shear resistance of GFRP bars in 20 large scale push-off specimens. It was concluded that a minimum interface reinforcement ratio of 0.405%, or in other words a minimum reinforcement stiffness of 29.44 ksi, is required to activate the GFRP bars to resist transverse shear. (The reinforcement stiffness, $E\rho$, is the elastic modulus times reinforcement ratio of bars). The mechanical properties, such as elastic modulus, of the GFRP bars differ from one manufacturer to another. Therefore, the reinforcement stiffness is a more general term, which can be used for any GFRP type. The use of GFRP bars as shear reinforcement in prestressed concrete girders has been very limited mainly due to the lack of research, sourcing and availability, and their high initial cost. Also, the mentioned design codes and specifications do not include any equations to determine the shear capacity of a prestressed concrete girder with GFRP bars as shear reinforcement.

10.2.2 Stainless steel rebars

Stainless steel rebars have high corrosion resistance and have been used in the construction industry for many decades. Stainless steel rebars have comparable, mostly higher, mechanical characteristics as carbon steel rebars. Stainless steel rebars have been used as main reinforcement in deck-slabs in bridges in cold regions where deicing salts are used. More information about stainless steel rebars can be found in Section 2.7.1.

10.3 Experimental program

10.3.1 Material properties

10.3.1.1 Glass Fiber Reinforced Polymer rebars

GFRP bars were selected because of their lower cost compared to CFRP and AFRP rebars. Information about mechanical properties of the GFRP bars used in this experimental program can be found in Section 4.2.4.2.

10.3.1.2 Stainless steel rebars

Duplex stainless steel rebars Grade 75 were selected because of their high strength and corrosion resistance compared to other stainless steel types. The stainless steel rebars used in this study satisfied the FDOT requirements per FDOT Standard Specifications for Road and Bridge Construction Section 931 (2020). Information about mechanical properties and chemical composition of the stainless steel bars used in this experimental program can be found in Section 4.2.4.2.

10.3.1.3 Prestressing strands

Two types of prestressing reinforcement were used, carbon steel and HSSS strands. Table 10-1 shows the mechanical properties of both types of strands, provided by the manufacturer. Note that the properties differ, especially the ultimate strain and modulus of elasticity. More information about the mechanical and bonds strength properties of HSSS strands can be found in Chapter 3.

10.3.1.1 Concrete

Two types of concrete were used, self-consolidating concrete (SCC) for the girders and normal-weight concrete for the deck slabs, with specified strengths of 10 ksi and 6.5 ksi, respectively. Several cylinders were taken from the concrete batches used to cast the girders and deck slabs and were tested on the day of the shear test.

Table 10-1 Mechanical properties of the HSSS and carbon steel strands

Mechanical properties	HSSS strands Grade 2205	Carbon steel strands Grade 270
Diameter (in.)	0.6	0.6
Area (in ²)	0.2328	0.2184
Yield strength (lb)	52,919	55,500
Breaking strength (lb)	59,755	60,900
Ultimate strain (in./in.)	1.90	6.33
Modulus of elasticity (ksi)	24,400	28,700

10.3.2 Specimen fabrication

Three of the eight 42-ft-long AASHTO Type II girders were tested in shear. Those were Girders A2, A3, and B3. More information about fabrication of the girders can be found in Section 4.2.5. Table 10-2 shows the testing matrix of this experimental program. Girders A2 and A3 had 11 0.6-in.-diameter, low-relaxation Grade 270 carbon steel strands as longitudinal prestressing. The transverse reinforcement of Girder A2 was GFRP rebars, while Girder A3 had stainless steel rebars. Girder B3 had 11 0.6-in.-diameter HSSS strands as longitudinal prestressing and stainless steel rebars as transverse reinforcement. Girders A2 and A3 had the same prestressing reinforcement type, ratio, and force, but different transverse reinforcement type and ratio. Girders A3 and B3 had different prestressing reinforcement type, ratio, and force, but the same transverse reinforcement type and ratio. Even though all girders had the same number of strands, the reinforcement ratio was different. The area of HSSS strands is larger than that of carbon steel strands. The prestressing ratio was 0.408% for Girders A2 and A3 and 0.438% for Girder B3. The total prestressing force was 482.9 kips for Girders A2 and A3 and 409.2 kips for Girder B3.

Table 10-2 Test matrix for shear testing

Reinforcement	Specimens	
<div style="display: flex; align-items: center;"> <div style="border-bottom: 1px solid black; width: 100%;"></div> <div style="border-right: 1px solid black; width: 100%;"></div> </div> Transverse	GFRP	Stainless steel
<div style="display: flex; align-items: center;"> <div style="border-bottom: 1px solid black; width: 100%;"></div> <div style="border-right: 1px solid black; width: 100%;"></div> </div> Longitudinal	Girder A2	Girder A3
Carbon steel strands		
HSSS strands	-	Girder B3

Figure 4-1 presents the confinement and vertical reinforcement layout. Note that they are not identical in the two end regions. The configuration in the narrow spacing end represents FDOT standardized end region reinforcement detailing. The confinement and vertical reinforcement spacings were increased at the other end, wide spacing end. The wide spacing end was detailed and tested to investigate a more extreme case and its effect on shear resistance for the girders. Three bar types for vertical reinforcement – bars 4K, 4Y, and 5Z – were used and bundled when spaced together as shown in Figure 4-1. Both the 4K and 5Z bars have 90-degree hooks at the bottom and top, and the direction of the 90-degree hook bars was alternated. Bars 4Y and 5Z were within the girder, and the 4K bars extended out of the top of the girder to provide interface shear resistance between the girder and deck slab. The use of 4Y and 5Z bars was limited to regions in which bursting and spalling stresses were of concern. The confinement reinforcement, bars 3D1, was placed along the first 56 in. from each end of the girder to resist bursting stresses when the strands were released. The confinement reinforcement was extended to more than the predicted transfer length to minimize cracking in the ends of the girder. The predicted transfer length was 36 in., which was calculated based on AASHTO LRFD design provisions. Minor web splitting cracks were noticed after releasing the strands. More information about transfer length of 0.6-in.-diameter carbon steel and HSSS strands can be found in Chapter 5.

Specimens were identified by the following naming convention: the first part is either A (for the specimen with carbon steel strands) or B (for the specimen with HSSS strands). The second part is either 2 (for the specimen with GFRP rebars as shear reinforcement) or 3 (for the specimen with stainless steel rebars as shear reinforcement). The last part is either 1 (for the first shear test, which had a wider shear spacing) or 2 (for the second shear test, which had narrow shear spacing for the first 36 in. from the edge of the specimen) or 3 (for the third shear test, mid span test of Girder A2). For example, A3_1 refers to the first shear test of a specimen that was prestressed with carbon steel strands and had stainless steel rebars as shear reinforcement.

10.3.3 Test setup

Girder A3 and Girder B3 were first tested in flexure (without breaking the specimen) and then in shear twice. However, Girder A2 was tested three times in shear. Figure 10-1, Figure 10-2, and Figure 10-3 show the test sequences of each girder. For Girder A3, a deck slab was cast before the flexure test, Figure 10-2. For Girder B3, a deck slab was cast after the flexure test, Figure 10-3. The flexure tests were terminated before failure of the members in the mid region. For the shear

tests, the specimen was simply supported and tested using a three-point loading scheme as shown in Figure 10-4. A thick reinforced neoprene bearing pad was put under the loading plates and over the supports to prevent any local failure and premature crushing. The dimensions of the bearing pad under the loading plates and over the supports were 15 in. x 10 in. x 3 in. and 12 in. x 10 in. x 2 in. (length, width and thickness), respectively. The load was applied incrementally using a 400-ton hydraulic jack and a loading rate of 0.25 kip/sec until failure. The loading was stopped when an audible noise happened, which was a sign of the origination of the first shear crack. The crack was marked, and the girder was reloaded until failure.

For the shear test at the ends (Figure 10-4), the clear and shear span lengths were 33 ft and 7 ft, respectively. The clear span length was set to ensure that the untested end remain undamaged throughout the first shear test and to ensure shear failure in the tested end. After the first end was tested, the girder was rotated, and external clamps were installed in the mid span region (only in Girder A3 and Girder B3) to prevent flexure failure. Then, the other side was tested in shear. Given that the mid-span region of Girder A2 was not affected during the first two shear tests, it was decided to continue with a third shear test as shown in Figure 10-1. The clear and shear span lengths for the third test were 14 ft and 7 ft, respectively.

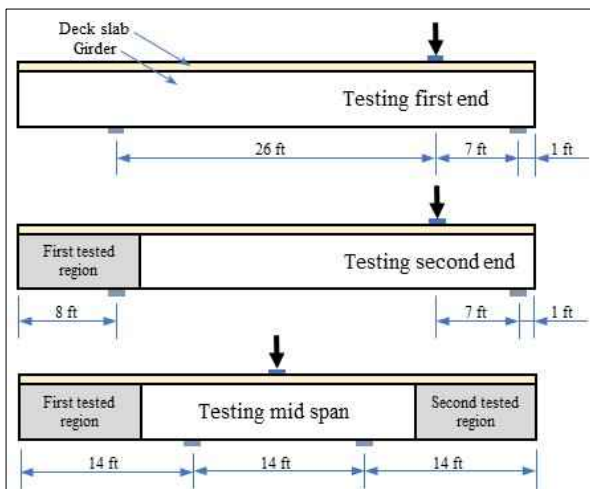


Figure 10-1 Test sequence Girder A2

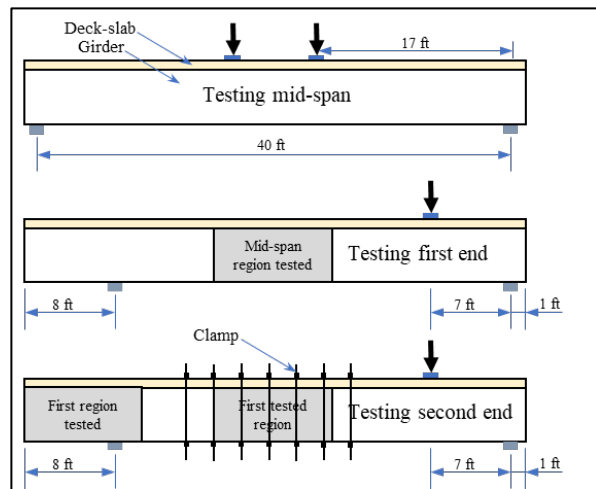


Figure 10-2 Test sequence Girder A3

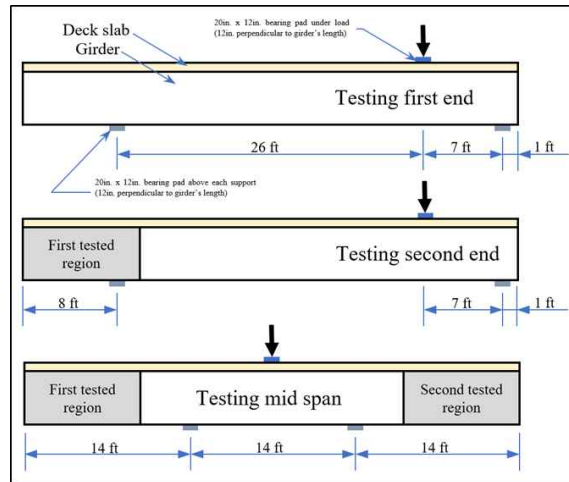


Figure 10-3 Test sequence Girder B3

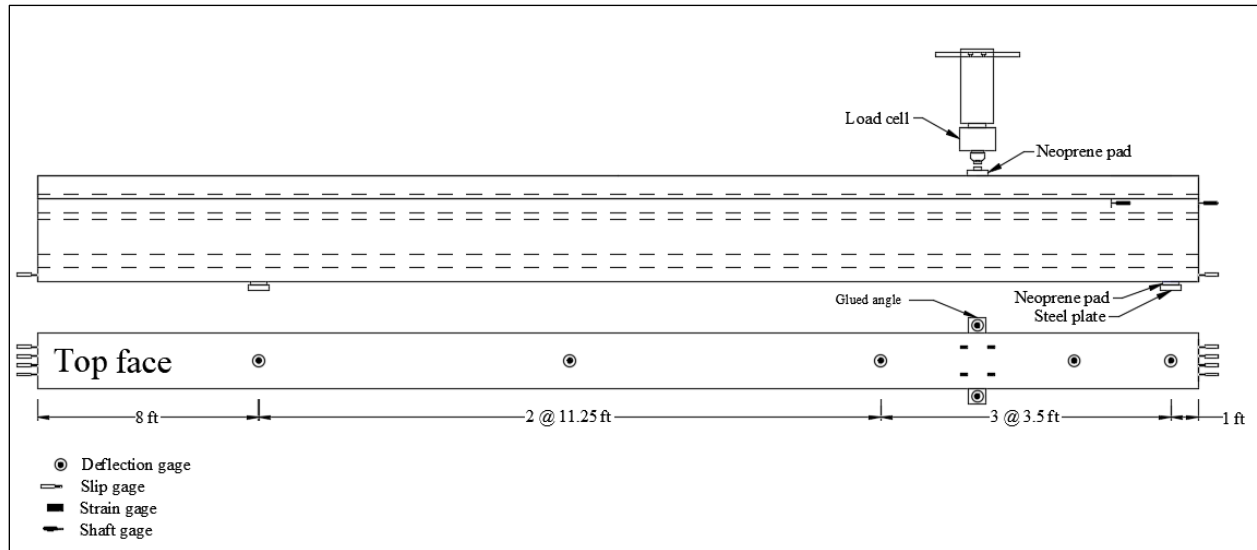


Figure 10-4 Shear test setup

10.3.4 Instrumentation

At the precast plant, seven stirrups at each end were instrumented with strain gages to monitor the development of strain in the stirrups during the shear test as shown in Figure 10-5. The strain gages on the stirrups were instrumented at mid height of the girder, 18 in. from the bottom face of the girder. In the testing lab, four strain gages were installed on the top of the slab, close to the loading point, to measure the concrete strain as shown in Figure 10-6. Rosette strain gages were placed on the web within the shear span to calculate the principal strains, which can be used to determine the cracking load, Figure 10-7. Four strands in the bottom layer were instrumented with end-slip gages to measure the strand slippage during the shear test as shown in Figure 10-8. For Girder A2, shaft gages were installed to measure relative displacement between the deck-slab and

girder as shown in Figure 10-9. No shaft gages were used in the first shear test (Girder A2_1). For the second shear test (Girder A2_2), four shaft gages were used; two were installed at the end face of the girder, and two were installed at 38 in. from the end face of the girder. For the third shear test (Girder A2_3), only one shear span was instrumented with shaft gages; two shaft gages were installed at the support, and the other two were installed at 38 in. from the support. The deflection of the girder was measured with laser-displacement sensors placed at the load point and at several locations along the girder as shown in Figure 10-10. A load cell was attached to the actuator to monitor load. Throughout testing, load, displacements, internal and external strains, strand slip, and relative displacement between the deck slab and girder were recorded using a 30-channel data acquisition system at a rate of 10 Hz. The specimens were loaded until failure occurred.



Figure 10-5 Strain gages attached to the stirrups



Figure 10-6 Strain gages at the top of the slab

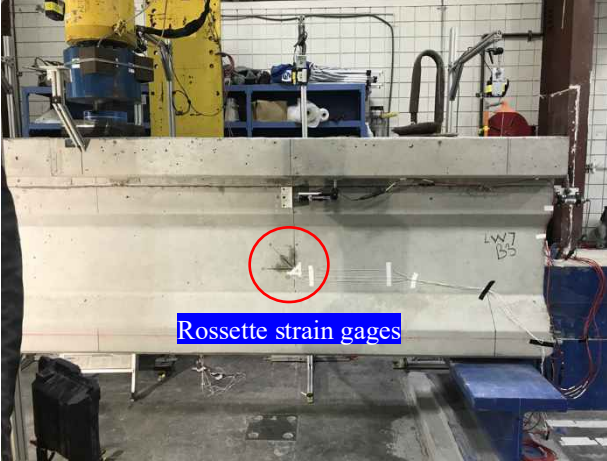


Figure 10-7 Rosette strain gages at the shear span

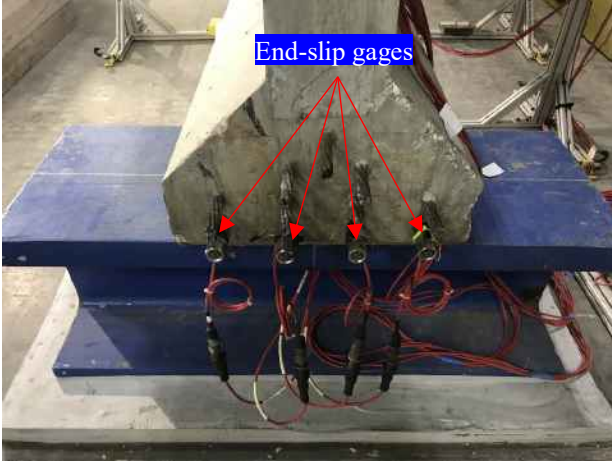


Figure 10-8 End-slip gages

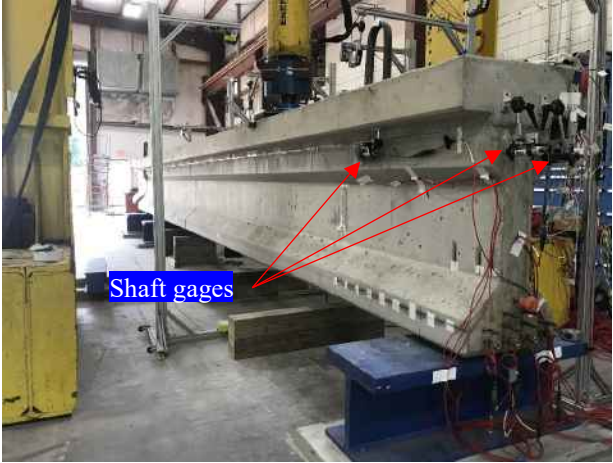


Figure 10-9 Shaft gages



Figure 10-10 Deflection gages

10.4 Interface shear reinforcement

The interface shear reinforcement ratio, which quantifies the amount of reinforcement along the interface shear plane, for the first 36 in. was greater than the rest of the specimen: 0.603% as opposed to 0.301%. In other words, in Girder A2_2, the first 36 in. had double the shear reinforcement than the rest of the beam. For Girder A3 and Girder B3, the interface shear reinforcement ratio was 0.278% for the 6-in. spacing region and 0.555% for the 3-in. spacing region.

Generally, shear stresses along the interface are resisted by the concrete surface and the shear reinforcement across the shear plane. According to AASHTO LRFD, the interface shear resistance (V_{ni}) can be calculated using AASHTO Equation 5.7.4.3-3, which is given in Equation 10-1

$$V_{ni} = cA_{cv} + \mu (A_{vf}f_y + P_c) \quad \text{Equation 10-1}$$

where c and μ are cohesion and friction factors, respectively; A_{cv} is area of concrete considered to be engaged in interface shear transfer; A_{vf} is area of interface shear reinforcement crossing the shear plane within the area A_{cv} ; f_y is the yield stress of reinforcement; and P_c is permanent net compressive force normal to the shear plane.

The concrete along the interface plane provides cohesion between the slab and girder, while the interface shear reinforcement provides clamping stresses to hold the slab and girder together. Note that the top fiber of the girder had a smooth surface, which does not provide significant cohesion stress. If the shear stresses are higher than the clamping stresses by the reinforcement, then the section fails at the interface. Otherwise, the shear resistance increases beyond the cracking load as the shear stirrups provide additional strength. Therefore, a minimum interface

reinforcement ratio, ρ , shall be provided to raise the shear resistance beyond the cracking load. (Mattock 1974) recommended a minimum reinforcement ratio in terms of clamping stress of 0.2 ksi for traditional steel rebars. This minimum clamping stress guarantees that additional shear strength is provided beyond the cracking load by the activation of the stirrups.

GFRP rebars have different mechanical properties than traditional steel rebars, therefore the value of the minimum reinforcement ratio shall be studied. (Alkatan 2016) concluded that an interface reinforcement ratio of 0.405% of GFRP rebars, which is approximately double that for traditional steel bars, is required to activate the GFRP shear stirrups. Because GFRP rebars do not have a yield point, it is better to represent the interface reinforcement ratio by the interface reinforcement stiffness perpendicular to the shear interface surface. The reinforcement stiffness, $E\rho$, is represented by the elastic modulus and interface reinforcement ratio of bars. (Alkatan 2016) recommended a minimum interface reinforcement stiffness of 29.44 ksi for GFRP rebars. The elastic modulus of GFRP bars might be different among manufacturers. If the elastic modulus of the GFRP bars is lower than that used by (Alkatan 2016), which was 7252 ksi, then the reinforcement ratio shall be increased to meet the minimum required interface reinforcement stiffness. (Alkatan 2016) found that the maximum strain of GFRP bars at the interface plane was approximately 5000 microstrain at ultimate load. Given the reinforcement stiffness and the maximum strain, the clamping stress was calculated. (Alkatan 2016) concluded that a minimum clamping stress of 0.148 ksi has to be provided to activate the GFRP shear stirrups to increase the shear strength beyond the cracking load. In this study, the interface reinforcement ratio and stiffness along the beam, except along the 36 in. at one end, were 0.301% and 21.19 ksi, which were lower than the minimum specified values recommended by (Alkatan 2016). Therefore, one can conclude that no additional shear strength was provided by the GFRP bars after cracking of concrete at the interface. According to the minimum GFRP interface shear reinforcement that will prevent interface shear failure, as reported by (Alkatan 2016), all three shear tests of Girder A2 in this study should fail at the interface. In this study, the lifting loop (Figure 4-9) may contribute to the interface shear resistance in the end regions, however, they are not considered in design.

10.5 Experimental results

All specimens were tested under static load up to failure. They exhibited linear behavior up to the formation of the first crack. The appearance of the first crack determines the limit of the concrete contribution to the total shear capacity of the specimen. Two methods were used to

determine the cracking load. The first method was based on the observation of the first crack during the shear test. Generally, a loud noise was accompanied by the appearance of the first crack. Once the first shear crack was spotted, the applied load was halted to document the cracking load, mark the crack, and measure the crack angle with respect to the horizontal axis. The second method used data from the rosette strain gages installed at the web of the girder at mid-point between the support and loading point. Maximum and minimum principal strains were calculated from the strains measured by the rosette gages. Figure 10-11 shows the minimum and maximum principal strains corresponding to the applied shear load. A rapid change, increase or decrease, in the minimum and maximum principal strains was a clear sign that the concrete cracked as shown in Figure 10-11. Table 10-3 presents the observed and calculated cracking loads of the specimens. The calculated shear forces are in good agreement with the observed ones.

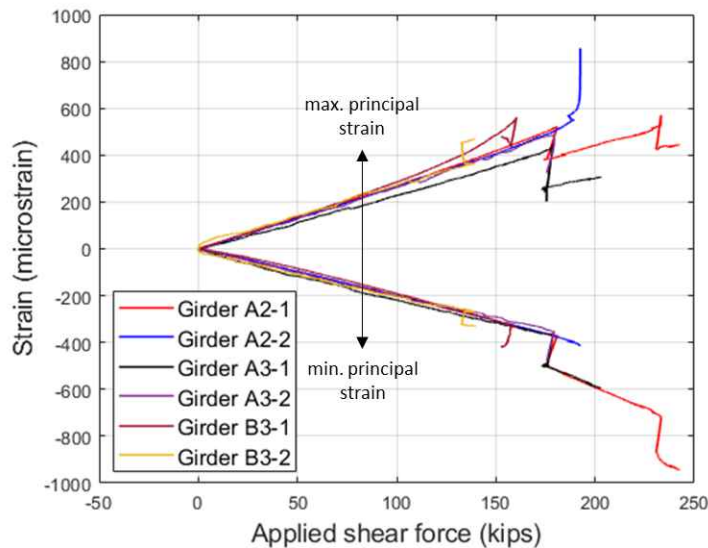


Figure 10-11 Principal strains for test specimens

Table 10-3 Cracking shear force

Specimen ID	Observed (kips)	Calculated using rosette gages (kips)
Girder A2_1 (wide spacing)	180.9	180.9
Girder A2_2 (narrow spacing)	192.6	187.8
Girder A2_3 (mid span)	138.9	138.8
Girder A3_1 (wide spacing)	178.7	178.8
Girder A3_2 (narrow spacing)	179.3	177.9
Girder B3_1 (wide spacing)	160.3	167.9
Girder B3_2 (narrow spacing)	139.3	148.1

The cracking and ultimate loads, deflection at cracking and ultimate loads, and angle of the first crack are presented in Table 10-4.

Table 10-4 Experimental shear results

Specimen ID	Cracking shear force (kips)	Ultimate shear load (kips)	Deflection at cracking shear force (in.)	Deflection at ultimate load (in.)	Angle of first crack (degrees)
Girder A2_1 (wide spacing)	180.9	281.9	0.28	2.31	32
Girder A2_2 (narrow spacing)	192.6	289.1	0.35	3.15	32
Girder A2_3 (mid span)	138.9	240.7	0.17	0.75	30
Girder A3_1 (wide spacing)	178.8	304.6	0.41	2.03	38
Girder A3_2 (narrow spacing)	177.9	297.0	0.38	1.66	38
Girder B3_1 (wide spacing)	167.9	288.2	0.26	2.65	30
Girder B3_2 (narrow spacing)	148.1	277.5	0.23	2.11	30

On average, three concrete cylinders were tested in compression for each member (girder and slab) on the day of the shear test except for Girder A2_3 and Girder B3_1. The specified concrete compressive strength for girder and slab were 10 ksi and 6.5 ksi, respectively. The average concrete compressive strengths of the members on the day of the shear tests are given in Table 10-5.

Table 10-5 Concrete compressive strength at testing day of shear tests

Specimen ID	Compressive strength (psi)	
	Girder	Deck slab
Girder A2_1	11,247	8,073
Girder A2_2	11,104	7,707
Girder A2_3	-	-
Girder A3_1	10,394	7,489
Girder A3_2	10,491	7,756
Girder B3_1	-	7,542
Girder B3_2	11,459	7,456

Experimental results are discussed in the following sections.

10.5.1 Girders prestressed with carbon steel strands

10.5.1.1 Specimens with GFRP shear reinforcement (Girder A2)

10.5.1.1.1 Load-deflection behavior

Figure 10-12 shows the applied shear load versus deflection for the three tests on Girders A2_1, A2_2, and A2_3. Deflections are relative to the support and measured under the load point. Before cracking, deflection increased linearly with the applied load, Figure 10-12. The slope of the elastic part can be used to determine the stiffness of the specimens. Once the concrete cracked, the stiffness of the member decreased. Girder A2_1 and Girder A2_2 exhibited non-linear behavior due to continued reduction in the girder's stiffness. A plateau in the shear load-deflection curve was reached, which indicated that the carbon steel strands had yielded. As the applied load increased, more cracks opened from the bottom flange, and existing cracks continued to propagate towards the top flange. Some of the cracks initiated from the support and propagated toward the top flange far from the point load, and these had a larger angle than that of the first crack. The largest measured crack angle was 52 degrees. Some flexural cracks began to form vertically in the bottom fiber around the applied load zone.

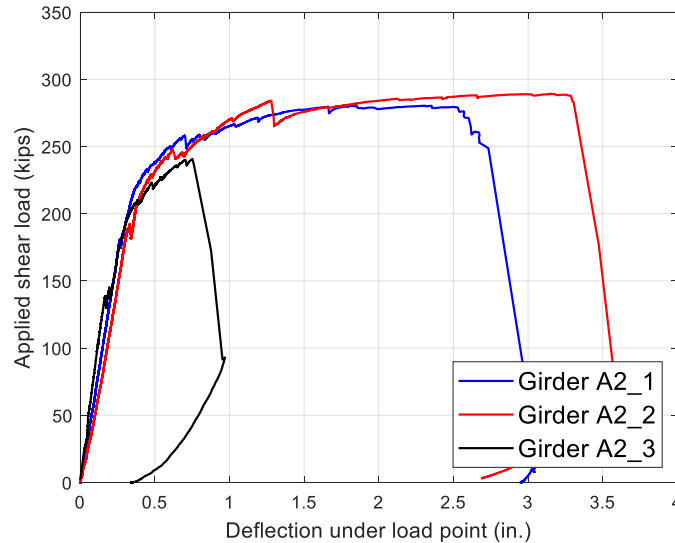


Figure 10-12 Load-deflection relationship for Girder A2

Girder A2_3 had completely different flexural behavior than that of Girder A2_1 and Girder A2_2. The difference was mainly due to the difference in clear span length, limited confinement and end region reinforcement at the supports, and possibly pre-existing flexural cracks from the previous shear tests. The clear span length of Girder A2_3 was 14 ft, while it was 33 ft for Girder

A2_1 and Girder A2_2. All three tests had the same shear span length of 7 ft. Ductility of members is significantly influenced by the clear span length as well as the shear reinforcement ratio. Ductility of the member is inversely proportional to the clear span length, while the ultimate strength of the member is directly proportional to the clear span length. The deflection of Girder A2_3 was reduced by approximately 39.3% and 51.4% from that of Girder A2_1 and Girder A2_2, respectively. The ultimate shear capacity of Girder A2_3 was also reduced by approximately 16% compared to both Girder A2_1 and Girder A2_2. A sudden failure occurred in Girder A2_3.

Girder A2_1 and Girder A2_2 had higher cracking loads than Girder A3_1 and A3_2, respectively, as shown in Table 10-4. This increase in cracking load is attributed to the difference in the concrete compressive strength of the girders on the day of the shear test, Table 10-5. The effect of different concrete strengths was eliminated by normalizing the measured shear forces with respect to the square root of measured concrete compressive strengths times bd , where the web width of the specimen (b) was 6 in., and the depth from the top fiber to the centroid of the strands (d) was 41.2 in. After normalization, the shear force was reduced approximately by 8% when transverse reinforcement changed from Grade 75 stainless steel rebars to GFRP rebars.

10.5.1.1.2 Strain in the stirrups

Seven stirrups, at each end of the girder, were instrumented with strain gages, installed during girder fabrication. For Girder A2, three strain gages were damaged: one strain gage AGF11, which was the middle gage in Girder A2_1 (Figure 10-13); and two strain gages AGF2 and AGF5 in Girder A2_2 (Figure 10-14). Note that as a concrete crack passed through or around a strain gage, the measured strain increased. Thus, the measured strain readings do not necessarily represent the strains along the entire stirrup.

Figure 10-13 and Figure 10-14 show the applied shear load-strain response for stirrups in Girder A2_1 and Girder A2_2, respectively. Experimental results showed that stirrups were not stressed until the first shear crack occurred. Once the concrete cracked, the initiation of stress in the stirrups started. In Girder A2_1, the stirrups (AGF8, AGF9 and AGF10) closest to the support were engaged with the initiation of the first crack as shown in Figure 10-13. The stirrups close to the point load were engaged when the applied load reached approximately 90% of the ultimate load. The lifting hooks likely contributed to the shear resistance of the member: the stirrups closer to the lifting hooks, AGF1 and AGF8, had lower strain at failure.

The strain in each stirrup was affected by the position of the stirrup within the shear span and the position of the strain gage with respect to the concrete crack, as mentioned above. Generally, the stirrups exhibited a higher strain at all loading levels in Girder A2_1, which had a lower shear reinforcement ratio than Girder A2_2. The recorded strain values at failure in the GFRP bars ranged from 0.00616 to 0.01376 and 0.00619 to 0.01394 for Girder A2_1 and Girder A2_2, respectively. Figure 10-13 and Figure 10-14 show that the stirrups closer to the support had lower ultimate strains than those closer to the applied load in both tests. The ultimate strain capacity of the No. 4 GFRP bars used in this study was 0.0172. The maximum recorded strain at failure was approximately equal to 80% of the ultimate strain capacity of the GFRP bars. The strains in all GFRP bars at ultimate load exceeded the allowable strain limit of 0.004 by ACI 440.1R-15 (2015); this limit is equal to 23.2% of the ultimate strain capacity of the GFRP bars. The first strain gages to reach 0.004 were AGF10 at 271 kips for Girder A2_1 and AFG7 at 340 kips for Girder A2_2.

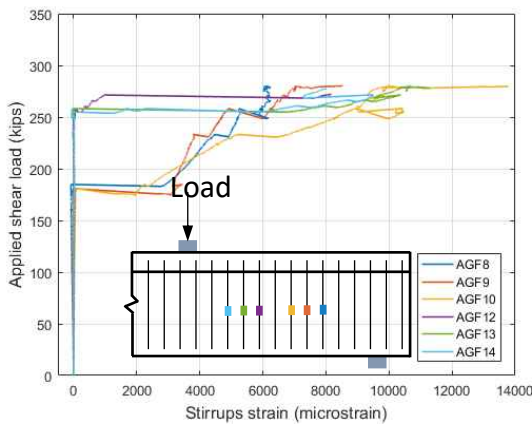


Figure 10-13 Load-stirrups strain for Girder A2_1

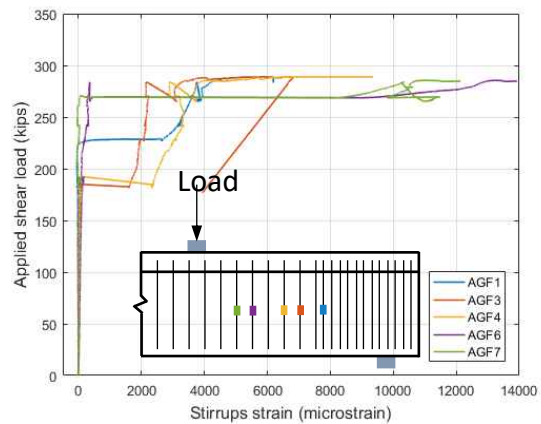


Figure 10-14 Load-stirrups strain for Girder A2_2

10.5.1.1.3 Strand slippage

The amount or distribution of confinement reinforcement influences the anchorage of prestressing strands at the girder ends (Patzlaff et al. 2012). Confinement reinforcement at the girder ends gets activated once the concrete cracks. Lower confinement reinforcement increases the probability of strand slippage.

Four strands at the bottom layer were instrumented with strand slip gages. Figure 10-15 and Figure 10-16 present the applied shear load versus the strand slippage in Girder A2_1 and Girder A2_2, respectively. For A2_3, no strands were monitored due to continuity of concrete at the supports. In Girder A2_1, one strand started to slip before the formation of the first crack; the other

three strands slipped at an applied shear load of 256.8 kips, approximately 91% of the ultimate shear load. This was correlated with a drop in the applied load. The slip of those three strands was accompanied by an audible sound. As the applied load increased, the slip in the strands increased as shown in Figure 10-15. The minimum and maximum strand slips were 0.0198 in. and 0.0383 in., respectively, which occurred at an ultimate shear load of 280.3 kips.

Figure 10-16 shows strand slip in Girder A2_2. Only two strands are plotted for clarity. The other two strands had lower ultimate slip at failure load. The first slip occurred in all four strands at an applied load of 278.9 kips, which is 96.5% of the ultimate load. The initiation of the strand slip happened simultaneously with a significant drop in the applied load, Figure 10-12. The minimum and maximum strand slips at failure load were 0.0160 in. and 0.0225 in., respectively. Although no significant gain in the applied shear load occurred after slip initiation of all strands, the deflection at ultimate increased to more than double as shown in Figure 10-12.

The anchorage of the prestressing strands at the girder's end is controlled by the amount or distribution of the confinement reinforcement (Patzlaff et al. 2012). The maximum strand slippage in Girder A2_1 was approximately 70% higher than in Girder A2_2, which can be attributed to the smaller confinement reinforcement ratio in Girder A2_1.

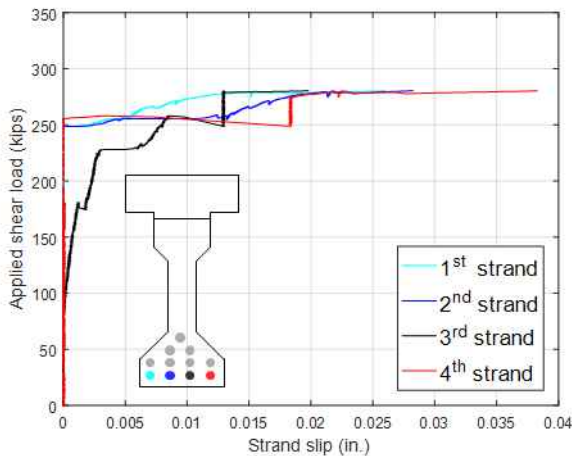


Figure 10-15 Strand slip response in Girder A2_1

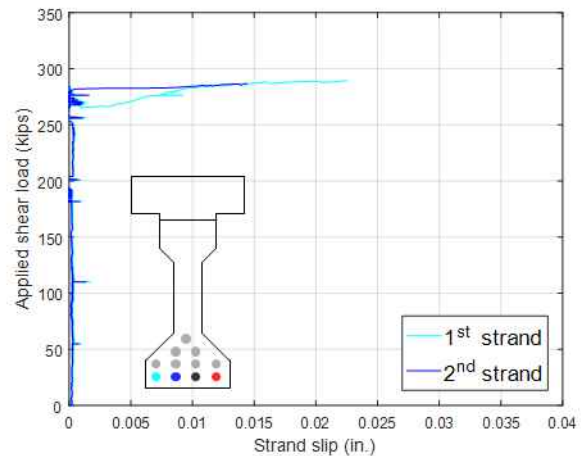


Figure 10-16 Strand slip response in Girder A2_2

10.5.1.1.4 Failure mode

The interface shear behavior and load transfer mechanism of shear forces of concrete composite sections are controlled by concrete-to-concrete cohesion and dowel contribution. The ultimate interface shear capacity depends on the surface condition and transverse stirrups (Kahn and Slapkus 2004). A roughened surface and higher number of stirrups result in higher horizontal

shear capacity. The roughened finish strengthens the bond between the deck slab and girder as it interlocks the two sections. However, in this study, the surface of the girder's top flange was smooth when the deck slab was cast.

Girder A2_1 and Girder A2_2 failed in interface shear failure. As the applied load increased, the diagonal cracks propagated and reached the girder's top flange. The concrete at the interface region started to lose adhesion mainly due to the smooth interface. The loss of adhesion resulted in engagement of the transverse reinforcement. With further loading, most of the cracks reached the deck slab, and the concrete at the interface region started to flake. Spalling of concrete from the interface region was observed during the shear test, before ultimate failure, which was due to slip of the deck slab. At that moment, the GFRP stirrups held together the two sections thru dowel action and friction. Once slippage occurred, the section lost its composite behavior. The separation of the composite section resulted in a decrease in the stiffness of the member, which limited the ultimate shear capacity. The girder alone was not able to resist the applied load, and web shear failure occurred. Interface shear failure happened first, and as a result of that failure, web shear failure occurred. The interface shear failure happened due to the low transverse shear capacity of GFRP rebars.

As mentioned before, no shaft gages were installed to measure interface displacement in Girder A2_1. However, the slip of the deck slab at failure can be visually seen and measured as shown in Figure 10-17 and Figure 10-18. The ultimate horizontal and lateral slips in Girder A2_1 were approximately 2 in. and 0.5 in., respectively. In Girder A2_2, slip of the deck slab was monitored using four shaft displacement gages. Shaft gages E3 and E4 were mounted at the end face of the girder, while shaft gages E1 and E2 were placed at 38 in. from the end of the girder towards the point load, one at each side. The deck slab started to slip at an approximate load of 283.6 kips, which was approximately 98% of the ultimate failure load. This is a clear reason that failure happened shortly after initiation of the slip of the deck slab. The maximum measured slip of the deck slab at failure load was 0.14 in. and 0.03 in. for E1 and E2 shaft gages, respectively. The deck slab slipped more at the gage closest to the loading point.



Figure 10-17 Horizontal interface displacement (Girder A2_1)



Figure 10-18 Horizontal interface displacement (Girder A2_2)

Figure 10-19a and Figure 10-20b show the Girder A2_1 and Girder A2_2, respectively, immediately after failure. After finishing both tests, concrete was removed in the shear span region to evaluate GFRP rebar integrity at the interface region as shown in Figure 10-19b and Figure 10-20b. Seven GFRP bars were found broken in the Girder A2_1 as shown in Figure 10-19c. For Girder A2_2, four GFRP bars were found ruptured at the interface region as shown in Figure 10-20c. The decrease in the number of ruptured GFRP bars between Girder A2_1 and Girder A2_2 is attributed to the increase in the shear reinforcement ratio at the end region in Girder A2_2. The lifting hook, made from strands, likely contributed to the specimen's interface shear capacity. All ruptured GFRP bars were beyond the lifting hooks towards the loading point in both tests. Figure 10-21 shows the different types of failure of GFRP bars, ranging from fiber breakage to rupture.

The two horizontal GFRP 5A bars in the girder's top flange ruptured at ultimate load. At failure load, the concrete at the girder's top flange on both sides split, and this mechanism may have resulted in the rupture of the GFRP bars. This failure indicated that the GFRP bars were not able to resist the applied load. Concrete spalling happened in the bottom flange close to the support at the level of the bottom layer of prestressing strands. The concrete spall was due to a post-failure effect. Visual inspection showed that one of the GFRP confinement bars broke at the bend region in Girder A2_1. As noted previously, GFRP rebars lose some of their strength at their bends due to the unidirectional characteristics of FRP material.



Figure 10-19 Concrete crushing and rupture of GFRP for Girder A2_1

Figure 10-20 Concrete crushing and rupture of GFRP for Girder A2_2

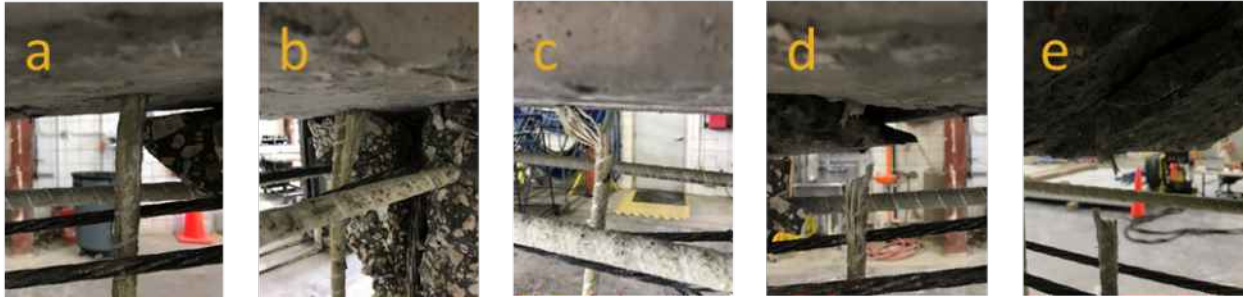


Figure 10-21 Types of failure of GFRP bars

Girder A2_3 failed in bond shear. Bond-shear failure is characterized by inclined cracks that initiate in the web and bottom flange near the support (Naji et al. 2016). Those cracks decrease the bond between the prestressing strands and the surrounding concrete and ultimately lead to slippage of strands. Some of the main reasons a member may fail in bond shear are limited confinement and end region reinforcement (Ross et al. 2011). Girder A2_3 was an academic exercise only as it included long overhangs, 14 ft, on both ends. Girders usually have only a few inches of overhang in the field. It has been reported that increasing the overhang length results in a nontraditional type of failure (Garber et al. 2016).

Due to continuity of concrete over the supports, no strand slip gages were installed to monitor the strand slippage. Even though Girder A2_2 had confinement reinforcement, a significant slip of strand happened, Figure 10-16. For Girder A2_3, only GFRP stirrups, 4K bars, were provided. Therefore, there was a high possibility of strand slip to occur. The first crack occurred at an applied shear load of 138.9 kips, Figure 10-12, to the left of the load actuator. The crack formed from the top of the bottom flange above the support to the center of the top flange near the loading point. Slightly after the formation of the first crack on the left side, another crack occurred at the right side of the actuator at an applied load of 145 kips. The orientation of this crack was similar to the other side. As the load increased, multiple cracks formed on both sides of the actuator. These cracks propagated towards the support because of the unavailable confinement and end region reinforcements and possibly due to flexural cracks from previous shear tests. One of the cracks was horizontally aligned with the strands in the bottom flange near the support. This crack resulted in bond loss of some strands. As shown in Figure 10-22, multiple cracks propagated and reached the bearing support. The ultimate capacity of the member was limited by the available tension force in the strands, and it was reduced when strand slip occurred. Figure 10-22 is a photo of the right side of Girder A2_3 at failure. The failure of Girder A2_3 was abrupt and could be

categorized as bond-shear failure. The ultimate shear capacity of Girder A2_3 was approximately 84% of the average of Girder A2_1 and Girder A2_2. Contrary to Girder A2_1 and Girder A2_2, no concrete spalled from the bottom flange at failure in Girder A2_3.



Figure 10-22 Girder A2_3 at failure

10.5.1.2 Specimens with stainless steel shear reinforcement (Girder A3)

10.5.1.2.1 Load-deflection behavior

Figure 10-23 shows the applied shear force versus deflection at the load point for the two tests. Deflection increased linearly with the applied load up to the formation of the first crack. The concrete contribution to the total shear capacity of the specimen was determined by the appearance of the first crack. The first crack was observed at shear forces of 178.7 kips and 179.3 kips for Girder A3_1 and Girder A3_2, respectively. After formation of the first crack, Girder A3_1 and Girder A3_2 exhibited non-linear behavior due to constant reduction in the girder's stiffness. As load increased, a plateau in the shear force-deflection curve was reached, which was a sign that the longitudinal reinforcement had yielded as shown in Figure 10-23. The ultimate shear force for Girder A3_1 and Girder A3_2 was 304.6 kips and 279.0 kips, respectively.

10.5.1.2.1 Strain in the stainless steel stirrups

Seven stirrups, at each end of the girder, were instrumented with strain gages, installed during girder fabrication. The strain measurements were collected throughout the shear tests. Figure 10-24 and Figure 10-25 show the location and name of each gage. Two strain gages malfunctioned from the beginning of the test: ASS1 in specimen A3_1 (Figure 10-24) and ASS10 in specimen A3_2 (Figure 10-25).

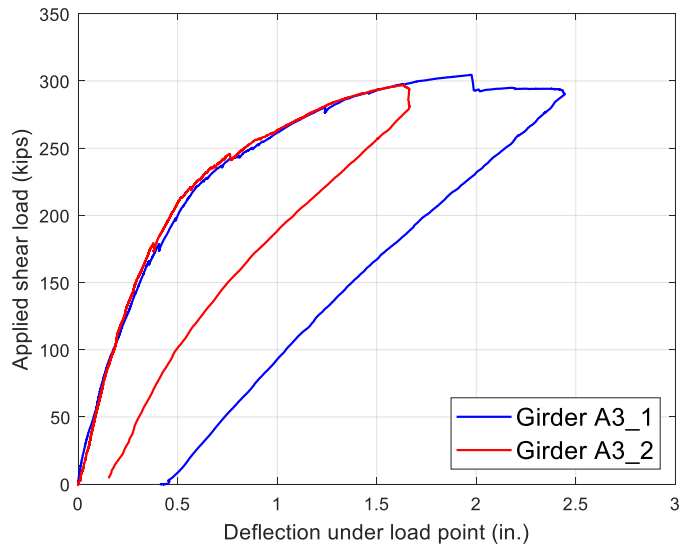


Figure 10-23 Load-deflection relationship for Girder A3

Before reaching the cracking load, no strain was measured in the stirrups (Figure 10-24 and Figure 10-25), which means the stirrups did not contribute to resist the applied load. After cracking, the stirrups were involved in resisting the applied load. As the applied load increased, the strain in the stirrups increased and eventually reached yielding. After yielding of one stirrup, the load transferred to another stirrup, and so on, until all stirrups yielded. The strain in almost all stirrups was beyond the yield strain, around 0.0028, at failure load. Generally, reducing the shear reinforcement ratio increases demand on the stirrups. The effect is clear in Girder A3. Strains in some stirrups in Girder A3_1 (Figure 10-24) were higher than those in Girder A3_2 (Figure 10-25).

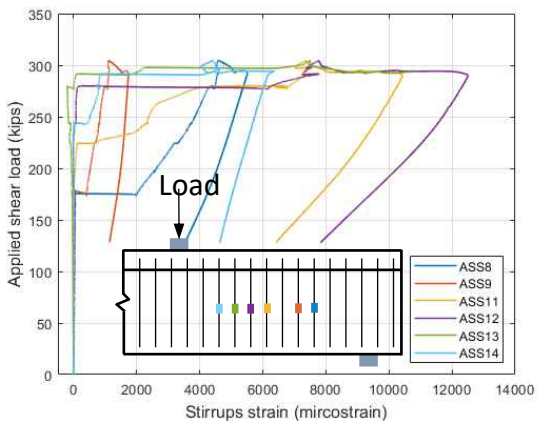


Figure 10-24 Load-stirrups strain for Girder A3_1

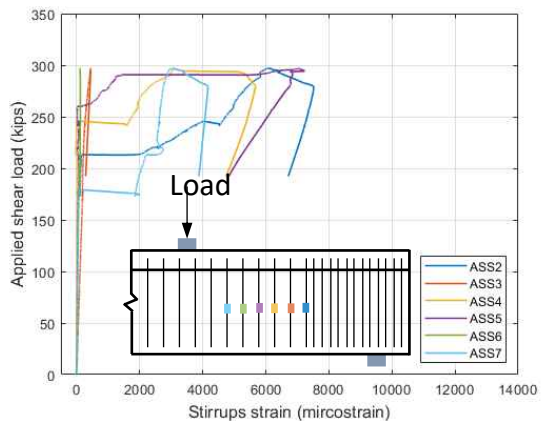


Figure 10-25 Load-stirrups strain for Girder A3_2

10.5.1.2.2 Strand slippage

Four strands at the bottom layer were instrumented with strand slip gages. Significant strand slip occurred only in Girder A3_1, which had wider confinement reinforcement compared to Girder A3_2. Strand slippage was observed only in one strand in both shear tests of Girder A3. In Girder A3_1, the strand started to slip at 228 kips shear force. A significant drop in the load-carrying capacity occurred when the strand slip reached 0.0069 in. at a shear force of 304 kips. The strand kept slipping while the member deformed with no increase in the shear force. The strand slip at failure was 0.0150 in. After finishing testing Girder A3_1, the girder was rotated, and the other end, Girder A3_2, was tested. The maximum measured strand slip in Girder A3_2 was 0.00016 in. The strand that slipped in Girder A3_1 was the same one that slipped in Girder A3_2. Despite the strand slip in both Girder A3_1 and Girder A3_2, the failure mode was the same, which was flexure-shear.

Results showed that direct replacement of confinement reinforcement from Grade 75 stainless steel rebars (Girder A3) to GFRP rebars (Girder A2) resulted in a large increase in the strand's slip at ultimate load. The confinement reinforcement stiffness of Girder A3 was approximately 3.8 times more than that of Girder A2. Thus, it can be concluded that the anchorage of the prestressing reinforcement is significantly influenced by the confinement reinforcement stiffness.

10.5.1.2.3 Failure mode

Girder A3_1 and Girder A3_2 failed in flexure-shear, where concrete at the top fiber crushed around the load point. Inclined shear cracks propagated toward the point load, and failure occurred. Flexure-shear failure for Girder A3_1 is shown in Figure 10-26. Figure 10-27 shows the top of Girder A3_1 after failure where concrete was crushed.

Experimental results show that direct replacement of the Grade 75 stainless steel stirrups (Girder A3) with GFRP stirrups (Girder A2) altered the failure mode from flexure-shear to interface shear failure.



Figure 10-26 Flexure-shear failure of Girder A3_1



Figure 10-27 Crushing of concrete of Girder A3_1

10.5.2 Girder prestressed with stainless steel strands

10.5.2.1 Specimens with stainless steel shear reinforcement (Girder B3)

10.5.2.1.1 Load-deflection behavior

The shear force (calculated from the measured applied load) versus vertical deflection at the load point for both shear tests is shown in Figure 10-28. The shear force-deflection curves are divided into two regions, pre- and post-cracking. For the pre-cracking region, both specimens exhibited linear behavior up to the formation of the first crack. The appearance of the first crack determines the limit of the concrete contribution to the total shear capacity of the specimen. The first crack was observed at shear forces of 167.3 kips and 139.3 kips for Girder B3_1 and Girder B3_2, respectively. The slope of the pre-cracking stiffness deviated once the concrete cracked. For the post-cracking region, both specimens exhibited non-linear behavior due to constant reduction in the girder's stiffness. A constant increase in the shear force-deflection curve was observed as shown in Figure 10-28. This behavior reflects the stress-strain shape of the HSSS strands. In case of girders prestressed with carbon steel strands (Girder A2), a plateau in the shear force-deflection curve was observed when the carbon steel strands have yielded as shown in Figure 10-12. The ultimate shear force for Girder B3_1 and Girder B3_2 was 288 kips and 278 kips, respectively.

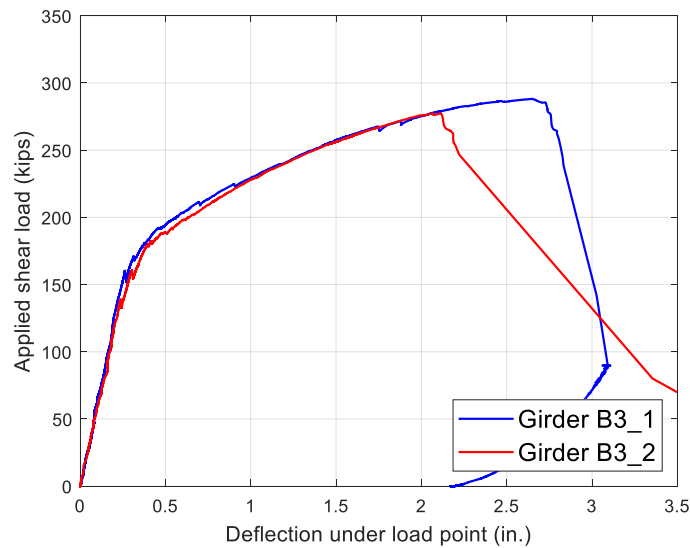


Figure 10-28 Shear force versus deflection for Girder B3

10.5.2.1.2 Strain in the stainless steel stirrups

Seven stirrups within the shear span were instrumented with strain gages before casting concrete. The strain measurements were collected throughout the shear tests. Figure 10-29 and Figure 10-30 show the location and name of each gage.

Figure 10-29 and Figure 10-30 show the shear force versus strain in the stirrups for Girder B3_1 and Girder B3_2, respectively. The data indicates that the stirrups did not contribute to resist the applied load before formation of the first crack. In other words, no strain was measured in the stirrups before reaching the cracking load. After reaching the cracking load, the stirrups were involved in resisting the applied load. Location and time of the formation of an inclined crack determined the appearance of the strain plateau in each bar. The length of the plateau varies depending on the location of the rebar and its contribution in resisting the applied load. As the applied load increased, the strain in the stirrups increased and eventually reached yielding. After yielding of one stirrup, the load transferred to another stirrup, and so on, until all stirrups yielded. From Figure 10-29 and Figure 10-30, the strain in almost all stirrups was beyond the yield strain, around 0.0028, at failure load. In Girder B3_2, one stirrup, BSS3, almost reached its ultimate strain, 0.0265. Multiple stirrups had strains in the strain hardening range. Several strain gages malfunctioned before reaching the specimen's failure load, especially in Girder B3_1, Figure 10-29. After shear tests, concrete was removed from the web in the shear span region to evaluate

the stirrups' integrity. In Girder B3_2 specimen, rebar BSS3 was found broken, likely due to post-failure effects.

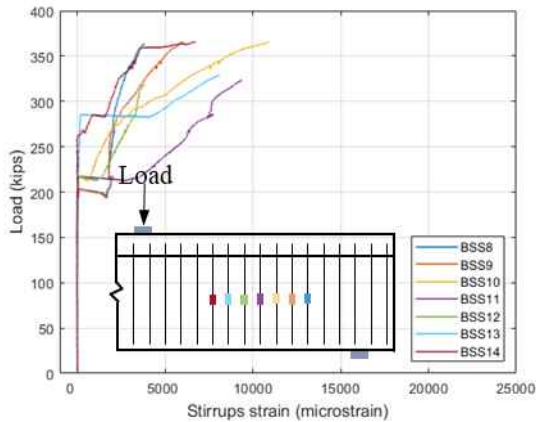


Figure 10-29 Load-stirrups strain for Girder B3_1

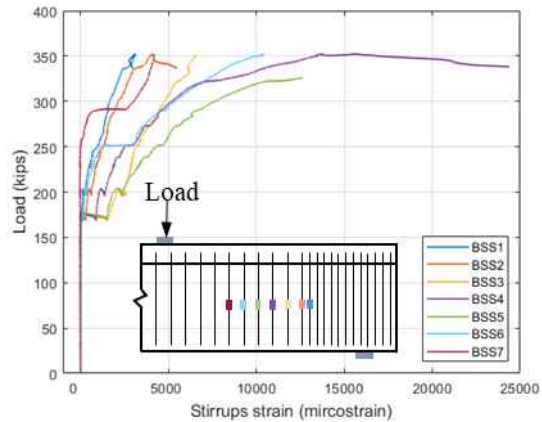


Figure 10-30 Load-stirrups strain for Girder B3_2

10.5.2.1.3 Strand slippage

Strand slip was monitored using shaft gages on the bottom four strands. Strand slip occurred only in the specimen with the wider-spaced confinement reinforcement, Girder B3_1. The bottom corner strand in Girder B3_1 started to slip at 268 kips shear force, which was 93% of the ultimate shear force. The strand kept slipping until the member failed by crushing of the web. The strand slip at failure was 0.0145 in. The maximum recorded slippage in the other three strands was 0.0007, 0.0017, and 0.0007 in. No significant strand slip occurred in Girder B3_2; the maximum slip at failure among the four instrumented strands was 0.0002 in.

10.5.2.1.4 Failure mode

Girder B3_1 and Girder B3_2 failed in web shear, where concrete in the web crushed as shown in Figure 10-31 and Figure 10-32. Crushing of concrete occurred along the concrete strut throughout the height of the web. Concrete damage in the web was observed to be more extensive in Girder B3_2 than in Girder B3_1. A large portion of concrete disintegrated from the web at failure in Girder B3_2 as shown in Figure 10-32. After failure, concrete was removed from the web to investigate the integrity of the stainless steel shear stirrups. It was found that one stainless steel shear rebar was broken in Girder B3_2. Although transverse shear reinforcement exhibited higher strain before failure, the stainless steel rebar broke due to post-failure effects. Additional damage due to post-failure effects was spalling of concrete from the bottom flange.



Figure 10-31 Web shear failure of Girder B3_1



Figure 10-32 Web shear failure of Girder B3_2

10.6 Code predictions

The experimental cracking and ultimate shear capacity are presented in Table 10-6; the reported values include the effect of self-weight of the tested specimens. The shear capacity of a concrete member has two components: concrete strength and stirrup strength. From the experiments, the concrete contribution was determined from the cracking load, while the stirrups' contribution was calculated by subtracting the concrete contribution from the shear capacity of the girder.

Table 10-6 Experimental results for test specimens

Specimen	V_c , kips	V_{ult} , kips	$V_{ult} - V_c$, kips	V_{ult}/V_{cr}	Failure mode
Girder A2_1	189.0	290.0	101.0	1.50	interface shear failure
Girder A2_2	200.7	297.2	96.5	1.48	interface shear failure
Girder A2_3	142.2	244.0	101.2	1.71	bond-shear failure
Girder A3_1	186.9	312.7	125.8	1.67	flexure shear failure
Girder A3_2	186.0	305.1	117.1	1.64	flexure shear failure
Girder B3_1	176.0	296.3	120.3	1.68	web shear failure
Girder B3_2	156.2	285.6	129.4	1.83	web shear failure

The measured experimental shear capacities were compared with the predicted values to verify the applicability of the code design expressions. *AASHTO LRFD Bridge Design Specifications* and

ACI 318 and ACI 440 were used to predict the shear strength of the tested specimens. The following sections demonstrate their use.

10.6.1 AASHTO LRFD Bridge Design Specifications

10.6.1.1 Concrete contribution (V_c)

The concrete contribution (V_c) was calculated using AASHTO Equation 5.7.3.3-3, which is given in Equation 10-2, where concrete density (λ) was 1.0, web width (b_v) was 6 in., effective shear depth (d_v) was 36.9 in, and concrete compressive strengths on testing day (f'_c) are given in Table 10-5. In this study, f_{po} was taken equal to f_{ps} , where f_{ps} is the jacking stress of the strands. The factor relating to the effect of longitudinal strain on the shear capacity of concrete (β_c) was calculated using AASHTO Equation 5.7.3.4.2-4, which is given in Equation 10-3. The net longitudinal tensile strain at the centroid of the tension reinforcement (ϵ_s) was calculated using AASHTO Equation 5.7.3.4.2-1, which is given in Equation 10-4. The ultimate shear force (V_u) and ultimate moment (M_u) were calculated at distance d_v from face of support. Table 10-7 presents the predicted concrete contribution of all specimens by AASHTO LRFD.

$$V_c = 0.0316\beta_c\lambda\sqrt{f'_c}b_vd_v \quad \text{Equation 10-2}$$

$$\beta_c = \frac{4.8}{(1+750\epsilon_s)} \quad \text{Equation 10-3}$$

$$\epsilon_s = \frac{\frac{M_u+V_u-A_{ps}f_{po}}{d_v}}{E_{ps}A_{ps}+E_cA_{ct}} \quad \text{Equation 10-4}$$

10.6.1.2 Stirrups contribution (V_s)

For Girder A3 and Girder B3, the stainless steel stirrups' contribution (V_s) was calculated using AASHTO Equation 5.7.3.3-4, which is given in Equation 10-5, where area of stirrups (A_v) was 0.2 in², yield stress of stainless steel stirrups (f_y) was 75 ksi, and spacing of stirrups (s) was 6 in. The angle of inclination of diagonal compressive stresses (θ) was calculated using AASHTO Equation 5.7.3.4.2-3, which is given in Equation 10-6. The AASHTO LRFD prediction of the stirrup contribution (V_s) was found to be 164.2 kips and 164.5 kips for Girder A3_1 and A3_2, respectively, and 163.7 kips and 164.0 kips for Girder B3_1 and B3_2, respectively.

$$V_s = \frac{A_vf_yd_v\cot\theta}{s} \quad \text{Equation 10-5}$$

$$\theta = 29 + 3500\epsilon_s \quad \text{Equation 10-6}$$

For Girder A2, the limitations of stirrup strength, provided in *AASHTO LRFD Bridge Design Guide Specifications for GFRP-Reinforced Concrete* Section 2.7.3.5, were considered. The GFRP

stirrups' contribution (V_f) was calculated using AASHTO Equation 2.7.3.5-1, which is given in Equation 10-7, where area of stirrups (A_{fv}) was 0.217 in² and spacing of stirrups (s) was 6 in. The tensile stress of GFRP stirrups (f_{fv}) was calculated using AASHTO equation 2.7.3.5-2, which is given in Equation 10-8, where the tensile modulus of elasticity of GFRP rebars (E_f) was 7042.6 ksi. The design tensile stress of the bent portion of GFRP rebars (f_{fb}) was calculated using AASHTO Equation 2.7.3.5-3, which is given in Equation 10-9, where the internal radius of the bent GFRP rebar (r_b) was 2 in., and the diameter (d_b) was 0.5257 in. The design tensile stress of GFRP rebars (f_{fd}) was 51.5 ksi, which was calculated using AASHTO Equation 2.4.2.1-1. The AASHTO LRFD prediction of the stirrup contributions (V_f) was found to be 67.2 kips, 67.1 kips and 65.9 kips for Girders A2_1, A2_2, and A2_3, respectively.

$$V_f = \frac{A_{fv} f_{yv} d_v \cot \theta}{s} \quad \text{Equation 10-7}$$

$$f_{fv} = 0.004 E_f \leq f_{fb} \quad \text{Equation 10-8}$$

$$f_{fb} = (0.05 \frac{r_b}{d_b} + 0.3) f_{fd} \leq f_{fd} \quad \text{Equation 10-9}$$

AASHTO LRFD (Article 5.7.4) was used to evaluate the interface shear capacity of Girder A2_1 and Girder A2_2 because they failed in interface shear. The limitations of stirrup strength, provided in *AASHTO LRFD Bridge Design Guide Specifications for GFRP-Reinforced Concrete* Section 2.7.4, were considered. The interface shear resistance (V_{ri}) was calculated using AASHTO Equation 5.7.4.3-3, which is given in Equation 10-10. Note that the surface of the girder's top flange was smooth when the deck slab was cast. Therefore, as specified in AASHTO Section 5.7.4.4, the cohesion factor (c) was 0.075 ksi, friction factor (μ) was 0.6 ksi, friction of concrete strength available to resist interface shear (K_1) was 0.2, and limiting interface shear resistance (K_2) was 0.8 ksi. The area of concrete considered to be engaged in interface shear (A_{cv}) equals $b_{vi} L_{vi}$, where the interface width (b_{vi}) was 12 in., and the interface length (L_{vi}) was 6 in. The area of interface shear reinforcement crossing the shear plane (A_{vf}) with the area (A_{cv}) was 0.217 in². The permanent net compressive force normal to the shear plane (P_c) was assumed equal to zero. As specified in *AASHTO LRFD Bridge Design Guide Specifications for GFRP-Reinforced Concrete* Section 2.7.4, the yield stress (f_y) in Equation (9) was replaced with the design tensile strength of GFRP (f_{fd}), which was 131.4 ksi. By substituting all the values in Equation 10-10, the AASHTO LRFD prediction for the interface shear capacity (V_{ri}) was found to be 22.5 kips, which satisfied

the requirements given in AASHTO LRFD Equation 2.7.4.3-4 and Equation 2.7.4.3-5. The interface shear capacity (V_{ri}) per unit length was equal to 3.75 kip/in. Note that, during experiments, bars in the lifting hook likely contributed to the specimen's interface shear capacity.

$$V_{ri} = cA_{cv} + \mu(A_{vf}f_y + P_c) \quad \text{Equation 10-10}$$

The experimental shear force at the loading point (V_u) was 287.1 kips and 294.3 kips for Girder A2_1 and Girder A2_2, respectively. The required interface shear force (V_{ui}) was calculated using Equation 10-11, where the effective shear depth (d_v) was 36.9 in. The experimental interface shear force (V_{ui}) was found to be 7.78 kip/in. and 7.98 kip/in. for Girder A2_1 and Girder A2_2, respectively.

$$V_{ui} = \frac{V_u}{d_v} \quad \text{Equation 10-11}$$

Calculations indicate that the experimental interface shear at failure load was more than double the interface shear capacity for both Girder A2_1 and Girder A2_2, which was calculated by the AASHTO LRFD design provisions given the condition of the girder. Even though Girder A2 failed by interface shear failure, the AASHTO LRFD design provisions conservatively predicted the interface shear force because Girder A2_1 and Girder A2_2 failed at an interface shear force more than double the predicted interface shear force. Based on AASHTO LRFD calculations, interface shear failure would have not occurred in Girder A2 if the surface condition at the interface region between the girder's top flange and deck slab had been intentionally roughened.

10.6.1.3 Results

Table 10-7 presents the experimental and AASHTO LRFD predicted shear capacities of the specimens. Overall, AASHTO LRFD conservatively estimated the ultimate shear capacity of all specimens. Due to different mechanical properties of the HSSS strands, the prediction of the ultimate shear capacity of specimens prestressed with HSSS strands (Girder B3_1 and Girder B3_2) was less conservative than those prestressed with carbon steel strands (Girder A3_1 and Girder A3_2) as shown in Table 10-7. Moreover, the prediction of ultimate shear capacity of specimens reinforced with GFRP stirrups (Girder A2_1 and Girder A2_2) was more conservative than those reinforced with stainless steel stirrups (Girder A3_1 and Girder A3_2).

Table 10-7 Experimental and AASHTO LRFD predicted capacities for test specimens

Specimen	Experimental			AASHTO LRFD			$\frac{V_{ult}}{V_{n,AASHTO}}$
	V_c , kips	V_s , kips	V_{ult} , kips	V_c , kips	V_s , kips	V_n , kips	
Girder A2_1	193.1	97.0	290.1	107.1	67.2	174.9	1.66
Girder A2_2	200.7	96.6	297.3	106.3	67.1	173.4	1.71
Girder A2_3	141.3	101.8	243.1	97.6	65.9	163.6	1.49
Girder A3_1	186.9	125.8	312.7	101.2	164.2	265.4	1.18
Girder A3_2	186.0	119.2	305.2	102.4	164.5	266.9	1.14
Girder B3_1	176.0	120.4	296.4	104.5	163.7	268.2	1.11
Girder B3_2	156.2	129.5	285.7	105.5	164.0	269.5	1.06

10.6.2 ACI 318-19

10.6.2.1 Concrete contribution (V_c)

First, the concrete strength (V_c) was calculated using the approximate method in Section 22.5.6.2 of ACI 318-19, which is given in Equation 10-12, where concrete density (λ) was 1.0, web width (b_w) was 6 in., the distance from the extreme compression fiber to the centroid of prestressed reinforcement (d) was 41.2 in., and concrete compressive strengths on testing day (f'_c) are given in Table 10-5. The ultimate shear force (V_u) and ultimate moment (M_u) were calculated at a distance d from the face of the support. Table 10-8 presents the predicted concrete strengths, using ACI 318-19 approximate method, of all specimens.

$$V_c = \min \begin{cases} (0.6\lambda\sqrt{f'_c} + 700 \frac{V_u d}{M_u}) b_w d \\ (0.6\lambda\sqrt{f'_c} + 700) b_w d \\ 5\lambda\sqrt{f'_c} b_w d \end{cases} \quad \text{Equation 10-12}$$

Second, the concrete strength (V_c) was calculated using the detailed method in Section 22.5.6.3 of ACI 318-19. The flexure-shear strength (V_{ci}) was calculated using ACI 318-19 Equation 22.5.6.3.1a, which is given in Equation 10-13; the distance from the extreme compression fiber to the centroid of prestressed reinforcement (d_p) was 41.2 in. The shear forces due to unfactored dead load (V_d), ultimate shear force (V_i), cracking moment (M_{cre}), and ultimate moment (M_{max}) were calculated at a distance d_p from the face of the support.

$$V_{ci} = (0.6\lambda\sqrt{f'_c}b_wd_p + V_d + \frac{V_iM_{cre}}{M_{max}}) \quad \text{Equation 10-13}$$

The web-shear strength (V_{cw}) was calculated using ACI 318-19 Equation 22.5.6.3.2, which is given in Equation 10-14. The compressive strength at the centroid of the composite section was calculated using Equation 10-15; f_{pe} is the effective tensile stress of the strands in ksi, A_{ps} is area of strands in in², and A_g is area of the composite section in in².

$$V_{cw} = (3.5\lambda\sqrt{f'_c} + 0.3f_{pc})b_wd_p + V_d \quad \text{Equation 10-14}$$

$$f_{pc} = \frac{f_{pe}A_{ps}}{A_g} \quad \text{Equation 10-15}$$

Table 10-8 presents the predicted concrete strengths (V_c), which was the minimum of (V_{ci}) and (V_{cw}), of all specimens.

10.6.2.2 Stirrups contribution (V_s)

For Girder A3 and Girder B3, the stainless steel stirrups' contribution (V_s) was calculated using ACI Equation 22.5.8.5.3, which is given in Equation 10-16, where the area of stirrups (A_v) was 0.2 in², specified yield strength of stainless steel stirrups (f_{yt}) was 75 ksi, distance from the extreme compression fiber to the centroid of the prestressed reinforcement (d) was 41.2 in., and spacing of stirrups (s) was 6 in. The ACI 318-19 prediction of the stirrups' contribution (V_s) was found to be 103.0 kips for Girder A3 and Girder B3.

$$V_s = \frac{A_v f_{yt} d}{s} \quad \text{Equation 10-16}$$

For Girder A2, the transverse reinforcement contribution was calculated using ACI 440.1 R-15, as the specimens were reinforced with GFRP stirrups. The GFRP stirrups' contribution (V_f) was calculated using Equation 10-17, where the area of stirrups (A_{fv}) was 0.217 in² and spacing of stirrups (s) was 6 in. The tensile stress in the GFRP stirrups (f_{yv}) was equal 0.004 E_f , where the tensile modulus of elasticity of GFRP rebars (E_f) was 7,043 ksi. The ACI 440.1 prediction of the stirrup strength (V_f) was found to be 42 kips for Girder A2.

$$V_f = \frac{A_f f_{yv} d}{s} \quad \text{Equation 10-17}$$

10.6.2.3 Results

Table 10-8 presents the experimental and ACI predicted shear capacities of the specimens. The ACI detailed method predicts the experimental results better than the ACI approximate method. Overall, ACI detailed method conservatively estimated the ultimate shear capacity of all

specimens. The prediction of the ultimate shear capacity of specimens prestressed with HSSS strands (Girder B3_1 and Girder B3_2) was less conservative than those prestressed with carbon steel strands (Girder A3_1 and Girder A3_2) as shown in Table 10-8. This difference is attributed to the differences in the mechanical properties of HSSS and carbon steel strands. Moreover, the prediction of the ultimate shear capacity of specimens reinforced with GFRP stirrups (Girder A2_1 and Girder A2_2) was more conservative than those reinforced with stainless steel stirrups (Girder A3_1 and Girder A3_2).

Table 10-8 Experimental and ACI predicted capacities for test specimens

Specimen	Experimental			ACI approximate method			ACI detailed method			$\frac{V_{ult}}{V_{n,ACI,det.}}$
	V_c , kips	V_s , kips	V_{ult} , kips	V_c , kips	V_s , kips	V_n , kips	V_c , kips	V_s , kips	V_n , kips	
Girder A2_1	193.1	97.10	290.1	131.0	42.0	173.0	152.9	42.0	194.8	1.49
Girder A2_2	200.7	96.6	297.3	130.2	42.0	172.1	152.3	42.0	194.2	1.53
Girder A2_3	141.3	101.8	243.1	130.6	42.0	172.6	152.6	42.0	194.5	1.25
Girder A3_1	186.9	125.8	312.7	126.0	103.0	228.9	149.1	103.0	252.0	1.24
Girder A3_2	186.0	119.2	305.2	126.5	103.0	229.5	149.5	103.0	252.4	1.21
Girder B3_1	176.0	120.4	296.4	132.3	103.0	235.2	145.5	103.0	248.5	1.19
Girder B3_2	156.2	129.5	285.7	132.3	103.0	235.2	145.5	103.0	248.5	1.15

10.7 Summary

The durability of concrete structures can be enhanced by implementing corrosion-resistant and/or corrosion-free materials for both longitudinal and transverse reinforcement. Corrosion-resistant strands, i.e. HSSS, can address corrosion issues in horizontal reinforcement, but corrosion also occurs in transverse reinforcement. Some of the available options for the transverse reinforcement are GFRP and stainless steel rebars.

Three 42-ft-long AASHTO Type II concrete girders were constructed. A deck slab was cast on top of the girder and made composite with the girder. One girder (Girder A3), the control, was prestressed with carbon steel strands and had Grade 75 stainless steel rebars as transverse reinforcement. The transverse reinforcement in the second girder (Girder A2) was changed from

Grade 75 stainless steel rebars to GFRP rebars to quantify the effect of GFRP stirrups on the shear behavior. The longitudinal reinforcement in the third girder (Girder B3) was changed from carbon steel strands to stainless steel strands to investigate the effect of using stainless steel strands on the shear behavior. The results were also compared with predicted capacities according to ACI and AASHTO LRFD. The following conclusions were made:

10.7.1 Effect of using GFRP rebars

- Both ends of one prestressed concrete girder reinforced with GFRP stirrups were tested in shear. This experimental program only provides preliminary results for the use of GFRP stirrups in prestressed concrete girders. More testing is needed to develop a full design guideline and detailing for prestressed girders reinforced with GFRP stirrups.
- The confinement reinforcement spacing for the first 12 in. at one end of the girder was double the current FDOT standard end region reinforcement detailing, the other end. Strand slippage occurred when the confinement reinforcement spacing was doubled. Therefore, increasing confinement reinforcement spacing is not recommended.
- Direct replacement of confinement reinforcement from Grade 75 stainless steel rebars (Girder A3) to GFRP rebars (Girder A2) resulted in an increase in the strand slippage during shear tests.
- The effect of the mechanical properties of the GFRP rebars is clear in the experimental data. Experimental results showed that direct replacement of shear reinforcement from Grade 75 stainless steel rebars (Girder A3) to GFRP rebars (Girder A2) reduced the ultimate shear capacity by approximately 8% and changed the failure mode from flexure shear to interface shear. The interface shear failure happened due to the low transverse shear capacity of GFRP bars and smooth interface between the girder and deck slab. At failure, multiple GFRP bars were found broken at the interface between the deck slab and girder.
- No design code or specification has been developed yet to cover the use of GFRP rebars as stirrups in prestressed concrete members. ACI 318 and ACI 440 were used to predict the concrete and stirrups' contributions to shear strength, respectively. Similarly, *AASHTO LRFD Bridge Design Specifications* and *AASHTO LRFD Bridge Design Guide Specifications for GFRP-Reinforced Concrete* were used to predict the concrete and

stirrups' contributions to shear strength. Both ACI and AASHTO LRFD conservatively estimated the shear capacity of the tested specimens.

- *AASHTO LRFD Bridge Design Specifications* and *AASHTO LRFD Bridge Design Guide Specifications for GFRP-Reinforced Concrete* were used to predict the interface shear resistance of Girder A2. Calculations indicate that the experimental interface shear force at failure load was more than double what was calculated by the design provisions based on the condition of the girder. Even though Girder A2 failed by interface shear failure, the AASHTO LRFD design provisions conservatively predicted the interface shear force because Girder A2 failed at more than double the predicted interface shear force.
- Based on AASHTO LRFD calculations, interface shear failure would have not occurred in Girder A2 if the surface condition at the interface region between the girder's top flange and deck slab had been intentionally roughened.
- The interface reinforcement stiffness for Girder A2 was 21.19 ksi, which was lower than the minimum specified values recommended by (Alkatan 2016), 29.44 ksi. Also, the cohesion factor was very low at the interface region due to the smooth surface condition of the concrete. Therefore, limited bond strength could be provided by the concrete. As a result, multiple GFRP rebars broke at failure as no additional shear strength could be provided by the GFRP rebars after cracking of concrete initiated at the interface.

10.7.2 Effect of using stainless steel strands

- Both ends of one HSSS prestressed concrete girder were tested in shear. This experimental program only provides preliminary results for the use of HSSS strands as main longitudinal prestressing reinforcement in prestressed concrete girders. Due to a limited sample size, more testing is needed to develop shear design guidelines for concrete girders prestressed with HSSS strands.
- The effect of the mechanical characteristics, stress-strain behavior, of the HSSS strands is clear in the experimental data. A constant increase in the shear force-deflection curve was seen in Girder B3 with no sign of a plateau, which reflected the stress-strain behavior of the HSSS strands.
- The shear capacity estimated by ACI 318 and AASHTO LRFD Bridge Design Specifications was in good agreement with experimental results obtained from testing Girder B3, which was prestressed with HSSS strands. Until further research, both ACI 318

and AASHTO LRFD equations can be used to design concrete girders prestressed with HSSS strands in shear.

- Both Girder A3 and Girder B3 were reinforced with stainless steel stirrups. Direct comparison cannot be made between Girder A3 and Girder B3 because they had different initial prestressing force, which affects the deflection behavior and shear cracking angle, which in turns affects the shear reinforcement contribution.

CHAPTER 11 SUMMARY AND CONCLUSIONS

11.1 Summary

This research program investigated the following: mechanical properties of 0.6-in.-diameter HSSS strand; bond strength of 0.6-in.-diameter HSSS strand; fabrication of full-scale 42-ft-long AASHTO Type II girders prestressed with HSSS strands; transfer length of 0.6-in.-diameter HSSS strands; prestress losses of 0.6-in.-diameter HSSS strands; flexural behavior of girders prestressed with 0.6-in.-diameter HSSS strands; shear behavior of a girder prestressed and reinforced with stainless steel reinforcing materials; and shear behavior of a girder reinforced with GFRP stirrups.

The research objectives were accomplished by conducting several tests. The research activities and tests were as follows.

1. Twenty (20) 50-in.-long HSSS strands from two spools were tested in direct tension following ASTM A1061. Five (5) 50-in.-long HSSS strands from one spool were tested in direct tension using regular wedges.
2. Six (6) HSSS strands from one spool were tested for bond strength following ASTM A1081.
3. Ten (10) and three (3) 42-ft-long AASHTO Type II girders prestressed with HSSS strands and carbon steel strands, respectively, were fabricated at Dura-Stress, Inc., casting yard in Leesburg, FL.
4. Transfer length tests were performed on eight (8) girders prestressed with HSSS strands and on three (3) girders prestressed with carbon steel strands.
5. Two (2) and one (1) non-composite girders prestressed with HSSS strands and carbon steel strands, respectively, were tested in flexure. One of the two girders prestressed with HSSS strands was unloaded before failure and was tested later in shear at both ends after adding a deck-slab. Eight (8) composite girders prestressed with HSSS strands were tested in flexure. One (1) composite girder prestressed with carbon steel strands was tested in flexure; however, it was unloaded before failure and was tested later in shear at both ends. One (1) composite girder prestressed with carbon steel strands was tested in shear at both ends and at mid span.

11.2 Conclusions

11.2.1 Conclusions drawn from experimental testing

11.2.1.1 Tensile tests

The mechanical properties of the HSSS strands are different from those of carbon steel strands. FDOT's Standard Specification for Road and Bridge Construction (Section 933) and ASTM A1114 specify the minimum guaranteed mechanical properties for HSSS strands. The current available HSSS strands have lower ultimate strain and stress and elastic modulus than those of carbon steel strands. The most significant difference is in elongation. The minimum required elongation of HSSS strands is 40% of that of carbon steel strands.

All tested strands satisfied FDOT and ASTM A1114 requirements. The stress-strain behavior of the HSSS strands was different between the two spools. A stress-strain equation is proposed for the 0.6-in.-diameter HSSS strands. The proposed equation fits the lower-bound curve of the tested strands in the elastic region, has a stress-strain shape similar to those of the tested strands, and satisfies FDOT and ASTM A1114 requirements.

The mechanical properties of the HSSS strands tested using regular chucks were not significantly affected in the elastic region. Therefore, regular wedges can be used to tension HSSS strands in the casting yard.

11.2.1.2 Bond strength tests

The minimum and average strand bond strengths, following ASTM A1081, of six 0.6-in.-diameter HSSS strands were 15,800 lb and 17,883 lb, respectively. Only 0.6-in.-diameter HSSS strands were tested for bond strength in this project. Therefore, experimental results obtained in this project were compared with bond strengths values recommended by PCI Strand Bond Task Group. The minimum and average experimental ASTM A1081 bond strengths were 23.4% and 19.8% greater than the recommended values by PCI Strand Bond Task Group. It can be concluded that the 0.6-in.-diameter HSSS strand has an acceptable bond strength.

11.2.1.3 Fabrication of girders prestressed with HSSS strands

Two sets of girders prestressed with 0.6-in.-diameter HSSS strands were fabricated; each set consisted of five girders that were constructed in one casting bed using the long-line method of precasting. Girders prestressed with HSSS strands were fabricated using the same apparatus and procedure that were used for girders prestressed with carbon steel strands. One incident occurred during fabrication of the first five girders prestressed with HSSS strands, which were cast in one

bed. During cutting of the penultimate HSSS strand at one of the external ends, the last HSSS strand fractured at the chuck device. Two factors may have contributed to this incident. First, as each strand is cut, elastic shortening of the beam causes additional tension in the remaining uncut strands, between the end of the girder and the abutment. The last HSSS strand to be cut experiences the most accumulation of these tensile stresses. Because an HSSS strand has low ductility, it reached its ultimate strain and broke. A second factor that may have contributed to the breakage is the deviation of that HSSS strand. The end abutments in the casting bed used for the girders were made for only three layers of strands, while the girders were designed with four layers of HSSS strands. Therefore, one strand had to be deviated from the girder ends to the abutments. Changing the orientation of the strand creates force concentration from the grips on one side of the fractured HSSS strand. Due to the impact force from the strand failure, the external girder moved approximately 2 in., and the internal spacing between the girders was reduced. Based on this incident, it is recommended that HSSS strands not be deviated until further studies can be done to establish HSSS strand's tolerance to kinks or deviations. Also, special attention shall be taken while cutting HSSS strands. The fabrication of the other five girders prestressed with HSSS strands went smoothly.

11.2.1.4 Transfer length

Girders were fabricated in the casting bed using the long-line method of precasting. The internal ends are more dominant in the long-line method. An analysis of the transfer length tests indicates that the measured transfer length at the first cut end (external end) is longer than that at the other cut ends (internal ends).

The maximum-measured transfer length of 0.6-in.-diameter HSSS strands at 35 days was 21.5 in., which was 40% less than that calculated by AASHTO. Therefore, it can be concluded that HSSS strand has good bonding with the surrounding concrete and that the AASHTO equation conservatively predicts the transfer length of 0.6-in.-diameter HSSS strands.

Results revealed that the transfer length of HSSS strands increases with an increase in the initial prestressing force. The initial jacking force for each HSSS strand was 37.2 kips in the first set of girders and 36.0 kips in the second set of girders. The maximum transfer length at release at the first cut end (external end) in the first and second sets of girders was 21.5 in. and 19.7 in., respectively. Also, the average transfer length at release at the internal end in the first and second sets of girders was 15.9 in. and 13.0 in., respectively.

Multiple sensing technologies (DEMEC points, strain gages, and fiber optic sensors) were used in this research program to measure strains at the end regions to determine transfer length. DEMEC points and strain gages have been used by researchers to measure transfer length for many years. Fiber optic sensors are another type of technology available to measure transfer length. Strain distribution at the end regions obtained by internal and external fiber optic sensors were in good agreement with the strains measured using strain gages. Thus, the fiber optic sensor is another viable option that can be used to measure transfer length.

11.2.1.5 Prestress losses

Prestress losses in the strands were measured using vibrating wire strain gages. Vibrating wire strain gages cannot detect changes in the strands strain caused by relaxation of strands; therefore, AASHTO Equation 5.9.3.4.2c-1 was used to estimate the stress-relaxation losses. The estimated stress-relaxation loss was 1.49 ksi and 0.52 ksi for carbon steel and HSSS strands, respectively. The estimated stress-relaxation loss for HSSS was significantly lower than that for carbon steel strands because the stress in the HSSS strands immediately after transfer was lower than that in carbon steel strands. The measured stress losses by vibrating wire strain gages (not including losses due to relaxation of strands) in composite Girder A2 (prestressed with carbon steel strands) and Girder C2 (prestressed with HSSS strands) was 21.2 ksi and 21.0 ksi, respectively. The initial stress was 202.3 ksi for carbon steel strands and 161.7 ksi for HSSS strands. Thus, the measured prestress loss was 10.5% for carbon steel strands and 13.0% for HSSS strands. Even though the measured prestress losses were almost equal in carbon steel and HSSS strands, the percentage of prestress losses was larger for HSSS strands. Thus, it can be concluded that HSSS strands exhibited greater prestress losses than carbon steel strands.

In the second set of girders, the initial stress in the HSSS strands was 156.5 ksi. The averaged-measured prestress losses using vibrating wire strain gages (not including losses due to relaxation of strands) was 16.2 ksi, 14.0 ksi, and 10.7 ksi for girders prestressed with 11, 9, and 7 HSSS strands, respectively. The maximum measured total prestress losses in HSSS strands was 12.1% of the initial stress. The AASHTO LRFD approximate method was used to estimate the prestress losses in HSSS strands. The estimated total prestress loss by AASHTO approximate method was found to be on average 25.3% greater than the measured values. Until further studies, AASHTO equations can be used to estimate the prestresses losses of HSSS strands.

11.2.1.6 Flexural tests

The post-cracking behavior of girders prestressed with HSSS strands continued to increase up to failure with no discernible plateau, which is different compared to girders prestressed with carbon steel strands. The differences in the post-cracking behavior are attributed to the differences in stress-strain behavior (mechanical properties) between the two strands.

The flexural strength was higher for the girder prestressed with HSSS strands compared to the girder prestressed with carbon steel strands (control) when both girders had the same initial prestressing force (greater prestressing reinforcement ratio). The flexural strength of the non-composite and composite girders prestressed with HSSS strands was approximately 11.7% and 23.7%, respectively, greater than girders prestressed with carbon steel strands. This increase is attributed to the increase, 25.3%, in the prestressing reinforcement ratio in the HSSS girders.

All composite girders failed due to rupture of strands where the bottom layer of HSSS strands reached their ultimate tensile strain before the concrete strain in the extreme compression fiber reached its assumed ultimate strain of 0.003. Even though the flexural behavior of the composite girders was controlled by the low ductility of the HSSS strands, the girders exhibited large reserve deflection and strength beyond the cracking load and provided significant and substantial warning through large deflection, as well as well-distributed and extensive flexural cracking, before failure. All composite girders prestressed with HSSS strands had ultimate deflection ranging from $L/125$ to $L/84$; the denominator value decreases as the reinforcement ratio increases. Regardless of failure mode, girders prestressed with HSSS strands can achieve ultimate capacity and deformability as high as those prestressed with carbon steel strands. Therefore, based on these experimental results, the recommended failure mode of I-girders prestressed with HSSS strands is rupture of strand.

11.2.1.7 Shear tests

Experimental results showed that direct replacement of shear reinforcement from Grade 75 stainless steel rebars (Girder A3) to GFRP rebars (Girder A2) reduced the ultimate shear capacity by approximately 8% and changed the failure mode from flexure shear to interface shear. The interface shear failure happened due to the low transverse shear capacity of GFRP bars and smooth interface between the girder and deck slab. At failure, multiple GFRP bars were found broken at the interface between the deck slab and girder. Based on AASHTO LRFD calculations, interface shear failure would not have occurred in Girder A2 if the surface condition at the interface region between the girder's top flange and deck slab had been intentionally roughened.

Strand slippage occurred during the shear test when the confinement reinforcement spacing for the first 12 in. was double the current FDOT standard end region reinforcement detailing. Therefore, it is not recommended to change/increase the current FDOT standard end region reinforcement detailing. Also, direct replacement of confinement reinforcement from Grade 75 stainless steel rebars (Girder A3) to GFRP rebars (Girder A2) resulted in an increase in the strand slippage during shear tests.

Both ACI and AASHTO LRFD conservatively estimated the shear capacity of the tested specimens. The average shear strength of Girder A2 (reinforced with GFRP stirrups) was 69% greater than AASHTO and 51% greater than ACI predictions. The average shear strength of Girder A3 (reinforced with stainless steel stirrups) was 16% higher than AASHTO and 23% higher than ACI predictions. The prediction of shear strength by design provisions (ACI and AASHTO) of Girder A2 is more conservative than that of Girder A3.

A constant increase in the shear force-deflection curve was observed in Girder B3 (prestressed with HSSS strands and reinforced with stainless steel Grade 75 stirrups) with no sign of a plateau, which reflected the stress-strain behavior of the HSSS strands. Both ACI and AASHTO LRFD conservatively estimated the shear capacity of the tested specimens. The average shear strength of Girder B3 was 9% higher than AASHTO and 17% higher than ACI predictions.

11.2.2 Conclusions drawn from analytical model

1. Two failure modes (crushing of concrete and rupture of strands) are feasible when HSSS strands are used in flexural members. Rupture of strands failure requires a smaller number of prestressing strands than crushing of concrete failure. In one example, to change the failure mode from rupture of strand to crushing of concrete, the number of HSSS strands was increased by 7 strands (equivalent to a prestressing reinforcement area increase of 50%). The ultimate deflection at mid span was 7.3% greater, and the flexural strength was 38.3% greater, for the section that failed by crushing of concrete than for the section that failed by rupture of strands. Although more strength was achieved with the addition of seven strands, if the additional strength were not needed, then one could argue that it is not worth the expense to gain only 7.3% more deflection.
2. For I-girder sections, it is recommended to design the member to fail due to rupture of strand (for better economy). To ensure adequate deformability at failure, it is recommended that the concrete strain at the extreme compression fiber be greater than $(f'_c+5)/10,000$ at failure.

3. For slab girders, it is recommended to design the member to fail due to crushing of concrete. To ensure adequate deformability at failure, it is recommended that the net tensile strain in the bottom layer of HSSS strands be greater than 0.005 at failure. Net tensile strain lower than 0.005 is acceptable after ensuring that the designed section exhibits large deformability at failure equivalent to the same section designed with carbon steel strands. Further research is needed to establish this net tensile strain limit for design purposes.
4. Numerical equations are proposed to compute the nominal flexural resistance for rectangular sections prestressed with HSSS strands. Development of numerical equations can be found in Chapter 7. For flanged sections prestressed with HSSS strands, simple iterative approaches are proposed. Design flowcharts are given in Chapter 9.
5. The recommended strength resistance factor is 0.75 for both crushing of concrete and rupture of strand failure modes.
6. The recommended maximum allowable stress in HSSS strands at jacking and immediately prior to transfer is 75% and 70%, respectively, of their guaranteed ultimate strength.

11.3 Suggestions for future research

1. Relaxation losses of both sizes of HSSS strands need to be experimentally studied. AASHTO Equation 5.9.3.4.2c-1 needs to be modified for HSSS strands.
2. Investigate tolerance to kinks or deviations of HSSS strands.
3. A robust reliability analysis needs to be done to determine the strength resistance factors for concrete members prestressed with HSSS strands.
4. Investigate the use of HSSS strands in post-tensioned concrete members.

REFERENCES

- EN 1992-1-1. 2004. "Eurocode 2: Design of Concrete Structures: Part 1-1: General Rules and Rules for Buildings", British Standards Institution (BSI),
- PCI Industry Handbook Committee. 2010. "PCI Design Handbook: Precast and Prestressed Concrete", Precast/Prestressed Concrete Institute, Chicago, IL.
- ASTM D7205. 2011. "Standard Test Method for Tensile Properties of Fiber Reinforced Polymer Matrix Composite Bars", American Society for Testing and Materials, West Conshohocken, PA.
- ASTM D7617. 2011. "Standard Test Method for Transverse Shear Strength of Fiber-reinforced Polymer Matrix Composite Bars", American Society for Testing and Materials, West Conshohocken, PA.
- CSA S806. 2012. "Design and Construction of Building Structures with Fibre-Reinforced Polymers", Canadian Standards Association, ON, Canada.
- KCI. 2012. "The Korean Concrete Structure Design Code", Korea Concrete Institute, Seoul, Korea.
- ASTM E328. 2013. "Standard Test Methods for Stress Relaxation for Materials and Structures", American Society for Testing and Materials, West Conshohocken, PA.
- ASTM A751. 2014. "Standard Test Methods, Practices and Terminology for Chemical Analysis of Steel Products", American Society for Testing and Materials, West Conshohocken, PA.
- ACI 440. 2015. "Guide for the Design and Construction of Structural Concrete Reinforced with Fiber Reinforced Polymer (FRP) Bars", ACI 440, American Concrete Institute, Farmington Hills, MI.
- ASTM A1081. 2015. "Standard Test Method for Evaluating Bond of Seven-Wire Steel Prestressing Strand", American Society for Testing and Materials, West Conshohocken, PA.
- ASTM A1061. 2016. "Standard Test Methods for Testing Multi-Wire Steel Prestressing Strand.", American Society for Testing and Materials, West Conshohocken, PA.
- AASHTO LRFD. 2017. "AASHTO LRFD Bridge Design Specifications", *8th Ed.*, American Association of State Highway and Transportation Officials, Washington, DC.
- ASTM A955. 2017. "Standard Specification for Deformed and Plain Stainless-Steel Bars for Concrete Reinforcement", American Society for Testing and Materials, West Conshohocken, PA.
- ASTM A276. 2017. "Standard Specification for Stainless Steel Bars and Shapes", American Society for Testing and Materials, West Conshohocken, PA.
- ASTM A416. 2017. "Standard Specification for Steel Strand, Uncoated Seven-Wire for Prestressed Concrete", American Society for Testing and Materials, West Conshohocken, PA.
- AASHTO. 2018. "Bridge Design Guide Specifications for GFRP-Reinforced Concrete Bridge Decks and Traffic Railings", American Association of State Highway and Transportation Officials, Washington, DC.
- ACI 318-19. 2019. "Building Code Requirements for Structural Concrete (ACI 318-19) and Commentary", American Concrete Institute, Farmington Hills, MI.
- NCHRP Report 907. 2019. "Design of Concrete Bridge Beams Prestressed with CFRP Systems", Washington, DC.

- Florida Department of Transportation (FDOT). 2020. "Standard Specifications for Road and Bridge Construction", Florida Department of Transportation, Tallahassee, FL.
- Florida Department of Transportation (FDOT). 2020. "Structures Design Guidelines", Florida Department of Transportation, Tallahassee, FL.
- Abreu, C. M., Cristóbal, M. J., Montemor, M. F., Nóvoa, X. R., Pena, G., and Pérez, M. C. 2002. "Galvanic Coupling Between Carbon Steel and Austenitic Stainless Steel in Alkaline Media." *Electrochimica Acta*, 47, 13-14, 2271-2279
- Ahmed, E. A., El-Salakawy, E. F., and Benmokrane, B. 2009. "Shear Performance of RC Bridge Girders Reinforced with Carbon FRP Stirrups." *Journal of Bridge Engineering*, 15, 1, 44-54
- Ahmed, E. A., El-Salakawy, E. F., and Benmokrane, B. 2010. "Fibre-Reinforced Polymer Composite Shear Reinforcement: Performance Evaluation in Concrete Beams and Code Prediction." *Canadian Journal of Civil Engineering*, 37, 8, 1057-1070
- Ahmed, E. A., El-Salakawy, E. F., and Benmokrane, B. 2010. "Performance Evaluation of Glass Fiber-Reinforced Polymer Shear Reinforcement for Concrete Beams." *ACI structural Journal*, 107, 1, 53-62
- Alkatan, J. 2016. "FRP Shear Transfer Reinforcement for Composite Concrete Construction." MS thesis, University of Windsor, ON, Canada.
- Baddoo, N. R. 2008. "Stainless Steel in Construction: A Review of Research, Applications, Challenges and Opportunities." *Journal of Constructional Steel Research*, 64, 11, 1199-1206
- Baddoo, N. R., and Kosmac, A. 2010. "Sustainable Duplex Stainless Steel Bridges." *Duplex 2010*, Barnes, R. W., Grove, J. W., and Burns, N. H. 2003. "Experimental Assessment of Factors Affecting Transfer Length." *ACI Structural Journal*, 100, 6, 740-748
- Belarbi, A., and Hsu, T. T. 1994. "Constitutive Laws of Concrete in Tension and Reinforcing Bars Stiffened by Concrete." *ACI Structural Journal*, V. 91, No. 4, July, pp. 465-474
- Brandes, M. R., and Kurama, Y. C. 2018. "Effect of Recycled Concrete Aggregates on Strength and Stiffness Gain of Concrete and on Bond Strength of Steel Prestressing Strand." *PCI Journal*, 63, 87-105
- Brown, K. 2018. "Production of Prestressed Concrete Piles Using Stainless Steel Strands." *Aspire Magazine*,
- Bruce, R. N., Russell, H. G., Roller, J. J., and Martin, B. T. 1994. "Feasibility Evaluation of Utilizing High-Strength Concrete in Design and Construction of Highway Bridge Structures." Louisiana Transportation Research Center, Baton Rouge, LA.
- Carroll, J. C., Cousins, T. E., and Roberts-Wollmann, C. L. 2017. "The Use of Grade 300 Prestressing Strand in Pretensioned, Prestressed Concrete Beams." *PCI Journal*, 62, 1, 49-65
- Castro-Borges, P., Troconis-Rincón, O., Moreno, E. I., Torres-Acosta, A. A., Martinez-Madrid, M., and Knudsen, A. 2002. "Performance of a 60-Year-Old Concrete Pier with Stainless Steel Reinforcement." *Materials Performance*, 41, 10, 50-55
- Chehab, A. I., Eamon, C. D., Parra-Montesinos, G. J., and Dam, T. X. 2018. "Shear Testing and Modeling of AASHTO Type II Prestressed Concrete Bridge Girders." *ACI Structural Journal*, V. 15, No. 3, May, pp. 801-811
- Collins, M. P., and Mitchell, D. 1991. *Prestressed Concrete Structures*, Prentice Hall, Englewood Cliffs, NJ.

- Dang, C. N., Floyd, R. W., Hale, W. M., and Martí-Vargas, J. R. 2016. "Measured Transfer Lengths of 0.7 in.(17.8 mm) Strands for Pretensioned Beams." *ACI Structural Journal*, 113, 1, 85
- Dang, C. N., Hale, W. M., and Martí-Vargas, J. R. 2018. "Quantification of Bond Performance of 18-mm Prestressing Steel." *Construction and Building Materials*, 159, 451-462
- Devalapura, R. K., and Tadros, M. K. 1992. "Stress-Strain Modeling of 270 ksi Low-Relaxation Prestressing Strands." *PCI Journal*, 37, 2, 100-106
- Dundu, M. 2018. "Evolution of Stress–Strain Models of Stainless Steel in Structural Engineering Applications." *Construction and Building Materials*, 165, 413-423
- El-Sayed, A. K., El-Salakawy, E. F., and Benmokrane, B. 2006. "Shear Capacity of High-Strength Concrete Beams Reinforced with FRP Bars." *ACI Structural Journal*, 103, 3, 383-389
- Garber, D., Gallardo, J., Deschenes, D., and Bayrak, O. 2016. "Nontraditional shear failures in bulb-t prestressed concrete bridge girders." *Journal of Bridge Engineering*, 21, 7, 04016030
- Garber, D. B., Gallardo, J. M., Deschenes, D. J., and Bayrak, O. 2015. "Experimental Investigation of Prestress Losses in Full-scale Bridge Girders." *ACI Structural Journal*, 112, 5, 553
- Gardner, L. 2005. "The Use of Stainless Steel in Structures." *Progress in Structural Engineering and Materials*, 7, 2, 45-55
- Gedge, G. 2008. "Structural Uses of Stainless Steel—Buildings and Civil Engineering." *Journal of Constructional Steel Research*, 64, 11, 1194-1198
- Grace, N. F. 2000. "Transfer Length of CFRP/CFCC Strands for Double-T Girders." *PCI journal*, 45, 5, 110-126
- Guadagnini, M., Pilakoutas, K., and Waldron, P. 2006. "Shear Resistance of FRP RC Beams: Experimental Study." *Journal of Composites for Construction*, 10, 6, 464-473
- Hwan, O. B., Sung, K. E., and Choi, Y. C. 2006. "Theoretical Analysis of Transfer Lengths in Pretensioned Prestressed Concrete Members." *Journal of engineering mechanics*, 132, 10, 1057-1066
- Ji, J., Darwin, D., and Browning, J. 2005. "Corrosion Resistance of Duplex Stainless Steels and MMFX Microcomposite Steel for Reinforced Concrete Bridge Decks." University of Kansas Center for Research, Inc.
- Johnson, D. T., and Sheikh, S. A. 2016. "Experimental Investigation of Glass Fiber-Reinforced Polymer-Reinforced Normal-Strength Concrete Beams." *ACI Structural Journal*, 113, 6, 1165-1174
- Kaar, P. H., LaFraugh, R. W., and Mass, M. A. 1963. "Influence of Concrete Strength on Strand Transfer Length." *PCI Journal*, 8, 2, 47-67
- Kahl, S. 2011. "Stainless and Stainless-Clad Reinforcement for Highway Bridge Use." Michigan Department of Transportation, Lansing, MI.
- Kahn, L. F., and Slapkus, A. 2004. "Interface Shear in High Strength Composite T-Beams." *PCI journal*, 49, 4, 102-111
- Kim, J. K., Yang, J. M., and Yim, H. J. 2016. "Experimental Evaluation of Transfer Length in Pretensioned Concrete Beams Using 2,400-MPa Prestressed Strands." *Journal of Structural Engineering*, 142, 11, 04016088
- Kim, Y. J., and Nickle, R. W. 2016. "Strength Reduction Factors for Fiber-Reinforced Polymer-Prestressed Concrete Bridges in Flexure." *ACI Structural Journal*, 113, 5, 1043
- Kose, M. M., and Burkett, W. R. 2005. "Formulation of New Development Length Equation for 0.6 in. Prestressing Strand." *PCI Journal*, 50, 96-105

- Lane, S. N. 1998. "A New Development Length Equation for Pretensioned Strands in Bridge Beams and Piles." Federal Highway Administration, McLean, VA.
- Lee, J. K. 2018. "Estimated Transfer Lengths of 0.6 in. (15.4 mm) Grade 350 (2400 MPa) Strands in High-Strength Concrete Pretensioned Members." *ACI Structural Journal*, 15, 3
- Lu, Z., Boothby, T. E., Bakis, C. E., and Nanni, A. 2000. "Transfer and Development Lengths of FRP Prestressing Tendons." *PCI Journal*, 45, 2, 84-95
- Maldonado, L., and Veleza, L. 1999. "Corrosivity Category Maps of a Humid Tropical Atmosphere: The Yucatán Peninsula, México." *Materials and Corrosion*, 50, 5, 261-266
- Maranan, G. B., Manalo, A. C., Benmokrane, B., Karunasena, W., and Mendis, P. 2017. "Shear Behavior of Geopolymer Concrete Beams Reinforced with Glass Fiber-Reinforced Polymer Bars." *ACI Structural Journal*, 114, 2, 337-348
- Markeset, G., Rostam, S., and Klinghoffer, O. 2006. "Guide for the Use of Stainless Steel Reinforcement in Concrete Structures." Norges byggforskningstitutt.
- Mattock, A. H. 1974. "Shear Transfer in Concrete Having Reinforcement at an Angle to the Shear Plane." *ACI Special Publication*, 42, 17-42
- Mattock, A. H. 1979. "Flexural Strength of Prestressed Concrete Sections by Programmable Calculator." *PCI Journal*, 24, 32-54
- Medina, E., Medina, J. M., Cobo, A., and Bastidas, D. M. 2015. "Evaluation of Mechanical and Structural Behavior of Austenitic and Duplex Stainless Steel Reinforcements." *Construction and Building Materials*, 78, 1-7
- Mitchell, D., Cook, W. D., Khan, A. A., and Tham, T. 1993. "Influence of High Strength Concrete on Transfer and Development Length of Pretensioning Strand." *PCI Journal*, 38, 3, 52-66
- Morcous, G., Assad, S., Hatami, A., and Tadros, M. K. 2014. "Implementation of 0.7 in. Diameter Strands at 2.0× 2.0 in. Spacing in Pretensioned Bridge Girders." *PCI Journal*, 59, 3, 145-158
- Morcous, G., Hatami, A., Maguire, M., Hanna, K. E., and Tadros, M. K. 2011. "Mechanical and Bond Properties of 18-mm-(0.7-in.-) Diameter Prestressing Strands." *Journal of Materials in Civil Engineering*, 24, 6, 735-744
- Moser, R. D. 2011. "High-Strength Stainless Steels for Corrosion Mitigation in Prestressed Concrete: Development and Evaluation." PhD diss., Georgia Institute of Technology.
- Moser, R. D., Kahn, L. F., Singh, P. M., and Kurtis, K. E. 2013. "Preliminary Studies of High-Strength Stainless Prestressing Steels." *ACI Special Publication*, 291, 1-10
- Moser, R. D., Singh, P. M., Kahn, L. F., and Kurtis, K. E. 2012. "Chloride-Induced Corrosion Resistance of High-Strength Stainless Steels in Simulated Alkaline and Carbonated Concrete Pore Solutions." *Corrosion Science*, 57, 241-253
- Mullins, G., Sen, R., and Sagüés, A. 2014. "Design and Construction of Precast Piles with Stainless Reinforcing Steel." Florida Department of Transportation, Tallahassee, FL.
- Nabipay, P., and Svecova, D. 2013. "Shear Behavior of CFRP Prestressed Concrete T-Beams." *Journal of Composites for Construction*, 18, 2, 04013049
- Naji, B., Ross, B. E., and W. Floyd, R. 2016. "Characterization of Bond-Loss Failures in Pretensioned Concrete Girders." *Journal of Bridge Engineering*, 22, 4, 06016013
- NBI. 2020. "National Bridge Inventory." <<https://www.fhwa.dot.gov/bridge/nbi/ascii.cfm>>. (November 1st, 2020).
- Nürnbergger, U., and Wu, Y. 2008. "Stainless Steel in Concrete Structures and in the Fastening Technique." *Materials and Corrosion*, 59, 2, 144-158

- Oh, B. H., and Kim, E. S. 2000. "Realistic Evaluation of Transfer Lengths in Pretensioned, Prestressed Concrete Members." *ACI Structural Journal*, 97, 6, 821-830
- Oh, B. H., Lim, S. N., Lee, M. K., and Yoo, S. W. 2014. "Analysis and Prediction of Transfer Length in Pretensioned, Prestressed Concrete Members." *ACI Structural Journal*, 111, 3, 549
- Park, H., Din, Z. U., and Cho, J.-Y. 2012. "Methodological Aspects in Measurement of Strand Transfer Length in Pretensioned Concrete." *ACI Structural Journal*, 109, 5, 625
- Patnaik, A. K. 2001. "Behavior of Composite Concrete Beams with Smooth Interface." *Journal of Structural Engineering*, 127, 4, 359-366
- Patzlaff, Q., Morcous, G., Hanna, K., and Tadros, M. K. 2012. "Bottom Flange Confinement Reinforcement in Precast Prestressed Concrete Bridge Girders." *Journal of Bridge Engineering*, 17, 4, 607-616
- Paul, A., Gleich, L. B., and Kahn, L. F. 2017a. "Structural Performance of Prestressed Concrete Bridge Piles Using Duplex Stainless Steel Strands." *Journal of Structural Engineering*, V. 143, No.7, Ju;y, pp. 04017042.doi: 10.1061/(ASCE)ST.1943-541X.0001770
- Paul, A., Gleich, L. B., and Kahn, L. F. 2017b. "Transfer and Development Length of High-Strength Duplex Stainless Steel Strand in Prestressed Concrete Piles." *PCI Journal*, V. 62, No. 3, May-June, pp. 59-71
- Paul, A., Kahn, L. F., and Kurtis, K. 2015. "Corrosion-Free Precast Prestressed Concrete Piles Made With Stainless Steel Reinforcement: Construction, Test and Evaluation." Georgia Department of Transportation, Atlanta, GA.
- Pessiki, S., Kaczinski, M., and Wescott, H. H. 1996. "Evaluation of Effective Prestress Force in 28-year-old Prestressed Concrete Bridge Beams." *PCI Journal*, 41, 6, 78-89
- Polydorou, T., Riding, K. A., and Peterman, R. J. 2016. "Interlaboratory Study of the Standard Test Method for Evaluating Bond of Seven-Wire Steel Prestressing Strand." *PCI Journal*, 61, 4, 53-64
- Rabi, M., Cashell, K. A., and Shamass, R. 2019. "Flexural Analysis and Design of Stainless Steel Reinforced Concrete Beams." *Engineering Structures*, 198, 109432
- Ramberg, W., and Osgood, W. R. 1943. "Description of Stress-Strain Curves by Three Parameters."
- Rambo-Roddenberry, M., Joshi, K., Fallaha, S., Herrera, R., Kampmann, R., Chipperfield, J., and Mtenga, P. 2016. "Construction, Strength, and Driving Performance of Carbon-Fiber-Reinforced Polymer Prestressed Concrete Piles." *PCI Journal*, 61, 24-37
- Ramirez-Garcia, A. T., Floyd, R. W., Hale, W. M., and Martí-Vargas, J. R. 2016. "Effect of Concrete Compressive Strength on Transfer Length." *Structures*, 5, 131-140
- Ramirez, J. A., and Russell, B. W. 2008. "Transfer, Development, and Splice Length for Strand/Reinforcement in High-Strength Concrete." Transportation Research Board, Washington, D.C.
- Riding, K. A., Peterman, R. J., and Polydorou, T. 2016. "Establishment of Minimum Acceptance Criterion for Strand Bond as Measured by ASTM A1081." *PCI Journal*, 61, 3, 86-103
- Rizkalla, S. H., and Tadros, G. 1995. "A Smart Highway Bridge in Canada." *Concrete International*, 16, 6, 42-44
- Ross, B. E., Ansley, M., and Hamilton, H. R. 2011. "Load Testing of 30-year-old AASHTO Type III Highway Bridge Girders." *PCI journal*, 56, 4, 152-163

- Rossini, M., and Nanni, A. 2019. "Composite Strands for Prestressed Concrete: State-of-the-Practice and Experimental Investigation into Mild Prestressing with GFRP." *Construction and Building Materials*, 205, 486-498
- Russell, B. W., and Burns, N. H. 1993. "Design Guidelines for Transfer, Development and Debonding of Large Diameter Seven Wire Strands in Pretensioned Concrete Girders.", Texas Department of Transportation, Austin, TX.
- Russell, B. W., and Burns, N. H. 1996. "Measured Transfer Lengths of 0.5 and 0.6 in. Strands in Pretensioned Concrete." *PCI Journal*, 41, 5, 44-65
- Salazar, J., Yousefpour, H., Abyaneh, R. A., Kim, H., Katz, A., Hrynyk, T., and Bayrak, O. 2018. "End-Region Behavior of Pretensioned I-Girders Employing 0.7 in.(17.8 mm) Strands." *ACI Structural Journal*, 115, 1, 91-14
- Salomon, A. L., and Moen, C. D. 2014. "Structural Design Guidelines for Concrete Bridge Decks Reinforced with Corrosion-Resistant Reinforcing Bbars." Virginia Department of Transportation, Richmond, VA.
- Schuetz, D. P. 2013. "Investigation of High Strength Stainless Steel Prestressing Strands." MSc thesis, Georgia Institute of Technology.
- Shahawy, M. A., Issa, M., and Batchelor, B. 1992. "Strand Transfer Lengths in Full Scale AASHTO Prestressed Concrete Girders." *PCI Journal*, 37, 3, 84-96
- Troconis, B. C., Sharp, S. R., Ozyildirim, H. C., Demarest, C. R., Wright, J., and Scully, J. R. 2020. "Corrosion-Resistant Stainless Steel Strands for Prestressed Bridge Piles in Marine Atmospheric Environments." Virginia Department of Transportation, Richmond, VA.
- Yang, J.-M., Kim, J.-K., and Yoo, D.-Y. 2018. "Transfer Length in Full-Scale Pretensioned Concrete Beams with 1.4 m and 2.4 m Section Depths." *Engineering Structures*, 171, 433-444
- Zia, P., and Mostafa, T. 1977. "Development Length of Prestressing Strands." *PCI Journal*, 22, 5, 54-65
- Zollman, C. C., Depman, F., Nagle, J., and Hollander, E. F. 1992. "A 40-Year Saga Building and Rebuilding of Philadelphia's Walnut Lane Memorial Bridge." *PCI Journal*, 37, 3

Appendix A – Mill certificates for HSSS strands and carbon steel strands

This appendix contains mill certificates, provided by manufacturer, for the two Duplex High-Strength Stainless Steel (HSSS) spools used in this study. The mill certificate includes information about the mechanical properties of the HSSS strands. The last three pages in this appendix are mill certificates for the carbon steel strands used in this study.



MILL CERTIFICATE OF INSPECTION

Order Number: SLPC170857-1

Page No : 1 OF 1

B/L No: SIPC172222

Issue Date : 10/18/2017

Commodity: Steel Strand, Uncoated Seven Wire for Prestressed Concrete

Size & Grade: 6/10" x 250 KSI Stainless

Specification: None - Low Relaxation

Customer Name: FLORIDA DEPT OF TRANSPORTATION

Customer P.O.: PO1504995-PR10206240

Destination: FLDOT

State Job No:

No Pack #	Heat #	B.S.	Elong.	Y.P.	Area	E-Modulus	CURVE#	
		(LB)	(%)	(LB)	(IN ²)	(MPSI)		
1	D430001-1D	DNA452D-2	59,755	1.9	52,919	0.2328	24.4	D430001

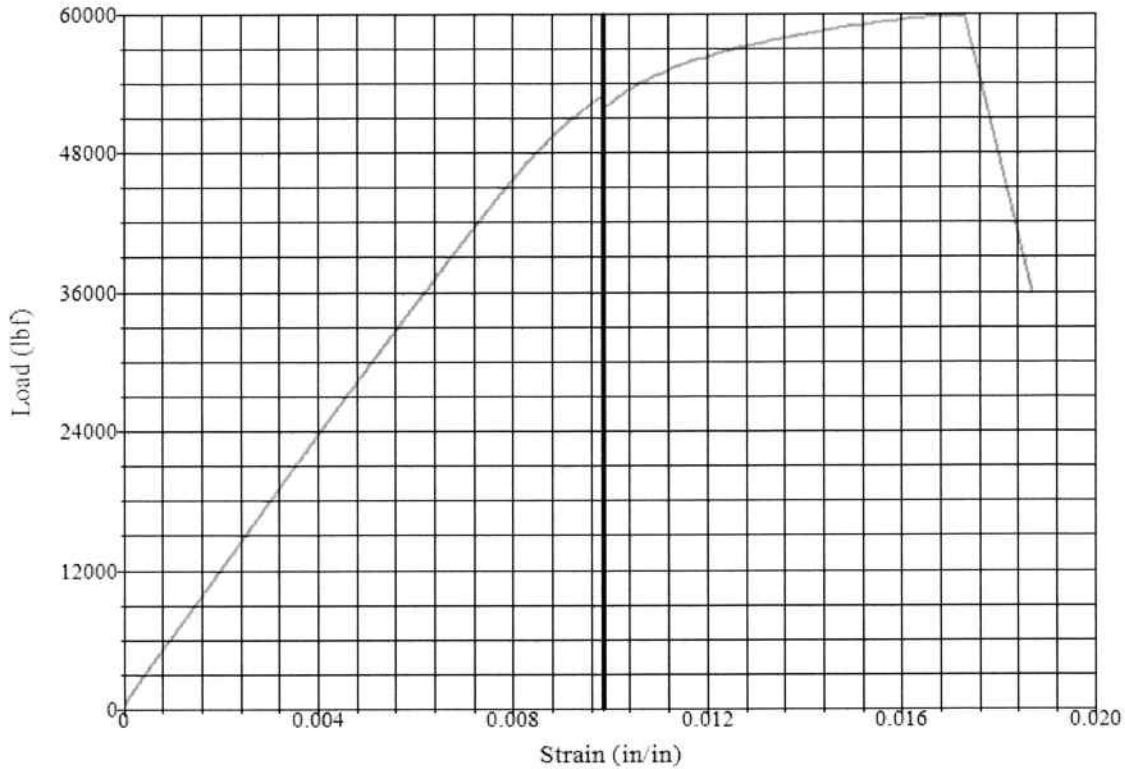
Note 1: Total elongation is below the expected minimum elongation of 3.5%.
Note 2: Diameter is larger than typical at 0.620" (15.75mm).

We hereby certify that:

- * We have accurately carried out the inspection of COMMODITY.
- * The raw material, and all manufacturing processes used in the production of the COMMODITY described above occurred in the USA, in compliance with the Buy America requirements of 23 CFR 635.410.
- * The material described above will bond to concrete of a normal strength and consistency in conformance with the prediction equations for transfer and development length given in the ACI/AASHTO specifications.
- * The individual below has the authority to make this certificate legally binding for SWPC.

Load - Elongation Curve

For Uncoated Seven Wire Steel Strand for Prestressed Concrete



* Vertical Line is drawn at 1% Extension Under Load
 * Tested to ASTM A1061 Standards

Curve Number D430001

Size	0.6	in
Grade	270	Ksi
Yield Point	52,919	lbf
Actual Area	0.2328	in²
As Tested Modulus	24.4	Msi
Breaking Strength	59,755	lbf
Elongation	1.90	%
Diameter OW 1	5.16	mm
Diameter OW 2	5.16	mm
Diameter OW 3	5.16	mm
Diameter OW 4	5.16	mm
Diameter OW 5	5.16	mm
Diameter OW 6	5.16	mm
Diameter CW	5.43	mm
Date Tested	10/12/2017	
Tested By	darryl	



[Signature]
 Approval

Curve D430001



MILL CERTIFICATE OF INSPECTION

Order Number: SLPC200183-1

Page No : 1 OF 1

B/L No: SIPC200318

Issue Date : 01/27/2020

Commodity: Steel Strand, Uncoated Seven Wire for Prestressed Concrete
 Size & Grade: 6/10" x 250 KSI Stainless
 Specification: None - Low Relaxation
 Customer Name: FLORIDA STATE UNIVERSITY
 Customer P.O.: FS20018925
 Destination: UNIVFSU
 State Job No:

No Pack #	Heat #	B.S.	Elong.	Y.P.	Area	E-Modulus	CURVE#	
		(LB)	(%)	(LB)	(IN ²)	(MPSI)		
1	D430018-2	DNAA10L	55,472	1.6	50,590	0.2306	23.9	D430018

Note 1: Total elongation is below the expected minimum elongation of 3.5%.

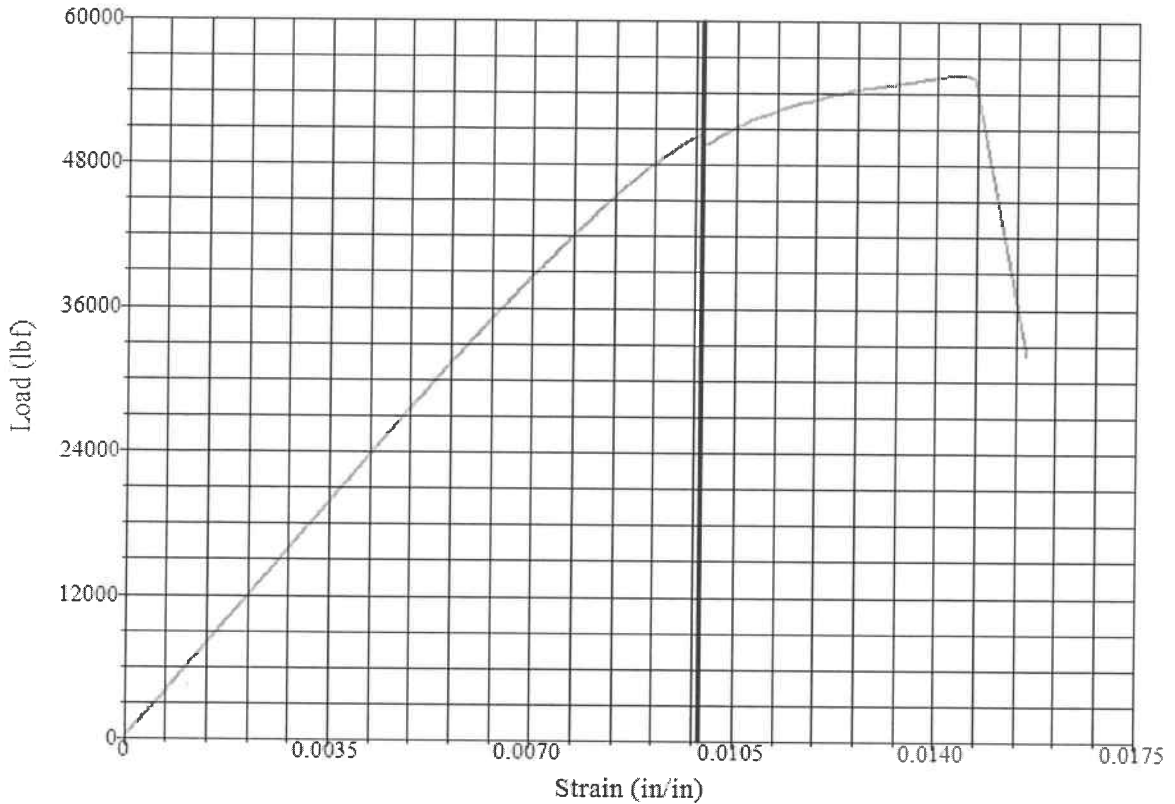
We hereby certify that:

- * We have accurately carried out the inspection of COMMODITY.
- * The raw material, and all manufacturing processes used in the production of the COMMODITY described above occurred in the USA, in compliance with the Buy America requirements of 23 CFR 635.410. The steel was melted and manufactured in the USA.
- * The material described above will bond to concrete of a normal strength and consistency in conformance with the prediction equations for transfer and development length given in the ACI/AASHTO specifications.
- * The individual below has the authority to make this certificate legally binding for SWPC.

Quality Assurance Section

Load - Elongation Curve

For Uncoated Seven Wire Steel Strand for Prestressed Concrete



* Vertical Line is drawn at 1% Extension Under Load
 * Tested to ASTM A1061 Standards

Curve Number D430018

Size	0.6	in
Grade	250	Ksi
Yield Point	50,590	lbf
Actual Area	0.2306	in²
As Tested Modulus	23.9	Msi
Breaking Strength	55,472	lbf
Elongation	1.60	%
Diameter OW 1	5.14	mm
Diameter OW 2	5.14	mm
Diameter OW 3	5.13	mm
Diameter OW 4	5.13	mm
Diameter OW 5	5.13	mm
Diameter OW 6	5.13	mm
Diameter CW	5.41	mm
Date Tested	2/18/2019	
Tested By	darryl	



[Signature]
 Approval

Curve D430018



CUSTOMER: DURASTRESS, INC
LOCATION: LEESBURG, FL 34788
PURCHASE ORDER: 12875

DATE: 08/28/2018
CERTIFICATION NUMBER: QA71855
CERTIFICATION STANDARD: ASTM A 416/A416M

PRODUCT DESCRIPTION

.600" (15.24 mm) DIAMETER 270 (1860) GRADE LOW RELAXATION SEVEN WIRE STRAND

COIL IDENTIFICATION

COIL # 'S	HEAT #
002829.009	82325S
002829.011	82325S
002900.001	82329S
002900.004	82329S
002900.005	82329S
002900.006	82329S
002900.007	82329S

TESTS AND SAMPLE INFORMATION

ATTACHED ARE ACTUAL TEST RESULTS FOR SAMPLES TAKEN FROM THE MATERIAL BEING PROVIDED. ADDITIONAL TESTS AND MANUFACTURING DATA AVAILABLE AS REQUIRED BY ASTM. ROD HEAT AND CHEMISTRY INFORMATION ON FILE.

COMMENTS

Prestressed concrete strand identified on this certification was produced by Strand Tech Martin Inc. and meets the requirements for "Domestic Origin" as defined by the Surface Transportation Act of 1978, and amended 1982, and meets all of the requirements set forth in Federal Highway Administration rules and regulations with regard to "Domestic Origin." All materials listed above was produced and fabricated in the United States of America. Meets certification ASTM A416/A416M

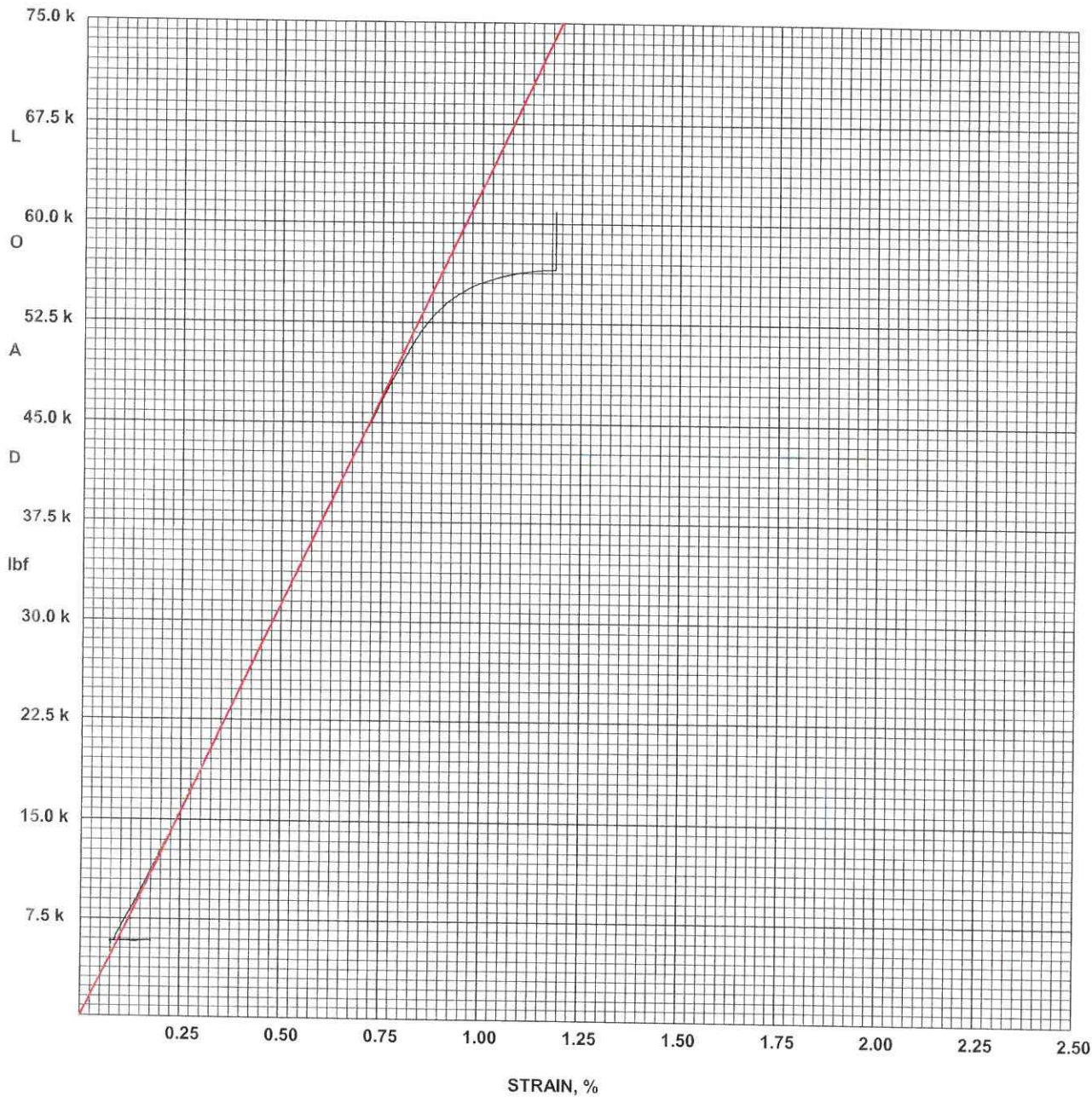
COMMENTS

"THE MATERIAL DESCRIBED IN THIS CERTIFICATION WILL BOND TO CONCRETE OF A NORMAL STRENGTH AND CONSISTENCY IN CONFORMANCE WITH THE PREDICTION EQUATIONS FOR TRANSFER AND DEVELOPMENT LENGTH GIVEN IN THE ACI/AASHTO SPECIFICATIONS."

STRAND-TECH MARTIN, INC.
P.O. BOX 2220
SUMMERVILLE, SC 29484
TOLL FREE (877) 783-3305

CERTIFICATION PREPARED BY:

CHRIS LEWIS



Strand-Tech Manufacturing, Inc.
Manufacturer of PC Strand & Wire
258 Deming Way
Summerville, SC 29483

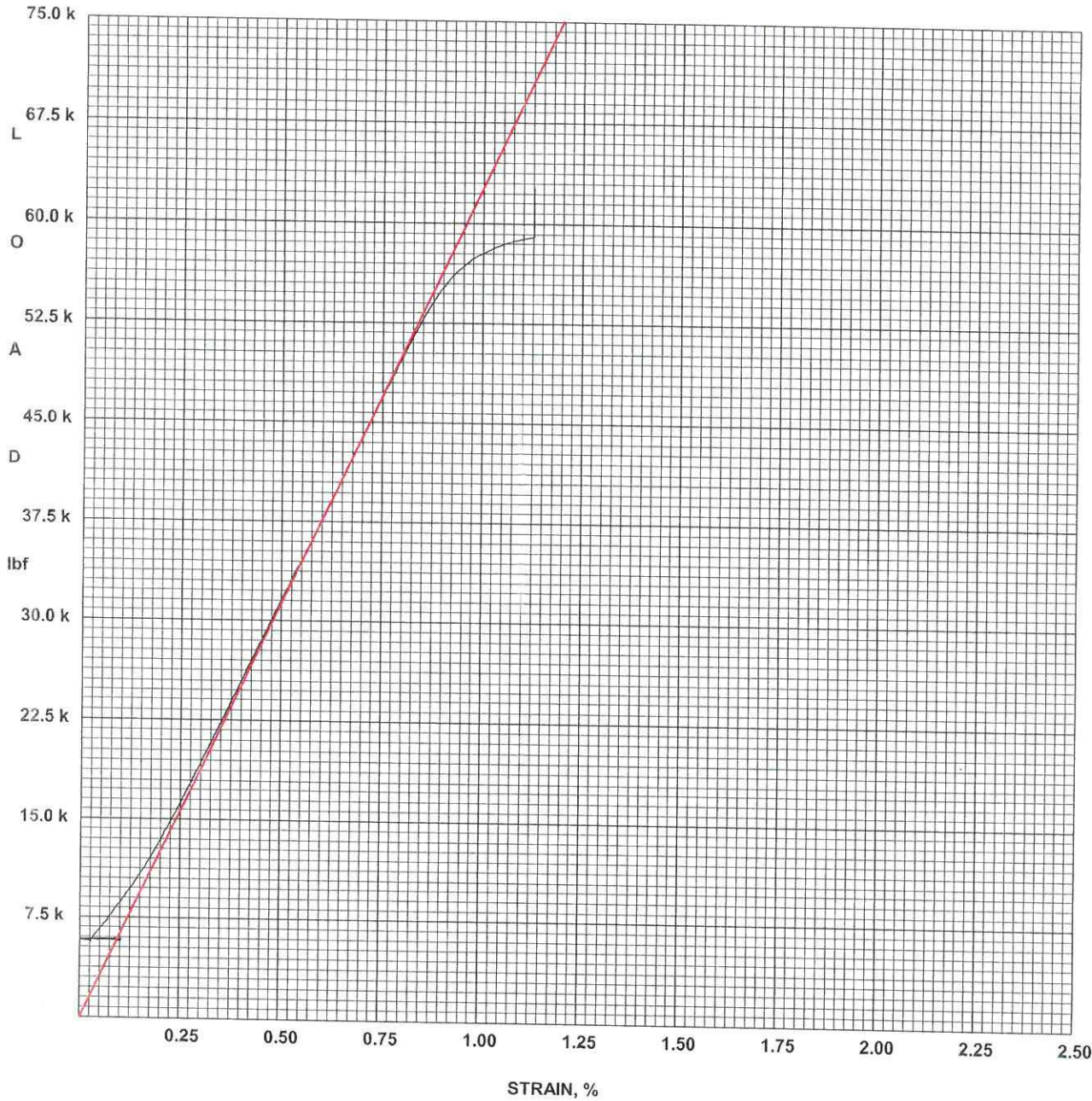
7-Wire Strand ASTM A416

Test Date 08/16/2018
 Size .600" 270 LR

Lot: 002829
 Sample: 05
 Heat Number: 82325S
 Test #: 1
 Tested By: 203 AW
 Ultimate, lbf: 60900
 Ultimate, kN: 271
 Load @, lbf: 55500
 Load @, kN: 247
 Elongation, %: 6.33
 Nominal Area, in²: 0.217
 Nominal Area, mm²: 140
 Actual, in²: 0.2184
 Actual, mm²: 140.91
 Strand Diameter, in: 0.604
 Modulus, Mpsi: 28.7
 Modulus, MPa: 197700
 Minimum, in: 0.0098

002829.009

002829.011



Strand-Tech Manufacturing, Inc.
Manufacturer of PC Strand & Wire
258 Deming Way
Summerville, SC 29483

7-Wire Strand ASTM A416

Test Date 08/26/2018
 Size .600" 270 LR

Lot: 002900
 Sample: 01
 Heat Number: 82329S
 Test #: 1
 Tested By: 203 AW
 Ultimate, lbf: 62700
 Ultimate, kN: 279
 Load @, lbf: 57800
 Load @, kN: 257
 Elongation, %: 5.29
 Nominal Area, in²: 0.217
 Nominal Area, mm²: 140
 Actual, in²: 0.2186
 Actual, mm²: 141.03
 Strand Diameter, in: 0.604
 Modulus, Mpsi: 28.7
 Modulus, MPa: 197800
 Minimum, in: 0.0093

- 002900.001
- 002900.004
- 002900.005
- 002900.006
- 002900.007

Appendix B – Design details drawings

This appendix contains design details drawings for the girders. The drawings included all the information needed for construction. The first set of drawings is for Girders A1-A3, B2-B3, and C1-C3. The second set of drawings is for Girders E1-E5.

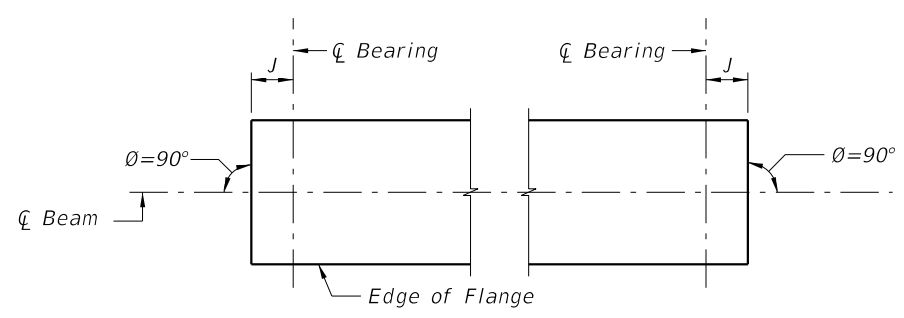
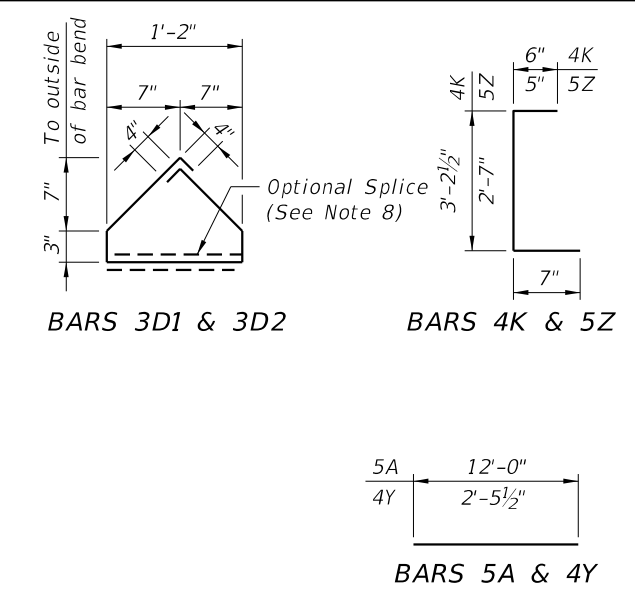
BEAM NOTES

1. Work Bar Bending Diagrams provided on this sheet with Index 415-001 for Beams A1, A3, B3, C1, C3, D1 and D2. Work Bar Bending Diagrams provided on this sheet with Developmental Design Standards Index D21310 for Beams A2, B2 and C2.
2. All bar bend dimensions are out-to-out.
3. Concrete cover: 2 inches minimum.
4. Strands N: $\frac{3}{8}$ " \emptyset minimum, stressed to 10,000 lbs. each. Strands N shall be Carbon Steel Strands.
5. Place one (1) Bar 4K or 5Z at each location. Alternate the direction of the ends for each bar.
6. Tie Bars 4K and 5Z to the fully bonded strands in the bottom or center row (see "STRAND PATTERN" on the Table of Beam Variables Sheet).
7. Place Bars 3D1 in beam END 1, and Bars 3D2 in beam END 2.
8. Contractor Options:
A. Bars 3D1 and 3D2 may be fabricated as a two-piece bar with a 1'-0" minimum lap splice of the bottom legs.
9. Cut wedges and Prestressing Strands at the end of the beam without damaging the surrounding concrete. See "STRAND CUTTING DETAIL."
10. Provide material certifications to FDOT Structures Research Center.
11. Carbon Steel and Stainless Steel reinforcing bars shall be Grade 60 per Specification Section 931.
12. GFRP reinforcing bars shall be in accordance with Specification Section 932.
13. Researchers and FDOT personnel shall be allowed to instrument the beams and monitor them during detensioning. Time required for instrumenting is approximately one day per casting bed setup.

BILL OF REINFORCING STEEL FOR ONE BEAM ONLY

MARK	NOTE NUMBERS	SIZE	NUMBER REQUIRED	LENGTH
A	—	5	4	12'-0"
D1	8	3	12	3'-11 $\frac{3}{4}$ "
D2	8	3	10	3'-11 $\frac{3}{4}$ "
K	5 & 6	4	80	4'-3 $\frac{1}{2}$ "
N	4 & 9	$\frac{3}{8}$ " \emptyset Strand	2	42'-5"
Y	—	4	6	2'-5 $\frac{1}{2}$ "
Z	5 & 6	5	6	3'-7"

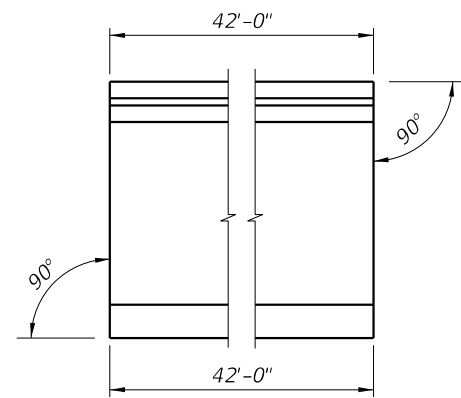
BENDING DIAGRAMS (See Notes 1 & 2)



END 1 END 2

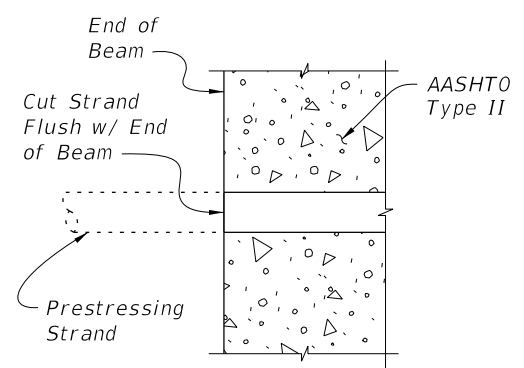
**PLAN VIEW
CASE 1**

(Standard Orientation for New Construction)



**END ELEVATION
CONDITION 1**

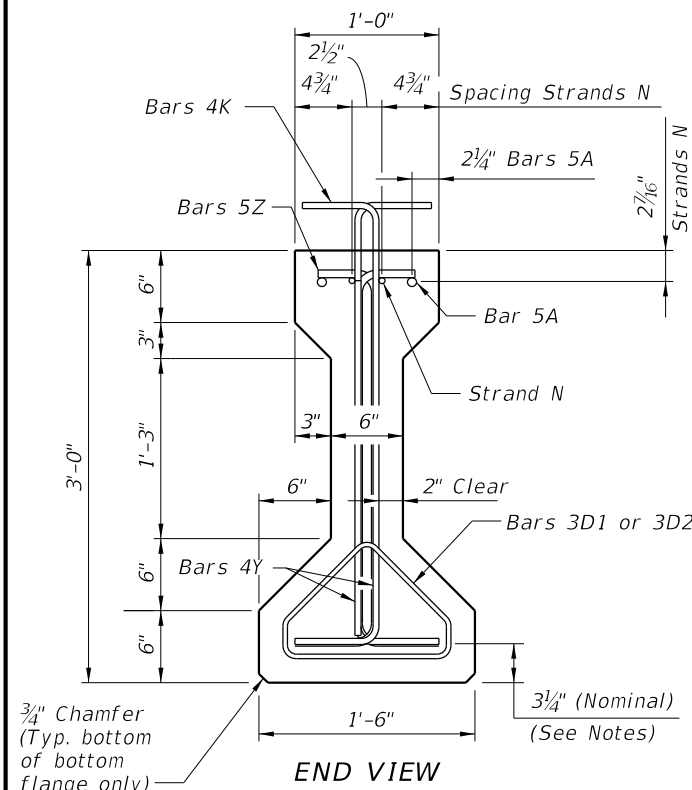
(Dim P = 0.0)



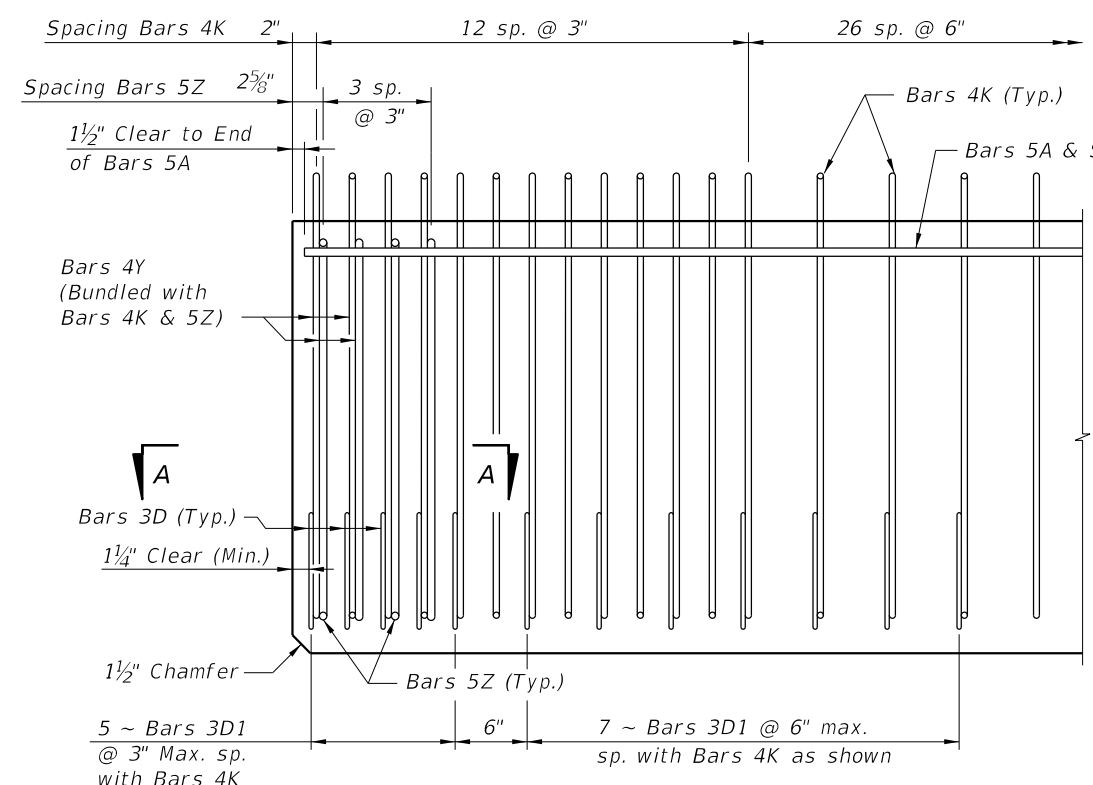
**TYPICAL SECTION
SHOWING CUT STRAND**

STRAND CUTTING DETAIL

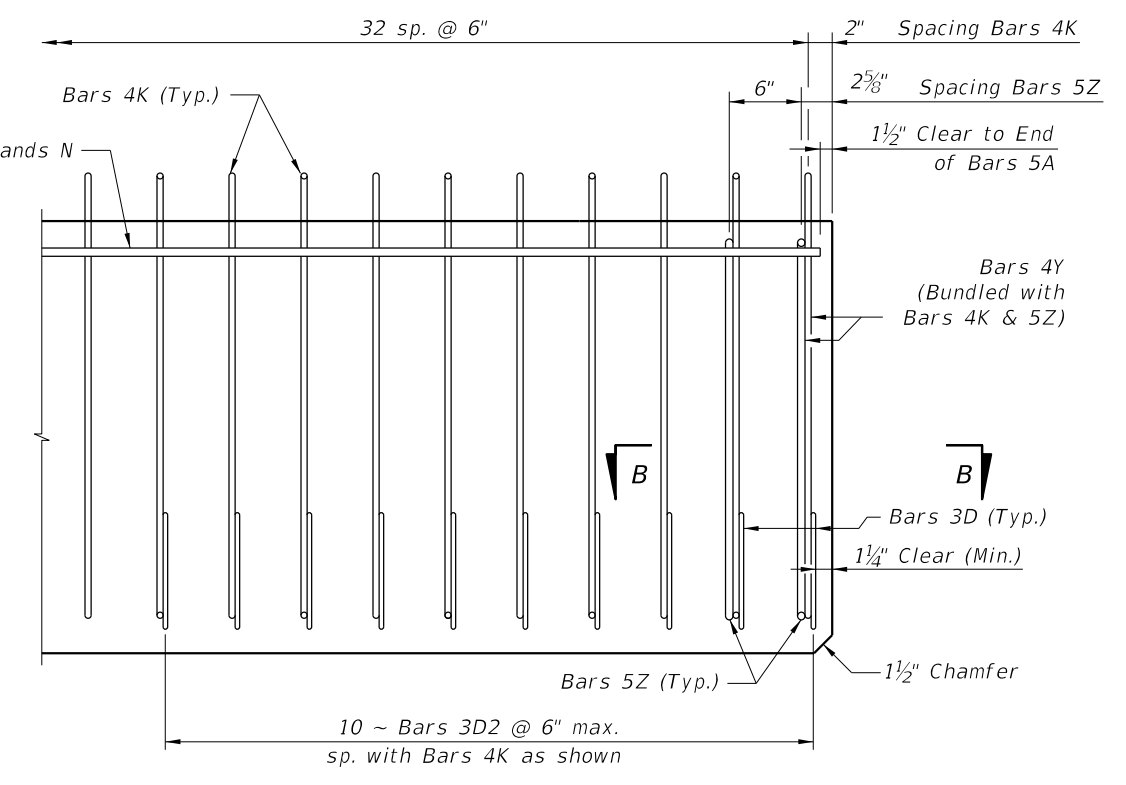
REVISIONS						B2	STATE OF FLORIDA DEPARTMENT OF TRANSPORTATION			SHEET TITLE:		REF. DWG. NO.
DATE	BY	DESCRIPTION	DATE	BY	DESCRIPTION		ROAD NO.	COUNTY	FINANCIAL PROJECT ID	AASHTO TYPE II BEAM - DETAILS AND NOTES		
										PROJECT NAME: Stainless Steel Strands for Prestensioned Concrete Girders		SHEET NO.
												1



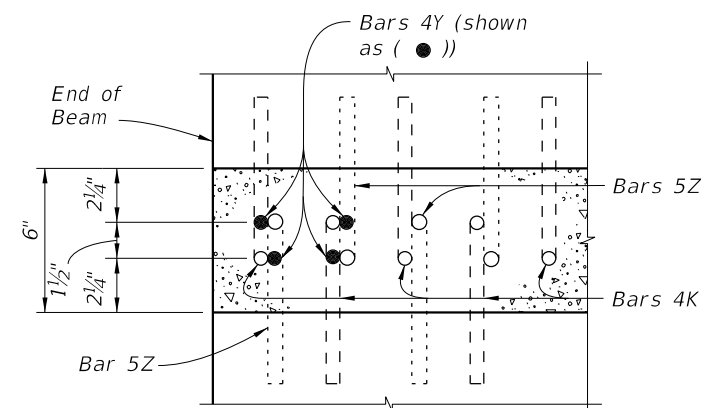
END VIEW



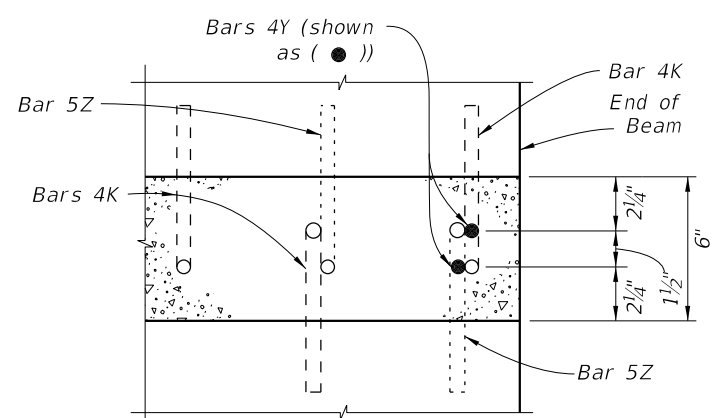
**ELEVATION AT END 1 OF BEAM
(Flanges Not Shown For Clarity)**



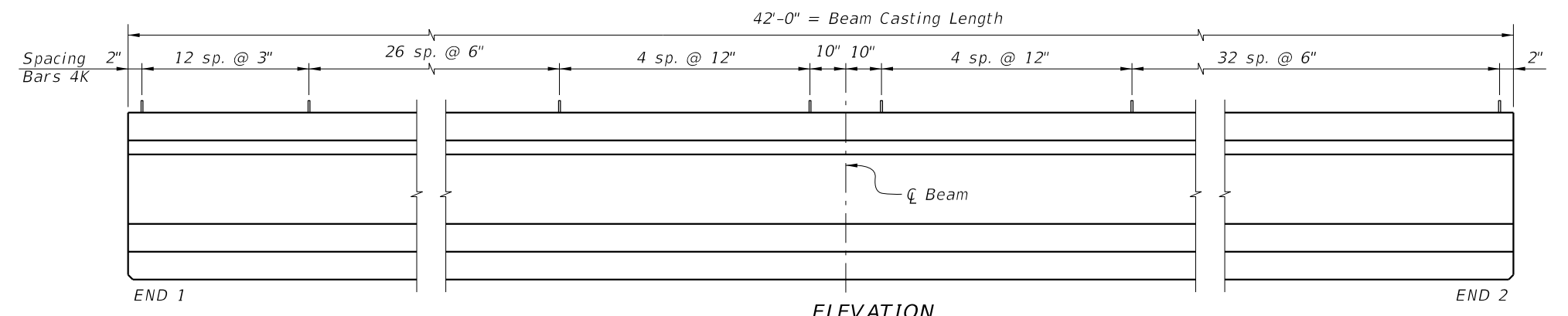
**ELEVATION AT END 2 OF BEAM
(Flanges Not Shown For Clarity)**



**SECTION A-A
(Showing Bars 4K, 4Y & 5Z Only)**



**SECTION B-B
(Showing Bars 4K, 4Y & 5Z Only)**



ELEVATION

GIRDERS A1, A2, A3, B2, B3, C1, C2, C3, D1 & D2

NOTES:
Work this Sheet with the AASHTO Type II Beam - Table of Beam Variables.
For referenced notes, see Sheet 1.

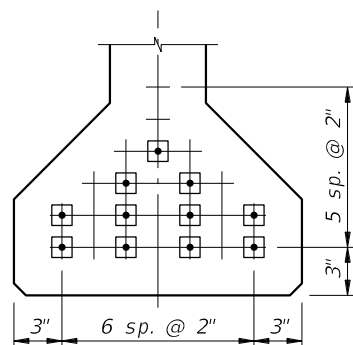
REVISIONS						B3	DRAWN BY: JKF 12/17 CHECKED BY: VAY 12/17 DESIGNED BY: CHECKED BY:	STATE OF FLORIDA DEPARTMENT OF TRANSPORTATION			SHEET TITLE: AASHTO TYPE II BEAM - DETAILS PROJECT NAME: Stainless Steel Strands for Pretensioned Concrete Girders	REF. DWG. NO.	
DATE	BY	DESCRIPTION	DATE	BY	DESCRIPTION			ROAD NO.	COUNTY	FINANCIAL PROJECT ID		SHEET NO.	
													2

AASHTO TYPE II BEAM - TABLE OF BEAM VARIABLES

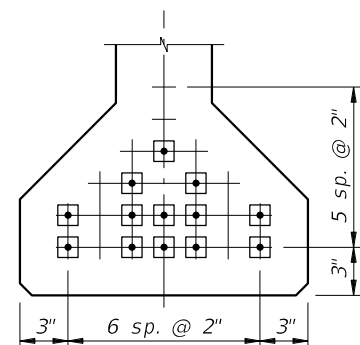
LOCATION		CONCRETE PROPERTIES		MATERIALS FOR BARS 4K, 4Y, 5Z 3D1, 3D2 & 5A	STND. PTRN. TYPE	END ELEV. COND.	PLAN VIEW CASE		BRG. PLATE MARK		END OF BEAM & BEARING DIMENSIONS					
SPAN NO.	BEAM NO.	CLASS	STRENGTHS (psi) 28 Day Release				END 1	END 2	END 1	END 2	END 1	END 2	ANGLE Ø	DIM P	DIM J	DIM K1
	A1	NWC	10000 6000	CARBON STEEL	3	1	1	1	-	-	90°	90°	-	-	-	-
	A2	NWC	10000 6000	GFRP	3	1	1	1	-	-	90°	90°	-	-	-	-
	A3	NWC	10000 6000	STAINLESS STEEL	3	1	1	1	-	-	90°	90°	-	-	-	-
	B2	NWC	10000 6000	GFRP	1	1	1	1	-	-	90°	90°	-	-	-	-
	B3	NWC	10000 6000	STAINLESS STEEL	1	1	1	1	-	-	90°	90°	-	-	-	-
	C1	NWC	10000 6000	CARBON STEEL	2	1	1	1	-	-	90°	90°	-	-	-	-
	C2	NWC	10000 6000	GFRP	2	1	1	1	-	-	90°	90°	-	-	-	-
	C3	NWC	10000 6000	STAINLESS STEEL	2	1	1	1	-	-	90°	90°	-	-	-	-
	D1	LWC	10000 6000	CARBON STEEL	3	1	1	1	-	-	90°	90°	-	-	-	-
	D2	LWC	10000 6000	CARBON STEEL	3	1	1	1	-	-	90°	90°	-	-	-	-

NOTES:

1. Work this Sheet with Sheets 1 and 2.
2. Use Carbon Steel Strands for Beams A1, A2, A3, D1 and D2.
Use Stainless Steel Strands for Beams B2, B3, C1, C2 and C3.
3. For Beams B2, B3, C1, C2 and C3, FDOT will supply an adequate length of Stainless Steel Strand to extend length of casting bed and additional length as needed for stressing.
4. Return unused Stainless Steel Strand to FDOT Structures Research Center.
5. FDOT will cut Stainless Steel Strand samples from the beginning, middle and end of spool as needed for testing purposes.
6. Use Normal Weight Concrete (NWC) for Beams A1, A2, A3, B2, B3, C1, C2 and C3.
7. Use Light Weight Concrete (LWC) for Beams D1 and D2.
8. Beams B2, B3, C1, C2 and C3 may be cast with one set of 13 strands in the casting bed. This will require sheathing of two strands for the entire beam length for Beams B2 and B3.



TYPE ① 11 STRANDS



TYPE ② 13 STRANDS

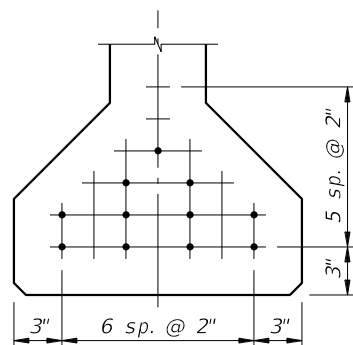
STRAND DESCRIPTION: Use 0.6" Diameter, Stainless Steel Strands. Area per strand equals 0.2328 sq. in.

STAINLESS STEEL STRAND PATTERNS

STRAND STRESSING LEGEND

- - Strands stressed at 43.9 kips each.
- ◻ - Strands stressed at 37.2 kips each.

NOTE: ALL STRANDS FULLY BONDED.

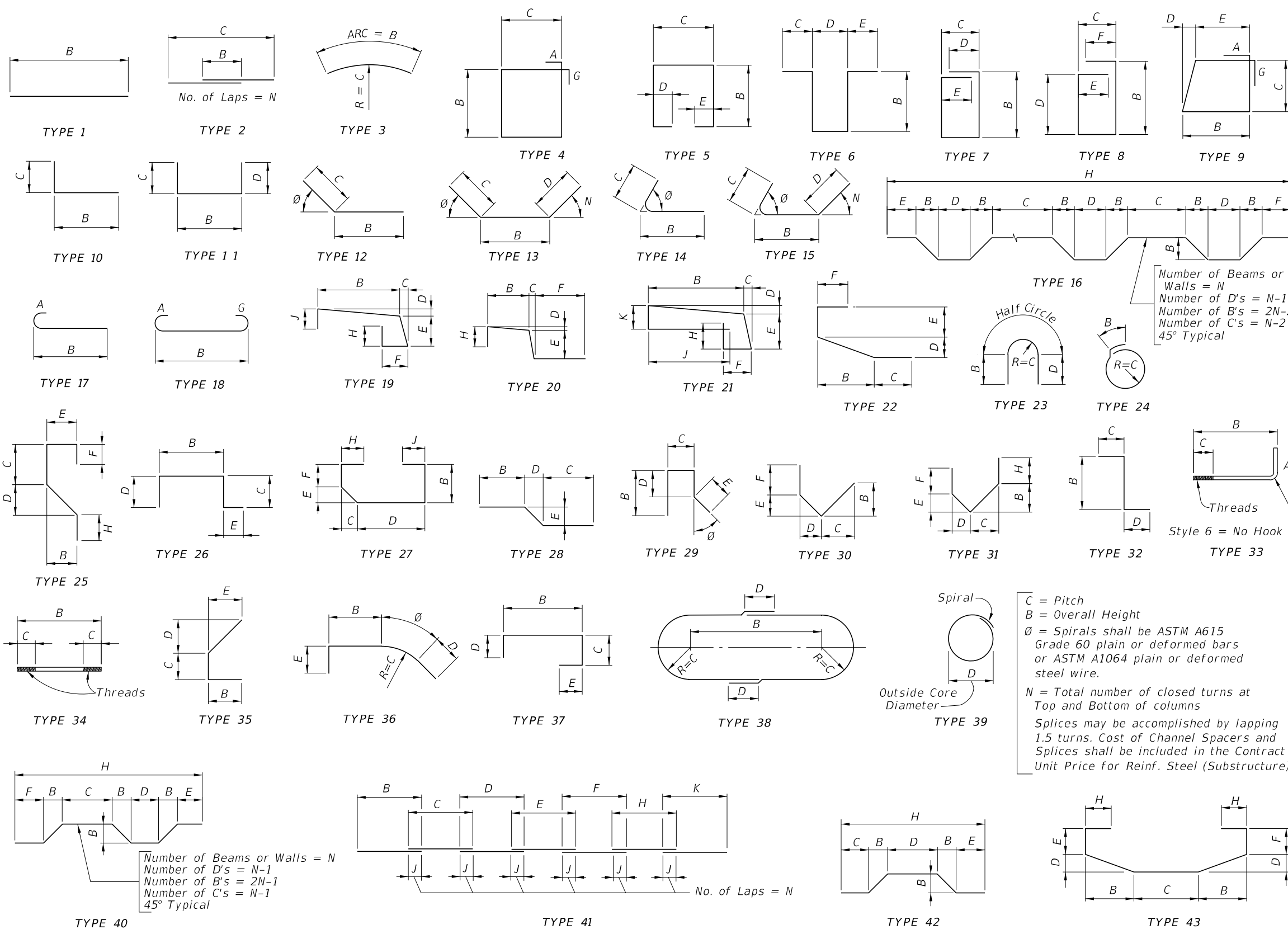


TYPE ③ 11 STRANDS

STRAND DESCRIPTION: Use 0.6" Diameter, Grade 270 Low-Relaxation Carbon Steel Strands. Area per strand equals 0.217 sq. in.

CARBON STEEL STRAND PATTERNS

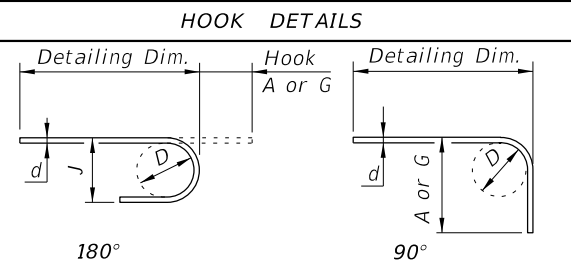
REVISIONS						B4	STATE OF FLORIDA DEPARTMENT OF TRANSPORTATION			SHEET TITLE:		REF. DWG. NO.
DATE	BY	DESCRIPTION	DATE	BY	DESCRIPTION		ROAD NO.	COUNTY	FINANCIAL PROJECT ID	AASHTO TYPE II BEAM - TABLE OF BEAM VARIABLES		
										PROJECT NAME: Stainless Steel Strands for Pretensioned Concrete Girders		SHEET NO.
												3



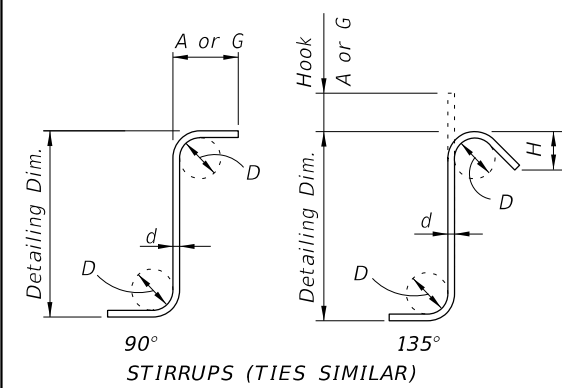
Number of Beams or Walls = N
 Number of D's = N-1
 Number of B's = 2N-1
 Number of C's = N-1
 45° Typical

Number of Beams or Walls = N
 Number of D's = N-1
 Number of B's = 2N-2
 Number of C's = N-2
 45° Typical

C = Pitch
 B = Overall Height
 Ø = Spirals shall be ASTM A615 Grade 60 plain or deformed bars or ASTM A1064 plain or deformed steel wire.
 N = Total number of closed turns at Top and Bottom of columns
 Splices may be accomplished by lapping 1.5 turns. Cost of Channel Spacers and Splices shall be included in the Contract Unit Price for Reinf. Steel (Substructure)



BAR SIZE	D	180° HOOKS		90° HOOKS
		A OR G	J	A OR G
#3	2 1/4"	5"	3"	6"
#4	3"	6"	4"	8"
#5	3 3/4"	7"	5"	10"
#6	4 1/2"	8"	6"	1'-0"
#7	5 1/4"	10"	7"	1'-2"
#8	6"	11"	8"	1'-4"
#9	9 1/2"	1'-3"	11 3/4"	1'-7"
#10	10 3/4"	1'-5"	1'-1 1/4"	1'-10"
#11	12"	1'-7"	1'-2 3/4"	2'-0"
#14	18 1/4"	2'-3"	1'-9 3/4"	2'-7"
#18	24"	3'-0"	2'-4 1/2"	3'-5"
STYLE		1		3



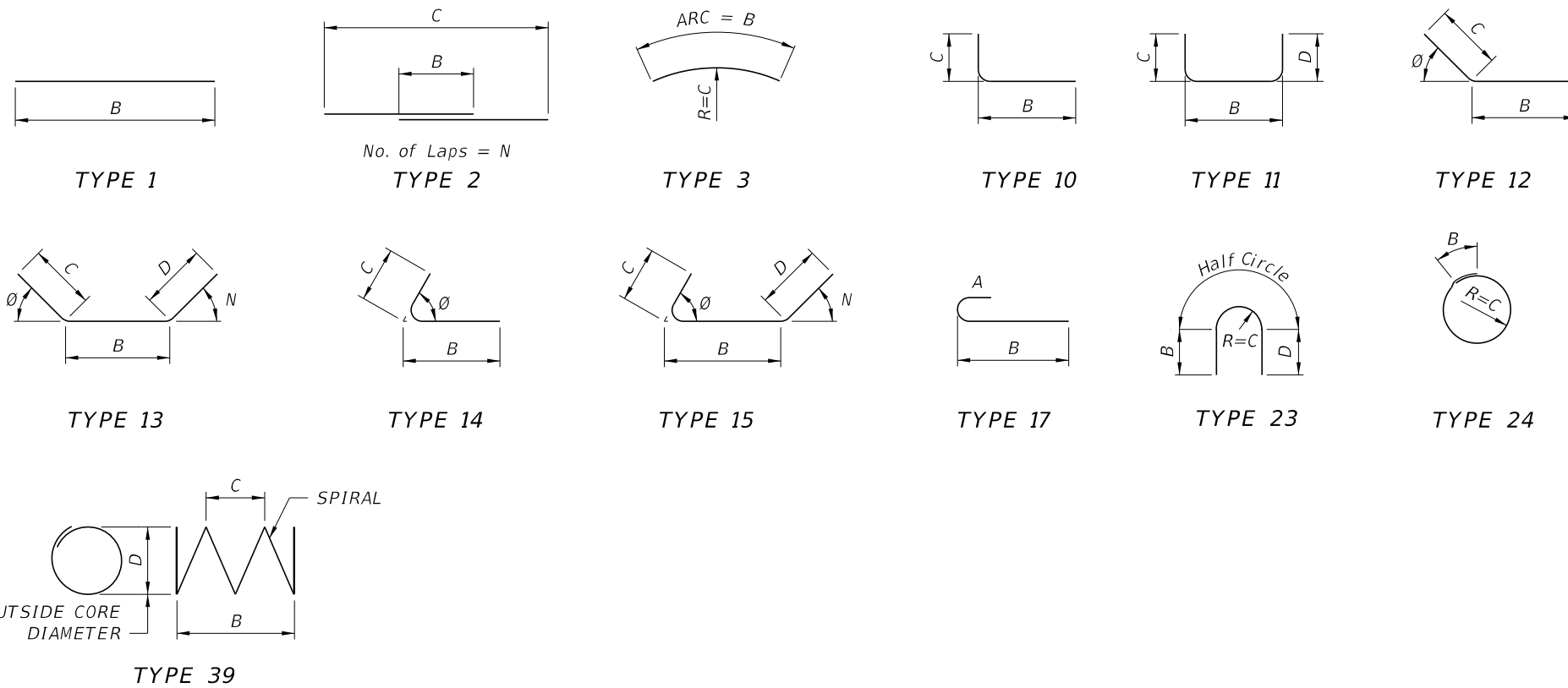
BAR SIZE	D	90° HOOKS		135° HOOKS	
		A or G	A or G	A or G	H *
#3	1 1/2"	4"	4"	4"	2 1/2"
#4	2"	4 1/2"	4 1/2"	4 1/2"	3"
#5	2 1/2"	6"	5 1/2"	5 1/2"	3 3/4"
#6	4 1/2"	1'-0"	8"	8"	4 1/2"
#7	5 1/4"	1'-2"	9"	9"	5 1/4"
#8	6"	1'-4"	10 1/2"	10 1/2"	6"
STYLE		4		5	

STYLE 6 = NO HOOK
 * Dimension is approximate.
 Hook Styles Detailed on this sheet are for Illustration Only.
 Actual Hook Style for any particular bar will be shown under A or G Heading on REINFORCING BAR LIST sheet(s) in Structures Plans.
 All Dimensions are out-to-out.

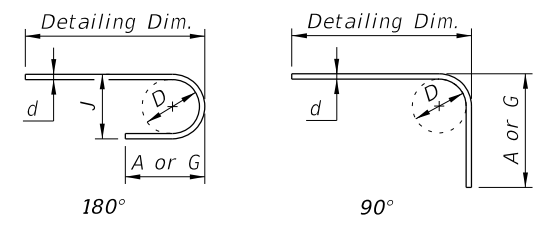
NOTE: For Bar Dimensions See REINFORCING BAR LIST Sheet(s) in Structures Plans.

10/26/2017 8:32:17 AM

FRP REBAR HOOK DETAILS



SINGLE BAR BENDING DETAILS



BAR SIZE	D	180° HOOKS		90° HOOKS
		A or G	J	A or G
#2	3"	4½"	3½"	4¾"
#3	4½"	6¾"	5¼"	7⅛"
#4	4½"	8¼"	5½"	8¾"
#5	4½"	9¾"	5¾"	10⅝"
#6	4½"	11½"	6"	1'-0"
#7	6"	1'-1½"	7¾"	1'-2"
#8	6"	1'-3"	8"	1'-4"
STYLE		1		3

NOTES

GENERAL

All dimensions are out-to-out.
For Bar Dimensions See REINFORCING BAR LIST Sheet(s) in Structures Plans.

SPIRALS (TYPE 39 BARS)

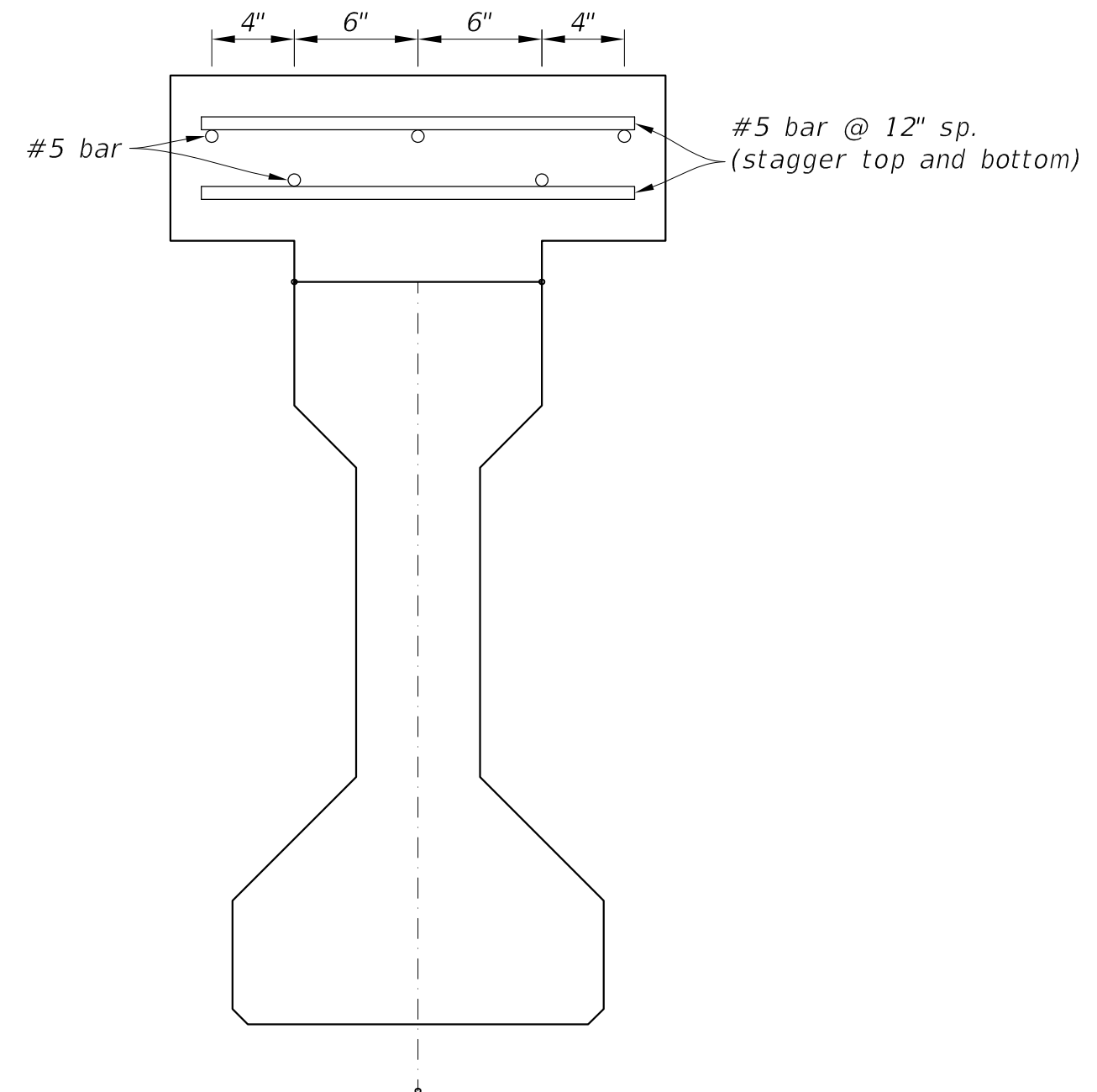
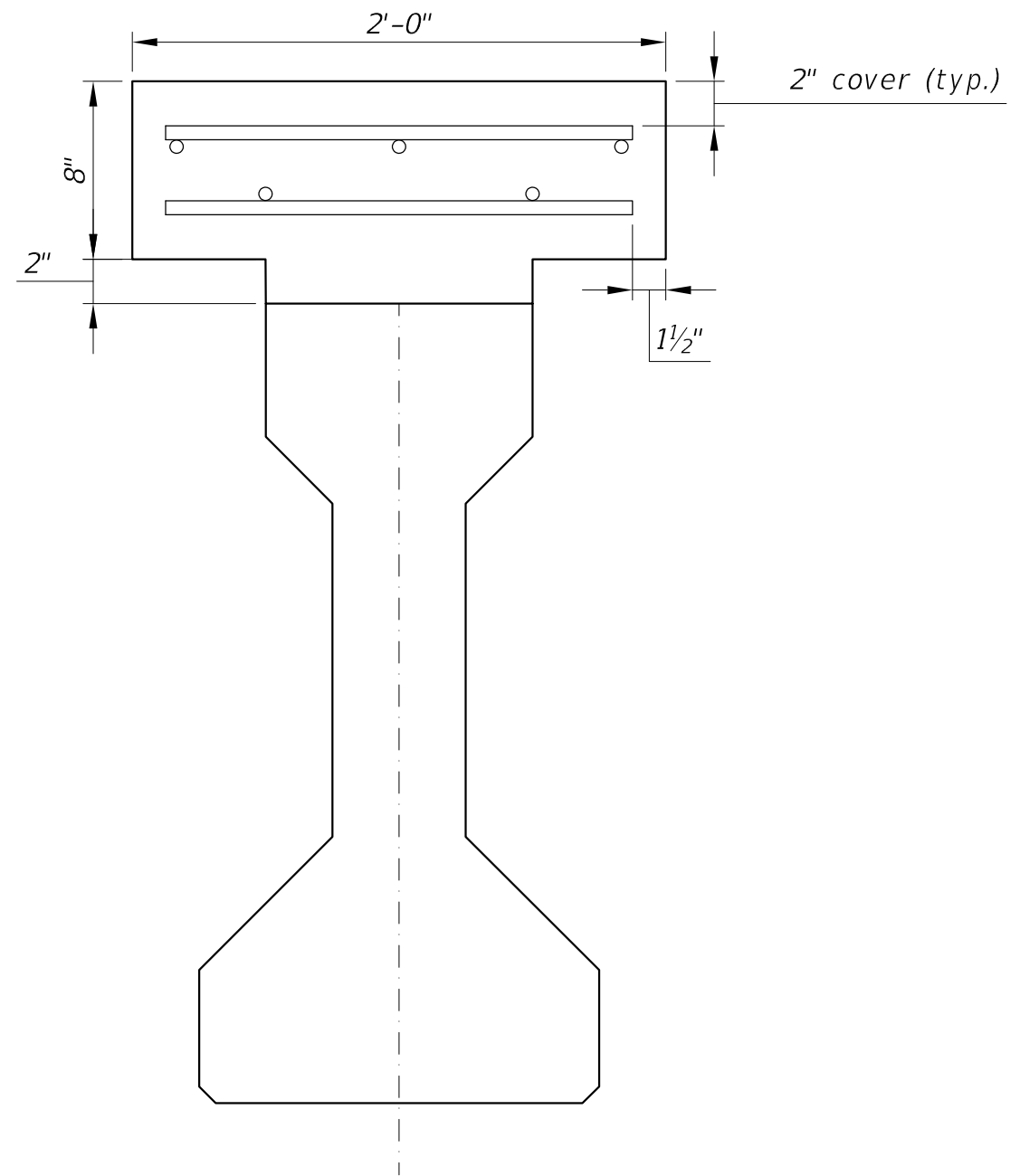
C = Pitch
B = Overall Height
N = Total number of closed turns at Top and Bottom of spiral
Splices = 1.5 turns
Include spiral splice in the Contract Unit Price for FRP Reinforcing.

HOOKS

All dimensions are approximate.
Hook Styles Detailed on this sheet are for Illustration Only.
Actual Hook Style for any particular bar will be shown under A or G Heading on REINFORCING BAR LIST sheet(s) in Structures Plans.

12/18/2017 1:29:58 PM

LAST REVISION 12/01/17	DESCRIPTION:	DEVELOPMENTAL DESIGN STANDARDS	B6	PULTRUDED FRP BAR BENDING DETAILS	INDEX NO. D21310	SHEET NO. 1 of 1
---------------------------	--------------	--------------------------------	----	-----------------------------------	---------------------	---------------------



- Notes:
- Splice longitudinal bars with a 12" lap splice.
 - Locate lap splice outside the spreader beam supports.
 - Concrete: Class IV (5,500 psi)

REVISIONS						B7	STATE OF FLORIDA DEPARTMENT OF TRANSPORTATION			Deck Details		REF. DWG. NO.
DATE	BY	DESCRIPTION	DATE	BY	DESCRIPTION		ROAD NO.	COUNTY	FINANCIAL PROJECT ID.	PROJECT NAME:		SHEET NO.
----	----	-----	----	----	-----		RD #	COUNTY	FPID #	SS Strand Project - FAMU/FSU		1
----	----	-----	----	----	-----							

AASHTO TYPE II BEAM - TABLE OF BEAM VARIABLES

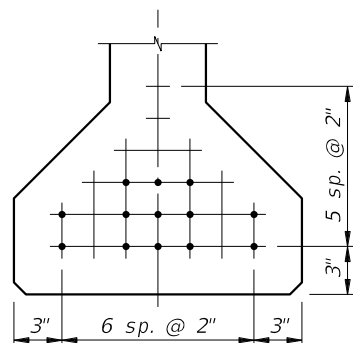
LOCATION	CONCRETE PROPERTIES				MATERIALS FOR BARS 5K, 4Y, 5Z 3D1, 3D2 & 5A	STND. PTRN. TYPE	END ELEV. COND.	PLAN VIEW CASE		BRG. PLATE MARK		END OF BEAM & BEARING DIMENSIONS								
	SPAN NO.	BEAM NO.	CLASS	STRENGTHS (psi)				END 1	END 2	END 1	END 2	END 1	END 2	ANGLE θ		DIM P	DIM J	DIM K1	DIM K2	
				28 Day										Release	END 1					END 2
	E1	NWC	8500	6800	CARBON STEEL	1	1	1	1	-	-	90°	90°	-	-	-	-			
	E2	NWC	8500	6800	CARBON STEEL	1	1	1	1	-	-	90°	90°	-	-	-	-			
	E3	NWC	8500	6800	CARBON STEEL	2	1	1	1	-	-	90°	90°	-	-	-	-			
	E4	NWC	8500	6800	CARBON STEEL	2	1	1	1	-	-	90°	90°	-	-	-	-			
	E5	NWC	8500	6800	CARBON STEEL	3	1	1	1	-	-	90°	90°	-	-	-	-			

BEAM NOTES:

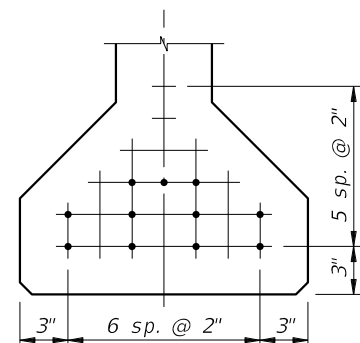
1. Work Bar Bending Diagrams provided on this sheet with Index 415-001.
2. All bar bend dimensions are out-to-out.
3. Concrete cover: 2 inches minimum.
4. Strands N: $\frac{3}{8}$ " \emptyset minimum, stressed to 10,000 lbs. each. Strands N shall be Carbon Steel Strands.
5. Place one (1) Bar 5K or 5Z at each location. Alternate the direction of the ends for each bar.
6. Tie Bars 5K and 5Z to the fully bonded strands in the bottom or center row (see "STRAND PATTERN").
7. Place Bars 3D1 in beam END 1, and Bars 3D2 in beam END 2.
8. Contractor Options:
 - A. Bars 3D1 and 3D2 may be fabricated as a two-piece bar with a 1'-0" minimum lap splice of the bottom legs.
9. Cut wedges and Prestressing Strands at the end of the beam without damaging the surrounding concrete. See "STRAND CUTTING DETAIL."
10. Provide material certifications to FDOT Structures Research Center.
11. Carbon Steel reinforcing bars shall be Grade 60 per Specification Section 931.
12. Researchers and FDOT personnel shall be allowed to instrument the beams and monitor them during detensioning. Time required for instrumenting is approximately one day per casting bed setup.

STRAND NOTES:

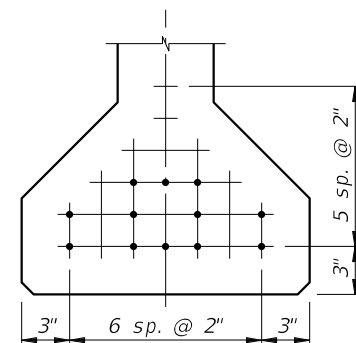
1. Use Stainless Steel Strands. FDOT will supply an adequate length of Stainless Steel Strand to extend length of casting bed and additional length as needed for stressing.
2. Return unused Stainless Steel Strand to FDOT Structures Research Center.
3. FDOT will cut Stainless Steel Strand samples from the beginning, middle and end of spool as needed for testing purposes.
4. Beams E1 and E2 may be cast with one set of 13 strands in the casting bed. This will require sheathing two strands for Beams E3 and E4 and sheathing one strand for Beam E5.



TYPE ① 13 STRANDS



TYPE ② 11 STRANDS



TYPE ③ 12 STRANDS

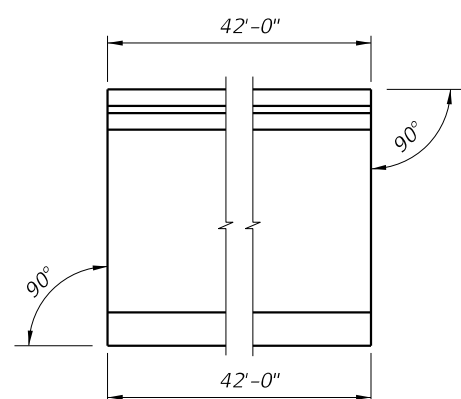
STRAND DESCRIPTION: Use 0.6" Diameter, Stainless Steel Strands. Area per strand equals 0.2328 sq. in.

STAINLESS STEEL STRAND PATTERNS

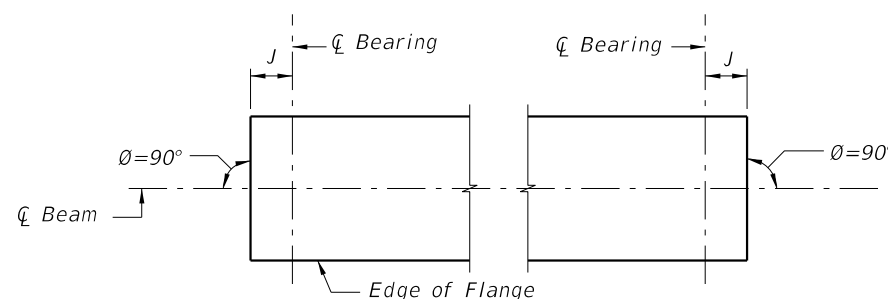
STRAND STRESSING LEGEND

- - Strands stressed at 38.9 kips each.

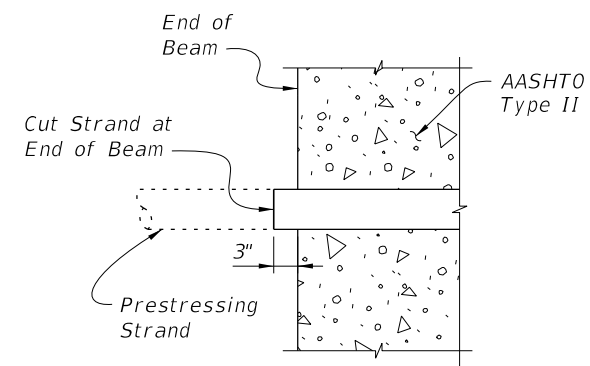
NOTE: ALL STRANDS FULLY BONDED.



**END ELEVATION
CONDITION 1
(Dim P = 0.0)**



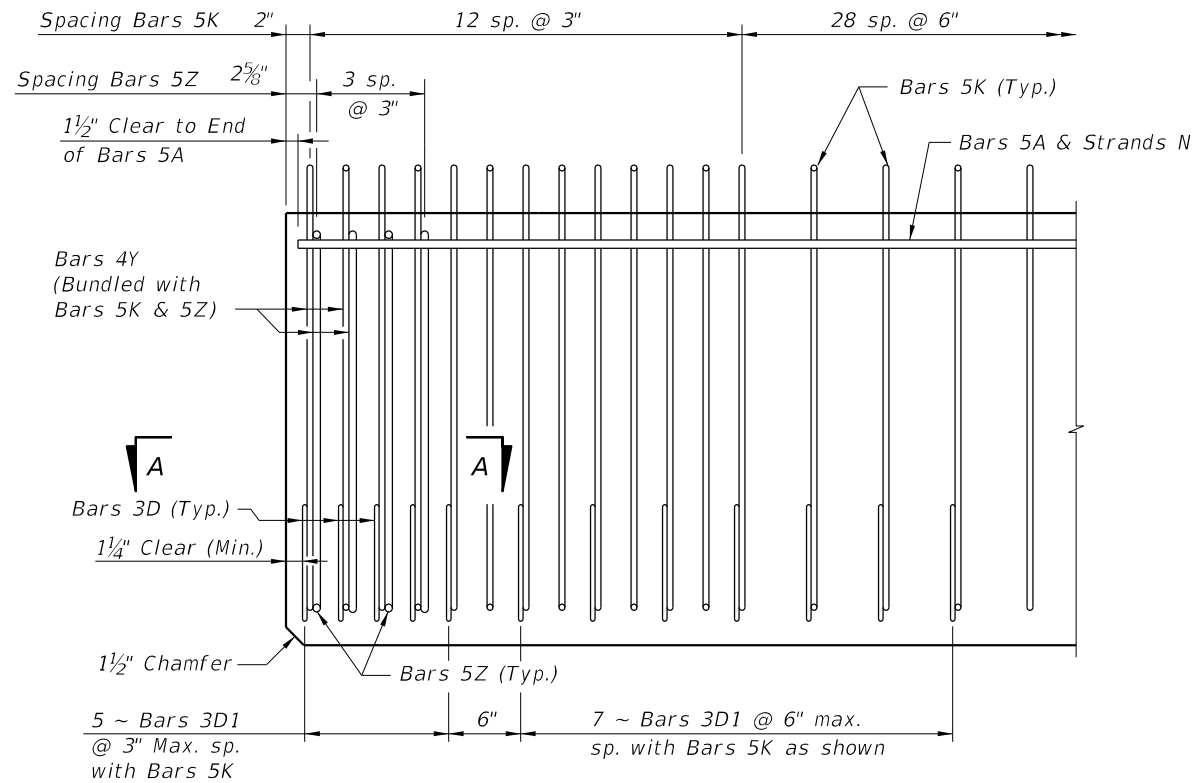
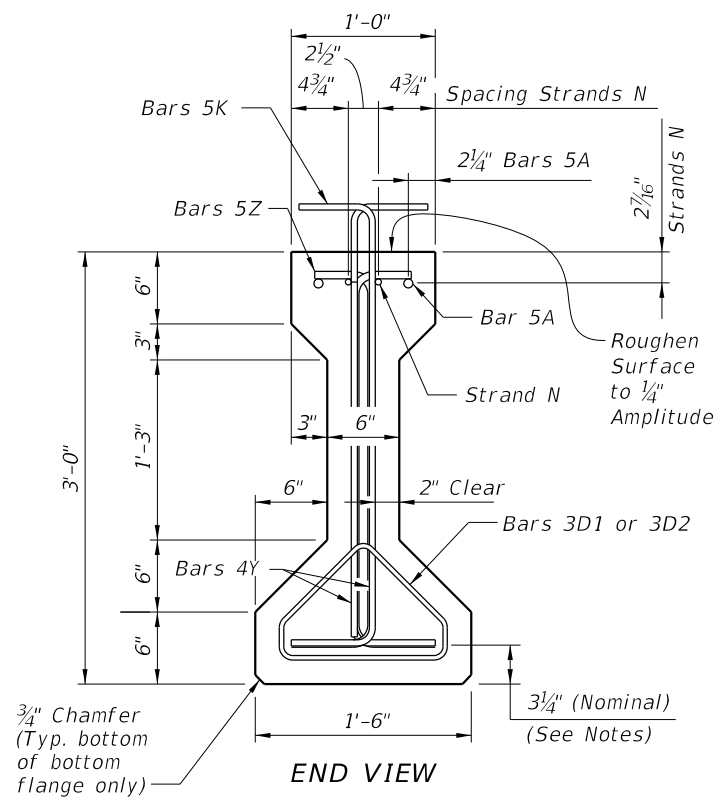
**PLAN VIEW
CASE 1**



**TYPICAL SECTION
SHOWING CUT STRAND**

STRAND CUTTING DETAIL

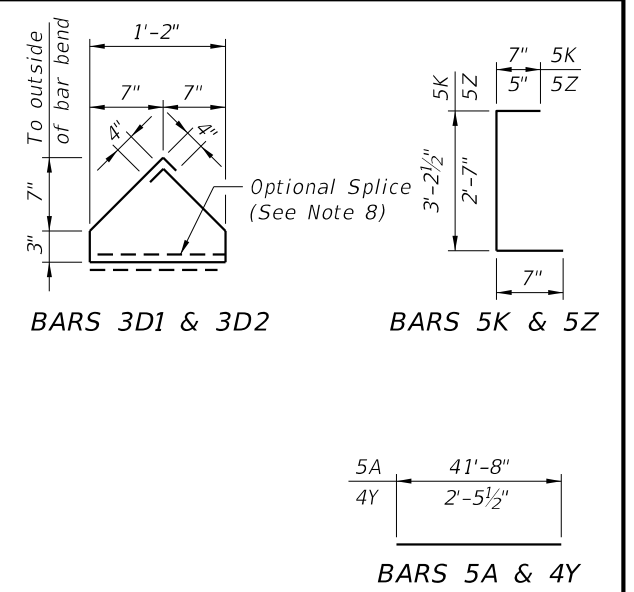
REVISIONS						B8	STATE OF FLORIDA DEPARTMENT OF TRANSPORTATION	SHEET TITLE: AASHTO TYPE II BEAM - NOTES, TABLE OF BEAM VARIABLES, & DETAILS	PROJECT NAME: Stainless Steel Strands for Pretensioned Concrete Girders - Part II	REF. DWG. NO.	
DATE	BY	DESCRIPTION	DATE	BY	DESCRIPTION						



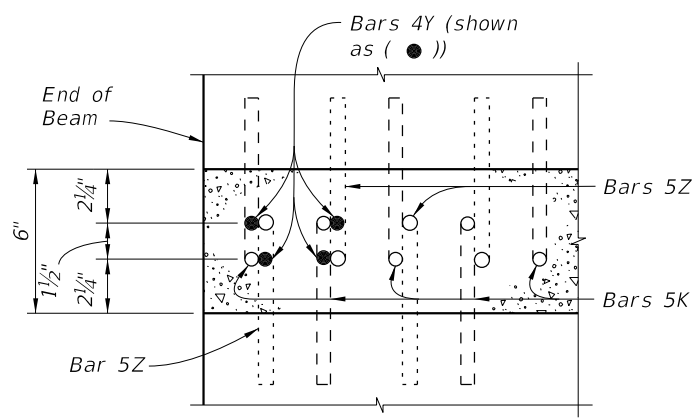
ELEVATION AT END OF BEAM
(Flanges Not Shown For Clarity)

BILL OF REINFORCING STEEL FOR ONE BEAM ONLY				
MARK	NOTE NUMBERS	SIZE	NUMBER REQUIRED	LENGTH
A	—	5	2	41'-9"
D1	8	3	12	3'-11 3/4"
D2	8	3	10	3'-11 3/4"
K	5 & 6	5	94	4'-4 1/2"
N	4 & 9	3/8" Ø Strand	2	42'-5"
Y	—	4	8	2'-5 1/2"
Z	5 & 6	5	8	3'-7"

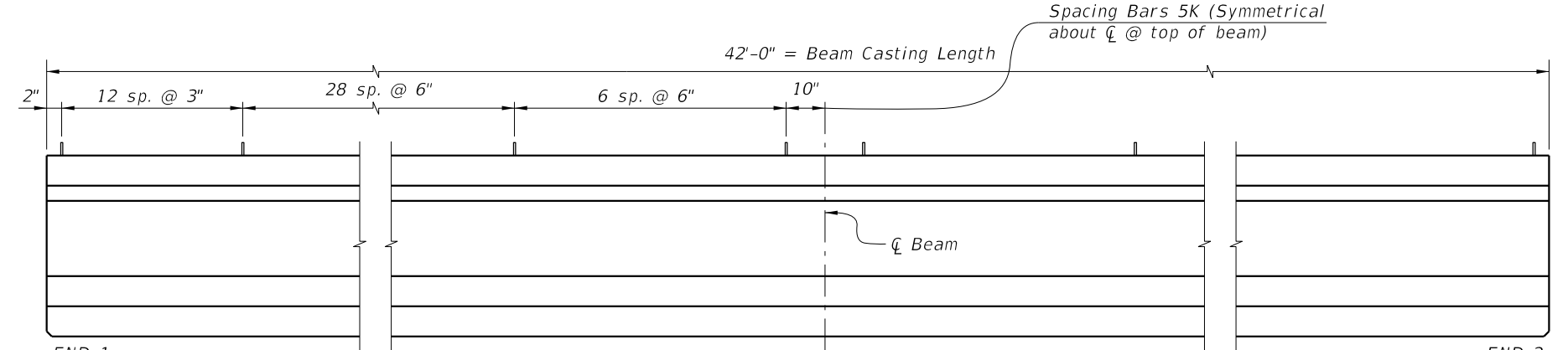
BENDING DIAGRAMS (See Notes 1 & 2)



NOTES:
Work this Sheet with the AASHTO Type II Beam - Table of Beam Variables.
For referenced notes, see Sheet 1.



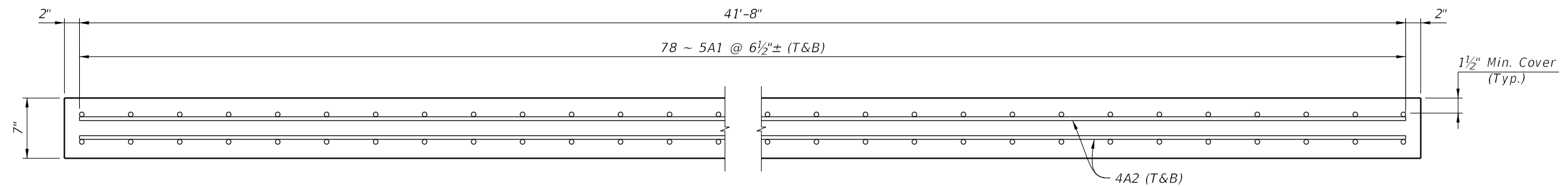
SECTION A-A
(Showing Bars 5K, 4Y & 5Z Only)



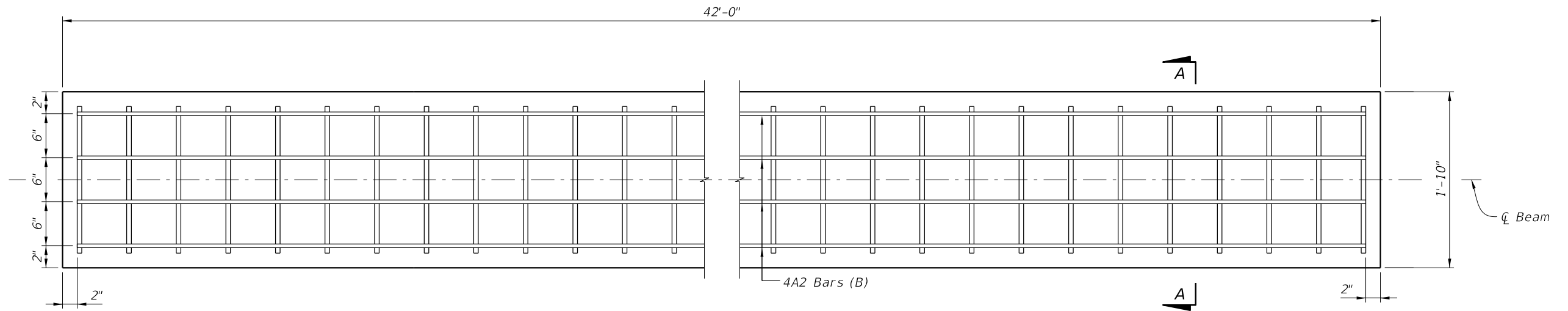
ELEVATION

GIRDERS E1, E2, E3, E4 & E5

REVISIONS						B9	DRAWN BY: JKF CHECKED BY: VAY DESIGNED BY: CHECKED BY:	STATE OF FLORIDA DEPARTMENT OF TRANSPORTATION			SHEET TITLE: AASHTO TYPE II BEAM - DETAILS Stainless Steel Strands for Pretensioned Concrete Girders - Part II	REF. DWG. NO.			
DATE	BY	DESCRIPTION	DATE	BY	DESCRIPTION			ROAD NO.	COUNTY	FINANCIAL PROJECT ID					
														PROJECT NAME:	
															SHEET NO. 2

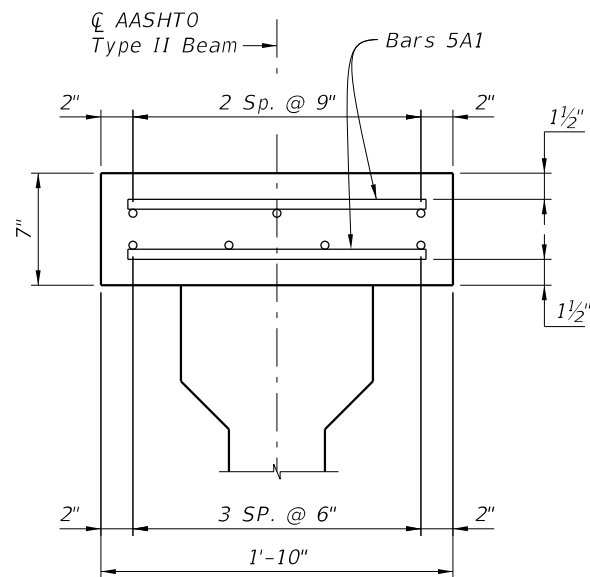


ELEVATION



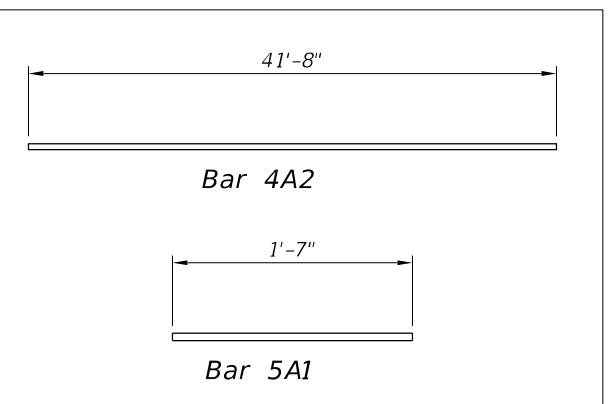
PLAN

(Bottom Mat of Reinforcement Shown,
Top Mat of Reinforcement Not Shown for Clarity)



SECTION A-A
(Bars 5K Not Shown)

Bill of Reinforcing Steel Per Deck			
Mark	Size	No. Reqd.	Length
A1	5	156	1'-7"
A2	4	7	41'-8"



REINFORCING BAR LIST

REVISIONS						B10	DRAWN BY: JKF	STATE OF FLORIDA DEPARTMENT OF TRANSPORTATION	SHEET TITLE: AASHTO TYPE II BEAM - C.I.P. DECK SLAB DETAILS AND NOTES	REF. DWG. NO.
DATE	BY	DESCRIPTION	DATE	BY	DESCRIPTION					

Appendix C – Construction of girders

This appendix contains information about fabrication of the girders. All girders were fabricated at Dura-Stress, Inc., casting yard in Leesburg, FL. Girders were fabricated at different casting beds and at different times. The girders were divided into three sets. The first set included Girders A1-A3 (references to Girders D1-D2 are lightweight concrete girders and are relevant to Part B of this report), the second set included Girders B2-B3 and C1-C3, and the third set included Girders E1-E5. Dura-Stress provided fabrication checklists for each set, which included the following:

1. Measured concrete fresh properties
2. Stress information
3. Rebar material/mechanical properties
4. Strand stress calculations
5. Pre-pour production sheet
6. Concrete mix designs
7. Concrete batch tickets
8. Casting bed diagram
9. Concrete compressive strength

Mill certificates for the strands are provided in Appendix A.

CHECK LIST

- TABLE SHEET
- STRESS
- REBAR/SPIRAL
- STRESS CALCS
- STRESS RESULTS
- PREPOUR
- BATCH TICKETS
- CASTING DIAGRAM

JOB # B1789
FDOT # TEST BEAM
PRODUCT TYPE TYPE II
MARK # 1-D1, 1-D2, 1-A3, 1-A2, 1-A1
SERIAL # LW1-LW5
BED # 31N
MIX DESIGN LIGHTWEIGHT (10,000 mix)
05-2056 (10,000 mix)

Check Off!

Cast Date: 9-12-18

Entered in Great Production: Janey

Entered in MAC (initials) N/A

Scanned: _____

Ready To File: _____

Sample #'s TEST01

REBAR REPORT

JOB # B1789

BED # 31N

MARK # 1-D1, 1-D2, 1-A3, 1-A2, 1-A1

TYPE OF PRODUCT GIRT 2

BAR SIZE 3 HEAT # BR1812076879

BAR SIZE 4 HEAT # BR1810121101

BAR SIZE 5 HEAT # ~~7579136~~

BAR SIZE _____ HEAT # ID 7578475, (5214503702)? HT

BAR SIZE _____ HEAT # _____

BAR SIZE _____ HEAT # _____

BAR SIZE _____ HEAT # _____

BAR SIZE _____ HEAT # _____

STRAIGHT BILL OF LADING - NOT NEGOTIABLE

Page: 1 of

Bill of Lading No
507382 Rev 0

PICKED: 07-06-2018 12:17 PM
PRINT: 6-Jul-2018 12:44 PM

Rebar

Nucor Steel Birmingham, Inc.
3900 NE 10TH Way
Pompano Beach, FL 33064
954-942-9400

BOLD TO: 000

SHIP TO: 010

DURA-STRESS INC
PO BOX 490779
LEESBURG, FL 34743
(352) 787-1422

DURA-STRESS INC
11325 COUNTY RD 44E
LEESBURG, FL 34788
(352) 787-1422

RECEIVED

JUL 09 2018

DURA-STRESS, INC.

Freight Mode: Truck

Subject to section 7 of the terms and conditions of this bill of lading, if this shipment is to be delivered to the consignee without receipt on the consignor, the consignor shall sign the following statement:

The carrier may decline to make delivery of this shipment with payment of freight and all other charges.

NUE

(Signature of Consignor)

Freight Charges are PREPAID unless marked collect.

CHECK BOX IF COLLECT:
To Be Prepaid

CUSTOMER NO.	CUSTOMER ORDER NUMBER	OUR ORDER NUMBER	SHIPPER NUMBER	TERMS
10099	See Below	See Below	P1-41856	Prepaid
SHIP VIA		VEHICLE NUMBER	ROUTING	
Fast Florida Freight		109 Julio		

NO. OF BUNDS.	NO. OF PIECES	DESCRIPTION	PRODUCT CODE	WEIGHT
9	3024	SPECIAL INSTRUCTIONS ALL BUNDLES MUST HAVE TAGS ALL MATERIAL MUST BE CLEAN/NO PITTING/NO RUST DOT INSPECTION AS TRUCK ARRIVES ALL DELIVERIES B/4 2:00 FRIDAYS B/4 10 AM ****SPECIAL TIE WIRE TAGGING**** FAST FLORIDA DELIVERY NEEDED 7/10 AM - PRELOAD 7/9		
		10/#3 Rebar 40' A615M GR420 (Gr60) OUR ORDER NUMBER - 360655/1 CUSTOMER PO# - 13289 SOUTHSIDE Tag# 1 : BR1812076878 Tag# 2 : BR1812076879 Tag# 3 : BR1812076880 Tag# 4 : BR1812076887 Tag# 5 : BR1812076888 Tag# 6 : BR1812076889 Tag# 7 : BR1812076857 Tag# 8 : BR1812076868 Tag# 9 : BR1812076871	900000104804200 Pieces: 336 Pieces: 336 Pieces: 336 Pieces: 336 Pieces: 336 Pieces: 336 Pieces: 336 Pieces: 336 Pieces: 336 Pieces: 336	45,477 5,053 5,053 5,053 5,053 5,053 5,053 5,053 5,053 5,053
		Total Tags: 9	Total Pieces: 3024	45,477

2 TAGS MISSING

Frank Wilkes

ENTERED SEP 07 2018

Name of Carrier: **Fast Florida Freight** Carrier's No. **109 Julio**
 RECEIVED, subject to the terms and conditions of this Bill of Lading, AT

If the shipment moves between two ports by a carrier by water, the law requires that the bill of lading shall state whether it is "carrier's weight" or "shipper's weight".

The property described above in apparent good order, except as noted (contents and condition of contents of packages unknown), marked, consigned, and destined as indicated above, which said carrier (the word carrier being understood throughout this contract as meaning any person or corporation in possession of the property under the contract) agrees to carry to its usual place of delivery at said destination, if on its route, otherwise to deliver to another carrier on the route to said destination. It is mutually agreed that every service to be performed hereunder shall be subject to all the terms and conditions of this bill of lading. THIS BILL OF LADING IS NOT SUBJECT TO ANY CLASSIFICATION OR TARIFFS, WHETHER INDIVIDUALLY DETERMINED OR FILED WITH ANY FEDERAL OR STATE REGULATORY AGENCY, EXCEPT AS SPECIFICALLY AGREED TO IN WRITING BY THE SHIPPER AND CARRIER.

The agreed-on declared value of the property is hereby specifically stated by the shipper to be not exceeding

_____ per _____

Carrier Certification:
 Carrier acknowledges receipt of the property described above in good order and condition. Per *[Signature]*

Shipper hereby certifies that he is familiar with all the terms and conditions of this bill of lading, including those on the back hereof, and the said terms and conditions are hereby agreed to by the shipper and accepted for itself and its assigns

SOLD DURA-STRESS INC
 PO BOX 490779
TO: LEESBURG, FL 34749-

NUCOR
 NUCOR STEEL BIRMINGHAM, INC.

CERTIFIED MILL TEST REPORT

SHIP DURA-STRESS INC
 11325 COUNTY RD 44E
TO: LEESBURG, FL 34788-

Ship from:
 MTR #: 0000182011
 Nucor Steel Birmingham, Inc.
 3900 NE 10TH Way
 Pompano Beach, FL 33064
 954-942-9400

Date: 6-Jul-2018
 B.L. Number: 507382
 Load Number: 41856

Material Safety Data Sheets are available at www.nucorbar.com or by contacting your inside sales representative.

NBMG-08 January 1, 2012

LOT # HEAT #	DESCRIPTION	PHYSICAL TESTS					CHEMICAL TESTS									
		YIELD P.S.I.	TENSILE P.S.I.	ELONG % IN 8"	BEND	WT% DEF	C Ni	Mn Cr	P Mo	S V	Si Cb	Cu Sn	C.E.			
	ALL BUNDLES MUST HAVE TAGS ALL MATERIAL MUST BE CLEAN/NO PITTING/NO RUST DOT INSPECTION AS TRUCK ARRIVES ALL DELIVERIES B/4 2:00 FRIDAYS B/4 10 AM PO# => 13289 SOUTHSIDE BR1810307901 Nucor Steel - Birmingham Inc 69,700 107,500 11.0% OK -2.7% .34 1.22 .012 .037 .24 .30 BR18103079 10/#3 Rebar 481MPa 741MPa .026 .14 .22 .032 .005 .001 40' A615M GR420 (Gr60) ASTM A615/A615M-16 GR 60 AASHT O M31-15 PO# => 13289 SOUTHSIDE BR1810308001 Nucor Steel - Birmingham Inc 75,500 110,900 13.0% OK -2.9% .34 1.32 .017 .049 .21 .29 BR18103080 10/#3 Rebar 521MPa 765MPa .026 .12 .24 .033 .006 .001 40' A615M GR420 (Gr60) ASTM A615/A615M-16 GR 60 AASHT O M31-15															

I hereby certify that the material described herein has been manufactured in accordance with the specifications and standards listed above and that it satisfies those requirements.
 1.) Weld repair was not performed on this material.
 2.) Melted and Manufactured in the United States.
 3.) Mercury, Radium, or Alpha source materials in any form have not been used in the production of this material.

C6

QUALITY

George Miller

George F. Miller

STRAIGHT BILL OF LADING - NOT NEGOTIABLE

NUCOR
 NUCOR STEEL BIRMINGHAM, INC.

Nucor Steel Birmingham, Inc.
 2060 Avenue A
 KISSIMMEE, FL 34758
 321-219-0191

Page: 1 of 1

Bill of Lading No.:
 502262 Rev 0

PICKED: 04-12-2018 11:21 AM
 PRINT: 12-Apr-2018 11:36 AM



SENT

APR 13 2018

Kelly Kelly

SOLD TO 000

DURA-STRESS INC
 PO BOX 490779
 LEESBURG, FL 34749
 (352) 787-1422

SHIP TO: 010

DURA-STRESS INC
 11325 COUNTY RD 411
 LEESBURG, FL 34788
 (352) 787-1422

Subject to section 7 of the terms and conditions of this bill of lading if this shipment is to be delivered to the consignee without recourse on the consignor, the consignor shall sign the following statement:

The carrier may decline to make delivery of this shipment without payment of freight and all other lawful charges.

Freight Mode: Truck

NUE

(Signature of Consignor)

Freight Charges are PREPAID unless marked collect.

CHECK BOX IF COLLECT:
 To Be Prepaid

CUSTOMER NO.	CUSTOMER ORDER NUMBER	OUR ORDER NUMBER	SHIPPER NUMBER	TERMS
10099	See Below	See Below	01-114348	Prepaid
SHIP VIA		VEHICLE NUMBER	ROUTING	
FREEDOM TRUCKING		1 DENNIS		

NO. OF BUNDS.	NO. OF PIECES	DESCRIPTION	PRODUCT CODE	WEIGHT
		SPECIAL INSTRUCTIONS ALL BUNDLES MUST HAVE TAGS ALL MATERIAL MUST BE CLEAN/NO PITTING/NO RUST DOT INSPECTION AS TRUCK ARRIVES ALL DELIVERIES B/4 2:00 FRIDAYS B/4 10 AM		
9	1701	13/#4 Rebar 40' A615M GR420 (Gr60) OUR ORDER NUMBER - 358732/2 CUSTOMER PO# - 11811 SOUTHSIDE Tag# 1 : BR1812030844 Heat #: BR18101207 Lot #: BR1810120701 Tag# 2 : BR1812030796 Heat #: BR18101209 Lot #: BR1810120901 Tag# 3 : BR1812030772 Heat #: BR18101210 Lot #: BR1810121001 Tag# 4 : BR1812030778 Heat #: BR18101210 Lot #: BR1810121001 Tag# 5 : BR1812030781 Heat #: BR18101210 Lot #: BR1810121001 Tag# 6 : BR1812030782 Heat #: BR18101210 Lot #: BR1810121001 Tag# 7 : BR1812030759 Heat #: BR18101211 Lot #: BR1810121101 Tag# 8 : BR1812030764 Heat #: BR18101211 Lot #: BR1810121101 Tag# 9 : BR1812031001 Heat #: BR18101288 Lot #: BR1810128801	900000134804200 Pieces: 189 Pieces: 189 Pieces: 189 Pieces: 189 Pieces: 189 Pieces: 189 Pieces: 189 Pieces: 189 Pieces: 189	45,450 5,050 5,050 5,050 5,050 5,050 5,050 5,050 5,050
		SCANNED	Total Tags: 9	Total Pieces: 1701
		<i>Brandon</i>	ENTERED SEP 06 2018	

Name of Carrier **FREEDOM TRUCKING** Carrier's No. **1 DENNIS**

RECEIVED, subject to the terms and conditions of this Bill of Lading.

If the shipment moves between two ports by a carrier by water, the law requires that the bill of lading shall state whether it is "carrier's weight" or "shipper's weight".

The property described above in apparent good order, except as noted (contents and condition of contents of packages unknown), marked, consigned, and destined as indicated above, which said carrier (the word carrier being understood throughout this contract as meaning any person or corporation in possession of the property under the contract) agrees to carry to its usual place of delivery at said destination, if on its route, otherwise to deliver to another carrier on the route to said destination. It is mutually agreed that every service to be performed hereunder shall be subject to all the terms and conditions of this bill of lading. THIS BILL OF LADING IS NOT SUBJECT TO ANY CLASSIFICATION OR TARIFFS, WHETHER INDIVIDUALLY DETERMINED OR FILED WITH ANY FEDERAL OR STATE REGULATORY AGENCY, EXCEPT AS SPECIFICALLY AGREED TO IN WRITING BY THE SHIPPER AND CARRIER.

The agreed-on declared value of the property is hereby specifically stated by the shipper to be not exceeding _____ per _____

Carrier Certification:

Carrier acknowledges receipt of the property described above in good order and condition.

Per *Brandon*

Shipper hereby certifies that he is familiar with all the terms and conditions of this bill of lading, including those on the back hereof, and the said terms and conditions are hereby agreed to by the shipper and accepted for itself and its assigns.

SOLD DURA-STRESS INC
 PO BOX 490779
TO: LEESBURG, FL 34749-



CERTIFIED MILL TEST REPORT

SHIP DURA-STRESS INC
 11325 COUNTY RD 44E
TO: LEESBURG, FL 34788-

Ship from:
 MTR #: 0000168857
 Nucor Steel Birmingham, Inc.
 2060 Avenue A
 KISSIMMEE, FL 34758
 321-219-0191

Date: 12-Apr-2018
 B.L. Number: 502262
 Load Number: 114348

Material Safety Data Sheets are available at www.nucorbar.com or by contacting your inside sales representative.

NBMG-08 January 1, 2012

LOT # HEAT #	DESCRIPTION	PHYSICAL TESTS					CHEMICAL TESTS											
		YIELD P.S.I.	TENSILE P.S.I.	ELONG % IN 8"	BEND	WT% DEF	C	Ni	Mn	Cr	P	Mo	S	V	Si	Cb	Cu	Sn
	ALL BUNDLES MUST HAVE TAGS ALL MATERIAL MUST BE CLEAN/NO PITTING/NO RUST DOT INSPECTION AS TRUCK ARRIVES ALL DELIVERIES B/4 2:00 FRIDAYS B/4 10 AM PO# => 11811 SOUTHSIDE BR1810120701 Nucor Steel - Birmingham Inc 66,400 102,200 12.0% OK -4.3% .39 .91 .011 .035 .20 .45 BR18101207 13/#4 Rebar 458MPa 705MPa .033 .12 .18 .036 .005 .017 40' A615M GR420 (Gr60) ASTM A615/A615M-16 GR 60 AASHT O M31-15 PO# => 11811 SOUTHSIDE BR1810120901 Nucor Steel - Birmingham Inc 67,400 98,200 11.0% OK -4.0% .41 .81 .014 .050 .20 .36 BR18101209 13/#4 Rebar 465MPa 677MPa .034 .14 .14 .032 .004 .016 40' A615M GR420 (Gr60) ASTM A615/A615M-16 GR 60 AASHT O M31-15 PO# => 11811 SOUTHSIDE BR1810121001 Nucor Steel - Birmingham Inc 61,500 92,800 11.0% OK -4.2% .38 .83 .016 .050 .18 .33 BR18101210 13/#4 Rebar 424MPa 640MPa .036 .12 .18 .039 .004 .016 40' A615M GR420 (Gr60) ASTM A615/A615M-16 GR 60 AASHT O M31-15 PO# => 11811 SOUTHSIDE BR1810121101 Nucor Steel - Birmingham Inc 65,900 97,300 10.0% OK -3.6% .40 .84 .013 .046 .22 .32 BR18101211 13/#4 Rebar 454MPa 671MPa .034 .11 .14 .037 .004 .016 40' A615M GR420 (Gr60) ASTM A615/A615M-16 GR 60 AASHT O M31-15																	

I hereby certify that the material described herein has been manufactured in accordance with the specifications and standards listed above and that it satisfies those requirements.
 1.) Weld repair was not performed on this material.
 2.) Melted and Manufactured in the United States.
 3.) Mercury, Radium, or Alpha source materials in any form have not been used in the production of this material.

C8

QUALITY ASSURANCE:

George Miljus

SOLD DURA-STRESS INC
 PO BOX 490779
TO: LEESBURG, FL 34749-



CERTIFIED MILL TEST REPORT

SHIP DURA-STRESS INC
 11325 COUNTY RD 44E
TO: LEESBURG, FL 34788-

Ship from:
 MTR #: 0000168857
 Nucor Steel Birmingham, Inc.
 2060 Avenue A
 KISSIMMEE, FL 34758
 321-219-0191

Date: 12-Apr-2018
 B.L. Number: 502262
 Load Number: 114348

Material Safety Data Sheets are available at www.nucorbar.com or by contacting your inside sales representative.

NBMG-08 January 1, 2012

LOT #	HEAT #	DESCRIPTION	PHYSICAL TESTS					CHEMICAL TESTS												
			YIELD P.S.I.	TENSILE P.S.I.	ELONG % IN 8"	BEND	WT% DEF	C	Ni	Mn	Cr	P	Mo	S	V	Si	Cb	Cu	Sn	C.E.
PO# =>		11811 SOUTHSIDE																		
BR1810128801		Nucor Steel - Birmingham Inc	62,700	90,900	13.0%	OK	-3.7%	.38	.83	.009	.045	.22	.32							
BR18101288		13/#4 Rebar	432MPa	627MPa			.036	.10	.11	.042	.004	.014								
		40' A615M GR420 (Gr60)																		
		ASTM A615/A615M-16 GR 60 AASHT																		
		O M31-15																		

I hereby certify that the material described herein has been manufactured in accordance with the specifications and standards listed above and that it satisfies those requirements.
 1.) Weld repair was not performed on this material.
 2.) Meltec and Manufactured in the United States.
 3.) Mercury, Radium, or Alpha source materials in any form have not been used in the production of this material.

C9

QUALITY
 ASSURANCE:

RECEIVED

Straight Bill of Lading



GERDAU SEP 04 2018

Rebar Road JACKSONVILLE, FL 32234 US



Shippers No. 1324-0000130464

Shipment Doc. No. 9919554

The property described below, in apparent good order, except for the contents and weight of contents of package unknown, marked, consigned, and destined as indicated below, which said carrier (the word carrier being understood throughout this contract as meaning any person or corporation in possession of the property under the contract) agrees to carry to its usual place of delivery as said description, if on its route, otherwise to deliver to another carrier on the route to said destination. It is mutually agreed, as to each carrier of all or any portion of said property over all or any portion of said route to destination, and as to each party at any time interested in all or any of said property, that every service to be performed hereunder shall be subject to all the terms and conditions of the Uniform Domestic Straight Bill of Lading set forth (1) in Uniform Freight Classification, in effect on the date hereof, if this is a rail or rail-water shipment, or (2) in the applicable motor carrier classification or tariff if this is a motor carrier shipment. Shipper hereby certifies that he is familiar with all the terms and conditions of the said bill of lading, including those on the back thereof, set forth in the classification or tariff which governs the transportation of this shipment, and the said terms and conditions are hereby agreed to by the shipper and accepted for himself and his assigns.

CONSIGNEE TO DURA STRESS INC 11325 CR 44 EAST LEESBURG, FL, 34788	INVOICE TO SOUTHWESTERN SUPPLIERS INC GENERAL ACCOUNT 6815 E 14TH AVE TAMPA, FL, 33619-2917	SHIP DATE 04-SEP-18 CUST.ACCOUNT NO 100415512	APPROVAL CODE OPERACAO
--	---	--	---------------------------

CARRIER: 100367341 COME GET IT TRUCKING LLC	CAR / VEHICLE INITIALS: 1030
DESTINATION: SEE CONSIGNED TO	DELIVERY ADDRESS: SEE CONSIGNED TO
ROUTE: T-1324-FL-LEESBURG	DELIVERY CARRIER: 100367341 COME GET IT TRUCKING LLC
SPECIAL INSTRUCTIONS : CONTAC # 352-787-1422 DELIVERY TO BE MADE AT SOUTHSIDE OF YARD	

DESCRIPTION OF ARTICLES: 11 BUNDLES, IRON OR STEEL RODS OR BARS, DESCRIBED BELOW

Freight Charges are to be PREPAID, unless marked Collect. Check Box if Collect. []

SHAPE AND SIZE PART #	DRAW #	GRADE BUNDLE ID	MILL	LENGTH	CUST PO # HEAT / BATCH	SALES ORDER # WEIGHT (LB)	ITEM # WEIGHT (KG)	DELIVERY # PCS	ITEM #	CUSTOMER MATERIAL NUMBER
Rebar #6 (19MM)	60 (420)	11324250000017571969	1324	40'00"	023902	6897855	20	8113251273	10	
					56145039/02	4,326 LB	1,962 KG	72		
					56145039/02	4,326 LB	1,962 KG	72		
					56145039/02	4,326 LB	1,962 KG	72		
					56145039/02	4,326 LB	1,962 KG	72		
SUBTOTAL				4 BUNDLES	17,304 LB	7,848 KG	288			
Rebar #5 (16MM)	60 (420)	11324250000017549108	1324	40'00"	023902	6897855	10	8113276415	10	
					56144609/02	4,005 LB	1,817 KG	96		
					56144609/02	4,005 LB	1,817 KG	96		

	AGENT
	DATE

Gerdau Corporation Shipper, per
 Permanent post office address of shipper Rebar Road JACKSONVILLE FL 32234 US

Time of Day 09/04/2018 07:30:31



WARNING: This product can expose you to chemicals, including nickel, which are known to the State of California to cause cancer, and lead, which is known to the State of California to cause cancer and birth defects or other reproductive harm. For more information go to www.P65Warnings.ca.gov



Straight Bill of Lading

Shippers No. 1324-0000130464

Shipment Doc. No. 9919554

Rebar Road JACKSONVILLE, FL 32234 US

RECEIVED, subject to the classification and tariffs in effect on the date of the issue of this Bill of Lading.

The property described below, in apparent good order, except as noted (contents and condition of contents of package unknown), marked, consigned, and destined as indicated below, which said carrier (the word carrier being understood throughout this contract as meaning any person or corporation in possession of the property under the contract) agrees to carry to its usual place of delivery as said description, if on its route, otherwise to deliver to another carrier on the route to said destination. It is mutually agreed, as to each carrier of all or any of said property over all or any portion of said route to destination, and as to each party at any time interested in all or any of said property, that every service to be performed hereunder shall be subject to all the terms and conditions of the Uniform Domestic Straight Bill of Lading set forth (1) in Uniform Freight Classification, in effect on the date hereof, if this is a rail or rail-water shipment, or (2) in the applicable motor carrier classification or tariff if this is a motor carrier shipment. Shipper hereby certifies that he is familiar with all the terms and conditions of the said bill of lading, including those on the back thereof, set forth in the classification or tariff which governs the transportation or this shipment, and the said terms and conditions are hereby agreed to by the shipper and accepted for himself and his assigns.

CONSIGNEE TO DURA STRESS INC 11325 CR 44 EAST LEESBURG, FL, 34788	INVOICE TO SOUTHWESTERN SUPPLIERS INC GENERAL ACCOUNT 6815 E 14TH AVE TAMPA, FL, 33619-2917	SHIP DATE 04-SEP-18 CUST.ACCOUNT NO 100415512	APPROVAL CODE OPERACAO
---	--	--	----------------------------------

CARRIER: 100367341 COME GET IT TRUCKING LLC	CAR / VEHICLE INITIALS: 1030
DESTINATION: SEE CONSIGNEE TO	DELIVERY ADDRESS: SEE CONSIGNEE TO
ROUTE: T-1324-FL-LEESBURG	DELIVERY CARRIER: 100367341 COME GET IT TRUCKING LLC
SPECIAL INSTRUCTIONS : CONTAC # 352-787-1422 DELIVERY TO BE MADE AT SOUTHSIDE OF YARD	

DESCRIPTION OF ARTICLES: 11 BUNDLES, IRON OR STEEL RODS OR BARS, DESCRIBED BELOW

Freight Charges are to be PREPAID, unless marked Collect. Check Box if Collect. []

SHAPE AND SIZE PART #	DRAW #	GRADE BUNDLE ID	MILL	LENGTH	CUST PO # HEAT / BATCH	SALES ORDER # WEIGHT (LB)	ITEM # WEIGHT (KG)	DELIVERY # PCS	ITEM #	CUSTOMER MATERIAL NUMBER
		11324250000017578431	1324		56145184/03	4,005 LB	1,817 KG	96		
		11324250000017578434	1324		56145184/03	4,005 LB	1,817 KG	96		
		11324250000017578445	1324		56145184/03	4,005 LB	1,817 KG	96		
		11324250000017578451	1324		56145184/03	4,005 LB	1,817 KG	96		
		11324250000017578475	1324		56145037/02	4,005 LB	1,817 KG	96		
SUBTOTAL				7 BUNDLES		28,035 LB	12,719 KG	672		
TOTAL				11 BUNDLES		45,339 LB	20,567 KG			

Note -- Where the rate is dependent on value, shippers are required to state specifically in writing the agreed or declared value of the property. The agreed or declared value of the property is hereby specifically stated by the shipper to be not exceeding _____ per _____	Subject to Section 7 of the conditions, if this shipment is to be delivered to the consignee without recourse on the consignor, the consignor shall sign the following statement. The carrier shall not make delivery of this shipment without payment of freight and all other lawful charges.	Shippers Total Net Weight (LB) 45,339	AGENT
		Shippers Total Net Weight (KG) 20,567	DATE

Gerdau Corporation Shipper, per
 Permanent post office address of shipper Rebar Road JACKSONVILLE FL 32234 US

Time of Day 09/04/2018 07:30:31



WARNING: This product can expose you to chemicals, including nickel, which are known to the State of California to cause cancer, and lead, which is known to the State of California to cause cancer and birth defects or other reproductive harm. For more information go to www.P65Warnings.ca.gov



CERTIFIED MATERIAL TEST REPORT

DOCUMENT ID:
0000049505

US-ML-JACKSONVILLE
16770 Rebar Road
JACKSONVILLE, FL 32234
USA

CUSTOMER SHIP TO
DURA STRESS INC
11325 CR 44 EAST
LEESBURG, FL 34788
USA

CUSTOMER BILL TO
SOUTHWESTERN SUPPLIERS INC
6815 E 14TH AVE
TAMPA, FL 33619-2917
USA

GRADE
60 (420)

SHAPE / SIZE
Rebar / #6 (19MM)

LENGTH
40'00"

WEIGHT
17,304 LB

HEAT / BATCH
56145039/02

SALES ORDER
6897855/000020

CUSTOMER MATERIAL N#

SPECIFICATION / DATE or REVISION
ASTM A615/A615M-16

CUSTOMER PURCHASE ORDER NUMBER
023902

BILL OF LADING
1324-0000130464

DATE
09/04/2018

CHEMICAL COMPOSITION

C %	Mn %	P %	S %	Si %	Cu %	Ni %	Cr %	Mo %	Sn %	V %
0.46	0.85	0.019	0.061	0.20	0.34	0.12	0.19	0.027	0.013	0.004

MECHANICAL PROPERTIES

YS PSI	YS MPa	UTS PSI	UTS MPa	G/L Inch	G/L mm
65712	453	104212	719	8.000	200.0
66132	456	104922	723	8.000	200.0

MECHANICAL PROPERTIES

Elong. %	BendTest
10.40	OK
10.50	OK

GEOMETRIC CHARACTERISTICS

%Light %	Def Hgt Inch	Def Gap Inch	DefSpace Inch
3.71	0.049	0.136	0.440
3.71	0.048	0.136	0.440

COMMENTS / NOTES

The above figures are certified chemical and physical test records as contained in the permanent records of company. We certify that these data are correct and in compliance with specified requirements. This material, including the billets, was melted and manufactured in the USA. CMTR complies with EN 10204 3.1.

BHASKAR YALAMANCHILI
QUALITY DIRECTOR

ALEX RENOSTO
QUALITY ASSURANCE MGR.

Phone: (409) 267-1071 Email: Bhaskar.Yalamanchili@gerdau.com

C12

Phone: 904-266-1468 Email: Alexander.Renosto@gerdau.com



CERTIFIED MATERIAL TEST REPORT

DOCUMENT ID:
0000049507

US-ML-JACKSONVILLE
16770 Rebar Road
JACKSONVILLE, FL 32234
USA

CUSTOMER SHIP TO DURA STRESS INC 11325 CR 44 EAST LEESBURG, FL 34788 USA	CUSTOMER BILL TO SOUTHWESTERN SUPPLIERS INC 6815 E 14TH AVE TAMPA, FL 33619-2917 USA
--	--

GRADE 60 (420)	SHAPE / SIZE Rebar / #5 (16MM)
-------------------	-----------------------------------

LENGTH 40'00"	WEIGHT 8,010 LB	HEAT / BATCH 56144609/02
------------------	--------------------	-----------------------------

SALES ORDER 6897855/000010	CUSTOMER MATERIAL N#
-------------------------------	----------------------

SPECIFICATION / DATE or REVISION
ASTM A615/A615M-16

CUSTOMER PURCHASE ORDER NUMBER 023902	BILL OF LADING 1324-0000130464	DATE 09/04/2018
--	-----------------------------------	--------------------

CHEMICAL COMPOSITION											
C %	Mn %	P %	S %	Si %	Cu %	Ni %	Cr %	Mo %	Sn %	V %	
0.46	0.83	0.014	0.042	0.19	0.35	0.10	0.11	0.027	0.011	0.003	

MECHANICAL PROPERTIES						
YS PSI	YS MPa	UTS PSI	UTS MPa	G/L Inch	G/L mm	
75000	517	113100	780	8.000	200.0	
74000	510	111200	767	8.000	200.0	


MECHANICAL PROPERTIES	
Elong. %	BendTest
14.50	OK
11.50	OK

GEOMETRIC CHARACTERISTICS			
%Light %	Def Hgt Inch	Def Gap Inch	DefSpace Inch
2.20	0.040	0.124	0.387
3.05	0.039	0.125	0.387

COMMENTS / NOTES

The above figures are certified chemical and physical test records as contained in the permanent records of company. We certify that these data are correct and in compliance with specified requirements. This material, including the billets, was melted and manufactured in the USA. CMTR complies with EN 10204 3.1.

 **BHASKAR YALAMANCHILI**
QUALITY DIRECTOR

 **ALEX RENOSTO**
QUALITY ASSURANCE MGR.

Phone: (409) 267-1071 Email: Bhaskar.Yalamanchili@gerdau.com

C13

Phone: 904-266-1468 Email: Alexander.Renosto@gerdau.com



CERTIFIED MATERIAL TEST REPORT

US-ML-JACKSONVILLE
16770 Rebar Road
JACKSONVILLE, FL 32234
USA

CUSTOMER SHIP TO DURA STRESS INC 11325 CR 44 EAST LEESBURG, FL 34788 USA		CUSTOMER BILL 1 SOUTHWESTERN SUPPLIERS INC 6815 E 14TH AVE TAMPA, FL 33619-2917 USA		GRADE 60 (420)	SHAPE / SIZE Rebar / #5 (16MM)	DOCUMENT ID: 0000049507
SALES ORDER 6897855/000010		CUSTOMER MATERIAL N#		LENGTH 40'00"	WEIGHT 4,005 LB	HEAT / BATCH 56145037/02
CUSTOMER PURCHASE ORDER NUMBER 023902		BILL OF LADING 1324-0000130464		DATE 09/04/2018		
SPECIFICATION / DATE or REVISION ASTM A615/A615M-16						

CHEMICAL COMPOSITION											
C %	Mn %	P %	S %	Si %	Cu %	Ni %	Cr %	Mo %	Sn %	V %	
0.48	0.94	0.016	0.038	0.19	0.34	0.12	0.11	0.028	0.010	0.004	


MECHANICAL PROPERTIES						
YS PSI	YS MPa	UTS PSI	UTS MPa	G/L Inch	G/L mm	
66854	461	106339	733	8.000	200.0	
67834	468	106077	731	8.000	200.0	

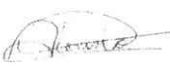
MECHANICAL PROPERTIES	
Elong. %	BendTest
10.00	OK
13.80	OK

GEOMETRIC CHARACTERISTICS			
%Light	Def Hgt Inch	Def Gap Inch	DefSpace Inch
3.61	0.036	0.124	0.388
3.05	0.037	0.112	0.388

COMMENTS / NOTES

The above figures are certified chemical and physical test records as contained in the permanent records of company. We certify that these data are correct and in compliance with specified requirements. This material, including the billets, was melted and manufactured in the USA. CMTR complies with EN 10204 3.1.


 BHASKAR YALAMANCHILI
 QUALITY DIRECTOR


 ALEX RENOSTO
 QUALITY ASSURANCE MGR.

Phone: (409) 267-1071 Email: Bhaskar.Yalamanchili@gerdau.com

C14

Phone: 904-266-1468 Email: Alexander.Renosto@gerdau.com

JS-ML-JACKSONVILLE
6770 Rebar Road
ACKSONVILLE, FL 32234
JSA

CUSTOMER SHIP TO
DURA STRESS INC
11325 CR 44 EAST
LEESBURG, FL 34788
USA

CUSTOMER BILL TO
SOUTHWESTERN SUPPLIERS INC
6815 E 14TH AVE
TAMPA, FL 33619-2917
USA

GRADE
60 (420)

SHAPE / SIZE
Rebar / #5 (16MM)

DOCUMENT ID:
0000049507

LENGTH
40'00"

WEIGHT
16,020 LB

HEAT / BATCH
56145184/03

SALES ORDER
6897855/000010

CUSTOMER MATERIAL N#

SPECIFICATION / DATE or REVISION
ASTM A615/A615M-16

CUSTOMER PURCHASE ORDER NUMBER
023902

BILL OF LADING
1324-0000130464

DATE
09/04/2018

CHEMICAL COMPOSITION

C %	Mn %	P %	S %	Si %	Cu %	Ni %	Cr %	Mo %	Sn %	V %
0.48	0.98	0.024	0.053	0.19	0.35	0.09	0.19	0.021	0.021	0.005

MECHANICAL PROPERTIES

YS PSI	YS MPa	UTS PSI	UTS MPa	G/L Inch	G/L mm
68439	472	108748	750	8.000	200.0
68538	473	108802	750	8.000	200.0

MECHANICAL PROPERTIES

Elong. %	Bend Test
9.20	OK
11.00	OK

GEOMETRIC CHARACTERISTICS

%Light %	Def Hgt Inch	Def Gap Inch	Def Space Inch
3.33	0.036	0.120	0.385
3.33	0.036	0.119	0.385

COMMENTS / NOTES

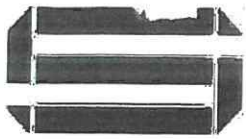
The above figures are certified chemical and physical test records as contained in the permanent records of company. We certify that these data are correct and in compliance with specified requirements. This material, including the billets, was melted and manufactured in the USA. CMTR complies with EN 10204 3.1.



BHASKAR YALAMANCHILI
QUALITY DIRECTOR



ALEX RENOSTO
QUALITY ASSURANCE MGR.



DELIVERY TICKET
SOUTHWESTERN
 SUPPLIERS, INC.

6815 East 14TH Avenue
 TAMPA, FL 33619-2917

Delivery Ticket No.	200676	
Delivery Date	8/16/2018	
Page	1	
Who Printed	warehouse	
Date/Time Printed	8/15/2018	4:40:24 PM

TAMPA (813) 626-2193
 WATS (800) 282-2867
 FAX (813) 628-0511
 www.sowes.com

Sold To:

DURA-STRESS, INC.
 PO BOX 490779

 LEESBURG FL 34749-0779
RECEIVED

Ship To:

DURA-STRESS, INC.
 "NORTHSIDE" ENTRANCE
 11325 CR 44 EAST
 LEESBURG FL 34788
 (352) 787-1422 Ext. 0000
 AUG 16 2018
 SCANNED

Purchase Order No.	Customer ID	Salesperson ID	Shipping Via	Special Instructions
13237	DURAS	DURA-STRESS, INC.	OUR TRUCK/DLVD	MTCs REQ'D / HEAT# ON ALL TAGS
Lift/Pkg/Pallet	Quantity	Unit	Description of Merchandise	
	1	EA	MISCELLANEOUS PRODUCT/SVC FIBERGLASS FABRICATED REBAR INCLUDES: 12pcs - A2 #5, 132pcs - D2 #3 240pcs - K2 #4, 18pcs - Y2 #4, 18pcs - Z2 #5 *** JOB# B1789 / PIECE # TYPE II BEAM	
Comments:			Total Weight	Total Units
			5	2

(EXCEPTIONS FOR DAMAGE OR SHORTAGES MUST BE TAKEN AT TIME OF DELIVERY)

[Signature]
 DELIVERED BY

X *[Signature]*
 RECEIVED - SIGNATURE

C16

[Signature]
 RECEIVED - PRINT NAME

Per ASTM D7205-06 Tensile Testing of GFRP Rebar



**Owens Corning
Infrastructure
Solutions**

Production
 Experimental
Tested By R Kruse
Test Date 7/23/2018

Rebar Size RB5
Sales Order
Work Order 833922
Date Produced 7/13/2018
Matrix VE
Formulation RBVE2567-600
Lot Color Code
Test Temp 75.8°F
Test R/H 29%
Load Rate 0.50"/min

Lot Type
Reinforcement ECR-Glass
Filament Diameter 23 Micron
Sizing Silane
Yield 113
of Ends 75
Sample Length 48.00"
Anchor Length 10.00"
Free Length 28.00"
Potting Material Hydrostone

TEST MACHINE

Baldwin Model 120 CS S/N: 1005
 Electromechanical 120,000 lbs Capacity
 Tension/Compression
 Certification Number 148101216100627
 By Instron 12-October-2016

Sample #	Load @ Failure (lbs)	Tensile Strength (psi)	Tensile Strength (MPa)	Ultimate Strain (in/in)	Modulus of Elasticity (psi)	Modulus of Elasticity (GPa)
1	41.070.6	133.867.7	923.0	0.0177	7.574.557	52.2
2	41.556.0	135.449.8	933.9	0.0177	7.635.148	52.6
3	38.904.7	126.808.0	874.3	0.0165	7.666.031	52.9
4	39.567.1	128.967.1	889.2	0.0168	7.666.945	52.9
5	41.589.4	135.558.7	934.7	0.0178	7.625.944	52.6
6	41.318.2	134.674.7	928.6	0.0171	7.870.031	54.3
7	40.109.5	130.735.0	901.4	0.0168	7.766.442	53.5
		Averages		0.0172	7.686.443	53.0

	PSI	MPa	Strain
Average Tensile	132.294.4	912.2	
Sigma	3.215.1	22.2	0.0005
3 Sigma	9.645.2	66.5	0.0014
Lot Only -3 Sigma	122.649.2	845.7	0.0158

Extensometer Epsilon Model 3543
 Certification Number 148101216140227
 Calibrated by Instron 12-October-2016

Distance from Anchors
LBS of Load at Removal 14.573
Percent of Load at Removal 50%
Span 6.0"

As of 1 Jan 2012: Tensile Strength and Modulus of Elasticity on this sheet are NOT calculated using Actual Cross Sectional Area, but are calculated using a standard Cross Sectional Area.

Surface: Undulated Externally Wrapped
 Spacing of Wrap .75 - 1.0"
 Silica Sand applied to Surface During Process

Sample	Mode of Failure	Line Traceability
1		
2		
3		
4		
5		
6		

* Samples cut using Diamond Blade Cutoff Saw
 ** Anchorages are cut to length and wheel labrated
 Schedule 40 Pipe **Additional Lab Test Data**

Rebar Size	Required Tensile Strength (psi / MPa)	Load Cell Min (lbs / N)	Standard ϕ (in / mm)	Standard CSA A \square (in / mm)
5	105 000	32 214	0.6250	0.3068
16	724 0	143 298	1.5 88	1.97 9

Glass to Matrix 77.79 / 22.21 By Weight
Barcol Hardness 63.8 ASTM D2583
Transverse Shear 27.313.4 psi ASTM D7617
Apparent Shear 7.527.8 psi ASTM D4475
Water Absorption Average 24 Hour 0.2267 % ASTM D570 P7.7

Metric Reference

Per ASTM D7205-06 Tensile Testing of GFRP Rebar



**Owens Corning
Infrastructure
Solutions**

● Production
○ Experimental

Tested By R Kruse
Test Date 7/18/2018

Rebar Size RB4
Sales Order
Work Order 834557
Date Produced 7/10/2018
Matrix PE
Formulation RBPE2234-600
Lot Color Code
Test Temp 77.2°F
Test R/H 31%
Load Rate 0.40"/min

Lot Type
Reinforcement ECR-Glass
Filament Diameter 23 Micron
Sizing Silane
Yield 113
of Ends 44
Sample Length 48.00"
Anchor Length 10.00"
Free Length 28.00"
Potting Material hydrostone

TEST MACHINE

Baldwin Model 120 CS S/N: 1005
Electromechanical 120,000 lbs Capacity
Tension/Compression
Certification Number 148101216100627
By Instron 12-October-2016

Sample #	Load @ Failure (lbs)	Tensile Strength (psi)	Tensile Strength (MPa)	Ultimate Strain (in/in)	Modulus of Elasticity (psi)	Modulus of Elasticity (GPa)
1	26.389.1	134.432.5	926.9	0.0191	7.026.830	48.4
2	25.768.0	131.268.5	905.1	0.0187	7.028.713	48.5
3	26.281.0	133.881.8	923.1	0.0190	7.038.677	48.5
4	26.153.2	133.230.8	918.6	0.0189	7.065.963	48.7
4	26.216.1	133.551.2	920.8	0.0189	7.069.301	48.7
5	23.971.6	122.117.2	842.0	0.0174	7.026.294	48.4
6	Averages			0.0187	7.042.630	48.6
Tensile Strength Average		131.413.7	906.1	Strain		
Sigma		4.272.4	29.5	0.0006		
3 Sigma		12.817.3	88.4	0.0018		
Lot Only -3 Sigma		118.596.4	817.7	0.0169		

Extensometer Epsilon Model 3543
Certification Number 148101216140227
Calibrated by Instron 12-October-2016

Distance from Anchors
LBS of Load at Removal 9.815
Percent of Load at Removal 50%
Span 6.0"

As of 1 Jan 2012: Tensile Strength and Modulus of Elasticity on this sheet are NOT calculated using Actual Cross Sectional Area, but are calculated using a standard Cross Sectional Area.

Surface: Undulated Externally Wrapped
Spacing of Wrap .75 - 1.0"
Silica Sand applied to Surface During Process

Sample	Mode of Failure	Line Traceability
1		
2		
3		
4		
5		

* Samples cut using Diamond Blade Cutoff Saw

** Anchorages are cut to Additional Test Data
Schedule 40 Pipe

Rebar Size	Required Tensile Strength (psi / MPa)	Load Cell Min (lbs / N)	Standard ϕ (in / mm)	Standard CSA A \square (in / mm)
4	110,000	21,593	0.5000	0.1963
13	758.4	96,078	12.70	126.7

Glass to Matrix 75.34 / 24.66 By Weight
Barcol Hardness 60.4 ASTM D2583
Transverse Shear 29.997.5 psi ASTM D7617
Apparent Shear 6.450.9 psi ASTM D4475
Water Absorption Average 24 Hour 0.3048 % ASTM D570 P7.7

Metric Reference

Per ASTM D7205-06 Tensile Testing of GFRP Rebar



**Owens Corning
Infrastructure
Solutions**

Production
 Experimental

Tested By R Kruse
Test Date 3/20/2018

TEST MACHINE

Baldwin Model 120 CS S/N: 1005
Electromechanical 120,000 lbs Capacity
Force/Strain
Certification Number 148102617163454
By Instron October 26, 2017

Rebar Size	BRB4
Sales Order	900368
Work Order	833817
Date Produced	3/8/2018
Matrix	VE
Formulation	BRBVEA20-922
Test Temp	72.9°F
Test R/H	19%
Load Rate	0.40"/min

Lot Type

Reinforcement	ECR-Glass
Filament Diameter	23 Micron
Sizing	Silane
Yield	113
# of Ends	44
Sample Length	48.00"
Free Length	28.00"
Anchor Length	10.00"
Potting Material	HydroStone

Sample #	Load @ Failure (lbs)	Tensile Strength (psi)	Tensile Strength (MPa)	Ultimate Strain (in/in)	Modulus of Elasticity (psi)	Modulus of Elasticity (GPa)
1	27.666.6	140.940.4	971.8	0.0201	7.023.234	48.4
2	28.802.6	146.727.5	1.011.7	0.0209	7.018.063	48.4
3	28.918.5	147.317.9	1.015.8	0.0208	7.066.594	48.7
4	28.657.2	145.986.8	1.006.6	0.0209	6.968.941	48.0
5	28.855.7	146.998.0	1.013.5	0.0208	7.068.954	48.7
6	28.810.5	146.767.7	1.012.0	0.0208	7.063.744	48.7
7	28.061.6	142.952.6	985.7	0.0204	7.014.530	48.4
7	29.362.7	149.580.7	1.031.4	0.0216	6.936.139	47.8
Averages				0.0208	7.020.025	48.4

Tensile Strength Average	PSI 145.908.9	MPa 1.006.0	Strain 0.0004
σ Sigma	2.537.0	17.5	0.0012
3σ Sigma	7.611.1	52.5	0.0196
Lot Only -3σ Sigma	138.297.8	953.6	

Extensometer Epsilon Model 3543
Certification Number 148101216140227
Calibrated by Instron 12-October-2016

Distance from Anchors	11.000"
LBS of Load at Removal	9.815
Percent of Load at Removal	50%
Span	6.0"

As of 1 Jan 2012: Tensile Strength and Modulus of Elasticity on this sheet are NOT calculated using Actual Cross Sectional Area, but are calculated using a standard Cross Sectional Area.

Sample	Mode of Failure	Line Traceability
1	Delam Center	
2	Delam Center	
3	Delam Center	
4	Delam Center	
5	Delam Center	
6	Delam Center	

Surface: Undulated Externally Wrapped
Spacing of Wrap .75 - 1.0"
Silica Sand applied to Surface During Process
* Samples cut using Diamond Blade Cutoff Saw
** Anchorages are cut to length and wheel abraded

Additional Lab Test Data

% Glass to Matrix	75.58 / 24.42	ASTM D2584
Barcol Hardness	63.0	ASTM D2583
Transverse Shear	35.694.3 psi	ASTM D7617
Apparent Shear	8.480.8 psi	ASTM D4475
Water Absorption Average 24 Hour	0.1141 %	ASTM D570 P7.7

Rebar Size	Required Tensile Strength (psi / MPa)	Load Cell Min (lbs / N)	Standard (in / mm)	Standard CSA A□ (in / mm)
4	110 000	21 593	0 5000	0 1963
13	758 4	96 078	12 70	126 7

Metric References



**NORTH AMERICAN
STAINLESS**

METALLURGICAL TEST REPORT

6870 Highway 42 East
Ghent, KY 41045-9615
(502) 347-6000

B1187

Certificate: 413533 01 Mail To: Ship To: Date: 5/22/2018 Page: 1 OF 2
 CORROSION RESISTANT REINFORCING, LLC CORROSION RESISTANT REINFORCING, LLC
 ACCOUNTS PAYABLE 935 WENSTRUP LANE Steel: 2304/EN1.4362
 CINCINNATI OH 45241 WALTON KY 41094 Finish: HR- Pickled
 Customer: 4666 001 Heat Treat Code: 47,110 Dia/Thk: .5000 in
 NAS Order: LP 83744 1 Leg Length:
 Your Order: 247 Item Code: 048S2304 Length:
 Corrosion: ASTM A1084 Method A

PRODUCT DESCRIPTION:

Reinforcing Bar
 UNS S32304
 ASTM A955/18 Grade 75, ASTM A276/17 (Chem Only)
 Heat Treat Condition: Hot rolled, Pickled & Passivated.

REMARKS:

COMPLIES W/REQUIREMENTS OF D FAR 252.225-7009 EU DIRECTIVE
 2011/65/EU. RoHS. EAF+AOD+CC. NO WELD REPAIR. MELTED AND MFG
 IN USA FREE FROM MERCURY AND LOW MELTING ALLOY CONTAMINATION

Bundle Weight	Bundle Weight	Bundle Weight	Bundle Weight	Bundle Weight	Bundle Weight	Bundle Weight	Bundle Weight	Bundle Weight	Bundle Weight
RA31967 3406	RA31968 3414	RA31970 3416	RA31972 3406	RA31975 3400	RA31976 3370	RA31977 3386	RA31978 3406	RA31985 3400	

CHEMICAL ANALYSIS CM(Country of Melt) ES(Spain) US(United States) ZA(South Africa) JP(Japan) ANAB, ISO/IEC 17025, Certificate# L2323
 Chemical Analysis per ASTM A751/14a

NAS Heat	Supplier Heat	CM	C %	CO %	CR %	CU %	MN %	MO %	N %	NI %	P %	S %
819B		US	.018	.09	22.55	.32	1.78	.206	.150	4.41	.034	.0007
			SI %									
			.58									

MECHANICAL PROPERTIES

	l d	HB	.2YS	UTS	Bend	Elo-8"	YS Grade
	o i	No.	KSI	KSI	P/F	%	ksi
	c r						
RA31967	R L	218.0	83.39	119.84	Pass	26.46	75.00
RA31968	R L	218.0	83.39	119.84	Pass	26.46	75.00
RA31970	R L	218.0	83.39	119.84	Pass	26.46	75.00
RA31972	R L	218.0	83.39	119.84	Pass	26.46	75.00
RA31975	R L	218.0	83.39	119.84	Pass	26.46	75.00
RA31976	R L	218.0	83.39	119.84	Pass	26.46	75.00
RA31977	R L	218.0	83.39	119.84	Pass	26.46	75.00
RA31978	R L	218.0	83.39	119.84	Pass	26.46	75.00
RA31985	R L	218.0	83.39	119.84	Pass	26.46	75.00

NAS hereby certifies that the analysis on this certification is correct. Based upon the results and the accuracy of the test methods used, the material meets the specifications stated. These results relate only to the items tested and this report cannot be reproduced, except in its entirety, without the written approval of NAS

Technical Dept. Mgr. KRIS LARK



METALLURGICAL TEST REPORT

6870 Highway 42 East
Ghent, KY 41045-9615
(502) 347-6000

Certificate: 413533 01 Mail To: CORROSION RESISTANT REINFORCING, LLC Ship To: CORROSION RESISTANT REINFORCING, LLC Date: 5/22/2018 Page: 2 Of 2
 Accounts Payable CINCINNATI OH 45241 935 WENSTRUP LANE WALTON KY 41094 Steel: 2304/EN1.4362
 Customer: 4666 001 Your Order: 247 Heat Treat Code: 47,110 Finish: HR- Pickled
 Dia/Thk: .5000 in
 Leg Length:
 Length:
 Corrosion: ASTM A1084 Method A

PRODUCT DESCRIPTION:

Reinforcing Bar
 UNS S32304
 ASTM A955/18 Grade 75, ASTM A276/17 (Chem Only)
 Heat Treat Condition: Hot rolled, Pickled & Passivated.

REMARKS:

COMPLIES W/REQUIREMENTS OF DPAR 252.225-7009 EU DIRECTIVE
 2011/65/EU.RoHS. EAF+AOD+CC. NO WELD REPAIR. MELTED AND MFG
 IN USA FREE FROM MERCURY AND LOW MELTING ALLOY CONTAMINATION

Bundle Weight	Bundle Weight	Bundle Weight	Bundle Weight	Bundle Weight	Bundle Weight	Bundle Weight	Bundle Weight	Bundle Weight	Bundle Weight	Bundle Weight
RA31993	3384									

CHEMICAL ANALYSIS

CM(Country of Melt) ES(Spain) US(United States) ZA(South Africa) JP(Japan) ANAB, ISO/IEC 17025, Certificate# L2323
 Chemical Analysis per ASTM A751/14a

NAS Heat	Supplier Heat	CM	C %	CO %	CR %	CU %	MN %	MO %	N %	NI %	P %	S %
819B		US	.018	.09	22.55	.32	1.78	.206	.150	4.41	.034	.0007
			SI %									
			.58									

MECHANICAL PROPERTIES

1 d o i o r	HB No.	.2YS KSI	UTS KSI	Bend P/F	Elc-8" %	YS Grade ksi
RA31993 R L	218.0	83.39	119.84	Pass	26.46	75.00

NAS hereby certifies that the analysis on this certification is correct. Based upon the results and the accuracy of the test methods used, the material meets the specifications stated. These results relate only to the items tested and this report cannot be reproduced, except in its entirety, without the written approval of NAS

Technical
Dept. Mgr.

KRIS LARK



METALLURGICAL TEST REPORT

6870 Highway 42 East
Ghent, KY 41045-9615
(502) 347-6000

Certificate: 427945 01 Mail To: CORROSION RESISTANT REINFORCING, LLC
 Accounts Payable Cincinnati OH 45241 Ship To: CORROSION RESISTANT REINFORCING, LLC
 935 WENSTRUP LANE WALTON KY 41094 Date: 7/12/2018 Page: 1 Of 1
 Customer: 4666 001 Heat Treat Code: 47,798 Steel: 2304/EN1.4362
 NAS Order: LP 87757 1 Item Code: 05SS2304 Finish: HR- Pickled
 Your Order: 265 Corrosion: ASTM A1064 Method A Dia/Thk: .6250 in
 Leg Length: Length:

PRODUCT DESCRIPTION:

Reinforcing Bar
UNS S32304
ASTM A955/18 Grade 75, ASTM A276/17 (Chem Only)
Heat Treat Condition: Hot rolled, Pickled & Passivated.

REMARKS:

COMPLIES W/REQUIREMENTS OF D FAR 252.225-7009 EU DIRECTIVE
2011/65/EU. RoHS. HAF+AOD+CC. NO WELD REPAIR. MELTED AND MFG
IN USA FREE FROM MERCURY AND LOW MELTING ALLOY CONTAMINATION

Bundle Weight	Bundle Weight	Bundle Weight	Bundle Weight	Bundle Weight	Bundle Weight	Bundle Weight	Bundle Weight	Bundle Weight	Bundle Weight
RA34040 3428	RA34041 3382	RA34042 3398	RA34043 3446						

CHEMICAL ANALYSIS

CM(Country of Melt) ES(Spain) US(United States) ZA(South Africa) JP(Japan) ANAB, ISO/IEC 17025, Certificate# L2323
Chemical Analysis per ASTM A751/14a

NAS Heat	Supplier Heat	CM	C %	CO %	CR %	CU %	MN %	MO %	N %	NI %	P %	S %
866Y		US	.018	.11	22.50	.26	1.70	.172	.143	4.19	.031	.0013
			SI %									
			.55									

MECHANICAL PROPERTIES

	id o i c r	HB No.	.2YS KSI	UTS KSI	Bend P/F	Elo-8" %	YS Grade ksi
RA34040	R L	260.0	87.86	120.55	Pass	24.79	75.00
RA34041	R L	260.0	87.86	120.55	Pass	24.79	75.00
RA34042	R L	260.0	87.86	120.55	Pass	24.79	75.00
RA34043	R L	260.0	87.86	120.55	Pass	24.79	75.00

NAS hereby certifies that the analysis on this certification is correct. Based upon the results and the accuracy of the test methods used, the material meets the specifications stated. These results relate only to the items tested and this report cannot be reproduced, except in its entirety, without the written approval of NAS

Technical Dept. Mgr. KRIS LARK



**NORTH AMERICAN
STAINLESS**

METALLURGICAL TEST REPORT

6870 Highway 42 East
Ghent, KY 41045-9615
(502) 347-6000

Certificate: 326128 04

Mail To:
CORROSION RESISTANT REINFORCING, LLC
ACCOUNTS PAYABLE
CINCINNATI OH 45241

Ship To:
CORROSION RESISTANT REINFORCING, LLC
935 WESTRUP LANE
WALTON KY 41094

Date: 8/23/2017 Page: 1 OF 1
Steel: 2304/EN1.4362
Finish: HR- Pickled
Dia/Thk: .3750 in
Leg Length:
Length:
Corrosion: ASTM A1084 Method A

Customer: 4666 001

NAS Order: LP 70026 3

Your Order: 176

Item Code: 03882304

PRODUCT DESCRIPTION:

Reinforcing Bar
UNS S32304
ASTM A955/17 Grade 75, ASTM A276/17 (Chem Only)
Heat Treat Condition: Hot rolled, Pickled & Passivated.

REMARKS:

COMPLIES W/REQUIREMENTS OF DFR 252.225-7009 EU DIRECTIVE
2011/65/EU. RoHS. EAF+ADD+CC. NO WELD REPAIR. MELTED AND MPG
IN USA FREE FROM MERCURY AND LOW MELTING ALLOY CONTAMINATION

Bundle Weight	Bundle Weight	Bundle Weight	Bundle Weight	Bundle Weight	Bundle Weight	Bundle Weight	Bundle Weight	Bundle Weight	Bundle Weight
RA26348	2280	RA26349	2280	RA26374	2536				

CHEMICAL ANALYSIS

Lab Accreditation Bureau, ISO/IEC 17025, Certificate# L2323
CM(Country of Mkr) ES(Spain) US(United States) ZA(South Africa) JP(Japan) Chemical Analysis per ASTM A751/16a

NAS Heat	Supplier Heat	CM	C %	CO %	CR %	CU %	NI %	MO %	N %	SI %	P %	S %
S05L		US	.013	.09	22.57	.32	1.64	.18	.161	4.03	.030	.0006
			SI %							.46		

MECHANICAL PROPERTIES

	1 0 0	0 1 r	HR No.	.2YS KSI	UTS KSI	Band P/F	Elo-8° %	YS Grade ksi
RA26348	R	L	266.0	92.25	125.04	Pass	20.28	75.00
RA26349	R	L	266.0	92.25	125.04	Pass	20.28	75.00
RA26374	R	L	266.0	92.25	125.04	Pass	20.28	75.00

NAS hereby certifies that the analysis on this certification is correct. Based upon the results and the accuracy of the test methods used, the material meets the specifications stated. These results relate only to the items tested and this report cannot be reproduced, except in its entirety, without the written approval of NAS

Technical
Dept. Mgr.

VDTC TADV



**NORTH AMERICAN
STAINLESS**

METALLURGICAL TEST REPORT

6870 Highway 42 East
Ghent, KY 41045-9615
(502) 347-6000

Certificate: 326128 04 Mail To:

CORROSION RESISTANT REINFORCING, LLC
ACCOUNTS PAYABLE
CINCINNATI OH 45241

Ship To:

CORROSION RESISTANT REINFORCING, LLC
935 WENSTROP LANE
WALTON KY 41094

Date: 8/23/2017 Page: 1 OF 1

Steel: 2304/KM1.4362

Finish: HR- Pickled

Dia/Thk: .3750 in

Leg Length:

Length:

Corrosion: ASTM A1084 Method A

Customer: 4666 001

NAS Order: LP 70026 3

Your Order: 176

Item Code: 03882304

PRODUCT DESCRIPTION:

Reinforcing Bar
UNS S32304
ASTM A955/17 Grade 75, ASTM A276/17 (Chem Only)
Heat Treat Condition: Hot rolled, Pickled & Passivated.

REMARKS:

COMPLIES W/REQUIREMENTS OF DPAR 252.225-7009 EU DIRECTIVE
2011/65/EU.ROHS. EAF+AOD+CC. NO WELD REPAIR. MELTED AND MFG
IN USA FREE FROM MERCURY AND LOW MELTING ALLOY CONTAMINATION

Bundle Weight	Bundle Weight	Bundle Weight	Bundle Weight	Bundle Weight	Bundle Weight	Bundle Weight	Bundle Weight	Bundle Weight
RA26348 2280	RA26349 2288	RA26374 2536						

CHEMICAL ANALYSIS

CM(Country of Mfg) ES(Spain) US(United States) ZA(South Africa) JP(Japan)

Lab Accreditation Bureau, ISO/IEC 17025, Certificate# L2323

Chemical Analysis per ASTM A751/14a

NAS Heat	Supplier Heat	CM	C %	CO %	CR %	CU %	NI %	MO %	N %	NI %	P %	S %
S05L		US	.013	.09	22.57	.32	1.64	.18	.161	4.03	.030	.0006
			SI %									
			.46									

MECHANICAL PROPERTIES

Lot No.	HR No.	.2YS KSI	UTS KSI	Bend P/F	Elo-8° %	YS Grade ksi	
RA26348	R L	266.0	92.25	125.04	Pass	20.28	75.00
RA26349	R L	266.0	92.25	125.04	Pass	20.28	75.00
RA26374	R L	266.0	92.25	125.04	Pass	20.28	75.00

NAS hereby certifies that the analysis on this certification is correct. Based upon the results and the accuracy of the test methods used, the material meets the specifications stated. These results relate only to the items tested and this report cannot be reproduced, except in its entirety, without the written approval of NAS

Technical
Dept. Mgr.

VDTC TADU



Pack Slip: 71855

Packing Slip

Page: 1 of 1

Ship To:
 DURA-STRESS, INC
 11325 CR 44 EAST
 LEESBURG FL 34788

RECEIVED

Phone: AUG 29 2018
Fax:
Email: DURA-STRESS, INC.

Sold To:
 DURA-STRESS, INC
 11325 CR 44 EAST
 LEESBURG FL 34788

Phone:
Fax:
Email:

SCANNED
 8-29-18

Ship Date: 8/28/2018 F.O.B.: FOB Summerville
 Ship Via: MOL TRUCKING

CUSTOMER SPECIFICATIONS

- No Covers
- Tarped
- Spaced for Straps
- Load to Side
- Load Down Center
- Load Eye to the Sky
- Certify with Domestic Statement
- P.O. No. Must Appear on Packing Slip
- Representative Curve
- Chemical Analysis

Shipments must be 7 pack shipments. Packs must be with no welds 1/13/2014 10:33> They can only take delivery of truckloads between the following hours! Monday ♦ Thursday 7:00 am to 3:30 pm Friday- 7:00 am to 12:00 pm If a driver arrives before 7:00 am they can use the West gate at the traffic light for overnight or early parking.

Line	Part Number / Description	Planned Qty
Sales Order: 60816 Your PO: 12875		

Salesperson(s): Aldo Bassi

Line 1 Rel 39
 4600.270.D

Back Order Qty: 66,500 FT
 3,148 FT

.600 7 WIRE 270 LOW RELAXATION

ENTERED AUG 29 2018

Lot	Shipped Qty	Net Weight
002829.009	9,066 FT	6,709 LB
002829.011	9,057 FT	6,702 LB
002900.001	9,110 FT	6,741 LB
002900.004	9,053 FT	6,699 LB
002900.005	9,063 FT	6,707 LB
002900.006	9,069 FT	6,711 LB
002900.007	8,934 FT	6,611 LB
Total Qty:	63,352 FT	Total Net Weight: 46,880 LB

Time: 830 am
Temp: _____
Taken by: _____

1 DAY POUR:
2 DAY POUR: _____
OTHER: _____

STRESS INFORMATION SLIP



F.D.O.T. PROJECT YES NO (CIRCLE ONE)

DATE 9-10-18 INITIAL TENSION 5,000

JOB# 1789 NUM OF STRAND 11 FINAL TENSION 13,900

BED# 31 JACK# _____ PAK# OR COIL# 002829.009
002900.004

LIST MARK#S 1-D1, 1-D2, 1-A3, 1-A2, 1-A1

PRODUCT TYPE Girt 2 TYPE OF CABLE 6

MUST BE SIGNED BY PERSON FILLING OUT SLIP: [Signature]

WILL NOT BE PROCESSED WITHOUT ALL PROPER INFORMATION AND SIGNATURE!

Stress Prepared by: [Signature]
Checked by: _____

Setup prepared by: [Signature]
Checked by: _____

6,000 psi - 10,000 psi
no sheathing

9/10/2018 7:58

JOB#:	B1789	
DATE:	9/10/2018	
BED #:	31N	
JACK #		
STRAND SIZE	.600 7W 270 LR ASTM A416	
COIL/PACK/REEL #	002829009-0	0
	002900004-0	0
	0	0
	0	0
BED LENGTH (L):	3811.375	0
STRAND SIZE: (A)	0.2170	0
FINAL TEN. (P)	43900	0
PRE TEN. : (Pi)	5000	0
M.O.E. (E):	28.70	0
		0
		0

PRODUCT

GIRT 2

MARK #

1-D1, 1-D2, 1-A3, 1-A2, 1-A1

CORRECTION INFO.	
Number of cable #	11
Exp. Conc temp @ Placement:	85
Ambient temperature(at):	73
Abutment rotation (ar): N/A	0
Live end seating (les):	0.2362
Dead end slippage (des):	0.08858
anchorage movement:	0.375

ELONGATION

delta.a.t (Pt_{xdb}/P_b)= 0
delt.(Pi x L)/(A x E) = 3.0599
delta'b.(P x L)/(A x E)= 23.8062
delta'bed shortning
(bs/2)+(bs/#strand)= 0.2216

GROSS ELONG. 24.353

NET ELONG. **24 1/8**

RANGE + 2.5%	24 11/16
RANGE - 2.5%	23 1/2

FORCE ADJUSTMENTS

P_b (P - P_i) = 38900
P_t(= 0
P_{ar} (ar x A x E)/(L)= 0
P_{les}(les x A x E)/(L)= 385.9578
P_{des} no adj. required 0
P_{bs} (d_{bs} x A x E)/(L)= 362.101
TOTAL FORCE ADJ. 748.0588
ADJUSTED FORCE = 39648.0588

JACKING FORCE = 44648

TOTAL ADJ. FORCE **44648**

AASHTO MAX =	46872
RANGE +2.5% =	45764
RANGE -2.5% =	43532

31N

9/12/2018 9:34

JOB#:	B1789	
DATE:	9/12/2018	
BED #:	54M	
JACK #		
STRAND SIZE	.6 ST TEST	
COIL/PACK/REEL #	D430001-1D	0
	0	0
	0	0
	0	0
BED LENGTH (L):	3021.5	0
STRAND SIZE: (A)	0.2328	0
FINAL TEN. (P)	37200	0
PRE TEN. : (Pi)	5000	0
M.O.E. (E):	24.40	0
		0
		0

PRODUCT
TYPE II
MARK #
TEST

CORRECTION INFO.	
Number of cable #	13
Exp. Conc temp @ Placement:	85
Ambient temperature(at):	85
Abutment rotation (ar): N/A	0
Live end seating (les):	0.3438
Dead end slippage (des):	0.1093
anchorage movement:	0.625

ELONGATION

delta.a.t (Ptxdb/Pb)= 0
delt.(Pi x L)/(A x E) = 2.6596
delta'b.(PxL)/(AxE)= 17.128
delta'bed shortning
(bs/2)+(bs/#strand)= 0.3606

GROSS ELONG. 17.942

NET ELONG.	17 9/16
------------	----------------

RANGE + 2.5%	18
RANGE - 2.5%	17 1/8

FORCE ADJUSTMENTS

Pb (P - Pi) = 32200
Pt(= 0
Par (arxAxE)/(L)= 0
Ples(lesxAxE)/(L)= 646.3326
Pdes no adj. required 0
Pbs (dbsxAxE)/(L)= 677.9161
TOTAL FORCE ADJ. 1324.2487
ADJUSTED FORCE = 33524.2487

JACKING FORCE = 38524

TOTAL ADJ. FORCE	38524
------------------	--------------

AASHTO MAX =	46560
RANGE +2.5% =	39487
RANGE -2.5% =	37561

54M

PREPOUR PRODUCTION SHEET

JOB# B1789
 F.D.O.T.# TEST BEAM
 CAST DATE _____

PRODUCT TYPE II
 BED# 31 N
 MIX # LIGHTWEIGHT (10,000 mix)
05-2056

COMMENT KEYS / = OK, O = ACCEPTABLE, X = NOT ACCEPTABLE

SERIAL #'S	LW1	LW2	LW3	LW4	LW5
MARK #'S	D1	D2	A3	A2	A1
DATE:	9-10-18	9-10-18	9-10-18	9-10-18	9-10-18
INSPECTOR:	KS				
WIDTH	O	O	O	O	O
LENGTH	O	O	O	O	O
HEIGHT	O	O	O	O	O
CABLE HOLES	O	O	O	O	O
"L" BAR HOLES	O	O	O	O	O
CHAMFER	O	O	O	O	O
SKEW	NA				
INSERTS	NA				
BLOCK OUTS	NA				
FORM CLEANNESS	O	O	O	O	O
PLATES FORM FACE	NA				

COMMENTS

SERIAL #'S	LW1	LW2	LW3	LW4	LW5
MARK #S	D1	D2	A3	A2	A1
DATE:	9-10-18	9-10-18	9-10-18	9-10-18	9-10-18
INSPECTOR:	KS				
REINFORCEMENT	O	O	O	O	O
STEEL SPACING	O	O	O	O	O
PLATES	NA				
CLEARANCE	O	O	O	O	O
LINER	O	O	O	O	O
LIFTING LOOPS	O	O	O	O	O
SHEATHING	NA				

COMMENTS

SERIAL #'S	LW1	LW2	LW3	LW4	LW5
MARK #S	D1	D2	A3	A2	A1
INSPECTOR:	KS				
DATE :	9-11-18	9-11-18	9-11-18	9-11-18	9-11-18
DROP IN PLATES	NA				
BLOCK OUTS	NA				
INSERTS	NA				
HEADERS	O	O	O	O	O
LENGTH	O	O	O	O	O
FORMS	O	O	O	O	O

COMMENTS

CONCRETE MIX DESIGN

05-2056

Producer: Dura-Stress, Inc.

Class VI (8500 PSI) / Self-Consolidating

Effective Date: 7/16/2018

Aggregate Correction Factor: 0.9

Environment: Extremely Aggressive

Hot Weather

Source of Materials

Product	Quantity	Production Facility
921: Cement - Type II (MH)	703 Pound(s)	CMT29 - Suwannee American Cement - Branford, FL
929: Fly Ash - Class F	167 Pound(s)	FA01 - Separation Technologies - Crystal River, FL
929: Metakaolin	74 Pound(s)	MK03 - BASF Middle Georgia
901: C12 - #67 Stone	1340 Pound(s)	10645 - VULCAN MATERIALS COMPANY
902: F01 - Silica Sand (Concrete)	1180 Pound(s)	11057 - VULCAN MATERIALS COMPANY
MasterAir AE 90 (MB-AE 90) [924-000-014 - Admixture for Concrete - Air Entraining]	2.36 FL OZ	BASF Construction Chemicals, LLC
MasterSet DELVO (Delvo) [924-003-021 - Admixture for Concrete Type D]	28 FL OZ	BASF Construction Chemicals, LLC
MasterGlenium 7920 [924-001-070 - Admixture for Concrete Type A]	57 FL OZ	BASF Construction Chemicals, LLC
MasterLife CI 30 (Rheocrete CNI) [924-009-002 - Admixture for Concrete - Corrosion Inhibiting]	320 FL OZ	BASF Construction Chemicals, LLC
Water	34.1 GAL	
Water	284 LB	

Calculated Values

Theoretical Unit Weight	139.9	PCF
Theoretical Yield	26.99	CF
Water Contributed from Admixture(s)	18.1	LB

Producer Data

Method of measuring	Pressure Meter
Air Content - Pressure	1.7 %
Temperature	95 degree F
Slump Flow	26.5 in
J-Ring Slump Flow	27.0 in
Passing Ability	0.5 in
Static Segregation	11.0 %
Average Chloride Content	0.196 lbs/yd ³
Water to Cementitious Materials Ratio	0.31
Age	13 Days
Compressive Strength	10,860 PSI
Slump Flow Cut Off Time	12 min
Age	21 Days
Surface Resistivity	37.56 kOhm-cm
Density (Unit Weight)	144.2 lbs/ft ³
VSI	0
T ₅₀	3.0 seconds
Penetration Depth (Pd)	1 mm

Mix Design Limits*

Slump Flow = 27 +/- 2.5 in
 Water to Cementitious Materials Ratio <= 0.32
 Slump Flow Cut Off Time <= 12 min
**See Contract Documents for Limits not displayed*

Special Use Instructions:

```

*****
Job:      31-10KMETA   Date: Sep 12, 2018   Start:05:35 Disch:--:--
Operator: W62342488   Duration/Wait: 2:28/0:00   Batch#:41840   Mixer#: 1
Mix:      05-2056     Mix Name: 10k psi         *ABORTED*
Required: 12.00      Batched: 6.00
Amount:   6.00 CY
PreWet:  70%

```

Material	Bin	Moist/ABS%	Design	Target	Actual	%Err	*Note	Jogs
67 10-645	3	2.00/0.00	1360	8323	8260 Lb	-0.8	-----	7
SAND 11-057	1	4.00/0.00	1202	7501	26080 Lb	247.7	O----	
SUWANEE	3		703	4218	3905 Lb	-7.4	----A	
STI FLYASH	4		167	1002	0 Lb	-100.0	-----	
MB AE90	1		0.25	1.50	2.00 Oz	33.3	-----	
gLENIUM 7920	4		69.00	414.00	556.00 Oz	34.3	O----	
DELVO	2		28.00	168.00	240.00 Oz	42.9	O----	
Prewet				692	685 Lb	-1.0	-----	
Water				303	0 Lb	-100.0	-----	
Prewet Mixing			0:01		0:00 s			
Dry Mixing			0:01		0:00 s			
Wet Mixing			2:00		0:00 s			
Total Moisture:			240	1440	1850 Lb	28.5		
Water/Cement:			0.276	0.474				

Job: 31-10KMETA Date: Sep 12, 2018 Start:06:14 Disch:06:27
Operator: W62342488 Duration/Wait: 13:39/0:30 Batch#:41844 Mixer#: 1
Mix: 05-2056 Mix Name: 10k psi
Required: 12.00 Batched: 6.00
Amount: 6.00 CY
PreWet: 70%

1 BW

Material	Bin	Moist/ABS%	Design	Target	Actual	%Err	*Note	Jogs
67 10-645	3	2.00/0.00	1360	8323	8240 Lb	-1.0	-----	
SAND 11-057	1	4.00/0.00	1202	7501	7460 Lb	-0.5	-----	3
SUWANEE	3		703	4218	4220 Lb	0.0	-----	2
STI FLYASH	4		167	1000	1025 Lb	2.5	-C----	3
MB AE90	1		0.25	1.50	2.00 Oz	33.3	-----	
gLENIUM 7920	4		69.00	414.00	416.00 Oz	0.5	-----	
DELVO	2		28.00	168.00	166.00 Oz	-1.2	-----	
Prewet				692	686 Lb	-0.9	-----	
Water				302	298 Lb	-1.3	-----	
Prewet Mixing			0:01		0:01 s			
Dry Mixing			0:01		0:01 s			
Wet Mixing			2:00		2:32 s			
Total Moisture:			240	1440	1432 Lb	-0.5		
Water/Cement:			0.276	0.273				

.27

+444 lb metamax
+1920 oz ^{NI} C~~130~~ (C130)



 Job: 31-10KMETA Date: Sep 12, 2018 Start:06:24 Disch:06:42
 Operator: W62342488 Duration/Wait: 18:19/0:20 Batch#:41845 Mixer#: 1
 Mix: 05-2056 Mix Name: 10k psi
 Required: 12.00 Batched: 12.00
 Amount: 6.00 CY
 PreWet: 70%

Z BW

Material	Bin	Moist/ABS%	Design	Target	Actual	%Err	*Note	Jogs
67 10-645	3	2.00/0.00	1360	8323	8260 Lb	-0.8	-----	10
SAND 11-057	1	4.00/0.00	1202	7501	7460 Lb	-0.5	-----	2
SUWANEE	3		703	4218	4205 Lb	-0.3	-----	7
STI FLYASH	4		167	1015	995 Lb	-2.0	-C---	9
MB AE90	1		0.25	1.50	3.00 Oz	100.0	-----	
gLENIUM 7920	4		69.00	414.00	416.00 Oz	0.5	-----	
DELVO	2		28.00	168.00	166.00 Oz	-1.2	-----	
Prewet				692	686 Lb	-0.9	-----	
Water				302	317 Lb	5.0	OF---	
Prewet Mixing			0:01		0:01 s			
Dry Mixing			0:01		0:01 s			
Wet Mixing			2:00		2:13 s			
Total Moisture:			240	1440				
Water/Cement:			0.276	0.279	1452 Lb	0.8		

+ 444 lb metamax
 + 1920oz CNI (C130)



 Job: 31-10KMETA Date: Sep 12, 2018 Start:07:03 Disch:07:08
 Operator: W62342488 Duration/Wait: 6:50/0:30 Batch#:41847 Mixer#: 1
 Mix: 05-2056 Mix Name: 10k psi
 Required: 14.00 Batched: 14.00
 Amount: 2.00 CY
 PreWet: 70%

3 BW

Material	Bin	Moist/ABS%	Design	Target	Actual	%Err	*Note	Jogs
67 10-645	3	2.00/0.00	1360	2774	2800 Lb	0.9	-----	7
SAND 11-057	1	4.00/0.00	1202	2500	2640 Lb	5.6	0----	
SUWANEE	3		703	1406	1410 Lb	0.3	-----	8
STI FLYASH	4		167	330	370 Lb	12.1	OC----	7
MB AE90	1		0.25	0.50	1.00 Oz	100.0	-----	
gLENIUM 7920	4		69.00	138.00	140.00 Oz	1.4	-----	
DELVO	2		28.00	56.00	56.00 Oz	0.0	-----	
Prewet				231	225 Lb	-2.6	-----	
Water				104	124 Lb	19.2	0----	
Prewet Mixing			0:01		0:01 s			
Dry Mixing			0:01		0:01 s			
Wet Mixing			2:00		2:01 s			
Total Moisture:			240	490	505 Lb	5.3		
Water/Cement:			0.276	0.284				

0.284

.28

BEAM PLACEMENT DIAGRAM

JOB NO.: B1789
 FDOT NO.: TEST BEAM
 MIX DESIGN: LIGHTWEIGHT (10,000 Mix) / 05-2056

BED: 31N
 PRODUCT: TYPE II

INSPECTOR: JCB/DK
 TEST LOAD(S):
 TOTAL YARDS: 1995

DATE CAST: 9-12-18

COVERED? OR CUR. COMPOUND
 CUR EXP DATE

SIN MARK	LW1 D1	LW2 D2	LW3 A3	LW4 A2	LW5 A1
	Truck #4 767 - AIR High Rejected (9)	Truck #6 767 - 906 AIR = 1.	767-636-IN Full Truck #1	767-648 OUT 1 1/2 yd From Truck #1	765-705 OUT OUT Truck #2 3yd
	Truck #5 765-838 - 8:46 AIR = 1			Truck #2 765-650 IN Full	Truck #3 767 7:16 IN 7:21 OUT 1 1/2 yds
	LIGHTWEIGHT	LIGHTWEIGHT	05-2029	05-2029	05-2029

W/C MAX 0.3

READY MIX TRUCK(S) MEET QCM BATCH PLANT CRITERIA

E

W

PROJECT NO.: B1789
TEST BEAM

BED #: 31N

DATE DETENSIONED: 9-14-18

DATE CAST: 9-12-18

TYPE: TYPE II

CYLINDER PSI: 6532/6641 - LW mix.
9023/8922 - 2054 mix.
REQUIRED RELEASE: 6000 PSI

SERIAL NO.:	LW1	LW2	LW3	LW4	LW5	
MARK NO.:	D1	D2	A3	A2	A1	
SIDE LENGTH RIGHT:	42'-1/8"	42'-1/8"	42'-1/4"	42'-1/4"	42'-1/8"	
SIDE LENGTH LEFT:	42'-1/8"	42'-1/8"	42'	42'	42'-1/8"	
AVG. LENGTH:	42'-1/8"	42'-1/8"	42'-1/8"	42'-1/8"	42'-1/8"	
DESIGN LENGTH:	42' 0"	42' 0"	42' 0"	42' 0"	42' 0"	
HORIZONTAL ALIGNMENT						
CAMBER (INCH)	0/3/16	0/3/16	0/1/4	0/1/4	0/3/16	
REMARKS:						



CHECK LIST

- TABLE SHEET
- STRESS
- REBAR/SPIRAL
- STRESS CALCS
- STRESS RESULTS
- PREPOUR
- BATCH TICKETS
- CASTING DIAGRAM

JOB # B1789
FDOT # TEST02-SS
PRODUCT TYPE Type II
MARK # 1-C3, 1-B3, 1-C2, 1-B2, 1-C1
SERIAL # LW6 - LW10
BED # 54M
MIX DESIGN 05-2056

Check Off!

Cast Date:

9-18-18

Entered in Great Production:

Jerry

Entered in MAC (initials)

N/A

Scanned:

Ready To File:

Sample #'s

TEST02-SS

TABLE SHEET

PROJECT NO.: B1789
TEST BEAM-SS
 BED #: 54M
 DATE CAST: 9-18-18

PRODUCT: Type II
 SERIAL NOS.: LW6-LW10 ✓
 MIX DESIGN: 05-2056
 CLASS: Metakaolin

9:52 @ 91° unit weight 42.85
 Temp 98° Pen 1
 T50 2 VSI 0
 Air 4 Slump/spread 29/29

CY TOTAL: 19.95
 DAY 1: _____
 DAY 2: _____

MIX DESIGN TOLERANCES

SLUMP: 24.5 MIN. AIR: 1 TO 6 AGG CORR FACTOR: 0.9
 RELEASE: 6000 PSI SHIP: 10,000 PSI PENETRATION: 25MM Max
 # OF REL. CYL'S: 10 MADE FROM RANDOM# 1 W/C RATIO: 0.3

SAMPLE #	LOT # / LAB #	AIR TEMP / TIME	CONC. TEMP	T50	SLUMP	VSI	PEN.	AIR %	BUCKET VOLUME	MEASURE WEIGHT	MEASURE WITH CONCRETE	W RA
INITIAL		9:43/90°	98°	2 ^{5sec}	28/28'	1	2 ^{mm}	5%	.25 ^{cu ft}	8.40 ^{lb}	42.55	.28
TEST02-SS	R#1	10:11 92	98	2 ^{5sec}	27/27	0	3	2%	.25 ^{cu ft}	8.40 ^{lb}	43.55	
	TRUCK #3											
	R#1											
	TRUCK #											
LOT SIZE	R-1		R-			R-						
LOAD NUMBER	20											
SERIAL NUMBER	LW6-LW10											
TEST LOAD NUMBER												

C42

TESTING TECH: BW/KK ES/KK

Time: 5am - Mon. 9/17
Temp: _____
Taken by: _____

1 DAY POUR: _____
2 DAY POUR: _____
OTHER: _____

STRESS INFORMATION SLIP



F.D.O.T. PROJECT

YES NO (CIRCLE ONE)

DATE 9-14-18

INITIAL TENSION 5000

JOB# B-1789

NUM OF STRANDS 13 C-3
C-2
C-1
B-3-B-2

FINAL TENSION 37,200

BED# 54"

JACK# _____ PAK# OR COIL# _____

LIST MARK#S ① C-3 ① B-3 ① C-2 ① B-2 ① C-1

PRODUCT TYPE II-Ashto

TYPE OF CABLE 6/10

MUST BE SIGNED BY PERSON FILLING OUT SLIP:

[Signature]

WILL NOT BE PROCESSED WITHOUT ALL PROPER INFORMATION AND SIGNATURE !

Stress Prepared by: [Signature]
Checked by: _____

Setup prepared by: [Signature]
Checked by: _____

SS - cable

REBAR REPORT

JOB # _____ B1789

BED # _____ 54M

MARK # _____ TEST

TYPE OF PRODUCT _____ TYPE II

BAR SIZE 3 HEAT # BR 1812076879

BAR SIZE 4 HEAT # BR 1812031001

BAR SIZE? 5 HEAT # ~~BR 18120~~ BR 5614503720

BAR SIZE _____ HEAT # _____

BAR SIZE _____ HEAT # _____

BAR SIZE _____ HEAT # _____

BAR SIZE _____ HEAT # _____

BAR SIZE _____ HEAT # _____

9/12/2018 9:34

JOB#:	B1789	
DATE:	9/12/2018	
BED #:	54M	
JACK #		
STRAND SIZE	.6 ST TEST	
COIL/PACK/REEL #	D430001-1D	0
	0	0
	0	0
	0	0
BED LENGTH (L):	3021.5	0
STRAND SIZE: (A)	0.2328	0
FINAL TEN. (P)	37200	0
PRE TEN. : (Pi)	5000	0
M.O.E. (E):	24.40	0
		0
		0

PRODUCT
TYPE II
MARK #
TEST
1-C3, 1-B3, 1-C2, 1-B2, 1-C1

CORRECTION INFO.	
Number of cable #	13
Exp. Conc temp @ Placement:	85
Ambient temperature(at):	85
Abutment rotation (ar):	N/A
Live end seating (les):	0.3438
Dead end slippage (des):	0.1093
anchorage movement:	0.625

ELONGATION

delta.a.t (Ptxdb/Pb)= 0
delt.(Pi x L)/(A x E) = 2.6596
delta'b.(PxL)/(AxE)= 17.128
delta'bed shortning
(bs/2)+(bs/#strand)= 0.3606

GROSS ELONG. 17.942

NET ELONG.	17 9/16
------------	---------

RANGE + 2.5%	18
RANGE - 2.5%	17 1/8

FORCE ADJUSTMENTS

Pb (P - Pi) = 32200
Pt(= 0
Par (arxAxE)/(L)= 0
Ples(lesxAxE)/(L)= 646.3326
Pdes no adj. required 0
Pbs (dbsxAxE)/(L)= 677.9161
TOTAL FORCE ADJ. 1324.2487
ADJUSTED FORCE = 33524.2487

JACKING FORCE = 38524

TOTAL ADJ. FORCE	38524
------------------	-------

AASHTO MAX =	46560
RANGE +2.5% =	39487
RANGE -2.5% =	37561

54M

PREPOUR PRODUCTION SHEET

JOB# B1789
 F.D.O.T.# TEST BEAM-SS
 CAST DATE 9-18-2018

PRODUCT Type II
 BED# 544
 MIX# 05-2056

COMMENT KEYS / = OK, O = ACCEPTABLE, X = NOT ACCEPTABLE

SERIAL #'S	LW6	LW7	LW8	LW9	LW10	
MARK #'S	C3	B3	C2	B2	C1	
DATE:						
INSPECTOR:						
WIDTH						
LENGTH						
HEIGHT						
CABLE HOLES						
"L" BAR HOLES						
CHAMFER						
SKEW						
INSERTS						
BLOCK OUTS						
FORM CLEANNESS						
PLATES FORM FACE						

COMMENTS No hay out

SERIAL #'S	LW6	LW7	LW8	LW9	LW10	
MARK #S	C3	B3	C2	B2	C1	
DATE:	9-17-18					
INSPECTOR:	KS					
REINFORCEMENT	O					
STEEL SPACING	O					
PLATES	NA					
CLEARANCE	O					
LINER	O					
LIFTING LOOPS	O					
SHEATHING	O					

COMMENTS Asked university about sheathed cables and if they were glad with it they said yes / B2, B3 had 2 extra cable in them to match other cable patterns in same pour extra cables were completely sheathed over from end to end.

SERIAL #'S	LW6	LW7	LW8	LW9	LW10	
MARK #S	C3	B3	C2	B2	C1	
INSPECTOR:	KS					
DATE :	9-17-18					
DROP IN PLATES	NA					
BLOCK OUTS	NA					
INSERTS	NA					
HEADERS	O					
LENGTH	O					
FORMS	O					

COMMENTS

 Job: 54-45FIB Date: Sep 18, 2018 Start:09:16 Disch:09:26
 Operator: W62342488 Duration/Wait: 10:56/1:30 Batch#:42079 Mixer#: 1
 Mix: 05-2056 Mix Name: 10k psi
 Required: 18.00 Batched: 6.00
 Amount: 6.00 CY
 PreWet: 70%
 Project#: FSU, Chloride:

Material	Bin	Moist/ABS%	Design	Target	Actual	%Err	*Note	Jogs
67 10-645	3	2.00/0.00	1360	8323	8300 Lb	-0.3	-----	8
SAND 11-057	1	4.50/0.00	1202	7537	7480 Lb	-0.8	-----	3
SUWANEE	2		703	4218	4190 Lb	-0.7	-----	5
STI FLYASH	4		167	1030	1025 Lb	-0.5	-C---	7
MB AE90	1		0.25	1.50	3.00 Oz	100.0	-----	
gLENIUM 7920	4		69.00	414.00	412.00 Oz	-0.5	-----	
DELVO	2		28.00	168.00	166.00 Oz	-1.2	-----	
Prewet				667	665 Lb	-0.3	-----	
Water				287	286 Lb	-0.3	-----	
Prewet Mixing			0:01		0:01 s			
Dry Mixing			0:01		0:01 s			
Wet Mixing			2:00		3:33 s			
Total Moisture:			240	1440	1436 Lb	-0.3		
Water/Cement:			0.276	0.275				

#44 / 6 meta max

71920 oz CNI



 Job: 54-45FIB Date: Sep 18, 2018 Start:09:34 Disch:09:46
 Operator: W62342488 Duration/Wait: 12:11/1:50 Batch#:42081 Mixer#: 1
 Mix: 05-2056 Mix Name: 10k psi
 Required: 18.00 Batched: 18.00
 Amount: 6.00 CY
 PreWet: 70%
 Project#: FSU, Chloride:

Material	Bin	Moist/ABS%	Design	Target	Actual	%Err	*Note	Jogs
67 10-645	3	1.90/0.00	1360	8315	8280 Lb	-0.4	-----	13
SAND 11-057	1	3.00/0.00	1202	7428	7380 Lb	-0.6	-----	3
SUWANEE	2		703	4218	4185 Lb	-0.8	-----	5
STI FLYASH	4		167	1035	1020 Lb	-1.4	-C---	7
MB AE90	1		0.25	1.50	2.00 Oz	33.3	-----	
gLENIUM 7920	4		69.00	414.00	416.00 Oz	0.5	-----	
DELVO	2		28.00	168.00	166.00 Oz	-1.2	-----	
Prewet				748	741 Lb	-0.9	-----	
Water				328	322 Lb	-1.8	-----	
Prewet Mixing			0:01		0:01 s			
Dry Mixing			0:01		0:01 s			
Wet Mixing			2:00		2:03 s			
Total Moisture:			240	1440	1432 Lb	-0.5		
Water/Cement:			0.276	0.275				

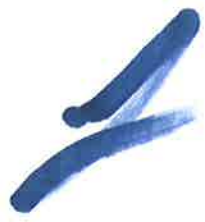
+444 Lb meta

+1920 oz CNI



 Job: 54-45FIB Date: Sep 18, 2018 Start:09:48 Disch:10:07
 Operator: W62342488 Duration/Wait: 19:08/0:55 Batch#:42083 Mixer#: 1
 Mix: 05-2056 Mix Name: 10k psi
 Required: 18.00 Batched: 18.00
 Amount: 6.00 CY
 PreWet: 70%
 Project#: FSU, Chloride:

Material	Bin	Moist/ABS%	Design	Target	Actual	%Err	*Note	Jogs
67 10-645	3	1.90/0.00	1360	8315	8300 Lb	-0.2	-----	7
SAND 11-057	1	3.00/0.00	1202	7428	7360 Lb	-0.9	-----	1
SUWANEE	2		703	4218	4185 Lb	-0.8	-----	5
STI FLYASH	4		167	1035	1060 Lb	2.4	-C---	7
MB AE90	1		0.25	1.50	3.00 Oz	100.0	-----	
gLENIUM 7920	4		69.00	414.00	412.00 Oz	-0.5	-----	
DELVO	2		28.00	168.00	166.00 Oz	-1.2	-----	
Prewet				748	741 Lb	-0.9	-----	
Water				328	322 Lb	-1.8	-----	
Prewet Mixing			0:01		0:01 s			
Dry Mixing			0:01		0:01 s			
Wet Mixing			2:00		2:02 s			
Total Moisture:			240	1440	1432 Lb	-0.5		
Water/Cement:			0.276	0.273				



BEAM PLACEMENT DIAGRAM

JOB NO.: B1789
 FDOT NO.: TEST BEAM-SS
 MIX DESIGN: 05-2056

BED: 54M
 PRODUCT: Type II

INSPECTOR: JUB
 TEST LOAD(s): 12, 3, 4, 5
 TOTAL YARDS: 14.95

DATE CAST: 9-18-18
 COVERED? OR CUR. COMPOUND
 CUR EXP DATE

S/N MARK	LW7 B3 ✓	LW8 C2 ✓	LW9 B2 ✓	LW10 C1 ✓
767-Truck#2 766-9:46	765- 10:00 10:00 → 766-1 1/2 yd - 10:02	765-3yds - 10:09 767-10:15	767-10:27	767 1yd 10:27 765-10:33-10:38

W/C MAX

0.3

READY MIX TRUCK(S) MEET QCM BATCH PLANT CRITERIA

Truck #1 - Rejected.

CHECK LIST

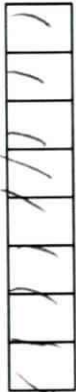


TABLE SHEET
STRESS
REBAR/SPIRAL
STRESS CALCS
STRESS RESULTS
PREPOUR
BATCH TICKETS
CASTING DIAGRAM

JOB # B1826
FDOT # 0
PRODUCT TYPE TYPE II
MARK # 1@E1,1@E3,1@E5,1@E4,1@E2
SERIAL # UC1 - UC5
BED # 42S
MIX DESIGN 05-1880-03

Check Off!

Cast Date:

21/2.13/2.18.20

Entered in Great Production:

YBY

Entered in MAC (initials)

n/A

Scanned:

Ready To File:

Sample #'s

UC01

0

UC02

UC03

TABLE SHEET

PROJECT NO. : B1826
 0
 BED # : 42S
 DATE CAST : 2-11-20

PRODUCT : TYPE II
 SERIAL NOS. : UC1 - UC5
 MIX DESIGN : 05-1880-03

CLASS : CLASS VI 8500 PSI

CY TOTAL : 30.25
 DAY 1 : 28.75
 DAY 2 : 0.50
 DAY 3 : 1

MIX DESIGN TOLERANCES			
SLUMP : <u>24.5 Min.</u>	AIR : <u>0 TO 6</u>	AGG CORR FACTOR : <u>0.8</u>	
RELEASE : <u>6800 PSI</u>	SHIP : <u>8500 PSI</u>	PENATRATION : <u>25MM Max</u>	
# OF REL. CYL'S : <u>8</u>	MADE FROM RANDOM# <u>1</u>	W/C : RATIO <u>0.33</u>	

SAMPLE #	LOT # / LAB #	AIR TEMP / TIME	CONC. TEMP	T50	SLUMP	VSI	PEN.	AIR %	BUCKET VOLUME	MEASURE WEIGHT	MEASURE WITH CONCRETE	W/C RATIO
Q.C. DAY 1	INITIAL											
UC01	R#1 Truck 1	73 / 10:00	85	3	32 / 31	1	12	4.0	.25	8.45	43.40	.26
21w SEP 20-024	TRUCK #2	73 / 10:10	85	3	31 1/2 / 31	1	12	2.4	.25	8.45	43.65	.27
	# 3	73 / 10:23	85	3	31 / 30	1	3	2.00	.25	8.45	44.20	.27
	# 4	74 / 10:32	86	3	33 1/2 / 32	1	20	1.3	.25	8.45	44.60	.26
	TRUCK #5	/			/				.25	8.45		
	# 6	/			/							
	R-		R-			R-						
LOT SIZE												
LOAD NUMBER												
SERIAL NUMBER												
ST LOAD NUMBER												

TESTING TECH: JR
 REMARKS : _____

Q/C NOTIFIED BATCH PLANT OF TEST RESULTS ? (YES) (NO)

TABLE SHEET

PROJECT NO. : B1826
 BED # : 42S
 DATE CAST : 2-13-20

PRODUCT : TYPE II
 SERIAL NOS. : UC1 - UC5
 MIX DESIGN : 05-1880-03
 CLASS : CLASS VI 8500 PSI

CY TOTAL : 30.25
 DAY 1 : 28.75
 DAY 2 : 0.50
 DAY 3 : 1

MIX DESIGN TOLERANCES

SLUMP : 24.5 Min. AIR : 0 TO 6 AGG CORR FACTOR : 0.8
 RELEASE : 4500 SHIP : SS00 PENATRATION : 25MM Max
 # OF REL. CYL'S : 16 MADE FROM RANDOM# 1 W/C : RATIO : 0.33

SAMPLE #	LOT # / LAB #	AIR TEMP / TIME	CONC. TEMP	T50	SLUMP	VSI	PEN.	AIR %	BUCKET VOLUME	MEASURE WEIGHT	MEASURE WITH CONCRETE	W/C RATIO
Q.C. DAY 2	INITIAL											
UC02	R#1	81/12:33	89	2	20/20	0	0	5.4	.25	8.45	42.25	.43
	TRUCK #											
	R#2											
	TRUCK #											
		R-	R-	R-								
LOT SIZE												
LOAD NUMBER												
SERIAL NUMBER												
ST LOAD NUMBER												

TESTING TECH: JR
 REMARKS :

Q/C NOTIFIED BATCH PLANT OF TEST RESULTS ? (YES) (NO)

Time: _____
Temp: _____
Taken by: _____

1 DAY POUR: _____
2 DAY POUR: _____
OTHER: _____

STRESS INFORMATION SLIP



F.D.O.T. PROJECT YES NO (CIRCLE ONE)

DATE 2.10.20

INITIAL TENSION 5.00

JOB# B1826

NUM OF STRAND 11

FINAL TENSION 36,000

BED# 425

JACK# _____

PAK# OR COIL# _____

LIST MARK#S E1 UC1 E3 UC2 E5 UC3 E4 UC4 E2 UC5

PRODUCT TYPE II Post Beam

TYPE OF CABLE Stainless Steel

MUST BE SIGNED BY PERSON FILLING OUT SLIP:

DT

WILL NOT BE PROCESSED WITHOUT ALL PROPER INFORMATION AND SIGNATURE !

Stress Prepared by: Jane
Checked by: _____

Setup prepared by: [Signature]
Checked by: _____

4 Better Row No (-2)
7 Post O/D (-10)

REBAR REPORT

JOB # B1826

BED # 42S

MARK # E1, E3, E5, E4, E2

TYPE OF PRODUCT Type II

BAR SIZE 3 HEAT # 3701001 64714

BAR SIZE 4 HEAT # 370100 194861

BAR SIZE 5 HEAT # BR 1812037670

BAR SIZE _____ HEAT # _____

BAR SIZE _____ HEAT # _____

BAR SIZE _____ HEAT # _____

BAR SIZE _____ HEAT # _____

BAR SIZE _____ HEAT # _____

DURA-STRESS INC. STRAND STRESS REPORT

New

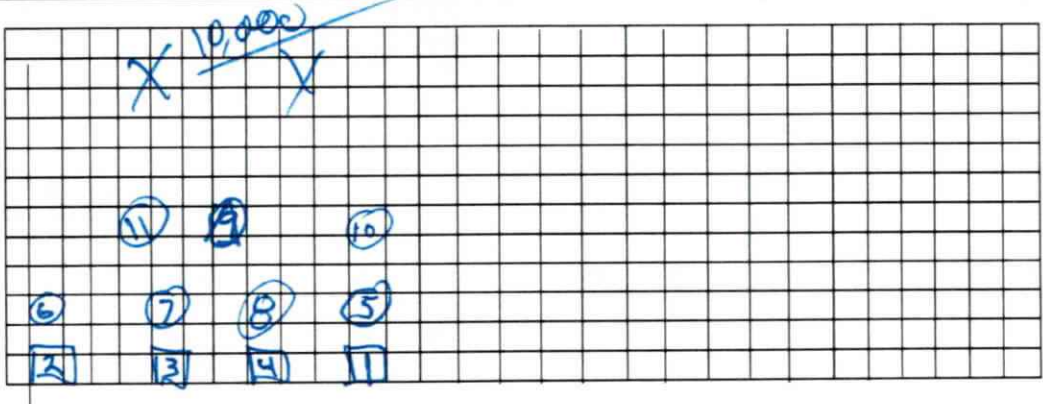
DATE:	2/10/2020	ITEM NO'S:	Type II	MARK #
PROJECT NO.	B1826			E1, E3, E5, E4, E2
PRODUCT	Type II			
BED NO.	42S			
NO. OF CABLE:	117	JACK CAL DATES:	11-18-17	
TECHNICIAN:	DT	Ambient temperature(at):	60	
DATE:	2-10-20	AMBIENT TEMP:	61	
		JACK #:	T-12	
		CABLE TYPE:	.600 / 10" KSI LR S.S. Bottom = 36700	

CHUCK SLIPPAGE			
LIVE		DEAD	
$3/8$ $7/8$ $3/8$ $1/4$			
		$1/8$ $1/8$ $1/8$ $1/8$	
AVERAGE:		AVERAGE:	
TOTAL:			

FINAL TENSION	36697
FINAL ELONGATION	21 7/8
+2.5%	22 7/16
-2.5%	21 3/8
AASHTO MAX =	49810

IF TARGET = AASHTO ELONGATION MAY NOT WORK

GAUGE	ELO	GAUGE	ELO	GAUGE	ELO	GAUGE	ELO	GAUGE	ELO	GAUGE	ELO	GAUGE	ELO
1	36700	2 1/4	12			23		34		45		56	
2	36700	2 1 3/8	13			24		35		46		57	
3	36700	2 1/2	14			25		36		47		58	
4	36700	2 1/4	15			26		37		48		59	
5	36750	2 0 3/4	16			27		38		49		60	
6	36750	2 0 3/4	17			28		39		50		61	
7	36750	2 0 1/2	18			29		40		51		62	
8	36750	2 1/4	19			30		41		52		63	
9	36750	2 1/4	20			31		42		53		64	
10	36750	2 1/4	21			32		43		54		65	
11	36750	2 0 1/2	22			33		44		55		66	



42S

2/10/2020 7:19

JOB#:	B1826	
DATE:	2/10/2020	
BED #:	42S	
JACK #		
STRAND SIZE	.600 / 10" KSI LR S.S.	
COIL/PACK/REEL #	D430018-2	0
	0	0
	0	0
	0	0
BED LENGTH (L):	3818.5	0
STRAND SIZE: (A)	0.2306	0
FINAL TEN. (P)	36000	0
PRE TEN. : (Pi)	5000	0
M.O.E. (E):	23.90	0
		0
		0

PRODUCT
Type II
MARK #
E1, E3, E5, E4, E2

CORRECTION INFO.	
Number of cable #	11
Exp. Conc temp @ Placement:	78
Ambient temperature(at):	60
Abutment rotation (ar):	N/A
Live end seating (les):	0.1875
Dead end slippage (des):	0.125
anchorage movement:	0.5

ELONGATION
 $\Delta a.t (Pt \times db / Pb) = 0$
 $\Delta t. (Pi \times L) / (A \times E) = 3.4642$
 $\Delta b.(PxL) / (Ax E) = 21.4782$
 $\Delta b / \text{bed shortning} (bs/2) + (bs/\#strand) = 0.2955$

FORCE ADJUSTMENTS
 $Pb (P - Pi) = 31000$
 $Pt(= 0$
 $Par (ar \times Ax E) / (L) = 0$
 $Ples (les \times Ax E) / (L) = 270.6236$
 $Pdes \text{ no adj. required} = 0$
 $Pbs (dbs \times Ax E) / (L) = 426.5028$
 TOTAL FORCE ADJ. = 697.1264
 ADJUSTED FORCE = 31697.1264

GROSS ELONG. 22.086

JACKING FORCE = 36697

NET ELONG.	21 7/8
------------	--------

36700

TOTAL ADJ. FORCE	36697
------------------	-------

RANGE + 2.5%	22 7/16
RANGE - 2.5%	21 3/8

AASHTO MAX =	49810
RANGE +2.5% =	37614
RANGE -2.5% =	35780

21.90	22.45	21.35
-------	-------	-------

New

42S

2/10/2020 7:20

JOB#:	B1826	
DATE:	2/10/2020	
BED #:	42S	
JACK #		
STRAND SIZE	.600 / 10" KSI LR S.S.	
COIL/PACK/REEL #	D430001-1D	0
	0	0
	0	0
	0	0
BED LENGTH (L):	3818.5	0
STRAND SIZE: (A)	0.2328	0
FINAL TEN. (P)	36000	0
PRE TEN. : (Pi)	5000	0
M.O.E. (E):	24.40	0
		0
		0

PRODUCT
Type II
MARK #
E1, E3, E5, E4, E2

CORRECTION INFO.	
Number of cable #	11
Exp. Conc temp @ Placement:	78
Ambient temperature(at):	60
Abutment rotation (ar):	N/A
Live end seating (les):	0.1875
Dead end slippage (des):	0.125
anchorage movement:	0.5

ELONGATION
 $\Delta a t (P_{txdb}/P_b) = 0$
 $\Delta t (P_i \times L)/(A \times E) = 3.3612$
 $\Delta a' b (P \times L)/(A \times E) = 20.8392$
 $\Delta a' \text{bed shortning} (bs/2) + (bs/\#strand) = 0.2955$

FORCE ADJUSTMENTS
 $P_b (P - P_i) = 31000$
 $P_t(= 0$
 $P_{ar} (ar \times A \times E)/(L) = 0$
 $P_{les} (les \times A \times E)/(L) = 278.921$
 $P_{des} \text{ no adj. required} = 0$
 $P_{bs} (dbs \times A \times E)/(L) = 439.5796$
 TOTAL FORCE ADJ. = 718.5006
 ADJUSTED FORCE = 31718.5006

GROSS ELONG 21.447

JACKING FORCE = 36719

NET ELONG.	21 1/4
------------	--------

TOTAL ADJ. FORCE	36719
------------------	-------

RANGE + 2.5%	21 13/16
RANGE - 2.5%	20 3/4

AASHTO MAX =	50285
RANGE +2.5% =	37637
RANGE -2.5% =	35801

42S

21.26	21.79	20.73
-------	-------	-------

CIP

PREPOUR PRODUCTION SHEET

JOB# B1826
 F.D.O.T.# 0
 CAST DATE 11-20-2000

PRODUCT TYPE II
 BED# 42S
 MIX # 05-1880-03

COMMENT KEYS / = OK, O = ACCEPTABLE, X = NOT ACCEPTABLE

SERIAL #S	UC1	UC2	UC3	UC4	UC5	
MARKS	E1	E3	E5	E4	E2	
DATE						
INSPECTOR						
WIDTH						
LENGTH						
HEIGHT						
CABLE HOLES						
REINFORCE						
PLATES						
BLACK OUTS						
FORM CLEANNESS						
REINFORCING FACE						

COMMENTS

SERIAL #S	UC1	UC2	UC3	UC4	UC5	
MARKS	E1	E3	E5	E4	E2	
DATE						
INSPECTOR						
REINFORCEMENT						
STEEL BRACING						
PLATES						
CLEARANCE						
REINFORCING						
CASTING COFFERS						
SHEATHING						

COMMENTS

SERIAL #S	UC1	UC2	UC3	UC4	UC5	
MARKS	E1	E3	E5	E4	E2	
DATE						
INSPECTOR						
BROCK IN PLATES						
BLACK OUTS						
REINFORCE						
WIDTH						
LENGTH						

COMMENTS

Job: 42BEM1 Date: Feb 11, 2020 Start:09:48 Disch:09:54
 Operator: W62342488 Duration/Wait: 7:23/1:00 Batch#:10076 Mixer#: 1
 Mix: 05-1880-03 Mix Name: CLASS VI 8500
 Required: 24.00 Batched: 6.00
 Amount: 6.00 CY
 Moist Target:(MANUAL) DryMix:-0.04 WetMix:12.62 Disch:13.03

Material	Bin	Moist/ABS%	Design	Target	Actual	%Err	*Note	Jogs
67 10-645	2	3.20/0.00	1308	8099	8125 Lb	0.3	-----	
SAND 11-057	1	4.45/0.00	1264	7922	7860 Lb	-0.8	-----	7
SUWANEE tl-2	1		735	4410	4390 Lb	-0.5	-----	2
ARGOS FLYASH	3		165	1010	1102 Lb	9.1	OC---	7
DAREX	1		1.00	6.00	6.00 Oz	0.0	-----	
ZYLA 610	2		18.00	108.00	108.00 Oz	0.0	-----	
ADVA 600	3		54.00	324.00	326.00 Oz	0.6	-----	
Water				911	824 Lb	-9.5	H----	
Trim Water					23 Lb			
HoldBack				0	90 Lb			
Dry Mixing			0:01		0:01 s			
Wet Mixing			2:00		2:54 s			
Total Moisture:			250	1500	1434 Lb	-4.4		
Water/Cement:			0.278	0.257/0.261	(MANUAL/TRIM)			

#1 Regor
JR

 Job: 42BEAM Date: Feb 11, 2020 Start:09:54 Disch:09:59
 Operator: W62342488 Duration/Wait: 6:07/0:05 Batch#:10077 Mixer#: 1
 Mix: 05-1880-03 Mix Name: CLASS VI 8500
 Required: 24.00 Batched: 12.00
 Amount: 6.00 CY
 Moist Target: (MANUAL) DryMix:-0.22 WetMix:13.12 Disch:13.17

Material	Bin	Moist/ABS*	Design	Target	Actual	%Err	*Note	Jogs
67 10-645	2	3.20/0.00	1308	8099	8080 Lb	-0.2	-----	5
SAND 11-057	1	4.45/0.00	1264	7922	7875 Lb	-0.6	-----	5
SUWANEE t1-2	1		735	4410	4460 Lb	1.1	O----	3
ARGOS FLYASH	3		165	940	930 Lb	-1.1	-C----	1
DAREX	1		1.00	6.00	6.00 Oz	0.0	-----	
ZYLA 610	2		18.00	108.00	110.00 Oz	1.9	-----	
ADVA 600	3		54.00	324.00	324.00 Oz	0.0	-----	
Water				911	836 Lb	-8.2	H----	
Trim Water					12 Lb			
HoldBack				0	75 Lb			
Dry Mixing			0:01		0:01 s			
Wet Mixing			2:00		2:04 s			
Total Moisture:			250	1500	1434 Lb	-4.4		
Water/Cement:			0.278	0.264/0.266	(MANUAL/TRIM)			


 A handwritten signature consisting of a large, stylized 'A' followed by '#2' and 'Mike' written below it.

Job: 42BEAM Date: Feb 11, 2020 Start:10:06 Disch:10:17
 Operator: W62342488 Duration/Wait: 11:23/5:20 Batch#:10078 Mixer#: 1
 Mix: 05-1880-03 Mix Name: CLASS VI 8500
 Required: 24.00 Batched: 18.00
 Amount: 6.00 CY
 Moist Target: (MANUAL) DryMix:0.34 WetMix:12.97 Disch:13.19

Material	Bin	Moist/ABS%	Design	Target	Actual	%Err	*Note	Jogs
67 10-645	2	3.20/0.00	1308	8099	8210 Lb	1.4	O----	
SAND 11-057	1	4.45/0.00	1264	7922	7915 Lb	-0.1	-----	7
SUWANEE t1-2	1		735	4410	4372 Lb	-0.9	-----	3
ARGOS FLYASH	3		165	1028	1036 Lb	0.8	-C---	
DAREX	1		1.00	6.00	7.00 Oz	16.7	-----	
ZYLA 610	2		18.00	108.00	110.00 Oz	1.9	-----	
ADVA 600	3		54.00	324.00	326.00 Oz	0.6	-----	
Water				911	840 Lb	-7.8	H----	
Trim Water					6 Lb			
HoldBack				0	75 Lb			
Dry Mixing			0:01		0:01 s			
Wet Mixing			2:00		7:22 s			
Total Moisture:			250	1500	1438 Lb	-4.1		
Water/Cement:			0.278	0.265			(MANUAL/TRIM)	

#3

Truck
765

B9

 Job: 42BEAM Date: Feb 11, 2020 Start:10:18 Disch:10:27
 Operator: W62342488 Duration/Wait: 9:35/3:30 Batch#:10079 Mixer#: 1
 Mix: 05-1880-03 Mix Name: CLASS VI 8500
 Required: 30.00 Batched: 24.00
 Amount: 6.00 CY
 Moist Target:(MANUAL) DryMix:0.42 WetMix:13.04 Disch:13.24

Material	Bin	Moist/ABS*	Design	Target	Actual	%Err	*Note	Jogs
67 10-645	2	3.20/0.00	1308	8099	8075 Lb	-0.3	-----	7
SAND 11-057	1	4.45/0.00	1264	7922	7885 Lb	-0.5	-----	1
SUWANEE t1-2	1		735	4410	4378 Lb	-0.7	-----	7
ARGOS FLYASH	3		165	1022	1078 Lb	5.5	OC---	
DAREX	1		1.00	6.00	6.00 Oz	0.0	-----	
ZYLA 610	2		18.00	108.00	110.00 Oz	1.9	-----	
ADVA 600	3		54.00	324.00	324.00 Oz	0.0	-----	
Water				911	840 Lb	-7.8	H----	
Trim Water					6 Lb			
HoldBack				0	75 Lb			
Dry Mixing			0:01		0:01 s			
Wet Mixing			2:00		5:33 s			
Total Moisture:			250	1500	1432 Lb	-4.5		
Water/Cement:			0.278	0.261/0.263	(MANUAL/TRIM)			

Potter

#4

BA

Day 1

Day 1

BEAM PLACEMENT DIAGRAM

JOB NO.: B1826
 FDOT NO.: 0
 MIX DESIGN: 05-1880-03
 CLASS VI 8500 PSI

BED: 42S
 PRODUCT: TYPE II

INSPECTOR: Kelly
 TEST LOAD(s):
 TOTAL YARDS: 30.25

DATE CAST: 2.11.20

COVERED? OR
 CUR COMPOUND
 CUR EXP DATE

S/N	UC1	UC2	UC3	UC4	UC5
MARK	E1	E3	E5	E4	E2
	42' 0"	42' 0"	42' 0"	42' 0"	42' 0"
	① 10:03 Start	① 10:13 End ② 10:12 start	② Continued ③ 10:24 Start	③ Continued ② 10:30 End	④ 10:35 Start 10:48 End ③ 10:36 Start End
	6.05	6.05	6.05	6.05	6.05

W/C MAX

0.33

READY MIX TRUCK(S) MEET QCM BATCH PLANT CRITERIA

 Job: CLASS2 Date: Feb 13, 2020 Start:12:43 Disch:12:47
 Operator: W62342488 Duration/Wait: 4:20/0:00 Batch#:58786 Mixer#: 1
 Mix: CLASS2MILES Mix Name: CLASS2MILES
 Required: 5.00 Batched: 5.00
 Amount: 2.00 CY
 PreWet: 70%

Material	Bin	Moist/ABS%	Design	Target	Actual	%Err	*Note	Jogs
67 10-645	5	2.80/0.00	1765	3629	3620 Lb	-0.2	-----	4
SAND 11-057	1	4.35/0.00	1385	2891	2880 Lb	-0.4	-----	3
SUWANEE	2		490	980	965 Lb	-1.5	-----	5
ARGOS FLYASH	4		122	259	250 Lb	-3.5	-C---	1
MB AE90	1		0.61	1.22	5.00 Oz	309.8	O----	
gLENIUM 7920	4		27.54	55.08	52.00 Oz	-5.6	-----	
DELVO	2		18.00	36.00	34.00 Oz	-5.6	-----	
Prewet				222	216 Lb	-2.7	-----	
Water				101	124 Lb	22.8	O----	
Dry Mixing			0:01		0:01 s			
Wet Mixing			2:00		2:01 s			
Total Moisture:			268	536	559 Lb	4.2		
Water/Cement:			0.438	0.460				

Job: CLASS2 Date: Feb 13, 2020 Start:13:05 Disch:--1--
 Operator: W62342488 Duration/Wait: 3:04/0:00 Batch#:58788 Mixer#: 1
 Mix: CLASS2MILES Mix Name: CLASS2MILES *ABORTED*
 Required: 3.00 Batched: 3.00
 Amount: 3.00 CY
 PreWet: 70%

Material	Bin	Moist/ABS*	Design	Target	Actual	%Err	*Note	Jogs
67 10-645	5	3.60/0.00	1765	5486	5440 Lb	-0.8	-----	4
SAND 11-057	1	5.50/0.00	1385	4384	4380 Lb	-0.1	-----	
SUWANEE	2		490	1470	1465 Lb	-0.3	-----	4
ARGOS FLYASH	4		122	377	380 Lb	2.4	-C----	5
MB AE90	1		0.61	1.83	7.00 Oz	282.5	O-----	
gLENIUM 7920	4		27.54	82.62	80.00 Oz	-3.2	-----	
DELVO	2		18.00	54.00	52.00 Oz	-3.7	-----	
Prewet				269	259 Lb	-3.7	-----	
Water				126	135 Lb	7.1	-----	
Dry Mixing			0:01		0:01 s			
Wet Mixing			2:00		1:13 s			
Total Moisture:			268	804	811 Lb	0.9		
Water/Cement:			0.438	0.443				

#2
 Roger

 Job: CLASS2 Date: Feb 13, 2020 Start:12:18 Disch:12:23
 Operator: W62342488 Duration/Wait: 5:12/0:05 Batch#:58785 Mixer#: 1
 Mix: CLASS2MILES Mix Name: CLASS2MILES
 Required: 3.00 Batched: 3.00
 Amount: 3.00 CY
 PreWet: 70%

Material	Bin	Moist/ABS%	Design	Target	Actual	%Err	*Note	Jcgs
67 10-645	5	2.80/0.00	1765	5443	5400 Lb	-0.8	-----	4
SAND 11-057	1	4.35/0.00	1385	4336	4300 Lb	-0.8	-----	2
SUWANEE	2		490	1470	1555 Lb	5.8	0----	7
ARGOS FLYASH	4		122	281	300 Lb	6.8	-C----	2
MB AE90	1		0.61	1.83	4.00 Cz	118.6	0----	
gLENIUM 7920	4		27.54	82.62	80.00 Cz	-3.2	-----	
DELVO	2		18.00	54.00	52.00 Cz	-3.7	-----	
Prewet				333	327 Lb	-1.8	-----	
Water				148	149 Lb	0.7	-----	
Dry Mixing			0:01		0:01 s			
Wet Mixing			2:00		2:07 s			
Total Moisture:			268	804	802 Lb	-0.2		
Water/Cement:			0.438	0.433				

1

Day 2

Day 2

BEAM PLACEMENT DIAGRAM

Dave - Truck 1, 2

Kelly Truck 3

2.13.20

JOB NO.: B1826
FDOT NO.: 0
MIX DESIGN: 05-1880-03
CLASS VI 8500 PSI

BED: 42S
PRODUCT: TYPE II

INSPECTOR: Kelly Truck 3
TEST LOAD(s): Any
TOTAL YARDS: 30.25

DATE CAST: 2.13.20
COVERED? OR CUR. COMPOUND
CUR EXP DATE

S/N	UC1	UC2		
MARK	E1	E3		
	42' 0"	42' 0"		
	①	①		
		② Sent Away		
		③		
	0.25	0.25		

W/C MAX

0.33

READY MIX TRUCK(S) MEET QCM BATCH PLANT CRITERIA

Job: 42 Date: Feb 18, 2020 Start:12:38 Disch:12:47
Operator: W62342488 Duration/Wait: 11:08/3:50 Batch#:58933 Mixer#: 1
Mix: CLASS2MILES Mix Name: CLASS2MILES
Required: 6.00 Batched: 6.00
Amount: 6.00 CY
PreWet: 70%

Material	Bin	Moist/ABS%	Design	Target	Actual	%Err	*Note	Jogs
67 10-645	5	2.40/0.00	1765	10844	10860 Lb	0.1	-----	7
SAND 11-057	1	4.30/0.00	1385	8667	8620 Lb	-0.5	-----	3
SUWANEE	2		490	2940	2930 Lb	-0.3	-----	7
ARGOS FLYASH	4		122	742	745 Lb	0.4	-C---	
DAREX	1		0.61	3.66	9.00 Oz	145.9	O----	
ADVA 600	4		27.54	165.24	164.00 Oz	-0.8	-----	
ZYLA 610	2		18.00	108.00	108.00 Oz	0.0	-----	
Prewet				698	685 Lb	-1.9	-----	
Water				312	314 Lb	0.6	-F---	
Dry Mixing			0:01		0:01 s			
Wet Mixing			2:00		2:47 s			
Total Moisture:			268	1698	1609 Lb	0.1		
Water/Cement:			0.438	0.438				

[Handwritten signature]

#1

LEWIS

Day 3

Day 3

BEAM PLACEMENT DIAGRAM

JOB NO.: B1826
FDOT NO.: 0
MIX DESIGN: 05-1880-03
CLASS VI 8500 PSI

BED: 42S
PRODUCT: TYPE II

INSPECTOR: LV
TEST LOAD(s):
TOTAL YARDS: 30.25

DATE CAST: 2-18-20
COVERED? OR CUR COMPOUND
CUR EXP DATE

S/N	UC3	UC4	UC5
MARK	E5	E4	E2
	42' 0"	42' 0"	42' 0"
	① 766-1256 →	① →	① → 108
	0.33	0.33	0.33

W/C MAX 0.33

READY MIX TRUCK(S) MEET QCM BATCH PLANT CRITERIA

PROJECT NO.: B1826
0

BED #: 42S

DATE DETENSIONED: 2-13-20

DATE CAST: 2-11-20

TYPE: TYPE II

CYLINDER PSI: 6836/6958
REQUIRED RELEASE: 6800

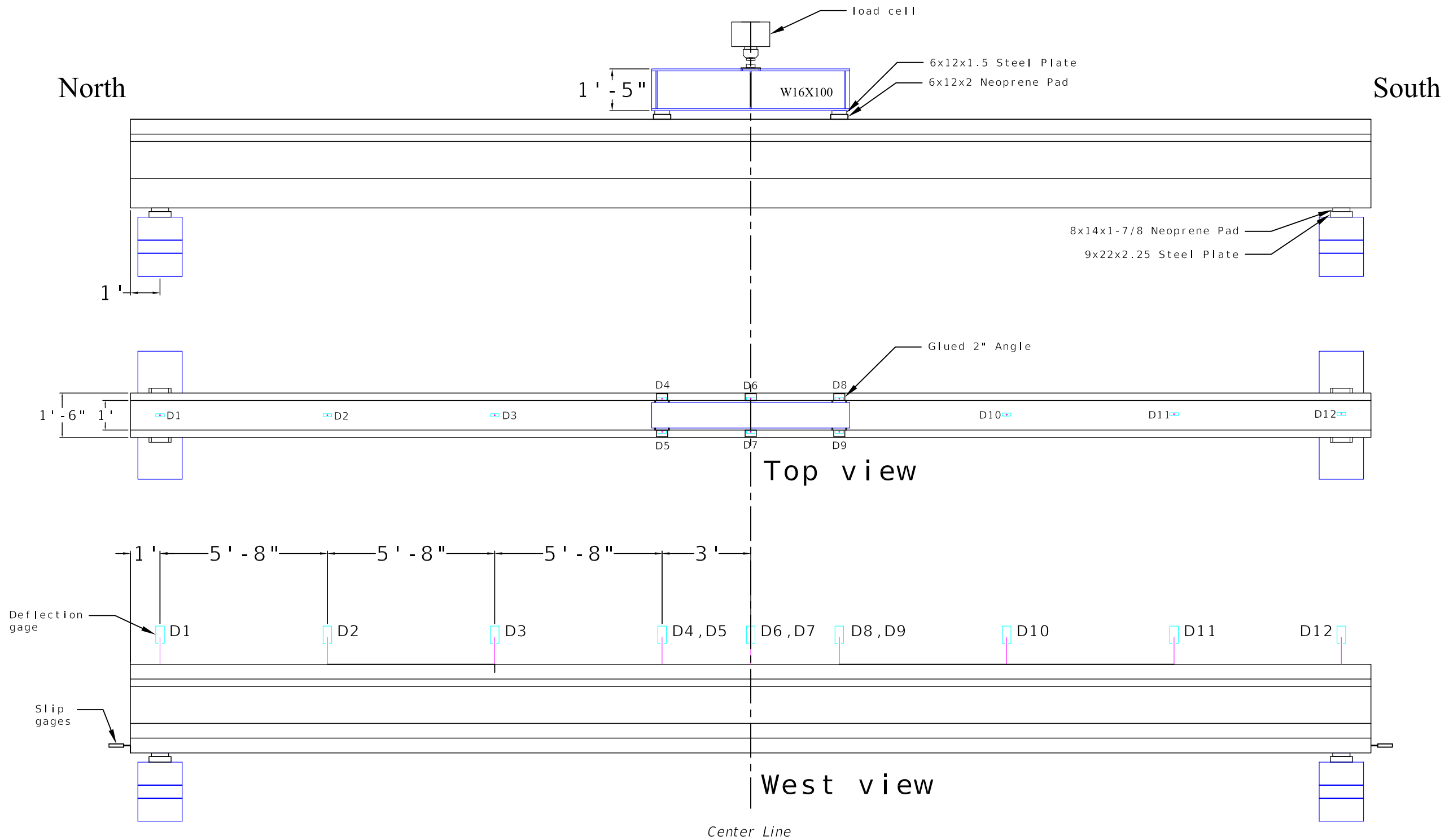
SERIAL NO.:	UC1	UC2	UC3	UC4	UC5	
MARK NO.:	E1	E3	E5	E4	E2	0
SIDE LENGTH RIGHT:	41 11 ³ / ₄	42-0	42-	42-	42-0 ¹ / ₄	
SIDE LENGTH LEFT:	41 11 ³ / ₄	42-	42-	41-11 ⁷ / ₈	42-0	
AVG. LENGTH:						
DESIGN LENGTH :	42' 0"	42' 0"	42' 0"	42' 0"	42' 0"	
HORIZONTAL ALIGNMENT	0	0	0	0	0	
CAMBER (INCH)	1/4"	1/6"	0	0	0	
REMARKS:	FSU					

Appendix D – Test setup and instrumentation plans

This appendix contains drawings of the test setup and instrumentation plans for the tested girders. It includes drawings for the flexural and shear tests. Only external instrumentation (done at the lab) is shown. Table D-1 shows the testing matrix. Some girders were tested more than one time. One (x) indicates the first test, two (xx) indicates the second test type, and three (xxx) indicates the third test type.

Table D-1 Testing matrix

Girder designation	Flexural test		Shear test (composite)		
	Non-composite	Composite	End 1	End 2	Midspan
A1	x				
A2			x	xx	xxx
A3		x	xx	xxx	
B2		x			
B3	x		xx	xxx	
C1	x				
C2		x			
C3		x			
E1		x			
E2		x			
E3		x			
E4		x			
E5		x			



Notes:-

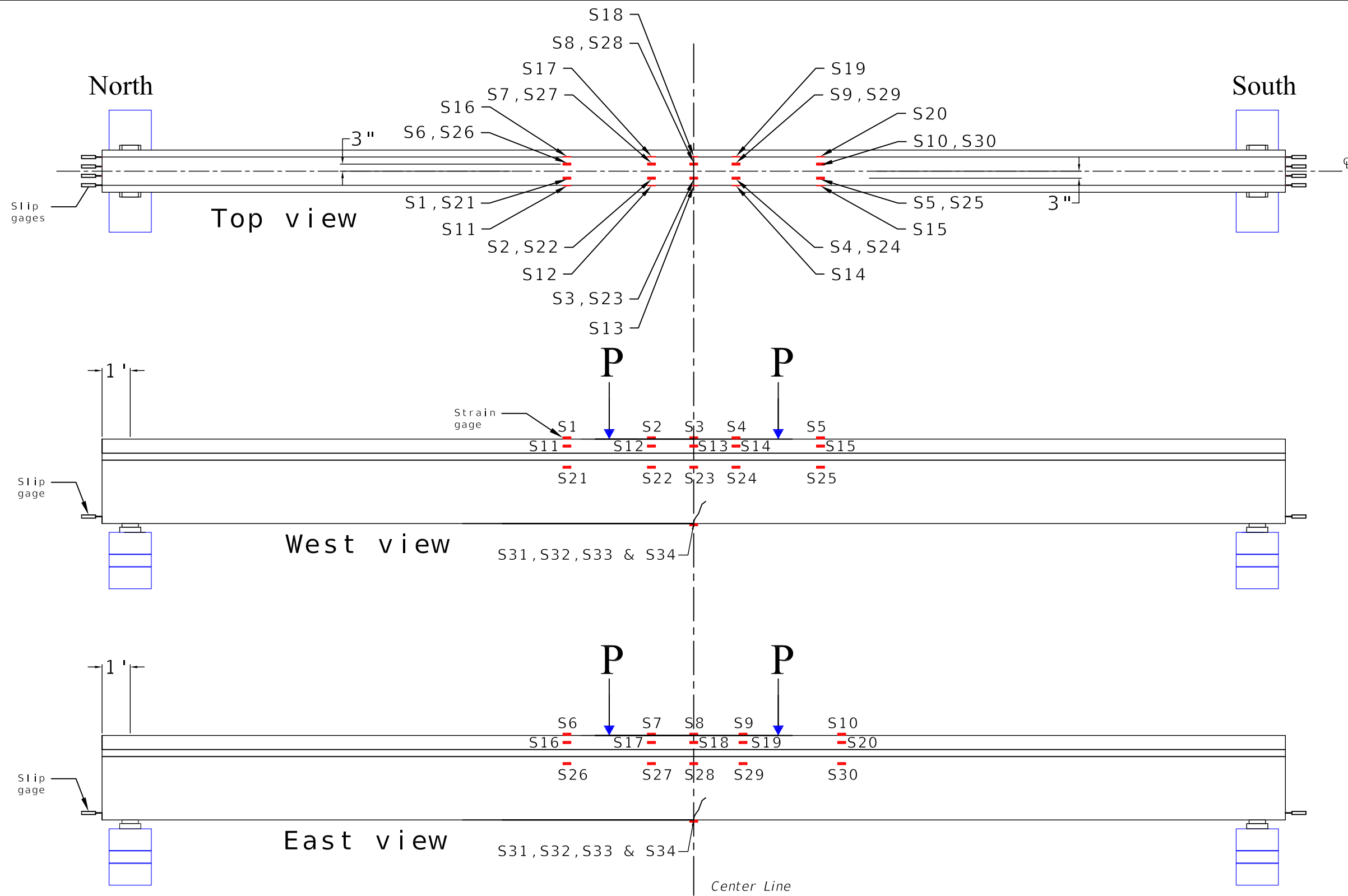
1. All dimensions are to center of deflection gages.
2. All deflection gages are symmetrical about girder's center line.
3. D4, D5, D6, D7, D8 and D9 may need an angle glued to top flange of specimen due to interference from the spreader beam supports.
4. 12.5 mm slip gages shall be used for all strand slip locations. See Sheet No. 4 for slip gages locations.
5. See Sheet No. 2 for strain gages locations.

Stainless Steel Strands and Lightweight Concrete for Pretensioned Concrete Girders

FAMU-FSU College of Engineering

Flexural test setup and instrumentation plan for non-composite girders (Girders A1, B3, and C1)

Sheet No.1



Notes:-

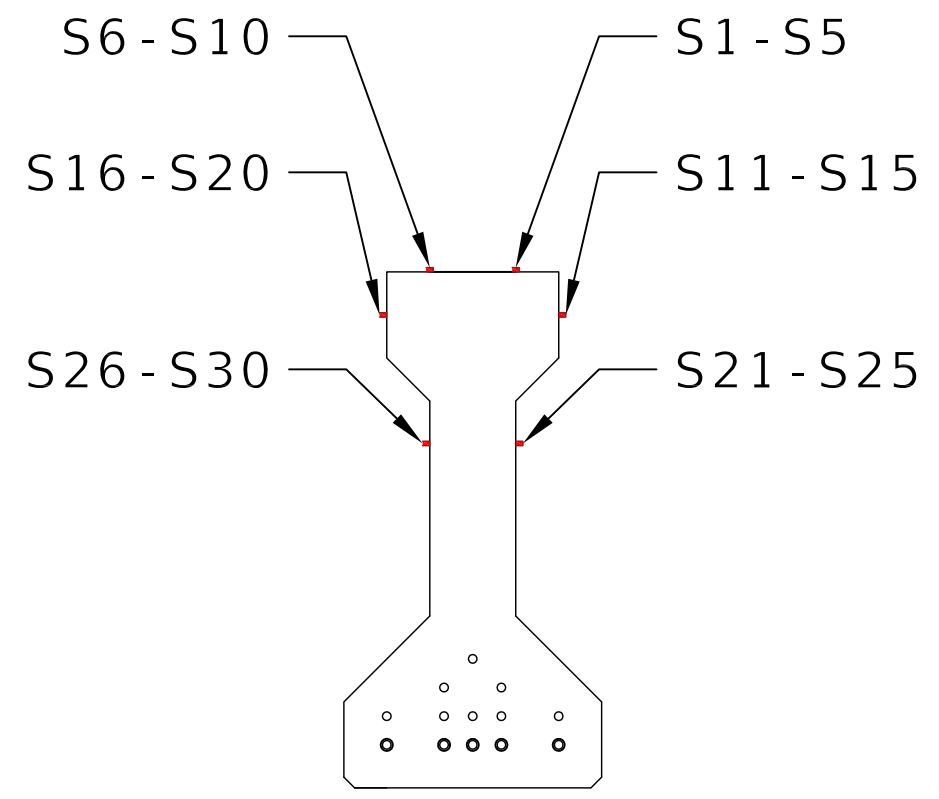
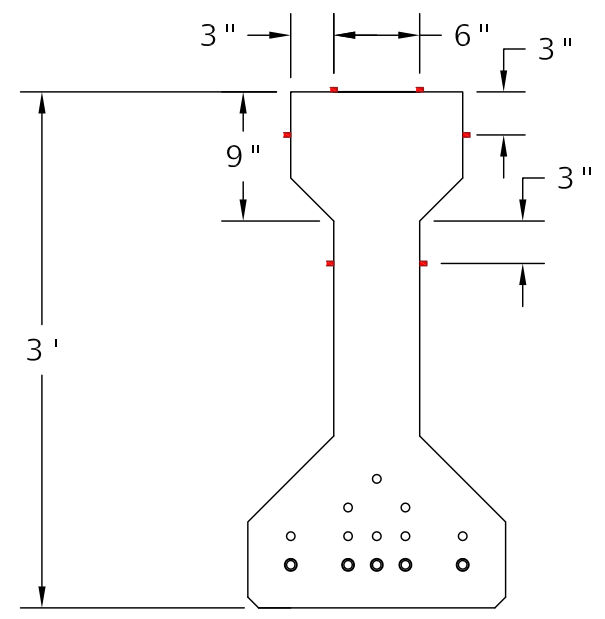
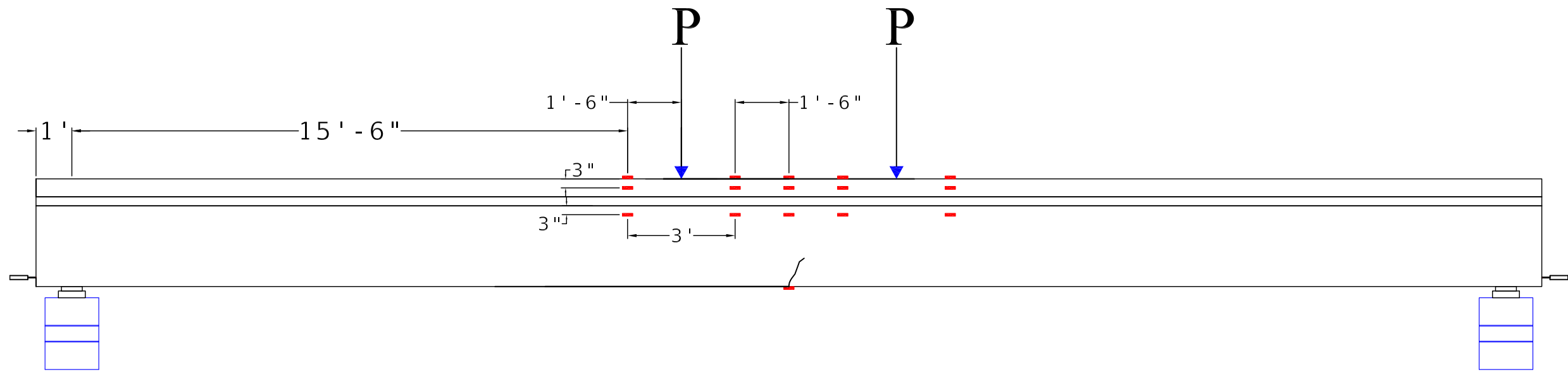
1. All dimensions are to center of strain gages.
2. All strain gages are symmetrical about girder's center line.
3. S31 - S34 shall be instrumented on bottom of girder after the first crack is observed.
4. One pair shall be placed on right of center line; other pair shall be placed on left of center line.
5. See sheet No.3 for more details and dimensions.

Stainless Steel Strands and Lightweight Concrete for Pretensioned Concrete Girders

FAMU-FSU College of Engineering

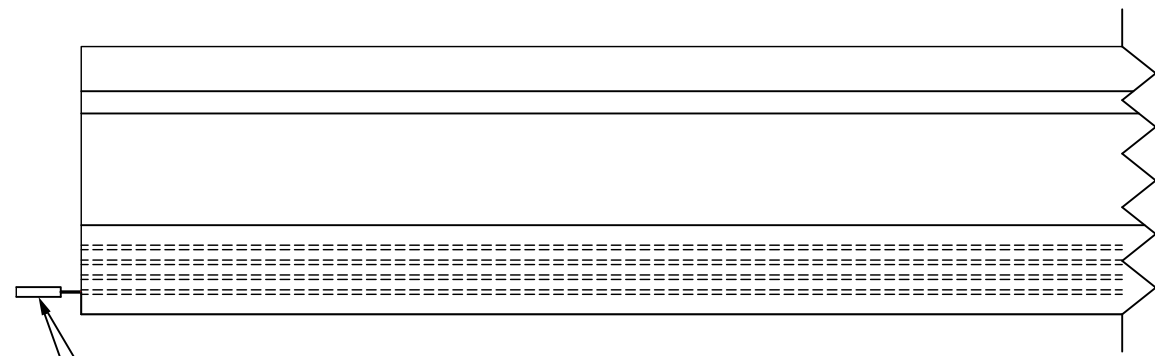
Flexural test setup and instrumentation plan for non-composite girders (Girders A1, B3, and C1)

Sheet No.2

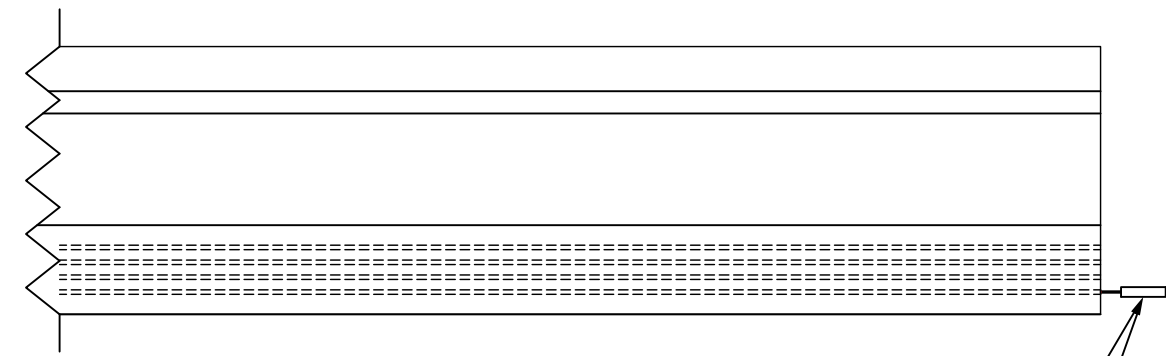


- Notes:-
1. All dimensions are to center of strain gages.
 2. All strain gauges are 60 mm foil gages.

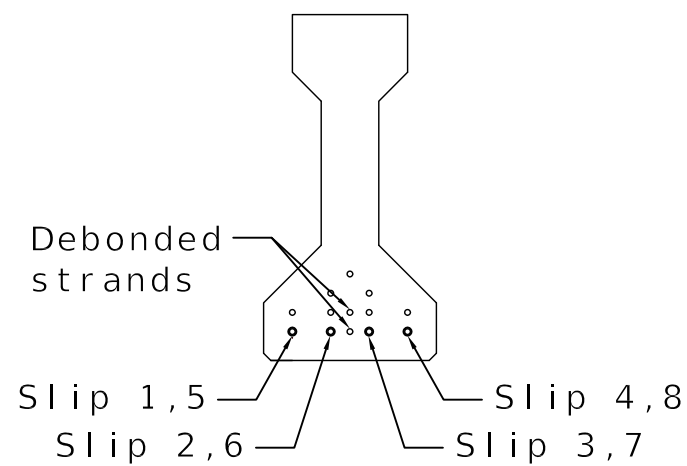
Stainless Steel Strands and Lightweight Concrete for Pretensioned Concrete Girders
FAMU-FSU College of Engineering
Flexural test setup and instrumentation plan for non-composite girders (Girders A1, B3, and C1)
Sheet No.3



Type 1 & Type 3 (slip 1-4)
 Type 2 (slip 1-5)



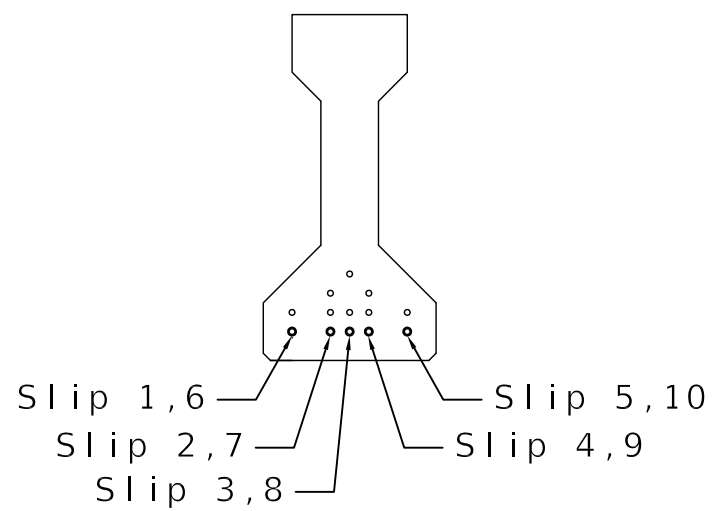
Type 1 & Type 3 (slip 5-8)
 Type 2 (slip 6-10)



Debonded strands

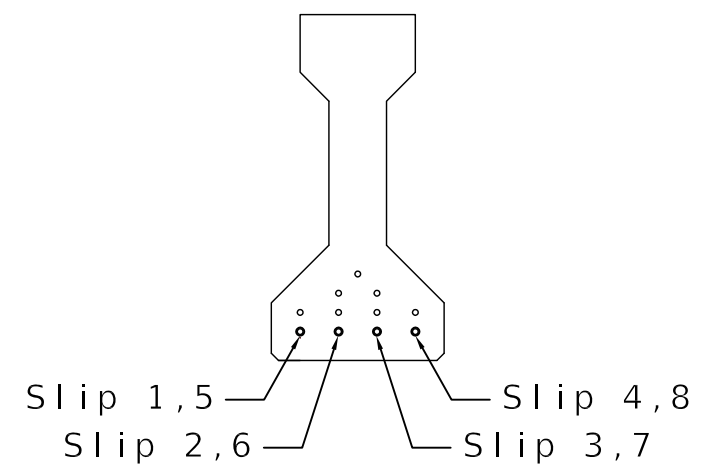
Slip 1,5
 Slip 2,6
 Slip 4,8
 Slip 3,7

Type 1
 (Girders B2 & B3)



Slip 1,6
 Slip 2,7
 Slip 3,8
 Slip 5,10
 Slip 4,9

Type 2
 (Girders C1, C2 & C3)



Slip 1,5
 Slip 2,6
 Slip 4,8
 Slip 3,7

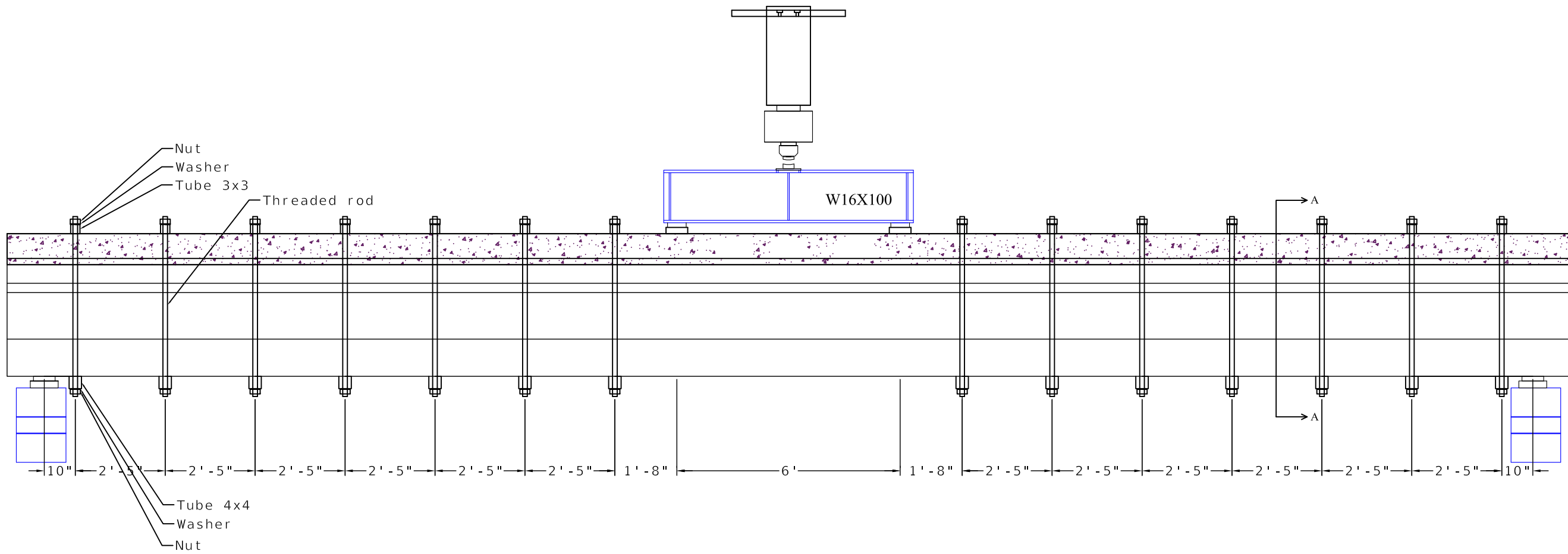
Type 3
 (Girders A1, A2 & A3)

Stainless Steel Strands and Lightweight Concrete for
 Pretensioned Concrete Girders

FAMU-FSU College of Engineering

Flexural test setup and instrumentation plan

Sheet No.4



Notes:-

1. See sheet No.5 for more details.
2. All tubes above the slab are 3x3.
3. All tubes under the girder are 4x4.
4. Minimum length of the threaded rod is 4' 10". Longer than that is ok.

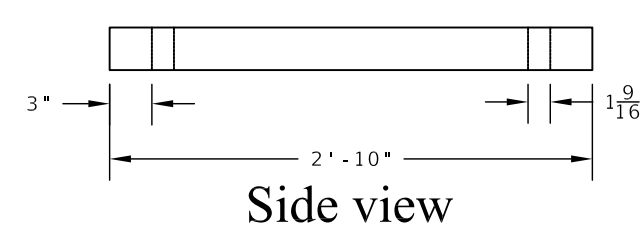
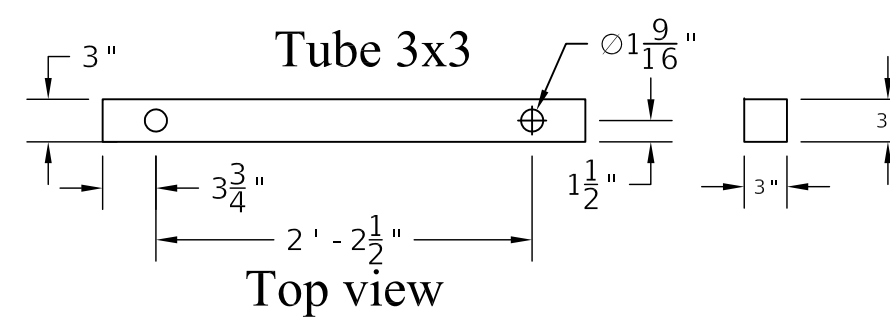
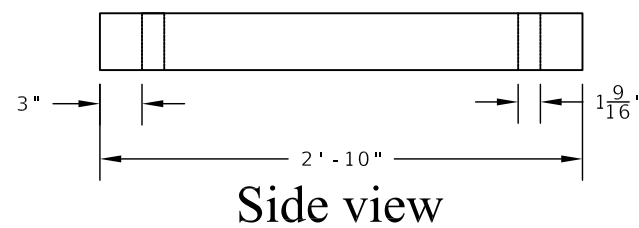
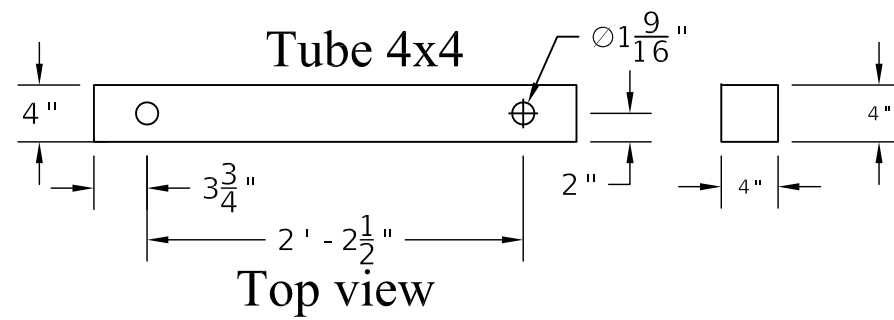
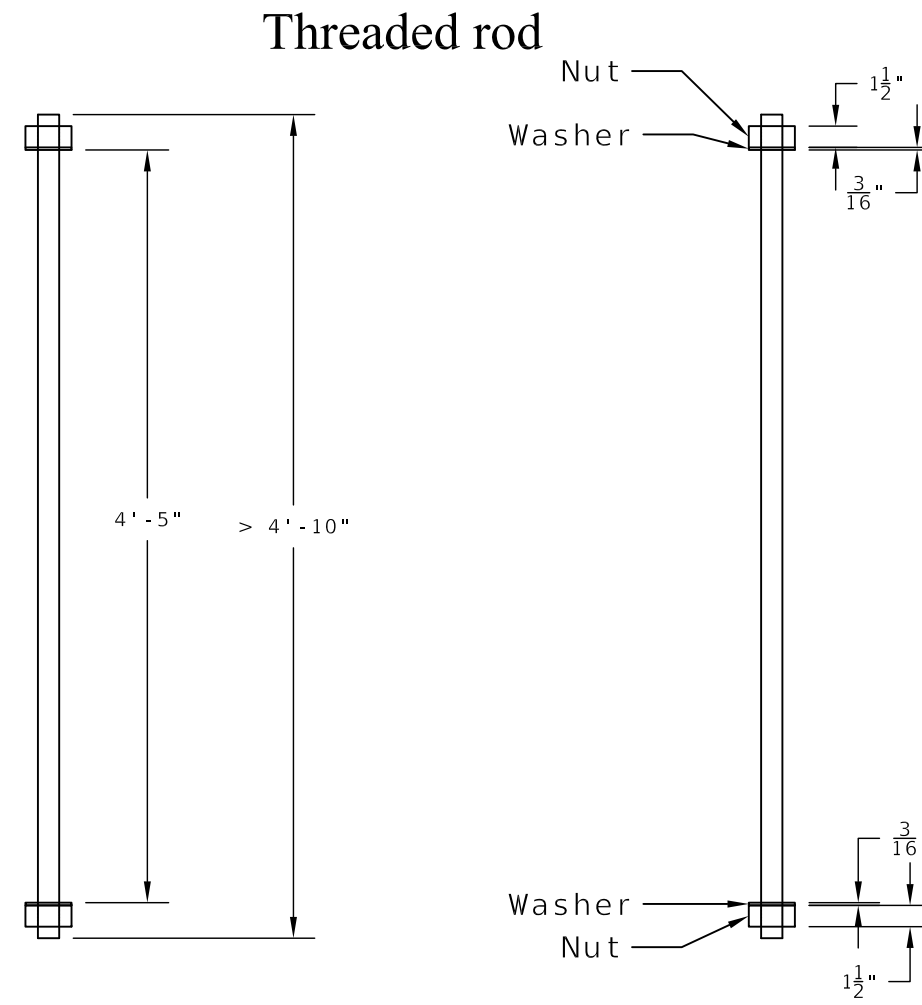
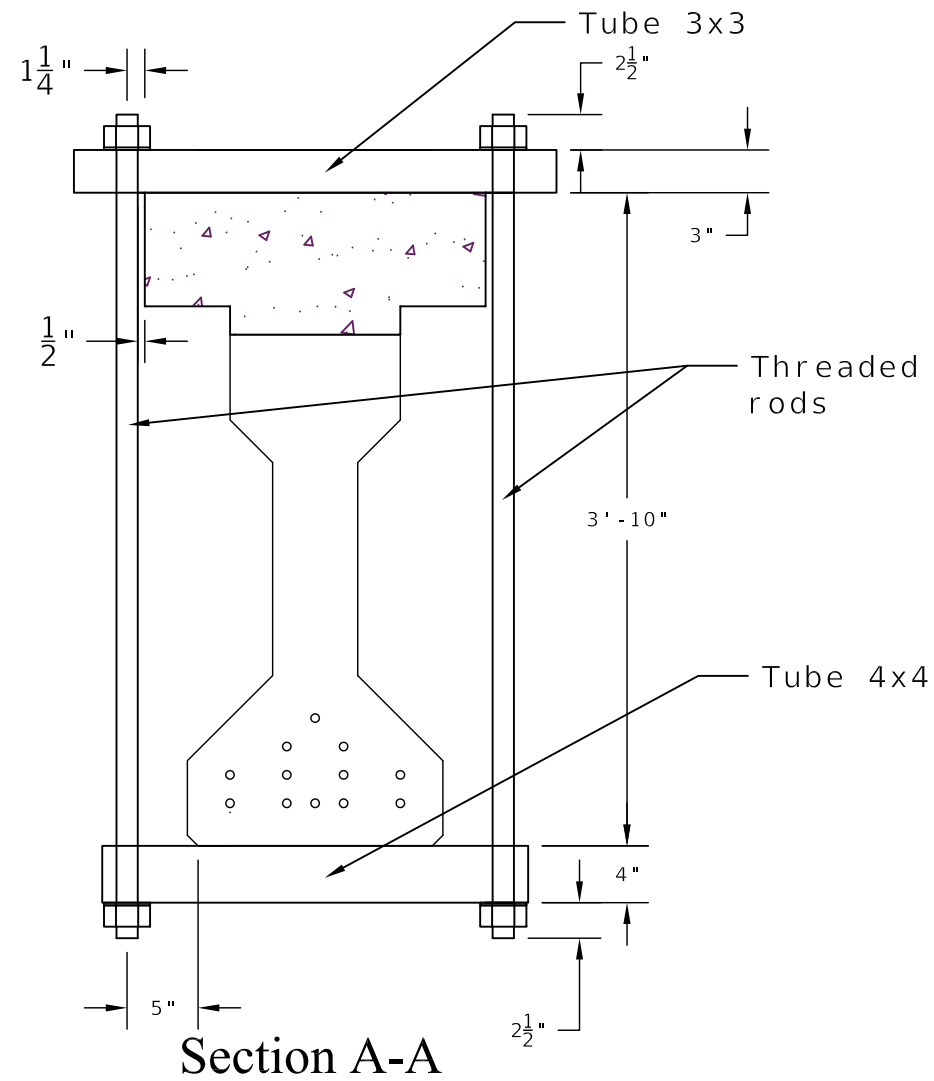
Part	Length	Quantity
Tube 3x3	34 in.	14
Tube 4x4	34 in.	14
Threaded rod	> 4ft10in.	28
Nut	size 1.5 in.	56
Washer	size 1.5 in.	56

Stainless Steel Strands and Lightweight Concrete for
 Pretensioned Concrete Girders

FAMU-FSU College of Engineering

Flexural test setup and instrumentation plan for
 composite girders (Girders A3, B2, C2 and C3)

Sheet No.5

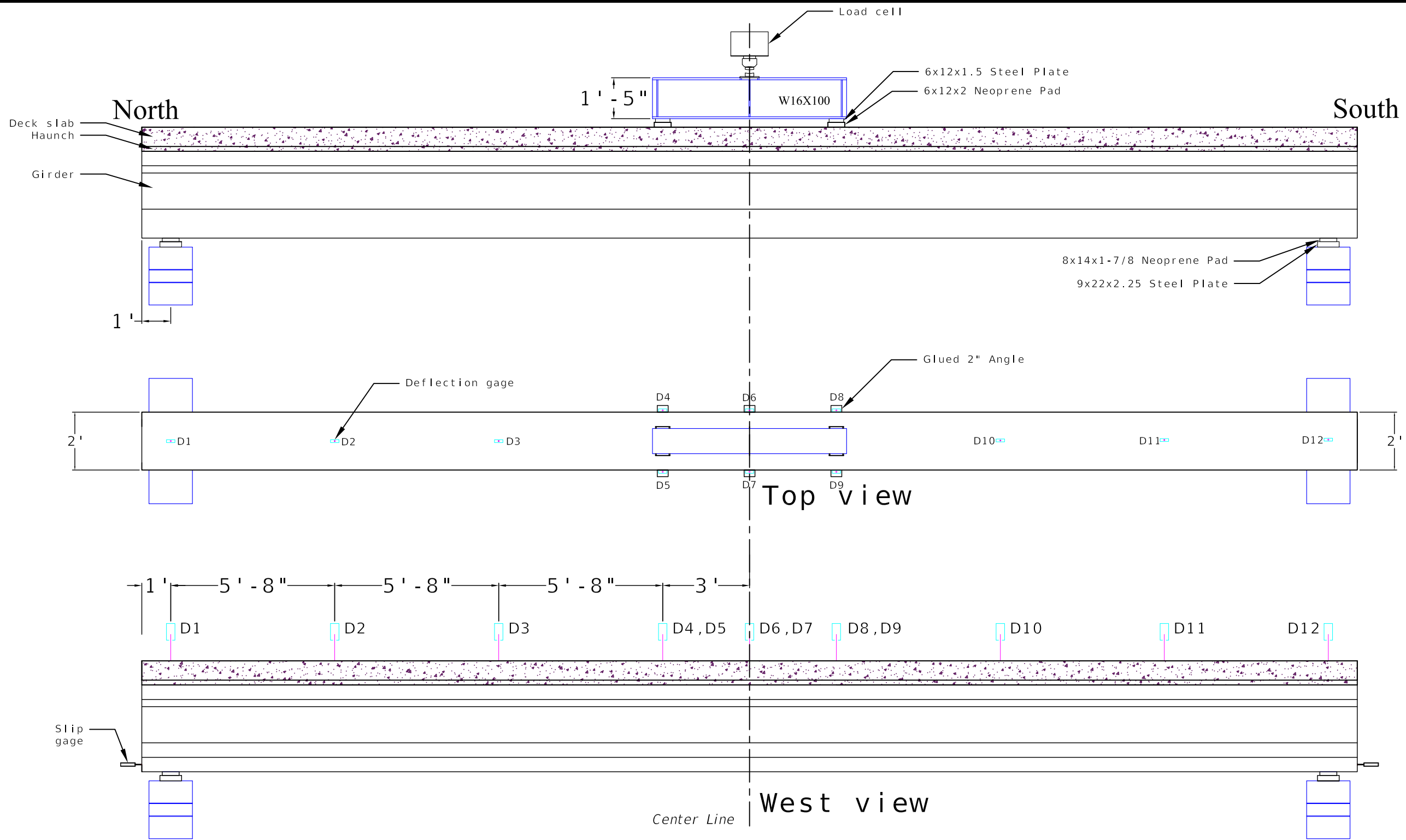


Stainless Steel Strands and Lightweight Concrete for Pretensioned Concrete Girders

FAMU-FSU College of Engineering

Flexural test setup and instrumentation plan for composite girders (Girders A3, B2, C2 and C3)

Sheet No.6



Notes:-

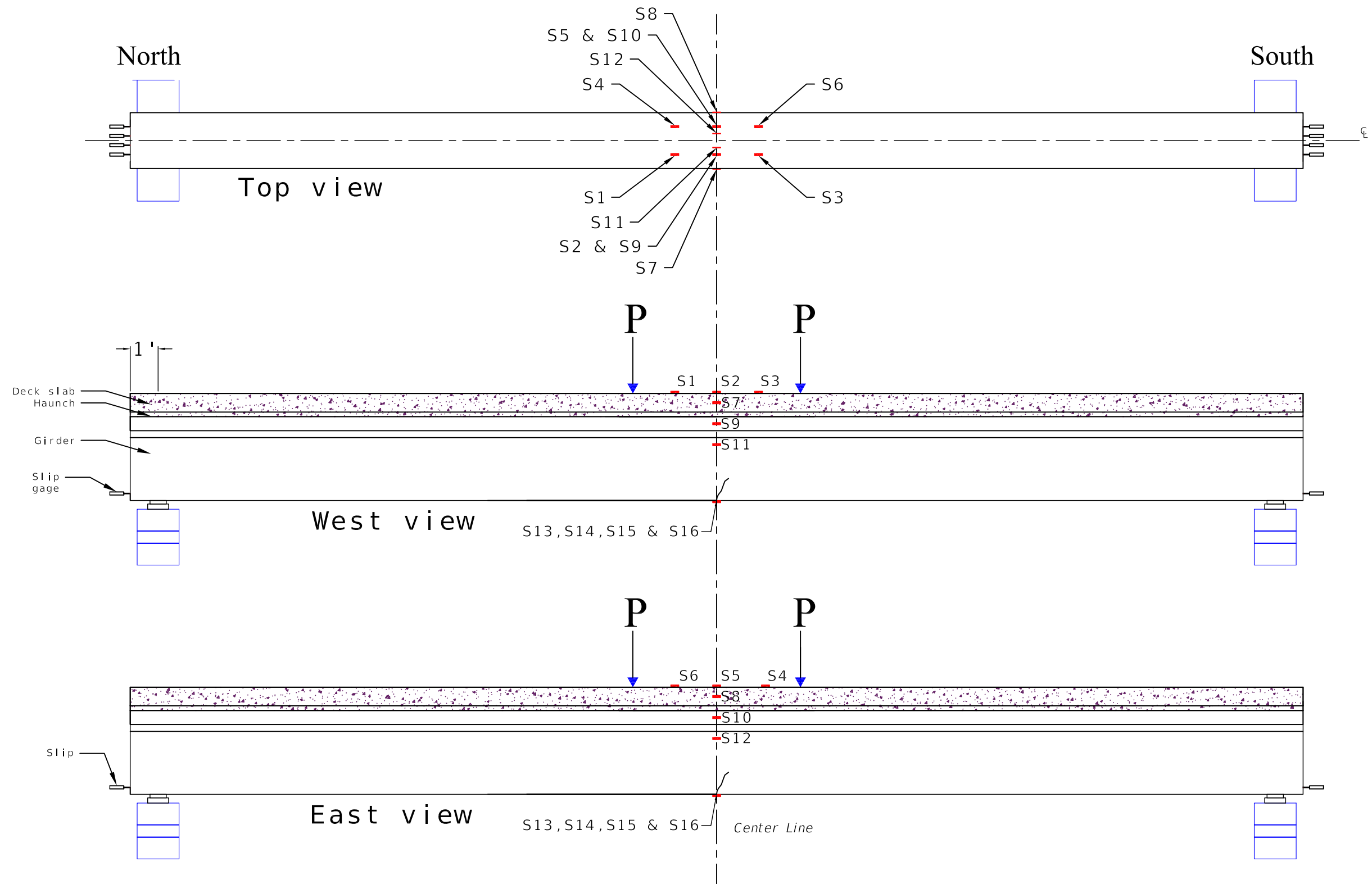
1. All dimensions are to center of deflection gages.
2. All deflection gauges are symmetrical about girder's center line.
3. D4, D5, D6, D7, D8 and D9 may need an angle glued to top flange of specimen due to interference from the spreader beam supports.
4. 12.5 mm slip gages shall be used for all strand slip locations. See Sheet No. 4 for slip gauges locations.
5. See Sheet No. 8 for strain gages locations.
6. External clamps are not shown for clarity.

Stainless Steel Strands and Lightweight Concrete for
Pretensioned Concrete Girders

FAMU-FSU College of Engineering

Flexural test setup and instrumentation plan for
composite girders (Girders A3, B2, C2 and C3)

Sheet No.7



Notes:-

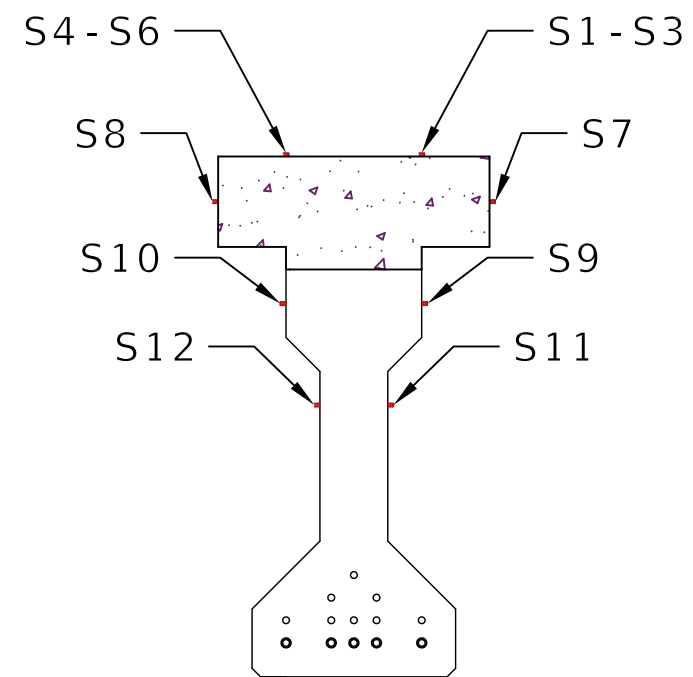
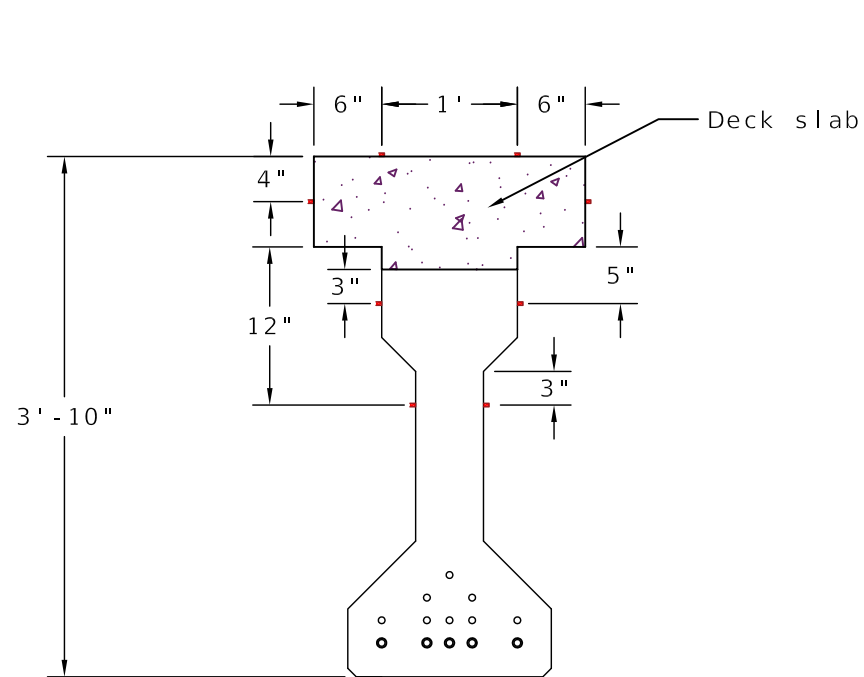
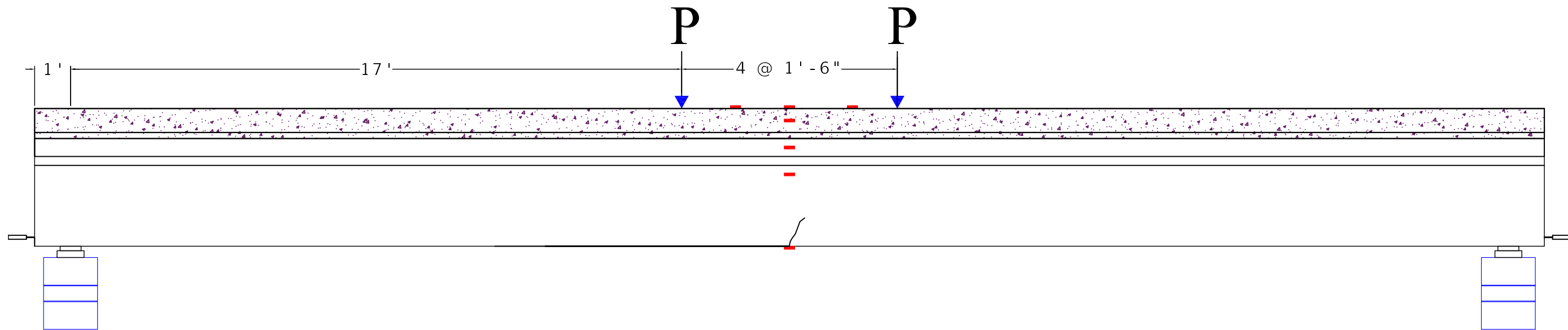
1. All dimensions are to center of strain gages.
2. All strain gages are symmetrical about girder's center line.
3. S13 - S16 shall be instrumented on bottom of girder after the first crack is observed.
4. One pair shall be placed on right of center line; other pair shall be placed on left of center line.
5. See Sheet No.9 for more details and dimensions.
6. External clamps are not shown for clarity.

Stainless Steel Strands and Lightweight Concrete for
Pretensioned Concrete Girders

FAMU-FSU College of Engineering

Flexural test setup and instrumentation plan for
composite girders (Girders A3, B2, C2 and C3)

Sheet No.8



Notes:-

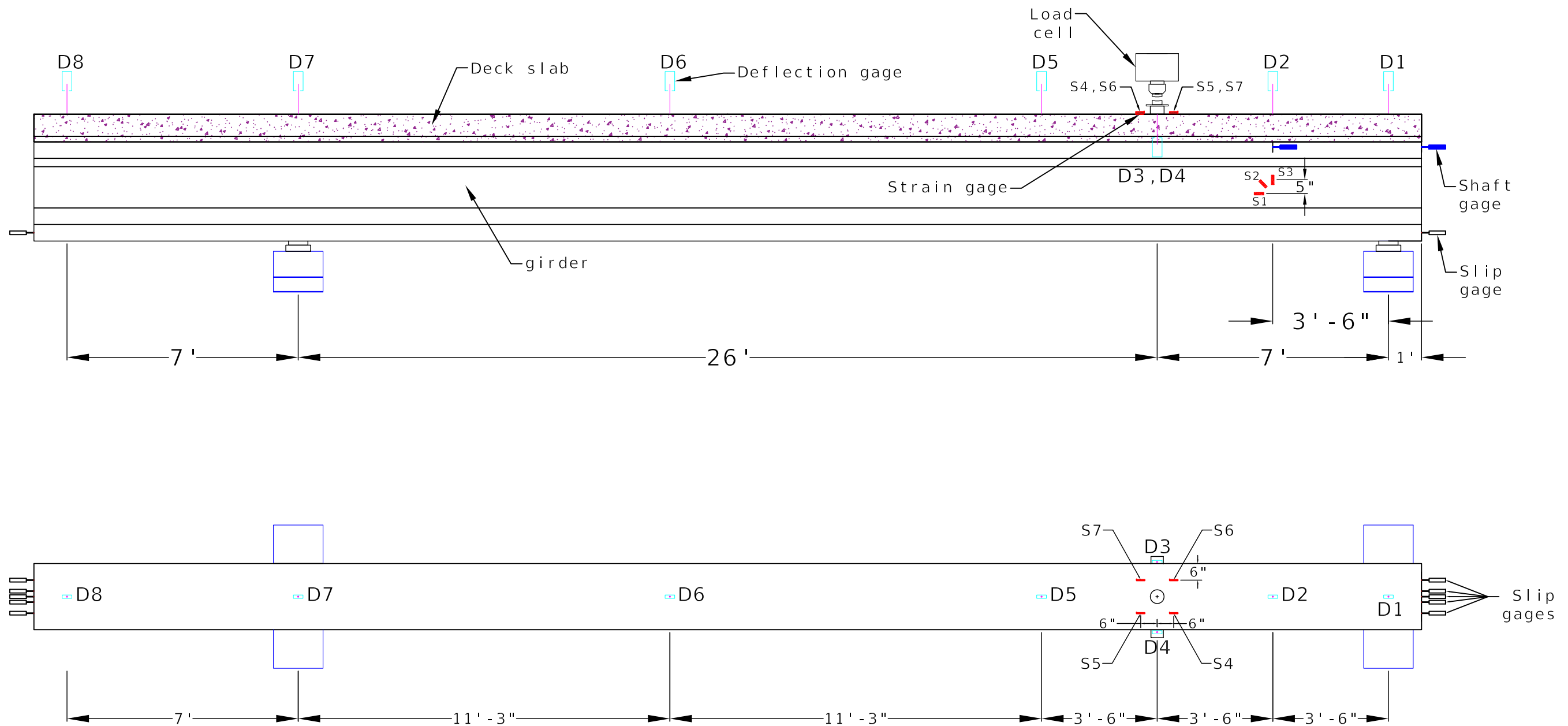
1. All dimensions are to center of strain gages.
2. All strain gages are 60 mm foil gages.
3. External clamps are not shown for clarity.

Stainless Steel Strands and Lightweight Concrete for
Pretensioned Concrete Girders

FAMU-FSU College of Engineering

Flexural test setup and instrumentation plan for
composite girders (Girders A3, B2, C2 and C3)

Sheet No.9



Notes:-

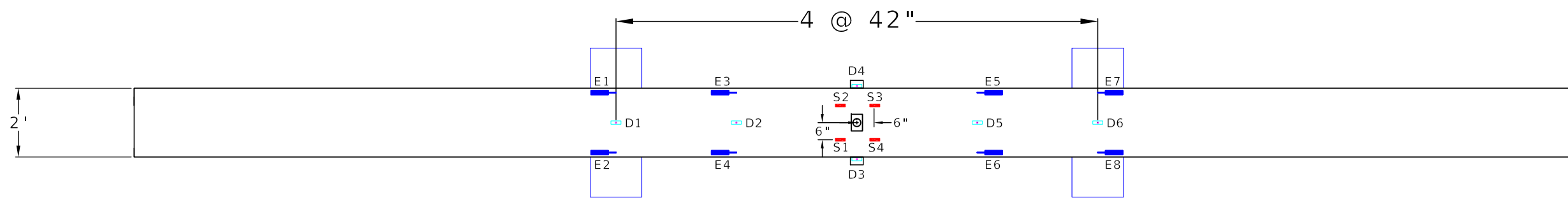
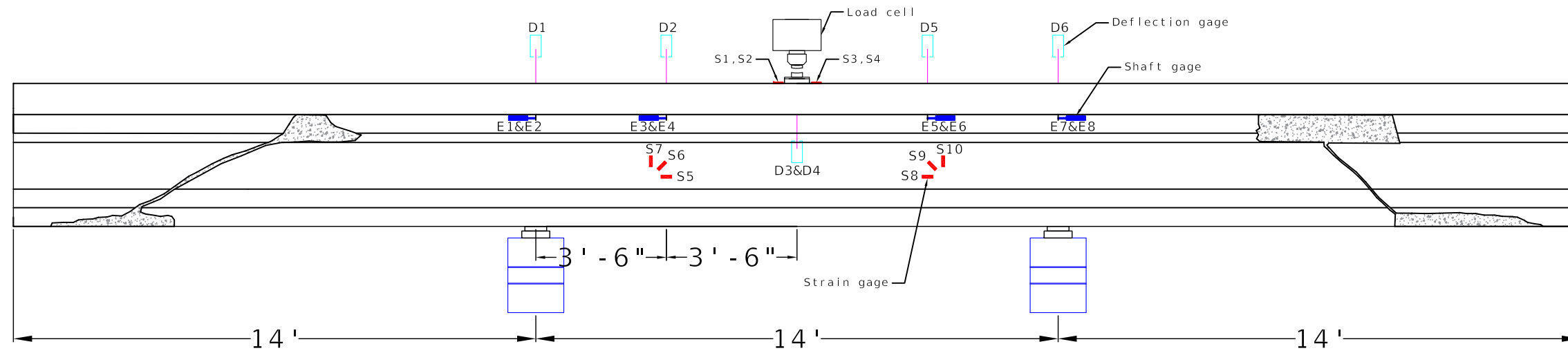
1. All dimensions are to center of strain and deflection gages.
2. All strain gages are 60 mm foil gages.
3. D3 and D4 may need an angle glued to slab of specimen due to interference with load cell.
4. 12.5 mm slip gages shall be used for all strand slip locations.
5. Only Girder B3 was shaft gages.
6. See Sheet No.11 for more information about midspan shear test for Girder A2.

Stainless Steel Strands and Lightweight Concrete for
Pretensioned Concrete Girders

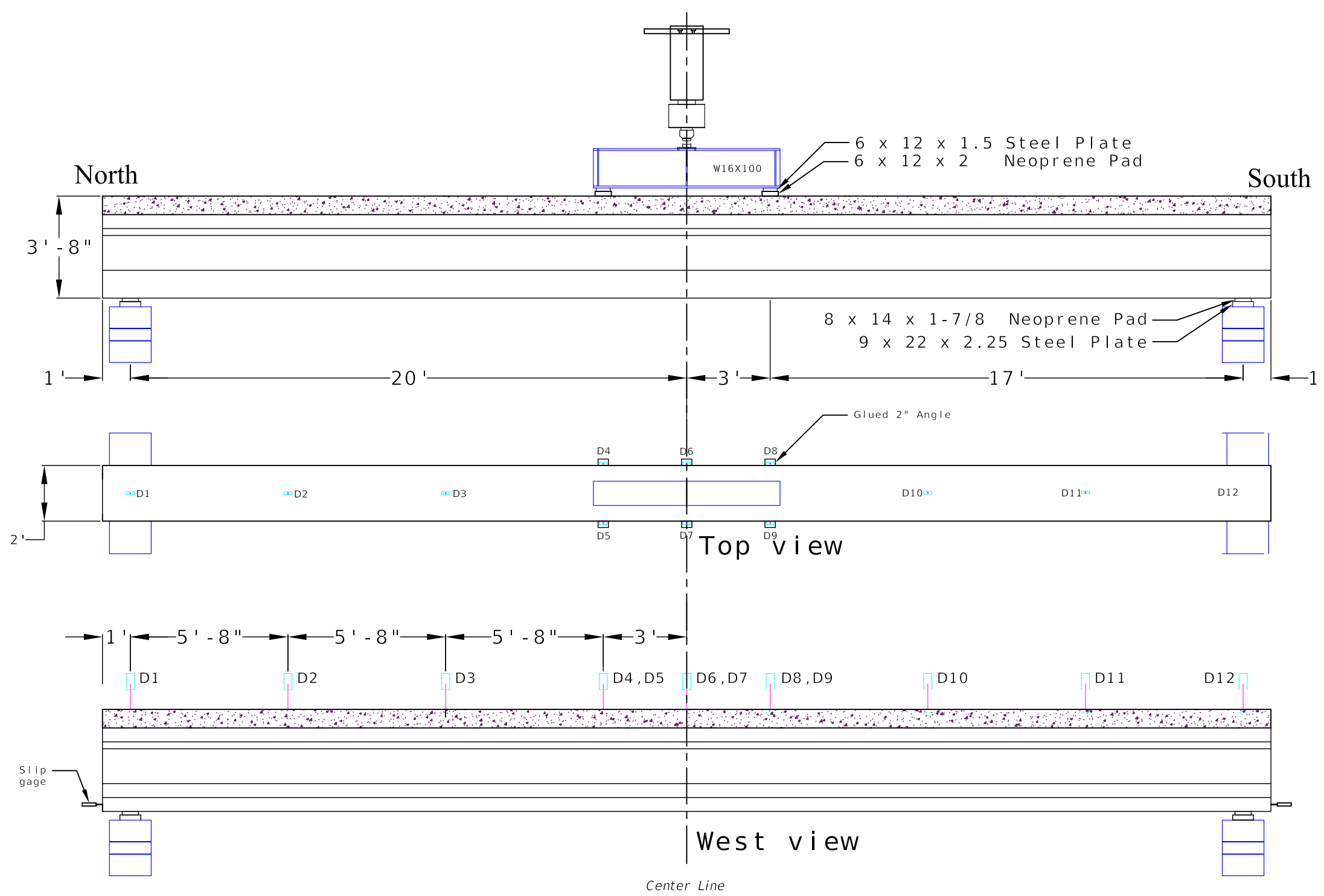
FAMU-FSU College of Engineering

Shear test setup and instrumentation plan for composite
girders (Girders A2, A3 and B3)

Sheet No.10



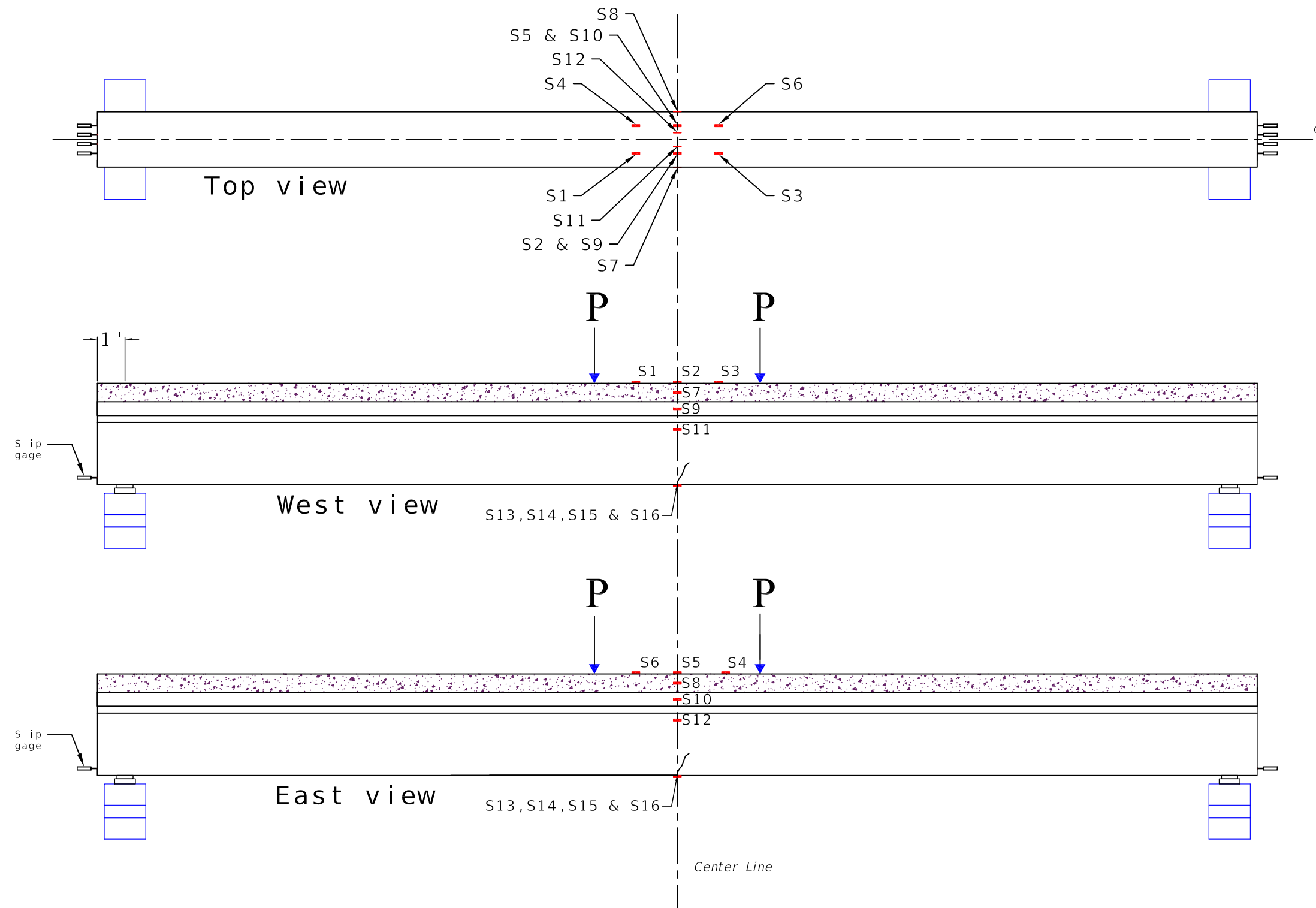
Stainless Steel Strands and Lightweight Concrete for
 Pretensioned Concrete Girders
 FAMU-FSU College of Engineering
 Shear test setup and instrumentation plan for Girder A2
 Sheet No.11



Notes:-

1. All dimensions are to center of deflection gages.
2. All deflection gages are symmetrical about girder's center line.
3. D4, D5, D6, D7, D8 and D9 may need an angle glued to top flange of specimen due to interference from the spreader beam supports.
4. 12.5 mm slip gauges shall be used for all strand slip locations. See Sheet No.14 for slip gages locations.
5. See Sheets No. 13 and 14 for strain gages locations.

Stainless Steel Strands and Lightweight Concrete for Pretensioned Concrete Girders
FAMU-FSU College of Engineering
Shear test setup and instrumentation plan for composite Girders E1-E5
Sheet No.12



Notes:-

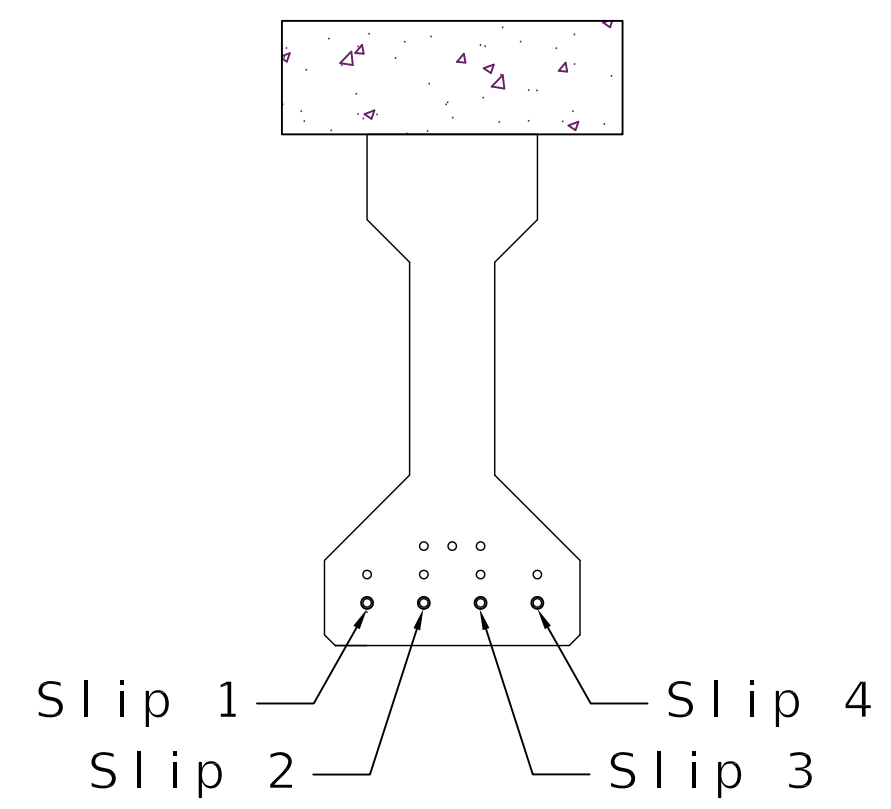
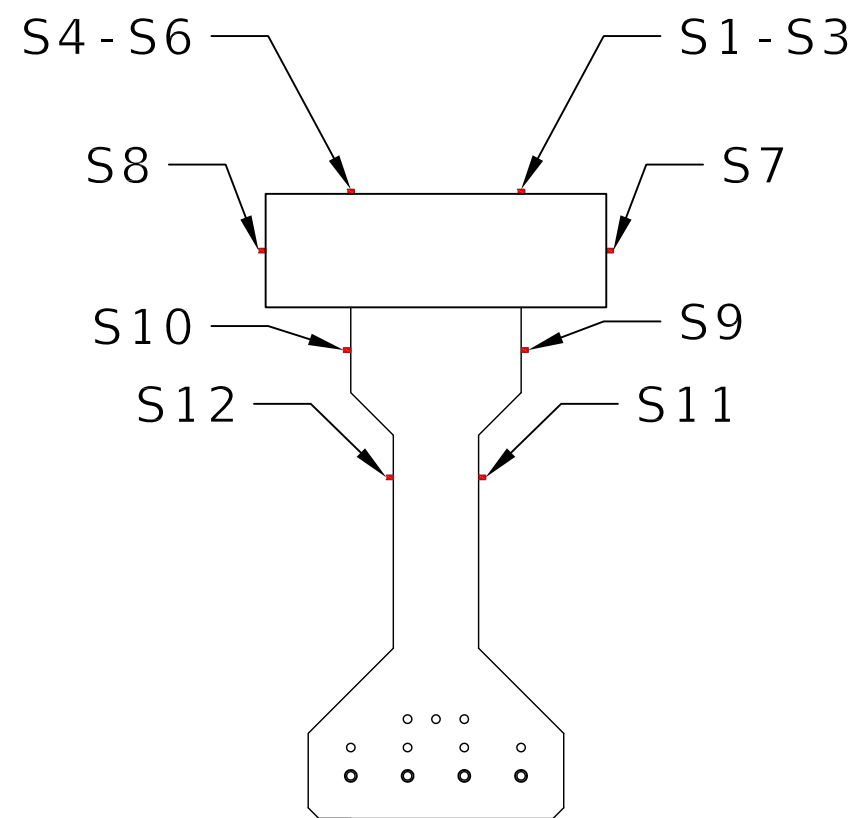
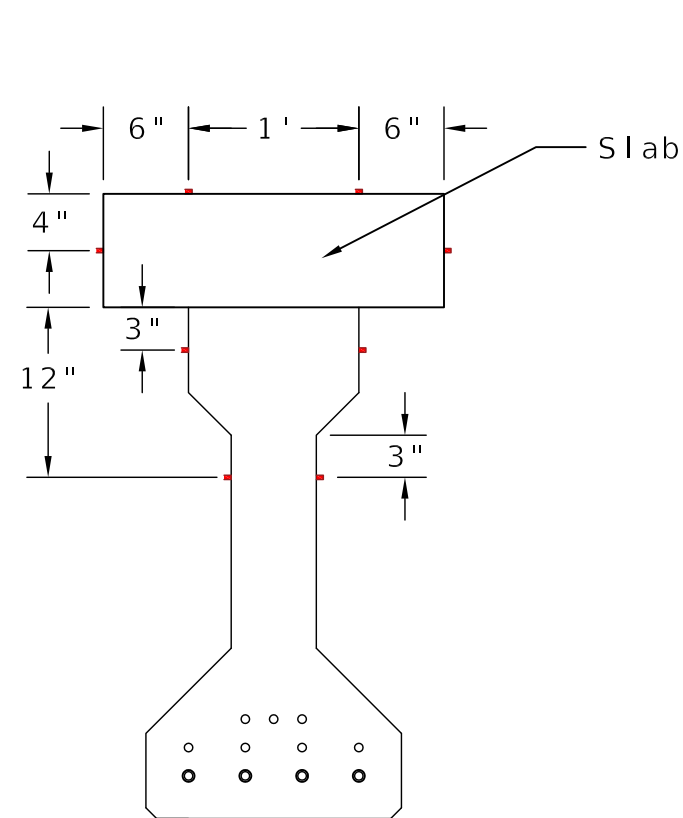
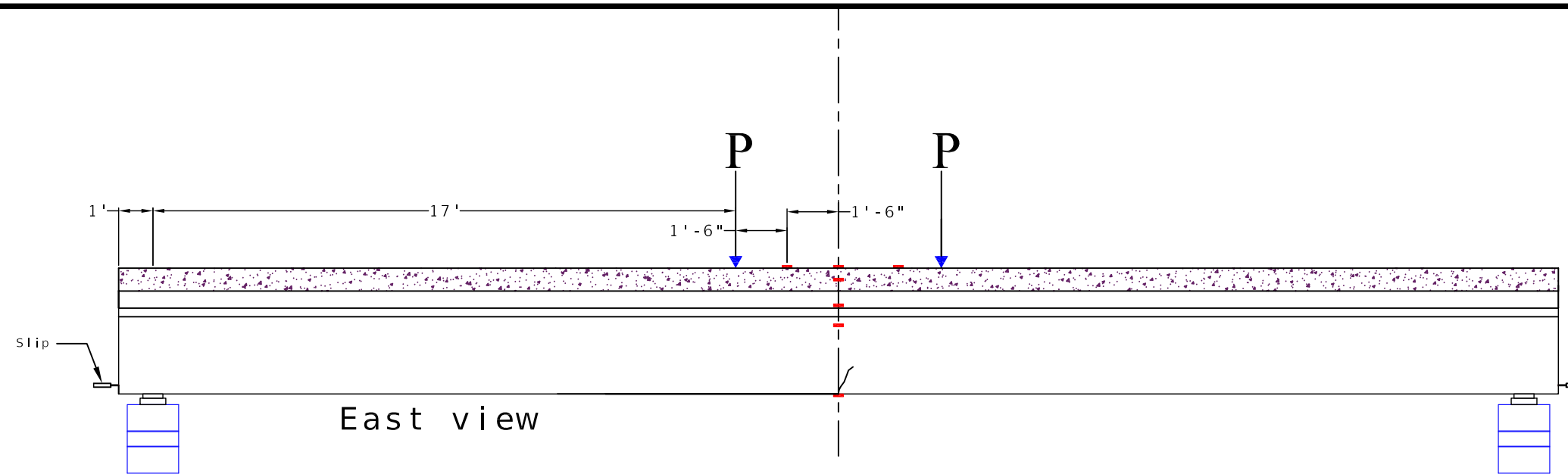
1. All dimensions are to center of strain gages.
2. All strain gages are symmetrical about girder's center line.
3. S13 - S16 shall be instrumented on bottom of girder after the first crack is observed.
4. One pair shall be placed on right of center line; other pair shall be placed on left of center line.
5. See sheet No.14 for more details and dimensions.

Stainless Steel Strands and Lightweight Concrete for
Pretensioned Concrete Girders

FAMU-FSU College of Engineering

Shear test setup and instrumentation plan for composite
Girders E1-E5.

Sheet No.13



Notes:-

1. All dimensions are to center of strain gages.
2. All strain gauges are 60 mm foil gages.

Stainless Steel Strands and Lightweight Concrete for Pretensioned Concrete Girders

FAMU-FSU College of Engineering

Shear test setup and instrumentation plan for composite Girders E1-E5

Sheet No.14

Appendix E – Concrete strain measurements

This appendix contains concrete strain measurements of each girder during flexural and/or shear tests. Locations of gages can be found in Appendix D.

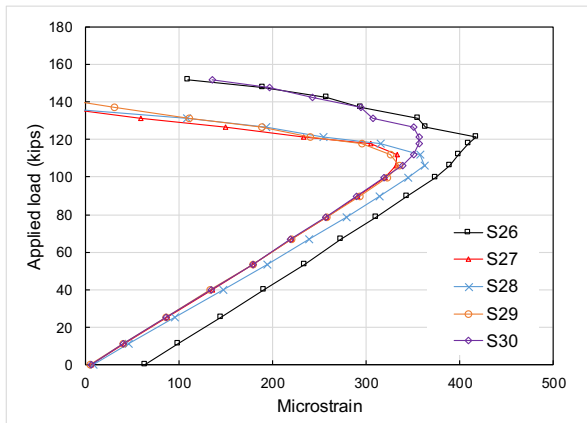
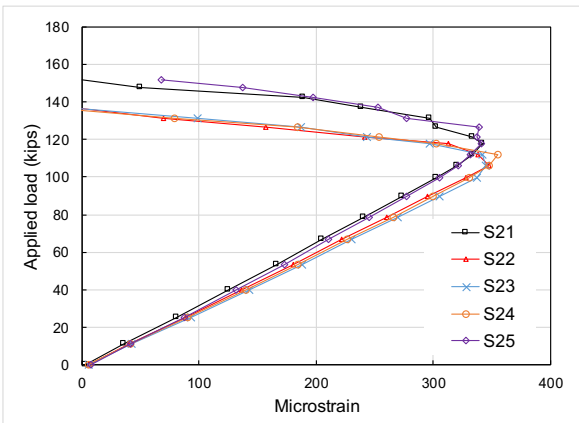
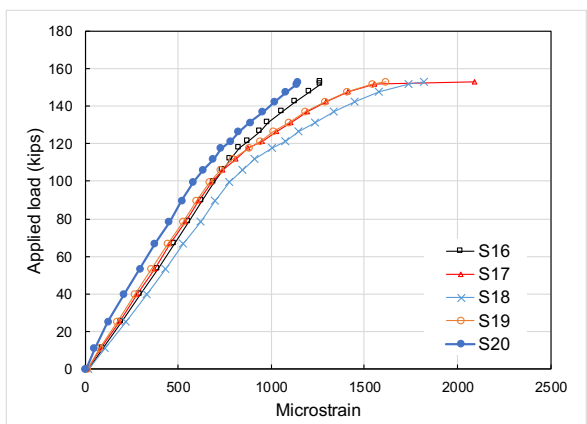
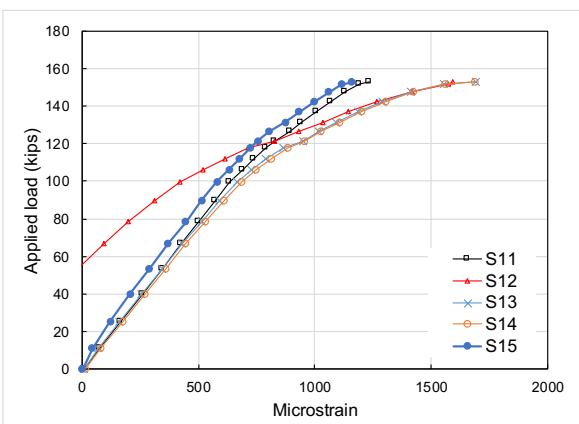
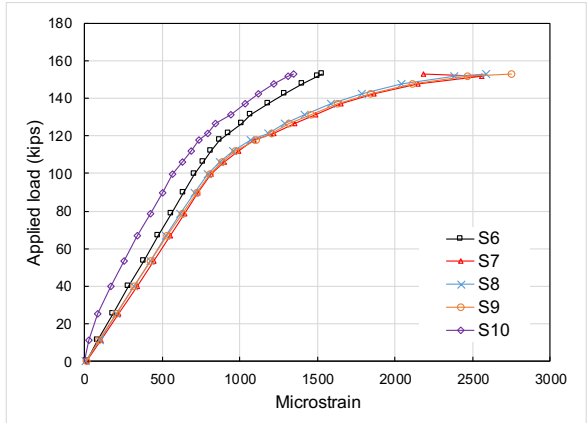
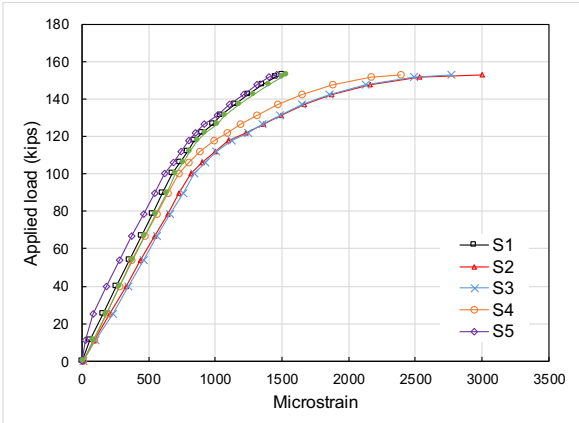


Figure E-1 Strain measurements at top fiber during flexural test of Girder A1

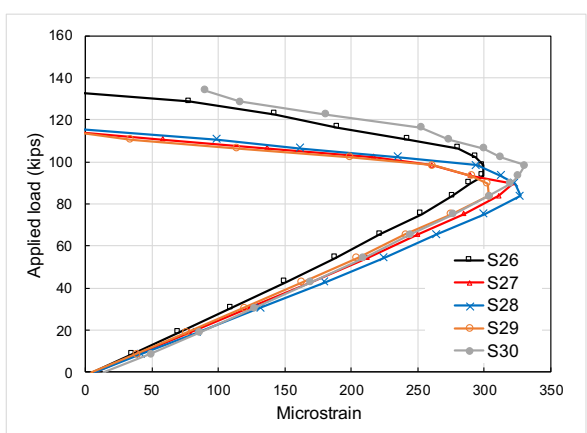
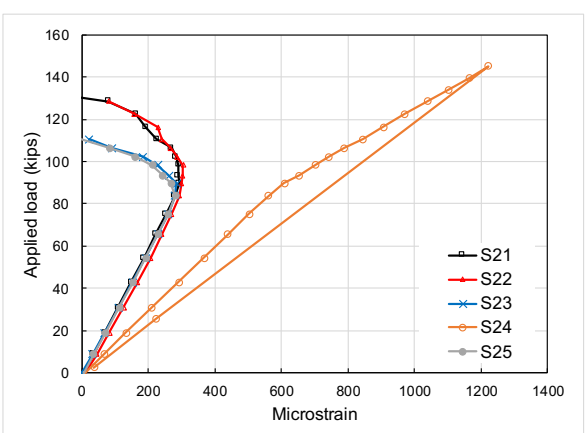
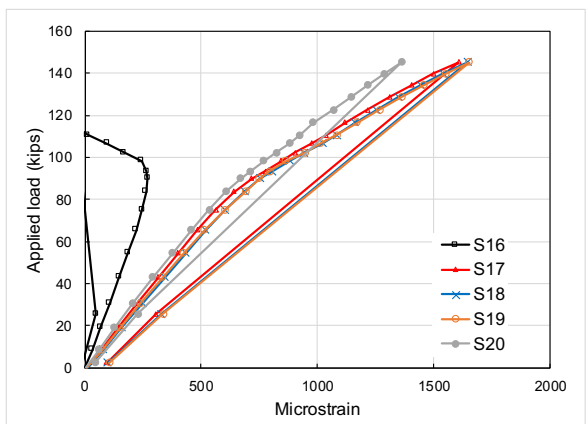
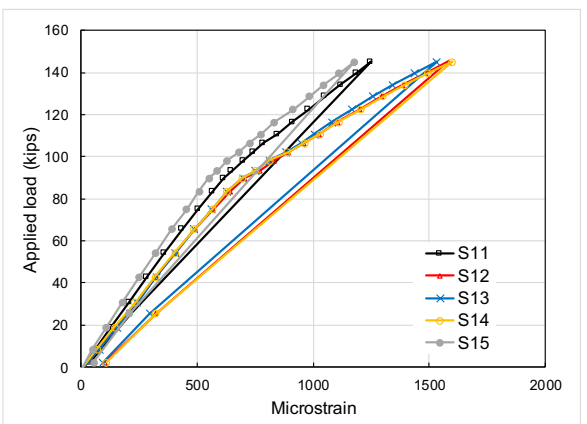
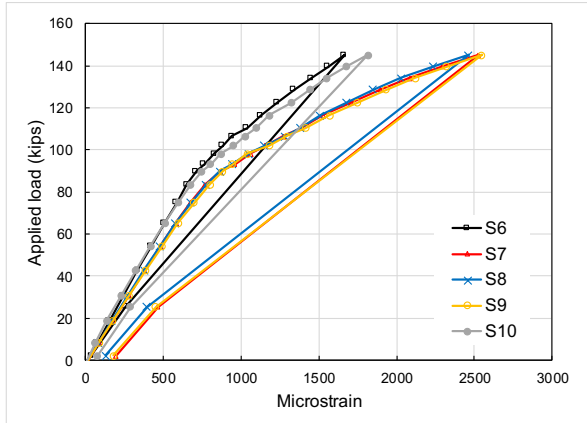
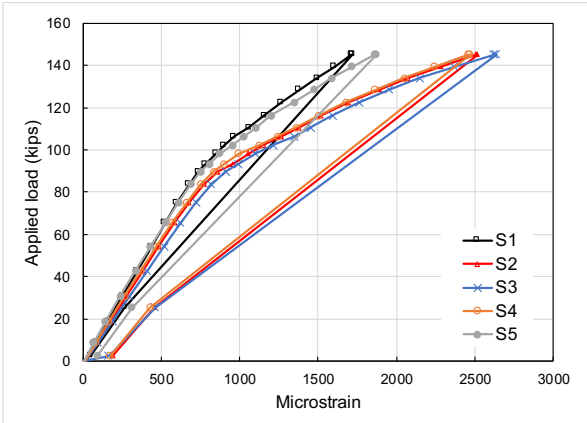


Figure E-2 Strain measurements during flexural test of Girder B3

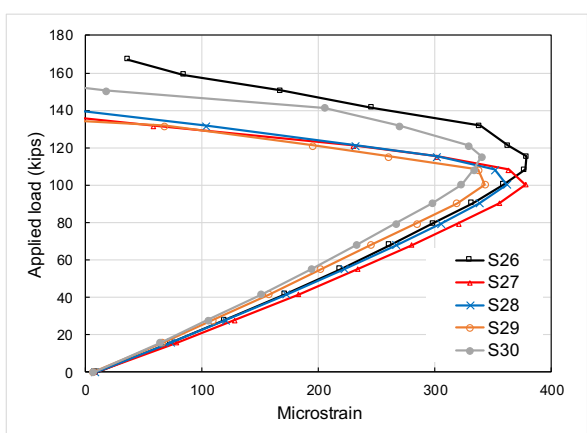
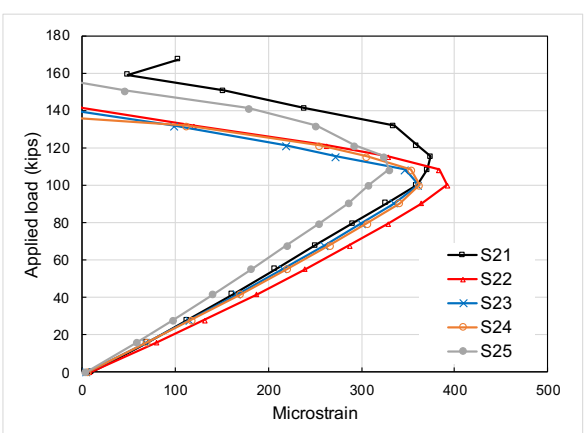
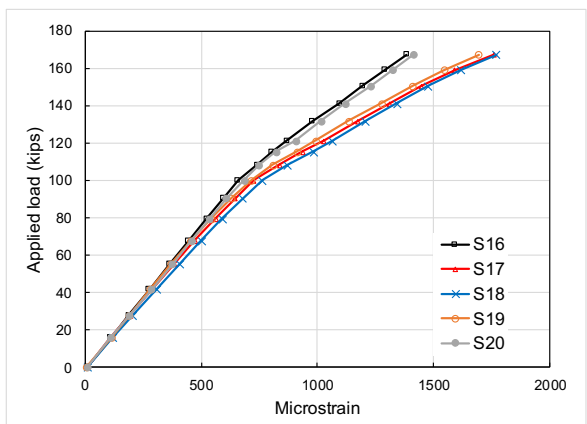
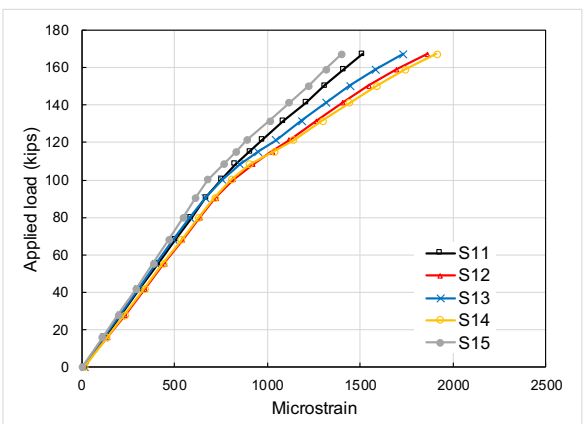
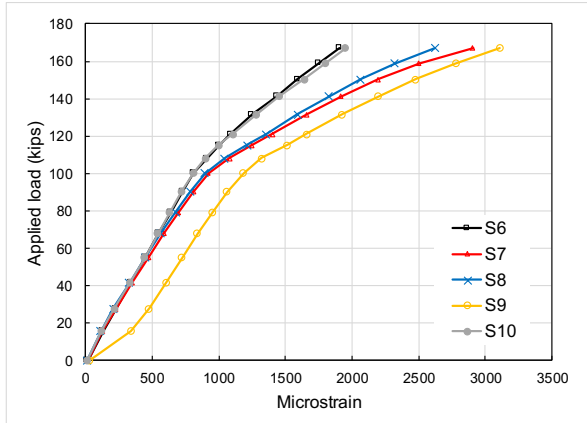
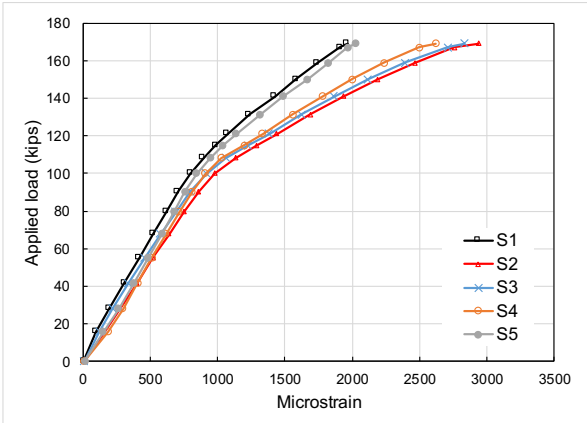


Figure E-3 Strain measurements during flexural test of Girder C1

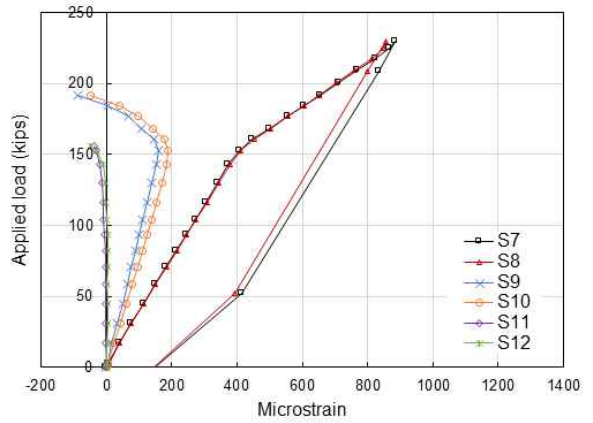
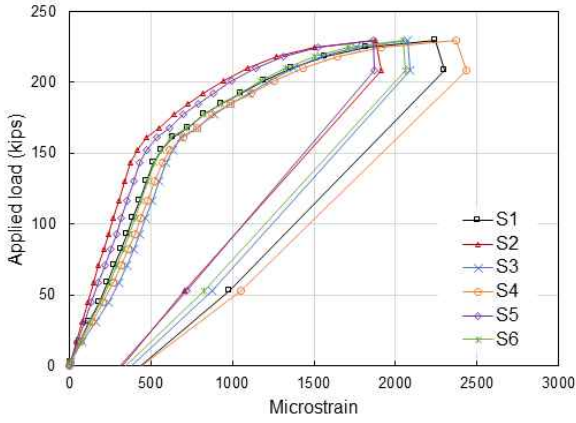


Figure E-4 Strain measurements during flexural test of Girder A3

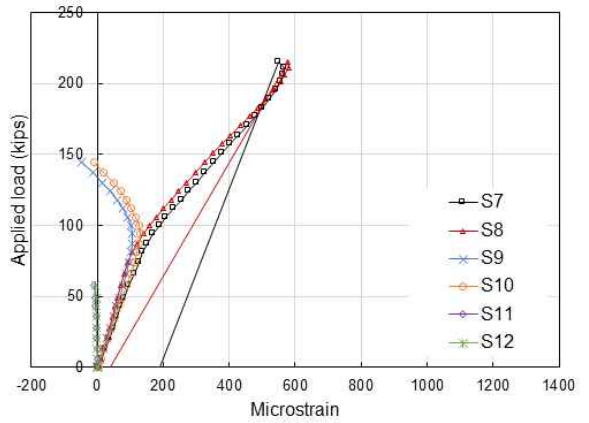
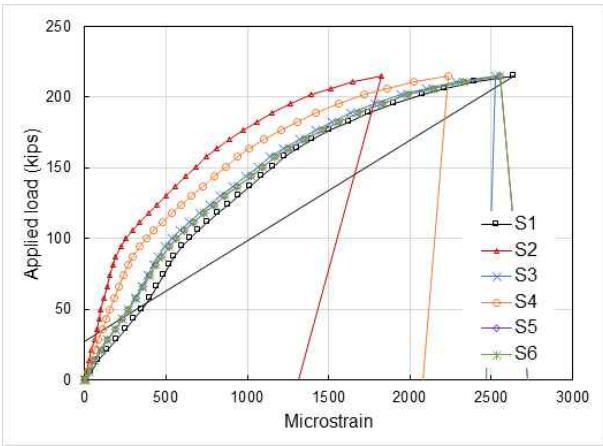


Figure E-5 Strain measurements during flexural test of Girder B2

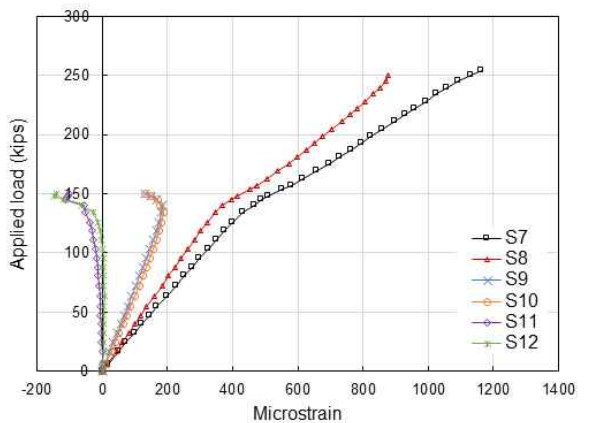
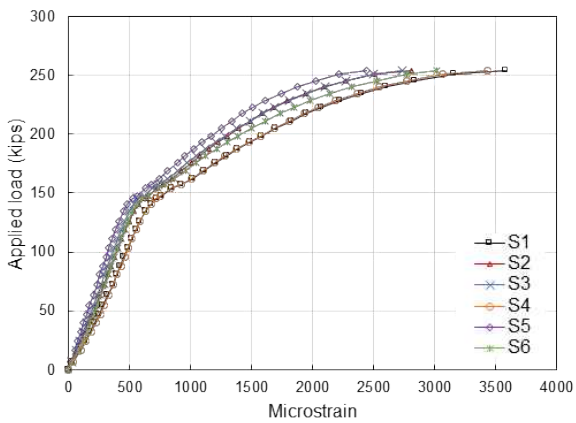


Figure E-6 Strain measurements during flexural test of Girder C2

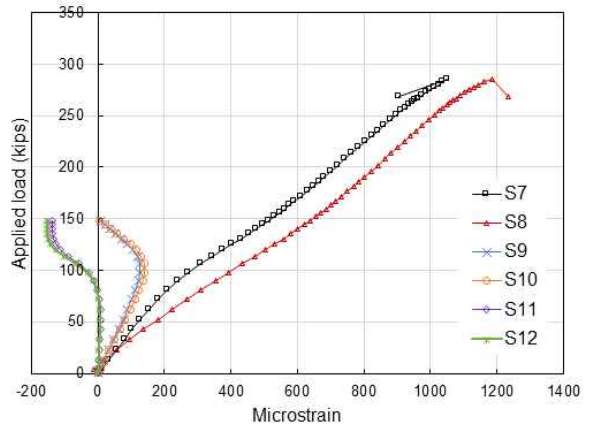
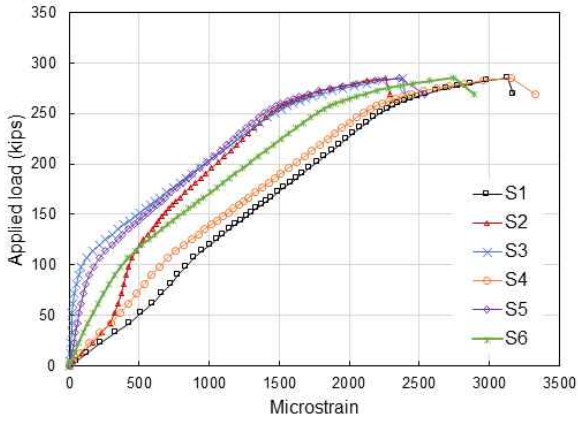


Figure E-7 Strain measurements during flexural test of Girder C3

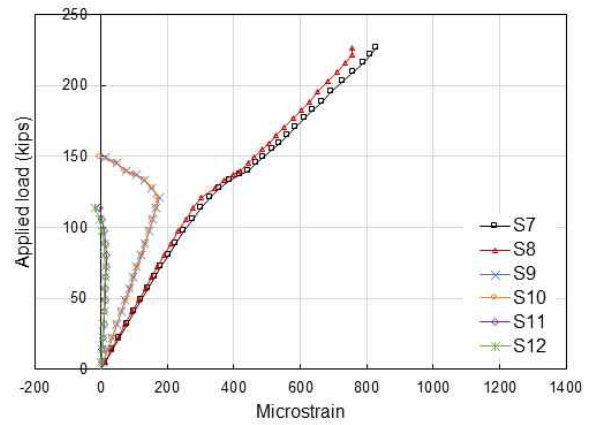
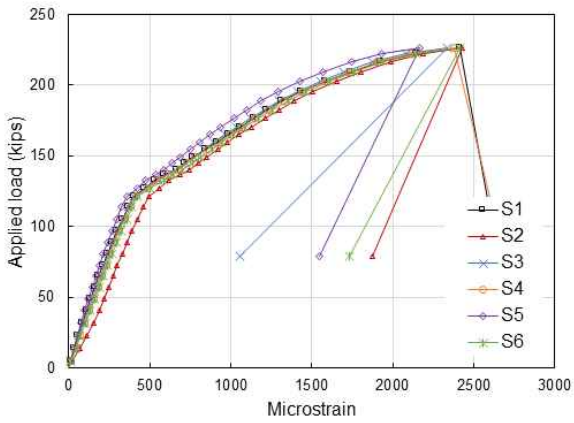


Figure E-8 Strain measurements during flexural test of Girder E1

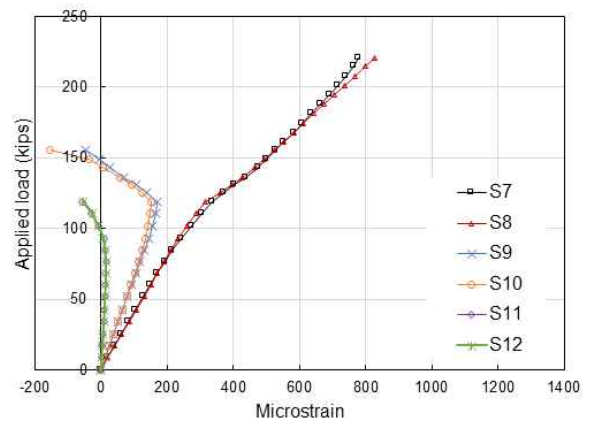
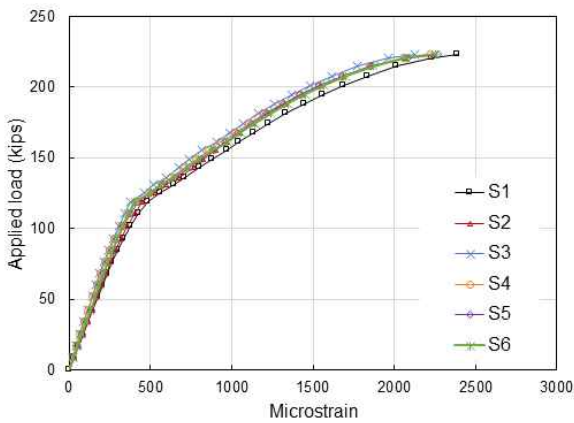


Figure E-9 Strain measurements during flexural test of Girder E2

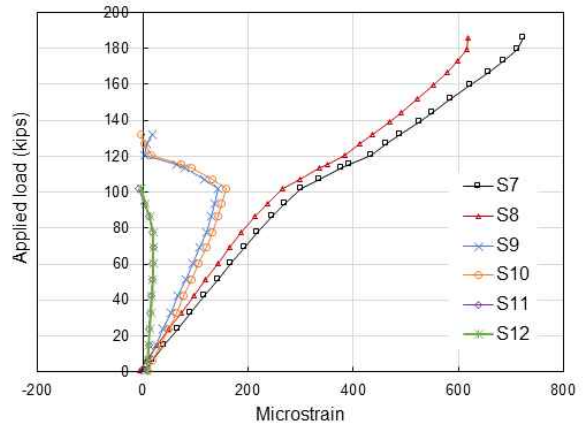
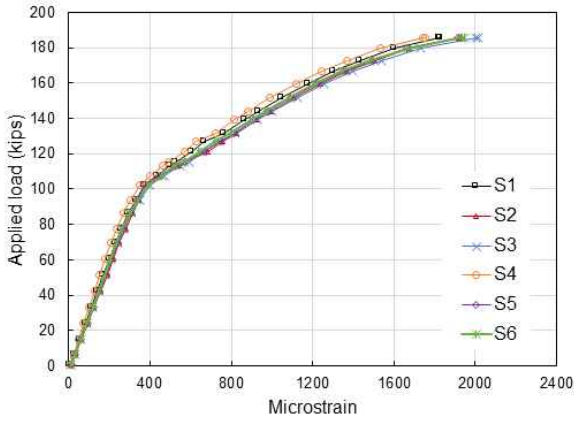


Figure E-10 Strain measurements during flexural test of Girder E3

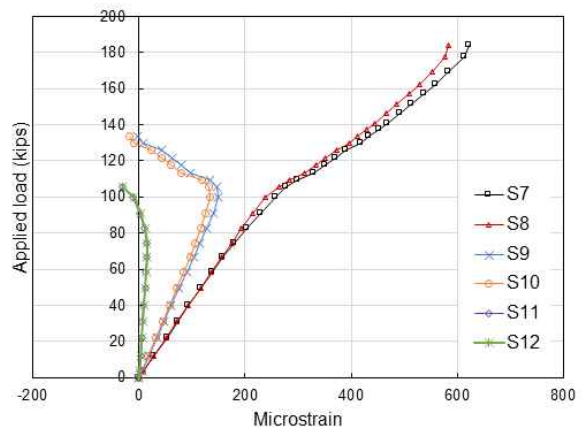
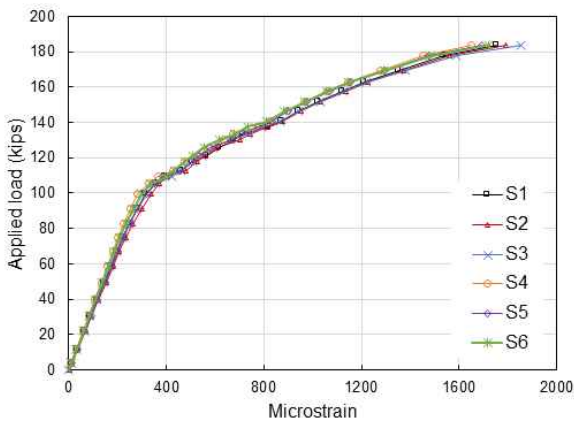


Figure E-11 Strain measurements during flexural test of Girder E4

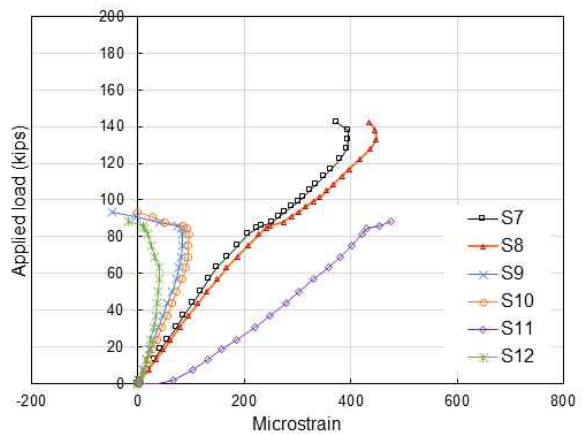
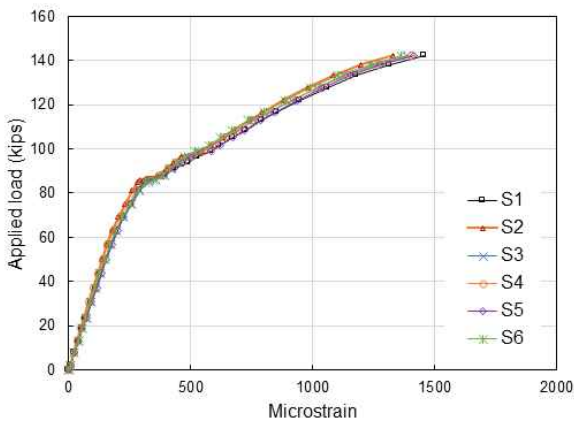


Figure E-12 Strain measurements during flexural test of Girder E5

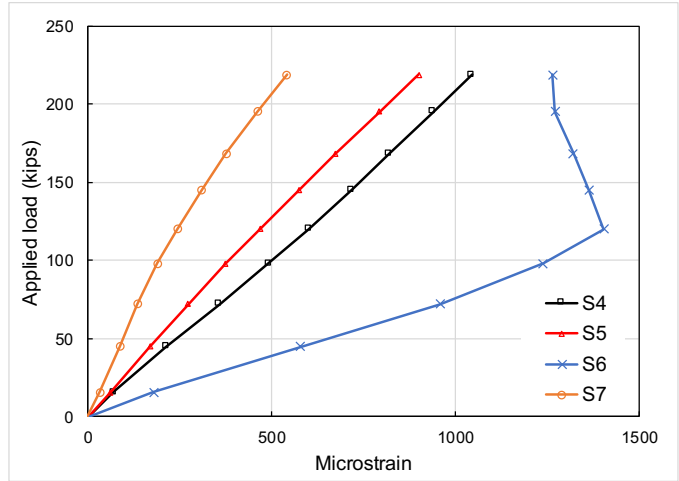


Figure E-13 Strain measurements at top fiber during first (wide spacing) shear test of Girder A2

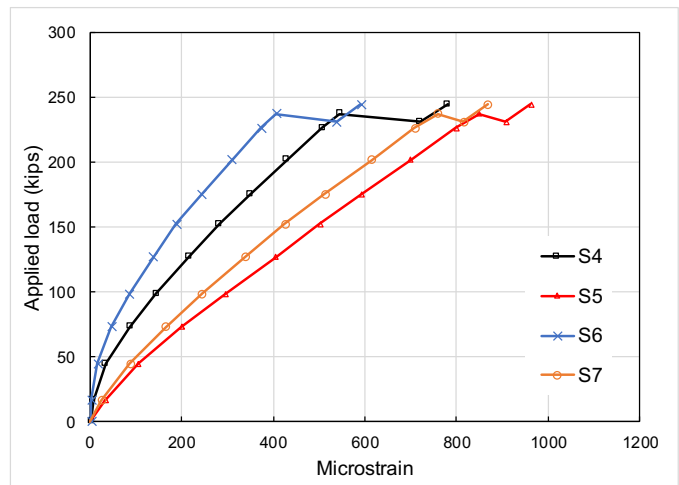


Figure E-14 Strain measurements at top fiber during second (narrow spacing) shear test of Girder A2

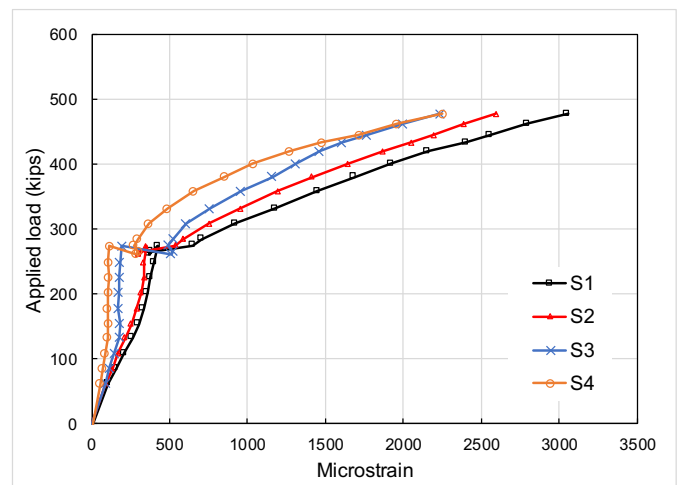


Figure E-15 Strain measurements at top fiber during third (midspan) shear test of Girder A2

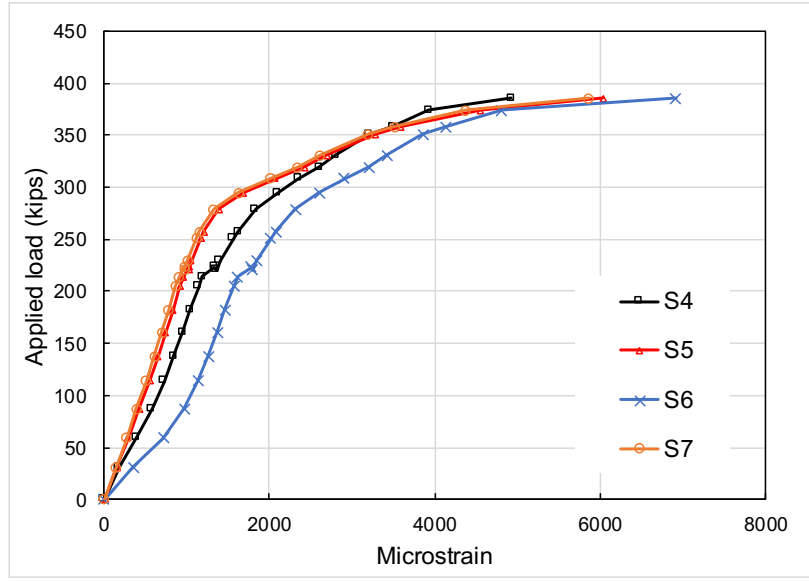


Figure E-16 Strain measurements at top fiber during first (wide spacing) shear test of Girder A3

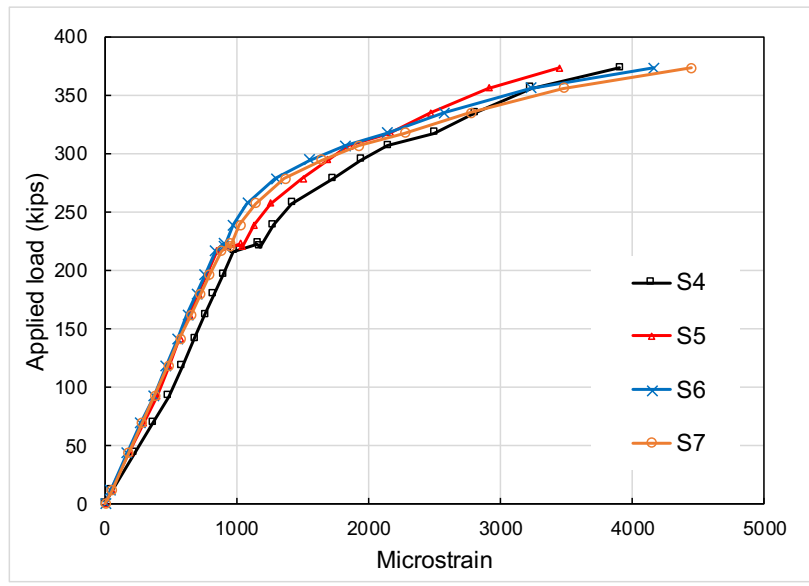


Figure E-17 Strain measurements at top fiber during second (narrow spacing) shear test of Girder A3

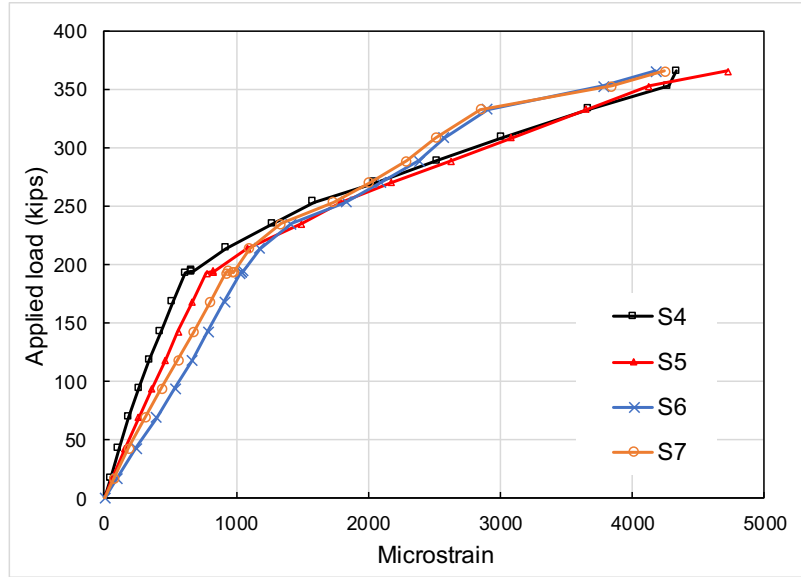


Figure E-18 Strain measurements at top fiber during first (wide spacing) shear test of Girder B3

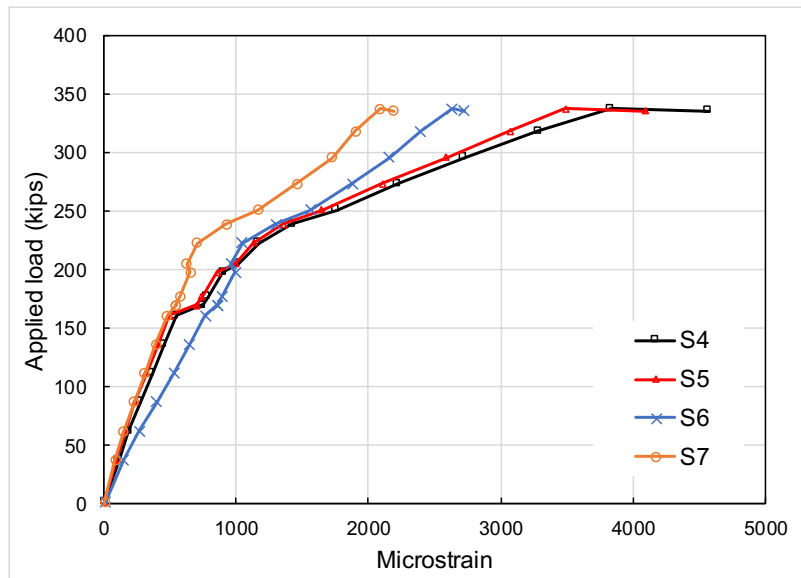


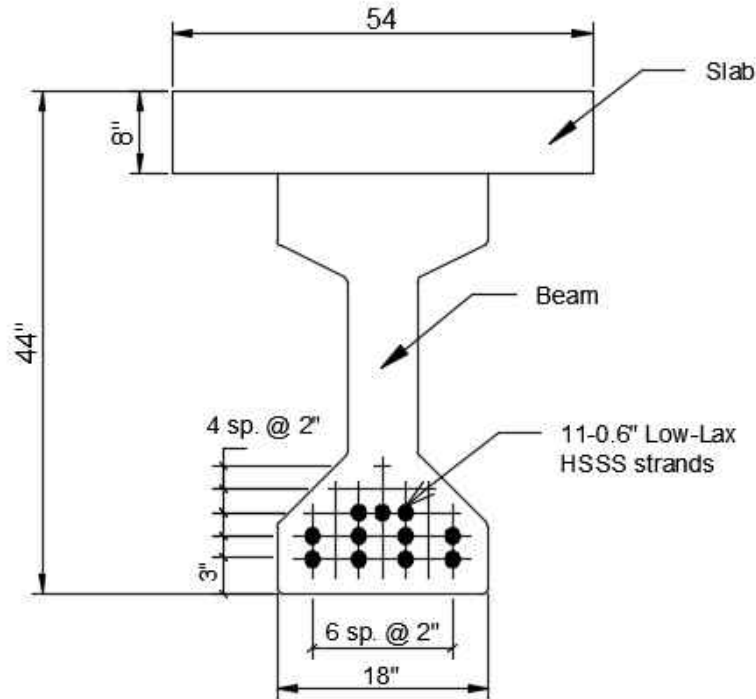
Figure E-19 Strain measurements at top fiber during second (narrow spacing) shear test of Girder B3

Appendix F – Design examples

This appendix contains examples to compute the flexural strength of concrete members prestressed with HSSS strands.

a. Analysis of concrete member prestressed with HSSS strands

Girder E1 was chosen and it is shown in the figure below.



Given:

Two spools of HSSS strands were used. Strands in the bottom layer were taken from the second spool while the strands in the second and third layers were taken from first spools. The mechanical properties for the two spools are given in Table 3-5.

$$\epsilon_{pu1} = 0.0163 \text{ in./in. (bottom layer of strands)}$$

$$\epsilon_{pu2} = 0.0181 \text{ in./in. (second and third layers of strands)}$$

$$\epsilon_{cu} = 0.003 \text{ in./in.}$$

$$f_{pu1} = 249.5 \text{ ksi (bottom layer of strands)}$$

$$f_{pu2} = 261.6 \text{ ksi (second and third layers of strands)}$$

$$E_{ps1} = 24,788 \text{ ksi (bottom layer of strands)}$$

$$E_{ps2} = 24,950 \text{ ksi (second and third layers of strands)}$$

$$f_{pe} = 137.6 \text{ ksi}$$

$$\epsilon_{pe} = 0.00555 \text{ in./in.}$$

$$f'_c \text{ (deck slab)} = 6.44 \text{ ksi}$$

$$f'_c (\text{girder}) = 10.06 \text{ ksi}$$

$$d_1 = 41 \text{ in. (distance from top fiber to bottom layer of strands)}$$

The flexural strength of Girder E1 was calculated using three different approaches as follows:

1. Using detailed iterative approach, following flowchart given in Figure 7-25

1. Assume top fiber strain, ε_{cf}

- $\varepsilon_{cf} = 0.0005$

2. Calculate the first neutral axis depth, c_1 , from strain distribution using Equation 7-22

- $c_1 = \left(\frac{\varepsilon_{cf}}{\varepsilon_{cf} + \varepsilon_{pu} - \varepsilon_{pe}} \right) \times d_1 = \left(\frac{0.0005}{0.0005 + 0.0163 - 0.00555} \right) \times 41 = 1.82 \text{ in.} < \text{slab thickness of } 8 \text{ in. (rectangular section)}$

3. Calculate the concrete stress block parameters β and α using Equations 7-18 and 7-19, respectively, where ε'_c is calculated using Equation 7-20

- $\varepsilon'_c = \left(\frac{f'_c}{11} + 1.6 \right) \times 10^{-3} = \left(\frac{6.44}{11} + 1.6 \right) \times 10^{-3} = 0.00219 \text{ in./in.}$
- $\beta = \frac{4 - \frac{\varepsilon_{cf}}{\varepsilon'_c}}{6 - 2 - \frac{\varepsilon_{cf}}{\varepsilon'_c}} \left(-\frac{f'_c}{50} + 1.1 \right) = \frac{4 - \frac{0.0005}{0.00219}}{6 - 2 - \frac{0.0005}{0.00219}} \left(-\frac{6.44}{50} + 1.1 \right) = 0.6608 \geq 0.65$
- $\alpha = \left(\frac{1}{\beta} \right) \left(\frac{\varepsilon_{cf}}{\varepsilon'_c} - \frac{1}{3} \left(\frac{\varepsilon_{cf}}{\varepsilon'_c} \right)^2 \right) \left(-\frac{f'_c}{60} + 1 \right) = \left(\frac{1}{0.6608} \right) \left(\frac{0.0005}{0.00219} - \frac{1}{3} \left(\frac{0.0005}{0.00219} \right)^2 \right) \left(-\frac{6.44}{60} + 1 \right) = 0.2849$

4. Calculate strain in the layers of HSSS strands using similar triangle

- $\varepsilon_{ps1} = \varepsilon_{pe} + \varepsilon_{cf} \left(\frac{(d_1 - c_1)}{c_1} \right) = 0.00555 + 0.0005 \left(\frac{(41 - 1.82)}{1.82} \right) = 0.0163 \text{ in./in. strain in the strands in the bottom layer}$

- $\varepsilon_{ps2} = \varepsilon_{pe} + \varepsilon_{cf} \left(\frac{(d_2 - c_1)}{c_1} \right) = 0.00555 + 0.0005 \left(\frac{(39 - 1.82)}{1.82} \right) = 0.0158 \text{ in./in. strain in the strands in the second layer}$

- $\epsilon_{ps3} = \epsilon_{pe} + \epsilon_{cf} \left(\frac{(d_3 - c_1)}{c_1} \right) = 0.00555 + 0.0005 \left(\frac{(37 - 1.82)}{1.82} \right) = 0.0152 \text{ in./in. strain}$

in the strands in the third layer

5. Calculated stress in the layers of HSSS strands using stress-strain model given in Equation 3-1 after substituting A , B , and C coefficients from Table 3-8 and elastic modulus from Table 3-5

- $f_{ps1} = E_{ps1} \times \epsilon_{ps1} \left(A + \frac{1-A}{(1+(B \times \epsilon_{ps1})^C)^{\frac{1}{C}}} \right) = 24,788 \times 0.0163 \left(0.05 + \frac{1-0.05}{(1+(102 \times 0.0163)^7)^{\frac{1}{7}}} \right) = 250 \text{ ksi}$

- $f_{ps2} = E_{ps2} \times \epsilon_{ps2} \left(A + \frac{1-A}{(1+(B \times \epsilon_{ps2})^C)^{\frac{1}{C}}} \right) = 24,920 \times 0.0158 \left(0.065 + \frac{1-0.065}{(1+(100 \times 0.0158)^{6.5})^{\frac{1}{6.5}}} \right) = 257 \text{ ksi}$

- $f_{ps3} = E_{ps2} \times \epsilon_{ps3} \left(A + \frac{1-A}{(1+(B \times \epsilon_{ps3})^C)^{\frac{1}{C}}} \right) = 24,920 \times 0.0152 \left(0.065 + \frac{1-0.065}{(1+(100 \times 0.0152)^{6.5})^{\frac{1}{6.5}}} \right) = 255 \text{ ksi}$

6. Calculate second neutral axis depth, c_2 , from force equilibrium

- $c_2 = \frac{\sum_{i=1}^n A_{psi} \times f_{psi}}{\alpha f'_c \beta b} = \frac{(4 \times 0.23 \times 250) + (4 \times 0.23 \times 257) + (3 \times 0.23 \times 255)}{0.2849 \times 6.44 \times 0.6608 \times 24} = 22.03 \text{ in.}$

7. Terminate the iteration if $c_1 - c_2 = 0$, otherwise go to step (1) and increase the top fiber strain for the next iteration.

- $c_1 - c_2 = 1.82 - 22.03 = -20.21 \text{ in.}$
- Because $c_1 - c_2 \neq 0$, go to step (1) and increase ϵ_{cf}
- A macro was created in excel program to find ϵ_{cf} that results in $c_1 - c_2 = 0$

1. New top fiber strain where equilibrium is achieved

- $\varepsilon_{cf} = 0.002198$

2. Calculate the first neutral axis depth, c_1 , from strain distribution

- $c_1 = \left(\frac{\varepsilon_{cf}}{\varepsilon_{cf} + \varepsilon_{pu} - \varepsilon_{pe}} \right) \times d_1 = \left(\frac{0.002198}{0.002198 + 0.0163 - 0.00555} \right) \times 41 = 6.960 \text{ in.} < \text{slab}$
thickness of 8 in. (rectangular section)

3. Calculate the concrete stress block parameters, β and α , using Equations 7-18 and 7-19, respectively, for the new top fiber strain

- $\beta = \frac{4 - \frac{\varepsilon_{cf}}{\varepsilon'_c}}{6 - 2 - \frac{\varepsilon_{cf}}{\varepsilon'_c}} \left(-\frac{f'_c}{50} + 1.1 \right) = \frac{4 - \frac{0.002198}{0.00219}}{6 - 2 - \frac{0.002198}{0.00219}} \left(-\frac{6.44}{50} + 1.1 \right) = 0.729$

- $\alpha = \left(\frac{1}{\beta} \right) \left(\frac{\varepsilon_{cf}}{\varepsilon'_c} - \frac{1}{3} \left(\frac{\varepsilon_{cf}}{\varepsilon'_c} \right)^2 \right) \left(-\frac{f'_c}{60} + 1 \right) = \left(\frac{1}{0.729} \right) \left(\frac{0.002198}{0.00219} - \frac{1}{3} \left(\frac{0.002198}{0.00219} \right)^2 \right) \left(-\frac{6.44}{60} + 1 \right) = 0.818$

4. Calculate strain in the layers of HSSS strands using similar triangle

- $\varepsilon_{ps1} = \varepsilon_{pe} + \varepsilon_{cf} \left(\frac{(d_1 - c_1)}{c_1} \right) = 0.00555 + 0.002198 \left(\frac{(41 - 6.96)}{6.96} \right) = 0.0163 \text{ in./in.} =$

ε_{pu} (rupture of strands)

- $\varepsilon_{ps2} = \varepsilon_{pe} + \varepsilon_{cf} \left(\frac{(d_2 - c_1)}{c_1} \right) = 0.00555 + 0.002199 \left(\frac{(39 - 6.96)}{6.96} \right) = 0.0157 \text{ in./in.}$

- $\varepsilon_{ps3} = \varepsilon_{pe} + \varepsilon_{cf} \left(\frac{(d_3 - c_1)}{c_1} \right) = 0.00555 + 0.002199 \left(\frac{(37 - 6.96)}{6.96} \right) = 0.0150 \text{ in./in.}$

5. Calculated stress in the layers of HSSS strands using stress-strain model given in Equation 3-1 after substituting A , B , and C coefficients from Table 3-8 and elastic modulus from Table 3-5

- $f_{ps1} = 24,788 \times 0.0163 \left(0.05 + \frac{1 - 0.05}{(1 + (102 \times 0.0163)^7)^{\frac{1}{7}}} \right) = 250.2 \text{ ksi}$

- $f_{ps2} = 24,920 \times 0.0157 \left(0.065 + \frac{1 - 0.065}{(1 + (100 \times 0.0157)^{6.5})^{\frac{1}{6.5}}} \right) = 256.5 \text{ ksi}$

- $f_{ps3} = 24,920 \times 0.0150 \left(0.065 + \frac{1-0.065}{(1+(100 \times 0.0150)^{6.5})^{\frac{1}{6.5}}} \right) = 254.9 \text{ ksi}$

6. Calculate second neutral axis depth, c_2 , from force equilibrium

- $c_2 = \frac{(4 \times 0.23 \times 250.2) + (4 \times 0.23 \times 256.5) + (3 \times 0.23 \times 254.9)}{0.818 \times 6.44 \times 0.729 \times 24} = 6.966 \text{ in.}$

7. Terminate the iteration if $c_1 - c_2 = 0$, otherwise go to step (1) and increase the top fiber strain for the next iteration.

- $c_1 - c_2 = 6.960 - 6.966 = -0.006 \cong 0$

8. Calculate the flexural strength, M_n , by summing tension forces about centroid of the compression depth.

- $a = \beta \times c_1 = 0.729 \times 6.96 = 5.074 \text{ in.}$
- $M_n = \sum_{i=1}^n A_{psi} \times f_{psi} \left(d_i - \frac{a}{2} \right) = \left\{ 4 \times 0.23 \times 250.2 \times \left(41 - \frac{5.074}{2} \right) \right\} + \left\{ 4 \times 0.23 \times 256.5 \times \left(39 - \frac{5.074}{2} \right) \right\} + \left\{ 3 \times 0.23 \times 254.9 \times \left(37 - \frac{5.074}{2} \right) \right\} = 1961 \text{ kip-ft}$

The measured experimental moment for Girder E1 was *2051 kip-ft*. The calculated moment using detailed iterative approach was 95.6%.

2. Using simplified iterative approach, following flowchart given in Figure 7-27

1. Assume top fiber strain, ε_{cf}

- $\varepsilon_{cf} = 0.0005$

2. Calculate the first neutral axis depth, c_1 , from strain distribution using Equation 7-22

- $c_1 = \left(\frac{\varepsilon_{cf}}{\varepsilon_{cf} + \varepsilon_{pu} - \varepsilon_{pe}} \right) \times d_1 = \left(\frac{0.0005}{0.0005 + 0.0163 - 0.00555} \right) \times 41 = 1.82 \text{ in.} < \text{slab thickness of } 8 \text{ in. (rectangular section)}$

3. Calculate the concrete stress block parameters, β and α using Equations 7-18 and 7-19, respectively, where ε'_c is calculated using Equation 7-20

- $\varepsilon'_c = \left(\frac{f'_c}{11} + 1.6 \right) \times 10^{-3} = \left(\frac{6.44}{11} + 1.6 \right) \times 10^{-3} = 0.00219 \text{ in./in.}$

- $$\beta = \frac{4 - \frac{\epsilon_{cf}}{\epsilon_c}}{6 - 2 \frac{\epsilon_{cf}}{\epsilon_c}} \left(-\frac{f'_c}{50} + 1.1 \right) = \frac{4 - \frac{0.0005}{0.00219}}{6 - 2 \times \frac{0.0005}{0.00219}} \left(-\frac{6.44}{50} + 1.1 \right) = 0.6608$$
- $$\alpha = \left(\frac{1}{\beta} \right) \left(\frac{\epsilon_{cf}}{\epsilon_c} - \frac{1}{3} \left(\frac{\epsilon_{cf}}{\epsilon_c} \right)^2 \right) \left(-\frac{f'_c}{60} + 1 \right) = \left(\frac{1}{0.6608} \right) \left(\frac{0.0005}{0.00219} - \frac{1}{3} \left(\frac{0.0005}{0.00219} \right)^2 \right) \left(-\frac{6.44}{60} + 1 \right) = 0.2849$$

4. Calculate second neutral axis depth, c_2 , from force equilibrium using Equation 7-21. The ultimate stress, f_{pu} , in the strands shall be taken for those in the bottom layer because they reach their ultimate stress before the other layer

- $$c_2 = \frac{A_{ps} \times f_{pu}}{\alpha f'_c \beta b} = \frac{11 \times 0.23 \times 249.5}{0.2849 \times 6.44 \times 0.6608 \times 24} = 21.74 \text{ in.}$$

5. Terminate the iteration if $c_1 - c_2 = 0$, otherwise go to step (1) and increase the top fiber strain for the next iteration.

- $c_1 - c_2 = 1.82 - 21.74 = -19.12 \text{ in.}$
- Because $c_1 - c_2 \neq 0$, go to step (1) and increase ϵ_{cf}
- A macro was created in excel program to find ϵ_{cf} that results in $c_1 - c_2 = 0$

1. New top fiber strain where equilibrium is achieved

- $\epsilon_{cf} = 0.002168$

2. Calculate the first neutral axis depth, c_1 , from strain distribution

- $$c_1 = \left(\frac{\epsilon_{cf}}{\epsilon_{cf} + \epsilon_{pu} - \epsilon_{pe}} \right) \times d_1 = \left(\frac{0.002168}{0.002168 + 0.0163 - 0.00555} \right) \times 41 = 6.881 \text{ in.} < 8 \text{ in. slab thickness of 8 in. (rectangular section)}$$

3. Calculate the concrete stress block parameters, β and α , using Equations 7-18 and 7-19, respectively.

- $$\beta = \frac{4 - \frac{\epsilon_{cf}}{\epsilon_c}}{6 - 2 \frac{\epsilon_{cf}}{\epsilon_c}} \left(-\frac{f'_c}{50} + 1.1 \right) = \frac{4 - \frac{0.002168}{0.00219}}{6 - 2 \times \frac{0.002168}{0.00219}} \left(-\frac{6.44}{50} + 1.1 \right) = 0.727$$

- $\alpha = \left(\frac{1}{\beta}\right) \left(\frac{\epsilon_{cf}}{\epsilon_c} - \frac{1}{3} \left(\frac{\epsilon_{cf}}{\epsilon_c}\right)^2\right) \left(-\frac{f'_c}{60} + 1\right) = \left(\frac{1}{0.726}\right) \left(\frac{0.002168}{0.00219} - \frac{1}{3} \left(\frac{0.002168}{0.00219}\right)^2\right) \left(-\frac{6.44}{60} + 1\right) = 0.815$

4. Calculate second neutral axis depth, c_2 , from force equilibrium using Equation 7-21.

- $c_2 = \frac{A_{ps} \times f_{pu}}{\alpha f'_c \beta b} = \frac{11 \times 0.23 \times 249.5}{0.815 \times 6.44 \times 0.727 \times 24} = 6.893 \text{ in.}$

5. Terminate the iteration if $c_1 - c_2 = 0$, otherwise go to step (1) and increase the top fiber strain for the next iteration.

- $c_1 - c_2 = 6.881 - 6.893 = -0.012 \cong 0$

6. Calculate distance from top fiber to centroid of strands

- $d_{avg} = \frac{\sum_{i=1}^n A_{psi} \times d_i}{\sum_{i=1}^n d_i} = \frac{(4 \times 0.23 \times 41) + (4 \times 0.23 \times 39) + (3 \times 0.23 \times 37)}{(11 \times 0.23)} = 39.18 \text{ in.}$

7. Calculate the flexural strength, M_n , by summing tension forces about centroid of the compression depth.

- $a = \beta * c_1 = 0.726 * 6.926 = 5.028 \text{ in.}$
- $M_n = f_{pu} \times A_{ps} \left(d_{avg} - \frac{a}{2}\right) = \left\{249.5 \times 11 \times 0.23 \left(39.18 - \frac{5.028}{2}\right)\right\} = 1929 \text{ kip-ft}$

The measured experimental moment for Girder E1 was *2051 kip-ft*. The calculated moment using detailed iterative approach was 94.1%.

3. Using non-iterative approach, following flowchart given in Figure 9-1

1. Calculate stress block parameters using Equation 8-10

- $\beta_1 \alpha_1 = 0.77 - \frac{f'_c}{60} = 0.77 - \frac{6.44}{60} = 0.6626$

2. Calculate balanced reinforcement ratio using Equation 8-6

- $\rho_{ssb} = \alpha_1 \beta_1 \frac{f'_c}{f_{pu}} \frac{\epsilon_{cu}}{\epsilon_{cu} + \epsilon_{pu} - \epsilon_{pe}} = 0.6626 \frac{6.44}{249.5} \frac{0.003}{0.003 + 0.0163 - 0.00555} = 0.00373$

3. Calculate distance from top fiber to centroid of strands

- $d_{avg} = \frac{\sum_{i=1}^n A_{psi} \times d_i}{\sum_{i=1}^n A_{psi}} = \frac{(4 \times 0.23 \times 41) + (4 \times 0.23 \times 39) + (3 \times 0.23 \times 37)}{(11 \times 0.23)} = 39.18 \text{ in.}$

4. Calculate reinforcement ratio

$$\bullet \rho_{ss} = \frac{\sum_{i=1}^n A_{psi}}{b \times d_{avg}} = \frac{11 \times 0.23}{24 \times 39.18} = 0.00269 < \rho_{ssb} \text{ (rupture of strand failure mode)}$$

5. Calculate neutral axis depth at balanced condition using Equation 8-5

$$\bullet c_b = \left(\frac{\varepsilon_{cu}}{\varepsilon_{cu} + \varepsilon_{pu} - \varepsilon_{pe}} \right) \times d_1 = \left(\frac{0.003}{0.003 + 0.0163 - 0.00555} \right) \times 41 = 8.945 \text{ in.}$$

6. Calculate neutral axis using Equation 8-13

$$\bullet c = \left(0.7 \frac{\rho_{ss}}{\rho_{ssb}} + 0.26 \right) c_b = \left(0.7 * \frac{0.00269}{0.00373} + 0.26 \right) \times 8.945 = 6.841 \text{ in.}$$

7. Calculate top fiber strain using Equation 8-14

$$\bullet \varepsilon_{cf} = c \left(\frac{\varepsilon_{pu} - \varepsilon_{pe}}{d_1 - c} \right) = 6.841 * \frac{0.0163 - 0.00555}{41 - 6.841} = 0.00215$$

8. Calculate the concrete stress block parameter, β , using Equation 8-7 where ε'_c is calculated using Equation 8-9

$$\bullet \varepsilon'_c = \left(\frac{f'_c}{11} + 1.6 \right) * 10^{-3} = \left(\frac{6.44}{11} + 1.6 \right) * 10^{-3} = 0.00219 \text{ in./in.}$$

$$\bullet \beta = \frac{4 - (\varepsilon_{cf} / \varepsilon'_c)}{6 - 2 (\varepsilon_{cf} / \varepsilon'_c)} \left(-\frac{f'_c}{50} + 1.1 \right) = \frac{4 - \frac{0.00215}{0.00219}}{6 - 2 * \frac{0.00215}{0.00219}} \left(-\frac{6.44}{50} + 1.1 \right) = 0.726 \geq 0.65$$

9. Calculate the flexural strength, M_n , by summing tension forces about centroid of the compression depth using Equation 8-15

$$\bullet M_n = A_{ps} \times f_{pu} \left(d_{avg} - \frac{\beta c}{2} \right) = 11 \times 0.23 \times 249.5 * \left(39.18 - \frac{0.726 * 6.841}{2} \right) = 930 \text{ kip-ft}$$

The measured experimental moment for Girder E1 was *2051 kip-ft*. The calculated moment using detailed iterative approach was 94.1%.

b. Design of concrete member prestressed with HSSS strands

Design Example 1: Assume the required ultimate moment (M_u) = 900 ki p-ft.

Given:

The guaranteed mechanical properties for HSSS strands, which are specified by ASTM A1114 and given in Table 3-5, were used in this design example.

$$A_{ps} = 0.231 \text{ in}^2$$

$$\epsilon_{pu} = 0.014 \text{ in./in.}$$

$$E_{ps} = 24,000 \text{ ksi}$$

$$f_{pu} = 240 \text{ ksi}$$

$$f_{pi} = 0.7 * 240 = 168 \text{ ksi} \rightarrow \text{assume initial stress 70\% of the ultimate strength}$$

$$f_{pe} = 0.85 * 168 = 142.8 \text{ ksi} \rightarrow \text{assume prestress losses equal 15\%}$$

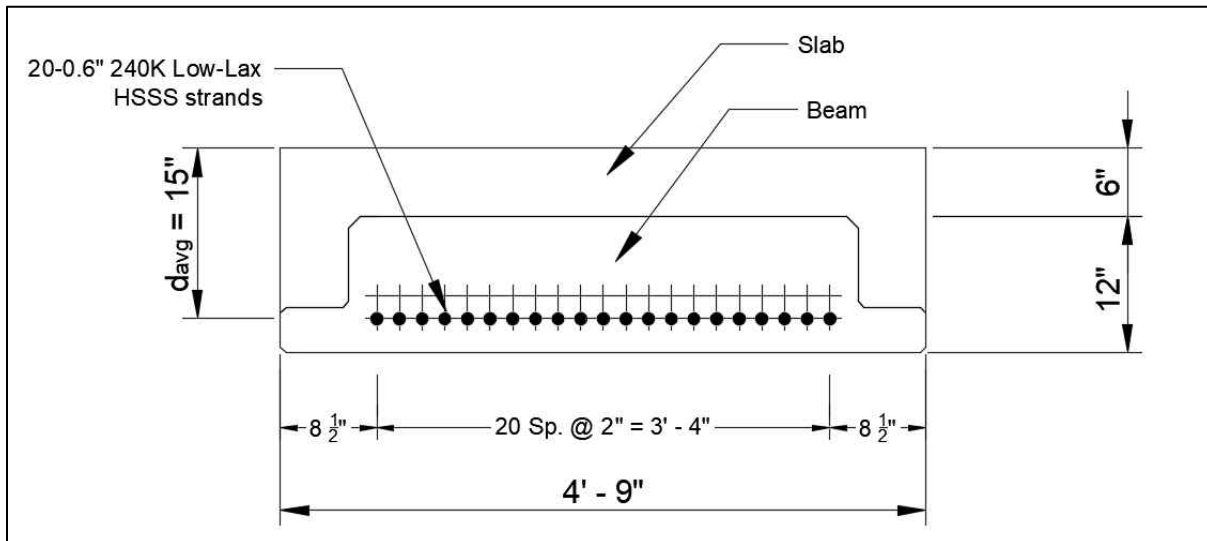
$$\epsilon_{pe} = 0.006 \text{ in./in.}$$

$$\epsilon_{cu} = 0.003 \text{ in./in.}$$

$$f'_c (\text{slab}) = 6.0 \text{ ksi}$$

$$f'_c (\text{beam}) = 8.5 \text{ ksi}$$

Choose Florida Slab Beam section (12x57) for the design



Using the design flowchart given in Figure 9-3

1. Calculate stress block parameters, $\beta_1 \alpha_1$, using Equation 8-10

$$\bullet \quad \beta_1 \alpha_1 = 0.77 - \frac{f'_c}{60} = 0.77 - \frac{6}{60} = 0.67$$

2. Calculate balanced reinforcement ratio using Equation 8-6

$$\bullet \quad \rho_{ssb} = \alpha_1 \beta_1 \frac{f'_c}{f_{pu}} \frac{\epsilon_{cu}}{\epsilon_{pu} + \epsilon_{pe}} = 0.67 \frac{6}{240} \frac{0.003}{0.003 + 0.014 - 0.006} = 0.00457$$

3. Assume 20 HSSS strands at the bottom layer of FSB as shown in Figure below

- $d_{avg} = 18 - 3 = 15$ in.

4. Calculate reinforcement ratio

- $\rho_{ss} = \frac{\sum_{i=1}^n A_{psi}}{b \times d_{avg}} = \frac{20 \times 0.231}{57 \times 15} = 0.00540$

- $\rho_{ss} > \rho_{ssb} \rightarrow$ failure mode is crushing of concrete; check maximum reinforcement limit using Equation 8-24

- $\rho_{ss,max} = \left(\frac{2 f_{pe}}{1,000} + 1.18 \right) \rho_{ssb} = \left(\frac{2 \times 142.8}{1000} + 1.18 \right) \times 0.00457 = 0.00670 > \rho_{ss}$ OK

5. Calculate neutral axis depth at balanced condition using Equation 8-5

- $c_b = \left(\frac{\varepsilon_{cu}}{\varepsilon_{cu} + \varepsilon_{pu} - \varepsilon_{pe}} \right) \times d_1 = \left(\frac{0.003}{0.003 + 0.014 - 0.006} \right) \times 15 = 4.091$ in.

6. Calculate neutral axis using Equation 8-20

- $c = \left(0.8 \frac{\rho_{ss}}{\rho_{ssb}} + 0.2 \right) c_b = \left(0.8 \times \frac{0.0054}{0.00457} + 0.2 \right) \times 4.091 = 4.684$ in.

7. Calculate strain in the layers of HSSS strands using similar triangle, Equation 8-21

- $\varepsilon_{p1} = \varepsilon_{pe} + \left(\varepsilon_{cu} \frac{d-c}{c} \right) = 0.006 + 0.003 \times \frac{15-4.684}{4.684} = 0.0126$

8. Calculated stress in the layers of HSSS using stress-strain model using Equation 3-2

- $f_{ps1} = 24,000 \times 0.0126 \left(0.06 + \frac{1-0.06}{(1+(101 \times 0.0126)^{6.45})^{\frac{1}{6.45}}} \right) = 235$ ksi

9. Calculate the concrete stress block parameter, β , using Equation 8-7 where ε'_c is calculated using Equation 8-9

- $\varepsilon'_c = \left(\frac{f'_c}{11} + 1.6 \right) \times 10^{-3} = \left(\frac{6}{11} + 1.6 \right) \times 10^{-3} = 0.00215$ in./in.

- $\beta = \frac{4 - (\varepsilon_{cf}/\varepsilon'_c)}{6 - 2 (\varepsilon_{cf}/\varepsilon'_c)} \left(-\frac{f'_c}{50} + 1.1 \right) = \frac{4 - \frac{0.00215}{0.003}}{6 - 2 \times \frac{0.00215}{0.003}} \left(-\frac{6}{50} + 1.1 \right) = 0.7 \geq 0.65$

10. Calculate the nominal flexural resistance, M_n , by summing tension forces about centroid of the compression depth using Equation 8-23

- $M_n = A_{ps} \times f_p \left(d_{avg} - \frac{\beta c}{2} \right) = 20 * 0.231 * 235 * \left(15 - \frac{0.7 * 4.684}{2} \right) = 1201 \text{ kip-ft}$
- Assume resistance factor (ϕ) equals 0.75 because of brittle nature of HSSS strands
- $\phi M_n = 0.75 * 1201 = 901 \text{ kip-ft}$
- $\phi M_n > M_u$; design is good otherwise go to step 3 and increase number of strands

Design Example 2: Assume the required ultimate moment (M_u) = 1600 kip-ft.

Given:

The guaranteed mechanical properties for HSSS strands, which are specified by ASTM A1114 and given in Table 3-5, were used in this design example.

$$A_{ps} = 0.231 \text{ in}^2$$

$$\varepsilon_{pu} = 0.014 \text{ in./in.}$$

$$E_{ps} = 24,000 \text{ ksi}$$

$$f_{pu} = 240 \text{ ksi}$$

$$f_{pi} = 0.7 * 240 = 168 \text{ ksi} \rightarrow \text{assume initial stress 70\% of the ultimate strength}$$

$$f_{pe} = 0.85 * 168 = 142.8 \text{ ksi} \rightarrow \text{assume prestress losses equal 15\%}$$

$$\varepsilon_{pe} = 0.006 \text{ in./in.}$$

$$\varepsilon_{cu} = 0.003 \text{ in./in.}$$

$$f'_c (\text{slab}) = 4.5 \text{ ksi}$$

$$f'_c (\text{beam}) = 8.5 \text{ ksi}$$

Choose AASHTO Type II section with slab thickness of 8" and width of 72".

Using the design flowchart given in Figure 9-1

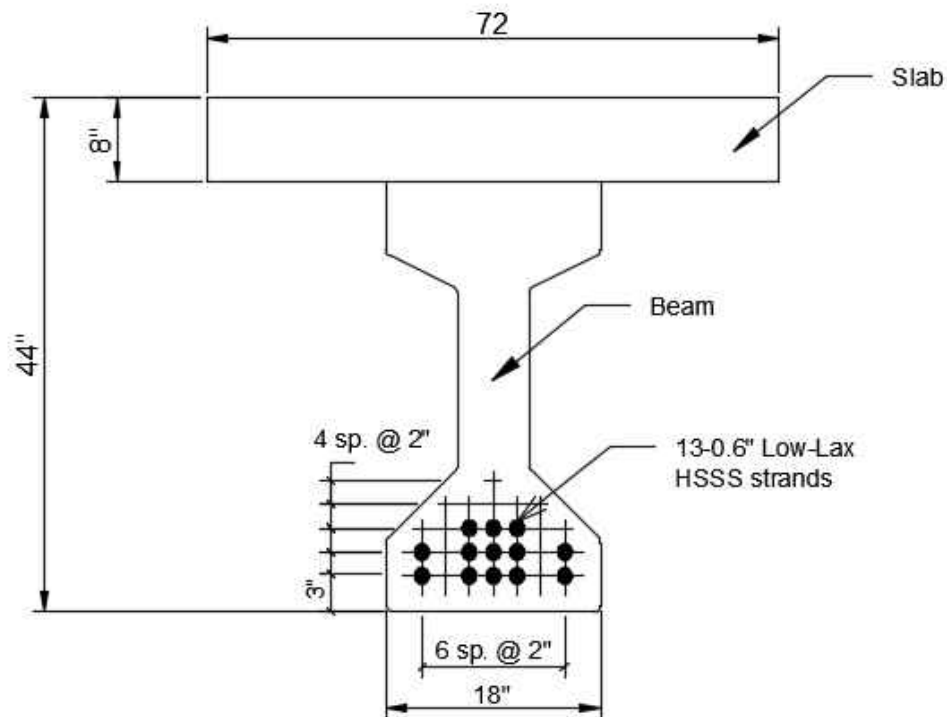
1. Calculate stress block parameters, $\beta_1 \alpha_1$, using Equation 8-10

$$\bullet \quad \beta_1 \alpha_1 = 0.77 - \frac{f'_c}{60} = 0.77 - \frac{4.5}{60} = 0.695$$

2. Calculate balanced reinforcement ratio using Equation 8-6

$$\bullet \quad \rho_{ssb} = \alpha_1 \beta_1 \frac{f'_c}{f_{pu}} \frac{\varepsilon_{cu}}{\varepsilon_{cu} + \varepsilon_{pu} - \varepsilon_{pe}} = 0.695 * \frac{4.5}{240} * \frac{0.003}{0.003 + 0.014 - 0.006} = 0.00355$$

3. Assume number of HSSS strands = 13 as shown in Figure below



4. Calculate distance from top fiber to centroid of strands

- $$d_{avg} = \frac{\sum_{i=1}^n A_{psi} \times d_i}{\sum_{i=1}^n A_{psi}} = \frac{(5 \times 0.231 \times 41) + (5 \times 0.231 \times 39) + (3 \times 0.231 \times 37)}{(13 \times 0.231)} = 39.31 \text{ in.}$$

5. Calculate reinforcement ratio

- $$\rho_{ss} = \frac{\sum_{i=1}^n A_{psi}}{b \times d_{avg}} = \frac{13 \times 0.231}{72 \times 39.31} = 0.00106$$

- $\rho_{ss} < \rho_{ssb} \rightarrow$ failure mode is rupture of strands; check minimum reinforcement limit using Equation 8-16

- $$\rho_{ss,min} = \frac{50 + 33 \times 4.5}{1000} \times 0.00355 = 0.0007 < \rho_{ss} \text{ OK}$$

6. Calculate neutral axis depth at balanced condition using Equation 8-5

- $$c_b = \left(\frac{\epsilon_{cu}}{\epsilon_{cu} + \epsilon_{pu} - \epsilon_{pe}} \right) \times d_1 = \left(\frac{0.003}{0.003 + 0.0163 - 0.006} \right) \times 41 = 11.182 \text{ in.}$$

7. Calculate neutral axis using Equation 8-13

- $c = \left(0.7 \frac{\rho_{ss}}{\rho_{ssb}} + 0.26\right) = \left(0.7 \times \frac{0.00106}{0.00355} + 0.26\right) \times 11.182 = 5.244 \text{ in.}$

8. Calculate top fiber strain using Equation 8-14

- $\epsilon_{cf} = c \left(\frac{\epsilon_{pu} - \epsilon_{pe}}{d_1 - c}\right) = 5.244 \times \frac{0.014 - 0.006}{41 - 5.244} = 0.00117$

- Another way to check minimum reinforcement ratio (top fiber strain must be within the inelastic region) $\rightarrow \epsilon_{cf} = 0.00117 > \frac{4.5+5}{10000} = 0.00095 \text{ OK}$

9. Calculate the concrete stress block parameter, β , using Equation 8-7 where ϵ'_c is calculated using Equation 8-9

- $\epsilon'_c = \left(\frac{f'_c}{11} + 1.6\right) \times 10^{-3} = \left(\frac{4.5}{11} + 1.6\right) \times 10^{-3} = 0.00201 \text{ in./in.}$

- $\beta = \frac{4 - (\epsilon_{cf}/\epsilon'_c)}{6 - 2(\epsilon_{cf}/\epsilon'_c)} \left(-\frac{f'_c}{50} + 1.1\right) = \frac{4 - \frac{0.00201}{0.003}}{6 - 2 \times \frac{0.00201}{0.003}} \left(-\frac{4.5}{50} + 1.1\right) = 0.6866$

10. Calculate the flexural strength, M_n , by summing tension forces about centroid of the compression depth.

- $M_n = A_{ps} \times f_{pu} \left(d_{avg} - \frac{\beta c}{2}\right) = 13 \times 0.231 \times 240 \times \left(39.31 - \frac{0.6866 \times 5.244}{2}\right) = 2253 \text{ kip-ft}$
- Assume resistance factor (ϕ) equals 0.75 because of brittle nature of HSSS strands
- $\phi M_n = 0.75 \times 2253 = 1690 \text{ kip-ft}$
- $\phi M_n > M_u$; design is good otherwise go to step 3 and increase number of strands